Université de Montréal

‘Investigating the Encoding of Visual Stimuli by forming Neural Circuits in the Cat Primary Visual Cortex’

par

Vishal Bharmauria

Département de Sciences Biologiques
Faculté des Arts et Sciences
Thèse présentée à la Faculté des études supérieures
en vue de l’obtention du grade de doctorat
en Sciences Biologiques

Avril 2016

Université de Montréal

Faculté des études supérieures

Cette thèse intitulée:

'Investigating the Encoding of Visual Stimuli by forming Neural Circuits in the cat Primary Visual Cortex'

présentée par:

Vishal Bharmauria

A été évaluée par un jury composé des personnes suivantes:

Dr. Annie Angers, président-rapporteur

Dr. Frédérique Dubois, membre du jury

Dr. Denis Boire, examinateur externe

Dr. Stéphane Molotchnikoff, directeur de recherche

Dr. Jean Rouat, co-directeur de recherche

RÉSUMÉ

Contexte

La connectomique, ou la cartographie des connexions neuronales, est un champ de recherche des neurosciences évoluant rapidement, promettant des avancées majeures en ce qui concerne la compréhension du fonctionnement cérébral. La formation de circuits neuronaux en réponse à des stimuli environnementaux est une propriété émergente du cerveau. Cependant, la connaissance que nous avons de la nature précise de ces réseaux est encore limitée. Au niveau du cortex visuel, qui est l'aire cérébrale la plus étudiée, la manière dont les informations se transmettent de neurone en neurone est une question qui reste encore inexplorée. Cela nous invite à étudier l'émergence des microcircuits en réponse aux stimuli visuels. Autrement dit, comment l'interaction entre un stimulus et une assemblée cellulaire est-elle mise en place et modulée?

Méthodes

En réponse à la présentation de grilles sinusoïdales en mouvement, des ensembles neuronaux ont été enregistrés dans la couche II/III (aire 17) du cortex visuel primaire de chats anesthésiés, à l'aide de multi-électrodes en tungstène. Des corrélations croisées ont été effectuées entre l'activité de chacun des neurones enregistrés simultanément pour mettre en évidence les liens fonctionnels de quasi-synchronie (fenêtre de ± 5 ms sur les corrélogrammes croisés corrigés). Ces liens fonctionnels dévoilés indiquent des connexions synaptiques putatives entre les neurones. Par la suite, les histogrammes peri-stimulus (PSTH) des neurones ont été comparés afin de mettre en évidence la collaboration synergique temporelle dans les réseaux fonctionnels révélés. Enfin, des spectrogrammes dépendants du taux de décharges entre neurones ou stimulus-dépendants ont été calculés pour observer les oscillations gamma dans les microcircuits émergents. Un indice de corrélation (Rsc) a également été calculé pour les neurones connectés et non connectés.

Résultats

Les neurones liés fonctionnellement ont une activité accrue durant une période de 50 ms contrairement aux neurones fonctionnellement non connectés. Cela suggère que les connexions entre neurones mènent à une synergie de leur inter-excitabilité. En outre, l'analyse du spectrogramme dépendant du taux de décharge entre neurones révèle que les neurones connectés ont une plus forte activité gamma que les neurones non connectés durant une fenêtre d'opportunité de 50ms. L'activité gamma de basse-fréquence (20-40 Hz) a été associée aux neurones à décharge régulière (RS) et l'activité de haute fréquence (60-80 Hz) aux neurones à décharge rapide (FS). Aussi, les neurones fonctionnellement connectés ont systématiquement un Rsc plus élevé que les neurones non connectés. Finalement, l'analyse des corrélogrammes croisés révèle que dans une assemblée neuronale, le réseau fonctionnel change selon l'orientation de la grille. Nous démontrons ainsi que l'intensité des relations fonctionnelles dépend de l'orientation de la grille sinusoïdale. Cette relation nous a amené à proposer l'hypothèse suivante : outre la sélectivité des neurones aux caractères spécifiques du stimulus, il y a aussi une sélectivité du connectome. En bref, les réseaux fonctionnels «signature » sont activés dans une assemblée qui est strictement associée à l'orientation présentée et plus généralement aux propriétés des stimuli.

Conclusion

Cette étude souligne le fait que l'assemblée cellulaire, plutôt que le neurone, est l'unité fonctionnelle fondamentale du cerveau. Cela dilue l'importance du travail isolé de chaque neurone, c'est à dire le paradigme classique du taux de décharge qui a été traditionnellement utilisé pour étudier l'encodage des stimuli. Cette étude contribue aussi à faire avancer le débat sur les oscillations gamma, en ce qu'elles surviennent systématiquement entre neurones connectés dans les assemblées, en conséquence d'un ajout de cohérence. Bien que la taille des assemblées enregistrées soit relativement faible, cette étude suggère néanmoins une intrigante spécificité fonctionnelle entre neurones interagissant dans une assemblée en réponse à une stimulation visuelle. Cette étude peut

être considérée comme une prémisse à la modélisation informatique à grande échelle de connectomes fonctionnels.

Mots-clés: Réseau fonctionnel, synergie, oscillations gamma, connectome, corrélations du bruit, cortex visuel, stimulus-discrimination, ensemble neuronal, microcircuit

ABSTRACT

Background

'Connectomics'— the mapping of neural connections, is a rapidly advancing field in neurosciences and it promises significant insights into the brain functioning. The formation of neuronal circuits in response to the sensory environment is an emergent property of the brain; however, the knowledge about the precise nature of these sub-networks is still limited. Even at the level of the visual cortex, which is the most studied area in the brain, how sensory inputs are processed between its neurons, is a question yet to be completely explored. Heuristically, this invites an investigation into the emergence of micro-circuits in response to a visual input — that is, how the intriguing interplay between a stimulus and a cell assembly is engineered and modulated?

Methods

Neuronal assemblies were recorded in response to randomly presented drifting sine-wave gratings in the layer II/III (area 17) of the primary visual cortex (V1) in anaesthetized cats using tungsten multi-electrodes. Cross-correlograms (CCGs) between simultaneously recorded neural activities were computed to reveal the functional links between neurons that were indicative of putative synaptic connections between them. Further, the peristimulus time histograms (PSTH) of neurons were compared to divulge the epochal synergistic collaboration in the revealed functional networks. Thereafter, perievent spectrograms were computed to observe the gamma oscillations in emergent microcircuits. Noise correlation (Rsc) was calculated for the connected and unconnected neurons within these microcircuits.

Results

The functionally linked neurons collaborate synergistically with augmented activity in a 50-ms window of opportunity compared with the functionally unconnected neurons suggesting that the connectivity between neurons leads to the added excitability between them. Further, the perievent spectrogram analysis revealed that the connected neurons

had an augmented power of gamma activity compared with the unconnected neurons in the emergent 50-ms window of opportunity. The low-band (20-40 Hz) gamma activity was linked to the regular-spiking (RS) neurons, whereas the high-band (60-80 Hz) activity was related to the fast-spiking (FS) neurons. The functionally connected neurons systematically displayed higher Rsc compared with the unconnected neurons in emergent microcircuits. Finally, the CCG analysis revealed that there is an activation of a salient functional network in an assembly in relation to the presented orientation. Closely tuned neurons exhibited more connections than the distantly tuned neurons. Untuned assemblies did not display functional linkage. In short, a 'signature' functional network was formed between neurons comprising an assembly that was strictly related to the presented orientation.

Conclusion

Indeed, this study points to the fact that a cell-assembly is the fundamental functional unit of information processing in the brain, rather than the individual neurons. This dilutes the importance of a neuron working in isolation, that is, the classical firing rate paradigm that has been traditionally used to study the encoding of a stimulus. This study also helps to reconcile the debate on gamma oscillations in that they systematically originate between the connected neurons in assemblies. Though the size of the recorded assemblies in the current investigation was relatively small, nevertheless, this study shows the intriguing functional specificity of interacting neurons in an assembly in response to a visual input. One may form this study as a premise to computationally infer the functional connectomes on a larger scale.

Key words: Functional network, synergy, gamma oscillations, connectome, noise correlations, visual cortex, stimulus-discrimination, cell-assembly, microcircuit

TABLE OF CONTENTS

ABBREVIATIONS

ACG:	Autocorrelogram
CCG	Cross-correlogram
EEG	Electroencephalogram
FF	Feed-forward
FS	Fast-spike
ING	Interneuron gamma
LFP	Local Field Potential
LGN	Lateral Geniculate Nucleus
MT	Middle Temporal
PCA	Principal Component analysis
PING	Pyramidal-interneuron gamma
PSTH	Peri-stimulus time histogram
V1	Primary visual cortex
V2	Secondary visual cortex
V3, V4, V5	Associative visual areas
RS	Regular-spike
Rsc	Noise correlation

..... I dedicate this thesis to my grandmother and my cousin, Ramansh,

.....who rest in heavens.....

ACKNOWLEDGEMENT

The sandal tree as if to prove, how sweet to conquer hate with love, perfumes the axe that lays it low.

— Rabindranath Tagore

First of all, I extend my sincere thanks to my thesis supervisor Dr. Stéphane Molotchnikoff, whose guidance and patience in directing me played a major role in completion of this thesis. Philosophically, I believe that one always goes through a process of construction and deconstruction in achieving his goals. I must acknowledge that his availability of time, suggestions, understanding, timely feedback and criticism during the progress of my project had been phenomenal in the completion of this investigation. On a similar note, I thank my thesis co-director Dr. Jean Rouat whose advice, guidance and critical evaluation, especially on the mathematical part of thesis had been the most beneficial. Having started a novice in neurosciences, and grasping the basics, it was essential to navigate and build upon their blueprints and translate them thereupon. Most importantly, once again I thank and appreciate them that they let me work freely and even explore my ideas, which I believe is inevitable for a budding career in Science.

Indeed, well-deserved big thanks to my colleagues, especially Lyes Bachatene, Sarah Cattan, and Nayan Chanauria with whom I have had numerous hours of discussion, troubleshooting problems and fine-tuning ideas. I also thank Simon Brodeur and Jeyabalaratnam Jeyadarshan for their experimental and intellectual contribution. Besides, I express that we have had memorable laughter and fun that always kept the ambience joyous. I owe a chunk of my success to them. I thank Ms. Claire Moran, a philanthropist, who in fact helped me in the understanding of the various aspects of the Western society. My thanks goes to Dr. Marc Pelletier, a Professor in University of Montreal, with whom I have had a fruitful exchange of letters that always motivated me during the various stages of my life as a doctoral student. I also thank Ms. Ligia Villarreal for the reverberant flux of letters that were always peppered with food for thought. I thank Ms. Margarita Costa, a

fellow doctoral student in adjacent lab, for numerous discussions on Science. I also thank Loveleen Singh, my roommate (and a great friend) for most of the time during my thesis. A special thanks to Ms. Louise Pelletier, especially for her home-made delicious cakes during the experiments. A note of thanks to Ms. Maud Morin and Dr. Bala Subramanian who helped me a lot during my initial time in Quebec.

I thank Yannick Passarelli, Afef Ouelhazi, Laurent Suissa, Lynn Megarbane, Massicylia Ait Yahia, Anastassia Al-Ezzi, Hidayate Mansouri, Vanessa Diab, Sarah Masson, Samir Masri, Malik Balti and others who had at different points been part of the lab. I also thank Gauri Patel, Anastassia Al-Ezzi, Amel Boudina, Riham Ayoubi, Sylvie Duchesne for their help with French. It goes without saying that the departmental administration had been the most helpful throughout my time as a graduate student. I thank the funding agencies for the scholarships that helped me in being financially independent. I thank all of them.

Finally, I thank my parents, all my family members and friends for their unprecedented support in achieving my goals. Words will not suffice their contribution in my being where I am today!

I thank everybody that had been directly or indirectly involved in the accomplishment of my thesis. I wish everyone success and happiness!

Vishal Bharmauria

CHAPTER 1. INTRODUCTION

Music begins to atrophy when it departs too far from the dance... poetry begins to atrophy when it gets too far from music.

— *Ezra Pound*

1.1 Overview

Brain is a vast jungle of connections (Cajal, 1923), and the complex behaviour of animals is attributed to the dense connectivity between neurons that comprise this amazing organ. In fact, most of the sensory, cognitive and motor faculties that animals and humans possess depend upon interactions between neurons (Buzsaki, 2010; Garner & Mayford, 2012; Herry & Johansen, 2014). Despite decades of research, many aspects of the brain have yet to be completely explored and understood. One of the central challenges in neurosciences is our ignorance of the micro-circuitry of the brain and its involvement in message encoding.

Many authors have opined that the understanding of dynamic interplay between neurons in relation to their sensory environment is only possible by extending the classical views of information processing in the brain (Buzsaki, 2010; Alivisatos *et al.*, 2012; Harris & Mrsic-Flogel, 2013; Scholl & Priebe, 2015). Traditionally, for decades researchers have relied on electrodes that could record the activity of one to few neurons in the brain, and thereby associating them to the external input (Alivisatos *et al.*, 2012). However, neuronal circuits can engage several thousand neurons, and the activity of that many neurons remains invisible to an investigator with single neuron recordings. Such a co-active group of neurons is termed a neuronal assembly (Hebb, 1948; Buzsaki, 2010; Miller *et al.*, 2014; Carrillo-Reid *et al.*, 2015). These simultaneously active neuronal cohorts have been named differently by different investigators; e.g. ensemble, synfire chains, songs, oscillators, attractors, flashes, bumps, clicks, and groups all refer to an assembly (Miller *et al.*, 2014).

Indeed, when a stimulus or a feature is presented within the sensory field of neurons, neurons form functional micro-circuits or sub-networks between themselves to encode the information present in the stimulus (Bartho *et al.*, 2004; Fujisawa *et al.*, 2008; Buzsaki, 2010; DiCarlo *et al.*, 2012; Harris & Mrsic-Flogel, 2013; Miller *et al.*, 2014; Carrillo-Reid *et al.*, 2015; Sadeh *et al.*, 2015). Understandably, it appears that functional micro-circuits are the fundamental bricks of information processing in the brain that make encoding possible. In other words, the formation of neural circuits in response to the sensory feature is an emergent, and thus a significant property of the brain (Bullmore & Sporns, 2009; Buzsaki, 2010; Rubinov & Sporns, 2010). However, to empirically gauge these functional sub-networks has been notoriously daunting for researchers, especially due to the technical limitations (Alivisatos *et al.*, 2012;). Nowadays, the advances in recording technology have made it possible to sample several hundred neurons simultaneously, and it seems that we are at the crossroads to fully comprehend these dynamically operating circuits.

Historically, the visual system has been the most studied area of the brain, and has provided us numerous insights into the brain functioning (visual cortex in particular). Despite the considerable progress since the seminal work of David Hubel and Torsten Wiesel (Hubel & Wiesel, 1959; 1962; 1965; 1968; 1969) on the visual cortex of cats, many questions still remain to be comprehensively explored in the visual cortex. One of the foremost questions, as discussed above, relates to the emergent formation of neuronal networks, so called the 'neural-codes' in the visual cortex in relation to the lived experience. This is the question that this thesis precisely attempts to answer — that is, how through the coordinated neuronal activity within a cell assembly different features are encoded.

At the outset, various approaches in deciphering the neural-code have been discussed. Thereafter, 'Connectomics' which is an emerging field in the brain mapping has been described briefly. Specifically, functional Connectomics is discussed as an approach for inferring neural codes. Since the investigations are done on the cat primary visual cortex, therefore, an overview of the cat visual cortex is presented briefly. Based upon the previous studies and what is not yet known, the next chapter pertains to the hypothesis for

the current experiments with the goal of unravelling the 'neural assembly dynamics'. The next chapters present the results of the investigation, and finally the results are discussed in an elaborate fashion.

1.2 Deciphering the Neural-Code: various approaches

Neural coding refers to characterizing the relationship between a stimulus and the activity of corresponding neuron(s) that is/are active in response to it. To decipher the neural code is a central challenge in neurosciences, and despite decades of dedicated research, we are yet to understand the anatomical and neurophysiologic aspects that make us interact with the environment to allow coherent behaviour. Neural coding is classified broadly into two main categories: the rate-code and the temporal-code (Johnson *et al.*, 2001).

1.2.1 Rate-Code

The rate-code is based on the frequency of the neuronal discharge (Adrian & Zotterman, 1926) and was the first formulation of a neural code. It was originally demonstrated in the somatosensory system, where the intensity of the stimulus is directly related to the frequency of neuronal discharge. The frequency encoding is also possible in the visual system (Molotchnikoff & Rouat, 2012). Simply speaking, in a rate-code the information is embedded in the number of spikes in a given time interval. As an example, a rate-code in the primary visual neurons, classically, refers to a tuning curve which is established in response to the orientation selectivity.

However, a complex scenario appears when neurons in the monkey temporal cortex respond to a multitude of features sharing traits (Steriade, 1997; Bullier, 2001). The biggest impediment to this code is that along the brain hierarchy, neurons become less selective to a specific feature and often respond to many features in an image. Along this line, an object-exclusive neuron must exist that may be implicated in integration of all the possible features in the target (Molotchnikoff & Rouat, 2012). Hypothetically, such neurons, if they exist, are currently termed *"grandmother cells"*. Therefore, a hierarchical system of coding seems to prevail as information flows along the cortical areas and ultimately converges onto a few grandmother cells. Several reasons militate

against the idea of cardinal cells. If there were grandmother cells in the brain operating uniquely to each stimulus, our brain would have been enormous as we are constantly bombarded by multitude of information. In addition, often cells that respond to the same stimulus, also respond weakly to other properties of the stimulus (Barth & Poulet, 2012). However, recently, neurons responding almost exclusively to pictures of a celebrity or a particular monument have been described in the median temporal lobe of humans, particularly in the hippocampus (Quiroga *et al.*, 2005).

1.2.2 Temporal-Code

The temporal-code implies that the information about the stimulus is encoded in the time-relationships of action-potentials of simultaneously active neurons. Milner (Milner, 1974) and Malsburg (Malsburg, 1981) were the initial proponents of the temporal-code. In other words, neurons sharing a same feature will have synchronized activity within a small time-window, that is, almost 1 ms period. However, the synchronized activity between neurons can be measured on different time scales ranging from 1-10 ms (Buzsáki 2010).

Indeed the time-related activity between neurons implies that "synchrony" dictates the neural code (Stanley, 2013). The initial proponents of synchrony (Milner, 1974; Grossberg, 1976; Malsburg, 1981) theoretically formulated synchrony as a potent coding mechanism to bind percepts coherently. It was until when Wolf Singer's laboratory in 1989 (Gray & Singer, 1989) experimentally showed spatially segregated neurons engaged in synchronous oscillatory activity. This suggested synchrony as a potential time related neural-code. Synchrony between two neurons is measured as a central peak in the cross-correlogram (CCG) (Perkel *et al.*, 1967; Ghisovan *et al.*, 2008). Put simply, neurons with spatially separate receptive fields will synchronize (central peak in CCG) their action potentials only to the presentation of a similar feature (e.g. same orientation) within their respective receptive fields, whereas the synchrony would disappear if the features are dissimilar or independent (Fries *et al.*, 2001). This led to the 'binding-by-synchrony' hypothesis, that is, neurons that synchronize their potentials are implicated in binding the similar features of the image.

1.2.3 Population encoding

The representation of a stimulus by joint activity of neurons is called population coding. When a feature is presented, in principle, cohorts of neurons become active at the same time. Such a group of simultaneously active neurons is termed an ensemble or a cell-assembly (Buzsaki, 2010; Kampa *et al.*, 2011; Miller *et al.*, 2014). They are referred by many names in the literature as mentioned previously. Such coding mechanism through synchronized activity of dynamic cell assemblies is termed as the *'neural distributive system'* (Bernardet & Verschure, 2010; Molotchnikoff & Rouat, 2012; Behrmann & Plaut, 2013). As a matter of fact, the CCG strategy can be employed to divulge the functional connectivity between neurons comprising a cell-assembly or even between neurons across assemblies.

Moreover, numerous oscillatory rhythms such as theta (4-7 Hz), alpha (8-12 Hz) and gamma (20-100 Hz) are prevalent for key operations (memory, perception etc) in the brain; however their range may vary slightly from one species to another species (Buzsaki & Watson, 2012; Fries, 2015). Even at rest, the brain exhibits spontaneous oscillatory reverberations (Drew *et al.*, 2008). When a stimulus is presented, it disturbs this ongoing oscillatory activity and regenerates a sparse oscillatory synchrony (Fries *et al.*, 2007; Buzsaki & Watson, 2012; Womelsdorf *et al.*, 2012; Fries, 2015). For example, in the gamma range a specific frequency might be encoding a particular property of the stimulus (Fries *et al.*, 2007). Therefore, in this framework, gamma oscillations and other oscillatory cycles (theta, alpha) are time-locked to a stimulus, and are thus potent information carriers, that is, a plausible neural-code. Indeed, it has been widely documented that inhibitory networks embedded among pyramidal neurons are involved in the generation of these task-dependent oscillatory rhythms in the brain (Carandini *et al.*, 1997; Chance *et al.*, 2002; Cardin *et al.*, 2009; Vinck *et al.*, 2013).

Having discussed these coding strategies in brief, it is to be mentioned that they are not immune to limitations (Gray *et al.*, 1990; Desimone & Duncan, 1995; Tiesinga & Sejnowski, 2009; Molotchnikoff & Rouat, 2012). As discussed above, if synchrony is the language of communication in the brain, neural populations must functionally collaborate. But how does anatomical connectivity relate to the images presented in the

receptive fields? Undoubtedly, the role of functional micro-circuitries has to be brought to the fore to understand the interplay between stimulus and the population of neurons involved in representing the stimulus.

1.3 Connectomics: An emerging field

'Connectomics' is an advanced branch of neurosciences that deals with the mapping of neuronal connections within the brain, possibly in all of the behavioural conditions (Sporns *et al.*, 2005; Sporns, 2011). Structural (anatomical) and functional descriptions of neuronal connections constitute the "connectome" of the brain (Sporns *et al.*, 2005; Hagmann *et al.*, 2010; Sporns, 2011; Alivisatos *et al.*, 2012; Leergaard *et al.*, 2012). In other words, there are two main approaches to studying the brain connectome: structural (anatomical) and functional.

1.3.1 The anatomical connectome

Neurons are densely connected to each other through synapses. This structural or the physical connectivity between neurons is referred to as the anatomical connectivity. The pioneer efforts of early investigators (Cajal, 1923; Sholl, 1956; Gilbert & Wiesel 1979) helped us in the basic understanding of the anatomical connectivity between neurons. In general, a neuron carries thousands of synapses on itself. For example, in the cat visual cortex, a neuron carries approximately 6000 synapses on it (Beaulieu & Colonnier, 1985). In fact, the spines on neuronal dendrites keep on growing and retracting in relation to experiences. Recently, the dynamics of changing synapses have been extensively studied — spines are rapidly created and destructed depending upon the input, whereas other may remain stable over a period of time (Kasai *et al.*, 2010; Dur-e-Ahmad *et al.*, 2011; Ebrahimi & Okabe, 2014; Jung & Herms, 2014; Hasegawa *et al.*, 2015; Kellner *et al.*, 2016). This renders the cortex the ability for short- and long-term plastic events, and as a consequence, the capacity for memory and cognition. Because of these dynamics, the time invariant description of synapses in neuronal circuits is precluded. However, the synaptic connectivity between neighbouring neurons has been quantified in terms of potential synapses by several investigators. For example, close neighbours (within 100 micrometer) in the supragranular layers of the cortex make up to 3-6 contacts with each

other (Hellwig, 2000; Frick *et al.*, 2008; Stepanyants *et al.*, 2008; Brown & Hestrin, 2009), whereas the probability of contacts may decrease considerably with distance (only one contact beyond 500 micrometer) (Hellwig, 2000). Similarly, an L4 neuron may also make up to 3 contacts with an L 2/3 neuron (Helmstaedter *et al.*, 2008). Notably, neurons may also make synaptic connections laterally in the brain. As an example, in the monkey prefrontal cortex, monosynaptic connections may exist between neurons across cortices for reverberating excitatory circuits (Melchitzky *et al.*, 2001).

The knowledge of the anatomical connectome is the first fundamental step to unravelling the brain connectome at other levels, because the emergence of functional and effective networks is closely associated to the neuro-anatomical layout of the brain regions (Leergaard *et al.*, 2012; Kuceyeski *et al.*, 2015). As Leergaard et al. 2012 have put it — 'a fundamental principle of the brain organization is that functional systems are formed by specific anatomical connections'. Therefore, the knowledge of the hodological organization of the brain may help in predicting the functional connectomes. Since majority of anatomical connections in the brain are local, it is imperative to understand the connectome on "microscale" (micrometer resolution). In simplest words, it is of immense importance to map anatomical micro-connectomes in the brain (Leergaard *et al.*, 2012).

From the classical histological studies to the modern technological investigations, there are many ways the neuro-anatomical microstructures in the brain can be studied. These modern day methods range from studying the histological sections through polarized imaging (PLI), to diffusion magnetic resonance imaging (dMRI), to scanning microscopy, to optogenetic functional MRI (ofMRI) (Leergaard *et al.*, 2012).

1.3.2 The functional connectome

As described above, it is essentially fundamental to map thousands of synaptic connections in the brain and relate them to the neuronal function (Seung, 2011; Leergaard *et al.*, 2012). This functional map of neuronal circuits is referred to as the functional connectome. The translation of sensory information for coherent representation in the brain is an outcome of emergent coordinated activity of groups of neurons (Alivisatos *et*

al., 2012). Such small groups of neurons, as mentioned above, that coordinate together to perform a computational task are referred to as cell assemblies (Hebb, 1949). As a matter of fact, neural spikes are a rapid medium by which neurons communicate with each other within these ensembles. Thus, the statistical prediction of such functional networks derived from the time series data is inevitable to reveal and define the brain connectome.

In a quest to capture this coordinated neural activity, several ambitious projects have been launched. For example, the Human Brain Project, the Human Connectome Project, and the Blue Brain Project. Despite decades of research with major technological advances on tracing the axonal connections (Saleem *et al.*, 2002; Sporns *et al.*, 2005; Hagmann *et al.*, 2010; Sporns, 2011; Alivisatos *et al.*, 2012; Leergaard *et al.*, 2012), the functional circuitry (Geerling & Loewy, 2006; Ugolini, 2011), the nature of synapses and the cellular level connections (Geerling & Loewy, 2006; Ugolini, 2011), the understanding of neuronal connectivity has still eluded us at all these levels. In order to better reveal the dynamics of this coordinated neural activity, an international public effort namely "the Brain activity map project" has been proposed by Alivisatos and colleagues (Alivisatos *et al.*, 2012), which underlines the challenges in functional connectomics and the major technological advances to overcome these challenges. According to them, a comprehensive measurement of neural activity would be carried out at time-scales corresponding to the behavioural output. The fact that neurons are interconnected and display plasticity, this ability renders them the ability to functionally switch from one ensemble to another depending on the task. Imperatively, the importance of divulged 'functional connectomes' would transcend the 'structural connectomes' because the same ensemble (in other words, the anatomical microconnectome) may lead to many functional connectomes depending upon the feature. Indeed, functional connections which are transiently active in the brain in response to the stimulus have to be dissociated from anatomical connections.

Several recent studies have reported the co-activation of small groups of neurons in the brain in response to applied stimuli (Fujisawa *et al.*, 2008; Buzsaki, 2010; Denman & Contreras, 2014; Schwindel *et al.*, 2014), and even pointed to the importance of functional networks within these assemblies (Buzsaki, 2010; Harris & Mrsic-Flogel,

2013; Singer, 2013; Miller *et al.*, 2014; Carrillo-Reid *et al.*, 2015; Sadeh *et al.*, 2015). For example, in a recent proposal, Singer (Singer, 2013) has suggested that a specific classifier (network) is recruited within a reservoir (assembly) of randomly coupled neurons to encode a particular stimulus. This is illustrated in **Figure 1A**. Along the same lines, Harris & Flogel (2013) **(Figure 1B)** have also suggested that cortical circuits comprise of inter-digitated sub-networks of interconnected principal neurons. In a study, Fujisawa et al. (2008) revealed the networks of functionally connected excitatory and inhibitory neurons in prefrontal cortex of rats that either ran in left or right direction. One such network is displayed in **Figure 1C.**

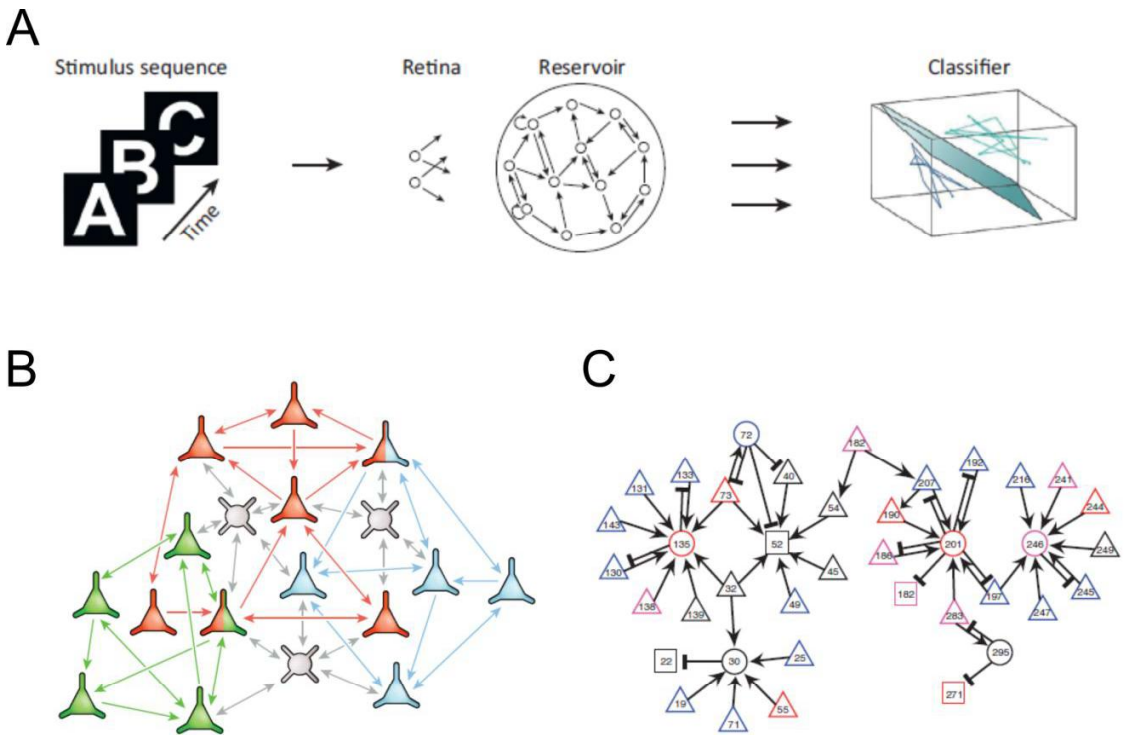

Figure 1. Functional connectomes. (A) A classifier is recruited to encode a specific stimulus from the reservoir of randomly coupled neurons (Singer, 2013). (B) An inter-digitated network of principal neurons (Harris & Mrsic-Flogel, 2013). (C) An inhibitory-excitatory network functional in the prefrontal cortex of a rat (Fujisawa *et al.*, 2008).

Indeed, many cutting-edge techniques including the classical approaches are employed to infer the functional connectivity in the brain. Many imaging techniques such as optical imaging and magnetic resonance imaging (MRI) based connectivity measures are used to reveal these maps (Leergaard *et al*., 2012). Other advanced techniques such as diffusion magnetic resonance imaging (dMRI), 3D interactive tractography-informed fMRI promise subject-specific imaging to intervene with the brain contingent upon the specific neuro-anatomy of an individual (Chamberland *et al.*, 2015). Moreover, several computation based approaches are commonly applied to estimate the functional networks (Just *et al.*, 1999; Sadeh *et al.*, 2015; Shimono & Beggs, 2015). A major advantage of computational modeling is that we can observe the networks on a bigger scale and even predict them. Calcium imaging is another widely employed technique nowadays to study key functions in cortical slices and in awake behaving animals (Grienberger & Konnerth, 2012).

Although, the above methods provide us variety of information about the brain functions, but they do not indicate the functional causalities between neurons, especially on a microscopic scale. This is only possible by correlating the activities of spike trains of simultaneously recorded neurons. In other words, the millisecond level interactions between neurons can only be revealed through the analysis of spike trains. Several correlational measures such as noise correlation (Rsc), signal correlation (r_{signal}) and cross-correlograms (CCG) are computed to investigate the functional interactions between neurons (Cohen & Kohn, 2011). In this study, CCGs are used to reveal the functional links. The details of CCG computation and interpretation are given below.

1.4 Cross-correlograms (CCG): a potent tool to infer functional connections

CCGs are an efficient way to study the time-related neural activity between two simultaneously sampled neurons (Bartho *et al.*, 2004; Fujisawa *et al.*, 2008; Ghisovan *et al.*, 2008; Buzsaki, 2010; Molotchnikoff & Rouat, 2012; Denman & Contreras, 2014). It has been shown that the CCG analysis of simultaneously recorded neurons reveals the functional linkage between them in response to a stimulus or a task (Bartho *et al.*, 2004; Fujisawa *et al.*, 2008; Denman & Contreras, 2014; Schwindel *et al.*, 2014; Sadeh *et al.*, 2015). These disclosed connections can be inferred as putative physiological connections

between neurons (Perkel *et al.*, 1967). Depending upon the latency between neuronal activities, these connections could be deemed direct or indirect. Smaller latency (< 5ms) may reflect monosynaptic projections, whereas latencies beyond 5 ms may indicate relatively disynaptic or indirect projections (Buzsaki, 2010).

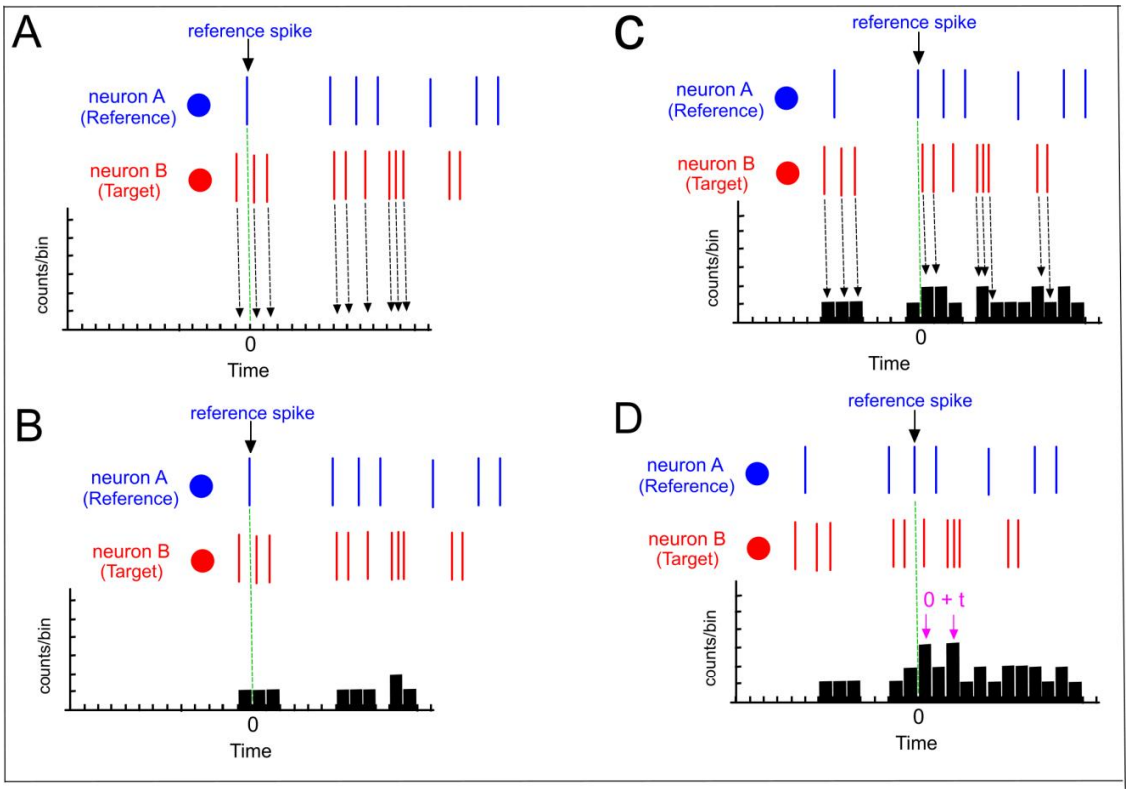

Figure 2. Cross-correlogram generation. (A-D) Progression of a CCG between two neurons.

A CCG is generated between the spikes trains of two neurons accumulated over different trials. The spikes of one of the neurons are set as reference one-by-one and a histogram is then computed for the spikes of the target neuron in relation to the reference spikes. This histogram is termed a cross-correlogram. **Figure 2** shows the cartooned progression of how a CCG is generated between the spike trains of two neurons under observation. The spikes of neuron A are set as reference, and then we observe when in time, the spikes of target neuron (neuron B) fall in the histogram. First (**Figure 2 A),** the first spike of neuron A (reference) is aligned at the time zero in the CCG (green broken

line). By doing so, the spikes of neuron B are filled in the CCG in relation to neuron A (**Figure 2B).** Gradually, by keeping every spike of neuron A as reference, the CCG is consequently filled up (**Figure 2C**). Thereafter, we observe when in relation to the spikes of neuron A, the spikes of neuron B most likely occur (this is calculated as a probability). For example, in **Figure 2C**, the maximal discharge for neuron B occured at time 0 + t. That is, when the neuron A fires at time zero, neuron B most likely fires at time 0 + t in relation to the spikes of neuron A. **Figure 2D** shows an example of an almost completely filled CCG.

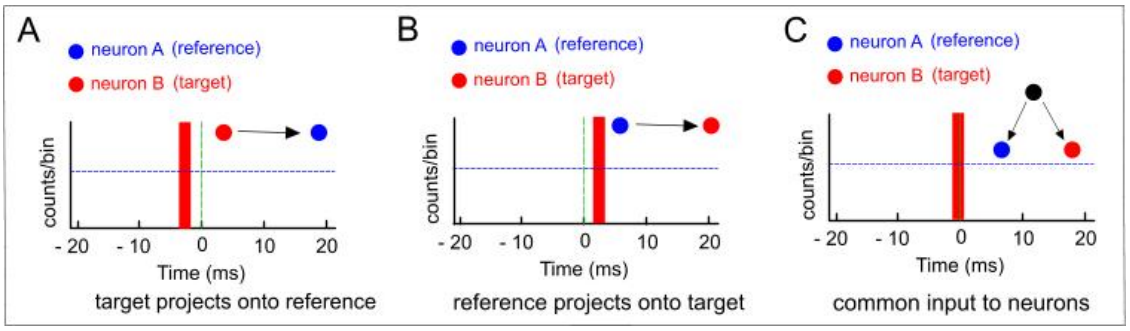

Figure 3. Interpretation of a cross-correlogram (CCG). (A) Target neuron projects onto the reference neuron. (B) Reference neuron projects onto the target neuron (C) Common input to both neurons.

Once the CCG between two neurons is computed, the next step is to interpret it. **Figure 3** explains the CCG analysis in a cartooned form. In **Figure 3A**, the spikes of neuron A are reference, and the spikes of neuron B are target. Since the histogram peaks before zero, this signifies that neuron B projects onto neuron A. This means that, the neuron B fires before neuron A, whereas it is otherwise in **Figure 3B**. However, to suggest a functional link between two neurons, peak-latencies on different scales (1−10 ms) could be observed (Buzsaki, 2010). A significant peak within 5 ms offset from zero might reflect a 'putative' relatively direct physiological connection between neurons (Perkel *et al.*, 1967; Bartho *et al.*, 2004; Denman & Contreras, 2014), because when one neuron fires and makes the another neuron fire, it usually takes 2-3 ms to communicate the message after it releases a neurotransmitter. **Figure 3C** corresponds to a common input to both neurons from other neuron(s) in the circuit since the CCG peaks at zero

(Perkel *et al.*, 1967; Denman & Contreras, 2014). The probability (p) of the connection between neurons can be computed from the significant peaks in the CCGs which is an indication of strength of the connection between neurons. Moreover, depending upon the physiology of the neuron, these connections can further be identified as exictatory or inhbitiory (Bartho *et al.*, 2004; Fujisawa *et al.*, 2008).

In short, by computing CCGs, one can reveal the functional-links and peak-probabilities (strength of connection) in response to a presented feature, either locally or distally in brain.

1.5 Visual system of the cat: Organization

1.5.1 Overview

Vision is one of the elementary senses that animals possess, and eyes are the incredible sense organs which act as an interface for us to interact with the external visual world, and behave accordingly in response to it. Since the pioneer investigations of Hubel and Wiesel on the cat visual cortex, wherein they discovered the orientation columns, cats have served as important animals of interest to understand the brain, primarily because of their high performance visual system that exhibits similarity to primates (Fox & Blake, 1971). In fact, a great deal of our knowledge about the neurophysiology of vision has come from the investigations on the cat visual system (Blake,1979; Swindale, 1997)

The cat visual cortex is divided mainly into three visual modules, namely, the primary visual cortex (Brodmann area 17 or V1), the secondary visual cortex (Brodmann area 18 or V2), and Brodmann area 19 (Blake, 1979; Felleman & Van Essen, 1991). The information encoding job is divided between these specialized regions and they process a multitude of information (such as orientation, spatial frequency etc.) resulting from the intricate networks within and between these involved areas (Schmolesky *et al.*, 1998; DiCarlo & Cox, 2007; DiCarlo *et al.*, 2012).

The cat visual cortex is arranged into domains of selectivity (e.g. the primary visual cortex is partitioned into orientation columns) — neurons sharing orientation selectivity are co-localized (Hubel & Wiesel, 1962; 1968; Kaschube *et al.*, 2010). That is, cells responding optimally to an orientation are grouped together into columns.

Classically, an electrode(s) is lowered into the area of interest in the brain to record the neural activity either in extracellular or intracellular fashion in response to a presented feature (that is, by stimulating neurons using different stimuli). The animals can be paralyzed during the experiment or the activity can even be recorded in awake, behaving animals. In the latter case, animals have to be trained for specific experiments. Notably, recently developed techniques — multi-electrode arrays, microscopy in conjunction with molecular techniques, imaging and optogenetics are currently being applied to study animal behavioral patterns (Kampa *et al.*, 2011; Ko *et al.*, 2011; Alivisatos *et al.*, 2012; Leergaard *et al.*, 2012; Tye & Deisseroth, 2012).

1.5.2 Lateral Geniculate Nucleus (LGN)

The cat LGN is a well defied laminar structure that consists of three major layers: dorsal, ventral and middle layers. They receive information from the retinal ganglion cells (Gilbert & Wiesel, 1979; Blake 1979) and pass on the information to the visual cortex.

1.5.3 Visual cortex

In cats, the axons of the LGN neurons project to the visual cortex. Visual pathways originate in the occipital lobe at the back of the brain; however some pathways originate in the parietal and temporal lobes too. The cat visual cortex is divided into three main visual areas: areas 17, 18 and 19. The areas 17 and 18 are also known as the primary visual cortex (V1) and the secondary visual cortex (V2) respectively (Blake,1979; Swindale, 1997). Area 19 comprises the associate visual areas. In addition to these areas, the cat visual cortex has another notable area that responds to visual stimulation. This is distinguished as the lateral wall of the suprasylvian gyrus (Clare & Bishop, 1954). Besides receiving inputs from the LGN, these areas are reciprocally connected to each

other (Swindale, 1997). A visual cortex is located in each hemisphere of the brain. The right visual cortex receives information from the left visual field, and the left visual cortex receives information from the right visual field. These areas form two major visual pathways in the brain that run parallel to each other in the visual system, and are inevitable for the coherent presentation of an object in the brain. These two routes are: the ventral pathway and the dorsal pathway (Grady *et al.*, 1992; DiCarlo *et al.*, 2012). The ventral pathway ends in the temporal lobe and is implicated in the processing of object recognition (color, shape) including faces; whereas, the dorsal pathway which ends in the parietal lobe relates to the spatial vision (action/location) of an object (Milner, 1974; DiCarlo *et al.*, 2012). In other words, the dorsal pathway is associated with processing of action in space.

1.5.4 Primary Visual Cortex (V1)

The cat primary visual cortex (V1) or Brodmann area 17 is one of the major areas of the neocortex which receives input from the retina. It is the major gateway to sensory information in cortex as thalamic relay cells project onto it (Gilbert & Wiesel, 1979). The primary visual cortex is organized into domains of specificity — neurons are clustered into specific columns with similar receptive fields (Hubel & Wiesel, 1962; 1965; Blasdel & Salama, 1986).

The cat primary visual cortex is divided into six layers, namely: I, II, III, IV, V, VI (Hubel & Wiesel, 1968). Each layer is characterized with specific cell types. Though numerous types of cells are present in these layers, but physiologically cells can be classified broadly into pyramidal cells and interneurons (Niell & Stryker, 2008; Bachatene *et al.*, 2012; Vinck *et al.*, 2013). Layers II, III, V, VI mainly contain the pyramidal cell types, whereas, layer IV consists of stellate cells. The LGN neurons project onto layer IV stellate cells (similar concentric receptive fields as to LGN neurons), though recently authors (Constantinople & Bruno, 2013) have demonstrated in rats that deeper cortical layers can be directly driven by thalamic input, suggesting that layer IV is not an obligatory intermediary hub of information pathway through the primary cortex. The layer II/III neurons display a radical transformation of receptive

fields — wherein cells fire maximally to the presentation of an edge or a bar within their receptive fields (Hubel & Wiesel, 1959). Besides, visual neurons also have other characteristic fundamental properties, namely — direction selectivity of layer IVβ neurons, and the selectivity for spatial frequency (Hubel & Wiesel, 1959; Movshon, 1975). Though the occurrence of spatial frequency maps is debatable, but recently authors have also demonstrated the occurrence of spatial frequency maps (Nauhaus *et al.*, 2012; Ribot *et al.*, 2013). There is another system of columnar organization in the cat visual cortex that relates to the afferent-separation from both eyes — the ocular dominance columns. An ocular dominance column corresponds to the cortical tissue that is alternately occupied by afferents either from the left eye or the right eye (Shatz & Stryker, 1978; Adams *et al.*, 2007). The ocular dominance columns are particularly defined at the cortical layer IV — to which the axonal endings of the LGN neurons project. In summary, the visual cortex is systematically organized into the maps of specific functional connectivity (orientation, ocular dominance, temporal frequency).

1.5.5 Secondary Visual Cortex (V2)

The secondary visual cortex (Brodmann area 18), which is also known as the prestriate cortex receives information from the V1. V2 exhibits strong reciprocal connections with area V1 (Symonds & Rosenquist, 1984; Salin *et al.*, 1995; Swindale, 1997) and projects strongly onto downstream area 19 (Blake 1979). Neurons in V2 share many of the properties with V1 area neurons (Blake, 1979; Bonhoeffer & Grinvald, 1993; Swindale, 1997), though they also have many differences (Sengpiel *et al.*, 1998; Kapadia *et al.*, 1999; Bair *et al.*, 2003). The major difference between V1 and V2 is that V1 receives its majority of input from the LGN, whereas V2, in addition to the input from the LGN, also receives input from the V1. That is, V1 and V2 have reciprocal relationships with each other (Symonds & Rosenquist, 1984; Cattan *et al.*, 2014).

1.6 Receptive fields and neuronal selectivity

The receptive field of a neuron is classically defined as a region in space in which the presence of a feature evokes maximum neuronal responses, that is, there is an augmentation in the firing of a neuron. The term was first coined in by Charles

Sherrington in 1906 (Sherrington, 1906). Neurons in the somatosensory system, the auditory system and the visual system have structured receptive fields. In other words, they are selective to a specific range of stimuli. Empirically, receptive fields are characterized by fixing the animal in space and presenting the feature systematically. Thus, contingent upon the stimuli presented in the receptive field, the selectivity of a neuron can be inferred — that is, to what feature the neuron fires maximal number of action potentials. For example, if a series of drifting sine-wave gratings tilting gradually in small angles is presented randomly to a primary visual neuron, it may respond best to a specific angle. In this framework, the neuron is selective for that angle or orientation. A Gaussian curve is fit on neuronal responses as a function of orientation to infer the precise value of neuronal orientation tuning (Swindale, 1998). In a similar fashion, other properties (spatial frequency, temporal frequency, speed, color etc) of neurons can also be characterized (Movshon, 1975; Heywood *et al.*, 1992).

In the visual cortex of cats, based on the receptive field properties, cells in these layers can be categorized as simple, complex and hyper-complex cells (Hubel & Wiesel, 1962; Gilbert & Wiesel, 1979). This classification is based on as to how neurons in these layers respond to dark or light edges (Hubel & Wiesel, 1962). Simple cells which were discovered by Hubel and Wiesel are mainly found in layers IV and VI of area 17 having ON-OFF sub fields. In other words, they respond to ON or OFF stimuli within their receptive fields and have flanking excitatory and inhibitory areas, that is, if a stimulus is present overlapping the excitatory and inhibitory areas, it would fail to evoke a strong response. Complex neurons do not have defined ON or OFF sub-fields, and a stimulus presented anywhere in the receptive field evokes a response, that is why complex cells have larger receptive fields than the simple cells. In other words, a complex cell does not exhibit adjacent excitatory and inhibitory zones within its receptive field. Layer II/II neurons are almost exclusively filled with complex cells (Gilbert & Wiesel, 1979). Hyper-complex cells which were discovered by Hubel and Wiesel in 1965 appear to emerge when complex neurons' axons interspersed with different orientations converge on it, that is, a hyper-complex cell transcends the behavior of a complex cell. When a line is presented within the receptive field of a hyper-complex cell, its response starts to

decline beyond a specific length of the line because of the antagonistic excitatory and inhibitory regions (Hubel & Wiesel, 1965).

1.7 Physiological classification of cells

Since the encoding job is divided amongst each neuron (or a selected group of neurons), one needs to associate the neurons implicated in the coherent encoding of various features (often very contrasting) present in an image to the obtained signal. In the cortex, there are mainly two different kinds of neurons, namely: the pyramidal cells that are excitatory in nature and the inhibitory interneurons that inhibit the activity of other neurons (Cardin *et al.*, 2009). Therefore, it becomes important to examine the isolated neurons and relate them to the signal within the context of an experiment. Electrophysiologically, based upon the ascending slope of the spike-waveform, neurons can be categorized into the regular spiking (RS) and the fast-spiking neurons (Niell & Stryker, 2008; Bachatene *et al.*, 2012; Vinck *et al.*, 2013). The RS neurons can be putatively linked to the pyramidal neurons, whereas the FS neurons may be associated to the inhibitory interneurons (Niell & Stryker, 2008; Bachatene *et al.*, 2012; Vinck *et al.*, 2013). Notably, in cats the dissociation of the interneurons and pyramidal cells based upon spike-width is not entirely possible as a fraction of pyramidal neurons may show the fast spiking pattern (Nowak *et al.*, 2003). Therefore, one has to be cautious while interpreting the data based on ascending-slope discrimination of spike-waveforms in cats. The major difference between an FS and an RS is that the FS has a steeper ascending slope than the RS (Niell & Stryker, 2008). In other words, the FS spike-width is smaller than the RS spike-width.

1.8 Similarity with the higher vertebrates

A majority of the sensory information (80%) that we receive is through our eyes. Characteristically, the cat visual system appears to exhibit similar properties among various species (Tyler *et al.*, 1998; Kaschube *et al.*, 2010), even with humans. Although neurons are dispersed in a salt-and-pepper fashion (lack the orientation columns) in the visual cortices of lower vertebrates (e.g. rats and mice), yet they exhibit neuronal selectivity. In other words, many axes of orientations are interspersed in a small tissue

volume in lower vertebrates (Ohki *et al.*, 2005; Van Hooser, 2007). However, in many respects the properties of cat visual neurons are similar to the primates. The receptive fields in the retina and the LGN are concentrically arranged in cats and monkeys (Blake, 1979; Swindale, 1997). Moreover, the X and Y classification follow the same rules in monkeys as in cats (Dreher *et al.*, 1976). In the cortices, the same array of neuronal types, that is, simple, complex and so on are found in primates as in cats (Hubel & Wiesel, 1968). In a similar fashion, through cat and human psycho-physical experiments, it has been well established that the human visual system shares the generalizations with the cat visual system (Blake, 1978). The only major difference being that the human visual system has much better color-discrimination power than the cat visual system (Loop & Bruce, 1978). Because of the striking similarity of the cat visual system to the primates, cats have been a favorite model for neuroscientists to study and investigate many aspects of the brain functioning.

CHAPTER 2. HYPOTHESIS AND OBJECTIVES

If a tree falls in a forest and no one is around to hear it, does it make a sound?

— George Berkeley

2.1 Hypothesis

Indeed, from the literature, it appears that it is of immense importance to understand the dynamics of a stimulus-encoding assembly. The various types of neurons (as discussed above) in the brain principally coordinate locally (Hellwig, 2000; Frick *et al.*, 2008; Brown & Hestrin, 2009; Petreanu *et al.*, 2009; Kampa *et al.*, 2011; Ko *et al.*, 2011; Perin *et al.*, 2011; Miller *et al.*, 2014; Carrillo-Reid *et al.*, 2015; Sadeh *et al.*, 2015), therefore, first, it is imperative to understand these local networks. Vision is an important sense that animals possess to interact with the environment, and the visual cortex is perhaps the most studied area of the brain in mammals. Nevertheless, the understanding of its neural circuits still eludes us. Thus, it is interesting to ask how neural circuits in visual cortex frame visual receptive fields.

As discussed above, orientation selectivity is a fundamental property of layer II/III primary visual neuron (Hubel & Wiesel, 1959). Neurons are arranged into orientation columns in cats. When a series of random drifting sine-wave gratings are presented tilting systematically within the receptive field of neurons under observation, orientation selectivity of neurons can be easily determined. Therefore, orientation was chosen as the tested stimulus because the functional connectivity could easily be inferred in relation to the property of the neuron. How a networking cell-assembly is organized within layer II/III orientation-selective neurons in response to different stimuli? This is the major goal of my investigation. To answer this question, neural activity from layer II/III neurons was recorded in anaesthetized cats using tungsten multi-electrodes.

Many studies (Fujisawa *et al.*, 2008; Miller *et al.*, 2014; Schwindel *et al.*, 2014) have investigated the functional interactions (on milliseconds scale) between the simultaneously recorded neurons in a bimodal fashion (either locally or distally in the

brain in relation to the stimulus or a very dissimilar condition, e.g. natural vs. artificial stimuli or stimulus vs. spontaneous conditions). However, until now, there has not been any report that has investigated the temporal relationships between neuronal impulses (indicative of functional interactions) in cell-assemblies in relation to the systematic change of a very similar stimulus. Simply speaking, how a functional network is selected in response to a particular feature by a cell-assembly.

Several techniques (Sporns *et al.*, 2005; Buzas *et al.*, 2006; Fujisawa *et al.*, 2008; Hagmann *et al.*, 2010; Kampa *et al.*, 2011; Ko *et al.*, 2011) such as optical imaging, fMRI, calcium imaging are employed to study the activity of neurons in response to a stimulus, however, the information from most of these techniques (except calcium imaging) is mainly global, and does not comprehensively reflect the patterns of fine-scale cell-assembly networks. In most cases, these methods do not allow measuring functional relationships between cells on a millisecond scale. In other words, no doubt they provide us information about the global activity of neurons, but fail to reveal the connectivity between neurons. Assuming that a synaptic delay is 0.5 ms and by adding the conductance time, one may assume that a peak disclosed within a time-window of 5 ms in a CCG is indicative of a relatively direct functional relationship between two neurons. Thus, the CCG strategy will be used to reveal the functional connections between cells, the relative weight of these connections, and their modifications when the stimulus condition changes.

2.2 Objectives:

The above hypothesis leads to the following objectives:

1. To study the functional dynamics of an assembly. Indeed many studies have proposed that network selection/formation is fundamental to encoding in distributed cortical networks. Therefore, the major goal of the investigation will be to reveal these carefully knit networks in relation to the stimulus (the systematic tilt of drifting sine-wave grating). The CCG strategy will be employed to reveal the functional networks and

the strength of connections at each presented orientation between the neurons comprising an assembly, that is, neurons recorded simultaneously. The role of different neuronal types and the structure of noise correlations will also be investigated.

2. To investigative the gamma oscillations in functional networks. Gamma oscillations are ubiquitous in brain across species. However, there is a debate on their role in cortical networks, especially due to their weak power. The dynamics of cortical ensembles is still not very well known. Another major goal of the investigation will be to analyse the gamma oscillatory power in emergent functional networks activated within these ensembles.

The neural-codes are still a highly debated question in the neuroscience community. As this study is targeted to understand the stimulus encoding by an assembly, this will be an important step further in unravelling the dynamics of emergent sub-networks in the visual cortex. Specifically, it will help in the understanding of the contribution of the temporal code within these functional microcircutis. Further, the in-vivo results could be used as a premise for comprehending the size of population codes using computational methods.

Neuronal circuits often go haywire in a diseased or a damaged brain**.** Therefore, understanding how the neuronal circuits function is immensely important, not only for fundamental reasons but equally inevitable for medical interventions, e.g. in the brain disorders. One of the central problems in any brain disease is that neurons lose their original functional properties and attain behaviours that are specific to the altered architecture, network, oscillations or state of the brain (Watson & Buzsaki, 2015). For example, an epileptic neuron fires action potentials well beyond the normal depolarization levels in healthy neurons. As a consequence of this change in properties, the neural syntax is perturbed. In fact, comprehending brain signals in form of networks may help in better understanding of the disease, in its diagnosis and therapy. As markers of collective behaviour of neurons in groups, they can be employed as specific inputs in damaged brain area to recalibrate the circuitry to proper functional mode.

CHAPTER 3. Synergistic activity between primary visual neurons

Vishal Bharmauria[a], Lyes Bachatene[a], Sarah Cattan[a], Jean Rouat[a,b], Stéphane Molotchnikoff[a,b]

a Département de Sciences Biologiques, Université deMontréal, Montréal, QC, Canada
b Universite´ de Sherbrooke, Sherbrooke, QC, Canada

Neuroscience (2014) ***268****: 255–264*

(Published article)

Neuroscience 268 (2014) 255–264

SYNERGISTIC ACTIVITY BETWEEN PRIMARY VISUAL NEURONS

V. BHARMAURIA,[a] L. BACHATENE,[a] S. CATTAN,[a] J. ROUAT[a,b] AND S. MOLOTCHNIKOFF[a,b]*

[a] *Département de Sciences Biologiques, Université de Montréal, Montreal, QC, Canada*

[b] *Université de Sherbrooke, Sherbrooke, QC, Canada*

Abstract—Cortical microcircuitry plays a pivotal role in encoding sensory information reaching the cortex. However, the fundamental knowledge concerning the mechanisms that govern feature-encoding by these sub-networks is still sparse. Here, we show through multi-electrode recordings in V1 of conventionally prepared anesthetized cats, that an avalanche of synergistic neural activity occurs between functionally connected neurons in a cell-assembly in response to the presented stimulus. The results specifically show that once the reference neuron spikes in a connected neuron-pair, it facilitates the response of its companion (target) neuron for 50 ms and, thereafter, the excitability of the target neuron declines. On the other hand, the functionally unconnected neurons do not facilitate each other's activity within the 50-ms time-window. The added excitation (facilitation) of connected neurons is almost four times the responsiveness of unconnected neurons. This suggests that connectedness confers the added excitability to neurons; consequently leading to feature-encoding within the emergent 50-ms-period. Furthermore, the facilitation significantly decreases as a function of orientation selectivity spread.

Key words: inter-neural relationships, primary visual cortex, functional network, microcircuit, synergy.

INTRODUCTION

Cortical neurons propagate information about the experience (input) through the complex temporal relationships of their action potentials (Alloway and Roy, 2002; Barthó et al., 2004; Kohn and Smith, 2005; Yoshimura et al., 2005; Samonds et al., 2006; Fujisawa et al., 2008; Ghisovan et al., 2008). Neurons principally coordinate in local sub-networks termed 'cell-assemblies' to represent distinct cognitive entities (Hebb, 1949; Buzsáki, 2010; Kampa et al., 2011; Ko et al., 2011, 2013; Perin et al., 2011). Visual cortex is perhaps the most studied area of the brain; yet, how local circuits emerge to encode specific information in response to a visual input, is a question to be deeply explored—that is, how the intriguing interplay between the stimulus and a microcircuit is engineered and modulated?

Rate coding and temporal coding seem to dominate the literature on population coding in response to a stimulating feature (Perkel and Bullock, 1968; Ainsworth et al., 2012; Ratté et al., 2013), and both appear to generate a code either as independent or mutually inclusive events (Ainsworth et al., 2012; Ratté et al., 2013). However, recently, authors (Ainsworth et al., 2012) have suggested a bias toward a precise temporal code (stimulus-driven-synchrony) that is a reflection of the anatomical architecture and synaptic biophysical properties of neurons (Ainsworth et al., 2012; Ratté et al., 2013). Synchronized neural activity implying specific functional connectivity has already been associated to the generation of coherent percepts (Gray and Singer, 1989; Barthó et al., 2004; Duret et al., 2006; Fujisawa et al., 2008; Ghisovan et al., 2008).

Cross-correlogram function is an efficient tool to study synchrony between the neural spike trains (Perkel et al., 1967; König et al., 1995; Barthó et al., 2004; Fujisawa et al., 2008). Employing cross-correlograms, we have already shown that co-active neurons in a V1 (layer II/III) cell-assembly frame a specific functional connectome in relation to a stimulus (Bretzner et al., 2001; Duret et al., 2006; Bharmauria et al., 2012). In other words, how a cell-assembly waxes and wanes as the visual stimulus varies. It is to be mentioned that these functional connections were revealed within a ±5-ms quasi-synchrony window in the cross-correlogram.

Building on the previous work, the goal of our current investigation is to observe and compare the most likely avalanche of neural activity between functionally connected, unconnected and untuned neuron-pairs in an assembly on a broader time-scale. That is, for how long, in relation to the spiking of one neuron, the discharge of the target neuron is modulated. We report that in V1 (layer II/III) of conventionally prepared anesthetized cats, the target neuron's discharge augments for 50 ms after reference neuron's spiking, and thereafter, the firing rate decreases. This is applicable to neurons (paired) that share orientation preference, as well as pairs exhibiting a large difference in orientation tunings. On the other hand, no significant increase was noticed for unconnected and untuned cell-pairs within the same

*Corresponding author. Address: Department of Biological Sciences, University of Montreal, C.P. 6128, succursale Centre-ville, Montréal, QC H3C 3J7, Canada. Tel: +1-514-343-6616; fax: +1-514-343-2293.

Abbreviations: OSI, orientation selectivity index; PSTH, peristimulus time histograms; SEM, standard errors of the mean.

http://dx.doi.org/10.1016/j.neuroscience.2014.03.027

time-window. Thus, our results indicate that a functional network in V1 is set within 50 ms as a result of maximal synergistic activity, after the onset of the activity of companion cells in the assembly.

EXPERIMENTAL PROCEDURES

Ethical approval

Nine cats (*Felis catus*) were prepared in a conventional fashion for electrophysiological recordings in the primary visual cortex, as per the guidelines of Canadian Council on Animal care and approved by the Institutional Animal care and Use committee of the Université de Montreal. The experiments were conducted in accordance with the Guide for Care and Use of Laboratory Animals of the National Institutes of Health (USA).

Animal preparation

Briefly, animals were sedated with acepromazine maleate (Atravet, Wyeth-Ayerst, Guelph, ON, Canada; 1 mg kg^{-1}, intramuscular) and atropine sulfate (ATRO-SA, Rafter, Calgary, AB, Canada; 0.04 mg kg^{-1}, intramuscular), and anesthetized with ketamine hydrochloride (Rogarsetic, Pfizer, Kirkland, QC, Canada; 25 mg kg^{-1}, intramuscular). The cats were then paralyzed with 40 mg and maintained with 10-mg kg^{-1} h^{-1} gallamine triethiodide (Flaxedil, Sigma Chemical, St. Louis, MO, USA; intravenous) administered in 5% dextrose lactated Ringer's nutritive solution. General anesthesia was maintained by artificial ventilation with a mixture of N_2O/O_2 (70:30) supplemented with 0.5% isoflurane (AErrane, Baxter, Toronto, ON, Canada). Electroencephalogram, electrocardiogram, rectal temperature and end-tidal CO_2 partial pressure were monitored throughout the experiment, and kept in physiological ranges. Pupils were dilated with atropine, and Plano lenses with artificial pupils (5 mm diameter) were fixed. The electroencephalogram pattern ensured that the animals were properly anesthetized. The loci of the area centrales were inferred from the position of the blind spots. At the end of the experiment, the cats were euthanized intravenously with Sodium Pentobarbital (CEVA, Sante Animale). The injecting dose was 1 ml/2 kg of animal weight.

Visual stimulation

Monocular stimulation was done. The multi-unit receptive fields (RF) were mapped as the minimum response field (Barlow et al., 1967) by using a hand-held ophthalmoscope after clearly detectable activity was obtained. These preliminary tests revealed qualitative properties such as dimensions, velocity, orientation and direction selectivity. Visual stimuli were generated with a VSG 2/5 graphic board (Cambridge Research Systems, Rochester, England) and displayed on a 21-inch monitor (Sony GDM-F520 Trinitron, Tokyo, Japan) placed 57 cm from the cat's eyes, with 1024 × 768 pixels, running at a 100-Hz frame refresh rate. Stimuli were sine-wave drifting gratings covering the excitatory RF of neurons at both electrode tips. Contrast was set at 80%. Mean luminance was 40 Cd m^{-2}. Optimal spatial and temporal frequencies were set at 0.24 cycles deg^{-1} and 1.0–2.0 Hz range respectively, where V1 neurons are driven maximally by sine-wave drifting gratings (Bardy et al., 2006).

Electrophysiological recording and single-unit selection from multi-unit activity

Multi-unit activity in the primary visual cortex was recorded at 410–820 μ apart by a tungsten multi-electrode (Frederick Haer & Co., Matrix Electrode). Recordings were performed in the supragranular layers (cortical depth < 1000 μm; mean = 650 μm). The signal from the microelectrodes was amplified, band-pass filtered (300 Hz–3 kHz), digitized and recorded with a 0.05-ms temporal resolution (Spike2, CED, Cambridge, England). All cells were discriminated on the basis of three criteria: (1) the spike-waveform difference, (2) principal component analysis (PCA) showing well-dissociated clusters, and, (3) auto-correlograms showing no events at central point (Csicsvari et al., 1998; Barthó et al., 2004; Fujisawa et al., 2008; Harris et al., 2001). The stability of each cell's activity across conditions was verified qualitatively by visual control of the disposition of the clusters and the shapes of the waveforms.

The cluster analysis was performed using Spike2, CED, Cambridge, England in a 3-dimensional plot. The isolation distance was calculated as the Mahalanobis distance. Mahalanobis distance is the distance from the center of the cluster within which as many events belong to the other clusters as many belong to the specified cluster (Harris et al., 2001). In other words, given multivariate data values for which the values in each variable are normally distributed around a mean, this measure allows us to define boundaries of constant probability around the multi-dimensional center of the distribution. This estimation allows the separation of a cluster from the nearest cluster. Units within Mahalanobis distance of 2.5 were considered for analysis.

Fig. 1 illustrates the protocol and isolation of neurons from a single electrode tip. Fig. 1A exemplifies the experimental protocol. Each drifting grating was presented 25 times lasting 180 s, with varying inter-stimulus (1–3 s) intervals. Each trial lasted 4 s. Orientations of gratings were presented in a random order. Fig. 1B depicts the separated and averaged waveforms of four units recorded simultaneously. Each waveform is distinct, well separated, and corroborated by Principal Component Analysis. Fig. 1C shows the respective auto-correlograms of the four separated neurons, and no event at zero (corresponding to the refractory period of neuron) ascertains the individuality of the neuron. Fig. 1D illustrates the cluster analysis as explained above.

Data analysis

Once single cells were sorted out off-line from multi-unit spike trains, orientation tuning curves of cells were obtained from raw data and fitted with the von Mises function (Swindale, 1998).

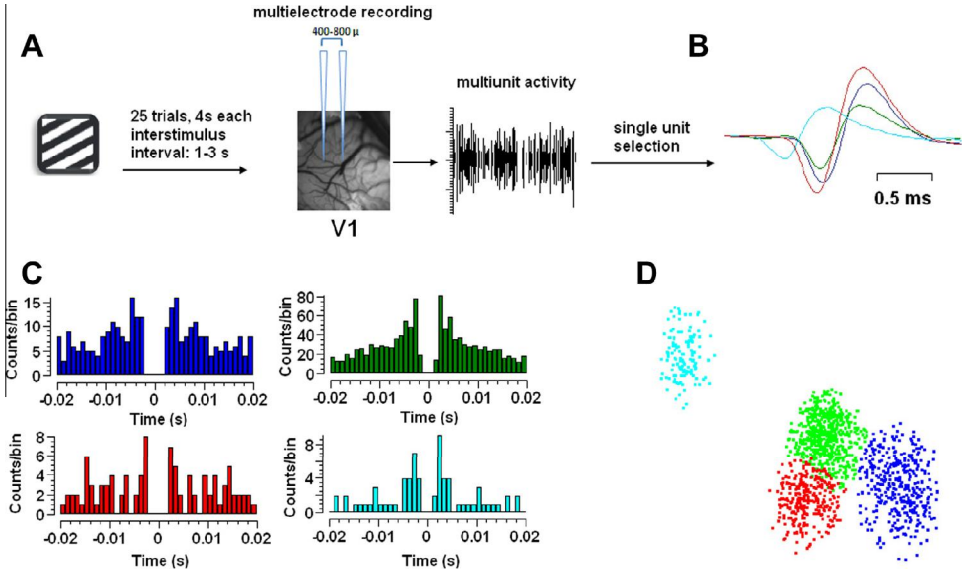

Fig. 1. Visual stimulation protocol and isolation of units. (A) Stimuli (drifting orientation-gratings) were presented in a random order. Each stimulus was presented 25 times and each trial lasted 4 s with a 1–3-ms inter-stimulus interval. Tungsten multi-electrodes (inter-electrode distance = 410 µ) were used to perform the multiunit recordings in layer II/III of V1 in cat. (B) Superimposed average waveforms of dissociated spikes from multi-unit recordings. (C) Auto-correlograms for the separated single units in (B). No event at zero representing the refractory period of neuron confirms the individuality of neuron. (D) Cluster analysis for the dissociated waveforms. The color scheme is respected in all figures.

$$M(\theta) = A \cdot e^{b(\cos(\theta - c))} + d \quad \text{(i)}$$

where '*A*' is the value of the function at the preferred orientation '*c*', and '*b*' is the width parameter. An additional parameter, '*d*', represents the spontaneous firing rate of the cell. $M(\theta)$ is the firing rate of the neuron at orientation, 'θ'. This allowed us to determine with precision the preferred orientation of every cell. An orientation selectivity index (OSI) was calculated to ensure the tuning of neurons. It was measured using the fitted tuning curves by dividing the firing rate at baseline (orthogonal orientations) by the firing rate at the preferred orientation, and subtracting the result from one (Ramoa et al., 2001; Liao et al., 2004; Bachatene et al., 2013). The closer the OSI is to one, the stronger the orientation selectivity. Neurons with OSI $\geqslant$ 0.7 were selected for further analysis.

Cross-correlograms and network-formation

Cross-correlograms were constructed between the spike trains of all the possible neuron-pairs at all the applied orientations to reveal the functional connections. We employed the shuffling minus subtraction algorithm based on the firing of the neurons, and it was subtracted from the raw cross-correlograms, which withdrew the evoked firing (Perkel et al., 1967). A significant peak of 2 ms (two adjacent 1 ms bins) or at least one significant bin (Alloway and Roy, 2002) was searched within a window of ±5 ms around zero in the shift-corrected cross-correlograms to reveal a functional connection between two neurons. The statistical threshold for the significant peak was set at 95% (red curved line in cross-correlogram), and the probability (*P*) of the neuron firing in a bin is calculated as follows (Abeles, 1982):

Considering the spike train is a Poisson train, the probability (*P*) of the neuron to fire in the small bin of the size *b* is:

$$P = F * b \quad \text{and} \quad F = N/T \quad \text{(ii)}$$

where '*F*' is the neuron frequency, '*T*' is the total time interval, and '*N*' is the number of spikes in that interval.

The confidence limit in the cross-correlogram was calculated as per Abeles (1982):

The expected bin count (*C*) for the histogram is:

$C = P * \text{NRef}$, where NRef is the number of the reference events.

The confidence limits for '*C*' are calculated using the assumption that *C* has a Poisson distribution.

Assuming that a random variable '*S*' has a Poisson distribution with parameter '*C*', then the 95% confidence limit is calculated as follows:

Low Conf. = x such that Prob ($S < x$) = 0.005
High Conf. = y such that Prob ($S > y$) = 0.005

In the case when two cells recorded from the same tip fired in synchrony, their respective waveforms might sum up and consequently the shape of the resultant waveform is rejected as it falls outside the range of the template. In the present investigation 'synchrony' of spikes from the same tip is excluded from the analysis. We considered only spikes that fell beyond ±1 ms after the central point in the cross-correlogram to make significant projections.

In addition, 'cumulative sums based on all histograms' of the firing rates indicated that the reference spike modulates the discharges of the target neuron. For every cross-correlogram the cumulative distribution of

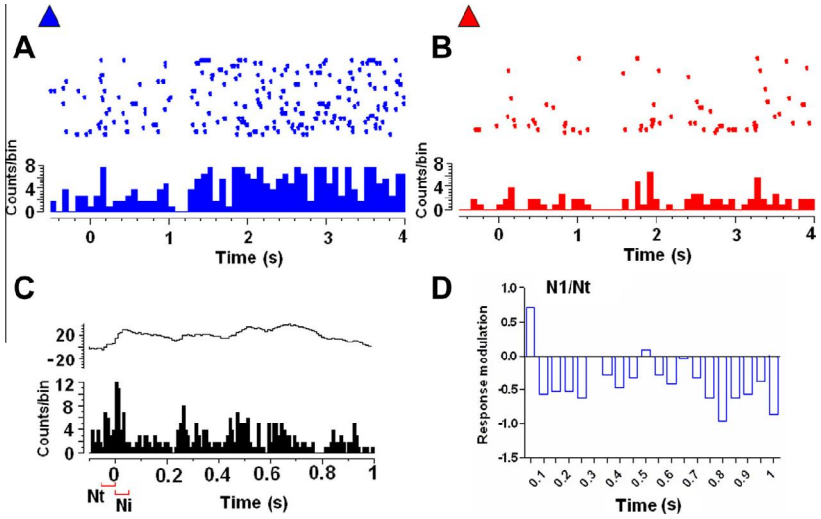

Fig. 2. Calculation of response-modulation. (A) Peristimulus time histogram (PSTH) of the reference neuron (blue) over 25 trials. (B) Peristimulus time histogram of the target neuron (red). (C) Histogram of the target neuron relative to the reference neuron spiking (spike-by-spike). (D) Response-modulation (*R*) histogram of the target neuron. 'Ni' stands for the mean response in every 50-ms bin after zero, whereas, 'Nt' represents the average firing within 50 ms before the zero mark. N1/Nt (R) is the modulated response of the target neuron in the first 50 ms after zero. (For interpretation of the references to color in this figure legend, the reader is referred to the web version of this article.)

spikes was computed (it is shown above each cross-correlogram). This spike-triggered increase further determines the functional connectivity between both cells since the activity of the target cell depends upon the activity of the companion unit (reference neuron).

The cumulative sum (cs) graphs above histograms are calculated as:

If we have a histogram with bin counts bc[*i*], $i = 1,\ldots,N$.
then the cumulative sum cs[*i*] for a bin is:
for bin 1: cs[1] = bc[1] − A
for bin 2: cs[2] = bc[1] + bc[2] − A ∗ 2
for bin 3: cs[3] = bc[1] + bc[2] + bc[3] − A ∗ 3, etc.

Calculation of the response-modulation

The 'response-modulation' following the spike of the reference cell is computed as a ratio. The ratio was calculated by considering the firing rates (counts/bin) derived from peristimulus time histograms (PSTH) of involved neurons. Fig. 2 illustrates the calculation of response-modulation (*R*) for two neurons. Fig. 2A corresponds to the raster plot of the blue neuron, whereas Fig. 2B represents the raster plot of the red neuron. The spikes of one neuron (blue[1]) were set as reference (spike-by-spike analysis) and the activity of second neuron (red) was calculated in relation to the reference neuron. This computation leads to the histogram in Fig. 2C. Thereafter, typically, several time-windows were considered for calculation of response-modulation. The first window is of 50 ms before reference spikes (zero mark), and second up to one second after the zero mark. This latter timescale was divided into 50-ms epochs to calculate the evolution of excitability modulation during the time-course of response up to one second after the zero mark. Thus, the ratio (*R*) is calculated as:

$$R = \mathrm{Ni}/\mathrm{Nt} \qquad \text{(iii)}$$

where Ni = Average response of target neuron after zero (after the reference neuron spiked) in each 50-ms epoch, and Nt = Average response of target neuron within 50 ms before the zero mark, that is, prior to spiking of the reference cell. Fig. 2D depicts the excitability modulation of the target cell in the respective time-windows. N1/Nt represents the modulated activity of the red neuron with respect to the blue neuron in the first 50 ms.

[1] For interpretation of color in Fig. 2, the reader is referred to the web version of this article.

RESULTS

The main goal of the current investigation is to examine the time-course of synergistic cross-influence between two simultaneously recorded neurons when one of them fires. In the current analysis, 363 pairs were investigated from 39 recording sites (each site corresponds to recording from an electrode tip). Table 1 summarizes the statistics for analyzed neuron-pairs. Out of analyzed pairs, 165 were connected; 120 were unconnected and 78 were untuned. In the context of this paper, it is emphasized that simultaneously recorded neurons from a tip (see Fig. 1) are termed as 'cell-assembly'. Unconnected neuron-pairs were also investigated from the same cell-assemblies. The untuned neurons-pairs were analyzed from the other five recordings. It is to be mentioned that neurons did not belong to more than one assembly.

Functional network revealed by cross-correlograms

The first objective was to reveal the functional links between neurons in an assembly. Fig. 3A illustrates the

Table 1. Assembly statistics for analyzed neuron-pairs

Total cell-assemblies (39 sites)			
Tuned neurons (**34 sites, 178 neurons**) Average neurons per cell-assembly: **5.2**			Untuned neurons (**5 sites, 28 neurons**) Average neurons per cell-assembly: **5.6**
Connected pairs		Unconnected pairs	**78**
165		**120**	
Unidirectional connections	Bi-directional connections		
111	**27**		

shift-corrected cross-correlograms (see Experimental procedures for details) based on which the functional network was disclosed between five simultaneously recorded neurons from a tip as shown in Fig. 3B. The first cross-correlogram represents the spike-triggered modulation of the green cell's (target, cell 2) activity in relation to the spiking of the blue neuron (reference, cell 1). The cross-correlogram significantly peaks within 5 ms after zero, implying that cell 1 functionally projects onto cell 2 (unidirectional connection). The probability (p) of the significant peak in the cross-correlogram is 0.023 (see Experimantal procedures). This relation can be interpreted as a putative excitatory connection between the neurons (blue cell excites the green cell in

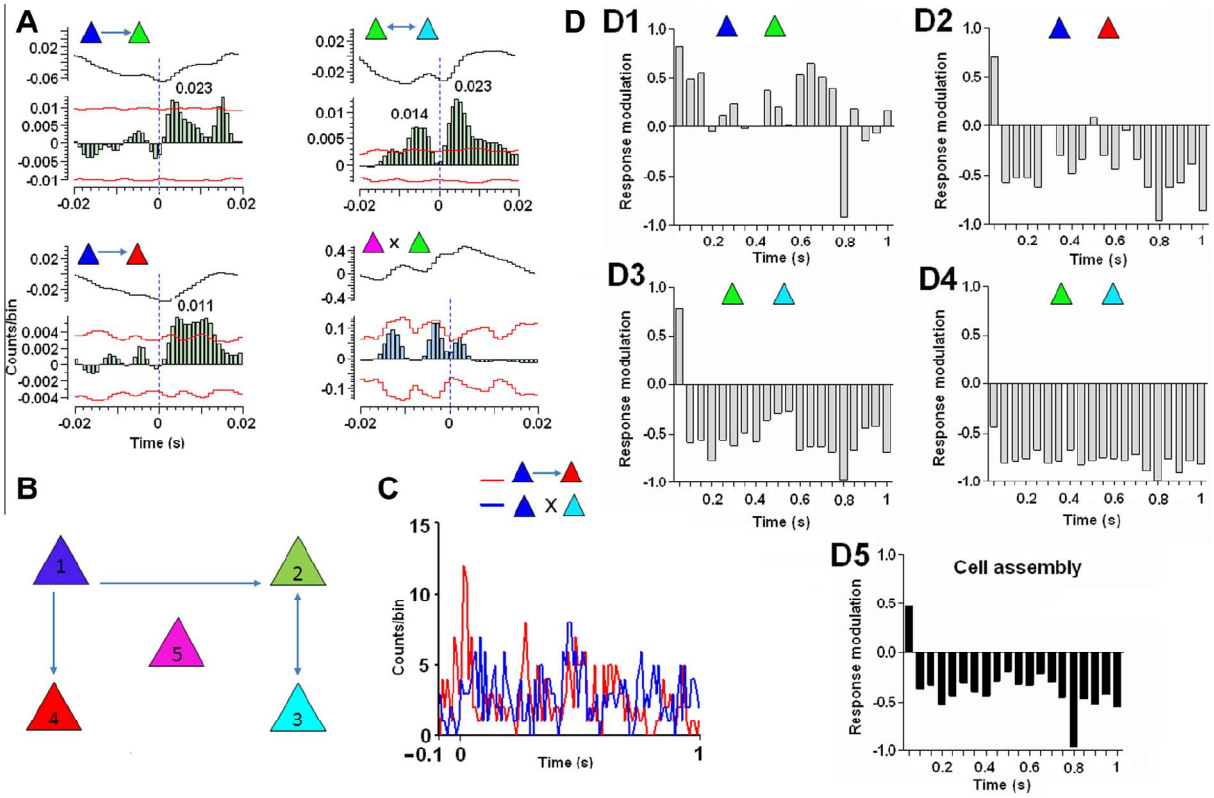

Fig. 3. Functional network and response-modulation in a cell-assembly. (A) Shift-corrected cross-correlograms to reveal the functional links between simultaneously recorded neurons shown in (B). The first cross-correlogram between the blue cell (reference) and the green cell (target) shows that target cell spikes within 5 ms once the reference cell fires and the probability of this discharge is 0.023. This means that the blue neuron projects onto the green neuron and signifies the functional link between them. The red curved line represents the significance level (95%). The curved line above the cross-correlogram corresponds to the cumulative sum based on histogram which further ascertains the functional link between neurons. The broken blue line depicts the zero in the cross-correlogram. The first neuron (colored triangle) in every cross-correlogram represents the reference neuron. (B) Functional network of simultaneously recorded neurons as disclosed from cross-correlogram analysis in (A). (C) A typical example of Peristimulus histogram comparison (PSTH) for neuron-pairs. Red curve stands for the connected pair whereas the blue curve depicts the unconnected pair. There is an augmented excitation of the target cell for the connected cell-pair. (D) Response-modulation of target cells in cell-pairs shown in (A). Note the surge of activity in the first 50 ms for all the histograms (D1–3) except (D4). (D5) Averaged histogram for a typical cell-assembly (D1–4).

the circuit). In addition, cumulative curve (shown above the cross-correlogram) of the firing rate shows the increased excitation of cell 2 almost immediately after cell 1 produced an action potential. This increased excitation further ascertains the functional link between the neurons. Similarly, cell 1 excites cell 4 ($p = 0.011$) within the assembly. Cells 2 and 3 are reciprocally connected (bidirectional connection), that is, firstly cell 2 excites cell 3 ($p = 0.023$) and after a brief period of inhibition characterized by a trough at zero in the histogram, cell 3 back-projects onto cell 2 ($p = 0.014$). The cross-correlogram between cell 5 and cell 2 is not significant, thus, no functional connection is inferred between them. The blue arrow depicts the direction of projection from one neuron to another.

Synergistic activity within an assembly

The analysis in Fig. 3A, B disclosed the functional connections in a short quasi-synchrony (±5 ms time-window) in cross-correlograms, and these links are indicative of putative and relatively direct synaptic links between the involved neurons. The next goal was to observe on a broader time-scale the evolution of the target cells' firing in the connected cell-pairs. To this aim, the PSTH's of neurons were compared to notice the modulation of the target cell's firing in relation to reference cell's spiking until one second (see Experimental procedures, Fig. 2 for details). A typical example of a connected and an unconnected neuron pair is shown in Fig. 3C. As revealed in Fig. 3A, cell 4 (red) receives a connection from cell 1 while cell 3 (cyan) is unconnected to cell 1 (blue). Quite interestingly, in response to the same stimulus, the evoked firing (red curve) of cell 4 is considerably higher shortly after cell 1 has produced an action potential at the zero mark. On the contrary, cell 1 failed to increase the evoked transient firing (blue curve) of cell 3, although the same stimulus was applied.

Fig. 3D displays the response-modulation histograms of the targets cells of the same cell-pairs as shown in Fig. 3A. The first histogram (Fig. 3D1) illustrates the firing modulation of cell 2 (target) in relation to the spiking of cell 1. An increase of 82% neural activity is noticed in the first 50 ms after the reference cell firing. This suggests the response-facilitation of cell 2 by cell 1 and advocates the synergistic coupling between them within this period. In a similar fashion, cell 1 promotes the neural discharge of cell 4 (Fig. 3D2) by 71% within 50 ms, and thereafter, the facilitation subsides gradually. Cells 2 and 3 are reciprocally connected to each other (see Fig. 3A). Cell 2 increases the activity of cell 3 by 78% in the same period (Fig. 3D3); however, there is no facilitation of cell 2 by cell 3 (Fig. 3D4) suggesting a unidirectional facilitatory influence. In addition, it may be worthwhile to notice that there is an increase of the target neuron's firing at different epochs with respect to the trigger (reference) spikes. For example, cell 2 in relation to cell 1 exhibits augmented activity beyond 50 ms—a facilitation by 49% at 100 ms, 55% at 150 ms, a down-regulation of activity at 200 ms, and again an increased activity corresponding to consequent bins. On the contrary, this does not apply to cell 1–cell 4 pair, and the facilitation is noticed only in the first 50 ms. However, when the connected cell-pairs are summed up into a single unique assembly (Fig. 3D5), the average maximal synergistic effort (increase of activity by 47%) was noticed within 50 ms. Thus, although the magnitude-modulation of the firing of neurons within a cell-assembly varies considerably, a significant trend seems to apply to most cells: shortly following the spiking of the reference cell, the firing of the target cell increases for about 50 ms and, following this period, the responses decline; see next section.

Difference between connected, unconnected and untuned units

Thereafter, the facilitation-magnitudes were averaged and compared for connected, unconnected and untuned cell-pairs across all recorded clusters comprising all orientation spreads. Fig. 4 illustrates these results. Neurons in an assembly frame a specific microcircuit for a particular orientation or, generally, any exciting feature (Bretzner et al., 2001; Duret et al., 2006; Bharmauria et al., 2012). For closely tuned orientation groups ($\leqslant \pm 22°$), an optimal or near-optimal orientation was chosen where most number of connections were found, since these orientations evoked the highest number of spikes. In the case of assemblies with larger orientation spreads ($\geqslant \pm 22°$), a random orientation with the highest number of connections was selected. In total, 165 connections were analyzed at all the selected orientations. Out of 165 connections, 111 were unidirectional and 27 were bidirectional/reciprocal (Table 1). It is to be mentioned that a bidirectional or reciprocal connection consists of two reverse projections (that is, two connections). Out of 165 connected pairs, a few pairs ($n = 37$) were analyzed at spontaneous activity, and the mean activity was found to be 0.87 ± 0.11 (mean ± SEM (standard errors of the mean)) in the 50-ms window, whereas, the same pairs exhibited a mean facilitation of 1.57 ± 0.30 upon stimulus presentation, that is, an increase of 57% in the chosen window. This suggests that stimulus presence leads to connections. Moreover, random unconnected neuron-pairs were also sampled ($n = 120$, total unconnected pairs = 619) across previously selected orientations. Additionally, untuned neuron-pairs ($n = 78$) were also analyzed to compare the excitability with connected and unconnected cell-pairs.

The average facilitation for connected cell-pairs amounted to 46% (Fig. 4A) within the 50-ms time-window, whereas for unconnected cells the average increase amounted to 11% only (Fig. 4B). This spike-triggered facilitation in discharge rate for connected pairs might be attributed to the enhanced evoked discharges in response to the drifting grating which is present while cells' activities are being recorded. The difference in excitation between connected and unconnected units was significant (unpaired t-test, $p < 0.05$), suggesting that connectivity increases the excitability in a significant fashion. Lastly, the activity of untuned cell-pairs ($n = 78$) remained unchanged within

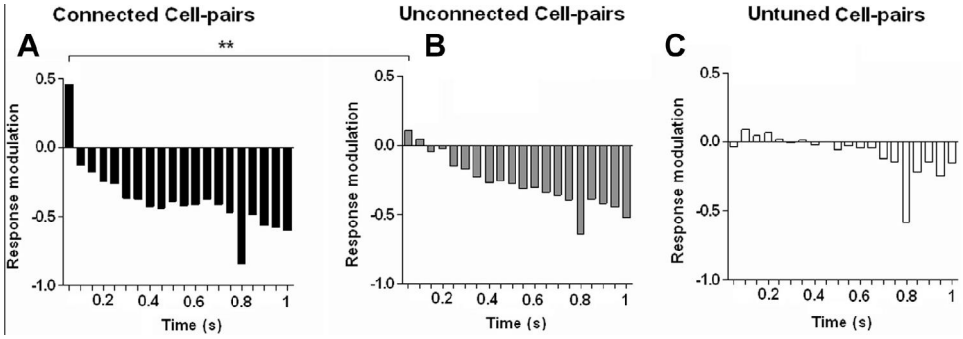

Fig. 4. Excitation comparison for connected, unconnected and untuned cell-pairs. (A) Average response modulation for pooled in connected cells across all recordings. There is 46% facilitation in the first 50-ms epoch for the target cells in connected cell-pairs. (B) Average response modulation for all unconnected cell-pairs. The excitation is 11% in the 50-ms time-window. There is a significant difference in facilitation for connected and unconnected units (unpaired *t*-test, $p < 0.05$). (C) Mean response modulation for untuned cell-pairs. The responses are down-regulated to 3%, that is, the firing of target neurons remains similar to their baseline firing.

the 50-ms window—a decrease in activity by 3% (Fig. 4C). In other words, the responsiveness of target cells in such cell-pairs was almost similar to the baseline firing.

Furthermore, neuron-pairs were grouped into orientation-class spreads to determine the relation between the facilitation and orientation range of the neurons (Fig. 5). As described in the Experimental procedures section, cells were tuned for orientation, and an orientation selectivity index (OSI) was calculated (Ramoa et al., 2001; Liao et al., 2004; Bachatene et al., 2013). The insert indicates the distribution of connections as a function of the orientation range of an assembly. The black part of the histogram corresponds to the number of connected pairs, whereas the gray part represents the number of unconnected pairs. The number above the histogram stands for the proportion of assemblies comprising that spread. The connections in all spreads are almost evenly distributed. This is attributed to a majority of closely tuned neurons (cell-pairs) that are present in all spreads.

However, on a cell-pair basis, as expected, there is a decrease in firing facilitation within 50 ms as the orientation spread increased. The mean facilitation for close orientation spread (44° or ±22°) was 1.53 ± 0.13 (mean ± SEM), that is, an increase of 53% from the baseline firing. The values of this upsurge in neural activity were found to be 1.35 ± 0.16 and 1.32 ± 0.13% respectively for 88°/±44° ($n = 24$) and 132°/±66° ($n = 10$) orientation ranges. It has to be mentioned that orientation spread beyond 132° was not taken into account, as the neural selectivity (cell-pairs) comprising this spread approaches the opposite direction of the sine-wave drifting gratings. The regression analysis excluding the fourth (unconnected, UC) and fifth (untuned, UT) groups shows the decreasing trend of excitation as the spread increases ($R^2 = 0.84$). Interestingly, this result seems to indicate that as the orientation selectivity diverges, the cooperation between the units is maintained, even though the magnitude of the facilitation is weaker. In other words, a group of neurons in an assembly is more salient than other neurons within the assembly. There is a significant difference in excitability between cell-pairs in 44° spread and unconnected units ($p < 0.05$, unpaired *t*-test).

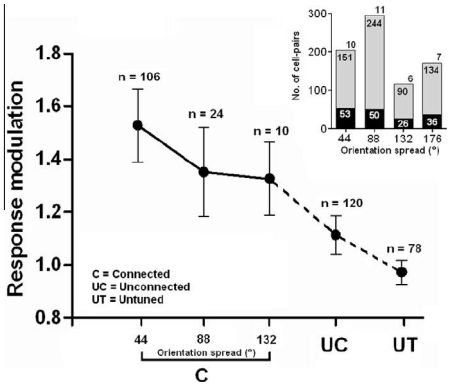

Fig. 5. Facilitation as a function of orientation spread. The first three points represent the connected (C) neuron-pairs in different orientation spreads. Linear regression analysis shows that there is a decrease in facilitation as the orientation range increases ($R^2 = 0.84$). The horizontal bars indicate the SEM. UC represents the unconnected cell-pairs, and UT corresponds to untuned cell-pairs. In general, the facilitation decreases from connected cell-pairs to untuned cell-pairs. *Note:* the last two dots (unconnected cells and untuned cells) are eliminated for regression analysis. Number of cell-pairs in each group is indicated by (n). The insert highlights the distribution of connected pairs as a function of the orientation range of an assembly. The black and gray part of the histogram represents the number of connected and unconnected pairs respectively. The number above the histogram indicates the number of assemblies within the spread.

Significant cross-correlograms, decreased excitability and time-course of response-modulation

Interestingly, a minority of cell-pairs displayed significant cross-correlograms (functional connections), but the respective target cells did not exhibit excitation within the 50-ms window of interest. Out of a total of 165 connected cell-pairs, 43 cells-pairs behaved in this fashion, that is, 26% of all the connected neuron-pairs. Fig. 6 illustrates a typical example. Fig. 6A shows a typical significant cross-correlogram for a connected neuron-pair. However, the activity of the same target cell is down-regulated by 19% within the 50-ms window, as evident from Fig. 6B.

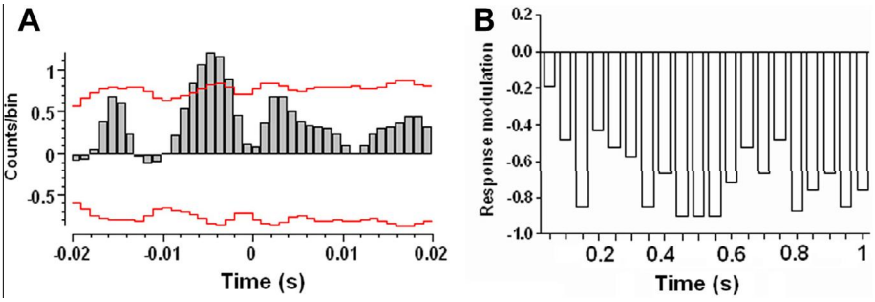

Fig. 6. A typical example of a cell-pair displaying a significant cross-correlogram (A), albeit, not exhibiting facilitation in the first 50-ms time-window (B).

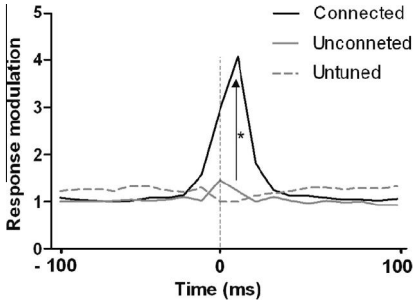

Fig. 7. Difference in excitation between connected, unconnected and untuned cell-pairs. Normalized facilitation curves for connected, unconnected and untuned cell-pairs. The black curve depicts the connected cells and shows a heightened activity for neurons in the 50-ms time-window in comparison to unconnected (gray curve) and untuned (broken gray curve) neuron-pairs. There is a significant increase (indicated by upright black arrow) in facilitatory activity for connected cell-pairs in comparison to unconnected pairs (asterisk represents the significance level, paired *t*-test for normalized responses, $p < 0.05$). The broken vertical black line indicates zero.

The normalized and averaged added increase of excitability that may be attributed to inter-neural connectivity is computed in Fig. 7. The normalized mean activities of connected, unconnected and untuned cell-pairs were calculated for 200 ms (−100 ms until 100 ms). The computation produced three curves: the bold black curve indicates responses of cells that exhibited connections ($n = 165$); the gray plot represents the cells lacking functional connectivity ($n = 120$); the dotted gray line stands for untuned pairs of cells ($n = 78$). Responses are aligned with the spikes of the reference cell at zero mark (vertical broken black line). The increase of cellular firing before zero mark is due to the presence of the stimulus in the receptive field as the stimulus is applied at the beginning of the trace. Thereafter, the transient-evoked responses emerge, followed by a decline of excitation. Interestingly, for connected pairs, the transient response is enhanced by almost 400%, whereas, there is a phasic increase of only 46% for unconnected pairs. Thus, there is almost 10 times significant (paired t-test for normalized responses, $p < 0.05$) increase (indicated by black arrow) in the activity of the connected neurons in comparison to the unconnected cell-pairs. Lastly, the activity of untuned neuron-pairs remains unmodulated as illustrated by the broken gray line. This spike-triggered difference in neural activity between connected and unconnected units underscores the avalanche of strong synergistic activity between connected cells.

DISCUSSION

In the current investigation, the synergistic cooperation between connected, unconnected and untuned cell-pairs recorded in anesthetized cat V1 (layer II/III), was investigated and compared. We found that after the onset of the reference neuron's spike, the target neuron fires at a higher rate in connected cell-pairs for a brief period of 50 ms, that is, the synergy is maximal within the 50-ms window, and thereafter this facilitation subsides. Secondly, the synergistic cross-influence decreases as a function of orientation spread.

Methodological considerations

Cellular excitation is certainly affected by anesthesia; however, it remained constant throughout the recording session. It has been demonstrated that spontaneous oscillations in anesthetized animals could induce correlations between neural firing (Poulet and Petersen, 2008). Likewise, varied oscillatory activities with different frequencies can be recorded in anesthetized animals (Gray and Singer, 1989; Gray et al., 1989). Previously, we have reported that connections were strongly related to a presented orientation; the pattern of cross-correlograms remained similar when a feature was presented repeatedly; and only a few connections (7%) were found at spontaneous activity. In addition, in the current analysis, connected cell-pairs did not exhibit facilitation when stimulus was absent. Moreover, neurons that shared orientation preference exhibited more connections (Bharmauria et al., 2012). Furthermore, as the synergistic effect occurs within a relatively brief time-window, such a short epoch does not support spontaneous modulation of excitability. Finally, targets were applied randomly. Collectively, these results suggest that connections are systematically established in response to a stimulus. One may argue that the increased activity for a brief period of time is simply due to co-activation of cells as the grating is presented, however, it is worthwhile to underline that the cross-correlations used to reveal the

functional connections were shift-corrected to remove the stimulus evoked and locked components.

Functional consequences

We report that V1 (layer II/III) neurons impinge upon each other's activity for about 50 ms in response to a stimulus, and thereafter the facilitation declines. The connected neuron-pairs exhibit heightened activity in this time-window than unconnected pairs. This time-window coincides with previous reports (Maunsell and Gibson, 1992; Rolls and Tovée, 1994) wherein authors have postulated that majority of sensory information seems to be encoded in the first 50 ms of neural activity, and this time-period is enough to discriminate even the complex stimuli.

The foremost question arises as whether the target neurons in connected pairs receive an input from other recorded or unrecorded neurons in the circuit. Since very few neurons were recorded from an electrode, it was not possible to quantitate other unrecorded neurons in the circuit. However, from results obtained, we infer that the input of the reference neuron most likely causes the upsurge in the activity of the target neuron. In other words, the magnitude of excitation of the target cell is predominantly related to the activity of the reference unit; otherwise the target cells in unconnected pairs might have shown a pronounced augmented activity in 50 ms, and as noticed, there is only 11% average facilitation in target cells of unconnected pairs in comparison to 46% for connected pairs.

A few pairs exhibited functional connections despite a down-regulation of activity in the 50-ms time-bin. This can be related to the characteristic sparse activity in cortical circuits (Molotchnikoff and Rouat, 2011; Jayakumar et al., 2012; Barth and Poulet, 2012). Even though no increase of firing rate was noticed in the 50-ms bin, yet cross-correlating their neural spike trains yielded a significant cross-correlogram between neurons. This reflects the precise temporal locking (temporal code) between neural activities.

Certainly through a distributive system (Bernardet and Verschure, 2002; Behrmann and Plaut, 2013), there are specific functional circuits dedicated to encoding processes. Such synergistic cross-influence between selected cells may assign specific roles and reduce multiple functions, hence, lessen ambiguities within the circuit. The augmented excitation for about 50 ms creates a 'window of opportunity' for downstream recipient assemblies to process the feature (Nádasdy, 2000; Wang et al., 2010). Such a model would modulate the excitability of involved pathways allowing the increased transmission of information and obliteration of irrelevant inputs. In other words, within this framework, the stimulus-dependent saliency of a microcircuit is promoted.

Although the excitation decreased as a function of the orientation spread, nevertheless, it persisted. This finding reflects that, in an assembly, neurons that share tuning properties collaborate vigorously than neurons exhibiting dissimilar tunings. This seems to be in line with investigations reporting that V1 (layer II/III) neurons receive a diversity of oriented inputs from surrounding neurons, however, there is an enhanced connectivity between neurons that share orientation preference (Monier et al., 2003; Jia et al., 2010; Ko et al., 2011). Recently, we have shown that cell-assemblies develop heightened functional connections to a suitable orientation, and may wax and wane contingent upon the presented orientation (Bretzner et al., 2001; Duret et al., 2006; Ghisovan et al., 2008; Bharmauria et al., 2012). Then the results of the present investigation suggest that the formation of an encoding assembly of excited neurons may rest on two global processes: firstly, to an appropriate stimulus, there is a development of functional connections leading to construction of a functional connectome particular to that stimulus; secondly, these connections allow enhanced responses leading to relevant and salient neural activities that participate in signaling a specific target. That is, some cells in an assembly stand out since they exhibit augmented excitation in comparison to other cells. Collectively, these results seem to support recent reviews wherein authors have postulated that stimulus-specific information is encoded within salient sub-networks of neurons (Singer, 2013; Harris and Mrsic-Flogel, 2013). Thus, we construe from our results that the augmented neural activity (synergy) for particular neurons within an assembly frames the premise for the formation of a specific network in response to the presented stimulus.

We conclude that within a stimulus-encoding assembly in layer II/III of V1, the effect of one neuron on companion neuron(s) lasts 50 ms, and thus the network is salient within this emergent period in relation to the stimulus. Our data also point to the fact that only a selected group of neurons within an assembly exhibits such increased excitation in response to a particular stimulus, while neighboring cells fail to show such a transient surge of excitation. Thus, we suggest that any given stimulus discriminates the linked neurons that may encode its presence and properties.

FUNDING

S.M. and J.R. were supported by CRSNG (Conseil de Recherches en Sciences Naturelles et en Génie) and FRQ-NT (Fonds de recherche du Québec – Nature et technologies).

AUTHOR CONTRIBUTIONS

V.B. did the experiments, analyzed the data and wrote the manuscript. L.B. and S.C. participated in experiments and analyses of data. J.R. contributed to the analyses of data. S.M. conceived the idea of study and contributed to data analyses and manuscript writing.

COMPETING INTERESTS

The authors declare no competing financial interests.

Acknowledgments—The authors thank the anonymous referees for extensive and constructive reviews that helped improve the manuscript significantly.

REFERENCES

Abeles M (1982) Quantification, smoothing, and confidence limits for single-units' histograms. J Neurosci Methods 5:317–325.

Ainsworth M, Lee S, Cunningham MO, Traub RD, Kopell NJ, Whittington MA (2012) Rates and rhythms: a synergistic view of frequency and temporal coding in neuronal networks. Neuron 75:572–583.

Alloway KD, Roy S (2002) Conditional cross-correlation analysis of thalamocortical neurotransmission. Behav Brain Res 135: 191–196.

Bachatene L, Bharmauria V, Cattan S, Molotchnikoff S (2013) Fluoxetine and serotonin facilitate attractive-adaptation-induced orientation plasticity in adult cat visual cortex. Eur J Neurosci 38:2065–2077.

Bardy C, Huang JY, Wang C, FitzGibbon T, Dreher B (2006) "Simplification" of responses of complex cells in cat striate cortex: suppressive surrounds and feedback inactivation. J Physiol 574:731–750.

Barlow HB, Blakemore C, Pettigrew JD (1967) The neural mechanism of binocular depth discrimination. J Physiol 193: 327–342.

Barth AL, Poulet JF (2012) Experimental evidence for sparse firing in the neocortex. Trends Neurosci 35:345–355.

Barthó P, Hirase H, Monconduit L, Zugaro M, Harris KD, Buzsáki G (2004) Characterization of neocortical principal cells and interneurons by network interactions and extracellular features. J Neurophysiol 92:600–608.

Behrmann M, Plaut DC (2013) Distributed circuits, not circumscribed centers, mediate visual recognition. Trends Cogn Sci 17: 210–219.

Bernardet U, Verschure PF (2002) Iqr: a tool for the construction of multi-level simulations of brain and behaviour. Neuroinformatics 8:113–134.

Bharmauria V, Bachatene L, Cattan S, Rouat J, Molotchnikoff S (2012) Network selectivity between primary visual neurons: Connectome Dynamics. Soc Neuros 572.07/FF8.

Bretzner F, Aïtoubah J, Shumikhina S, Tan YF, Molotchnikoff S (2001) Modulation of the synchronization between cells in visual cortex by contextual targets. Eur J Neurosci 14:1539–1554.

Buzsáki G (2010) Neural syntax: cell assemblies, synapsembles, and readers. Neuron 68:362–385.

Csicsvari J, Hirase H, Czurko A, Buzsáki G (1998) Reliability and state dependence of pyramidal cell-interneuron synapses in the hippocampus: an ensemble approach in the behaving rat. Neuron 21:179–189.

Duret F, Shumikhina S, Molotchnikoff S (2006) Neuron participation in a synchrony-encoding assembly. BMC Neurosci 7:72.

Fujisawa S, Amarasingham A, Harrison MT, Buzsáki G (2008) Behavior-dependent short-term assembly dynamics in the medial prefrontal cortex. Nat Neurosci 11:823–833.

Ghisovan N, Nemri A, Shumikhina S, Molotchnikoff S (2008) Synchrony between orientation-selective neurons is modulated during adaptation-induced plasticity in cat visual cortex. BMC Neurosci 9:60.

Gray CM, Singer W (1989) Stimulus-specific neuronal oscillations in orientation columns of cat visual cortex. Proc Natl Acad Sci U S A 86:1698–1702.

Gray CM, König P, Engel AK, Singer W (1989) Oscillatory responses in cat visual cortex exhibit inter-columnar synchronization which reflects global stimulus properties. Nature 338:334–337.

Harris KD, Hirase H, Leinekugel X, Henze DA, Buzsáki G (2001) Temporal interaction between single spikes and complex spike bursts in hippocampal pyramidal cells. Neuron 321:141–149.

Harris KD, Mrsic-Flogel TD (2013) Cortical connectivity and sensory coding. Nature 503:51–58.

Hebb DO (1949) The organization of behavior. New York: John Wiley and Sons.

Jayakumar J, Hu D, Vidyasagar TR (2012) Sparseness of coding in area 17 of the cat visual cortex: a comparison between pinwheel centres and orientation domains. Neuroscience 225:55–64.

Jia H, Rochefort NL, Chen X, Konnerth A (2010) Dendritic organization of sensory input to cortical neurons in vivo. Nature 464:1307–1312.

Kampa BM, Roth MM, Göbel W, Helmchen F (2011) Representation of visual scenes by local neuronal populations in layer 2/3 of mouse visual cortex. Front Neural Circuits 5:18.

Ko H, Hofer SB, Pichler B, Buchanan K, Sjöström PJ, Mrsic-Flogel TD (2011) Functional specificity of localsynaptic connections in neocortical networks. Nature 473:87–91.

Ko H, Cossell H, Baragli C, Antolik J, Clopath C, Hofer SB, Mrsic-Flogel TD (2013) The emergence of functional microcircuits in visual cortex. Nature 496:96–100.

Kohn A, Smith MA (2005) Stimulus dependence of neuronal correlation in primary visual cortex of the macaque. J Neurosci 25:3661–3773.

König P, Engel AK, Roelfsema PR, Singer W (1995) How precise is neuronal synchronization? Neural Comput 7:469–485.

Liao DS, Krahe TE, Prusky GT, Medina AE, Ramoa AS (2004) Recovery of cortical binocularity and orientation selectivity after the critical period for ocular dominance plasticity. J Neurophysiol 92:2113–2121.

Maunsell JHR, Gibson JR (1992) Visual response latencies in striate cortex of the macaque monkey. J Neurophysiol 68:1332–1344.

Molotchnikoff S, Rouat J (2011) Brain at work: time, sparseness and superposition principles. Front Biosci 17:583–606.

Monier C, Chavane F, Baudot P, Graham LJ, Frégnac Y (2003) Orientation and direction selectivity of synaptic inputs in visual cortical neurons: a diversity of combinations produces spike tuning. Neuron 37:663–680.

Nádasdy Z (2000) Spike sequences and their consequences. J Physiol Paris 94:505–524.

Perin R, Berger TK, Markram H (2011) A synaptic organizing principle for cortical neuronal groups. Proc Natl Acad Sci U S A 108: 5419–5424.

Perkel DH, Bullock TH (1968) Neural coding. Neurosci Res Prog Bull 6:221–348.

Perkel DH, Gerstein GL, Moore GP (1967) Neuronal spike trains and stochastic point processes. I. The single spike train. Biophys J 7:391–418.

Poulet JF, Petersen CCH (2008) Internal brain state regulates membrane potential synchrony in barrel cortex of behaving mice. Nature 454:881–885.

Ramoa AS, Mower AF, Liao D, Jafri SI (2001) Suppression of cortical receptor function prevents development of orientation selectivity in the primary visual cortex. J Neurosci 21:4299–4309.

Ratté S, Hong S, De Schutter E, Prescott SA (2013) Impact of neuronal properties on network coding: roles of spike initiation dynamics and robust synchrony transfer. Neuron 78:758–772.

Rolls ET, Tovée MJ (1994) Processing speed in the cerebral cortex, and the neurophysiology of backward masking. Proc R Soc Lond Biol 257:9–15.

Samonds JM, Zhou Z, Bernard MR, Bonds B (2006) Synchronous activity in cat visual cortex encodes collinear and cocircular contours. J Neurophysiol 95:2602–2616.

Singer W (2013) Cortical dynamics revisited. Trends Cogn Sci 17:616–626.

Swindale NV (1998) Orientation tuning curves: empirical description and estimation of parameters. Biol Cybern 78:45–56.

Wang Q, Webber RM, Stanley GB (2010) Thalamic synchrony and the adaptive gating of information flow to cortex. Nat Neurosci 13: 1534–1541.

Yoshimura Y, Dantzker JL, Callaway EM (2005) Excitatory cortical neurons form fine-scale functional networks. Nature 433: 868–873.

(Accepted 13 March 2014)
(Available online 21 March 2014)

CHAPTER 4. Stimulus-dependent augmented gamma oscillatory activity between the functionally connected cortical neurons in the primary visual cortex.

Vishal Bharmauria[a], Lyes Bachatene[a], Sarah Cattan[a], Nayan Chanauria[a], Jean Rouat[a,b], Stéphane Molotchnikoff[a,b]

a Département de Sciences Biologiques, Université deMontréal, Montréal, QC, Canada
b Universite´ de Sherbrooke, Sherbrooke, QC, Canada

European Journal of Neuroscience (2015) ***41****:1587-96*

(Published article)

EJN European Journal of Neuroscience

FENS

European Journal of Neuroscience, Vol. 41, pp. 1587–1596, 2015 doi:10.1111/ejn.12912

COGNITIVE NEUROSCIENCE

Stimulus-dependent augmented gamma oscillatory activity between the functionally connected cortical neurons in the primary visual cortex

Vishal Bharmauria,[1] Lyes Bachatene,[1] Sarah Cattan,[1] Nayan Chanauria,[1] Jean Rouat[1,2] and Stéphane Molotchnikoff[1,2]

[1]Neurophysiology of the Visual System, Département de Sciences Biologiques, Université de Montréal, CP 6128 Succursale centre-ville, Montréal, QC H3C 3J7, Canada

[2]Département de Génie Électrique et Génie Informatique, Université de Sherbrooke, Sherbrooke, QC, Canada

Keywords: coherence, functional connection, gamma oscillations, primary visual cortex, window of opportunity

Abstract

Neuronal assemblies typically synchronise within the gamma oscillatory band (30–80 Hz) and are fundamental to information processing. Despite numerous investigations, the exact mechanisms and origins of gamma oscillations are yet to be known. Here, through multiunit recordings in the primary visual cortex of cats, we show that the strength of gamma power (20–40 and 60–80 Hz) is significantly stronger between the functionally connected units than between the unconnected units within an assembly. Furthermore, there is increased frequency coherence in the gamma band between the connected units than between the unconnected units. Finally, the higher gamma rhythms (60–80 Hz) are mostly linked to the fast-spiking neurons. These results led us to postulate that gamma oscillations are intrinsically generated between the connected units within cell assemblies (microcircuits) in relation to the stimulus within an emergent '50-ms temporal window of opportunity'.

Introduction

Microcircuitries in the brain are fundamental in encoding information about the lived experience. Despite numerous investigations, a great deal has to be revealed about the mechanisms by which these networks process information. Coactive neurons with tightly correlated neural activities have been shown to be implicated in encoding processes, wherein neurons fire with close time relationships to each other (Singer, 1999; Barthó *et al.*, 2004; Fujisawa *et al.*, 2008; Buzsáki, 2010; Molotchnikoff & Rouat, 2012; Bharmauria *et al.*, 2014; Bachatene *et al.*, 2015).

Oscillatory rhythms are ubiquitous in cortical networks across different species (Fries *et al.*, 2007; Buzsáki *et al.*, 2013; Bosman *et al.*, 2014), and are believed to constitute an additional factor contributing to synchronised activity in encoding sensory stimuli. Neuronal assemblies typically synchronise in the gamma-frequency spectrum (30–80 Hz) (Gray & Singer, 1989; Gray & McCormick, 1996; Engel *et al.*, 2001; Womelsdorf *et al.*, 2006; Fries *et al.*, 2007), and these rhythms are widely postulated as constituting the fundamental precursor of computational mechanisms within brain networks. Recently, it has been suggested that neuronal coherence assigns oscillatory excitation rhythms in assemblies to eventually create windows of temporal communication (Bharmauria *et al.*, 2014; Siegle *et al.*, 2014). These oscillations subserve various cognitive aspects (perceptual binding, attention, and short-term and long-term memory). Despite a plethora of literature, the specific functions of gamma rhythms remain debatable (Fries *et al.*, 2007; Bosman *et al.*, 2014; Ray & Maunsell, 2014), and a great deal is yet to be determined about how these rhythms are generated and maintained.

A widely accepted hypothesis is that inhibitory interneurons embedded in networks are implicated in the generation of gamma-band synchrony (Wang & Buzsáki, 1996; Bartos *et al.*, 2002, 2007; Fries *et al.*, 2007; Cardin *et al.*, 2009; Tiesinga & Sejnowski, 2009); however, recurrent excitatory connections are characteristic features of neural circuits (Shu *et al.*, 2003; Douglas & Martin, 2004), and have also been linked to these chattering reverberations (Gray & McCormick, 1996; Tiesinga & Sejnowski, 2009).

Previously, we have reported that a specific functional network is activated within a cell assembly (simultaneously recorded neurons) that is contingent upon a particular orientation (Bharmauria *et al.*, 2012). The functionally connected neurons within these circuits synergistically cross-interact within a 50-ms emergent 'window of opportunity' to encode the presence of a stimulus (Bharmauria *et al.*, 2014). During this window of opportunity, the firing rate of the target neuron significantly increases following the spike occurrence of the reference neuron. With this latter finding as a premise, we sought to investigate how one neuron impinges upon the oscillatory rhythm of its simultaneously recorded companion neuron. First, we report that the connected neuron pairs in an assembly show

Correspondence: Dr S. Molotchnikoff, [1]Neurophysiology of the Visual System, as above.

Received 23 January 2015, revised 18 March 2015, accepted 1 April 2015

higher power than the unconnected neuron pairs in the gamma oscillatory range (20–40 and 60–80 Hz); second, there is increased coherence between them. Finally, the higher gamma oscillations (60–80 Hz) are exclusively related to the fast-spiking neurons. This finding leads us to postulate that gamma routing is specific within the cortical circuitry, and is an intrinsically generated substrate within an assembly for feature processing.

Materials and methods

Ethical approval

Four cats were prepared for electrophysiological recordings in the primary visual cortex (V1), according to the guidelines of the Canadian Council on Animal Care; the procedure was approved by the Institutional Animal Care and Use Committee of University of Montreal. The full description of the protocol is given below.

Animals, anesthesia, and surgical procedures

Cats premedicated with acepromazine maleate (Atravet; Wyeth-Ayerst, Guelph, ON, Canada; 1 mg/kg, intramuscular) and atropine sulfate (ATRO-SA; Rafter, Calgary, AB, Canada; 0.04 mg/kg, intramuscular), were anesthetised with ketamine hydrochloride (Rogarsetic; Pfizer, Kirkland, QC, Canada; 25 mg/kg, intramuscular). The cats were then paralyzed with 40 mg of gallamine triethiodide and maintained with 10 mg/kg/h gallamine triethiodide (Flaxedil; Sigma Chemical, St Louis, MO, USA; intravenous) administered in 5% dextrose lactated Ringer's nutritive solution. General anesthesia was maintained by artificial ventilation with N_2O/O_2 (70 : 30) supplemented with 0.5% isoflurane (AErrane; Baxter, Toronto, ON, Canada). Electroencephalogram, electrocardiogram, rectal temperature and end-tidal CO_2 partial pressure were monitored throughout the experiment, and kept within physiological ranges. Pupils were dilated with atropine, and Plano lenses with artificial pupils (diameter, 5 mm) were fixed. The loci of the area centrales were inferred from the positions of the blind spots.

Visual stimulation

Monocular stimulation was performed. The multiunit receptive fields (RFs) were mapped as the minimum response fields (Barlow *et al.*, 1967) by use of a hand-held ophthalmoscope after clearly detectable activity had been obtained. These preliminary tests revealed qualitative properties such as dimensions, velocity preference, orientation, and directional selectivity. Visual stimuli were generated with a VSG 2/5 graphic board (Cambridge Research Systems, Rochester, UK), and displayed on a 21-inch monitor (Sony GDM-F520 Trinitron; Sony, Tokyo, Japan) placed 57 cm from the cat's eyes, with 1024 × 768 pixels, running at 100-Hz frame refresh. Stimuli were sine-wave drifting gratings covering the excitatory RFs of neurons at both electrodes. Stimuli were presented randomly in eight different orientations. Contrast was set at 80%. The mean luminance was 40 Cd/m^2. Optimal spatial and temporal frequencies were set at 0.24 cycles/deg and a range of 1.0–2.0 Hz, respectively, where V1 neurons are driven maximally by sine-wave drifting gratings (Bardy *et al.*, 2006). Each drifting grating was presented 25 times (each trial lasted for 4.1 s) with varying interstimulus (1–3 s) intervals. Thus, the presentation of a stimulus lasted for 180 s (with all trials and interstimulus intervals).

Electrophysiological recording, single-unit selection, and orientation selectivity index (OSI)

Multiunit activity in V1 was recorded at positions 410–820 μm (laterally) apart with a tungsten multielectrode (matrix electrode; Frederick Haer & Co.). The multielectrode had four columns, and each column had one row). For each recording, only two contacts were used (spaced 410–820 μm apart). Fourteen recordings were performed across all cats in either the left or the right hemisphere. In total, 28 sites were obtained. Each site corresponds to a tip (contact). Recordings were performed in the supragranular layers (cortical depth, < 1000 μm; mean, 650 μm). The signal from the microelectrodes was amplified, bandpass-filtered (300 Hz to 3 kHz), digitised, and recorded with 0.05-ms temporal resolution (Spike2; CED, Cambridge, UK). Spike sorting from the multiunit signals was performed, and each electrode yielded isolated single units. All cells were discriminated on the basis of three criteria: (i) the spike waveforms' difference; (ii) principal component analysis showing well-dissociated clusters; (iii) and auto-correlograms showing no events at the central point (Csicsvari *et al.*, 1998; Barthó *et al.*, 2004; Fujisawa *et al.*, 2008). The stability of each cell's activity across conditions was verified qualitatively by the visual control of the disposition of clusters and the shapes of waveforms. The details are given in Bharmauria *et al.* (2014).

Cluster analysis was performed with Spike2 (CED) in a three-dimensional plot. The isolation distance was calculated as the Mahalanobis distance. The Mahalanobis distance is the distance from the cluster center within which as many events belong to the other clusters as to the specified cluster (Harris *et al.*, 2001). In other words, given multivariate data values for which the values in each variable are normally distributed around a mean, this measure allows us to define boundaries of constant probability around the multidimensional center of the distribution. This estimation allows the separation of a cluster from the nearest cluster. Units within a Mahalanobis distance of 2.5 were considered for the further analysis of the spike trains of neurons, to reveal the functional connections between them. Furthermore, the J3 values were calculated for every neuron pair (clusters); these indicate the separation of the clusters. Clusters with a J3 value of 1.5 were set as the benchmark for cluster separation. The insert in the figure shows an example of a neuron pair (clusters) that has a J3 value of 1.56. The respective waveforms are shown adjacent to the clusters. Across all recordings, 276 pairs were analysed. Figure 1A shows this meta-analysis.

Once single cells had been sorted out offline from multiunit spike trains accumulated during data acquisition, orientation tuning curves of cells were obtained from raw data and fitted with the von Mises function (Swindale, 1998).

$$M(\theta) = A.e^{b}[\cos(\theta - c)] + d \quad (1)$$

where A is the value of the function at the preferred orientation c, and b is the width parameter. An additional parameter, d, represents the spontaneous firing rate of the cell. $M(\theta)$ is the firing rate of the neuron at orientation θ. This allowed us to determine with precision the preferred orientation of every cell.

An OSI was calculated to ensure the tuning of neurons. It was measured from the fitted tuning curves by dividing the firing rate at baseline (orthogonal orientations) by the firing rate for the preferred orientation, and subtracting the result from 1 (Ramoa *et al.*, 2001; Liao *et al.*, 2004; Bachatene *et al.*, 2013). The closer the OSI is to 1, the stronger the orientation selectivity. Figure 1B shows the OSI

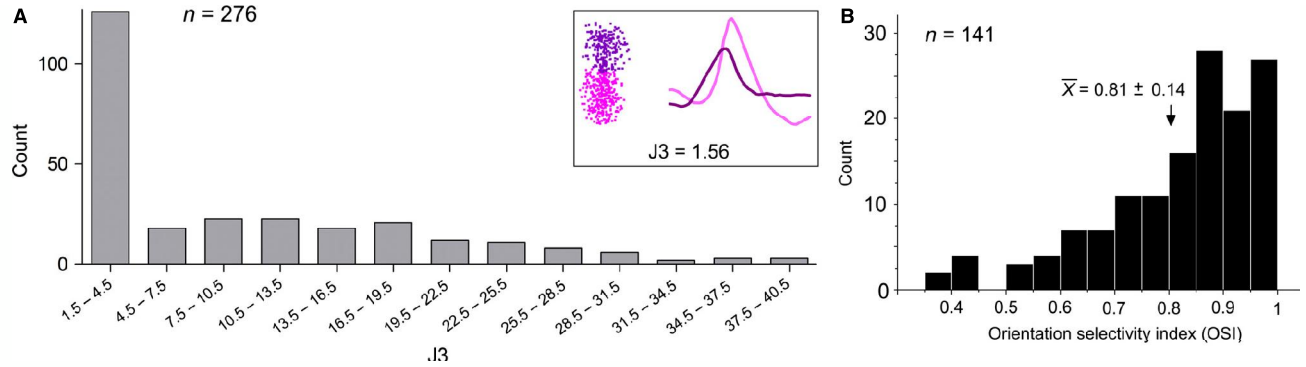

FIG. 1. Cluster separation and OSI. (A) Histogram of cluster separation based on J3 values for all of the neuron pairs. A typical example of cluster separation (J3 = 1.56) is shown as an insert with respective waveforms for the clusters. (B) Distribution of the OSI for all neurons.

for all of the analysed neurons (n = 141). The mean OSI ± standard deviation was found to be 0.81 ± 0.14.

Cross-correlograms and network formation

Cross-correlograms were constructed between the trains of action potentials of every recorded neuron at all of the sites and all of the applied orientations to reveal the functional connections. The raw cross-correlograms were shift-corrected to eliminate the putative significant peaks resulting from the simultaneous stimulation of both cells during each trial (to remove the stimulus-evoked and locked components) (Perkel *et al.*, 1967).

A significant peak of 2 ms (two adjacent 1-ms bins) or at least one significant bin (Alloway & Roy, 2002) was searched within a window of ± 5 ms around zero (excluding the ± 1-ms bins around zero) in the shift-corrected cross-correlograms to reveal a functional connection between two neurons. The statistical threshold for the significant peak was set at 95% (red curved line in cross-correlograms), and the probability of the neuron firing in a bin was calculated as follows (Abeles, 1982).

Considering the spike train as a Poisson train, the probability of the neuron firing in the small bin of size b is:

$$P = Fb \text{ and } F = N/T \qquad (2)$$

where F is the neuron frequency, T is the total time interval, and N is the number of spikes in that interval.

The confidence limit was calculated as in Abeles (1982), as follows.

The expected bin count (C) for the histogram is then:

$$C = PN_{\text{Ref}},$$

where N_{Ref} is the number of reference events.

The confidence limits for C were calculated on the assumption that C has a Poisson distribution.

Assume that a random variable S has a Poisson distribution with parameter C. Then, the 95% confidence limits are calculated as follows:

Low confidence = x, such that probability ($S < x$) = 0.005

High confidence = y, such that probability ($S > y$) = 0.005

On the basis of the shift-corrected cross-correlograms, functional networks between all neurons at all orientations were wired. In cases when two cells recorded from the same tip fired in synchrony, their respective waveforms were summed, and consequently the shape of the resultant waveform was rejected, as it fell outside the range of the template. In the present investigation, 'synchrony' of spikes from the same tip was excluded from the analysis. We considered only spikes that fell beyond ± 1 ms after the central point in the cross-correlogram to make significant projections. In addition, cumulative sums based on all histograms of the firing rates indicated that the reference spike modulates the discharge of the target neuron. For every cross-correlogram, the cumulative distribution of spikes was computed (it is displayed above every cross-correlogram). This computation indicates the modulation of the firing rate of the target cell after the reference cell has fired an action potential. The reference spike occurred at point zero, i.e. the central point in the cross-correlogram, and the corresponding cumulative distribution is shown above. This further illustrates the functional connectivity between both cells, as the activity of the target cell depends upon the activity of the companion unit (reference neuron).

The cumulative sum (cs) graphs above the histograms were calculated as follows.

If we have a histogram with bin counts bc(i), i = 1,. . .,N, then the cumulative sum cs(i) for a bin is as follows:

for bin 1: cs(1) = bc(1) – A
for bin 2: cs(2) = bc(1) + bc(2) – A × 2
for bin 3: cs(3) = bc(1) + bc(2) + bc(3) – A × 3, etc.

Peri-event spectrogram and coherence analysis

The analysis was performed with NEUROEXPLORER 4 (Nex Technologies). For each selected variable, this analysis results in multiple spectrograms that start at the specified time after the occurrence of each reference event (spike). These spectrograms are then averaged over all of the reference events. The power spectra were calculated by the use of 512 frequencies between 1 and 120 Hz, smoothed with a Gaussian kernel with a bin width of 3. The analysis window lasted from −0.75 s (relative to the reference event) until 0.75 s. The sliding window (shift) was set at 20 ms (i.e. 100 shifts for the window of analysis).

The power spectrum was calculated for the specified number (number of shifts) of windows as follows.

For a time-stamped variable, the rate histogram was calculated and copied into a signal array. The following parameters were used:

Histogram start = start + shift × (window number − 1)

Bin = 1/(2 × maximum frequency)

Number of bins = 2 × number of frequency values.

In other words, each time-stamp of the reference neuron (t) was taken, and then a bunch of histograms of another neuron in time intervals (t + histogram start, t + histogram start + bin × number of bins) was calculated.

For each interval, rate histograms are calculated and detrended, the ing window was applied, and fast Fourier transforms were calculated. Then, individual densities and cross-densities were calculated. Finally, the fast Fourier transform analysis on these rate histograms produced a single spectrogram for time-stamp ***t***. The same was repeated for another time-stamp of the reference neuron, and so on. In a similar fashion, the peri-event spectrograms were calculated for all of the analysed neurons (n = 141) in response to the stimulus (i.e. when the stimulus was set as trigger instead of the spike of the neuron).

Thereafter, the coherence was calculated. Coherence measures the correlation between two time series as a function of frequency (Pereda *et al.*, 2005; Sakkalis *et al.*, 2009). In our study, we computed the coherence between the time series (spike trains) of two neurons by using 512 frequencies between 1 and 120 Hz. The overlap window was set at 5%, and it was smoothed with a Gaussian kernel with a binwidth of 3. For each time-stamped variable, coherence was calculated in a similar fashion as above.

Results

Anesthetised cats were used for these experiments. Sine-wave drifting gratings were presented within the RFs of neurons in V1 to record their activities simultaneously with multielectrodes. Thereafter, neurons were spike-sorted from the multiunit activity, and traced at all of the orientations. As described in Materials and methods, the functional connections were revealed at the tested orientations between the recorded neurons (Bharmauria *et al.*, 2012). Such simultaneously recorded neurons from a single tip of a multielectrode were termed a cell assembly. Following this, the goal of the current investigation was to observe the changes in firing frequency of a neuron with reference to the firing of another simultaneously recorded neuron in the assembly. Some neurons in the assembly connect to each other, whereas others do not show connections (Bharmauria *et al.*, 2012, 2014), depending upon the applied orientation. In total, 198 pairs were analysed from 28 recording sites. The connected (n = 98) and unconnected (n = 100) neuron pairs were investigated across the same assemblies. Table 1 summarises the recordings. It should be noted that, in the current analysis, a single orientation where an assembly showed the highest number of connections was chosen for the peri-event spectrogram analysis, although the networks were revealed at of all the tested orientations.

Augmented gamma activity between functionally connected neurons

We began with the peri-event spectrogram analysis for the same pairs for which cross-correlations were computed. Figure 2 shows a typical example of cross-correlogram and peri-event spectrogram analysis of a neuron pair. The functional connection between the pair was revealed by computing a cross-correlogram (shift-corrected, see Materials and methods) between the spike trains of both neurons. In Figure 2A, the blue raster represents the reference neuron, and the cyan raster represents the target neuron. The cross-correlogram analysis (Fig. 2B) revealed a significant peak (95% statistical threshold, highlighted by the cyan background; see Materials and methods) within 5 ms after the zero (black broken line), thereby indicating that the blue neuron projected onto the cyan neuron (that is, it excited the blue neuron in the circuit). This is highlighted by the black horizontal arrow linking the two neurons (blue and cyan circles above the cross-correlogram). The probability of the significant peak was found to be 0.13, and indicated the strength of the connection. The black curved line above the cross-correlogram represents the cumulative sum based on the histogram, and further reveals the upsurge in spike activity of the target neuron after the reference neuron's firing, as described previously (Bharmauria *et al.*, 2014). This upsurge suggests augmented excitability. Thereafter, the peri-event spectrogram analysis (see Materials and methods) was performed for the same neuron pair (Fig. 2C). It was found that, once the reference neuron (blue) had spiked at zero (indicated by the red broken line), there was an increase in frequency power (indicated by the colored scale) of the target neuron (cyan) that straddled zero, and that there was a distinct zone of increased frequency that ranged approximately from 20 to 40 Hz (low-gamma oscillatory band), as indicated by the pink arrow in Fig. 2C.

Table 1. Statistics for the analysed neuron pairs

Total number of sites (cell assemblies)	Average number of cells isolated	Connected cell pairs analysed	Unconnected cell pairs analysed
28	5.1	98	100

Some neuron pairs did not show connections between them. In a similar fashion, the peri-event spectrogram analysis was performed for the unconnected neuron pairs. Figure 2D shows the respective spike trains for the unconnected neuron pair (the red neuron is the reference). The absence of a significant peak in the cross-correlogram (Fig. 2E) indicates that there was no functional link between neurons. The spectrogram analysis (Fig. 2F) for the pair shows that the activity of the target neuron was unmodulated, and this indicates the absence of a distinct gamma-activity band between neurons (note that all frequencies are almost equally represented).

Figure 2G shows that there was augmented gamma power in the 20–40-Hz range (highlighted by the shaded gray area) for the connected neuron pair (blue curve) as compared with the unconnected connected pair (pink curve). Note that these four neurons were isolated from a single tip, and thus constituted a cell assembly.

Significant difference between the connected and unconnected units

Figure 3 shows the averaged analysis for the connected (n = 98) and unconnected (n = 100) neuron pairs. Figure 3A shows that there was a significant difference between the time courses of evolution (0.75 s to +0.75 s) of the oscillatory activities between the connected (green curve, n = 98) and unconnected (red curve, n = 100) neuron pairs (unpaired t-test, $P < 0.0001$). The shaded area depicts the standard error of the mean (SEM). The curves are aligned with the responses of the reference neuron at the zero mark (indicated by the red broken line). To better compare the gain in activity, the raw curves were normalised. The normalisation was performed with the lowest value set to zero. Figure 3B shows the normalised curves for connected and unconnected pairs, which were significantly different (paired t-test, $P < 0.0001$). The power straddling zero for connected pairs was approximately twice (indicated by the black arrow) the activity for the unconnected neuron pairs. The shaded purple area

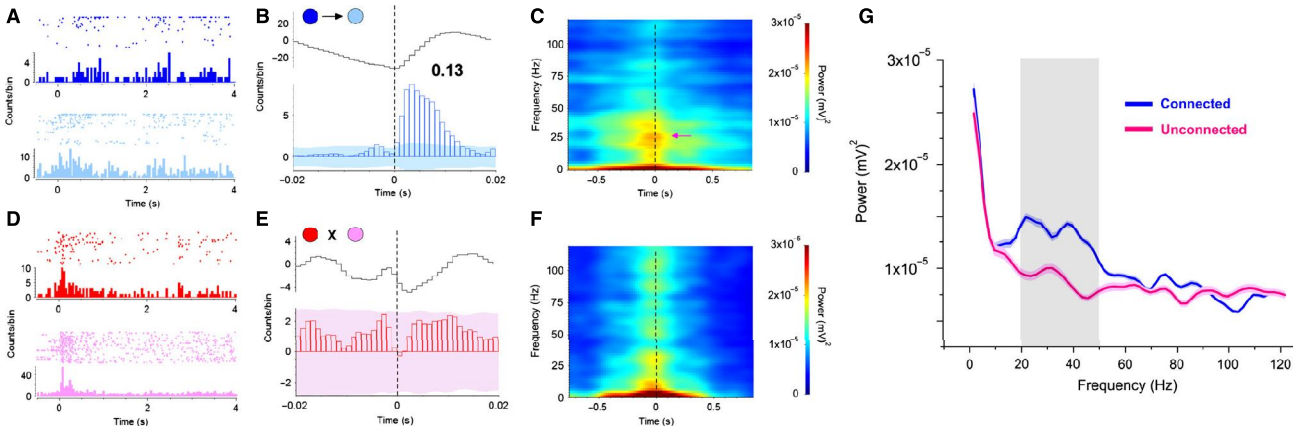

FIG. 2. Cross-corrrelogram and peri-event spectrogram analysis. (A) Respective rasters and peri-event histograms for two neurons isolated from the same tip of an electrode. (B) Cross-correlogram (shift-corrected) for the isolated neurons in A. The cross-correlogram for the target neuron (cyan) significantly peaks within 5 ms after zero (black broken line), indicating that the blue neuron projects onto the cyan neuron. The probability of the peak is 0.13. The black curve above the histogram stands for the cumulative sum based on the histogram that further confirms the upsurge in the activity of the target neurons once the reference neuron spikes at zero. (C) Peri-event spectrogram for the same neuron pair (the blue neuron is the reference) as in B. The pink arrow indicates the increase in gamma power straddling zero for the target neuron around 25 Hz. (D) Rasters and peri-event histograms for two neurons isolated from the same tip. (E) Cross-correlogram for the neurons in D. As there is no significant peak in the cross-correlogram within ± 5 ms around zero, this suggests that no functional relationship exists between neurons (the red neuron is the reference). (F) Peri-event spectrogram analysis for the same neuron pair (the red neuron is the reference) shows an absence of pronounced gamma activity in the 25-Hz range for the target neuron. (G) Comparison of the gamma power between the connected and unconnected neuron pairs analysed above. There is higher gamma power for the connected neuron pair (blue curve) than for the unconnected neuron pair (pink curve) in the gamma bandwidth highlighted by a gray background. Note that these four neurons were isolated from a single tip, and thus constitute a cell assembly.

represents the characteristic temporal window of opportunity, and coincides with the 50-ms epoch (the peak of the green curve is offset from the peak of the red curve by ~50 ms, and the increase in the rhythmic activity before zero is attributable to the application of the stimulus, as it is presented at the beginning of the trace) in our previous study (Bharmauria *et al.*, 2014).

One of the most significant results of the current investigation (Fig. 3C) was that there was augmented power of gamma activity (approximately 20–40 Hz and 60–80 Hz) between the connected (blue curve) pairs as compared with the unconnected (pink curve) pairs (unpaired *t*-test, $P < 0.0001$). The normalised curves (Fig. 3D) also show that the power was substantially different (paired *t*-test, $P < 0.0001$) in the low and high gamma bands (indicated by the gray shaded areas) for the connected and unconnected pairs. To further confirm that, indeed, the revealed connections and the consequent higher power between the connected neurons resulted from stimulus presentation (each spike of the reference neuron is aligned at zero), we investigated the same connected pairs for the frequency–power analysis at spontaneous (black curve) oscillations (Fig. 3E). The curves in both conditions were significantly different (unpaired *t*-test, $P < 0.0001$). Figure 3F shows the normalised curves, and reflect the significant difference in gamma activity (shaded gray area) between the spike-triggered activity of pairs at the presentation of the stimulus and during spontaneous oscillations (paired *t*-test, $P < 0.0001$). These distinct gamma bands in response to the presentation of a stimulus have been extensively reported in the literature (Fries, 2005; Fries *et al.*, 2007; Brunet *et al.*, 2014a; Miller *et al.*, 2014); thus, it was important to examine whether this spike-triggered gamma activity was also present when the stimulus was set as trigger. To this end, we calculated the peri-event spectrograms of all neurons ($n = 141$) with reference to the stimulus. Figure 3G (dark cyan curve) represents the mean power of spectrogram analysis, and shows that these two zones of gamma activity (shaded gray area) were also present when the stimulus was set as trigger. Figure 3I (normalised curves) shows that the spike-triggered power (blue) was significantly higher than and different from (paired *t*-test, $P < 0.0001$) the stimulus-triggered power (dark cyan). This reference neuron-triggered difference in spectral power between the two classes points to the fact that gamma activity is specifically routed between the functionally connected neurons in a stimulus-activated assembly. Moreover, it seems from the latter analysis that gamma activity is masked within microcircuits, so there is a contentious debate (Fries *et al.*, 2007; Bosman *et al.*, 2014; Ray & Maunsell, 2014) regarding their occurrence (as all previous studies are related to local field potentials, which capture the activity of the entire neuronal population within a volume).

Augmented coherence between the connected neuron pairs

We then calculated the coherence for all of the analysed pairs, as it has been suggested as an inevitable mechanism for the generation of oscillatory rhythms within an assembly (Fries, 2005). Coherence measures the relationship (correlation) between frequencies of two time series (Sakkalis *et al.*, 2009). If either the power or the phase of the signals changes, it leads to a change in the coherence value of the analysed signals. That is, if two signals have a phase or power relationship, they will have a higher value of coherence.

Figure 4 illustrates this analysis. Figure 4A shows the difference in coherence between a connected (purple curve) and an unconnected (orange curve) neuron pair. There was increased coherence (0.08) for the connected pair around 20–40 Hz, although the pair also showed coherence at higher frequencies. Note that these are the same pairs as in Fig. 2. Figure 4B shows the global trend for the connected (purple curve, $n = 98$) and unconnected (orange curve, $n = 100$) pairs, with SEMs (shaded area). The global coherence analysis between the two classes showed that there was an added

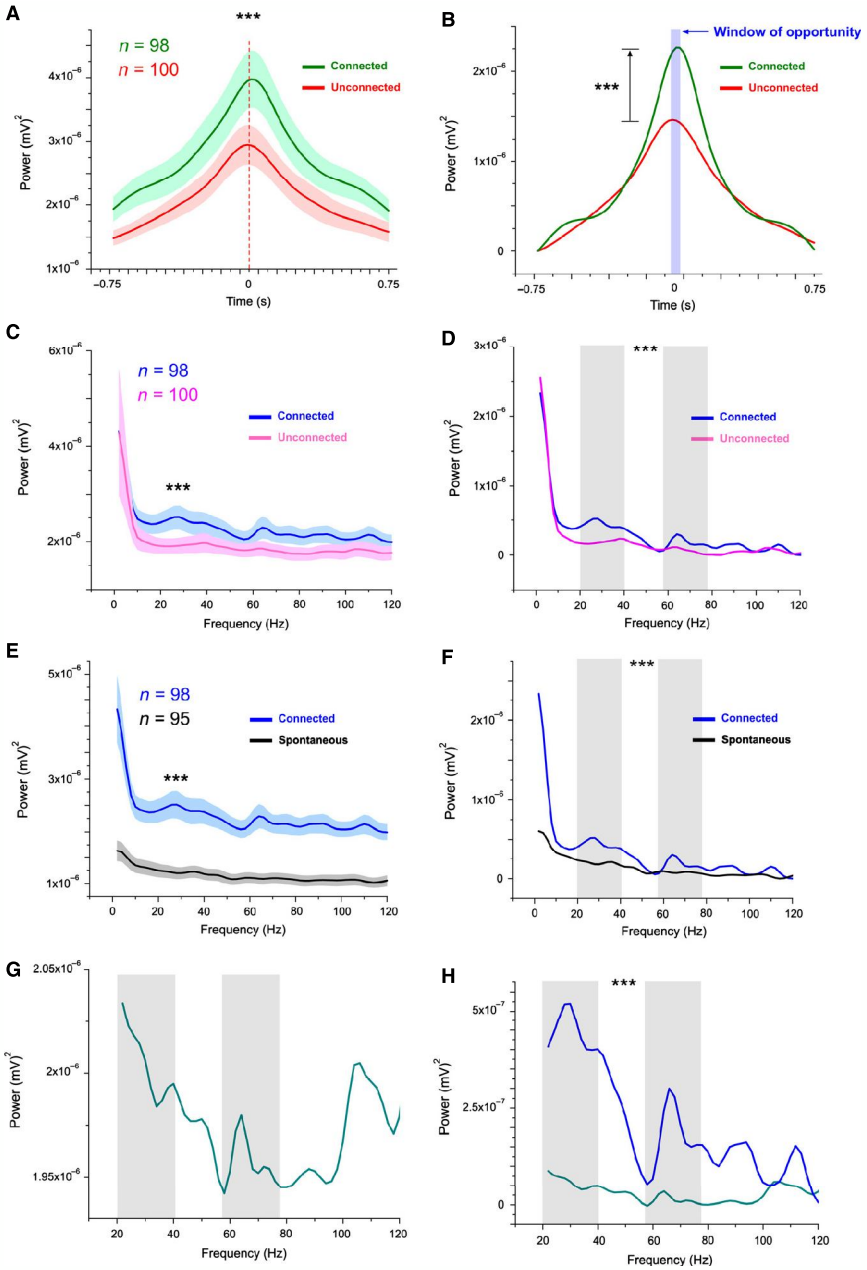

FIG. 3. Difference between the connected and the unconnected units. (A) Global comparison between the connected (green) and the unconnected (red) units during the time course of evolution of gamma power. The shaded area corresponds to the SEM. The curves are significantly different (unpaired *t*-test, $P < 0.0001$). The red broken line represents the spike occurrence of the reference neuron. (B) Normalised curves for the connected and unconnected neuron pairs. There is a significant difference between the connected and unconnected neuron pairs (paired *t*-test, $P < 0.0001$), and the rhythmic power for connected neurons is almost twice (black arrow) the activity for unconnected neurons. The purple shaded area corresponds to the characteristic window of opportunity for neuronal collaboration. (C) Global comparison of gamma power between the connected and unconnected neurons. The curves are significantly different (unpaired *t*-test, $P < 0.0001$). (D) Normalised curves show that the connected and unconnected neuron pairs are significantly different (paired *t*-test, $P < 0.0001$). The power is higher (almost twice) in the gamma band for the connected neurons, as indicated by the shaded gray areas. (E) Global comparison of gamma power for the connected neuron pairs at the presentation of the stimulus (blue curve) and during spontaneous activity (black curve). The curves are significantly different (unpaired *t*-test, $P < 0.0001$). (F) Normalised curves for the spike-triggered analysis at the presentation of stimulus and during spontaneous oscillations. The curves are significantly different (paired *t*-test, $P < 0.0001$). (G) Stimulus-triggered gamma activity for all of the recorded neurons ($n = 141$). The shaded areas correspond to the zones of low and high gamma activity. (H) Normalised curves for stimulus-triggered and spike-triggered gamma activity. The curves are significantly different (paired *t*-test, $P < 0.0001$). The normalisation was performed with the lowest value, set at zero.

coherence for the connected pairs in the gamma band, especially in the lower gamma band (the shaded gray area), as compared with the unconnected pairs, and it was significantly different (unpaired *t*-test, $P < 0.0001$). This suggests that interneuronal connections facilitate multiple rhythmic activities; however, it was more pronounced in the lower gamma band. On the other hand, unconnected neurons

appeared to lack these rhythmic oscillations. Figure 4C shows the normalised curves for connected (purple curve) and unconnected pairs (orange curve), and it also shows that the increase for connected pairs was significantly different from that for unconnected pairs in the gamma band (20–40 and 70 Hz, shaded gray areas) (paired *t*-test, $P < 0.0001$). This distinct augmented coherence in the low-frequency and high-frequency domains further points to the fact that connected neurons share an oscillatory phase.

Interaction between the regular spikes (RSs) and fast spikes (FSs)

Inhibitory interneurons embedded in excitatory neuron networks have been widely postulated to be generators of gamma oscillations (Wang & Buzsáki, 1996; Bartos *et al.*, 2002, 2007; Fries *et al.*, 2007). To investigate this, we categorised the spike waveforms on the basis of their ascending slope into RSs and FSs (Niell & Stryker, 2008; Vinck *et al.*, 2013), which are putatively linked to pyramidal neurons and inhibitory interneurons, respectively (Niell & Stryker, 2008; Bachatene *et al.* 2012; Vinck *et al.*, 2013). The histogram in Fig. 5A shows the division of spike waveforms into RSs (red) and FSs (gray) – waveforms with ascending slopes of ≤ 0.3 ms were categorised as FSs, and those with ascending slopes of > 0.3 ms were categorised as RSs. Of a total of 141 waveforms (neurons), 40 were categorised as FSs and 101 were categorised as RSs. Typical examples of an FS (putative inhibitory interneuron) and an RS (putative pyramidal cell) are shown as an insert in Fig. 5A.

Thereafter, all the connected pairs were divided into RS–RS connections, FS–RS connections, and FS–FS connections. The distribution is shown in Fig. 5B: 73 connections were RS–RS connections; 21 were FS–RS connections; and only four were FS–FS connections. We also analysed the respective peri-event spectrograms and coherence values for only RS–RS connections, and for FS–RS and FS–FS connections. Figure 5C shows the spectrogram analysis, and can be seen that RS–RS connections (red curves) only showed the low gamma oscillation, whereas, the high gamma rhythm was absent. Interestingly, in contrast, when a fast-spiking neuron was involved in a connection (FS–RS or FS–FS) the higher-gamma band around 60–80 Hz was pronounced, although the low gamma hump was still present. The raw curves were significantly different from each other (unpaired *t*-test, $P < 0.0001$). The results are further accentuated in the normalised curves (Fig. 5D), which were significantly different from each other (paired *t*-test, $P < 0.0001$). The shaded cyan areas indicate two distinct epochs of gamma activity. Furthermore, the coherence analysis on the same pairs yielded results that further corroborated the above findings. The RS–RS coherence (red curve) was present only in the low gamma band, whereas fast-spiking neurons showed higher coherence (black curve) with other neurons (FS–RS and FS–FS) at both low and high gamma rhythms. The curves were significantly different from each other (unpaired *t*-test, $P < 0.0001$). The significant difference (paired *t*-test, $P < 0.0001$) between normalised curves further emphasises the difference in low and high gamma rhythms between two classes, as highlighted by the shaded cyan areas. In summary, these latter analyses show that higher gamma rhythms are mostly linked to fast-spiking neurons or putative inhibitory interneurons.

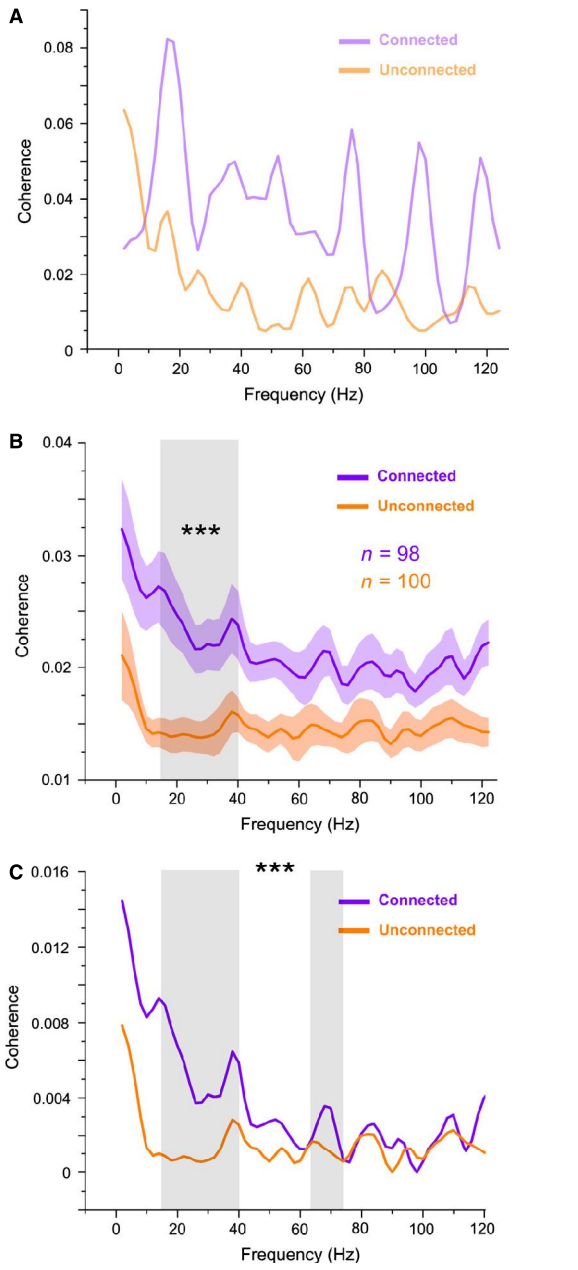

FIG. 4. Difference in coherence between the connected and the unconnected units. (A) Typical examples of a connected and an unconnected neuron pair. Note that these are the same pairs as in Fig. 1. There is higher coherence for the connected neuron pair than for the unconnected neuron pair in the gamma bandwidth. (B) Difference between the pooled activity of the connected and the unconnected neuron pairs. There is a significant difference between the curves (unpaired *t*-test, $P < 0.0001$), especially in the 20–40-Hz range. The shaded area corresponds to the SEM. (C) Normalised curves for the connected and unconnected neuron pairs show that the coherence is almost twice as high for the connected neuron pair (the shaded areas), and is significantly different (paired *t*-test, $P < 0.0001$) between the connected neuron pair and the unconnected neuron pair. The normalisation was performed with the lowest value, set at zero.

Discussion

In the present investigation, using peri-event spectrogram analysis, we have shown that once a neuron spikes in a connected neuron pair in an assembly, it switches the target neuron firing into the gamma oscillatory mode. The power of gamma oscillations in connected neuron pairs is significantly higher than that in unconnected neuron

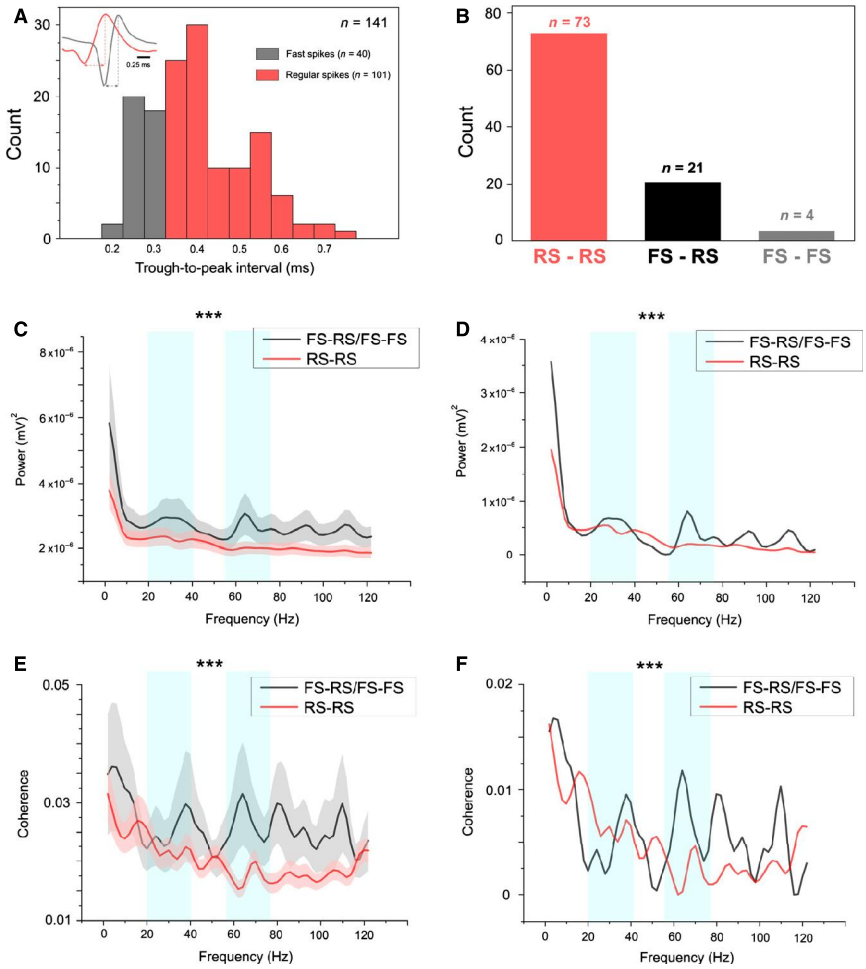

FIG. 5. Interaction between FSs and RSs. (A) Division and distribution of FSs and RSs according to the ascending slope of the action potential. The gray bars represent the FSs (n = 40), and the red bars represent the RSs (n = 101). Typical examples of an FS and an RS are shown superimposed as an insert. (B) Distribution of connections according to spike waveforms. (C) Raw frequency–power curves for FS–RS/FS–FS (black) and RS–RS connections. The curves are significantly different (unpaired t-test, $P < 0.0001$). (D) Comparison of normalised curves for FS–RS/FS–FS (black) and RS–RS connections. The curves are significantly different (paired t-test, $P < 0.0001$). There are distinct humps of low gamma activity (20–40 Hz) and high gamma activity (around 60–80 Hz) for FS connections. RS–RS connections show low gamma activity only. (E) Corresponding coherence analysis for the pairs in C. (F) Normalised curves for the coherence analysis in E. The curves are significantly different (paired t-test, $P < 0.0001$). The shaded cyan areas for spectrogram and coherence analyses show that the gamma activities are different for FS–RS/FS–FS (black) and RS–RS connections.

pairs, although all neurons were activated with the stimulus. The fact that there is added coherence for connected neuron pairs suggests that the oscillatory rhythms originate from this systematic phase relationship between the firing of connected neurons.

Anesthetised animals were used in the current experiments. A stimulating orientation grating was presented within the RFs of the neurons. It has already been shown that different oscillatory rhythms might be present in anesthetised animals, either spontaneously or in relation to the stimulus (Fries, 2005; Fries *et al.*, 2007; Brunet *et al.*, 2014a,b; Miller *et al.*, 2014). Moreover, we have already reported that the revealed connections between neurons are strongly related to the stimulus rather than to the spontaneous fluctuations in the brain (Bharmauria *et al.*, 2012, 2014).

Functional consequences

Previously, it has been shown by many authors that there is rhythmic gamma oscillatory activity that develops within the population in relation to the stimulus (Fries, 2005; Fries *et al.*, 2007; Brunet *et al.*, 2014a); however, all of these studies were performed on fast local field potentials, which provide the activity of all of the neurons captured in a local population. Interestingly, the major finding of the current investigation was that the connected neurons within an encoding population of neurons (a cell assembly) show higher gamma activity than the unconnected neurons within the same assembly. Moreover, there is an increased frequency coherence related to these connected neurons. Recently, we have reported that, after the reference neuron spikes in a connected pair, it leads to an upsurge in the excitation of the target neuron for a short time period of 50 ms (window of opportunity), and that, thereafter, the activity gradually subsides (Bharmauria *et al.*, 2014). Furthermore, comparison of the spectrograms of the same connected neurons in relation to the spike-triggered activity in the presence and absence of stimulus (spontaneous oscillations) shows that the reference neurons switch the target neurons into the gamma band.

A few decades ago, an emerging hypothesis (binding-by-synchrony) emerged, explaining the encoding of sensory signals. This hypothesis rests on the principle that selected neurons within an assembly synchronise their spikes within gamma oscillations to frame a specific network (Milner, 1974; Engel *et al.*, 1991; Singer, 1999; Salinas & Sejnowski, 2001). In general, precise synchrony is attributed to the common afferent input; however, quasi-synchronous delays (~5 ms) between neuronal spike trains are indicative of putative functional links between cells (Barthó *et al.*, 2004; Fujisawa *et al.* 2008; Bharmauria *et al.*, 2014). Thus, within the framework of a distributive system (Bernardet & Verschure, 2002; Behrmann & Plaut, 2013), wherein circuits are specifically programmed to encode a stimulus, we suggest the following process for information retrieval within circuits. In response to the presentation of a stimulus, a group of neurons (typically defined as a cell assembly, but this is synonymous with synfire chain, reservoir, and ensemble) become simultaneously active, whereby they share frequency coherence, eventually switching the neurons within the assembly into a recurrent gamma oscillatory mode (Fries, 2005; Miller *et al.*, 2014). Functional connections are then engineered between neurons in an assembly that have added coherence, as suggested by Fries (2005), because the input and output gates are open for these neurons at the same time. This ultimately cascades into the temporal window of opportunity (Fries, 2005; Bharmauria *et al.*, 2014; Siegle *et al.,* 2014) for neurons to encode the relevant information downstream and wire a specific network contingent upon the input [synonymous with a classifier, as postulated by Singer (2013)]. In other words, an intrinsically generated functional network is constructed by a cell assembly according to the input, as has been recently postulated by numerous authors (Harris & Mrsic-Flogel, 2013 Singer, 2013; Miller *et al.*, 2014). Sparse activity of neurons has emerged as a major phenomenon for neural coding within cortical circuits. Some authors have postulated that the temporal codes and sparseness may well arise from each other (Guyonneau *et al.*, 2004; Molotchnikoff & Rouat, 2012; Ratté *et al.*, 2013). Sparseness implies a low firing rate of neurons in response to a stimulus, and it explains very well the redundancy reduction and multiplexing (Molotchnikoff & Rouat, 2012; Ratté *et al.*, 2013) of neural codes (temporal and rate codes) within circuits; however, it has a few problems associated with it, based on the fragmented organisation of the sparse activity, and seems to contrast with the coherent perception of everyday events (Barth & Poulet, 2012; Jayakumar *et al.*, 2012; Molotchnikoff & Rouat, 2012). This so-called 'window of opportunity' (Bharmauria *et al.*, 2014; Siegle *et al.,* 2014) organised within oscillatory phases seems to overcome the problem that sparseness poses, i.e. the increase in firing during this period. Thus, the window of opportunity creates a burst of cooperative neuronal discharges that potentiate coding within sparse circuits. Indeed, this study differs from previous studies (Singer, 1999; Salinas & Sejnowski, 2001; Fries, 2005; Fries *et al.*, 2007; Brunet *et al.*, 2014a) in that it rests on the increased neuronal coherence between 'functionally connected' neurons within an assembly; however, it also integrates the synchrony (quasi-synchronous functional links within 5 ms) and coherence hypotheses that are at the heart of dynamic communication structure in cortical circuits. Recently, Womelsdorf *et al.* (2012) showed that a high OSI of neurons was linked to high gamma activity (although the experiments were performed in awake monkeys, so the gamma bands differed across monkeys), so we may infer that most of the firing of neurons in the current investigation was synchronised with gamma activity, as the mean OSI was high and gamma activity was present in relation to the stimulus.

Pyramidal-interneuron gamma (PING) or interneuron gamma (ING)?

Excitatory pyramidal neurons and inhibitory interneurons are two major classes of neurons that fill the cortex, and synchrony within a limited space volume (e.g. an orientation column) can be achieved by their specific interactions (Tiesinga & Sejnowski, 2009) – ING (related to mutually connected FS cells) or PING (related to mutually connected FS–RS cells). Because, in our investigation, we found that low and high gamma oscillations were simultaneously generated by the interaction of FSs with other spikes (as RS–RS interactions were at low gamma only), we suggest that PING gamma may be implicated in the generation of these synchronous outputs (Cardin *et al.*, 2009; Tiesinga & Sejnowski, 2009); whereas the RS–RS gamma synchrony might be an outcome of feedforward flow from the upstream areas (Tiesinga *et al.*, 2008).

Recently, the role of gamma oscillations has been questioned (Ray & Maunsell, 2014), mainly for the following reasons. The first is that they have low power, particularly during the first 200 ms after stimulus onset (Ray & Maunsell, 2014). The second is the irregularity of their occurrence, which appears to depend on several systemic (brain state) and stimulus factors. In contrast to these investigations, here we associated gamma oscillations with the neuronal activity of a companion cell instead of the stimulus onset. In our investigation, although the stimulus-triggered gamma was present (although weak) our strategy (spike-triggered spectrograms) enabled us to reveal the heightened power of these oscillations between connected units in this range. Thus, this study might help to reconcile the debate on the occurrence of gamma oscillations.

We conclude that, in response to a stimulus, coactive neurons feature a cell assembly; however, most importantly, it is the specific network and gamma routing between neurons within a characteristic temporal window of opportunity that eventually lead to the feature encoding. The intrinsically generated gamma oscillations are specifically spread between connected neurons within V1 circuits in relation to the stimulus; this consequently leads to preliminary processing of information, and then the passing of this information downstream in cortical areas through feedforward flow.

Conflict of interest

The authors declare no conflict of interest.

Acknowledgements

S. Molotchnikoff and J. Rouat were supported by CRSNG (Conseil de Recherches en Sciences Naturelles et en Génie) and FRQ-NT (Fonds de recherche du Québec – Nature et technologies).

Abbreviations

FS, fast spike; ING, interneuron gamma; OSI, orientation selectivity index; PING, pyramidal-interneuron gamma; RF, receptive field; RS, regular spike; SEM, standard error of the mean; V1, primary visual cortex.

References

Abeles, M. (1982) Quantification, smoothing, and confidence limits for single-units' histograms. *J. Neurosci. Meth.*, **5**, 317–325.

Alloway, K.D. & Roy, S. (2002) Conditional cross-correlation analysis of thalamocortical neurotransmission. *Behav. Brain Res.*, **135**, 191–196.

Bachatene, L., Bharmauria, V., Rouat, J. & Molotchnikoff, S. (2012) Adaptation-induced plasticity and spike waveforms in cat visual cortex. *NeuroReport*, **23**, 88–92.

Bachatene, L., Bharmauria, V., Cattan, S. & Molotchnikoff, S. (2013) Fluoxetine and serotonin facilitate attractive-adaptation-induced orientation plasticity in adult cat visual cortex. *Eur. J. Neurosci.*, **38**, 2065–2077.
Bachatene, L., Bharmauria, V., Cattan, S., Rouat, J. & Molotchnikoff, S. (2015) Modulation of functional connectivity following visual adaptation: homeostasis in V1. *Brain Res.*, **1594**, 136–153.
Bardy, C., Huang, J.Y., Wang, C., FitzGibbon, T. & Dreher, B. (2006) 'Simplification' of responses of complex cells in cat striate cortex: suppressive surrounds and 'feedback' inactivation. *J. Physiol.*, **574**, 731–750.
Barlow, H.B., Blakemore, C. & Pettigrew, J.D. (1967) The neural mechanism of binocular depth discrimination. *J. Physiol.*, **193**, 327–342.
Barth, A.L. & Poulet, J.F. (2012) Experimental evidence for sparse firing in the neocortex. *Trends Neurosci.*, **35**, 345–355.
Barthó, P., Hirase, H., Monconduit, L., Zugaro, M., Harris, K. & Buzsáki, G. (2004) Characterization of neocortical principal cells and interneurons by network interactions and extracellular features. *J. Neurophysiol.*, **92**, 600–608.
Bartos, M., Vida, I., Frotscher, M., Meyer, A., Monyer, H., Geiger, J.R. & Jonas, P. (2002) Fast synaptic inhibition promotes synchronized gamma oscillations in hippocampal interneuron networks. *Proc. Natl. Acad. Sci. USA*, **99**, 13222–13227.
Bartos, M., Vida, I. & Jonas, P. (2007) Synaptic mechanisms of synchronized gamma oscillations in inhibitory interneuron networks. *Nat. Rev. Neurosci.*, **8**, 45–56.
Behrmann, M. & Plaut, D.C. (2013) Distributed circuits, not circumscribed centers, mediate visual recognition. *Trends Cogn. Sci.*, **17**, 210–219.
Bernardet, U. & Verschure, P.F. (2002) Iqr: a tool for the construction of multi-level simulations of brain and behaviour. *Neuroinformatics*, **8**, 113–134.
Bharmauria, V., Bachatene, L., Cattan, S., Rouat, J. & Molotchnikoff, S. (2012) Network selectivity between primary visual neurons: connectome dynamics. *Soc. Neurosci.*, Poster abstract, Society for Neuroscience Annual meeting, 572.07/FF8.
Bharmauria, V., Bachatene, L., Cattan, S., Rouat, J. & Molotchnikoff, S. (2014) Synergistic activity between primary visual neurons. *Neuroscience*, **268**, 255–264.
Bosman, C.A., Lansink, C.S. & Pennartz, C.M.A. (2014) Functions of gamma-band synchronization in cognition: from single circuits to functional diversity across cortical and subcortical systems. *Eur. J. Neurosci.*, **39**, 1982–1999.
Brunet, N.M., Vinck, M., Bosman, C.A., Singer, W. & Fries, P. (2014a) Gamma or no gamma, that is the question. *Trends Cogn. Sci.*, **18**, 507–509.
Brunet, N.M., Bosman, C.A., Vinck, M., Roberts, M., Oostenveld, R., Desimone, R., De Weerd, P. & Fries, P. (2014b) Stimulus repetition modulates gamma-band synchronization in primate visual cortex. *Proc. Natl. Acad. Sci. USA*, **111**, 3626–3631.
Buzsáki, G. (2010) Neural syntax: cell assemblies, synapsembles, and readers. *Neuron*, **68**, 362–385.
Buzsáki, G., Logothetis, N.K. & Singer, W. (2013) Scaling brain size, keeping timing: evolutionary preservation of brain rhythms. *Neuron*, **80**, 751–764.
Cardin, J.A., Carlén, M., Meletis, K., Knoblich, U., Zhang, F., Deisseroth, K., Tsai, L.H. & Moore, C.I. (2009) Driving fast-spiking cells induces gamma rhythm and controls sensory responses. *Nature*, **459**, 663–667.
Csicsvari, J., Hirase, H., Czurko, A. & Buzsáki, G. (1998) Reliability and state dependence of pyramidal cell–interneuron synapses in the hippocampus: an ensemble approach in the behaving rat. *Neuron*, **21**, 179–189.
Douglas, R.J. & Martin, K.A.C. (2004) Neuronal circuits of the neocortex. *Annu. Rev. Neurosci.*, **27**, 419–451.
Engel, A.K., Kreiter, A.K., König, P. & Singer, W. (1991) Synchronization of oscillatory neuronal responses between striate and extrastriate visual cortical areas of the cat. *Proc. Natl. Acad. Sci. USA*, **88**, 6048–6052.
Engel, A.K., Fries, P. & Singer, W. (2001) Dynamic predictions: oscillations and synchrony in top-down processing. *Nat. Rev. Neurosci.*, **2**, 704–716.
Fries, P. (2005) A mechanism for cognitive dynamics: neuronal communication through neuronal coherence. *Trends Cogn. Sci.*, **9**, 474–480.
Fries, P., Nikolić, D. & Singer, W. (2007) The gamma cycle. *Trends Neurosci.*, **30**, 309–316.
Fujisawa, S., Amarasingham, A., Harrison, M.T. & Buzsáki, G. (2008) Behavior-dependent short-term assembly dynamics in the medial prefrontal cortex. *Nat. Neurosci.*, **11**, 823–833.
Gray, C.M. & McCormick, D.A. (1996) Chattering cells: superficial pyramidal neurons contributing to the generation of synchronous oscillations in the visual cortex. *Science*, **274**, 109–113.
Gray, C.M. & Singer, W. (1989) Stimulus-specific neuronal oscillations in orientation columns of cat visual cortex. *Proc. Natl. Acad. Sci. USA*, **865**, 1698–1702.
Guyonneau, R., Vanrullen, R. & Thorpe, S.J. (2004) Temporal codes and sparse representations: a key to understanding rapid processing in the visual system. *J. Physiology-Paris*, **98**, 487–497.
Harris, K.D. & Mrsic-Flogel, T.D. (2013) Cortical connectivity and sensory coding. *Nature*, **503**, 51–58.
Harris, K.D., Hirase, H., Leinekugel, X., Henze, D.A. & Buzsáki, G. (2001) Temporal interaction between single spikes and complex spike bursts in hippocampal pyramidal cells. *Neuron*, **32**, 141–149.
Jayakumar, J., Hu, D. & Vidyasagar, T.R. (2012) Sparseness of coding in area 17 of the cat visual cortex: a comparison between pinwheel centres and orientation domains. *Neuroscience*, **225**, 55–64.
Liao, D.S., Krahe, T.E., Prusky, G.T., Medina, A.E. & Ramoa, A.S. (2004) Recovery of cortical binocularity and orientation selectivity after the critical period for ocular dominance plasticity. *J. Neurophysiol.*, **92**, 2113–2121.
Miller, J.E., Ayzenshtat, I., Carrillo-Reid, L. & Yuste, R. (2014) Visual stimuli recruit intrinsically generated cortical ensembles. *Proc. Natl. Acad. Sci. USA*, **111**, E4053–E4061.
Milner, P.M. (1974) A model for visual shape recognition. *Psychol. Rev.*, **81**, 521–535.
Molotchnikoff, S. & Rouat, J. (2012) Brain at work: time, sparseness and superposition principles. *Front. Biosci.*, **17**, 583–606.
Niell, C.M. & Stryker, M.P. (2008) Highly selective receptive fields in mouse visual cortex. *J. Neurosci.*, **28**, 7520–7536.
Pereda, E., Quiroga, R.Q. & Bhattacharya, J. (2005) Nonlinear multivariate analysis of neurophysiological signals. *Prog. Neurobiol.*, **77**, 1–37.
Perkel, D.H., Gerstein, G.L. & Moore, G.P. (1967) Neuronal spike trains and stochastic point processes. I. The single spike train. *Biophys. J.*, **7**, 391–418.
Ramoa, A.S., Mower, A.F., Liao, D. & Jafri, S.I. (2001) Suppression of cortical receptor function prevents development of orientation selectivity in the primary visual cortex. *J. Neurosci.*, **21**, 4299–4309.
Ratté, S., Hong, S., De Schutter, E. & Prescott, S.A. (2013) Impact of neuronal properties on network coding: roles of spike initiation dynamics and robust synchrony transfer. *Neuron*, **78**, 758–772.
Ray, S. & Maunsell, J.H.R. (2014) Do gamma oscillations play a role in cerebral cortex? *Trends Cogn. Sci.*, **19**, 78–85.
Sakkalis, V., Doru Giurc Neanu, C., Xanthopoulos, P., Zervakis, M.E., Tsiaras, V., Yang, Y., Karakonstantaki, E. & Micheloyannis, S. (2009) Assessment of linear and nonlinear synchronization measures for analyzing EEG in a mild epileptic paradigm. *IEEE T. Inf. Technol. B.*, **13**, 433–441.
Salinas, E. & Sejnowski, T.J. (2001) Correlated neuronal activity and the flow of neural information. *Nat. Rev. Neurosci.*, **2**, 539–550.
Shu, Y., Hasenstaub, A. & McCormick, D.A. (2003) Turning on and off recurrent balanced cortical activity. *Nature*, **423**, 288–293.
Siegle, J.H., Pritchett, D.L. & Moore, C.I. (2014) Gamma-range synchronization of fast-spiking interneurons can enhance detection of tactile stimuli. *Nat. Neurosci.*, **17**, 1371–1379.
Singer, W. (1999) Neuronal synchrony: a versatile code for the definition of relations? *Neuron*, **24**, 49–65.
Singer, W. (2013) Cortical dynamics revisited. *Trends Cogn. Sci.*, **17**, 616–626.
Swindale, N.V. (1998) Orientation tuning curves: empirical description and estimation of parameters. *Biol. Cybern.*, **78**, 45–56.
Tiesinga, P.H. & Sejnowski, T.J. (2009) Cortical enlightenment: are attentional gamma oscillations driven by ING or PING? *Neuron*, **63**, 727–732.
Tiesinga, P.H., Fellous, J.M. & Sejnowski, T.J. (2008) Regulation of spike timing in visual cortical circuits. *Nat. Rev. Neurosci.*, **9**, 97–109.
Vinck, M., Womelsdorf, T., Buffalo, E.A., Desimone, R. & Fries, P. (2013) Attentional modulation of cell-class-specific gamma-band synchronization in awake monkey area v4. *Neuron*, **80**, 1077–1089.
Wang, X.J. & Buzsáki, G. (1996) Gamma oscillation by synaptic inhibition in a hippocampal interneuronal network model. *J. Neurosci.*, **16**, 6402–6413.
Womelsdorf, T., Fries, P., Mitra, P.P. & Desimone, R. (2006) Gamma-band synchronization in visual cortex predicts speed of change detection. *Nature*, **439**, 733–736.
Womelsdorf, T., Vinck, M., Oostenvelda, R., Singer, W., Neuenschwanderc, S. & Fries, P. (2012) Orientation selectivity and noise correlation in awake monkey area V1 are modulated by the gamma cycle. *Proc. Natl. Acad. Sci. USA*, **109**, 4302–4307.

CHAPTER 5. Network-selectivity and stimulus-discrimination in the primary visual cortex: cell-assembly dynamics

Vishal Bharmauria[a], Lyes Bachatene[a], Sarah Cattan[a], Simon Brodeur[b], Nayan Chanauria[a], Jean Rouat[a,b], Stéphane Molotchnikoff[a,b]

a Département de Sciences Biologiques, Université deMontréal, Montréal, QC, Canada
b Universite´ de Sherbrooke, Sherbrooke, QC, Canada

European Journal of Neuroscience (2016) ***43****: 204-219*

(Published article)

EJN European Journal of Neuroscience

FENS

European Journal of Neuroscience, Vol. 43, pp. 204–219, 2016 doi:10.1111/ejn.13101

NEUROSYSTEMS

Network-selectivity and stimulus-discrimination in the primary visual cortex: cell-assembly dynamics

Vishal Bharmauria,[1,2] Lyes Bachatene,[1,2] Sarah Cattan,[1,2] Simon Brodeur,[2,3] Nayan Chanauria,[1,2] Jean Rouat[1,2,3] and Stéphane Molotchnikoff[1,2,3]

[1]Neurophysiology of Visual System, Département de Sciences Biologiques, Université de Montréal, CP 6128 Succursale Centre-Ville, Montréal, QC, Canada H3C 3J7

[2]Neurosciences Computationnelles et Traitement Intelligent des Signaux (NECOTIS), Sherbrooke, QC, Canada

[3]Département de Génie Électrique et Génie Informatique, Université de Sherbrooke, Sherbrooke, QC, Canada

Keywords: assembly-dynamics, cat, functional connection, network-selectivity, primary visual cortex, stimulus-discrimination

Edited by László Acsády

Received 6 May 2015, revised 6 October 2015, accepted 10 October 2015

Abstract

Visual neurons coordinate their responses in relation to the stimulus; however, the complex interplay between a stimulus and the functional dynamics of an assembly still eludes neuroscientists. To this aim, we recorded cell assemblies from multi-electrodes in the primary visual cortex of anaesthetized cats in response to randomly presented sine-wave drifting gratings whose orientation tilted in 22.5° steps. Cross-correlograms revealed the functional connections at all the tested orientations. We show that a cell-assembly discriminates between orientations by recruiting a 'salient' functional network at every presented orientation, wherein the connections and their strengths (peak-probabilities in the cross-correlogram) change from one orientation to another. Within these assemblies, closely tuned neurons exhibited increased connectivity and connection-strengths compared with differently tuned neurons. Minimal connectivity between untuned neurons suggests the significance of neuronal selectivity in assemblies. This study reflects upon the dynamics of functional connectivity, and brings to the fore the importance of a 'signature' functional network in an assembly that is strictly related to a specific stimulus. It appears that an assembly is the major 'functional unit' of information processing in cortical circuits, rather than the individual neurons.

Introduction

'Connectomics', which refers to the mapping of neuronal circuits, is an emerging field in neurosciences, and it promises significant insights into the brain function and dynamics (Sporns *et al.*, 2005; Hagmann *et al.*, 2010; Sporns, 2011; Alivisatos *et al.*, 2012; Leergaard *et al.*, 2012). The developing consensus is that microcircuits (synonymous to sub-networks, cell-assemblies, co-active neurons, synfire chains, clicks, songs, ensembles) are fundamental to information processing in the brain (Buzsáki, 2010; Harris & Mrsic-Flogel, 2013); yet, knowledge about their functional dynamics in relation to the sensory environment remains sparse.

Many reports document that the mere co-activation of a neuronal group is not evidence of the functional interactions between them (Kenet *et al.*, 2003; Han *et al.*, 2008; Mohajerani *et al.*, 2013; Miller *et al.*, 2014). Neurons in primary visual cortex (V1) are exquisitely selective to a preferred edge of an orientation when it is presented within their receptive fields (Hubel & Wiesel, 1959; Bishop & Henry, 1972). In cats, V1 neurons are columned into homogeneous populations with similar response properties; yet, they exhibit abundant anatomical and functional connections with neurons in adjacent columns (DeAngelis *et al.*, 1999; Kisvárday *et al.*, 2000; Binzegger *et al.*, 2004; Stepanyants *et al.*, 2008; Martin & Schröder, 2013). Although V1 has been studied for decades, the functional interplay between an assembly and the applied orientation is still not completely understood. We thus sought to examine how an orientation-selective assembly in cat V1 (layer II/III, area 17) engineers functional connections between its neurons in response to different orientations.

In parallel with neuronal selectivity (Butts & Goldman, 2006), it has been shown that encoding sensory stimuli may be achieved by decoding sparsely firing neurons within assemblies that display time-relationships (functional synchrony) between their respective spike trains (König *et al.*, 1995; Csicsvari *et al.*, 1998; Barthó *et al.*, 2004; Fujisawa *et al.*, 2008; Bharmauria *et al.*, 2014; Schwindel *et al.*, 2014) within the rhythmic oscillations of the brain (Gray & Singer, 1989; Engel *et al.*, 2001; Fries *et al.*, 2007; Bharmauria *et al.*, 2015). Traditionally, cross-correlogram (CCG) analysis is an effective tool to reveal these functional causalities, which are indicative of putative synaptic contacts between neurons (Perkel *et al.*, 1967; König *et al.*,

Correspondence: Dr S. Molotchnikoff, [1]Neurophysiology of Visual System, as above.

1995; Csicsvari *et al.*, 1998; Shannon *et al.*, 2000; Barthó *et al.*, 2004; Fujisawa *et al.*, 2008; Vizuete *et al.*, 2012; Bharmauria *et al.*, 2014; Schwindel *et al.*, 2014).

Employing a CCG strategy, we report that a salient functional network is activated within a cell-assembly contingent upon the presented orientation, wherein connections are maintained, activated or inactivated with changing strengths as the orientation changes. Thus, along with our previous work (Bharmauria *et al.*, 2014, 2015), we suggest that an assembly is synergistically engaged within gamma oscillations in a characteristic 50-ms temporal 'window of opportunity' to frame a specific functional network in relation to the stimulus.

Here, we systematically presented orientated sine-wave gratings in 22.5° steps to examine the functional modulation (peak-modulation in CCG) in assemblies in relation to the applied axis of orientation, unlike previous reports (Kenet *et al.*, 2003; Ecker *et al.*, 2010; Talebi & Baker, 2012; Martin & Schröder, 2013; Miller *et al.*, 2014), wherein they compared two very dissimilar stimuli (e.g. gratings vs. natural images or gratings vs. no stimulus). As far as we know, this study is the first to show the dynamic formation of a unique functional network within an assembly in response to the systematic change of an input stimulus. In short, this work demonstrates that network-selectivity within an assembly is the underpinning of stimulus-discrimination in cortical circuits.

Materials and methods

Ethical approval

Nine adult cats (weight: 2.0 3.0 kg, ~ 12 24 months) of either sex were prepared for electrophysiological recordings in V1, as per the guidelines of Canadian Council on Animal Care. The protocol was approved by the Institutional Animal Care and Use committee of Université de Montréal. A full description of the procedure is given below.

Animal, anaesthesia and surgical procedures

Briefly, cats were premedicated with acepromazine maleate (Atravet; Wyeth-Ayerst, Guelph, ON, Canada; 1 mg/kg, i.m.) and atropine sulphate (ATRO-SA; Rafter, Calgary, AB, Canada; 0.04 mg/kg, i.m.), and anaesthetized with ketamine hydrochloride (Rogarsetic, Pfizer, Kirkland, QC, Canada; 25 mg/kg, i.m.). Lidocaine hydrochloride (2% Xylocaine; AstraZeneca, Mississauga, ON, Canada) was administered subcutaneously for local anaesthesia at the surgical site. For artificial ventilation, a tracheotomy was performed and during the surgery the cats were sustained using 2% isoflurane (AErrane; Baxter, Toronto, ON, Canada) ventilation. Xylocaine gel (5%; Astra Pharma, Mississauga, ON, Canada) was applied at the pressure points. Tribrissen (30 mg/kg/day, s.c.; Schering-Plough, Point-Claire, QC, Canada) and Duplocillin (0.1 mL/kg, i.m.; Intervet, Whitby, ON, Canada) were administered to prevent infection. After the surgery, the cats were fixed in a stereotaxic apparatus. Neuromuscular blockade was induced with 40 mg gallamine triethiodide and maintained with 10 mg/kg/h gallamine triethiodide (Flaxedil; Sigma Chemical, St. Louis, MO, USA; i.v.) administered in 5% dextrose lactated Ringer's nutritive solution. General anaesthesia was maintained by artificial ventilation with a mixture of N_2O/O_2 (70:30) supplemented with 0.5% isoflurane. Electroencephalogram, electrocardiogram, rectal temperature (using a heated pad to maintain a body temperature of 37.5 °C) and end-tidal CO_2 partial pressure (25 30 mmHg) were monitored throughout the experiment, and kept within physiological ranges. The pupils were dilated with atropine sulfate (1%, Isopto-Atropine; Alcon, Mississauga, ON, Canada) and the nictitating membranes were retracted with phenylephrine hydrochloride (2.5%, Mydfrin; Alcon). The loci of the area centrales were inferred from the position of the blind spots, which were opthalmoscopically focused and projected onto a translucent screen. Plano lenses with artificial pupils (5 mm in diameter) were fixed on the cat's eyes to prevent the cornea from drying and to improve the acuity. At the end of the experiment, the cats were killed with a dose (0.5 mL/kg, i.v.) of sodium pentobarbital (CEVA, Sante Animale).

Visual stimulation, electrophysiological recording and single-unit selection

Monocular stimulation was done. A schematic of the experimental setup is shown in Fig. 1. The multi-unit receptive fields (RFs) were mapped as the minimum response field (Barlow *et al.*, 1967) by using a hand-held ophthalmoscope after clearly detectable activity was obtained. These preliminary tests revealed qualitative properties such as dimensions, velocity preference, orientation and directional selectivity of neurons. Thereafter, the visual stimuli were generated with a VSG 2/5 graphic board (Cambridge Research Systems, Rochester, UK) and displayed on a 21-inch monitor (Sony GDM-F520 Trinitron, Tokyo, Japan) placed 57 cm from the cat's eyes, with 1024 × 768 pixels, running at 100-Hz frame refresh. The blank screen was uniformly grey (~ 35 cd/m^2). Contrast and mean luminance were set at 80% and 40 cd/m^2, respectively. Optimal spatial and temporal frequencies were set at 0.24 cycles/deg and in the range 1.0 2.0 Hz, respectively, where V1 neurons are driven maximally by sine-wave drifting gratings (Bardy *et al.*, 2006). The tested orientations were presented in a random order. Each drifting grating was presented in blocks of 25 trials (each trial lasted 4.1 s) with varying inter-stimulus (1 3 s) intervals during which no stimulus was presented (Fig. 1A). Thus, the presentation of a stimulus lasted 180 s (with all trials and inter-stimulus intervals).

Multi-unit activity in V1 (layer II/III, area 17) was recorded using a tungsten multi-electrode (Matrix Electrode; Frederick Haer & Co., Bowdoin, ME, USA) that had four columns (inter-column distance 410 μm) and each column had one row. For each recording, only two contacts were used as shown in Fig. 1B (spaced by 410 or 820 μm). The excitatory RFs (sine-wave drifting grating covering the excitatory RF of neurons at both electrodes) extended from 4° to 5°. The average overlap for the excitatory RF was 81 ± 11%. The RFs were located centrally within a 15° radius from fovea. Twenty-four recordings were done across all cats in the supragranular layers (cortical depth < 1000 μm; mean = 650 μm), either in the left or in the right hemisphere. Twenty-two recordings were tested once; two recordings were tested twice, i.e. the same stimulus was tested after ~ 1 h. The signal from the microelectrodes was amplified, band-pass filtered (300 Hz to 3 kHz), digitized and recorded with a 0.05-ms temporal resolution (Spike2, CED, Cambridge, UK). Spike sorting from the multi-unit activity was performed, and each microelectrode yielded isolated single units (Fig. 1C). The units were discriminated on the basis of three criteria: (1) the spike-waveform difference, (2) principal component analysis (PCA) showing well-dissociated clusters and (3) auto-correlograms (ACGs) with a characteristic refractory period (no events at zero) indicating the absence of contamination (Csicsvari *et al.*, 1998; Barthó *et al.*, 2004; Fujisawa *et al.*, 2008; Bharmauria *et al.*, 2014; Denman & Contreras, 2014). The stability of each cell's activity across conditions was verified qualitatively by visual control of the disposition of clusters and the shapes of waveforms. Cluster-analysis was done using Spike2 software in a three-dimensional plot. The isolation distance was

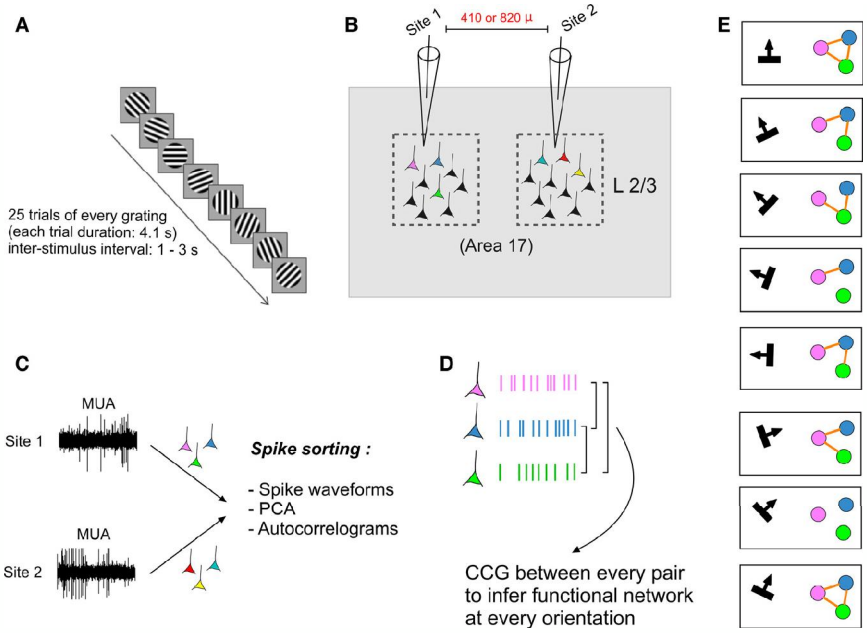

FIG. 1. Schematic of the experiment. (A) Randomly presented sine-wave drifting gratings. (B) Multi-electrode recordings in layer II/III (area 17). (C) Spike sorting from the multi-unit activity using spike waveforms, auto-correlograms and principal component analysis (PCA). (D) Cross-correlation between neural activities of isolated neurons to reveal the functional connections. (E) A hypothetical assembly displaying network-selectivity at each orientation.

calculated as the Mahalanobis distance. The Mahalanobis distance is the distance from the cluster centre within which as many events belong to the other clusters as belong to the specified cluster (Harris *et al.*, 2001). In other words, given the multivariate data values for which the values in each variable are normally distributed around a mean, this measure allows us to define boundaries of constant probability around the multi-dimensional centre of the distribution. Thus, this estimation allows the separation of a cluster from the nearest cluster. Units with Mahalanobis distance > 2.5 were considered for further analysis of the spike trains to reveal the functional connections between them. Once the clusters were computed using Mahalanobis distances, J3 values for neuron pairs were calculated indicating the distance separating the clusters:

$$J3 = J2/J1, \tag{1}$$

where J2 equals the sum of the squared distances of all the clustered points from the centroid of all the points, and J1 equals the sum of the squared distances of each point from the centroid of the cluster to which it belongs. A J3 value of 1.5 was set as the benchmark for the separation (Bharmauria *et al.*, 2015).

Orientation tuning and orientation selectivity index (OSI) computation

Once single cells had been sorted out offline from multi-unit spike trains accumulated during data acquisition, orientation tuning curves of cells were obtained from the raw data and fitted with the von Mises function (Swindale, 1998).

$$M(\Theta) = A.e^{b(\cos(\Theta - c))} + d, \tag{2}$$

where A is the value of the function at the preferred orientation c, and b is the width parameter. An additional parameter, d, represents the spontaneous firing rate of the cell. $M(\theta)$ is the firing rate of the neuron at orientation θ. This allowed us to determine the preferred orientation of every cell. An OSI was calculated to ensure the tuning of neurons. It was measured using the fitted tuning curves by dividing the firing rate at baseline (orthogonal orientations) by the firing rate at the preferred orientation, and subtracting the result from 1 (Ramoa *et al.*, 2001; Liao *et al.*, 2004; Bachatene *et al.*, 2013). The closer the OSI is to 1, the stronger the orientation selectivity. Note that within the context of this paper, we have considered neurons with OSI < 0.5 as untuned.

CCGs and network-formation

A CCG is a histogram of the spikes of the target neuron in relation to the spikes of the reference neuron (spike-by-spike analysis). CCGs were computed (binwidth = 1 ms) between the neural activities of all the possible neuron pairs at all the applied orientations to reveal the functional connections (Fig. 1D). The raw CCGs were shift-corrected to eliminate the putative significant peaks resulting from simultaneous stimulation of both cells during each trial (to remove the stimulus-evoked and locked components) (Perkel *et al.*, 1967). A significant peak of 2 ms (two adjacent bins) or at least one significant bin (Alloway & Roy, 2002) was searched within a window of ± 5 ms offset from zero (excluding the ± 1-ms bins around zero) in the shift-corrected CCG to reveal a functional connection between two neurons. The statistical threshold for the significant peak was set at 95%, and the probability of the neuron firing in a bin is calculated as follows (Abeles, 1982):

Considering the spike train is a Poisson process, the probability (p) of a neuron firing in the small bin of the size b is:

$$p = F * b, \tag{3}$$

$$F = N/T, \tag{4}$$

where F is the neuronal firing rate, T is the total time interval and N is the number of spikes in that interval.

The expected bin count C for the histogram is:

$$C = p * N_{\mathrm{Ref}}, \tag{5}$$

where N_{Ref} is the number of the reference events (spikes of the reference neuron, that is, at time zero in the CCG). We calculated 95% intervals for p and C according to Abeles (1982).

A hypothetical network between three neurons (isolated from a microelectrode) at every orientation is displayed in Fig. 1E. For every CCG, the cumulative distribution of spikes was computed. This computation further indicates the modulation of the firing rate of the target cell after the reference cell fired an action potential. The cumulative sum (*cs*) graphs above histograms are calculated for each bin i as:

$$cs[i] = \sum_{j=1}^{i} bc[j] - A^{i}; \qquad i = 1, 2, \ldots, N, \tag{6}$$

where *bc* is the bin counts (i.e. the number of spikes falling inside the histogram bin *j*) and *A* the average of all *bc*.

Discrimination index (DI) calculation

The DI for a cell-assembly was calculated as:

$$\mathrm{DI} = N^{s}/N^{t}, \tag{7}$$

where N^{s} is the number of significant connections found at an orientation, and N^{t} is the total number of possible connections if all the neurons in the group were to establish functional connections at that orientation.

Results

The main aim of our current investigation was to examine the functional relationships between neurons in a cell-assembly (within the context of this paper, neurons simultaneously recorded from a microelectrode are termed a cell-assembly) with orientation as the target property. We recorded data in 44 sites (tested once) in the primary visual cortex (area 17, layer II/III) of anaesthetized cats using a tungsten multi-electrode. Neurons were discriminated based on spike waveforms, ACGs and cluster analysis (see Materials and methods). In total, 174 neurons were identified as clean and a further 79 neurons were discarded (if they did not fit any of the above criteria for isolation). The meta-analysis for OSI of all neurons is shown in Fig. 2. The mean OSI was 0.74. Functional connections were disclosed within a quasi-synchrony time-window in CCGs, i.e. ± 5 ms around zero (see above).

Functional network between the closely tuned neurons

Neurons in the cat visual cortex are organized into orientation columns, and thus it is expected that neurons belonging to a column respond in unison, putatively implying the existence of specific connections between them (Shadlen & Newsome, 1998; Stepanyants *et al.*, 2008). Figure 3A shows five well-isolated single units (distinct waveforms with respective responses and orientation tuning curves computed from the firing levels at each orientation) from the tip of a tungsten multi-electrode. The individuality of neurons was further assured by their respective ACGs (Fig. 3B), PCA denoting the clear separation of clusters (Fig. 3C, waveforms superimposed as an inset) and J3 value for each pair (Fig. 3D), which represents the isolation distance between every cluster pair.

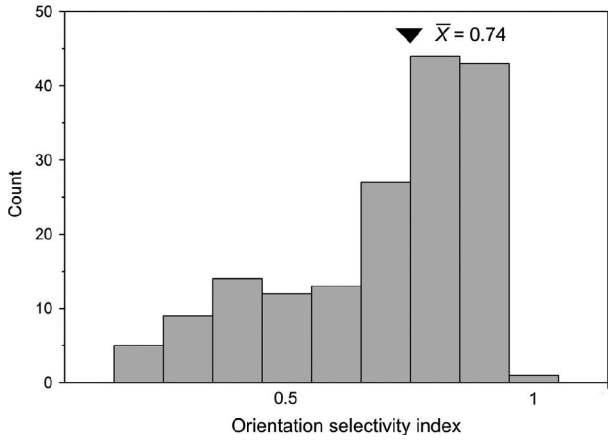

FIG. 2. Distribution of the orientation selectivity index (OSI) for all neurons.

Thereafter, the corresponding activities of all the pairs (10 for the above assembly) were cross-correlated to reveal the functional connections between them. Figure 3E shows the functional network between these neurons (similarly tuned, ~ 45°, see polar plots inside units) when an orientated sine-wave drifting grating of 22.5° was presented within their receptive field. Orange arrows depict the functional connections as revealed by CCGs (Fig. 3F) and are indicative of time-locked activity between the neurons. Because neurons physically close together are densely innervated to each other (Gilbert & Wiesel, 1989; Binzegger *et al.*, 2004; Stepanyants *et al.*, 2008; Kampa *et al.*, 2011), these time-relationships may be inferred as putative synaptic links between neurons (Barthó *et al.*, 2004; Fujisawa *et al.*, 2008; Bharmauria *et al.*, 2014; Schwindel *et al.*, 2014). Neuron 2 (reference) projects onto neuron 1 (target), as the CCG significantly peaks (p = 2.5%) within 5 ms after the zero mark. The cumulative histogram (above CCG) of the discharge rate of the target cell further illustrates that once the reference neuron produced a spike, the firing rate of the target unit was considerably modulated, thus signifying the functional link between neurons. Neurons 1 (reference) and 4 (target) are reciprocally connected to each other, implying the recurrent excitation between them (Schwindel *et al.*, 2014). First, the target neuron excites the reference neuron with a probability of 2% and then after a brief period of inhibition from third neuron(s) (the trough at zero in the CCG) the reference neuron back-projects and excites the target neuron with a probability of 1.7%. Neuron 4 receives two connections, indicating convergent input from several neurons in the microcircuit. Similarly, other connections were revealed, and consequently the whole network was disclosed at the applied orientation within an assembly.

Analogically, this seems to parallel to what Singer has opined in his review (Singer, 2013) – if we consider the recorded co-active neurons (assembly) as a reservoir with randomly coupled neurons, then the network framed within the reservoir could be compared to a classifier (network) that is stimulus-specific and emerges within this recurrent network. Notably, most of the peaks in CCGs were broad (beyond 2 ms) and were probably caused by the shared input to the target neuron, because many orientations are represented on the dendritic branches of a neuron. However, the synaptic drive related to the applied orientation dominates over others (Jia *et al.*, 2010; Bachatene *et al.*, 2013; Wertz *et al.*, 2015), and, moreover, it has been shown that the transient surge of the target neuron

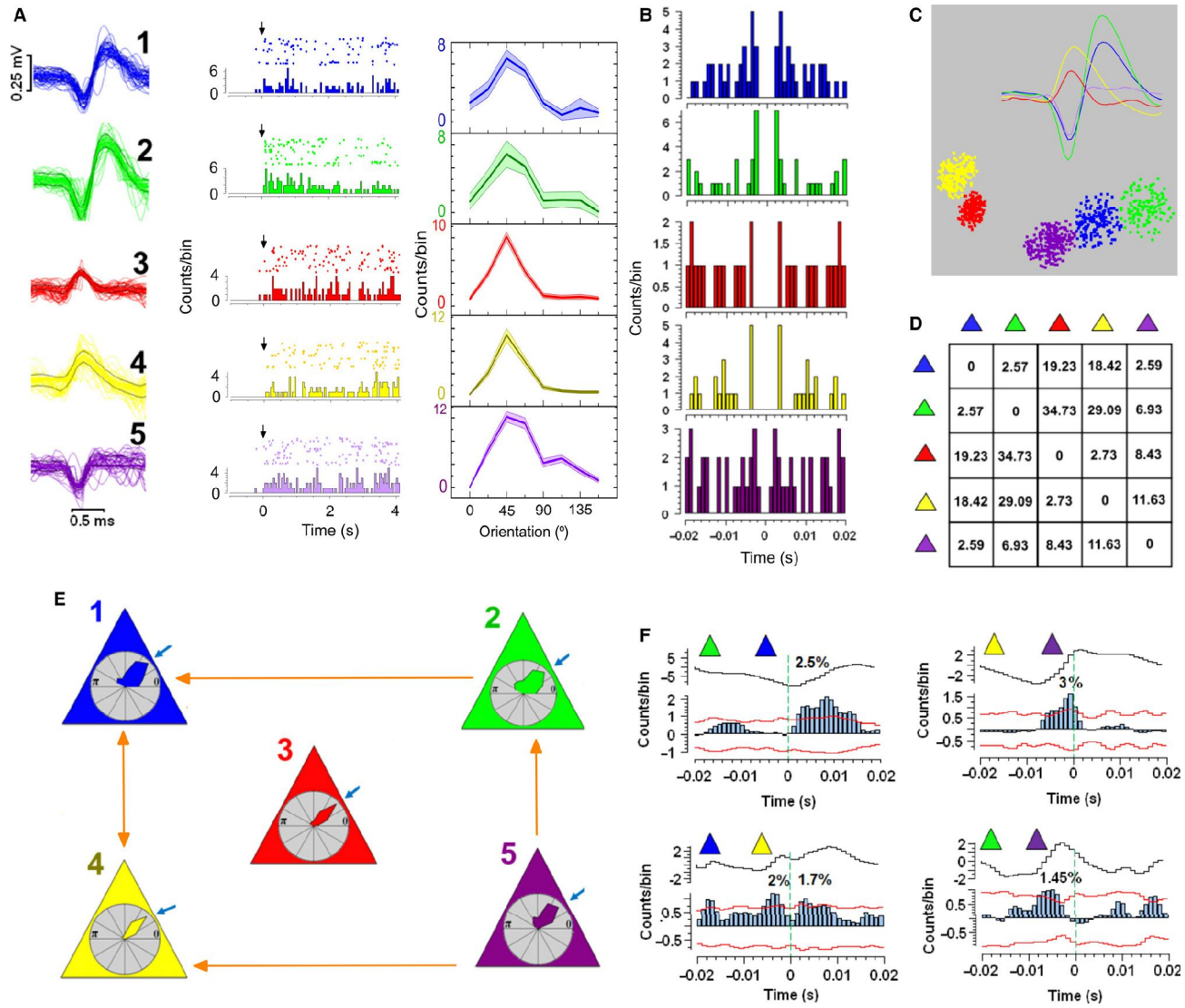

FIG. 3. Functional network between tightly tuned neurons. (A) Spike-waveforms of neurons isolated (labelled 1–5) recorded from a microelectrode. The respective visual responses (downward black arrow indicates the stimulus presentation) and tuning curves (shaded area represents the standard error of the mean, SEM; *x*-axis, orientation gratings; *y*-axis, firing level in counts per bin) are shown adjacent to each waveform. The colour scheme is respected throughout the figure. (B) Auto-correlograms of all the isolated units. (C) Principal component analysis indicates a distinct cluster for every neuron. Waveforms are superimposed as an insert. (D) The tabular matrix shows the J3 values between all pairs. (E) Functional network between neurons (all neurons are tuned to ~ 45°; blue arrow indicates the precise tuning of the neuron). The orange arrow depicts the direction of the projection from one neuron to another as revealed by the cross-correlogram (CCG). (F) Shift-corrected CCGs to show the functional connections between neurons. The number above the significant peak (red curved line indicates the significance level) in the CCG represents the probability (p) of the target neuron discharge. The significant peak suggests a functional link between neurons. The curve above the CCG depicts the cumulative sum histogram of the discharge of the target neuron. The left triangle above each CCG indicates the reference neuron in the pair and dotted green line marks the zero mark.

discharge is predominantly caused by the reference neuron (Bharmauria *et al.*, 2014).

Functional network between the differently tuned neurons

Neurons in an orientation column exhibit anatomical and functional connections with neurons from adjacent columns (Kisvárday *et al.*, 2000; Binzegger *et al.*, 2004; Stepanyants *et al.*, 2008); therefore, neurons recorded within a cortical subspace from an electrode might exhibit different orientation selectivity from each other. Figure 4A illustrates four simultaneously recorded neurons (differently tuned – neurons 2 and 3 are tuned similarly to ~ 67.5°; whereas neurons 1 and 4 are more responsive at 0° and 90°, respectively) with distinctive waveforms, the respective visual responses and orientation tuning curves calculated from the firing at each orientation. Figure 4B represents the cluster-separation of the dissociated spikes that are overlaid as an inset. The network between these neurons (in response to 45°) is shown in Fig. 4C. Figure 4D illustrates the CCGs for all the functionally connected pairs. In addition to the functional link between similarly tuned neurons (neuron 3 projects onto neuron 2, p = 3.3%), neurons 3 and 1, which display dissimilar tunings, are reciprocally connected to each other (neuron 1 projects onto neuron

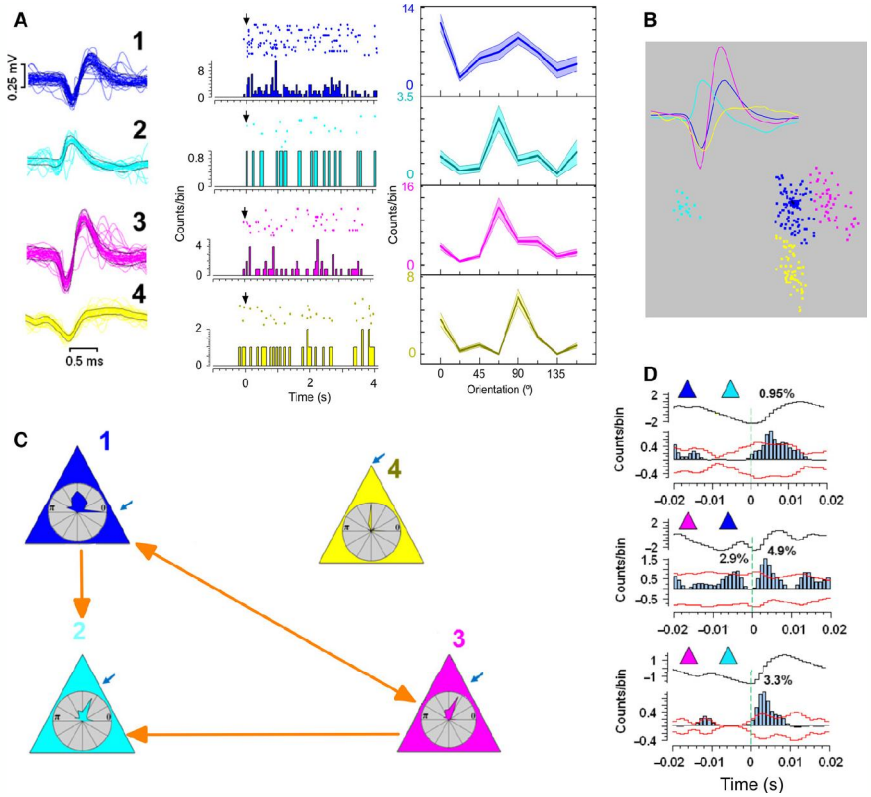

FIG. 4. Functional network in a high orientation-range assembly. (A) Waveforms of single-tip recorded neurons with corresponding visual responses and tuning curves. Same convention as in Fig. 3. (B) PCA for the isolated neurons. (C) The functional network between neurons. (D) Significant shift-corrected CCGs to reveal the functional connections. Neuron 1 with different orientation preference (~ 0°) connects to neuron 2 and neuron 3 (~ 67.5°), which exhibit different tunings. Neuron 4 (~ 90°) remains unconnected in the circuit.

3, p = 2.9%; neuron 3 back-projects onto neuron 1; p = 4.9%). The blue neuron (tuned at 0°) projects onto the cyan neuron (tuned at 67.5°) with a probability of 0.95%. Neuron 4, which is tuned to 90°, did not exhibit any connection. In summary, this shows that an assembly of differently orientation-selective neurons may feature a stimulus-encoding network between them.

Network-selectivity and assembly dynamics

As mentioned above, many reports have shown that a group of co-active neurons constitute a cell-assembly; however, how these neurons functionally connect with each other in response to different stimuli has not yet been fully explored. To this end, we systematically wired networks between co-active neurons (the assembly in Fig. 3) at every presented orientation and spontaneous activity (Fig. 5A). A unique network was activated at every presented orientation. A maximum of five connections were disclosed at 22.5°, and in relation to that, only three connections were revealed at the optimal orientation (45°, which elicited highest firing rates) – two connections were maintained (purple to yellow and purple to green); the connection between the blue–yellow pair changed to unidirectional from bidirectional; and the connection between the blue–green pair was deactivated. The orange connections were mostly maintained in spite of the change in orientation (e.g. yellow–purple pair), whereas the green links were activated only at some orientations. The connection from the blue to the yellow neuron was reversed at 135°. No connection was observed at 0° and spontaneous firing (last box).

Furthermore, the connections were characterized by a change in their probabilities (p) from one orientation to another as depicted in the connectivity matrices (Fig. 5B), for example the connection between the purple–yellow pair (p = 3% at 22.5°, p = 1.65% at 45° and p = 0.7% at 90°). This suggests changing synaptic weights between neurons (Alloway & Roy, 2002), and also shows the network-dynamics of the assembly as the orientation changes. A typical example of a CCG peak-modulation with orientation for a neuron pair (blue–yellow, blue is reference) is shown in Fig. 5C. In most cases (45°, 67.5°, 90° and 157.5°), the peak was maintained but the probability changed (p = 2.3, 0.7, 1.6 and 2%, respectively). At 22.5°, the pair exhibited a bidirectional connection (blue to yellow, p = 1.7%; yellow to blue, p = 2%). The position of the peak is reversed at 135° with p = 0.95%. At 0° and 112.5°, no peak was observed. Irrespective of the fact that firing rates of the neurons changed from one orientation to another (see counts/bin on the y-axis), significant CCGs emerged, but with changing strengths.

Taken together, we conclude that the activation of a specific functional network between co-active neurons (cell-assembly) is 'inevitable' for feature encoding as suggested by Miller *et al.* (2014) (intrinsically generated and visually evoked ensembles are similar in activation pattern of neurons with one major difference – that visually evoked stimuli are 'time-locked' to stimuli whereas the spontaneous ensembles repeat randomly). In short, this analysis shows the dynamics of functional connectivity and network-selectivity within an assembly in response to different orientations.

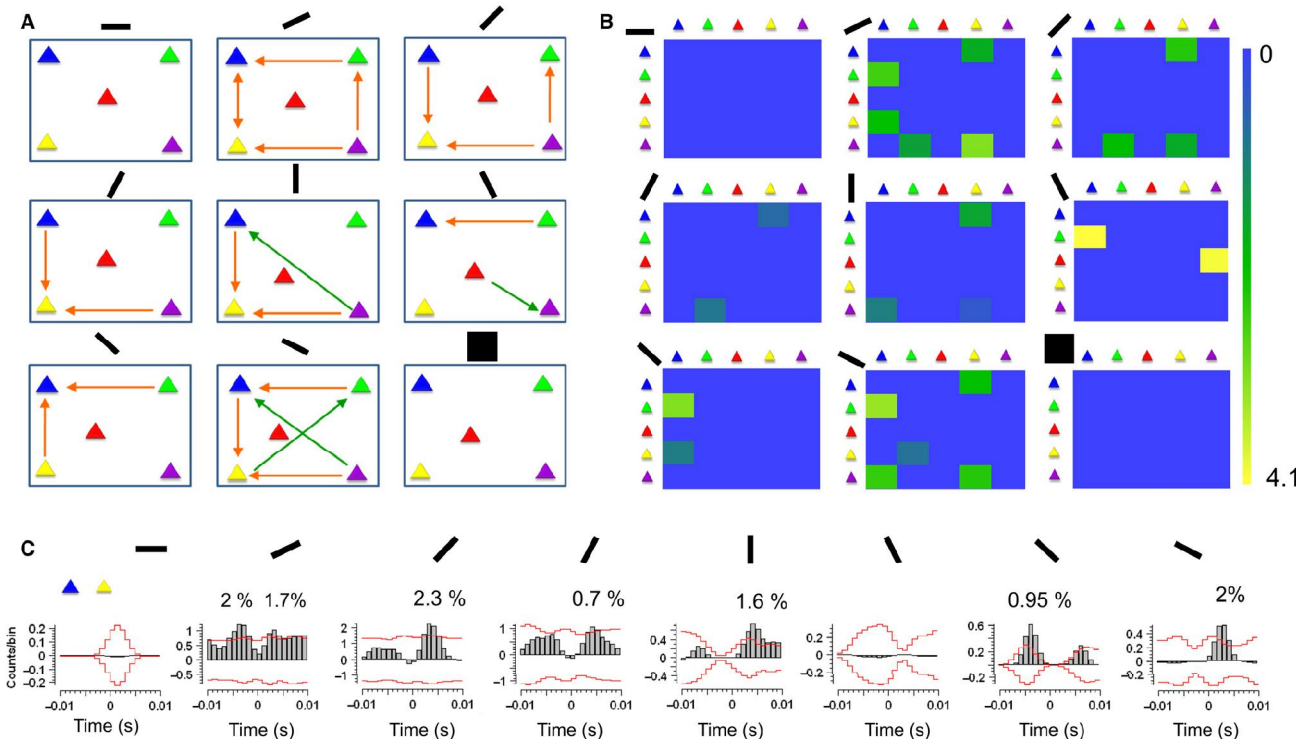

FIG. 5. Link-dynamics of the assembly. (A) Functional network in an assembly (in Fig. 3) at every presented orientated grating (bar above each box represents the angle). The solid triangle depicts a neuron. The orange arrows correspond to the unchanged connections, while the green arrows represent the new functional connections in relation to 22.5°. (B) Connectivity strength (peak-probability in CCG) matrices at all the tested gratings. The square in the matrix represents the strength of the connection; see coloured scale to the right. The neurons along the *y*-axis project on to neurons on the *x*-axis. (C) A typical example of a neuron pair showing the peak-modulation in the CCG from one orientation to another.

Peak-probability is independent of the firing rates of neurons

We then investigated if the peak-probability was related to the firing rate of the neurons involved in a connection (Fig. 6). Figure 6A illustrates this relationship for the connections (n = 22) in an assembly (in Fig. 5). The horizontal regression line (P = 0.58; R^2 = 0.02) indicates that p is independent of the cumulative firing (total number of spikes collected over 25 trials between a pair) of a neuron pair. Even globally, when neuron pairs (n = 101) across different assemblies were pooled randomly, no relationship (p = 0.71; R^2 = 0.001) was observed between p and the cumulative firing of neurons, which is in line with previous reports suggesting that these changes in peak-probability are independent of the firing rate of neurons (Duret *et al.*, 2006; Ghisovan *et al.*, 2008; Rolls & Treves, 2011). Because weakly firing neurons also exhibited connections, this implies that these neurons also have an important role in encoding stimuli.

Additionally (Fig. 6C), we randomly pooled unconnected pairs (n = 71) to compare their evoked cumulative firing with the connected pairs (n = 101). The mean (with SEM) cumulative firings for the connected and unconnected pairs were 9.61 ± 0.65 and 9.90 ± 1.63, respectively, and were non-significantly different, i.e. almost equivalent (unpaired t-test, P = 0.71). However, the firing of the same unconnected pairs was significantly different (unpaired t-test, p = 0.002) at the evoked (see above) and spontaneous (4.78 ± 0.57) conditions (i.e. when the responses of the same neurons were elicited with a stimulus exhibiting higher cumulative firings, yet displaying no connections). The connected and spontaneous classes were significantly different from each other too (unpaired t-test, p < 0.0001). Collectively, this latter analysis further suggests that irrespective of the fact that connected and unconnected pairs exhibited similar firing patterns, the specific interactions between connected neurons yield the precise temporal relationships between their activities. The functional connection is thus established in relation to the applied stimulus.

DI and orientation range

We then investigated whether the probability of finding connections is related to the orientation range of neurons in an assembly. To this aim, a DI was calculated for all assemblies (numbered on the x-axis) at every tested orientation (Fig. 7). A neuron is depicted as a solid circle (pink for tuned and black for untuned) with its preferred orientation (y-axis). The orientation range of an assembly is underlined by a black vertical line (for presentation purposes, the smaller ranges are positioned to the left of the figure). In line with previous studies (Shadlen & Newsome, 1998; Ko *et al.*, 2011, 2013; Cossell *et al.*, 2015; Wertz *et al.*, 2015), neurons in smaller ranges (assemblies 1 6) are frequently connected (even at different orientations), thus exhibiting higher DI (up to 1, see the DI colour scale, the DI values increase from blue to red) values. Assemblies 7 and 8 neurons display tight tuning but remain unconnected, suggesting that the selection of a functional network transcends their mere co-activation (Miller *et al.*, 2014). As the range increased, there was a tendency for neurons to remain unconnected (low DI); however, assemblies (e.g. 21, 26, 37) with larger orientation ranges (~ 75 150°) also exhibited abundant functional connections (high DI). The higher the DI at a specific orientation, the least selective the assembly is for that stimulus property (e.g. assembly 3 neurons that are

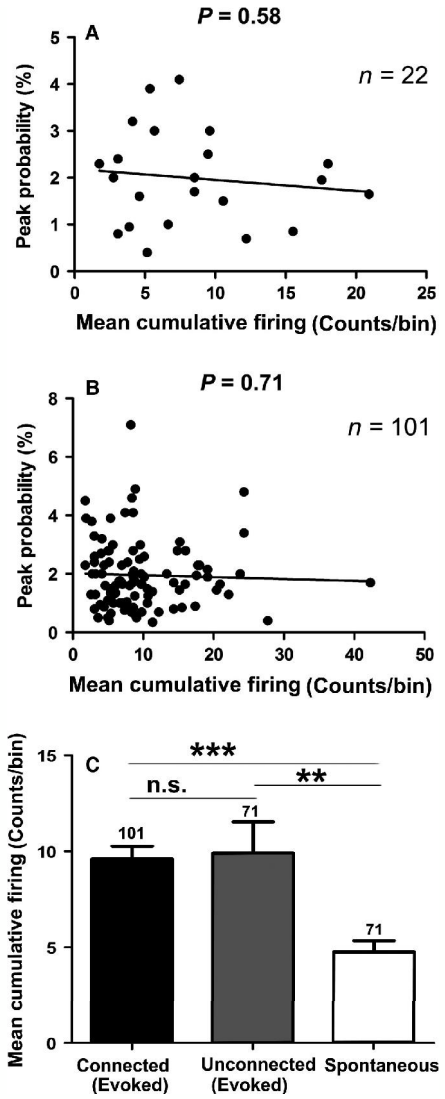

FIG. 6. Cumulative firing of connected neurons and peak-probability. (A) No relationship was found between the peak-probability and the summed firing ($P = 0.58$) in a cell-assembly (Fig. 3). (B) Globally, no relationship was inferred between the cumulative firing and peak-probability ($P = 0.71$). (C) Comparison of cumulative firing between connected (evoked), unconnected (evoked) and the evoked unconnected pairs at spontaneous activity. The connected (evoked) and unconnected (evoked) classes were insignificantly different (unpaired *t*-test, $P = 0.71$). The unconnected (evoked) and spontaneous classes were significantly different (unpaired *t*-test, $P = 0.002$). Also, the connected (evoked) and spontaneous classes were significantly different (unpaired *t*-test, $P < 0.0001$). The number at the top of the bar is the number of pairs analysed in that class. Asterisks (*) indicate the significance value (see text for details).

closely tuned have higher DI at all the orientations, and are therefore less selective and frequently connect to form a network); whereas, the lower the DI, the more selective the network. Finally, untuned neurons did not exhibit many connections (e.g. assembly 44 neurons with OSI < 0.5), suggesting that connectivity is largely dependent on orientation selectivity. Conclusively, this analysis shows that even though neurons in small-range assemblies (as if biased toward a particular orientation) connect more frequently to each other, importantly, high-range assemblies do exhibit connectivity too. Note that newly active cells (six in number) which are not shown in the figure were also considered for calculating the DI at that specific orientation. Please see Fig. 8 for analysis on a cell pair basis.

Global distribution of connections within assemblies

In total, 399 connections were found across all assemblies – 378 (236 unidirectional and 71 bidirectional, Fig. 8A) at all orientations (stimulus-locked) and 21 at spontaneous firing. Note that a bidirectional connection consisted of two connections. The proportions of stimulus-locked (0.19) and spontaneously active (0.08) connections are significantly different (*z*-test, $P < 0.00001$) from each other (Fig. 8B), implying that the disclosed connections are strongly linked to stimuli.

Indeed, the DI computation (Fig. 7) hinted at the general distribution of connections, but to further investigate whether connections were linked to the orientation spread of involved neurons, we computed the absolute number of connections in assemblies as a function of their orientation spread (Fig. 8C, the untuned (UT) group was eliminated from this analysis). We found that no such relationship (ANOVA, $p = 0.49$) exists, suggesting that all assemblies tend to exhibit numerous connections. Because an orientation spread comprises neurons with different tunings, one may assume that closely tuned neurons in an assembly might exhibit more connectivity between them. Thus, further analysis was targeted to infer connectivity on a neuron pair basis as a function of the orientation spread. The linear regression (Fig. 8D) showed a declining trend ($R^2 = 0.96$, $p = 0.12$) for the proportion of connections (mean: 0.25 at ± 22°, 0.19 at ± 44°, 0.16 at ± 66°) as the spread increased until ± 66° (although the analysis was performed for ± 88° this spread was excluded from statistical tests for this and all subsequent analysis, as neurons involved in the pair were tuned to opposite directions). The proportion increased to 0.27 at ± 88°. Interestingly, in a similar way, the peak-probabilities (*p*) also declined (mean ± SEM: 2.65 ± 0.17% at ± 22°; 2.02 ± 0.17% at ± 44° and 1.99 ± 0.23% at ± 66°) ($R^2 = 0.78$, $p = 0.30$) as a function of the orientation spread (Fig. 8E). The strength increased to 2.65 ± 0.42% at ± 88°. Furthermore, the proportion (0.23) of connected tuned pairs (T–T) was found to be significantly higher (*z*-test, $P < 0.00001$) than the proportion (0.025) of connections where an untuned (UT) neuron was involved in a connection with any other neuron (UT or T). In short, the above analyses point to the fact that neuronal selectivity is fundamental to functional connectivity, and closely tuned neurons connect more vigorously with each other than distantly tuned neurons in V1 microcircuits as reported previously (Stepanyants *et al.*, 2008; Ko *et al.*, 2011, 2013; Cossell *et al.*, 2015). However, the high connectivity and increased strength of connections at ± 88° could be attributed to specific connectivity pattern between neurons, as they have to process the contrasting features in the image.

Thereafter, we analysed the proportion of bidirectional and unidirectional connections in relation to the orientation spread (Fig. 8G). The unidirectional connections decreased from 0.15 to 0.14 to 0.12 at ± 22° to ± 44° to ± 66°, respectively, whereas the corresponding proportions for bidirectional connections were 0.09, 0.04 and 0.04. The ratio of bidirectional connections was significantly different between ± 22° and ± 44° (*z*-test, $P = 0.002$), and between ± 22° and ± 66° (*z*-test, $P = 0.012$), but it was insignificant between ± 44° and ± 66° (*z*-test, $P = 0.48$). The corresponding analyses for unidirectional connections between all the classes did not exhibit significant differences between them (*z*-test, $P > 0.05$).

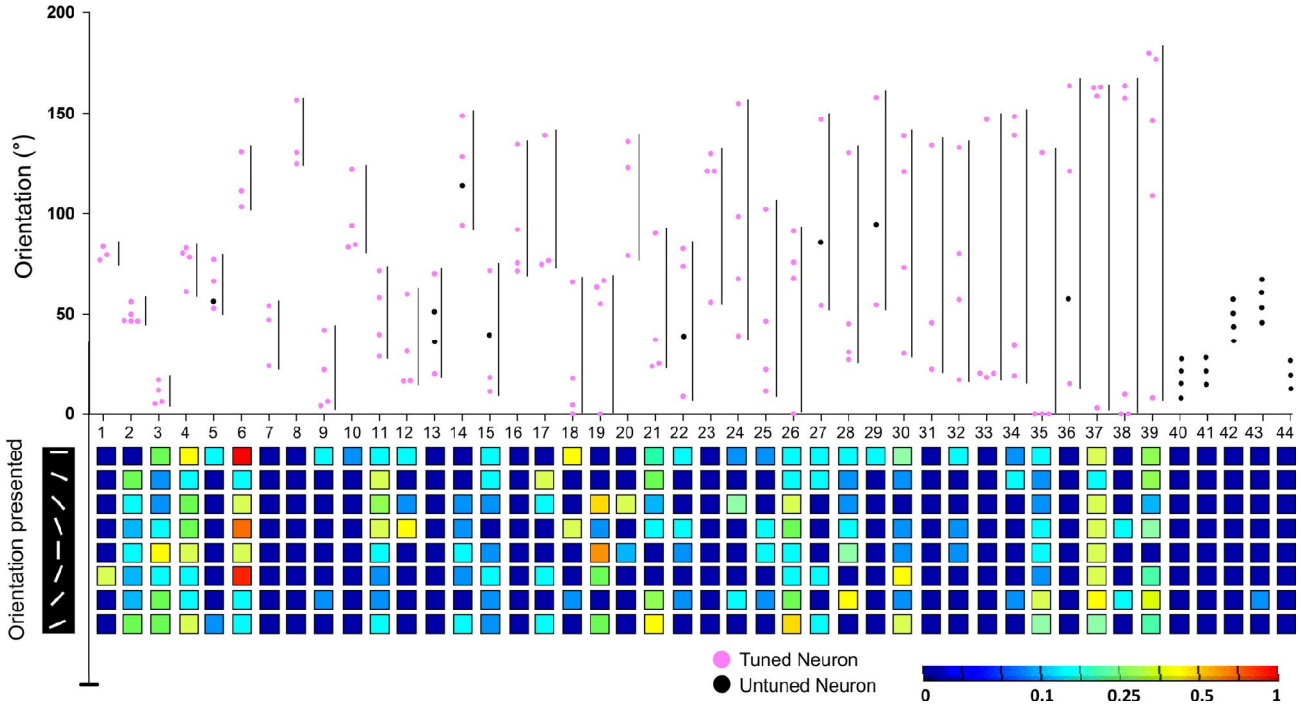

FIG. 7. Orientation spread and discrimination index (DI). Top: Assemblies (numbered on the *x*-axis) aligned according to the orientation scatter (black vertical line). Low-range assemblies are arranged to the left. Bottom: DI of the corresponding assembly at every orientation (*y*-axis). Solid circles represent neurons. Note: the newly active cells (not shown) and untuned cells have been included to calculate the DI. The color scale represents the DI values and increases from blue to red.

The ± 88° had a proportion of 0.12 and 0.14 unidirectional and bidirectional connections, respectively. Finally (Fig. 8H), the strength of the bidirectional connections (mean ± SEM: 3.04 ± 0.25%) was significantly (unpaired *t*-test, $P = 0.0007$) higher than the unidirectional connections (2.16 ± 0.12%). In brief, the bidirectional connections indicate strong recurrent excitation between neuronal circuits, suggesting that recurrent excitation between neurons in an assembly plays a pivotal role in feature encoding, as has been reported in the literature (Bopp *et al.*, 2014; Schwindel *et al.*, 2014; Cossell *et al.*, 2015). Note that the calculations for the bidirectional connections were performed over all possible connections representing bidirectional connections (i.e. if X represents a bidirectional connection, then the calculations were done over 2X).

Connections with distance

Lateral connectivity is a characteristic feature of visual neurons (Shadlen & Newsome, 1998), so we further sought to examine the connections between simultaneously recorded neurons from two microelectrodes (410 or 820 μm apart). A typical example of neuronal connectivity between electrodes (spaced laterally by 820 μm) is shown in Fig. 9A. CCG analysis revealed that the red neuron recorded from electrode-1 projects (blue arrow) onto the blue neuron recorded from electrode-2. In a similar fashion, the pink neuron recorded from electrode-2 projects onto the purple neuron recorded from electrode-1. The green stars beside the neurons (purple from electrode-1 and blue from electrode-2) indicate synchrony between these neurons (peak straddling zero in the CCG) and presumably receiving a common afferent input from a third neuron (König *et al.*, 1995; Ghisovan *et al.*, 2008; Denman & Contreras, 2014). A single orientation grating was positioned on the monitor screen covering the RFs of neurons at both sites. In total, only 48 connections (37 quasi-synchronous and 11 synchronous) were revealed between the electrodes (i.e. across assemblies). The proportion of local connections (0.19) was significantly higher (*z*-test, $P < 0.00001$) than the proportion of distal connections (0.02), which seems to be in line with a report (Fujisawa *et al.*, 2008) that connection-probability (number of connections) declines as a function of distance between recorded neurons. Collectively, this suggests that predominantly the interactions between neurons occur locally.

Interaction between the regular-spiking (RS) and fast-spiking (FS) neurons

In cortical circuits, inhibitory neurons are interspersed within networks of excitatory principal neurons (Nowak *et al.*, 2003; Fries *et al.*, 2007; Bopp *et al.*, 2014; Cossell *et al.*, 2015). Thus, we next investigated how these two peculiar classes of neurons might connect with each other within microcircuits. Electrophysiologically, based upon the ascending slope of the waveform, these two types can be dissociated from each other (Nowak *et al.*, 2003; Niell & Stryker, 2008; Vinck *et al.*, 2013) into RS and FS neurons, which are putatively linked to excitatory principal cells and inhibitory neurons, respectively. We thus categorized the neurons as RS and FS, wherein waveforms with slopes ≤ 0.3 were dissociated as FS, whereas waveforms with slopes > 0.3 were separated as RS. The dissociation is shown in Fig. 10A (FS, $n = 50$ and RS, $n = 124$; a typical example of an RS and an FS is shown superimposed as an inset). Thereafter, we investigated the connections among these two classes (i.e. RS–RS, the connections between RS neurons; RS–FS,

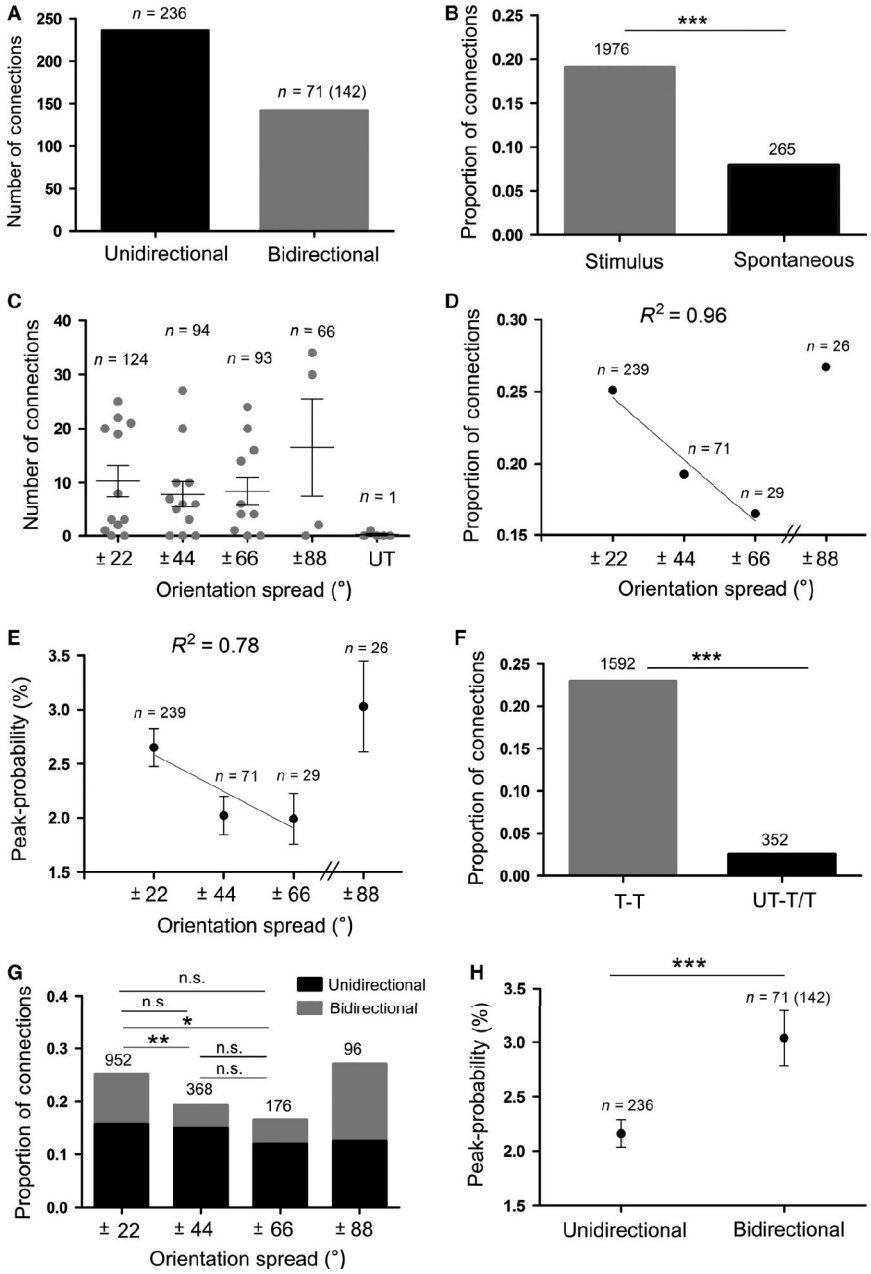

FIG. 8. Distribution of connections. (A) Distribution of connections (unidirectional and bidirectional) at stimulus-presentation. (B) Proportion of connections at the presentation of stimulus and spontaneous firing across all recordings. Both classes are significantly different (z-test, $P < 0.00001$). (C) No relation was observed for the number of connections as a function of the orientation scatter of the assembly (ANOVA, $P = 0.49$). (D) Proportion of connected cell pairs decreases in relation to the orientation spread ($R^2 = 0.96$, $P = 0.12$). (E) Peak-probability (P) decreased as a function of the orientation spread ($R^2 = 0.78$, $P = 0.30$). (F) Proportions of connections between tuned neuron pairs (T-T) and untuned-tuned/untuned (UT-T/UT) pairs were significantly different (z-test, $P < 0.00001$). (G) The ratio of unidirectional and bidirectional connections in relation to orientation spread of pairs. Bidirectional connections: significant difference between ± 22° and ± 44° (z-test, $P = 0.002$), significant difference between ± 22° and ± 66° (z-test, $P = 0.012$), non-significant between ± 44° and ± 66° (z-test, $P = 0.48$). The corresponding unidirectional classes were non-significant (z-test, $P > 0.05$). (H) Mean peak-probabilities for unidirectional and bidirectional connections were significantly different (unpaired t-test, $P = 0.0007$). It is to be underlined that ± 88° was eliminated from the analysis in D, E and G as the neurons in the pair approached opposite directions. The numbers at the top of the bars (in B, F and G) indicate the total number of possible pairs in that class.

the connections between RS and FS neurons; FS–FS, the connections between FS neurons). The proportion of connections declined (Fig. 10B) from RS–RS (0.22) to RS–FS (0.17) to FS–FS (0.12) and each of the classes was significantly different from each other (z-test, between RS–RS and RS–FS, $P = 0.005$; between RS–RS and FS–FS, $P = 0.0002$; between RS–FS and FS–FS, z-test, $P = 0.034$).

Furthermore, we labelled these interactions as excitatory or inhibitory depending upon the position of peaks or troughs in CCGs (Barthó *et al.*, 2004; Schwindel *et al.*, 2014). Out the RS–RS inter-

actions, 134 were deemed unidirectional (excitatory in one direction, e.g. connection between neurons 4 and 5 in Fig. 3) and 48 were identified as bidirectional (recurrent excitation, e.g. connection between neurons 1 and 4 in Fig. 3). Among FS–RS interactions, four major types of interactions occurred: inhibitory (FS to RS, unidirectional, n = 27); inhibitory–excitatory (FS to RS, bidirectional, n = 18); excitatory (FS to RS, unidirectional, n = 22) and excitatory (RS to FS, unidirectional, n = 33). A typical example of an inhibitory connection is shown in Fig. 11A. The reference neuron (FS, orange) completely suppressed the activity of the target neuron (RS, target) for a few milliseconds (~ 5 ms) after the zero point in the CCG. A typical example of inhibitory–excitatory connection is illustrated between neuron 3 (identified as FS, reference) and neuron 1 (RS) in Fig. 4. Note the strong suppression of the RS neuron at zero point in the CCG. This indicates inhibition of the RS neuron in one direction and excitation of the FS neuron in another direction (Barthó *et al.*, 2004). An example of an FS neuron exciting an RS neuron is signified by neuron 3 to neuron 2 in Fig. 4. In a similar fashion, RS neurons projected onto FS neurons. Finally, among FS–FS interactions, 20 were marked as unidirectional (Fig. 11B, the orange projected onto the brown neuron) and five were identified as bidirectional (Fig. 11C, the orange neuron and the blue neuron reciprocally excited each other). The modulation of connections with orientation is displayed in Fig. 5.

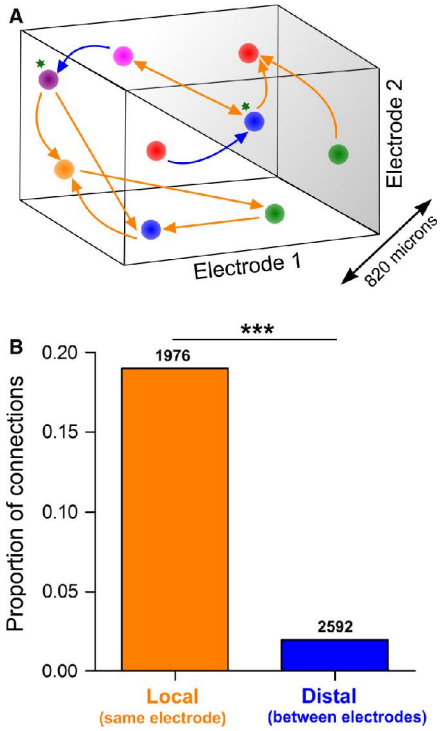

FIG. 9. Connections with distance. (A) Functional network between two simultaneously recorded assemblies (white and gray parts of the cuboid represent assemblies recorded from two separate tips that were 820 μm apart) in response to an orientation grating. The blue arrows depict the functional connections between assemblies. The green stars indicate the synchronized activity of neurons. Colored circles stand for neurons. (B) Proportions of local and distal connections were significantly different (z-test, $P < 0.00001$). At the top of the bar, the number represents total number of possible pairs in that class.

In summary, this analysis indicates that in cat primary visual microcircuits, the interactions between regular spiking cells (RS–RS) are predominant, which putatively may be attributed to the principal excitatory neurons. The FS neurons target a few RS neurons in cat visual cortex, unlike the mouse cortices where RS neurons weave on average more FS neurons. This seems to be in line with earlier reports (Hofer *et al.*, 2011; Bopp *et al.*, 2014; Cossell *et al.*, 2015) and these interactions point to the role of FS neurons in maintaining the orientation selectivity of RS neurons through distinct mechanisms (Tiesinga & Sejnowski, 2009). However, note that in cat visual cortex, the foolproof separation of spikes into putative pyramidal and inhibitory neurons based on ascending slopes is not entirely possible as a fraction of excitatory neurons may exhibit an FS pattern (Nowak *et al.*, 2003). Therefore, one has to be cautious when interpreting the above analysis, as this may not exhaustively suggest inhibitory and excitatory connections between these two classes of neurons in cat primary visual cortex.

Similarity pattern of CCGs (network stability)

To show that the revealed functional connections are indeed an outcome of specific coordinated activity between neurons rather than

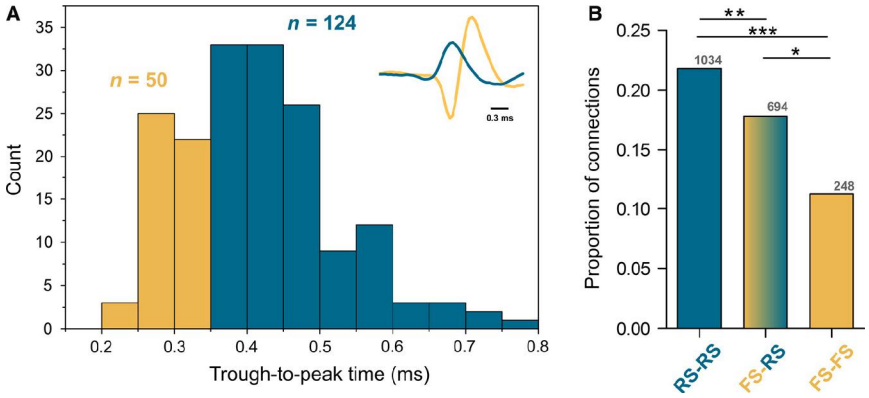

FIG. 10. Interaction between regular spikes (RS) and fast spikes (FS). (A) Dissociation of RSs and FSs based on the spike-width. A typical example of an RS and an FS is shown as a superimposed inset. (B) Proportion of connections according to spike waveforms. Each of the classes is significantly different from each other: RS/RS and FS/RS (z-test, P = 0.005); RS/RS and FS/FS (z-test, P = 0.0002); FS/RS and FS/FS (z-test, P = 0.034). The number at the top of the represents total number of possible pairs in that class.

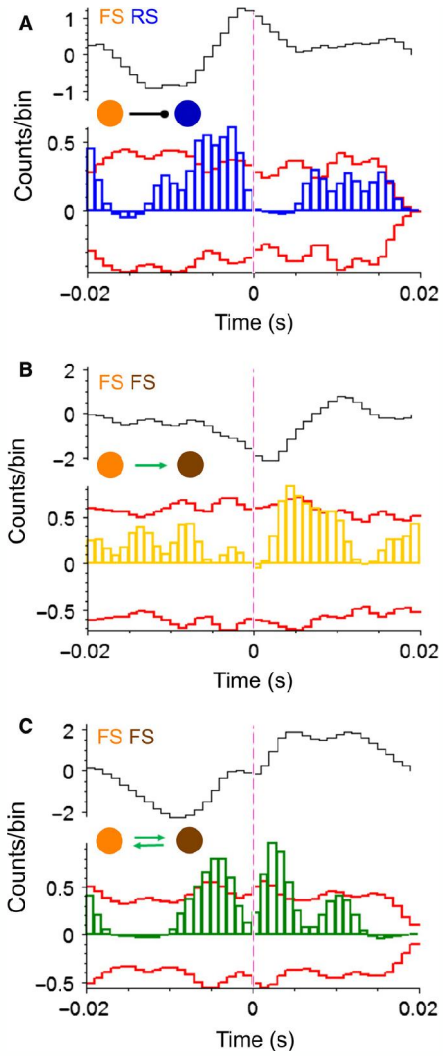

FIG. 11. Typical examples of excitatory and inhibitory connections. (A) A typical CCG (inhibitory connection) between an FS and an RS neuron. The FS neuron (reference) suppresses the activity of the RS neuron (target) for few milliseconds after zero time in the CCG. (B) An excitatory connection between FS neurons. The reference neuron (orange) excites the target (brown). (C) Recurrent excitation between FS neurons.

the result of random fluctuations, some neuron pairs recorded simultaneously were tested twice; that is, a particular test feature presentation was repeated after almost an hour. Two recordings were tested twice, i.e. four sites. Fourteen neurons were sorted from these recordings. An example of two simultaneously recorded neurons from a tip (red and blue waveforms) with their respective responses (raster and peristimulus histogram) at both attempts is shown in Fig. 12A. The black arrow pointing downwards indicates presentation of the stimulus. The CCG at each attempt in Fig. 12B shows that the red neuron projects on to the blue neuron in either case with noticeable similarity. In both attempts, the significant peak appeared at the same time (+4 ms, green line) with p equaling 1.4%. An example of a network that remains similar (same connections with similar p) in both attempts between three simultaneously recorded neurons is shown in Fig. 12C. A few connected neuron pairs (n = 26) were pooled, and no significant difference (paired t-test, P = 0.24) was found between the peak-probability at both attempts (Fig. 12D). This suggests that neurons establish specific functional connections in relation to a particular input that remain constant over time within an assembly, as suggested by Miller *et al.* (2014).

Discussion

We performed multi-electrode recordings to capture V1 assemblies in cats. The goal was to examine functional connectivity (by employing CCGs) between neurons in an assembly in response to different orientation gratings. Our main findings were as follows. (1) Most importantly, we found that an assembly structures a salient functional network at every orientation. (2) In addition to the closely tuned assemblies, high orientation-range assemblies also featured stimulus-encoding networks between themselves; however, within these assemblies, closely tuned neurons were connected more frequently and vigorously than distantly tuned neurons; untuned neurons did not exhibit many connections. (3) The connections between the RS neurons dominated the connections between RS–FS and FS–FS neurons. (4) The functional connections in assemblies remain stable over a period of time. (5) Despite low firing, neurons displayed connections.

Methodological considerations

The recordings were done in anaesthetized cats; therefore, the neuronal output cannot be attributed to attention parameters (de Kock & Sakmann, 2009). Spontaneous oscillations could induce time-locked neural activity in an anaesthetized animal (Poulet & Petersen, 2008); however, rhythmic oscillations that permit neuronal synchrony can also be recorded in the anaesthetized state (Gray & Singer, 1989; Xing *et al.*, 2012; Bharmauria *et al.*, 2015). In current experiments, the stimuli were applied in a random fashion with random inter-stimulus intervals. The assemblies exhibited more connections when visually evoked; connectivity and connection-strength decreased as a function of orientation spread as expected (Hofer *et al.*, 2011; Ko *et al.*, 2011; Denman & Contreras, 2014); and the interactions between neurons were predominantly local and the pattern of CCGs remained similar with time. Moreover, we have already documented that connected neurons in an assembly cooperate more synergistically than their unconnected companions within a characteristic 50-ms window of opportunity exhibiting heightened gamma power (Bharmauria *et al.*, 2014, 2015). All these significant trends along with our previous findings suggest that the functional connections were indeed strongly linked to the input stimulus.

Functional network: the encoding signature of an assembly

Many previous studies using different approaches such as calcium imaging (Hofer *et al.*, 2011; Miller *et al.*, 2014; Cossell *et al.*, 2015; Wertz *et al.*, 2015), electrophysiology (Barthó *et al.*, 2004; Fujisawa *et al.*, 2008; Ecker *et al.*, 2010; Denman & Contreras, 2014) and computational modelling (Binzegger *et al.*, 2004; Buzas *et al.*, 2006) have pointed to the significance of specific local connectivity in neural circuits; however, none of them explored the functional interactions in an assembly to the systematic presentation of a stimulus, as in this investigation (the systematic tilt of the orientated gratings). We found that a salient network is activated in an assembly at each orientation, wherein connections are activated or inactivated depending on the feature. To draw an analogy with Singer's postulation (Singer, 2013) – a reservoir (assembly in our case) recruits a specific classifier (network) within its randomly coupled neurons contingent upon the input.

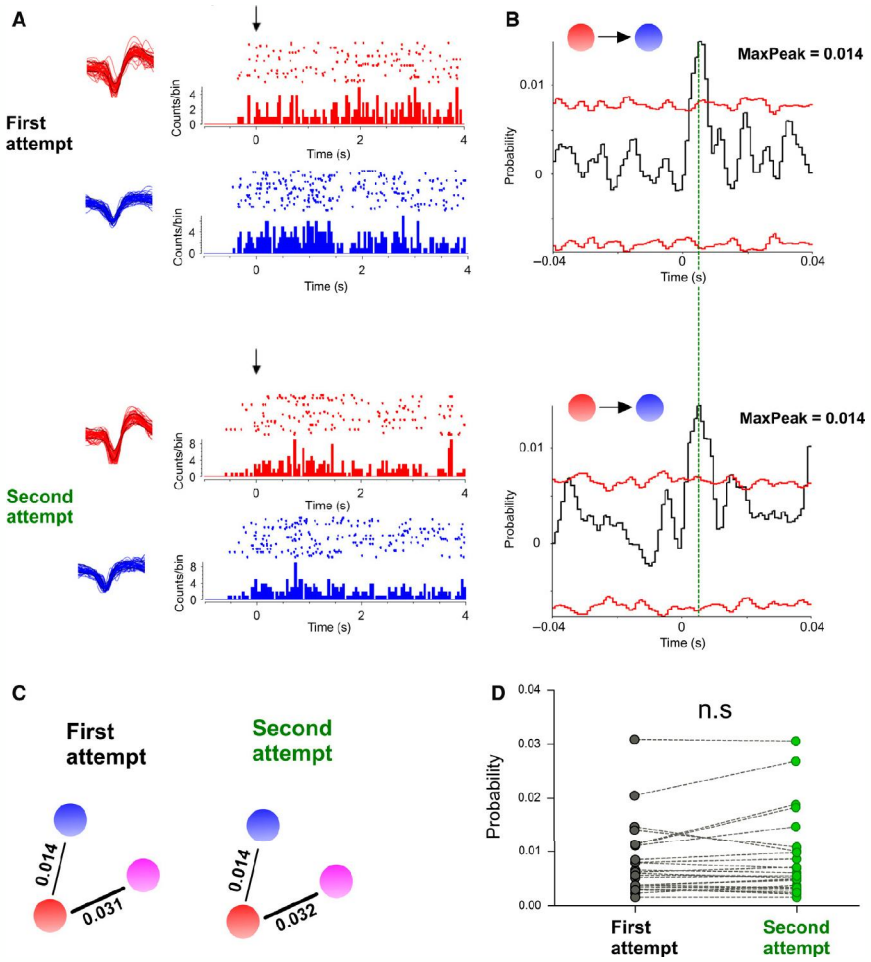

FIG. 12. Stability of the cross-correlogram (CCG). (A) Left: Respective waveforms and visual responses (downward black arrow indicates stimulus onset) of simultaneously recorded spikes from a microelectrode at the 'First' and the 'Second' attempt; time interval between both attempts was about 1 h. (B) Significant shift-corrected CCGs for the neuron pair. Notice the similarity of CCGs at both attempts. The green broken line in the CCGs represents the highest bins at the same time (P = 1.4% in both attempts). (C) A similar network of simultaneously recorded three neurons at both attempts. (D) Globally, no significant difference (paired t-test, P = 0.24) was found for peak-probability from the first attempt to the second attempt.

Moreover, some connections are frequently active as if embedded strongly in an assembly irrespective of the input. In addition, new cells might become active (start responding) and some may leave the assembly in relation to the grating. Along with previous reports (Barth & Poulet, 2012; Cossell *et al.*, 2015), we suggest that in an assembly there is a core group of active cells that interact synergistically (Bharmauria *et al.*, 2014) and may always remain connected, whereas the weakly connected neurons confer flexibility to the assembly as the input changes. In addition, the assemblies were active intrinsically (absence of input) too, as has been reported previously (Kenet *et al.*, 2003; Han *et al.*, 2008; Mohajerani *et al.*, 2013; Miller *et al.*, 2014), but did not display many connections in comparison with the visual stimulation. This reverberating activity may be a fundamental precursor for the organization of neural circuits that develops with past experience (during youth and adulthood), thereby keeping the circuit always prepared to receive the input efficiently. Any relevant input may then propel the intrinsically active circuit into a biased functional mode (Miller *et al.*, 2014). Lastly, the stability of connections with time reflects the specific time-locked neural activities in an assembly in relation to the same stimulus. Conclusively, all the above findings and arguments imply that a salient functional network within an emergent assembly is its 'encoding signature' to a particular input.

Firing rate of neurons, functional interactions and their strength

Neuronal selectivity (implying the firing rate) is the classical method to study feature encoding (e.g. in V1 neurons), and sparse firing is a characteristic feature of microcircuits (Barth & Poulet, 2012; Jayakumar *et al.*, 2012; Molotchnikoff & Rouat, 2012). We found that significant peaks (and their probabilities) in CCGs may emerge irrespective of the low firing of the involved pair. Thus, it can be inferred that connectivity between low firing neurons (and at non-optimal orientations) is attributed to the precise spike timing of the reference neuron to modulate the firing of the recipient cell. Indeed, several arguments militate against a possible bias of firing rates for significant CCGs (Duret *et al.*, 2006; Ghisovan *et al.*, 2008; Rolls & Treves, 2011). Moreover,

many studies (Pellionisz & Llinas, 1979; Hopfield, 1982; Buzsáki, 2010; Miller *et al.*, 2014) conclude that, in an assembly of interconnected neurons, the firing rate of an individual neuron is not as important as the whole network. Lastly, it has been shown that population responses decode the tasks better than individual neurons (as the response of a neuron is promiscuous even to the same stimulus) (Kampa *et al.*, 2011). One may also argue that the brain state of an anaesthetized animal might control the number of responsive neurons and suppress the response output (de Kock & Sakmann, 2009). Thus, time-locked events between neurons might go undetected due to low firing of neurons or insufficient trials (stimulus presentation) that may result in few spikes for CCG analysis. The number of trials and their duration may change from one experimental setup to another. In our case, the duration of stimulation was relatively long to allow enough spikes to be collected for CCG analysis; nevertheless, the possibility of some undetected connections cannot be eliminated. Indeed, the equivalent firing of connected and unconnected neurons (Fig. 6C) underlines the importance of precisely locked firing between neurons compared with the firing rate of neurons. The strongly embedded connections in circuits may consistently show such time-locked neural activities (Cossell *et al.*, 2015). In summary, we suggest that an assembly (and thus the activated network) is more important than its neurons as separate individuals, wherein the weakly firing neurons may also play an important role in stimulus encoding.

The importance of neuronal selectivity and RS–FS interactions

We found that the closely tuned neurons exhibited increased connectivity and connection strengths compared with the distantly tuned neurons within assemblies. This is in line with previous reports (Gilbert & Wiesel, 1989; Shadlen & Newsome, 1998; Kisvárday *et al.*, 2000; Stepanyants *et al.*, 2008; de Kock & Sakmann, 2009; Ecker *et al.*, 2010; Hofer *et al.*, 2011; Ko *et al.*, 2011, 2013; Wertz *et al.*, 2015), as neurons with similar response properties densely innervate each other, have correlated spike activities, and receive a common peripheral input (therefore having a maximal likelihood of being connected). This suggests that the network activity is biased towards a particular range of close orientation. The similarly tuned neurons encode the similar features in a target, whereas the differentially or oppositely tuned pairs may simultaneously bind the contrasting or opposing features, respectively, to establish the entirety of a complex target (Singer, 2001; Molotchnikoff & Rouat, 2012). Because closely tuned neurons have simultaneous high firing rates, such occurrence may allow a reduction of the overall space of possible trajectories or operating connections; otherwise, the population would not exhibit network-selectivity. The subset of neurons most closely tuned to a stimulus may thus drive the activity of the connected cell within the network, producing stable neuronal trajectories and network-selectivity. By contrast, in a higher orientation spread, we are likely to observe more contrast between the firing rates, eventually constraining the circuit to a limited number of functional connections. Lastly, the untuned neurons exhibited a few connections, implying that neuronal selectivity is an essential determinant of network-selection.

Finally, the predominance of RS–RS interactions alludes to the importance of recurrent excitatory connections within V1 assemblies between these particular cells, wherein FS neurons calibrate the selectivity of RS neurons (Hofer *et al.*, 2011; Bopp *et al.*, 2014; Cossell *et al.*, 2015).

Conclusions

In the current experiments, the neurons comprising assemblies were relatively few in number compared with the suggested size of population-codes (Alivisatos *et al.*, 2012). Indeed, the striking specificity of interacting neurons from one orientation to another reflects the temporal signature and dynamics of a stimulus-encoding assembly. This study further establishes the significance of cell-assembly as the main functional unit of information processing in cortical circuits and dilutes the importance of an individually firing neuron in encoding the stimulus. In short, this work could be a step toward the further unravelling of the neuronal codes governing cortical responses.

Competing interests

The authors declare no competing financial interests.

Acknowledgements

S.M. and J.R. were supported by CRSNG (Conseil de Recherches en Sciences Naturelles et en Génie) FRQ-NT (Fonds de recherche du Québec – Nature et technologies). S.B. was supported by a CRSNG Graduate scholarship (Grant No. NSERC, Canada 6943-1210). V.B. did the experiments, analysed the data and wrote the manuscript. L.B., S.C. and N.C. participated in experiments and analyses of the data. S.B. and J.R. contributed to analyses of the data. V.B. and S.M. conceived the idea of the study and contributed to data analyses and manuscript writing.

Abbreviations

ACG, auto-correlogram; CCG, cross-correlogram; DI, discrimination index; FS, fast spike; OSI, orientation selectivity index; PCA, principal component analysis; RF, receptive field; RS, regular spike; SEM, standard error of the mean; V1, primary visual cortex.

References

Abeles, M. (1982) Quantification, smoothing, and confidence limits for single-units' histograms. *J. Neurosci. Meth.*, **5**, 317–325.

Alivisatos, A.P., Chun, M., Church, G.M., Greenspan, R.J., Roukes, M.L. & Yuste, R. (2012) The brain activity map project and the challenge of functional connectomics. *Neuron*, **74**, 970–974.

Alloway, K.D. & Roy, S.A. (2002) Conditional cross-correlation analysis of thalamocortical neurotransmission. *Behav. Brain Res.*, **135**, 191–196.

Bachatene, L., Bharmauria, V., Cattan, S. & Molotchnikoff, S. (2013) Fluoxetine and serotonin facilitate attractive-adaptation-induced orientation plasticity in adult cat visual cortex. *Eur. J. Neurosci.*, **38**, 2065–2077.

Bardy, C., Huang, J.Y., Wang, C., FitzGibbon, T. & Dreher, B. (2006) 'Simplification' of responses of complex cells in cat striate cortex: suppressive surrounds and 'feedback' inactivation. *J. Physiol.*, **574**, 731–750.

Barlow, H.B., Blakemore, C. & Pettigrew, J.D. (1967) The neural mechanism of binocular depth discrimination. *J. Physiol.*, **193**, 327–342.

Barth, A.L. & Poulet, J.F. (2012) Experimental evidence for sparse firing in the neocortex. *Trends Neurosci.*, **35**, 345–355.

Barthó, P., Hirase, H., Monconduit, L., Zugaro, M., Harris, K.D. & Buzsáki, G. (2004) Characterization of neocortical principal cells and interneurons by network interactions and extracellular features. *J. Neurophysiol.*, **92**, 600–608.

Bharmauria, V., Bachatene, L., Cattan, S., Rouat, J. & Molotchnikoff, S. (2014) Synergistic activity between primary visual neurons. *Neuroscience*, **268**, 255–264.

Bharmauria, V., Bachatene, L., Cattan, S., Chanauria, N., Rouat, J. & Molotchnikoff, S. (2015) Stimulus-dependent augmented gamma oscillatory activity between the functionally connected cortical neurons in the primary visual cortex. *Eur. J. Neurosci.*, **41**, 1587–1596.

Binzegger, T., Douglas, R.J. & Martin, K.A. (2004) A quantitative map of the circuit of cat primary visual cortex. *J. Neurosci.*, **24**, 8441–8453.

Bishop, P.O. & Henry, G.H. (1972) Striate neurons: receptive field concepts. *Invest. Ophthalmol.*, **11**, 346–354.
Bopp, R., Macarico da Costa, N., Kampa, B.M., Martin, K.A. & Roth, M.M. (2014) Pyramidal cells make specific connections onto smooth (GABAergic) neurons in mouse visual cortex. *PLoS Biol.*, **12**, e1001932.
Butts, D.A. & Goldman, M.S. (2006) Tuning curves, neuronal variability, and sensory coding. *PLoS Biol.*, **4**, e92.
Buzas, P., Kovacs, K., Ferecsko, A.S., Budd, J.M., Eysel, U.T. & Kisvárday, Z.F. (2006) Model-based analysis of excitatory lateral connections in the visual cortex. *J. Comput. Neurosci.*, **499**, 861–881.
Buzsáki, G. (2010) Neural syntax: cell assemblies, synapsembles, and readers. *Neuron*, **68**, 362–385.
Cossell, L., Iacaruso, M.F., Muir, D.R., Houlton, R., Sader, E.N., Ko, H., Hofer, S.B. & Mrsic-Flogel, T.D. (2015) Functional organization of excitatory synaptic strength in primary visual cortex. *Nature*, **518**, 399–403.
Csicsvari, J., Hirase, H., Czurko, A. & Buzsáki, G. (1998) Reliability and state dependence of pyramidal cell-interneuron synapses in the hippocampus: an ensemble approach in the behaving rat. *Neuron*, **21**, 179–189.
DeAngelis, G.C., Ghose, G.M., Ohzawa, I. & Freeman, R.D. (1999) Functional micro-organization of primary visual cortex: receptive field analysis of nearby neurons. *J. Neurosci.*, **19**, 4046–4064.
Denman, D.J. & Contreras, D. (2014) The structure of pairwise correlation in mouse primary visual cortex reveals functional organization in the absence of an orientation map. *Cereb. Cortex*, **24**, 2707–2720.
Duret, F., Shumikhina, S. & Molotchnikoff, S. (2006) Neuron participation in a synchrony-encoding assembly. *BMC Neurosci.*, **7**, 72.
Ecker, A.S., Berens, P., Keliris, G.A., Bethge, M., Logothetis, N.K. & Tolias, A.S. (2010) Decorrelated neuronal firing in cortical microcircuits. *Science*, **327**, 584–587.
Engel, A.K., Fries, P. & Singer, W. (2001) Dynamic predictions: oscillations and synchrony in top-down processing. *Nat. Rev. Neurosci.*, **2**, 704–716.
Fries, P., Nikolic, D. & Singer, W. (2007) The gamma cycle. *Trends Neurosci.*, **30**, 309–316.
Fujisawa, S., Amarasingham, A., Harrison, M.T. & Buzsáki, G. (2008) Behavior-dependent short-term assembly dynamics in the medial prefrontal cortex. *Nat. Neurosci.*, **11**, 823–833.
Ghisovan, N., Nemri, A., Shumikhina, S. & Molotchnikoff, S. (2008) Synchrony between orientation-selective neurons is modulated during adaptation-induced plasticity in cat visual cortex. *BMC Neurosci.*, **9**, 60.
Gilbert, C.D. & Wiesel, T.N. (1989) Columnar specificity of intrinsic horizontal and corticocortical connections in cat visual cortex. *J. Neurosci.*, **9**, 2432–2442.
Gray, C.M. & Singer, W. (1989) Stimulus-specific neuronal oscillations in orientation columns of cat visual cortex. *Proc. Natl. Acad. Sci. USA*, **86**, 1698–1702.
Hagmann, P., Cammoun, L., Gigandet, X., Gerhard, S., Grant, P.E., Wedeen, V., Meuli, R., Thiran, J.P., Honey, C.J. & Sporns, O. (2010) MR connectomics: principles and challenges. *J. Neurosci. Meth.*, **194**, 34–45.
Han, F., Caporale, N. & Dan, Y. (2008) Reverberation of recent visual experience in spontaneous cortical waves. *Neuron*, **60**, 321–327.
Harris, K.D. & Mrsic-Flogel, T.D. (2013) Cortical connectivity and sensory coding. *Nature*, **503**, 51–58.
Harris, K.D., Hirase, H., Leinekugel, X., Henze, D.A. & Buzsáki, G. (2001) Temporal interaction between single spikes and complex spike bursts in hippocampal pyramidal cells. *Neuron*, **32**, 141–149.
Hofer, S.B., Ko, H., Pichler, B., Vogelstein, J., Ros, H., Zeng, H., Lein, E., Lesica, N.A. & Mrsic-Flogel, T.D. (2011) Differential connectivity and response dynamics of excitatory and inhibitory neurons in visual cortex. *Nat. Neurosci.*, **14**, 1045–1052.
Hopfield, J.J. (1982) Neural networks and physical systems with emergent collective computational abilities. *Proc. Natl. Acad. Sci. USA*, **79**, 2554–2558.
Hubel, D.H. & Wiesel, T.N. (1959) Receptive fields of single neurones in the cat's striate cortex. *J. Physiol.*, **148**, 574–591.
Jayakumar, J., Hu, D. & Vidyasagar, T.R. (2012) Sparseness of coding in area 17 of the cat visual cortex: a comparison between pinwheel centres and orientation domains. *Neuroscience*, **225**, 55–64.
Jia, H., Rochefort, N.L., Chen, X. & Konnerth, A. (2010) Dendritic organization of sensory input to cortical neurons in vivo. *Nature*, **464**, 1307–1312.
Kampa, B.M., Roth, M.M., Gobel, W. & Helmchen, F. (2011) Representation of visual scenes by local neuronal populations in layer 2/3 of mouse visual cortex. *Front. Neural. Circuits.*, **5**, 18.
Kenet, T., Bibitchkov, D., Tsodyks, M., Grinvald, A. & Arieli, A. (2003) Spontaneously emerging cortical representations of visual attributes. *Nature*, **425**, 954–956.
Kisvárday, Z.F., Crook, J.M., Buzas, P. & Eysel, U.T. (2000) Combined physiological-anatomical approaches to study lateral inhibition. *J. Neurosci. Meth.*, **103**, 91–106.
Ko, H., Hofer, S.B., Pichler, B., Buchanan, K.A., Sjostrom, P.J. & Mrsic-Flogel, T.D. (2011) Functional specificity of local synaptic connections in neocortical networks. *Nature*, **473**, 87–91.
Ko, H., Cossell, L., Baragli, C., Antolik, J., Clopath, C., Hofer, S.B. & Mrsic-Flogel, T.D. (2013) The emergence of functional microcircuits in visual cortex. *Nature*, **496**, 96–100.
de Kock, C.P. & Sakmann, B. (2009) Spiking in primary somatosensory cortex during natural whisking in awake head-restrained rats is cell-type specific. *Proc. Natl. Acad. Sci. USA*, **106**, 16446–16450.
König, P., Engel, K., Roelfsema, P.R. & Singer, W. (1995) How precise is the neuronal synchronization? *Neural Comput.*, **7**, 469–485.
Leergaard, T.B., Hilgetag, C.C. & Sporns, O. (2012) Mapping the connectome: multi-level analysis of brain connectivity. *Front. Neuroinform.*, **6**, 14.
Liao, D.S., Krahe, T.E., Prusky, G.T., Medina, A.E. & Ramoa, A.S. (2004) Recovery of cortical binocularity and orientation selectivity after the critical period for ocular dominance plasticity. *J. Neurophysiol.*, **92**, 2113–2121.
Martin, K.A. & Schröder, S. (2013) Functional heterogeneity in neighboring neurons of cat primary visual cortex in response to both artificial and natural stimuli. *J. Neurosci.*, **33**, 7325–7344.
Miller, J.E., Ayzenshtat, I., Carrillo-Reid, L. & Yuste, R. (2014) Visual stimuli recruit intrinsically generated cortical ensembles. *Proc. Natl. Acad. Sci. USA*, **111**, E4053–E4061.
Mohajerani, M.H., Chan, A.W., Mohsenvand, M., LeDue, J., Liu, R., McVea, D.A., Boyd, J.D., Wang, Y.T., Reimers, M. & Murphy, T.H. (2013) Spontaneous cortical activity alternates between motifs defined by regional axonal projections. *Nat. Neurosci.*, **16**, 1426–1435.
Molotchnikoff, S. & Rouat, J. (2012) Brain at work: time, sparseness and superposition principles. *Front Biosci.*, **17**, 583–606.
Niell, C.M. & Stryker, M.P. (2008) Highly selective receptive fields in mouse visual cortex. *J. Neurosci.*, **28**, 7520–7536.
Nowak, L.G., Azouz, R., Sanchez-Vives, M.V., Gray, C.M. & McCormick, D.A. (2003) Electrophysiological classes of cat primary visual cortical neurons in vivo as revealed by quantitative analyses. *J. Neurophysiol.*, **89**, 1541–1566.
Pellionisz, A. & Llinas, R. (1979) Brain modeling by tensor network theory and computer simulation. The cerebellum: distributed processor for predictive coordination. *Neuroscience*, **4**, 323–348.
Perkel, D.H., Gerstein, G.L. & Moore, G.P. (1967) Neuronal spike trains and stochastic point processes. I. The single spike train. *Biophys. J.*, **7**, 391–418.
Poulet, J.F. & Petersen, C.C. (2008) Internal brain state regulates membrane potential synchrony in barrel cortex of behaving mice. *Nature*, **454**, 881–885.
Ramoa, A.S., Mower, A.F., Liao, D. & Jafri, S.I. (2001) Suppression of cortical NMDA receptor function prevents development of orientation selectivity in the primary visual cortex. *J. Neurosci.*, **21**, 4299–4309.
Rolls, E.T. & Treves, A. (2011) The neuronal encoding of information in the brain. *Prog. Neurobiol.*, **95**, 448–490.
Schwindel, C.D., Ali, K., McNaughton, B.L. & Tatsuno, M. (2014) Long-term recordings improve the detection of weak excitatory-excitatory connections in rat prefrontal cortex. *J. Neurosci.*, **34**, 5454–5467.
Shadlen, M.N. & Newsome, W.T. (1998) The variable discharge of cortical neurons: implications for connectivity, computation, and information coding. *J. Neurosci.*, **18**, 3870–3896.
Shannon, R., Baekey, D.M., Morris, K.F., Li, Z. & Lindsey, B.G. (2000) Functional connectivity among ventrolateral medullary respiratory neurones and responses during fictive cough in the cat. *J. Physiol.*, **525**, 207–224.
Singer, W. (2001) Consciousness and the binding problem. *Ann. N.Y. Acad. Sci.*, **929**, 123–146.
Singer, W. (2013) Cortical dynamics revisited. *Trends Cogn. Sci.*, **17**, 616–626.
Sporns, O. (2011) The human connectome: a complex network. *Ann. N.Y. Acad. Sci.*, **1224**, 109–125.
Sporns, O., Tononi, G. & Kotter, R. (2005) The human connectome: a structural description of the human brain. *PLoS Comput. Biol.*, **1**, e42.

Stepanyants, A., Hirsch, J.A., Martinez, L.M., Kisvárday, Z.F., Ferecsko, A.S. & Chklovskii, D.B. (2008) Local potential connectivity in cat primary visual cortex. *Cereb. Cortex*, **18**, 13–28.

Swindale, N.V. (1998) Orientation tuning curves: empirical description and estimation of parameters. *Biol. Cybern.*, **78**, 45–56.

Talebi, V. & Baker, C.L. (2012) Natural versus synthetic stimuli for estimating Receptive field models: a comparison of predictive robustness. *J. Neurosci.*, **32**, 1560–1576.

Tiesinga, P. & Sejnowski, T.J. (2009) Cortical enlightenment: are attentional gamma oscillations driven by ING or PING? *Neuron*, **63**, 727–732.

Vinck, M., Womelsdorf, T., Buffalo, E.A., Desimone, R. & Fries, P. (2013) Attentional modulation of cell-class-specific gamma-band synchronization in awake monkey area V4. *Neuron*, **80**, 1077–1089.

Vizuete, J.A., Pillay, S., Diba, K., Ropella, K.M. & Hudetz, A.G. (2012) Monosynaptic functional connectivity in cerebral cortex during wakefulness and under graded levels of anesthesia. *Front. Integr. Neurosci.*, **6**, 90.

Wertz, A., Trenholm, S., Yonehara, K., Hillier, D., Raics, Z., Leinweber, M., Szalay, G., Ghanem, A., Keller, G., Rozsa, B., Conzelmann, K.K. & Roska, B. (2015) Single-cell-initiated monosynaptic tracing reveals layer-specific cortical network modules. *Science*, **349**, 70–74.

Xing, D., Shen, Y., Burns, S., Yeh, C.I., Shapley, R. & Li, W. (2012) Stochastic generation of gamma-band activity in primary visual cortex of awake and anesthetized monkeys. *J. Neurosci.*, **32**, 13873–13880a.

CHAPTER 6. High noise correlation between the functionally connected neurons in emergent V1 microcircuits.

Vishal Bharmauria[a], Lyes Bachatene[a], Sarah Cattan[a], Nayan Chanauria[a], Jean Rouat[a,b], Stéphane Molotchnikoff[a,b]

a Département de Sciences Biologiques, Université deMontréal, Montréal, QC, Canada
b Universite´ de Sherbrooke, Sherbrooke, QC, Canada

Experimental Brain Research (2015) ***234****: 523-532*

(Published article)

Exp Brain Res (2016) 234:523–532
DOI 10.1007/s00221-015-4482-7

RESEARCH ARTICLE

High noise correlation between the functionally connected neurons in emergent V1 microcircuits

Vishal Bharmauria[1,2] · Lyes Bachatene[1,2] · Sarah Cattan[1,2] · Nayan Chanauria[1,2] · Jean Rouat[1,2,3] · Stéphane Molotchnikoff[1,2,3]

Received: 26 May 2015 / Accepted: 19 October 2015 / Published online: 2 November 2015

Abstract Neural correlations (noise correlations and cross-correlograms) are widely studied to infer functional connectivity between neurons. High noise correlations between neurons have been reported to increase the encoding accuracy of a neuronal population; however, low noise correlations have also been documented to play a critical role in cortical microcircuits. Therefore, the role of noise correlations in neural encoding is highly debated. To this aim, through multi-electrodes, we recorded neuronal ensembles in the primary visual cortex of anaesthetized cats. By computing cross-correlograms, we divulged the functional network (microcircuit) between neurons within an ensemble in relation to a specific orientation. We show that functionally connected neurons systematically exhibit higher noise correlations than functionally unconnected neurons in a microcircuit that is activated in response to a particular orientation. Furthermore, the mean strength of noise correlations for the connected neurons increases steeply than the unconnected neurons as a function of the resolution window used to calculate noise correlations. We suggest that neurons that display high noise correlations in emergent microcircuits feature functional connections which are inevitable for information encoding in the primary visual cortex.

Keywords Cell-assembly · Cross-correlation (CCG) · Functional connection · Noise correlation (Rsc)

[1] Neurophysiology of Visual System, Département de Sciences Biologiques, Université de Montréal, Succ. centre-ville, CP 6128, Montreal, QC H3C 3J7, Canada

[2] Neurosciences Computationnelles et Traitement Intelligent des Signaux (NECOTIS), Sherbrooke, QC, Canada

[3] Département de Génie Électrique et Génie Informatique, Université de Sherbrooke, Sherbrooke, QC, Canada

Introduction

There is mounting evidence that understanding of information encoding in brain requires studying the correlation (noise correlation or Rsc; cross-correlations or CCG) between neurons (Perkel et al. 1967; Alloway and Roy 2002; Bach and Kruger 1986; Zohary et al. 1994; Averbeck and Lee 2003; Barthó et al. 2004; Uhlhaas et al. 2009; Cohen and Kohn 2011; Graf et al. 2011; Cotton et al. 2013; Denman and Contreras 2014; Cossell et al. 2015). Rsc is the trial-by-trial Pearson correlation of the spike counts of two neurons in response to the same stimulus, and it simply gives us information about the degree to which trial-by-trial fluctuations are shared by a neuronal pair (Averbeck et al. 2006; Cohen and Kohn 2011). On the other hand, a 'CCG' is a histogram of the firing rate of the target neuron with reference to the spiking of another simultaneously recorded neuron, and it provides the direction and type of functional link between neurons (Alonso and Martinez 1998; Barthó et al. 2004; Fujisawa et al. 2008; Bharmauria et al. 2014; 2015b). A peak offset from zero (quasi-synchrony) in a 'CCG' indicates a putative excitatory or inhibitory connection, whereas a peak straddling zero (synchrony) signifies a common input to neurons (Perkel et al. 1967; Shadlen and Newsome 1998; Dong et al. 2008; Bachatene et al. 2015).

On one hand, many previous studies (in the visual cortex of different species) have reported high Rsc between neurons (Gawne et al. 1996; Kohn and Smith 2005; Gutnisky and Dragoi 2008; Cohen and Kohn 2011; Cotton et al. 2013; Cossell et al. 2015), suggesting that highly correlated

neurons may share a great deal of sensory input (Zohary et al. 1994; Shadlen and Newsome 1998; Bair et al. 2001; Kohn and Smith 2005). On the other hand, decorrelated firing (low Rsc) has also been observed in V1 microcircuits (Ecker et al. 2010; Renart et al. 2010), implying that highly correlated variability may be detrimental to population coding (Zohary et al. 1994; Sompolinsky et al. 2001). Investigators have also reported in V1 that, a CCG between a neuronal pair fluctuates systematically with changing stimulus (orientation grating) irrespective of low or high Rsc between them (Gawne et al. 1996; Bair et al. 2001; Reich et al. 2001; Kohn and Smith 2005). Thus, a contentious debate persists concerning the precise nature of Rsc in microcircuits (Cohen and Kohn 2011; Averbeck et al. 2006).

A major factor while calculating Rsc is the counting window (resolution window, as we name it) that is employed to compute Rsc (Cohen and Kohn 2011; Hansen et al. 2012; Schulz et al. 2015). Shorter windows may underestimate the true Rsc between neurons, whereas bigger windows may add artificial correlation between spike trains (Cohen and Kohn 2011; Hansen et al. 2012).

Recently, we have shown that a salient functional network (microcircuit) is activated within an ensemble (Bharmauria et al. 2015b) in a characteristical 50-ms window of opportunity, wherein neurons cooperate synergistically exhibiting augmented power of gamma oscillations (Bharmauria et al. 2014, 2015a). In the current investigation, we report that, in such an emergent microcircuit framed by an ensemble (simultaneously recorded neurons from a microelectrode), the connected pairs exhibit significantly higher Rsc than the unconnected pairs at all the resolution windows. Moreover, consistent with the previous findings (Gawne et al. 1996; Bair et al. 2001; Reich et al. 2001; Kohn and Smith 2005), the value of Rsc between a pair is independent of the presented orientation in an ensemble irrespective of the activation or inactivation of a functional connection between them at that orientation. To our knowledge, this investigation is the first to systematically investigate the connected and unconnected pairs based on correlations (Rsc and CCG) in an emergent microcircuit. This report further corroborates the earlier finding (Cossell et al. 2015) that, high Rsc between the strongly connected neurons carries well defined and structured information in microcircuits. However, importantly, Rsc has to be calculated in optimal resolution windows to extract meaningful information from these microcircuits. We suggest that highly correlated (stable or strong connections) neuronal pairs are major junctions of information routing in quasi-simultaneously active cohorts of neurons.

Materials and methods

Ethical approval

Five adult animals (Cats) were prepared for electrophysiological recordings in the primary visual cortex (layer II/III, area 17), as per the guidelines of Canadian Council on Animal Care and approved by the Institutional Animal Care and Use committee of Université de Montreal. The procedure is as below.

Animals, anesthesia and surgical procedures

Animals premedicated with acepromazine maleate (Atravet, Wyeth-Ayerst, Guelph, ON, Canada; 1 mg/kg, intramuscular) and atropine sulfate (ATRO-SA, Rafter, Calgary, AB, Canada; 0.04 mg/kg, intramuscular) were anesthetized with ketamine hydrochloride (Rogarsetic, Pfizer, Kirkland, QC, Canada; 25 mg/kg, intramuscular). The cats were then paralyzed with 40 mg and maintained with 10 mg/kg/h of gallamine triethiodide (Flaxedil, Sigma Chemical, St. Louis, MO, USA; intravenous) administered in 5 % dextrose lactated Ringer's nutritive solution. General anesthesia was maintained by artificial ventilation with a mixture of N_2O/O_2 (70:30) supplemented with 0.5 % isoflurane (AErrane, Baxter, Toronto, ON, Canada). Electroencephalogram, electrocardiogram, rectal temperature and end-tidal CO_2 partial pressure were monitored throughout the experiment, and kept in physiological ranges. The pupils were dilated with atropine sulfate (1 %, Isopto-Atropine; Alcon, Mississauga, Ontario, Canada), and the nictitating membranes were retracted with phenylephrine hydrochloride (2.5 %, Mydfrin, Alcon). The loci of the area centrales were inferred from the position of the blind spots which were opthalmoscopically focused and projected onto a translucent screen. At the end of the experiment, the cats were euthanized intravenously with a dose (0.5 mL/kg) of Sodium Pentobarbital (CEVA, Sante Animale).

Visual stimulation

Monocular stimulation was done. The multi-unit receptive fields (RF) were mapped as the minimum response field (Barlow et al. 1967) by using a hand-held ophthalmoscope after clearly detectable activity had been obtained. These preliminary tests revealed qualitative properties such as dimensions, velocity-preference, orientation, and directional selectivity of neurons. Visual stimuli were generated with a VSG 2/5 graphic board (Cambridge Research Systems, Rochester, England) and displayed on a 21-inch monitor (Sony GDM-F520 Trinitron, Tokyo, Japan) placed 57 cm from the cat's eyes, with 1024 × 768 pixels, running

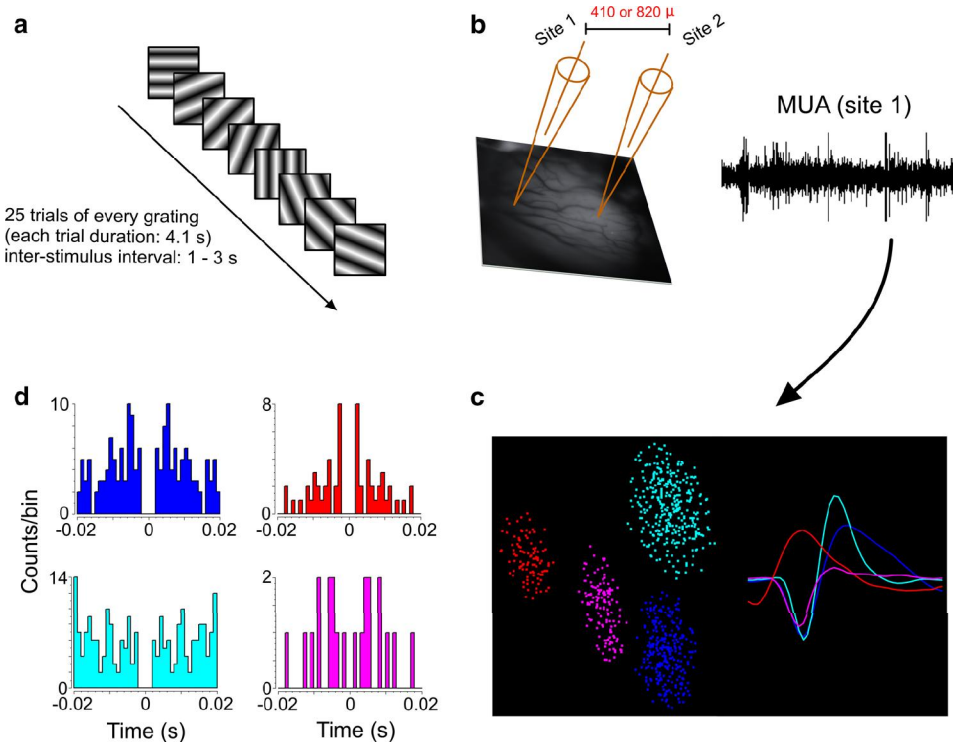

Fig. 1 A schematic of the experiment **a** presentation of sine-wave drifting gratings in a random fashion. **b** Multi-unit recording in layer II/III (area 17) in the primary visual cortex. **c** An example of four neurons sorted from multi-unit activity recorded from a microelectrode. Each neuron has a distinct waveform and a well-dissociated cluster. **d** Corresponding auto-correlograms (ACGs) for the isolated neurons

at 100-Hz frame refresh. The blank screen was uniformly gray (~35 Cd/m^2). Contrast was set at 80 %. Mean luminance was 40 cd/m^2. Optimal spatial and temporal frequencies were set at 0.24 cycles/deg and a range of 1.0–2.0 Hz, respectively, where V1 neurons are driven maximally by sine-wave drifting gratings (Bardy et al. 2006). The tested orientations were presented in a random order. Each drifting grating was presented in blocks of 25 trials (each trial lasted 4.1 s) with varying inter-stimulus (1–3 s) intervals during which no stimulus was presented (Fig. 1a). Thus the presentation of a stimulus lasted 180 s (with all the trials and inter-stimulus intervals).

Electrophysiological recording and single-unit selection

Multi-unit activity in the primary visual cortex was recorded by a tungsten multi-electrode (Frederick Haer & Co, Matrix Electrode; the multi-electrode had four columns, and each column had one row). The recordings were performed at locations 410 or 820 µm apart (Fig. 1b). Twelve recordings (24 sites) were done across all cats either in the left or the right hemisphere. Recordings were performed in the supragranular layers (cortical depth <1000 µm; mean = 650 µm). The signal from the microelectrodes was amplified, band-pass filtered (300 Hz–3 kHz), digitized and recorded with a 0.05 ms temporal resolution (Spike2, CED, Cambridge, England). Spike sorting from the multi-unit signals was done. Neurons were discriminated on the basis of three criteria: (1) the spike-waveform difference (2) principal component analysis (PCA) showing well-dissociated clusters (3) and auto-correlograms (ACG) showing no events (indicative of the refractory period of neuron) at the central point (Csicsvari et al. 1998; Barthó et al. 2004; Bharmauria et al. 2014). The stability of each cell's activity across conditions was verified qualitatively by the visual control of the disposition of clusters and the shapes of waveforms. Cluster analysis was performed using Spike2, CED, Cambridge, England in a 3-dimensional plot. The isolation distance was calculated as the Mahalanobis distance. The Mahalanobis distance is the distance from the cluster center within which as many events belong to the other clusters as to the specified cluster (Harris et al. 2001). In other words, given the multivariate data values for which the values in each variable are normally distributed around a mean, this measure allows to define boundaries of constant probability around the multidimensional center of the distribution. Thus, this estimation allows the separation of a cluster from the nearest cluster. Units within a Mahalanobis distance of 2.5 were considered for further analysis of the spike trains to reveal the functional connections between them. An example of dissociated spikes from multiunit activity is shown in Fig. 1c. The corresponding PCA and auto-correlograms are shown in Fig. 1d, e, respectively.

Cross-correlogram (CCG) computation

Cross-correlogarms were computed (binwidth = 1 ms) between the neural activities of all the possible neuron pairs at all the applied orientations to reveal the functional connections. The raw CCGs were shift-corrected (one spike train shifted over one stimulus period) to eliminate the putative significant peaks due to the simultaneous stimulation of both cells during each trial (to remove the stimulus-evoked and locked components) (Perkel et al. 1967). A significant peak of 2 ms (two adjacent bins) or at least one significant bin (Alloway and Roy 2002) was searched within a window of ±5 ms offset from zero (excluding the ±1 ms bins around zero) in the shift-corrected CCG to reveal a functional connection between two neurons. The statistical threshold for the significant peak was set at 95 %, and the probability (p) of the neuronal firing in a bin is calculated according to Abeles (1982). The details are present in Bharmauria et al. (2014).

Calculation of noise correlation (Rsc)

Noise correlation represents the trial-by-trial Pearson correlation-coefficient between the simultaneous firing of two neurons in response to the presentation of an identical stimulus (Cohen and Kohn 2011). Rsc was calculated for the connected and unconnected pairs across all ensembles at one selected orientation where the most number of connections were found. An optimal or near optimal orientation was chosen for closely tuned assemblies, whereas an orientation exhibiting maximum connections was selected for assemblies with wide orientation spreads. Rsc was calculated over all 25 trials for a neuron pair. The respective trials of the pair were correlated. The Rsc computation was performed over three different counting windows (resolution window) separately (5, 25 and 50 ms). A resolution window is the equally sized bin into which the whole trial duration is divided to perform the Rsc computation. For example, in our case, a trial of 4 s yielded 800 bins when the resolution window was set at 5 ms.

Results

The aim of the current investigation was to systematically compare the noise correlation between the functionally connected (as revealed from the CCGs, see methods) and unconnected neuronal pairs in V1 microcircuits activated within an ensemble in response to oriented sine-wave drifting gratings. It is to be noted that, within the context of this paper, simultaneously recorded neurons from a microelectrode are termed an ensemble (that is, coactive neurons as Miller et al. (2014) have defined them). It is to be underlined that a particular microcircuit activated within an ensemble at a specific orientation (for closely tuned ensembles an optimal or non-optimal orientation that exhibited numerous connections was chosen, and for distantly tuned ensembles an orientation that exhibited maximum connections was chosen) was selected to systematically compare the connected and unconnected neurons. Across twenty-four sites (ensembles), 94 neurons were recorded; 62 functionally connected and 47 unconnected pairs were analyzed.

Revealing the functional connection between neurons

Neurons in physical proximity share a great deal of peripheral input (Averbeck and Lee 2003; Shadlen and Newsome 1998); therefore, it is expected that they exhibit abundant functional connections with each other. Previously, we have shown that a 'signature' functional network is framed by an ensemble contingent upon the presented orientation (Bharmauria et al. 2015b). We computed CCGs to reveal these functional connections within an ensemble. A typical example of a connected and an unconnected neuron pair is shown in Fig. 2. Figure 2a illustrates the raster plots of two simultaneously recorded neurons with respective waveforms as insets. Figure 2b shows the CCG between the above spike trains (light green neuron is the reference), and the significant (the green background indicates the significance level, see methods) peak off-set from zero (within 5 ms) indicates that the reference neuron projects onto the target neuron (Barthó et al. 2004; Bharmauria et al. 2015a, b). The probability (p) of the peak that reflects the strength of connection is 0.016. The cumulative histogram of the target neuron (black curve above the CCG) further signifies that, once the reference neuron fires, it leads to an upsurge in the activity of the target neuron transiently. Figure 2c illustrates the raster plots (waveforms as insets) of an unconnected pair (absence of the significant peak) as inferred from the CCG (light red neuron is the reference) in Fig. 2d. It is to be noted that the above three neurons (same target neuron in both cases) were recorded simultaneously from a microelectrode, thus constitute an ensemble.

High noise correlation between the functionally connected neurons in an assembly

Recently, in mouse visual cortex, it has been shown that highly correlated (Rsc) neurons are strongly connected to each other (Cossell et al. 2015). After computing CCGs that revealed the functional connections, we calculated Rsc for the connected and unconnected pairs in an ensemble (at a specific microcircuit) at different resolution windows. Figure 3 shows an example of Rsc comparison between the connected and unconnected pairs in an ensemble (four

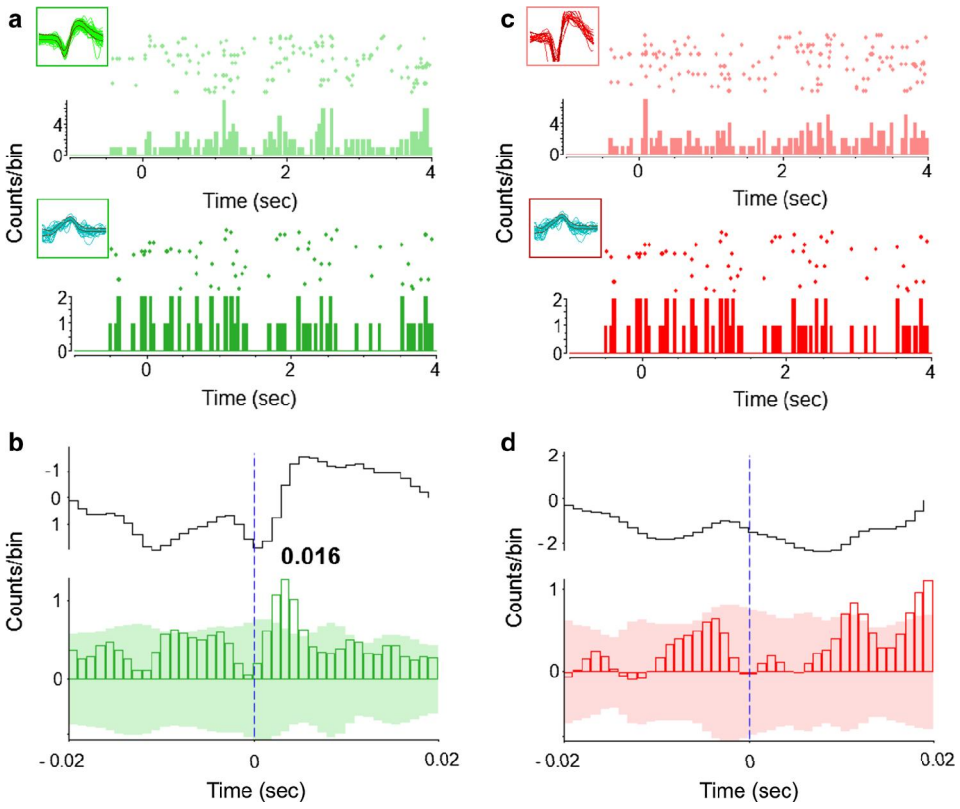

Fig. 2 Inferring functional connectivity (**a**) respective raster plots and perievent histograms of two simultaneously recorded neurons (waveforms as *insets*) from a microelectrode. **b** The cross-correlogram (CCG) between the spike trains of neurons (*light green* neuron is the reference) yielded a significant peak ($p = 0.016$) offset from zero (*blue broken line*), thus indicating that the reference neuron projects onto the target neuron. **c** Respective responses of two simultaneously recorded neurons (waveforms as *insets*) that did not exhibit a functional connection between them, as revealed from the non-significant CCG in (**d**). *Note*: The target neuron is same in both cases (color figure online)

simultaneously recorded neurons). The first matrix (Fig. 3a) illustrates the connectivity and the strength (colored scale) of the functional connections as divulged by CCGs. Out of the six possible pairs, three pairs (red–cyan; red–blue; blue–cyan) were connected, and the other three pairs were unconnected. It is to be noted that the matrix is symmetric along the diagonal (that is, the same connection is also represented on other side of diagonal). Figure 3b shows the Rsc values for the same pairs at 5-ms resolution window (see methods). The Rsc strength seems to be almost equivalent for all pairs. However, the Rsc values for the respective pairs increased systematically as we increased the resolution windows from 5–25 (Fig. 3c) to 50-ms (Fig. 3d). The strength of Rsc for the connected pairs increased steeply than the unconnected pairs. Figure 3e further shows the difference in increase in Rsc for the connected (green curves) and unconnected pairs (red curves). For example, the Rsc values for the blue–cyan (connected) pair increased steeply from 0.02 at 5-ms to 0.16 at 25-ms to 0.19 at 50-ms window, whereas for the red–purple (unconnected) pair, the respective Rsc values were found to be 0.00, 0.01 and 0.04. On a microcircuit basis (Fig. 3f), the mean correlation (with SD) for the connected pairs increased from 0.02 ± 0.00 at 5-ms to 0.12 ± 0.03 at 25-ms to 0.14 ± 0.03 at 50-ms window, whereas the corresponding values for the unconnected pairs were found to be 0.00 ± 0.00; 0.00 ± 0.13 and 0.04 ± 0.00. Both curves were significantly different (unpaired t test, $P < 0.05$). In summary, in a microcircuit activated within an ensemble, the connected neuron pairs systematically carry high Rsc than the unconnected neurons, implying that neurons with high Rsc may be strongly related to the presented feature.

Strength of connection (*P*), noise correlation (Rsc) and resolution window

Many investigators (Zohary et al. 1994; Graf et al. 2011; Hansen et al. 2012; Cossell et al. 2015) have suggested that high Rsc is directly related to the strength of the connection between neurons. We thus investigated how the probability of the peak (p) in the CCG might be related to Rsc between the same neurons. Figure 4a depicts that there is no relation between p and Rsc when Rsc was calculated in a low (5 ms) resolution window, as the regression curve did not deviate significantly from zero ($P > 0.05$). However, when the similar analysis was performed at 25-ms (Fig. 4b) and 50-ms (Fig. 4c) windows, the regression curves significantly deviated from zero in either case ($P < 0.05$), thus, indicating that as the Rsc value increases, the peak probability in the CCG tends to increase too. In short, this analysis points to the fact that Rsc has to be calculated in optimal resolution windows to undermine the true correlation between the

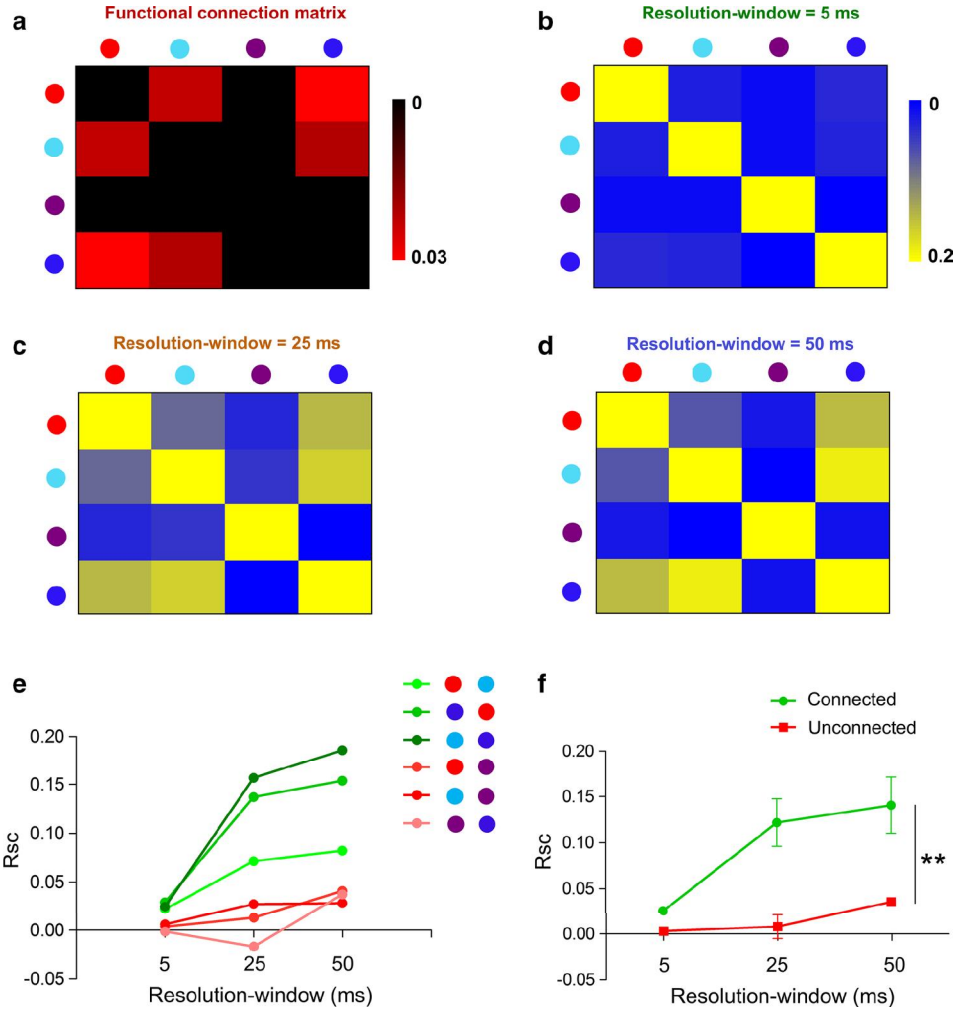

Fig. 3 High noise correlation between functionally connected neurons in a microcircuit (**a**) Functional connectivity matrix between four simultaneously recorded neurons from a microelectrode. Neurons along the *x* axis project onto the *y* axis neurons. *Note*: the matrix is symmetric along the diagonal, that is, the same connection is also represented on the other side of the diagonal. The *colored* scale stands for the strength of the connection. (**b–d**) Rsc matrices of the same neurons at 5, 25 and 50-ms resolution windows, respectively. The *colored* scale in '**b**' stands for all the matrices. **e** Noise correlation as a function of the resolution window for each pair in the microcircuit. The *green curves* represent the connected neuron pairs, and the *red lines* correspond to the unconnected pairs. **f** Mean noise correlation for connected and unconnected neuron pairs as a function of the resolution window. The mean correlation is higher and significantly different for the connected pairs than the unconnected pairs (unpaired *t* test, $P < 0.05$) (color figure online)

firing of two neurons. In other words, in optimal resolution windows, it is possible to associate the strength of the connections (p) to Rsc; if Rsc is high, p is high too.

Rsc dynamics within a microcircuit in relation to the presented orientation

As discussed above, we have already shown that an ensemble frames a specific functional network (microcircuit) that is strictly related to the presented orientation (Bharmauria et al. 2015b). We next examined the fluctuation of Rsc (at 50-ms resolution window) for the same neurons pairs in an ensemble (that is, from one microcircuit to another) as the orientation tilted in 22.5° steps. An example of an ensemble comprising four neurons (all neurons were tuned approximately to 90°) is shown in Fig. 5a. A specific network is activated at each presented orientation. The red–blue pair remains unconnected in all networks, exhibiting almost similar Rsc values (Fig. 5b). The red–green pair is connected at four orientations exhibiting high Rsc values, except at 135° where it displays a low Rsc value without a connection. Interestingly, in other four pairs, neurons remained unconnected regardless of the high values of Rsc in these microcircuits. For example, the red–orange pair exhibited highest Rsc (0.17) at 45°, but failed to display a connection. This seems to be in line with previous reports (Gawne et al. 1996; Bair et al. 2001; Reich et al. 2001; Kohn and Smith 2005) wherein investigators documented that the peak in CCG was orientation-dependent, whereas the respective Rsc of the involved neurons was independent of the tilt in orientation. Hence it appears that Rsc and CCGs have to be appropriately associated to each other in microcircuits. With this example and other analyses, we show that within an emergent microcircuit, the connected pairs always exhibit higher average Rsc values than the unconnected pairs (it is to be noted that in all the microcircuits, the connected pairs always had higher average Rsc than the unconnected pairs).

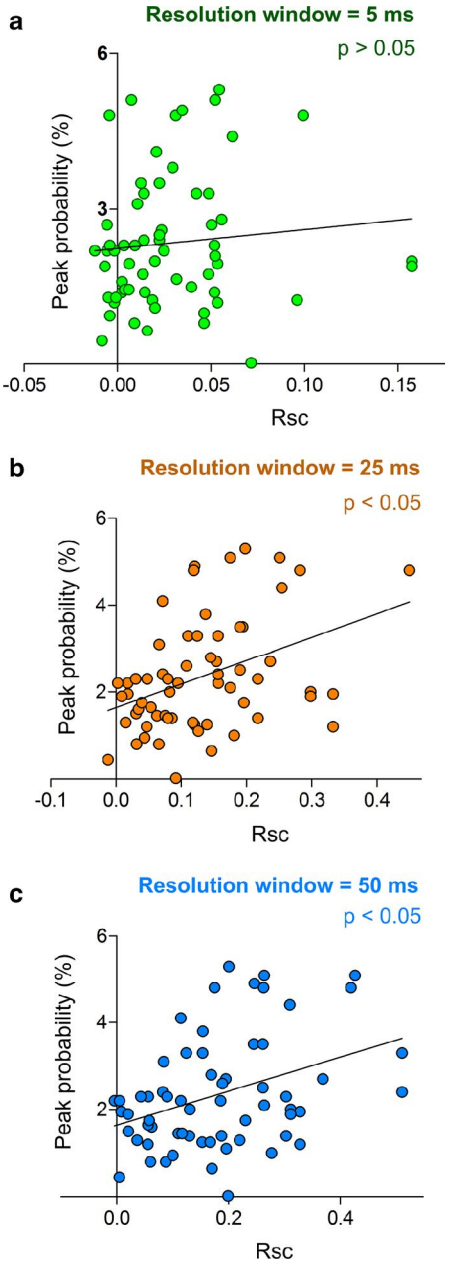

Fig. 4 Peak probability (p), noise correlation (Rsc) and the resolution window. **a** No relation is inferred between p and Rsc at 5-ms resolution window as the regression curve did not deviate significantly from zero ($P > 0.05$). **b**, **c** 'p' and Rsc in relation to the 25 and 50-ms resolution windows. 'p' showed a significant relation with Rsc at both resolution windows ($P < 0.05$)

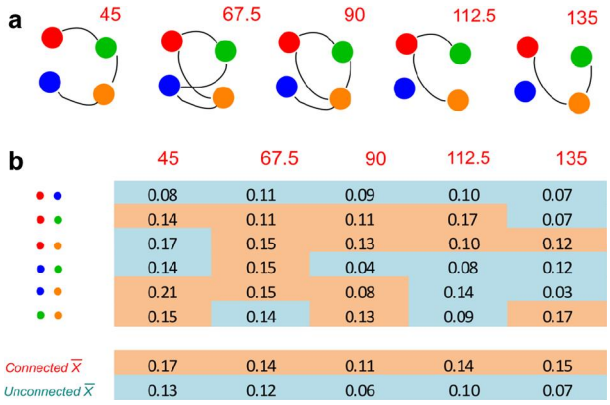

Fig. 5 An example of the dynamics of Rsc (calculated in 50-ms resolution window) in an ensemble in relation to the presented orientation. **a** Activation of an emergent microcircuit contingent upon the presented orientation within an ensemble. **b** Tabular matrix representing the mean Rsc (*red box* stands for the connected pair, *blue box* corresponds to the unconnected pair) for every pair at every presented orientation. $\bar{X}$ represents the mean (color figure online)

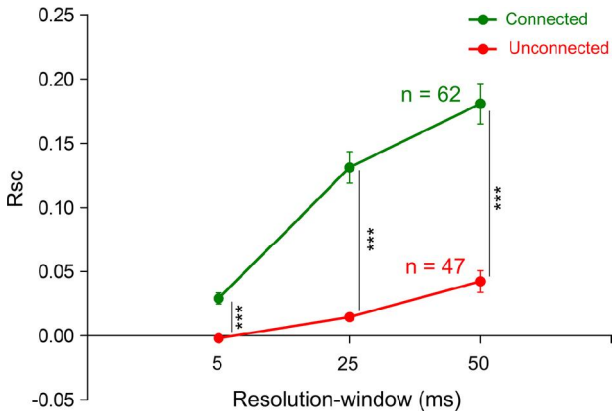

Fig. 6 Global trend for the functionally connected (*green*) and unconnected (*red*) pairs. Functionally connected neurons exhibited significantly higher noise correlation than the unconnected neuron pairs at all the resolution windows (Kolmogorov–Smirnov test, $P <$ at 0.05) (color figure online)

Significant difference between the connected and the unconnected pairs

Finally, all the connected and unconnected pairs were pooled as separate groups to observe the global trend of variation of Rsc as a function of the resolution window (Fig. 6). The mean Rsc (with SEM) for the connected pairs ($n = 62$) increased steeply from 5–25 to 50-ms window (0.02 ± 0.00 to 0.13 ± 0.01 to 0.18 ± 0.01, respectively) and significantly differed (respective values for the unconnected class were 0.00 ± 0.00; 0.01 ± 00 and 0.04 ± 00) from the unconnected pairs ($n = 47$) at every resolution window (Kolmogorov–Smirnov test, $P < 0.05$). This coincides with previous reports (Hansen et al. 2012; Schulz et al. 2015), wherein they reported that noise correlation increased with the resolution window. In summary, we may suggest that whenever two neurons in a "microcircuit" exhibit high Rsc, this may augur a functional connection between them.

Discussion

In this study, noise correlation (Rsc) was systematically compared for the connected and unconnected neuron pairs in V1 microcircuits. We found that Rsc values were significantly higher and different for the connected neuron pairs than the unconnected pairs. Further, we found that the peak probability (indicative of strength of the connection) in the CCG increases with Rsc at higher resolution windows.

Methodological considerations

The current experiments were done on anaesthetized cats, and we have already shown that the disclosed functional connections are strongly related to the presented stimulus rather than the spontaneous fluctuations in the brain—the proportion of connections was more at stimulus conditions than at spontaneous activity; the gamma power was high at stimulus presentation than at spontaneous oscillations (Bharmauria et al. 2015a, b). Many investigations have reported that nearby neurons carry high noise correlations between them (Zohary et al. 1994; Kohn and Smith 2005; Graf et al. 2011; Cossell et al. 2015). One may also argue that high noise correlation between the connected neurons in current investigation might be attributed to the artificial binning of spikes in wider resolution windows, but if it were the case we would not have obtained such trendy difference between the connected and the unconnected pairs. Moreover, Cohen and Kohn (2011) have suggested that noise correlation between the jittered spike trains (since the peaks in CCGs that revealed the functional connections were jittered in our case, that is, offset from zero) have to be calculated over higher resolution windows and longer trial durations in order to capture the full strength of Rsc. Because we used higher resolution windows and longer trial durations to calculate Rsc, we may infer that indeed the functionally connected neurons exhibit high noise correlation between their spike trains in emergent cortical microcircuits.

Functional consequences

Recently, through calcium imaging and electrode recordings in slices of mouse V1 (Cossell et al. 2015), investigators have shown that nearby neurons exhibiting high noise correlations are strongly connected to each other and are predominantly responsible for feature encoding. We found that, in general, the strength of connections increases as a function of Rsc (although in higher resolution windows) between neurons. Thus, we may suggest that neurons with higher Rsc were strongly connected to each other and played a major role in stimulus processing.

Along the same lines (as suggested by Cossell et al. 2015), we also suggest that in layer II/III, majority of the input to a strongly connected neuron (a reader neuron as postulated by Buzsáki 2010) is provided by other neurons that share the similar tuning property as the reader neuron. Indeed, this investigation extends the recent work on ensembles (Miller et al. 2014; Carrillo-Reid et al. 2015; Bharmauria et al. 2015b), wherein authors have shown that same ensembles are active in response to the stimulus and even at spontaneous oscillations. We have already reported that a signature microcircuit is activated in such an ensemble that is strictly related to the presented stimulus (Bharmauria et al. 2015b). Specifically, Carrillo-Reid et al. (2015) documented that within the sequential activation of ensembles in a Hebbian assembly, neurons fire with repeating firing patterns in an ensemble called 'doublet pathways'. Such recurring patterns of spiking activity were revealed through CCGs by us that were indicative of functional connections between neurons. Furthermore, building upon these investigations, herein, we show that within a particular microcircuit framed by an ensemble, the connected neurons systematically exhibit higher Rsc than the unconnected neurons. Moreover, we also report that Rsc between neurons is independent of the presented orientation and the neurons may or may not exhibit connections from one orientation to another irrespective of the strength of Rsc. We suggest that the "inherent" (Miller et al. 2014; Carrillo-Reid et al. 2015; Bharmauria et al. 2015b) temporal spiking pattern between neurons confers them almost equivalent Rsc along the presented orientations, but on occasions it may not be possible to reveal it through CCGs as the firing rate varies from one orientation to another. This study also relates to another recent study by Shimono and Beggs (2014), wherein they revealed such functional links in small clusters (3–6 neurons) using transfer entropy in rodent cortical slices. Collectively, this may imply that every presented stimulus drives the ensemble in such a way that, a group of neurons (connected) within it covaries its responses systematically than the group of cells (unconnected) whose firings are independent of each other. Such strongly connected neurons feature a small proportion of connected neurons in distributed cortical circuits and are implicated in major processing and transformation of information along the pathways. On the other hand, the weaker connections might be attributed to the plasticity based rules, that is, they can change (strengthen) contingent upon the input as has already been shown by Bharmauria et al. (2015b)—that a specific network between V1 neurons (layer II/III) is activated by a particular orientation. When the orientation changes, another network might be framed within the same ensemble—wherein, some connections may remain (strong) in relation to the previous orientation and other connections may become active.

From this study, we may conclude that high noise correlations between neurons in cortical microcircuits augur functional interactions between them; however, it is important to calculate noise correlations in appropriate resolution windows to extract meaningful information from these simultaneously active local cohorts of neurons. This study along with our previous studies might form a premise for computational modeling to further our understanding of neural circuits on a bigger scale.

Acknowledgments S.M and J.R were supported by CRSNG (Conseil de Recherches en Sciences Naturelles et en Génie) FRQ-NT (Fonds de recherche du Québec—Nature et technologies). Grant No. NSERC, Canada 6943-1210.

Author contribution V.B did the experiments, analyzed the data and wrote the manuscript. L.B, S.C and N.C participated in the experiments and analyses of data. J.R contributed to the analyses of data. V.B and S.M conceived the idea of study. S.M contributed to data analyses and manuscript writing.

Compliance with ethical standards

Conflict of interest The authors report no conflict of interest.

References

Abeles M (1982) Quantification, smoothing, and confidence limits for single-units' histograms. J Neurosci Methods 5:317–325

Alloway KD, Roy SA (2002) Conditional cross-correlation analysis of thalamocortical neurotransmission. Behav Brain Res 135:191–196

Alonso JM, Martinez LM (1998) Functional connectivity between simple cells and complex cells in cat striate cortex. Nat Neurosci 1:395–403

Averbeck BB, Lee D (2003) Neural noise and movement-related codes in the macaque supplementary motor area. J Neurosci 23:7630–7641

Averbeck BB, Latham PE, Pouget A (2006) Neural correlations, population coding and computation. Nat Rev Neurosci 7:358–366

Bach M, Kruger J (1986) Correlated neuronal variability in monkey visual cortex revealed by a multi-microelectrode. Exp Brain Res 61:451–456

Bachatene L, Bharmauria V, Cattan S, Rouat J, Molotchnikoff S (2015) Modulation of functional connectivity following visual adaptation: homeostasis in V1. Brain Res 1594:136–153

Bair W, Zohary E, Newsome WT (2001) Correlated firing in macaque visual area MT: time scales and relationship to behavior. J Neurosci 21:1676–1697

Bardy C, Huang JY, Wang C, FitzGibbon T, Dreher B (2006) 'Simplification' of responses of complex cells in cat striate cortex: suppressive surrounds and 'feedback' inactivation. J Physiol 574:731–750

Barlow HB, Blakemore C, Pettigrew JD (1967) The neural mechanism of binocular depth discrimination. J Physiol 193:327–342

Barthó P, Hirase H, Monconduit L, Zugaro M, Harris KD, Buzsáki G (2004) Characterization of neocortical principal cells and interneurons by network interactions and extracellular features. J Neurophysiol 92:600–608

Bharmauria V, Bachatene L, Cattan S, Rouat J, Molotchnikoff S (2014) Synergistic activity between primary visual neurons. Neuroscience 268:255–264

Bharmauria V, Bachatene L, Cattan S, Chanauria N, Rouat J, Molotchnikoff S (2015a) Stimulus-dependent augmented gamma oscillatory activity between the functionally connected cortical neurons in the primary visual cortex. Eur J Neurosci 41:1587–1596

Bharmauria V, Bachatene L, Cattan S, Brodeur S, Chanauria N, Rouat J, Molotchnikoff S (2015b) Network selectivity and stimulus discrimination in the primary visual cortex: cell-assembly dynamics. Eur J Neurosci. doi:10.1111/ejn.13101

Buzsáki G (2010) Neural syntax: cell assemblies, synapsembles, and readers. Neuron 68:362–385

Carrillo-Reid L, Miller JE, Hamm JP, Jackson J, Yuste R (2015) Endogeneous sequential cortical activity evoked by visual stimuli. J Neurosci 35:8813–8828

Cohen MR, Kohn A (2011) Measuring and interpreting neuronal correlations. Nat Neurosci 14:811–819

Cossell L, Iacaruso MF, Muir DR et al (2015) Functional organization of excitatory synaptic strength in primary visual cortex. Nature 518:399–403

Cotton RJ, Froudarakis E, Storer P, Saggau P, Tolias AS (2013) Three-dimensional mapping of microcircuit correlation structure. Front Neural Circuits 7:151

Csicsvari J, Hirase H, Czurko A, Buzsáki G (1998) Reliability and state dependence of pyramidal cell-interneuron synapses in the hippocampus: an ensemble approach in the behaving rat. Neuron 21:179–189

Denman DJ, Contreras D (2014) The structure of pairwise correlation in mouse primary visual cortex reveals functional organization in the absence of an orientation map. Cereb Cortex 24:2707–2720

Dong Y, Mihalas S, Qiu F, von der Heydt R, Niebur E (2008) Synchrony and the binding problem in macaque visual cortex. J Vis 8:1–16

Ecker AS, Berens P, Keliris GA, Bethge M, Logothetis NK, Tolias AS (2010) Decorrelated neuronal firing in cortical microcircuits. Science 327:584–587

Fujisawa S, Amarasingham A, Harrison MT, Buzsáki G (2008) Behavior-dependent short-term assembly dynamics in the medial prefrontal cortex. Nat Neurosci 11:823–833

Gawne TJ, Kjaer TW, Hertz JA, Richmond BJ (1996) Adjacent visual cortical complex cells share about 20% of their stimulus-related information. Cereb Cortex 6:482–489

Graf AB, Kohn A, Jazayeri M, Movshon JA (2011) Decoding the activity of neuronal populations in macaque primary visual cortex. Nat Neurosci 14:239–245

Gutnisky DA, Dragoi V (2008) Adaptive coding of visual information in neural populations. Nature 452:220–224

Hansen BJ, Chelaru MI, Dragoi V (2012) Correlated variability in laminar cortical circuits. Neuron 76:590–602

Harris KD, Hirase H, Leinekugel X, Henze DA, Buzsáki G (2001) Temporal interaction between single spikes and complex spike bursts in hippocampal pyramidal cells. Neuron 32:141–149

Kohn A, Smith MA (2005) Stimulus dependence of neuronal correlation in primary visual cortex of the macaque. J Neurosci 25:3661–3673

Miller JE, Ayzenshtat I, Carrillo-Reid L, Yuste R (2014) Visual stimuli recruit intrinsically generated cortical ensembles. Proc Natl Acad Sci USA 111:E4053–E4061

Perkel DH, Gerstein GL, Moore GP (1967) Neuronal spike trains and stochastic point processes. I. The single spike train. Biophys J 7:391–418

Reich DS, Mechler F, Victor JD (2001) Independent and redundant information in nearby cortical circuits. Science 294:2566–2568

Renart A, de la Rocha J, Bartho P, Hollender L, Parga N, Reyes A, Harris KD (2010) Science 327:587–590

Schulz DP, Sahani M, Carandini M (2015) Five key factors determining paiwise correlations in visual cortex. J Neurophysiol 114:1022–1033

Shadlen MN, Newsome WT (1998) The variable discharge of cortical neurons: implications for connectivity, computation, and information coding. J Neurosci 18:3870–3896

Shimono M, Beggs JM (2014) Functional clusters, hubs, and communities in the cortical microconnectome. Cereb Cortex 25:3743–3757

Sompolinsky H, Yoon H, Kang K, Shamir M (2001) Population coding in neuronal systems with correlated noise. Phys Rev E: Stat, Nonlin, Soft Matter Phys 64:051904

Uhlhaas PJ, Pipa G, Lima B, Melloni L, Neuenschwander S, Nikolić D, Singer W (2009) Neural synchrony in cortical networks: history, concept and current status. Front Integr Neurosci 3:17

Zohary E, Shadlen MN, Newsome WT (1994) Correlated neuronal discharge rate and its implications for psychophysical performance. Nature 370:140–143

Chapter 7. Interplay of orientation selectivity and the power of low- and high-gamma bands in the cat primary visual cortex

Vishal Bharmauria[a], Lyes Bachatene[a], Afef Ouelhazi[a], Sarah Cattan[a], Nayan Chanauria[a], Faustin Armel Etindele-Sosso[a], Stéphane Molotchnikoff[a,b]

a Département de Sciences Biologiques, Université deMontréal, Montréal, QC, Canada
b Universite´ de Sherbrooke, Sherbrooke, QC, Canada

Neuroscience Letters (2016) ***620*** *:14-19*

(Published article)

Neuroscience Letters 620 (2016) 14–19

Contents lists available at ScienceDirect

Neuroscience Letters

journal homepage: www.elsevier.com/locate/neulet

Research paper

Interplay of orientation selectivity and the power of low- and high-gamma bands in the cat primary visual cortex

Vishal Bharmauria[a,1], Lyes Bachatene[a,1], Afef Ouelhazi[a], Sarah Cattan[a], Nayan Chanauria[a], Faustin Armel Etindele-Sosso[a], Jean Rouat[a,b], Stéphane Molotchnikoff[a,b,*]

[a] Neurophysiology of Visual System, Université de Montréal, Département de Sciences Biologiques, Montréal, QC, Canada
[b] Département de Génie Électrique et Génie Informatique, Université de Sherbrooke, Sherbrooke, QC, Canada

HIGHLIGHTS

- The gamma-power is high for highly selective neurons in the low-gamma band.
- The gamma power is high for weakly selective neurons in the high-gamma band.
- The power in low-gamma band declines with decrease in OSI.
- The power in high-gamma band increases with decrease in OSI.
- The spike-width and OSI exhibit no relation with each other.

ARTICLE INFO

Article history:
Received 29 January 2016
Received in revised form 1 March 2016
Accepted 21 March 2016
Available online 23 March 2016

Keywords:
Gamma oscillations
Primary visual cortex
Orientation selectivity index
Ensemble

ABSTRACT

Gamma oscillations are ubiquitous in brain and are believed to be inevitable for information processing in brain. Here, we report that distinct bands (low, 30–40 Hz and high gamma, 60–80 Hz) of stimulus-triggered gamma oscillations are systematically linked to the orientation selectivity index (OSI) of neurons in the cat primary visual cortex. The gamma-power is high for the highly selective neurons in the low-gamma band, whereas it is high for the broadly selective neurons in the high-gamma band. We suggest that the low-gamma band is principally implicated in feed-forward excitatory flow, whereas the high-gamma band governs the flow of this excitation.

1. Introduction

Gamma oscillations are inevitable substrates of information processing in neural circuits [11,35], however, their role and exact mechanisms of origin are yet to be completely known [15,25]. Cell-assemblies typically reverberate in oscillatory cycles, wherein neurons synchronize their action potentials to encode the presence of the sensory stimulus within their receptive fields [16,33].

Stimulus selectivity is a fundamental property of a neuron which is indispensable for feature extraction. As a matter of fact, neurons in the primary visual cortex are orientation detectors, and thus exhibit selectivity to a specific orientation when a series of random sine-wave drifting gratings is presented within their receptive field [19,20]. The selectivity of a neuron can be inferred by computing an orientation selectivity index (OSI) that is a measure of the sharpness of its tuning [1,28]. Recently, authors [36] have shown that orientation selectivity is modulated in the gamma phase — neurons exhibit high selectivity in the rising phase of the gamma cycle. Furthermore, in the latest investigation, we have also shown that in a recurrent network of primary visual neurons, low-gamma band (30–40 Hz) is associated to regular-spiking (RS) neurons and high-gamma band (60–80 Hz) is putatively linked to fast-spiking (FS) neurons [9]. However, to date, no evidence exists between the orientation selectivity of neurons and the gamma power.

To this aim, in the present investigation, we recorded neuronal ensembles in the primary visual cortex of anaesthetized cats, and thereafter systematically examined the relation between the orientation selectivity of neurons and the power of gamma bands.

* Corresponding author at: Université de Montréal, Sciences Biologiques CP 6128 Succ. centre-ville Montréal, Québec H3C 3J7, Canada.

http://dx.doi.org/10.1016/j.neulet.2016.03.033
0304-3940/

We report that the broadly tuned neurons with low OSI exhibit high power in the high-gamma band (60–80 Hz). On the other hand, sharply tuned neurons with high OSI display high power in the low-gamma band (30–40 Hz). From these results, we may conclude that within a distributive network of layer II/III neurons, the sharply tuned neurons interact in a feed-forward excitatory flow within the low-gamma band, wherein the excitatory flow is modulated by the broadly tuned neurons in the high-gamma band.

2. Methods

2.1. Ethical approval and animal surgery

Four adult animals (Cats) were prepared for electrophysiological recordings in the primary visual cortex (area 17, layer II/III). The experiments followed the guidelines of the Canadian Council on Animal Care and were approved by the Institutional Animal Care and Use Committee of the University of Montreal. Animals were supplied by the Division of Animal Resources of the University of Montreal. The experiments were conducted in accordance with the Guide for Care and Use of Laboratory Animals of the National Institutes of Health (USA).

Briefly, cats were premedicated with acepromazine maleate (Atravet, Wyeth-Ayerst, Guelph, ON, Canada; 1 mg/kg, intramuscular) and atropine sulphate (ATRO-SA, Rafter, Calgary, AB, Canada; 0.04 mg/kg, intramuscular). Thereafter, the animals were anaesthetized with ketamine hydrochloride (Rogarsetic, Pfizer, Kirkland, QC, Canada; 25 mg/kg, intramuscular). Then the cats were paralyzed with 40 mg and maintained with 10 mg/kg/h of gallamine triethiodide (Flaxedil, Sigma Chemical, St. Louis, MO, USA; intravenous) administered in 5% dextrose lactated Ringer's nutritive solution. General anesthesia was maintained with a mixture of N_2O/O_2 (70:30) supplemented with 0.5% isoflurane (AErrane, Baxter, Toronto, ON, Canada). Electrocardiogram, electroencephalogram, rectal temperature and end-tidal CO_2 partial pressure were monitored and kept in physiological ranges throughout the experiment. The pupils were dilated with atropine sulphate (1%, Isopto-Atropine; Alcon, Mississauga, Ontario, Canada). The nictitating membranes were retracted with phenylephrine hydrochloride (2.5%, Mydfrin, Alcon). The loci of the area centrales were inferred from the position of the blind spots which were focused and projected onto a translucent screen using an ophthalmoscope. After the experiment, the cats were euthanized with an intravenous dose (0.5 mL/kg) of Sodium Pentobarbital (CEVA, Sante Animale).

2.2. Visual stimulation, electrophysiological recording, and single-unit selection

The stimulation was done in a monocular fashion. The multi-unit receptive fields (RF) were mapped as the minimum response field [6] by using an ophthalmoscope after clearly detectable neuronal activity had been obtained. These preliminary tests disclosed the qualitative properties such as dimensions, velocity-preference, orientation, and directional selectivity of neurons. A VSG 2/5 graphic board (Cambridge Research Systems, Rochester, England) was used to generate visual stimuli. Visual stimuli were displayed on a 21-inch monitor (Sony GDM-F520 Trinitron, Tokyo, Japan) placed 57 cm from the cat's eyes, with 1024 × 768 pixels, running at 100-Hz frame refresh. The blank screen was gray (~35 cd/m^2). Contrast was set at 80%. Mean luminance was 40 cd/m^2. Optimal spatial and temporal frequencies were set at 0.24 cycles/deg and a range of 1.0–2.0 Hz, respectively, where V1 neurons are known to be driven maximally by sine-wave drifting gratings [5]. Each drifting grating was presented in blocks of 25 trials (the duration of each 4.1 s) with varying inter-stimulus (1–3 s) intervals during which no stimulus was presented. Hence, the presentation of a stimulus lasted 180 s, with all the trials and inter-stimulus intervals. Multi-unit activity in the primary visual cortex was recorded by a tungsten multi-electrode (Frederick Haer & Co, Matrix Electrode; the multi-electrode had four columns, and each column had one row). The recordings were performed at locations 410 or 820 μm apart. The excitatory RFs were located centrally within a 15° radius from the fovea. Fourteen recordings (28 sites) were done across all cats either in the left or the right hemisphere. Recordings were performed in the supragranular layers (cortical depth < 1000 μm; mean = 650 μm). The signal from the microelectrodes was amplified, band-pass filtered (300 Hz–3 kHz), digitized and recorded with a 0.05 ms temporal resolution (Spike2, CED, Cambridge, England). Spike sorting from the multi-unit signals was done. Neurons were discriminated on the basis of three criteria: 1) the spike-waveform difference 2) principal component analysis (PCA) showing well dissociated clusters 3) and auto-correlograms (ACG) showing no events (indicative of the refractory period of neuron) at the central point [7,10,14].

2.3. Orientation tuning and OSI (Orientation Selectivity Index) computation

Once single cells had been sorted out offline from multi-unit spike trains accumulated during data acquisition, orientation tuning curves of cells were obtained from raw data and fitted with the von Mises function [31].

$$M(\theta) = A.e^{b(\cos(\theta - c))} + d \quad (1)$$

where, A is the value of the function at the preferred orientation 'c', and 'b' is the width parameter. An additional parameter 'd' represents the spontaneous firing rate of the cell. $M(\theta)$ is the firing rate of the neuron at orientation, 'θ'. This allowed us to determine the preferred orientation of every cell. An orientation selectivity index (OSI) was calculated to ensure the tuning of neurons. It was measured using the fitted tuning curves by dividing the firing rate at the baseline (orthogonal orientations) by the firing rate at the preferred orientation, and subtracting the result from one [3,23,27]. The closer the OSI is to one, the stronger the orientation selectivity.

2.4. Perievent spectrogram analysis

The analysis was performed with NEUROEXPLORER 4 (Nex Technologies). For each selected variable, this analysis results in multiple spectrograms that start at the specified time after the occurrence of each reference event (stimulus onset). These spectrograms are then averaged over all of the reference events. An optimal or a near optimal orientation for the neurons was chosen to generate the spectrograms. The power spectra were calculated by the use of 512 frequencies between 1 and 120 Hz, smoothed with a Gaussian kernel with a bin-width of 3. The analysis window lasted 4 s (1 s before the stimulus and 3 s after the stimulus onset). The sliding window (shift) was set at 20 ms (i.e. 200 shifts for the window of analysis). The power spectrum was calculated for the specified number (number of shifts) of windows. For a time-stamped variable, the rate histogram was calculated and copied into a signal array. The parameters were used as follows:

$$\text{Histogram start} = \text{start} + \text{shift} \times (\text{window number} - 1)$$

$$\text{Bin} = 1/(2 \times \text{maximum frequency})$$

$$\text{Number of Bins} = 2 \times \text{Number of Frequency Values}$$

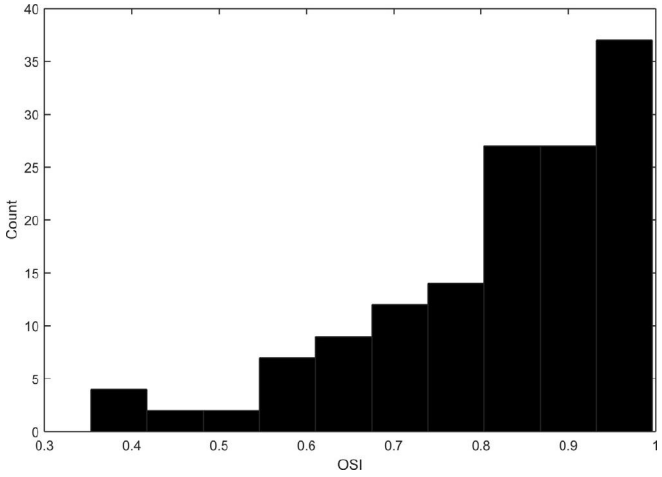

Fig. 1. Distribution of orientation selectivity index (OSI).

In other words, in response to a timestamp t, for a neuron under analysis, a bunch of histograms in time intervals (t + Histogram Start, t + Histogram Start + Bin × Number of bins) was calculated. For each interval, rate histograms were calculated and detrended, Hanning window was applied and FFTs (Fast Fourier transform) were calculated. Then the individual and cross-densities were computed. Finally, the FFT analysis on these rate histograms produced a single spectrogram for timestamp t.

3. Results

In this study, 141 neurons were analyzed across 28 sites in four cats. The major goal of the investigation was to distinguish the broadly tuned and narrowly tuned neurons and relate each of the classes to the power of gamma oscillations in response to the application of the stimulus.

3.1. Categorization of neurons

The OSI distribution of neurons in shown in Fig. 1. To begin with, based upon the literature [3,29,32], neurons were arbitrarily categorized as broadly and sharply tuned in relation to the OSI. To dissociate neurons, the OSI threshold was set at 0.7 — neurons with OSI ≥ 0.7 were considered narrowly tuned (n = 114), whereas neurons with OSI less than 0.7 were classified as broadly tuned (n = 27).

3.2. Sharply tuned neurons exhibit high power in low-gamma band and vice versa

Cortex is filled with many types of neurons and indeed visual neurons show varied selectivity in response to stimuli in the cortex [1]. Thus, we further sought to examine the relation of the power of gamma bands with the broadly tuned and sharply tuned neurons. Fig. 2a and b show typical examples of a broadly tuned neuron (OSI = 0.57) and a sharply tuned neuron (OSI = 0.95) respectively (the respective responses of neurons are shown in Fig. 2c and d). Further, we computed peri-event spectrograms on the visual responses of neurons until 3 s after the stimulus onset (see Section 2). Fig. 2e shows the spectrogram of the broadly tuned neuron and Fig. 2f illustrates the spectrogram of the sharply tuned neuron. The broadly tuned neuron reverberates principally at higher gamma frequency as indicated by the black arrows, and this is further accentuated in Fig. 2g. The shaded area highlights the peak at high-gamma band around 60–80 Hz. On the contrary, the sharply tuned neuron exhibits high power in the low-gamma band as depicted by the white arrows. The frequency-power curve in Fig. 2h further shows that the sharply tuned neuron exhibits high power in the low-gamma band (shaded gray area, approximately 30–40 Hz).

3.3. Interplay of gamma power and orientation selectivity

Thereafter, we pooled the respective spectrograms of the broadly tuned and sharply tuned neurons as separate classes (Fig. 3a) and we found that the power for sharply tuned neurons (black curve) is higher in the low-gamma band (approximately 30–40 Hz); whereas the power is high in the high-gamma band (around 60–70 Hz) for the broadly tuned neurons (gray curve). Both curves were found to be significantly different in both bands (Mann-Whitney *U* test, $p < 0.005$). The neuronal dissociation above was an arbitrary choice based on the literature [3,29,32]. To investigate whether the gamma power showed any systematic relationship with OSI, we computed the gamma power (low and high band) as a function of the OSI classes (Fig. 3b). We found the power of gamma (mean ± SEM) in low band systematically decreased with the decline in OSI (linear regression, $R^2 = 0.80$), whereas the power in the high gamma band increased with the decrease in OSI (linear regression, $R^2 = 0.92$). Note that two neurons were eliminated from this analysis as they exhibited OSI less than 0.4.

3.4. Spike-width and gamma power

Finally, we categorized neurons as regular spikes (RS) and fast-spikes (FS) based upon their spike-width and related them to the power of gamma oscillations in both bands. RS neurons are putatively linked to the excitatory neurons, whereas FS neurons are putatively associated with the inhibitory neurons [24,34]. In fact, the relationship was found to be opposite between the spike-width and the power of gamma in low and high-gamma bands (Fig. 4). The power of oscillations was found to be significantly higher (Mann-Whitney *U* Test, $p < 0.005$) for FS neurons than the RS neurons in the low-gamma band, whereas no significant difference was observed between these classes in the high-gamma band. Therefore, it seems that the systematic difference in gamma power between two distinct classes based on OSI does not relate to the distinction between neurons based upon their spike-width. This maybe particularly due to the fact that spike-width is not a reliable parameter to dissociate neurons into RS and FS in the cat visual cortex, as a fraction of excitatory neurons may exhibit FS pattern in cats [26].

4. Discussion

In this investigation we report that the orientation selectivity of a neuron is linked to the gamma power that it exhibits — highly orientation-selective neurons exhibit high power in the low-gamma band (30–40 Hz), whereas neurons displaying low orientation selectivity exhibit high power in the high-gamma band (60–80 Hz).

The current experiments were performed in the primary visual cortex of cats and it has been amply demonstrated that gamma oscillations that potentiate neural synchronization can be recorded in anaesthetized animals [16]. Moreover, we have already shown that these gamma oscillations recorded in our case are strongly linked to the presented stimulus [9], and cannot be associated to any attentional parameters.

4.1. Functional consequences

In an investigation, Womelsdorf et al. [36] have shown that orientation selectivity is modulated within the gamma cycle — a

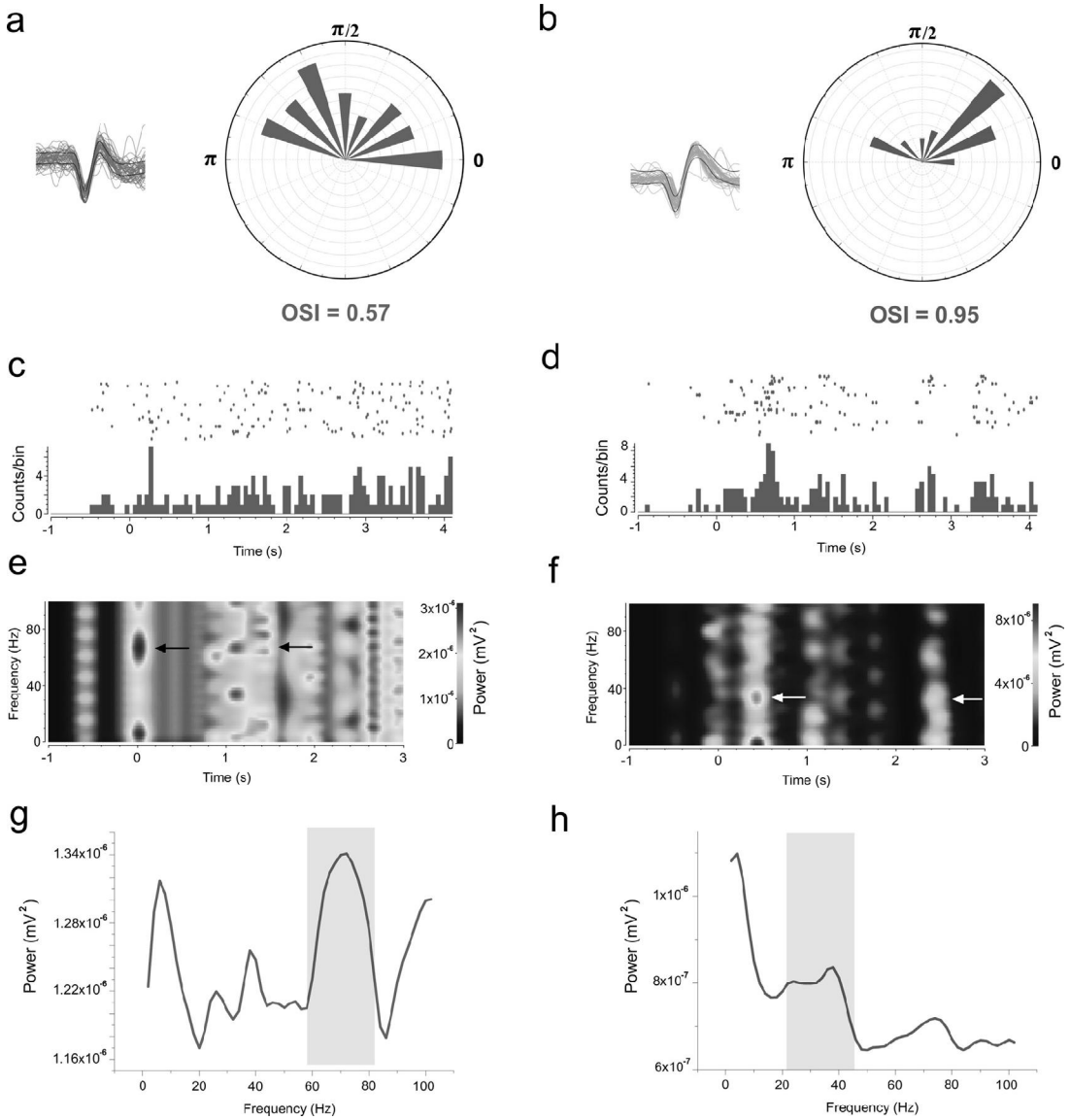

Fig. 2. Gamma power for broadly and sharply tuned neurons. (a) Polar plot of a broadly tuned neuron (OSI = 0.57) with its spike waveform. (b) Polar plot of a sharply tuned neuron (OSI = 0.95) with its spike waveform. (c, d) Respective visual responses for the broadly and sharply tuned neruons shown above. (e) Stimulus-triggered perievent spectrogram for the broadly tuned neuron. Notice the high gamma power in two epochs (60–70 Hz) as indicated by the black arrow. (f) Stimulus-triggered spectrogram for the sharply tuned neuron. The power of gamma is high in the low-band (30–40 Hz) as indicated by the white arrows. (g, h) Mean frequency-power curves for the broadly and sharply tuned neurons shown above. The gray shaded area corresponds to the distinct zone of high gamma activity.

neuron displays high orientation selectivity during the rising phase of gamma cycle, thereby carrying the maximum information about the stimulus. Indeed, along with previous investigations [17,33] and results demonstrated from our lab [9], there is evidence that gamma cycle creates a window of opportunity for coordinated neuronal firing through a cyclic loop of excitatory and inhibitory currents. Within this recurrent excitatory-inhibitory loop (wherein excitation leads inhibition), the maximum depolarization occurs at the mean phase of the gamma cycle which is crucial in triggering postsynaptic spikes. Pyramidal neurons are densely innervated with inhibitory neurons in the cortex. Many reports have concluded that neurons with high OSI are excitatory in nature, whereas neurons showing low OSI are inhibitory in nature [1,18]. Furthermore, we have also reported that the low-gamma band (30–40 Hz) power is linked predominantly to the interaction between regular-spiking (RS) neurons, whereas the high-band (60–80 Hz) gamma is associated mainly with the interactions of fast-spiking (FS) neurons with other neurons (FS or RS). Moreover, within V1 assemblies, on average RS neurons connect more RS neurons than FS neurons [9] and untuned neurons do not exhibit many functional connections [8]. However, in this study, no relation was found between the spike-width and the OSI of neurons. This may be due to the fact that in the cat visual cortex, spike-width dissociation of neurons is not a completely valid parameter as some excitatory neurons may show FS pattern [26]. But with our previous finding [9], it may also point to the fact that only specific interactions between FS and other neurons (RS/FS) give rise to the high-gamma band. Similar analysis on monkeys and mice may better reflect upon the relation between the OSI and the spike-width. Integrating all above findings we suggest that, within the window of opportunity [9,30] in a distributive network, the highly orientation-selective neurons depolarize steeply in the rising phase of low-gamma band leading to the triggering of spikes in nearby postsynaptic neurons. On the other hand, the weakly selective neurons depolarize within the mean phase of the

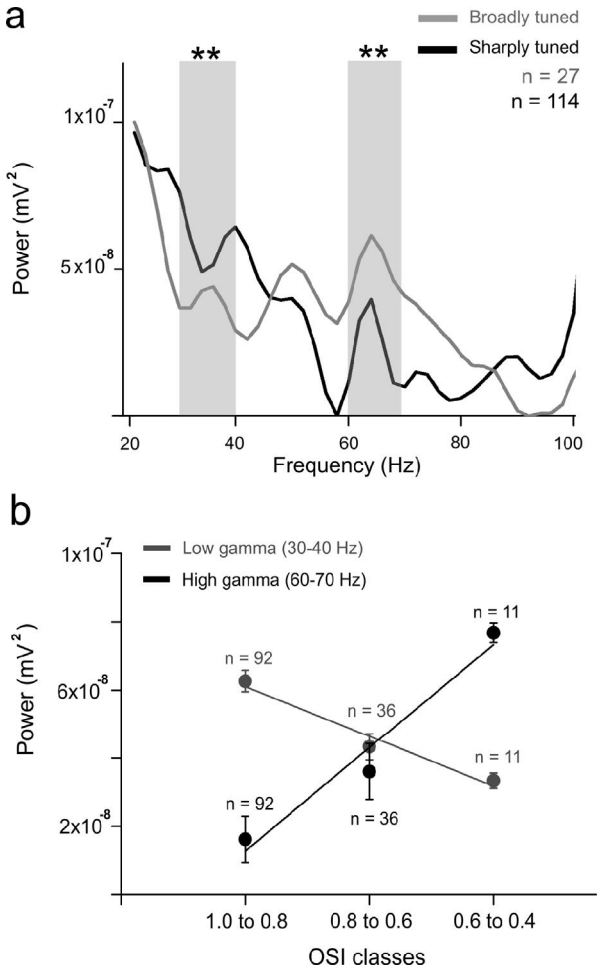

Fig. 3. Orientation selctvity index and gamma power. (a) Mean frequency-power curves for the broadly (gray) and sharply (black) tuned neurons. The broadly tuned neruons principally oscillate in the high-gamma band, whereas the sharply tuned neurons oscillate in the low band. (b) Frequency-power curves for the low and high gamma bands as a function of the OSI. Note: two neurons have been eliminated from this analysis as they exhibited OSI < 0.4. The bars represent the SEM.

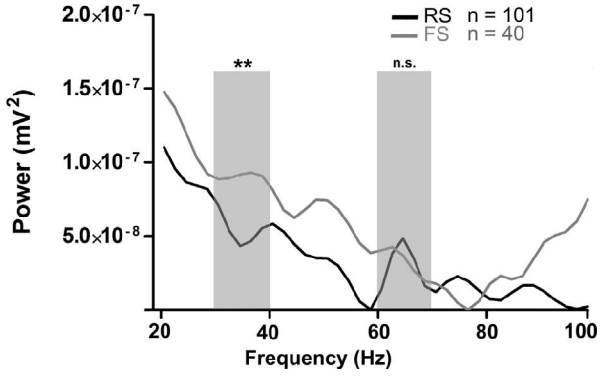

Fig. 4. Relationship between the spike-width and the power of oscillations in the low- and high-gamma bands.

high-gamma band, thereby regulating the activity of the RS neurons or depolarizing other neurons (RS or FS). Indeed, it has been postulated that a neuron contains synapses corresponding to every orientation on its dendrites [3,21]. However, when a particular orientation is presented, it may drive the neuronal response toward this specific orientation by activating the corresponding synapses, consequently making the neuron more selective to this orientation. Such highly selective neurons mainly receive the information from the lateral geniculate nucleus (LGN), thereby setting the orientation selectivity of a neuronal population [4]. On the other hand, when all the synapses are equally activated on neuronal dendrites, the selectivity of a neuron is low. These broadly tuned neurons maybe well situated to perform divisive normalization [12] and control the balance of excitation and inhibition in cortical circuits [13]. The more selective a neuron is, the more it is implicated in the excitatory flow; on the contrary, the least selective it is, the more it is involved in regulating the activity of a broad spectrum of neuronal population [2]. Within this context, sharply tuned neurons which are more involved in excitation fire sparsely [22], thus exhibiting pronounced activity in the low-gamma band, whereas broadly tuned neurons exhibit episodes of high firing, thereby reverberating in the high-gamma band. Put simply, in cortical circuits, the sharply tuned neurons are principally responsible for feed-forward excitation in the low-gamma band, wherein their activity is consistently modulated by broadly tuned neurons by creating regulatory feed-back loops in the high-gamma band.

5. Conclusion

In conclusion, in primary visual circuits, the highly selective and weakly selective neurons have salient roles to play in distinct gamma bands to systematically process the visual information.

Conflict of interest

The authors declare no conflict of interest.

Author contributions

VB did the experiments, analyzed the data and wrote the manuscript. LB prepared the figures. LB, JR, AO, SC, NC, FAE participated in experiments and analyses of data. VB conceived the idea of study. SM contributed to the manuscript writing.

Acknowledgements

SM and JR were supported by CRSNG (Conseil de Recherches en Sciences Naturelles et en Génie) and FRQ-NT (Fonds de recherche du Québec—Nature et technologies). Grant no: 6943-2010-RGPIN.

References

[1] B.V. Atallah, W. Bruns, M. Carandini, M. Scanziani, Parvalbumin-expressing interneurons linearly transform cortical responses to visual stimuli, Neuron 73 (2012) 159–170.
[2] L. Bachatene, V. Bharmauria, S. Cattan, N. Chanauria, J. Rouat, S. Molotchnikoff, Electrophysiological and firing properties of neurons: categorizing soloists and choristers in primary visual cortex, Neurosci. Lett. 604 (2015) 103–108.
[3] L. Bachatene, V. Bharmauria, S. Cattan, S. Molotchnikoff, Fluoxetine and serotonin facilitate attractive-adaptation-induced orientation plasticity in adult cat visual cortex, Eur. J. Neurosci. 38 (2013) 2065–2077.
[4] L. Bachatene, V. Bharmauria, J. Rouat, S. Molotchnikoff, Adaptation-induced plasticity and spike waveforms in cat visual cortex, Neuroreport 23 (2012) 88–92.
[5] C. Bardy, J.Y. Huang, C. Wang, T. FitzGibbon, B. Dreher, 'Simplification' of responses of complex cells in cat striate cortex: suppressive surrounds and 'feedback' inactivation, J. Physiol. 574 (2006) 731–750.
[6] H.B. Barlow, C. Blakemore, J.D. Pettigrew, The neural mechanism of binocular depth discrimination, J. Physiol. 193 (1967) 327–342.
[7] P. Bartho, H. Hirase, L. Monconduit, M. Zugaro, K.D. Harris, G. Buzsaki, Characterization of neocortical principal cells and interneurons by network interactions and extracellular features, J. Neurophysiol. 92 (2004) 600–608.
[8] V. Bharmauria, L. Bachatene, S. Cattan, S. Brodeur, N. Chanauria, J. Rouat, S. Molotchnikoff, Network-selectivity and stimulus-discrimination in the primary visual cortex: cell-assembly dynamics, Eur. J. Neurosci. 43 (2016) 204–219.
[9] V. Bharmauria, L. Bachatene, S. Cattan, N. Chanauria, J. Rouat, S. Molotchnikoff, Stimulus-dependent augmented gamma oscillatory activity between the

functionally connected cortical neurons in the primary visual cortex, Eur. J. Neurosci. 41 (2015) 1587–1596.
[10] V. Bharmauria, L. Bachatene, S. Cattan, J. Rouat, S. Molotchnikoff, Synergistic activity between primary visual neurons, Neuroscience 268 (2014) 255–264.
[11] G. Buzsaki, Neural syntax: cell assemblies, synapsembles, and readers, Neuron 68 (2010) 362–385.
[12] M. Carandini, D.J. Heeger, J.A. Movshon, Linearity and normalization in simple cells of the macaque primary visual cortex, J. Neurosci. 17 (1997) 8621–8644.
[13] F.S. Chance, L.F. Abbott, A.D. Reyes, Gain modulation from background synaptic input, Neuron 35 (2002) 773–782.
[14] J. Csicsvari, H. Hirase, A. Czurko, G. Buzsaki, Reliability and state dependence of pyramidal cell–interneuron synapses in the hippocampus: an ensemble approach in the behaving rat, Neuron 21 (1998) 179–189.
[15] P. Fries, D. Nikolic, W. Singer, The gamma cycle, Trends Neurosci. 30 (2007) 309–316.
[16] C.M. Gray, W. Singer, Stimulus-specific neuronal oscillations in orientation columns of cat visual cortex, Proc. Natl. Acad. Sci. U. S. A. 86 (1989) 1698–1702.
[17] B. Haider, D.A. McCormick, Rapid neocortical dynamics: cellular and network mechanisms, Neuron 62 (2009) 171–189.
[18] S.B. Hofer, H. Ko, B. Pichler, J. Vogelstein, H. Ros, H. Zeng, E. Lein, N.A. Lesica, T.D. Mrsic-Flogel, Differential connectivity and response dynamics of excitatory and inhibitory neurons in visual cortex, Nat. Neurosci. 14 (2011) 1045–1052.
[19] D.H. Hubel, T.N. Wiesel, Receptive fields of single neurones in the cat's striate cortex, J. Physiol. 148 (1959) 574–591.
[20] D.H. Hubel, T.N. Wiesel, Receptive fields, binocular interaction and functional architecture in the cat's visual cortex, J. Physiol. 160 (1962) 106–154.
[21] H. Jia, N.L. Rochefort, X. Chen, A. Konnerth, Dendritic organization of sensory input to cortical neurons *in vivo*, Nature 464 (2010) 1307–1312.
[22] M. Krupa, S. Gielen, B. Gutkin, Adaptation and shunting inhibition leads to pyramidal/interneuron gamma with sparse firing of pyramidal cells, J. Comput. Neurosci. 37 (2014) 357–376.
[23] D.S. Liao, T.E. Krahe, G.T. Prusky, A.E. Medina, A.S. Ramoa, Recovery of cortical binocularity and orientation selectivity after the critical period for ocular dominance plasticity, J. Neurophysiol. 92 (2004) 2113–2121.
[24] C.M. Niell, M.P. Stryker, Highly selective receptive fields in mouse visual cortex, J. Neurosci. 28 (2008) 7520–7536.
[25] D. Nikolic, P. Fries, W. Singer, Gamma oscillations: precise temporal coordination without a metronome, Trends Cogn. Sci. 17 (2013) 54–55.
[26] L.G. Nowak, R. Azouz, M.V. Sanchez-Vives, C.M. Gray, D.A. McCormick, Electrophysiological classes of cat primary visual cortical neurons in vivo as revealed by quantitative analyses, J. Neurophysiol. 89 (2003) 1541–1566.
[27] A.S. Ramoa, A.F. Mower, D. Liao, S.I. Jafri, Suppression of cortical NMDA receptor function prevents development of orientation selectivity in the primary visual cortex, J. Neurosci. 21 (2001) 4299–4309.
[28] D.L. Ringach, R.M. Shapley, M.J. Hawken, Orientation selectivity in macaque V1: diversity and laminar dependence, J. Neurosci. 22 (2002) 5639–5651.
[29] B. Scholl, A.Y. Tan, J. Corey, N.J. Priebe, Emergence of orientation selectivity in the Mammalian visual pathway, J. Neurosci. 33 (2013) 10616–10624.
[30] J.H. Siegle, D.L. Pritchett, C.I. Moore, Gamma-range synchronization of fast-spiking interneurons can enhance detection of tactile stimuli, Nat. Neurosci. 17 (2014) 1371–1379.
[31] N.V. Swindale, Orientation tuning curves: empirical description and estimation of parameters, Biol. Cybern. 78 (1998) 45–56.
[32] A.Y. Tan, B.D. Brown, B. Scholl, D. Mohanty, N.J. Priebe, Orientation selectivity of synaptic input to neurons in mouse and cat primary visual cortex, J. Neurosci. 31 (2011) 12339–12350.
[33] P. Tiesinga, T.J. Sejnowski, Cortical enlightenment: are attentional gamma oscillations driven by ING or PING? Neuron 63 (2009) 727–732.
[34] M. Vinck, T. Womelsdorf, E.A. Buffalo, R. Desimone, P. Fries, Attentional modulation of cell-class-specific gamma-band synchronization in awake monkey area V4, Neuron 80 (2013) 1077–1089.
[35] T. Womelsdorf, P. Fries, P.P. Mitra, R. Desimone, Gamma-band synchronization in visual cortex predicts speed of change detection, Nature 439 (2006) 733–736.
[36] T. Womelsdorf, B. Lima, M. Vinck, R. Oostenveld, W. Singer, S. Neuenschwander, P. Fries, Orientation selectivity and noise correlation in awake monkey area V1 are modulated by the gamma cycle, Proc. Natl. Acad. Sci. U. S. A. 109 (2012) 4302–4307.

8. GENERAL DISCUSSION

One must still have chaos in oneself to be able to give birth to a dancing star.

— *Friedrich Nietzsche*

This thesis investigated ensembles in the primary visual cortex of anaesthetized cats. The main findings of the current investigation are: 1) Neurons in these ensembles cooperate synergistically in a 50-ms window of opportunity. 2) Within these ensembles, the connected neurons exhibit high gamma power compared with the unconnected neurons in the 50-ms window of opportunity. 3) A 'signature' functional network is activated at every presented orientation within an ensemble. 4) The connected neurons systematically display high noise correlation than the unconnected neurons within these ensembles. 5) The orientation selectivity index (OSI) of neurons is systematically related to the power of oscillations in the low- and high-gamma bands.

8.1 Methodological considerations

8.1.1 State of the animal

Anaesthetized animals have widely been used as models to study the brain. Anaesthesia affects the frequency of neuronal discharge — in principle, neurons fire more sparsely, that is, with lower firing rates during anaesthesia than in behaving animals (Barth & Poulet, 2012). Indeed, many reports have documented that oscillatory activity that potentiates neural synchronization can be recorded in anaesthetized animals (Gray *et al.*, 1989; Gray & Singer, 1989). One may also argue as to whether these revealed micro-connectomes and the spread of gamma oscillations between neurons resulted from the co-stimulation of neurons. In other words, were the connections artificially induced between neurons because of simultaneous stimulation? As mentioned above, the CCG strategy was employed to disclose the functional connections between neurons. It is to be underlined that the spike trains of neurons were shifted by a few trials

to remove the stimulus-locked and evoked components. Moreover, the targets were applied in a random fashion to eliminate the notion of anticipation in the brain. On a different note, it has also been reported that spontaneous oscillations in anaesthetized animals could induce correlations between neuronal firing (Poulet & Petersen, 2008). However, only a few connections were divulged at the spontaneous activity. Moreover, a salient network was activated within an ensemble in response to a stimulus that remained stable over a period of time; the closely tuned neurons exhibited vigorous connectivity with augmented synergy; the connected neurons displayed heightened gamma activity than the unconnected neurons. Furthermore, as the synergistic cross-influence was effected within a relatively brief time-window of 50 ms, such a short epoch cannot accommodate spontaneous fluctuations of response modulations. All these trends along with other systematic patterns point to the fact that, indeed, the emergent functional micro-connectomes were strictly related to the applied orientation.

8.1.2 Spike sorting from the multiunit activity

The sorting of spikes from the multiunit activity is an important step in careful separation of neurons. Indeed, when many neurons are isolated from a microelectrode, one has to be cautious in determining the validity of a neuron because of the overlapping spikes and the bursting of neurons (Quiroga, 2012; Rey *et al.*, 2015). To further confirm the individuality of sorted spikes, autocorrelgrams (ACG) and principal component analysis (PCA) were computed (Csicsvari *et al.*, 1998; Bartho *et al.*, 2004; Fujisawa *et al.*, 2008). A blank period at zero time-lag in the ACG verified the refractory period of a neuron, whereas the PCA analysis ascertained a separate cluster corresponding to a spike within a Mahalanobis distance of 2.5.

8.1.3 Response output and CCGs

The CCG computation depends upon the number of spikes accumulated over the stimulus-duration to detect significant peaks. As described earlier, anaesthesia may also suppress the activity of neurons (de Kock & Sakmann, 2009; Barth & Poulet, 2012). In

this study, the responses were accumulated over 25 trials, each of which lasted 4.1 sec. This experimental time was relatively long to collect sufficient spikes for CCG generation. Indeed, in these findings, the connected and unconnected neurons exhibited comparable firing rates. This suggests that neurons fire in systematic time-relationships with each other irrespective of the firing rates. However, the possibility of some connections having gone undetected cannot be eliminated.

8.2 The stimulus encoding assembly and its characteristics

A prevalent hypothesis in neurosciences is that ephemerally active cohorts of neurons termed 'cell-assemblies' are fundamental to information processing in the brain — from encoding memories, to behaving, to reasoning or, in general, to almost everything (Drew *et al.*, 2008; Buzsaki, 2010; Garner & Mayford, 2012; Harris & Mrsic-Flogel, 2013; Herry & Johansen, 2014; Shimono & Beggs, 2015). However, a consensus on emergence and disbanding of these assemblies is an elusive 'Holy grail' for neuroscientists. Indeed, since the proposition of cell-assembly theory by Donald Hebb until now, many investigations (Csicsvari *et al.*, 1998; Bartho *et al.*, 2004; Fujisawa *et al.*, 2008; Buzsaki, 2010; Kampa *et al.*, 2011; Ko *et al.*, 2011; Denman & Contreras, 2014; Carrillo-Reid *et al.*, 2015) have sought to examine the origins and dynamics of these assemblies, and it appears that we are on the verge of disclosing these carefully knit neural processes. It is to be underlined that, within the context of this thesis, simultaneously recorded neurons from a microelectrode were termed an assembly or an ensemble. This type of encoding by neuronal assemblies has been defined as the distributive system of encoding (Bernardet & Verschure, 2010; Buzsaki, 2010; Molotchnikoff & Rouat, 2012; Behrmann & Plaut, 2013). Within the framework of distributive encoding, the results of this investigation have been discussed below.

8.2.1 Synergy and the 50-ms window of opportunity

In the first part of this investigation it was revealed that, within V1 ensembles, a neuron impinges significantly upon the activity of its companion neuron(s) for about 50-

ms period. This synergistic cross-influence was shown to be systematically higher for the connected neurons compared with the unconnected neurons in these ensembles. Further, the synergy between the connected neurons decreased as a function of the orientation spread of neurons. In addition, these connected neurons were swayed by an increase in the gamma oscillatory power compared with the unconnected neurons. Indeed, this augmented oscillatory power coincided with the 50-ms window of opportunity for synergistic cross-influence between them.

The visual cortex is involved in many tasks besides only object recognition (DiCarlo & Cox, 2007; DiCarlo *et al.*, 2012). These include tracking of the object, obstacle avoidance, grasping and many other tasks. To accomplish these tasks, studies on monkeys and humans suggest that it may take less than 200 ms to fully recognize the image, even without any attentional pre-cuing (Fabre-Thorpe *et al.*, 1998; Keysers *et al.*, 2001; Rousselet *et al.*, 2002). This typical "blink of the eye" epoch is sufficient to identify and process any vision related task. This has been termed as 'core recognition' by DiCarlo and Cox (DiCarlo & Cox, 2007). Moreover, this time period also coincided with the saccadic eye movements (Rubin & Turano, 1992; McMahon *et al.*, 1993). The information about the image is processed and conveyed through a retinotopic hierarchical stream in the visual system (Felleman & Van Essen, 1991; DiCarlo *et al.*, 2012). Within the conventional information flow from the thalamus (LGN) to the cortex, the first visually triggered response is recorded at about 50 ms from the retina (Felleman & Van Essen, 1991; Schmolesky *et al.*, 1998; DiCarlo *et al.*, 2012). The successive visual areas are systematically lagged by about 10 ms time interval. Therefore, it appears that the representation of an image does not stay any longer than 50 ms in any given cortical regime (Schmolesky *et al.*, 1998). Authors (Maunsell & Gibson, 1992; Logothetis *et al.*, 1994; Desimone & Duncan, 1995; DiCarlo *et al.*, 2012) have suggested that, it takes about 100 ms since the point image-photons impinge upon the retina until the first wave of activity hits the IT. This phenomenon encompasses a combination of intra- and inter-area processing of the visual image. Moreover, investigators have also previously postulated that 50-ms time window is sufficient to encode the 'majority' of information

about the stimulus (Maunsell & Gibson, 1992; Rolls & Tovee, 1994). In fact, this characteristic time-period is even large enough to process any complex stimuli.

The recordings in this study were performed in layer II/III of V1 in cats. Indeed, this corresponds to one of the layers of the visual flow as discussed above. Within the framework of a distributive system (Bernardet & Verschure, 2010; Molotchnikoff & Rouat, 2012; Behrmann & Plaut, 2013), specific intra-area computations between neurons are responsible for the processing of information through this stage, that is, there are dedicated V1 circuits for information retrieval from the image. A selected group of cells within an ensemble that exhibits synergistic collaboration may be entrusted with major and specific roles within the circuit. Reports have suggested that, within ensembles, there is a core group of neurons which is always active, and neurons comprising it are strongly connected to each other (Barth & Poulet, 2012). Hence, the redundant information routing resulting from enhanced connectivity between these neurons may lessen the communication ambiguity within the circuit. The 50-ms window creates an opportunistic epoch for the synergistic coupling between neurons — within this period of augmented excitation, the gates are open for the recipient assemblies to process the feature (Nadasdy, 2000; Tiesinga & Sejnowski, 2009; Wang *et al.*, 2010) and even transmit the information downstream (Tiesinga & Sejnowski, 2009; Siegle *et al.*, 2014). Such a model would only drive the information through the selection of specific routing channels within an assembly and obliteration of irrelevant inputs. In short, within this framework, the stimulus-dependent saliency of a microcircuit is promoted.

8.2.2 Gamma oscillations: the waves that an assembly rides on

Gamma oscillations (typically 30–100 Hz) in the brain are believed to be inevitable substrates of information processing across species (Buzsaki & Watson, 2012; Fries, 2015); however, their roles, origins and exact mechanisms are yet to be completely understood. On the other hand, there is even a contentious debate (Brunet *et al.*, 2014; Ray & Maunsell, 2015) on the role of gamma oscillations, as at times it is difficult to

empirically measure their strength, mainly because of their weak power. Undoubtedly, it seems that the causes of this debate have to be investigated in-depth.

Many decades ago, a hypothesis (binding-by-synchrony) emerged that rests on the principle that a particular group of neurons within an ensemble synchronizes its spikes within gamma oscillations for stimulus encoding (Milner, 1974; Singer, 1999; Salinas & Sejnowski, 2001). A peak straddling zero in the CCG is defined as precise synchrony (Singer, 1999), however, quasi-synchronous peaks indicating functional connections may also emerge in CCGs (Fujisawa *et al.*, 2008; Schwindel *et al.*, 2014). The backbone of neuronal communication through gamma oscillations underlines the importance of neuronal synchronization (Singer, 1999; Fries, 2015). Fries, in his latest communication through coherence (CHC) hypothesis (Fries, 2005; 2015) has formulated that an activated neuronal group engages in rhythmic synchronization, wherein excitation and inhibition flow in short temporal windows. Put simply, if two spike trains are coherent, that is, when they spike together within a coincident temporal window, they most likely will have effective connectivity. On the other hand, if inputs arrive randomly within the excitatory cycle, most likely the neurons will have lower effective connectivity.

In this investigation, using spike-triggered PSTH analysis, it was revealed that the reference neuron in a connected neuron pair in an assembly modulates the response of the target neuron, and switches it into the gamma oscillatory band with enhanced power. On the contrary, the unconnected neurons within these ensembles fail to exhibit such tendency — the power of gamma oscillations was much lower than the connected pairs. It is to be noted that all of the neurons were activated with the same stimulus. Furthermore, it was observed that there was an augmented coherence for the connected pairs compared with the unconnected pairs. These findings almost exclusively fit the CHC hypothesis (Fries, 2015). Indeed, when there is a systematic quasi-synchronous time-relationship between neuronal spike trains (that is, when one neuron makes another neuron fire), coherence emerges momentarily between their respective spike trains, eventually leading to the higher power of gamma oscillations between them. And as revealed before, all these dynamics occur within a 50-ms window of opportunity (that is, the input and output gates are open at the same time for neurons to collaborate) which is

almost indispensable for the coincident flow of excitatory and inhibitory loops (Tiesinga & Sejnowski, 2009; Siegle *et al.*, 2014). In short, gamma oscillations systematically emerge between the connected neurons in emergent circuits. This also suggests that, in general, different oscillatory rhythms originate from this systematic phase-relationship between neuronal firing.

8.2.2.1 Reconciling the debate on gamma oscillations

As mentioned already, there is a debate on the role of gamma oscillations in the cortex (Brunet *et al.*, 2014; Ray & Maunsell, 2015). This may be due to the fact that their power is usually inconsistent and weak. Moreover, they have a low dependence on low-level features of the stimulus, and even problems related to the conduction delays and contamination due to the spiking activity (Brunet *et al.*, 2014). In short, their occurrence and power depend on several systemic (brain state) and stimuli factors. Traditionally, gamma oscillations are measured using electroencephalogram (EEG) or local field potentials (LFP). The former employs surface electrodes on the brain, whereas the latter is measured using microelectrodes that are implanted within the region of interest in the brain. Characteristically, both techniques measure the activity of a local population of neurons.

By contrast, a different technique was used to measure the gamma-power in this investigation. At the outset, neurons (spike-waveforms) were separated from the neuronal activity by filtering out the LFPs (below 300 Hz). Understandably, the response output was in the form of spikes. Thereafter, the spike-triggered spectrograms were computed between the connected and unconnected neuronal pairs within these ensembles. This analysis showed a systematic relationship between the classes: the connected neurons exhibited high gamma-power, whereas the unconnected neurons displayed low gamma power. This dissociation would have been nearly impossible using any other technique. Moreover, the gamma peak for the connected neurons shared the synergistic 50-ms window of opportunity as revealed in an earlier investigation (Siegle *et al.*, 2014). It was also divulged that the spike-triggered gamma was significantly higher than the spike-triggered gamma at the spontaneous oscillations for the same connected pairs. As a matter of fact, the stimulus-triggered gamma (spectrograms generated on the stimulus-

triggered spike trains for all of the neurons) was obvious (weak) but not as pronounced as the spike–triggered oscillations. Thus, this hitherto unemployed strategy led to the unmasking of the power of gamma oscillations between the connected neurons in V1 circuits. Otherwise, with other techniques, it would not have been possible as the signal almost gets neutralized within the population. Thus, this study effectively helps to reconcile the debate on gamma. It also appears that gamma oscillations are intrinsically generated precursors of information processing within cortical circuits that emerge through synchronised activity between neurons in relation to the presented stimulus.

8.2.2.2 Orientation selectivity index (OSI) and gamma power

Recently, it has been shown that a visual neuron exhibits the highest power of gamma during the rising phase of the gamma cycle (Womelsdorf *et al.*, 2012). Further, in this investigation it was revealed that the power of gamma is modulated systematically in the low- and high-gamma bands as a function of the orientation selectivity index (OSI) of neurons. The more selective the neuron is, the more power it exhibits in the low-gamma (30-40 Hz) band, whereas the least selective the neuron is, the more power it exhibits in the high-gamma (60-70 Hz) band.

Many reports have shown that the gamma cycle creates a window of opportunity for neurons to collaborate within cyclical loops of excitatory and inhibitory currents (Wang & Buzsaki, 1996; Tiesinga & Sejnowski, 2009; Siegle *et al.*, 2014). Within this cyclical loop, maximum depolarization occurs at the rising phase of the gamma cycle. The highly orientation selective neurons have been linked to the pyramidal cells, whereas the broadly tuned neurons have been related to the inhibitory neurons (Bachatene *et al.*, 2012; Vinck *et al.*, 2013). Collectively this implies that, the sharply tuned neurons depolarize in the mean phase of the low-gamma band, whereas the broadly selective neurons depolarize in the mean phase of the high-gamma band. Indeed, all orientations are represented on the dendritic trees of a neuron (Jia *et al.*, 2010; Bachatene *et al.*, 2013; Wertz *et al.*, 2015); however, a specific input may trigger the drive toward a particular set of synapses, thereby tuning the output of the neuron toward that specific orientation resulting in high

OSI for that neuron. On the other hand, when all synapses are driven equally, this cascades into a broadly tuned neuron with high OSI. The highly selective neurons fire sparsely and mediate the feed-forward flow; therefore, they have pronounced activity in the low-gamma band. On the contrary, the broadly tuned neurons fire with higher rates in the high-gamma band and are well-suited for the roles of divisive normalization by maintaining the inhibitory-excitatory balance (Carandini *et al.*, 1997; Chance *et al.*, 2002).

8.2.2.3 Role of the spontaneous oscillations

Fast oscillations (20-60 Hz) are prevalent in the brain, even spontaneously, and are an intriguing domain for neuroscientists (Drew *et al.*, 2008). In principle, these oscillations persist during sleep or simply in absence of any input to the brain (Massimini *et al.*, 2004; Chauvette *et al.*, 2011). Although most of the information (action and perception) is processed within few milliseconds in the brain, these ultra-slow oscillations act on a time-scale of seconds in the brain (different species) as background activity to the stimulus-linked activity (Drew *et al.*, 2008). Investigators have linked them to their role in various cognitive tasks, inter-hemispheric communication (Nir *et al.*, 2008), perception and memory (Marshall *et al.*, 2006; Chauvette *et al.*, 2011).

What is the role of these spontaneous oscillations and what is their genesis? It is important to disentangle their exact mechanisms and roles for a fundamental understanding of the brain functions. Cholinergic activation of the cortex, spontaneous synaptic release, depolarization-induced changes in the recovery time lasting up to seconds, are the causes that have been put forward for their emergence in the brain (Drew *et al.*, 2008; Nir *et al.*, 2008).

In my study, it was revealed that the ensembles recorded in the presence of a stimulus were also active spontaneously. However, they exhibited fewer connections, decreased synergism and low power of the gamma oscillations. Indeed, using different techniques (Kenet *et al.*, 2003; Han *et al.*, 2008; Mohajerani *et al.*, 2013; Miller *et al.*, 2014), many

researchers have previously reported in the visual cortex that the same groups of neurons are active during visual stimulation and even in the absence of the input. Along with these findings and the results from my investigation, it is suggested that spontaneous oscillations in the brain always keep the brain prepared (as if a lubricant to a car) to receive the sensory input efficiently, and thereby processing it promptly for the organism to react immediately. Importantly, these ultra-slow oscillations may emerge from the strongly embedded connections between neurons in ensembles, whereas the weakly connected neurons may remain synaptically inactive. In other words, the spontaneous oscillations originate endogenously from inherently quasi-synchronized strong links between neurons. This validates the fact that some boutons remain stable on neuronal dendrites, whereas others may dynamically appear and disappear in relation to the lived experience (Stettler *et al.*, 2006). These strongly inscribed boutons may be the channels of repeating information relay between neurons in absence of inputs, thereby giving rise to ongoing oscillations.

One of the most fascinating facets of the slow oscillations is that their power has been reported to be high during sleep (Cox *et al.*, 2014). I speculate that selective communication between specific neurons with strong synapses renders the brain the opportunity to consolidate the lived experience by filtering out the weaker synapses. As a consequence, the experience is carefully stitched in the brain memoir. Notably, in this process, the newly active synapses may also be strengthened to give rise to novel intrinsically reverberating ensembles.

8.2.3 Interactions between the regular-spiking (RS) and the fast-spiking (FS) neurons

There is a variety of neurons present in the brain that play distinct roles in information processing (Vinck *et al.*, 2013; Kepecs & Fishell, 2014; Dehorter *et al.*, 2015). Indeed, the neuronal circuit functioning is dependent upon these specific classes of neurons. Neuronal identity is typically established during the youth, and it is generally accepted that the fate of a neuron once established, stays with it throughout its life.

Although, different experiences (such as adaptation) may change its properties (such as orientation selectivity in V1) but its role remains the same (Dehorter *et al.*, 2015). With the progress in modern techniques, it has now become possible to distinguish these different types of neurons (Markram *et al.*, 2004; Niell & Stryker, 2008; Vinck *et al.*, 2013; Kepecs & Fishell, 2014; Dehorter *et al.*, 2015). Generally, neurons in the cortex are categorized into two main classes: pyramidal cells and interneurons. Pyramidal neurons are excitatory in nature, whereas interneurons, in general, regulate the flow of excitation in the cortex by inhibiting the activity of principal neurons (Cardin *et al.*, 2009; Wang *et al.*, 2010). Electrophysiologically, these two distinct types of neurons can be dissociated from each other based on the ascending slope of their spike-waveforms (Niell & Stryker, 2008; Bachatene *et al.*, 2012; Vinck *et al.*, 2013). A steeper slope with smaller spike-width is associated to the interneurons, whereas a neuron with bigger spike-width is related to the excitatory neuron (Bachatene *et al.*, 2012).

Inhibitory interneurons are embedded in a web of pyramidal neurons (Wang & Buzsaki, 1996; Wang *et al.*, 2010), and it has been documented that specific interactions between these two classes potentiate the oscillatory rhythms in the brain (Cardin *et al.*, 2009). There are three prevalent theories that explain the information processing in gamma-bands by recruiting the excitatory (E) and inhibitory (I) populations in the locally synchronized cortical motifs (Tiesinga & Sejnowski, 2009). These three distinct mechanisms are: the feed-forward (FF) projections, the pyramidal-interneuron gamma (PING) and the interneuron gamma (ING).

The simplest way to achieve synchrony is by the feed-forward coincident inputs from the upstream areas, that is, the FF mechanism. In this case, simply, a pool of LGN neurons provides coincident input to a pool of L2/3 neurons through L4 neurons. Within the ING mechanism, synchrony is fashioned in two distant ways that have been confirmed even computationally (Tiesinga & Sejnowski, 2009). First, if all of the inhibitory neurons get the input at the same time, this will most likely cause a simultaneous increase in their firing rate. If more than average neurons fire in a recurrent inhibitory network, this eventually leads to an increased inhibition of the neighbouring

neurons, thereby delaying their spikes and consequently preparing them to fire synchronously in the next cycle of firing. Typically, inhibitory neurons fire at around 40 Hz (Fujisawa *et al.*, 2008). These neurons can acquire such high firing only when they are depolarized by strong excitatory inputs (Whittington *et al.*, 1995). In this way, the network achieves oscillatory state through synchronous activity of inhibitory neurons. Second, when a large number of inhibitory neurons fire randomly with firing rates as low as 1 Hz, this pushes the network into an asynchronous state. An external input or drive may disturb the asynchronous state and transform the network into an oscillatory rhythm (Brunel & Hakim, 1999). Therefore, within the ING mechanism, oscillations could be produced either starting from a synchronous or an asynchronous state involving the pyramidal cells. In the PING mechanism, the excitatory neurons have to be synchronized in order to drive the inhibitory neurons. If inhibitory neurons are not excited, this would eventually result in failure of an inhibitory volley.

In this study, based upon the spike-width analysis, it was revealed that a significant majority of interactions in the primary visual cortex were between the RS neurons that are linked putatively to the excitatory neurons. On the contrary, a minority of interactions were found with FS neurons. In parallel, it was also divulged that the RS interactions predominantly occur with increased power in the low gamma (30-40 Hz) band, whereas the FS-RS and FS-FS interactions were mainly associated to the high gamma band (60-80 Hz). That is, the former band was linked to the activity of the pyramidal neurons, whereas the latter was associated to the putative interneurons. The predominance of RS-RS interactions suggests that the low gamma band is simply generated by the feed-forward inputs from the upstream areas, that is, it seems that the FF mechanism is the most plausible way of acquiring synchrony in the cortical networks. However, the simultaneous occurrence of the high gamma band points to the fact that PING gamma may be involved in generation of the high gamma band. Within this framework, first, the RS neurons may collaborate quasi-synchronously between themselves. Once they are depolarized enough in a feed-forward fashion, they project onto the inhibitory neurons, thereby increasing their firing rate momentarily and consequently opening the top-down (activating a feedback loop) gates for the control of excitatory flow. This loop also fits

within the window of opportunity, as there is a relative phase difference between the activity of the pyramidal neurons and the interneurons (Wang & Buzsaki, 1996; Siegle *et al.*, 2014). Indeed, a very few inhibitory connections in the current study suggest that the pyramidal neuron activity precedes the excitation of inhibitory neurons in V1 microcircuits.

However, it is to be underlined that, in the cat visual cortex it is not entirely possible to classify neurons as excitatory and inhibitory based upon their spike-width (Nowak *et al.*, 2003), as a fraction of pyramidal neurons may exhibit fast spiking pattern. Therefore, while interpreting the results of the current study, one has to be cautious in exhaustively determining the significance of these results.

8.2.4 The importance of noise correlations (Rsc) in an ensemble

Noise correlation (Rsc) is the trial-by-trial Pearson correlation of the firing of two neurons in response to the repeated presentation of the same stimulus (Averbeck *et al.*, 2006; Cohen & Kohn, 2011), and it has been widely employed to study the stimulus structure. Rsc simply gives the information about the co-modulation of the spiking activity of two neurons, whereas a CCG reveals the functional relationship between neurons. Indeed, there has been a contentious debate on the precise nature of noise correlations, even at the level of the primary visual cortex — investigators have reported Rsc ranging from 0.001 to 0.35 across various studies (Averbeck *et al.*, 2006; Gutnisky & Dragoi, 2008; Smith & Kohn, 2008; Ecker *et al.*, 2010; Hansen *et al.*, 2012; Denman & Contreras, 2014; Ecker *et al.*, 2014). However, all studies have converged to the point that nearby and closely tuned neurons exhibit high Rsc. However, there are two exceptions to these studies (Ecker *et al.*, 2010; Renart *et al.*, 2010). A striking dissimilarity between Ecker et al. (Ecker *et al*., 2010) and the earlier studies is that in this study the stimulus presentation was for about 500 ms with a relatively low mean firing rate, which may have resulted in the underestimation of true correlation between neurons. Nevertheless, both studies (Ecker *et al.*, 2010; Renart *et al.*, 2010) showed that an appreciable number of pairs exhibited correlations on the positive side. Furthermore,

Ecker and colleagues found Rsc to be significantly high between the closely tuned neurons. Clearly, what if all above studies yielded varied values of average Rsc, but they are unified by similarities too. This suggests that high Rsc between pairs may certainly have an important role to play in the stimulus encoding.

Many recent reports (Carrillo-Reid *et al.*, 2015; Cossell *et al.*, 2015; Shimono & Beggs, 2015) along with my findings, if interpreted collectively, converge to a point that, within a space of 100 μm, neurons that project onto each other in a repeating firing pattern (usually ≤ 5 ms) may systematically display high Rsc between them than their unconnected companions. In short, in "emergent" microcircuits, Rsc obeys a simple rule: the strongly connected neurons exhibit highly correlated responses, whereas the unconnected neurons display on average low correlations.

In experimental conditions, lower firing rate binned into smaller calculation windows may further complicate the true estimation of Rsc, as the few related spikes could easily be assigned to different bins. This may be particularly valid for neurons interacting quasi-synchronously (jittered) in microcircuits (that is, within a small cortical distance) because majority of neuronal interactions occur within a limited volume. Importantly, because of the inherent (established during maturation of synapses) spiking pattern between a neuron pair, they may always exhibit similar values of Rsc in response to different set of stimuli. However, a stimulus engineers the microcircuit in such a fashion that a cohort of neurons (connected) covaries its responses systematically than a group of neurons (unconnected) whose firings fall out of the coincident window.

In conclusion, it is important to dissociate the connected and unconnected neurons while interpreting the Rsc, because by simply pooling the observed population of neurons in an experiment may always mask the contribution of the connected neurons. It may especially hold true for populations analyzed over long cortical distances as neurons are activated to different degrees over space.

8.2.5 Emergent functional network: the encoding 'signature' of an assembly

In 1949, the pioneering Canadian neuroscientist Donald Hebb published his book 'The Organization of Behaviour' in which he put forward his theory of the Hebbian learning in cell-assemblies. The central idea of his hypothesis was that neurons that 'fire together wire together'. Another important element of his theory was that, within these assemblies, when a neuron makes the other neuron(s) fire consistently or repetitively, it leads to the strengthening of synapses between them (Hebbs synapse). Milner and Marlsburg in 1981 (Milner, 1974; Marlsburg 1981) proposed their theory of 'binding by synchrony' in the brain that was further extended by Singer and colleagues in 1989 (Singer, 1999). The important determinant of this postulation was that, neurons that synchronize their action potentials are implicated in binding the features of an image, thus its coherent perception in the brain. Indeed, this theory encompassed Hebb's 'fire together wire together' principle in that neurons had to be simultaneously active to synchronize their action potentials. Recently, Buzsaki (Buzsaki, 2010) suggested a neural syntax for information processing in the brain. Fundamentally, in his hypothesis, it is important to examine the dynamics of causal relationships and the constellations of changing synaptic weights (termed synapsemle by him) between neurons in assemblies to understand their encoding phenomenon in form of neuronal output along the brain hierarchy. Further, Singer (2013) proposed that, within a reservoir of connections in a neuronal assembly, neurons recruit a specific classifier between themselves that is related to the input provided to them. Lately, within the framework of the Hebbian assemblies, Yuste and colleagues (Miller *et al.*, 2014; Carrillo-Reid *et al.*, 2015) have empirically reflected upon the emergence of endogenously active ensembles in relation to specific stimuli. Similarly, using transfer entropy, clusters of neurons (equivalent to ensembles) were shown to frame functional circuits between themselves (Shimono & Beggs, 2015). In a similar fashion, Sadra *et al*. (2015) have also shown that specific connectivity between orientation selective pyramidal cells emerges from a pool of random network in relation to a specific input. The weights between pyramidal neurones increase and decrease contingent upon the input, thus giving rise to a specific network.

In fact, these previous investigations used different approaches to study the dynamics of functional interactions within assemblies. These included the classical electrophysiological approaches (Bartho *et al.*, 2004; Fujisawa *et al.*, 2008; Ecker *et al.*, 2010; Denman & Contreras, 2014), calcium imaging (Miller *et al.*, 2014; Cossell *et al.*, 2015; Wertz *et al.*, 2015), transfer entrophy (Shimono & Beggs, 2015) and even predicting the networks by exploiting the computational tools (Binzegger *et al.*, 2004; Buzas *et al.*, 2006). These main hypotheses, recent findings, and many other investigations 'collectively' indicate that the emergence of functional connections in assemblies is an indispensable process for the stimulus encoding.

As already discussed, until now all of the investigations have largely been conducted in a bimodal fashion (e.g. natural vs artificial stimuli; stimuli vs spontaneous activity). In other words, the ensembles have been explored in response to very dissimilar stimuli. Indeed, in day-to-day life, we are bombarded with many different kinds of inputs, from very contrasting to even the most subtle ones. Therefore, it is important to examine how the brain discriminates these subtle variations. Here, in this investigation, the functional network of an orientation selective assembly was detected in response to the systematic tilt of an oriented drifting sine-wave grating. It was revealed that a 'salient' functional network is activated in an assembly in response to a particular orientation that remains stable over a period of time. Indeed, as the orientation changes, the connections in an assembly may wax and wane contingent upon the input. Moreover, cells may leave the assembly or new cells may start participating in the assembly with the novel orientation. In addition, the weights of connections may change from one orientation to another orientation.

These dynamics encompass most of the characteristics of an assembly that had been previously reported or suggested by authors. It entails the concept of synchrony in the brain (Singer, 1999), that is, the revealed quasi-synchronous functional links. The participation of newly active cells in relation a specific input hints at the transition of a neuron from one ensemble to another ensemble within the framework of a Hebbian assembly (It is to be noted that a Hebbian assembly is defined as transmission of

information between different constellations of neurons termed ensembles). The reader-centric definition of assembly postulated by Buzsaki (Buzsaki, 2010) also seems to fit well for the functionally active assemblies divulged in the current study. According to him, neurons become ephemerally active in time to produce a downstream effect, wherein synchrony is the major modus operandi by which they achieve this. However, this synchrony is only meaningful if it is read by a mechanism downstream. That is, there must be a reader-classifier mechanism to receive this input from the upstream assembly. He suggested that even a small neural network can give rise to multiple firing patterns. In my study, a uniquely activated network in relation to an orientation is a reflection of his hypothesis. He implies that, it is the calibration of synaptic weights (synapsemble) in an assembly which is the most important phenomenon for the stimulus encoding. In short, a particular synapsemle will project onto a specific reader, that is, a specific input will be processed in a certain fashion by an assembly. If the weight of the assembly changes, it may activate another reader in the downstream assembly. Importantly, these events should occur in a meaningful window for synaptic integration, such as the 50-ms window of opportunity revealed in this investigation. Further, these findings very well accommodate the suggestions that the recruitment of a specific network from the functional lexicon of an assembly is strictly related to an input (Singer, 2013; Sadeh *et al.*, 2015). In fact, some connections were frequently active from one orientation to another (although with changing strengths) implying that, within an assembly, there is a core group of cells (Barth & Poulet, 2012; Cossell *et al.*, 2015) that may always exhibit enhanced connectivity and synergism than its companion neurons. The frequently active (strong) connections may be the main junctions of information encoding within an assembly, whereas the changing connections (adaptable) may confer flexibility to an ensemble in order to receive and learn various inputs. This study also supports the finding by Miller *et al*. (2014) in that the evoked and spontaneously active ensembles are same (neurons comprising ensembles were active in relation to the input as well as ongoing activity). The peaks revealed in CCGs can be linked to the 'doublet pathways'— that is, the recurrent firing pattern of neurons, as documented in a recent finding by Carrillo-Reid *et al*. (2015). In a similar way, these revealed functional connections can be compared to

the links that were divulged using transfer entropy paradigm by Shimono and Beggs (Shimono & Beggs, 2015).

In short, all above findings and this study can be compared to each other. Collectively, they support the evidence that a functionally salient assembly is the neural signature of its encoding mechanisms. The intriguing interplay of an assembly in relation to the systematic tilt of the orientation throws light upon the dynamics of an assembly, and suggests that even subtle changes may drastically reconfigure the neuronal networks.

8.2.5.1 But why specific functional networks?

There is mounting evidence that chaos persists at the simplest to the most complex levels of the nervous system organization (Bob, 2007; Tsuda & Fujii, 2007). "Chaos" in general means the formless emptiness from which order springs. Chaos underlines the activity patterns for all of the perceptual processes and functions. In other words, it is a repository of the brain's functional lexicon, thereby enabling it to access previously learned sensory patterns and even learn new patterns (Korn & Faure, 2003). Indeed, the brain operates by biasing the external drive toward a particular set of neurons that may encode it efficiently through a carefully organized network between them. It has been widely reported that within distributed networks, the larger the connectivity matrix is, the more redundant the network is. In short, in relation to an input, the more redundant the network is (in other words, salient or specific), the more readily the information is processed within the circuit. Therefore, the saliency of a functional network renders an ensemble the opportunity to process and pass the information to the next level with minimal latency.

8.2.5.2 Size of assemblies

Indeed, one can record several hundred neurons simultaneously in the cortex; however, this involves recordings over a wide cortical spread. In other words, these recordings are performed over numerous sites, that is, on a parallel scale (Alivisatos *et*

al., 2012). In principle, neurons communicate locally while processing a feature. Therefore, understandably, it is important to unmask the dynamics of these local circuits. Despite major technological advances, it is yet not possible to monitor the activity of several neurons locally within the cortex (Alivisatos *et al.*, 2012; Quiroga, 2012; Rey *et al.*, 2015).

Over decades of neurophysiologic recordings at different scales, there is no clear evidence about the size of neuronal population codes that encode the sensory input. Nevertheless, researchers have suggested that an assembly may comprise tens to hundreds of neurons. For example, in hippocampus, authors have suggested that 150-300 CA3 pyramidal neurons firing within a gamma cycle may comprise an assembly (de Almeida *et al.*, 2007). Under special circumstances, when inputs converge on millisecond (<6 ms, that is, synchronously firing neurons) timescales, as few as 20 neurons (Losonczy & Magee, 2006) may be sufficient to trigger a spike in a downstream neuron (a reader neuron, according to Buzsaki, 2010). Interestingly, the activity of only a few hippocampal cells (even one) is more informative about the position of an animal than the entire population (Miles, 1990). In olfactory bulb, even though many mitral cells are active at the same time, but fewer than 10 % are implicated in generating discrete outputs (Niessing & Friedrich, 2010). Therefore, it appears that differently sized assemblies may originate depending upon the task in different brain regions.

In the current study, the electrophysiological recordings captured the activity of an exceedingly small number of local neurons, which is a relatively small number compared with the suggested size of population codes. Indeed, there were many hidden cells in the network whose activities could not be recorded with the microelectrodes used in this investigation. Although, a very few neurons were sampled, but certainly the results point to the specificity of information flow in cortical circuits. Notably, such rules may also apply to assemblies on a bigger scale.

Interestingly, these findings coincide with two previous findings, wherein authors reported that functional clusters of 3-6 neurons are essential building blocks of large scale

hubs and communities spreading across the cortex (Perin *et al.*, 2011; Shimono & Beggs, 2015). It is worthwhile to underline here that, the findings in this study relate to the systematic tilt of the oriented sine-wave drifting grating. Therefore, this study essentially reveals the subtle dynamics of these small clusters of neurons.

Indeed, the "Holy Grail" will be to record millions of neurons simultaneously, keeping the same bandwidth, and reducing the pitch of the electrodes to few microns with the ability to record at several centimetres of cortical volume in depth and laterally. This requires a significant leap in systems engineering.

8.2.5.3 The importance of neuronal selectivity in emergent functional networks

Since the seminal investigations of Hubel and Wiesel on the cat primary visual cortex, neuronal selectivity has been central to studying the visual neurons. Indeed, when a series of random drifting sine-wave gratings is presented within the receptive field of a visual neuron, the neuron is selective to a particular range of orientations. This is termed as the orientation selectivity of a neuron (Swindale, 1998).

After many investigations, the consensus is that closely tuned neurons exhibit numerous connections with each other than neurons with disparate tunings (Stepanyants *et al.*, 2008; Kampa *et al.*, 2011; Ko *et al.*, 2011; Ko *et al.*, 2014) irrespective of the organization of the visual cortex (that is, columned or salt-and-pepper). Moreover, the proponents of the binding hypothesis also suggest that neurons that share the orientation tuning and common peripheral input are implicated in binding the similar features of the image. In this study, it was revealed that the closely tuned neurons exhibited augmented connectivity between them accompanied by increased connection-weights. Investigators have documented and postulated that the dendritic branches of a neuron contain synapses corresponding to all the orientations (Jia *et al.*, 2010; Bachatene *et al.*, 2013; Wertz *et al.*, 2015). However, when a preferred orientation is flashed within the receptive field of a neuron, it potentiates corresponding synapses on the neuronal dendrites. Consequently, this specific drive tunes the whole neuronal ensemble toward a common goal.

Furthermore, the increased weight between these closely tuned neurons indicates strong connectivity pattern between them. Along the lines of a distributive network, it is suggested that the similarly tuned neurons with increased connectivity and strength within an assembly are principal precursors of information processing at the local level; whereas, synchronized neurons across different assemblies are fundamental to binding of similar features in the image, although present on different parts of the image (Singer, 1999). On the other hand, distantly tuned neurons that display connectivity are inevitable for processing dissimilar or opposite features in the image (Singer, 1999; Molotchnikoff & Rouat, 2012). Untuned neurons did not exhibit many connections between themselves, implying that neuronal selectivity with these ensembles is indispensable for the feature encoding.

8.2.5.4 Firing rate and the multiplexed code

Information propagates between neurons through their action potentials, that is, through the firing of a neuron. Indeed, many candidate neuronal encoding strategies have been identified but they broadly fall in two main categories: the rate code and the temporal code (Molotchnikoff & Rouat, 2012; Ratte *et al.*, 2013). The firing rate of a neuron implies the rate code. Indeed, a neuron may fire maximally to one stimulus, whereas it may fire weakly to another stimulus indicating that it encodes the presence of earlier stimulus than the latter one. On the other hand, the temporal code refers to the precisely locked firing between two neurons that is a reflection of synaptic biophysical properties of neurons (Ainsworth *et al.*, 2012). But what exactly is the operational mode of a neuron? Indeed, there are recent reports (Molotchnikoff & Rouat, 2012; Ratte *et al.*, 2013) which suggest that an average neuron operates somewhere between the rate code and the temporal code (that is, by multiplexing both modes). However, researchers (Ainsworth *et al.*, 2012; Ratte *et al.*, 2013) have shown a bias toward the temporal code.

In this investigation, it was found that neurons exhibited connections with each other irrespective of their low firing. This implies that the firing rate of a neuron is not as important as its precise spike timing to trigger a spike in another neuron. Moreover,

reports have shown that a population of neurons decodes a task better than the individual neurons comprising it (Miller *et al.*, 2014; Carrillo-Reid *et al.*, 2015). Spare activity is an important characteristic of neuronal circuits and it means that neurons fire with low firing rates in response to a stimulus (Barth & Poulet, 2012; Jayakumar *et al.*, 2012; Molotchnikoff & Rouat, 2012). However, there are certain problems associated with sparseness: its fragmented organization and it seems to not fit with daily perception of events (Molotchnikoff & Rouat, 2012). Indeed, the 50-ms window creates an opportunistic epoch for neurons to multiplex both codes. The transient synergistic burst of neuronal discharges implies the rate code, wherein the temporal code is almost exclusively embedded between the firing of involved neurons. Therefore, this opportunistic window also overcomes the problems that sparseness poses. In summary, this signifies that, in distributed networks, the firing of an individual neuron is not as important as the whole network is. This further corroborates the developing consensus that indeed an assembly is the major functional unit of information encoding in cortical circuits rather than a neuron working in isolation.

8.3 Future directions

Indeed, the size of assemblies recorded in this investigation is very small. Although, they suggest that neural codes are specific, but it would be interesting to explore them on a bigger scale. It will require multiple electrodes spaced by a few microns that can simultaneously sample many neurons. Moreover, in a similar fashion, neurons can also be recorded simultaneously between different areas of the visual cortex to divulge the functional connectivity patterns between their neurons. For example, if multiple electrodes that can sample several neurons are lowered in V1, V2 and V4 simultaneously, one may infer the functional connectomes that are conjointly processing the different properties in an image. Understandably, it may be a difficult task but certainly will help us in understanding the inter-regional connectomes. Similarly, other brain regions can also be explored. Until now, there is no clear consensus on the functioning of an emergent ensemble that is implicated in encoding a feature. In fact, by recording ensembles in different areas of the brain in response to different inputs, one maybe able

to further reveal their sizes and dynamics in various brain regions. This will also help us in comprehending the functional hierarchy of the brain. On a different level, the sizes of the encoding assemblies could be predicted using computational methods by exploiting the results of this investigation.

Moreover, in future it will be interesting to analyse the oscillatory rhythms in the brain on the neuronal spikes, as not many studies have explored them in this fashion. This will further help us in the understanding of inter-areal rhythms and the further development of the 'communication though coherence (CTC)' hypothesis.

It would be indeed advantageous to multiplex several techniques too and then map the brain. This will be particularly interesting in a diseased individual where one can lower the electrodes in a region of interest (e.g. tumor) that is identified by an imaging technique. For example, by using 3D interactive tractography (Chamberland *et al*., 2015), one can desirably and more specifically intervene with the pathological area and then perform electrophysiology. In one of imminent goals of multiplexing techniques, we may foresee in-vivo electrophysiology with matrix electrodes in conjunction with 3D interactive tractography-driven fMRI or other imaging techniques. The unifying goal of such experiments will be to synergistically employ many techniques to study a region-of-interest (ROI) in a subject-specific fashion.

Understandably, to achieve these goals, the first step would be to design probes which can record the activities of many neurons simultaneously (sampling every spike from every neuron as Alivisatos *et al*. 2012 have suggested). It maybe a challenging task, but the major technological advances have put us at cross-roads to achieve this!

9. CONCLUSION

The main result (saliency of a stimulus-specific network) of the current investigation suggests that indeed emergent functional microcircuits are the underpinnings of stimulus encoding in the cortex. A specifically framed neuronal circuit is the encoding signature of an assembly in response to a particular stimulus. The fact that neurons encode the information about the stimulus by framing networks between themselves, points to the importance of a cell-assembly as the major functional unit of information retrieval in the brain. Therefore, this study further dilutes the importance of an individually firing neuron.

The 50-ms window of opportunity maybe a general encoding window in most of the parts of the brain, whereby information is processed in a synergistic fashion giving rise to oscillatory rhythms in the brain. Indeed, such window exclusively accommodates the mechanisms for neural encoding: whether it is the excitatory-inhibitory volley of involved neurons, the sparse firing of neurons, the rate and the temporal codes, the gamma oscillatory patterns or even the plasticity rules that allow assemblies to recruit numerous network patterns between themselves. Lastly, noise correlations obey a simple rule in emergent microcircuits: neurons that display high noise correlation values are strongly connected to each other, and vice-versa.

The spike-triggered gamma analysis offers a new method to quantitate the strength of numerous oscillatory patterns in the brain. Exploiting this method, one can more specifically dig information from the cortical microcircuits.

A limitation of the current study was that with tungsten microelectrodes it was not possible to record many neurons. However, these small ensembles still reflected upon the specificity of operational modes of neuronal circuits. In fact, it will be interesting to record many neurons simultaneously in the brain and observe their connectivity patterns thereupon. Certainly, we are not far from the complete understanding of these emergent circuits.

Notably, it is not only the field of neurosciences where investigators are seeking answers to emergent-level problems. In fact, in many other complex-system fields (e.g. statistical mechanics, non-equilibrium thermodynamics, quantum physics and others) scintillating discoveries have been possible by shifting the focus of investigations to the emergent level. For example, in the biological systems, the genome sequencing and the analyses of genome-wide expression have led to many emergent models of gene regulation and developmental control with increased predictive accuracy. On a similar note, the multi-level analyses of connectomes, especially the emergent connectomes may trigger a new era in the further understanding of the brain. We may then harness these developments into the fields of robotics, engineering, building engineering, prosthetics and most importantly in discovering ourselves.

REFERENCES

Adams, D.L., Sincich, L.C. & Horton, J.C. (2007) Complete pattern of ocular dominance columns in human primary visual cortex. *The Journal of neuroscience : the official journal of the Society for Neuroscience*, **27**, 10391-10403.

Adrian, E.D. & Zotterman, Y. (1926) The impulses produced by sensory nerve-endings: Part II. The response of a Single End-Organ. *The Journal of physiology*, **61**, 151-171.

Ainsworth, M., Lee, S., Cunningham, M.O., Traub, R.D., Kopell, N.J. & Whittington, M.A. (2012) Rates and rhythms: a synergistic view of frequency and temporal coding in neuronal networks. *Neuron*, **75**, 572-583.

Alivisatos, A.P., Chun, M., Church, G.M., Greenspan, R.J., Roukes, M.L. & Yuste, R. (2012) The brain activity map project and the challenge of functional connectomics. *Neuron*, **74**, 970-974.

Averbeck, B.B., Latham, P.E. & Pouget, A. (2006) Neural correlations, population coding and computation. *Nature reviews. Neuroscience*, **7**, 358-366.

Bachatene, L., Bharmauria, V., Cattan, S. & Molotchnikoff, S. (2013) Fluoxetine and serotonin facilitate attractive-adaptation-induced orientation plasticity in adult cat visual cortex. *The European journal of neuroscience*, **38**, 2065-2077.

Bachatene, L., Bharmauria, V., Rouat, J. & Molotchnikoff, S. (2012) Adaptation-induced plasticity and spike waveforms in cat visual cortex. *Neuroreport*, **23**, 88-92.

Bair, W., Cavanaugh, J.R. & Movshon, J.A. (2003) Time course and time-distance relationships for surround suppression in macaque V1 neurons. *The Journal of neuroscience : the official journal of the Society for Neuroscience*, **23**, 7690-7701.

Barth, A.L. & Poulet, J.F. (2012) Experimental evidence for sparse firing in the neocortex. *Trends Neurosci*, **35**, 345-355.

Bartho, P., Hirase, H., Monconduit, L., Zugaro, M., Harris, K.D. & Buzsaki, G. (2004) Characterization of neocortical principal cells and interneurons by network interactions and extracellular features. *Journal of neurophysiology*, **92**, 600-608.

Beaulieu, C. & Colonnier, M. (1985) A laminar analysis of the number of round-asymmetrical and flat-symmetrical synapses on spines, dendritic trunks, and cell bodies in area 17 of the cat. *The Journal of comparative neurology*, **231**, 180-189.

Behrmann, M. & Plaut, D.C. (2013) Distributed circuits, not circumscribed centers, mediate visual recognition. *Trends Cogn Sci*, **17**, 210-219.

Bernardet, U. & Verschure, P.F. (2010) iqr: a tool for the construction of multi-level simulations of brain and behaviour. *Neuroinformatics*, **8**, 113-134.

Blake, R. (1979). The visual system of the cat. *Perception and Pyschophy.***26***,* 423-448.

Blasdel, G.G. & Salama, G. (1986) Voltage-sensitive dyes reveal a modular organization in monkey striate cortex. *Nature*, **321**, 579-585.

Bob, P. (2007) Chaos, brain and divided consciousness. *Acta Universitatis Carolinae. Medica. Monographia*, **153**, 9-80.

Bonhoeffer, T. & Grinvald, A. (1993) The layout of iso-orientation domains in area 18 of cat visual cortex: optical imaging reveals a pinwheel-like organization. *The Journal of neuroscience : the official journal of the Society for Neuroscience*, **13**, 4157-4180.

Born, R.T. & Bradley, D.C. (2005) Structure and function of visual area MT. *Annual review of neuroscience*, **28**, 157-189.

Braddick, O.J., O'Brien, J.M.D., Wattam-Bell, J., Atkinson, J., Hartley, T. & Turner, R. (2001) Brain areas sensitive to coherent visual motion. *Perception*, **30**, 61-72.

Brown, S.P. & Hestrin, S. (2009) Intracortical circuits of pyramidal neurons reflect their long-range axonal targets. *Nature*, **457**, 1133-1136.

Brunel, N. & Hakim, V. (1999) Fast global oscillations in networks of integrate-and-fire neurons with low firing rates. *Neural computation*, **11**, 1621-1671.

Brunet, N., Vinck, M., Bosman, C.A., Singer, W. & Fries, P. (2014) Gamma or no gamma, that is the question. *Trends Cogn Sci*, **18**, 507-509.

Bullier, J. (2001) Integrated model of visual processing. *Brain research. Brain research reviews*, **36**, 96-107.

Bullmore, E. & Sporns, O. (2009) Complex brain networks: graph theoretical analysis of structural and functional systems. *Nature reviews. Neuroscience*, **10**, 186-198.

Buzas, P., Kovacs, K., Ferecsko, A.S., Budd, J.M., Eysel, U.T. & Kisvarday, Z.F. (2006) Model-based analysis of excitatory lateral connections in the visual cortex. *The Journal of comparative neurology*, **499**, 861-881.

Buzsaki, G. (2010) Neural syntax: cell assemblies, synapsembles, and readers. *Neuron*, **68**, 362-385.

Buzsaki, G. & Watson, B.O. (2012) Brain rhythms and neural syntax: implications for efficient coding of cognitive content and neuropsychiatric disease. *Dialogues Clin Neurosci*, **14**, 345-367.

Carandini, M., Heeger, D.J. & Movshon, J.A. (1997) Linearity and normalization in simple cells of the macaque primary visual cortex. *The Journal of neuroscience : the official journal of the Society for Neuroscience*, **17**, 8621-8644.

Cardin, J.A., Carlen, M., Meletis, K., Knoblich, U., Zhang, F., Deisseroth, K., Tsai, L.H. & Moore, C.I. (2009) Driving fast-spiking cells induces gamma rhythm and controls sensory responses. *Nature*, **459**, 663-667.

Carrillo-Reid, L., Miller, J.E., Hamm, J.P., Jackson, J. & Yuste, R. (2015) Endogenous sequential cortical activity evoked by visual stimuli. *The Journal of neuroscience : the official journal of the Society for Neuroscience*, **35**, 8813-8828.

Cattan, S., Bachatene, L., Bharmauria, V., Jeyabalaratnam, J., Milleret, C. & Molotchnikoff, S. (2014) Comparative analysis of orientation maps in areas 17 and 18 of the cat primary visual cortex following adaptation. *The European journal of neuroscience*, **40**, 2554-2563.

Chamberland, M., Bernier, M., Fortin, D., Whittingstall, K. & Descoteaux, M. (2015) 3D interactive tractography-informed resting-state fMRI connectivity. *Frontiers in neuroscience*, **9**, 275.

Chance, F.S., Abbott, L.F. & Reyes, A.D. (2002) Gain modulation from background synaptic input. *Neuron*, **35**, 773-782.

Chauvette, S., Crochet, S., Volgushev, M. & Timofeev, I. (2011) Properties of slow oscillation during slow-wave sleep and anesthesia in cats. *The Journal of neuroscience : the official journal of the Society for Neuroscience*, **31**, 14998-15008.

Clare, M.H. & Bishop, G.H. (1954) Responses from an association area secondarily activated from optic cortex. *Journal of neurophysiology*, **17**, 271-277.

Cohen, M.R. & Kohn, A. (2011) Measuring and interpreting neuronal correlations. *Nature neuroscience*, **14**, 811-819.

Constantinople, C.M. & Bruno, R.M. (2013) Deep cortical layers are activated directly by thalamus. *Science*, **340**, 1591-1594.

Cossell, L., Iacaruso, M.F., Muir, D.R., Houlton, R., Sader, E.N., Ko, H., Hofer, S.B. & Mrsic-Flogel, T.D. (2015) Functional organization of excitatory synaptic strength in primary visual cortex. *Nature*, **518**, 399-403.

Cox, R., van Driel, J., de Boer, M. & Talamini, L.M. (2014) Slow oscillations during sleep coordinate interregional communication in cortical networks. *The Journal of neuroscience : the official journal of the Society for Neuroscience*, **34**, 16890-16901.

Csicsvari, J., Hirase, H., Czurko, A. & Buzsaki, G. (1998) Reliability and state dependence of pyramidal cell-interneuron synapses in the hippocampus: an ensemble approach in the behaving rat. *Neuron*, **21**, 179-189.

de Almeida, L., Idiart, M. & Lisman, J.E. (2007) Memory retrieval time and memory capacity of the CA3 network: role of gamma frequency oscillations. *Learning & memory*, **14**, 795-806.

de Kock, C.P. & Sakmann, B. (2009) Spiking in primary somatosensory cortex during natural whisking in awake head-restrained rats is cell-type specific. *Proceedings of the National Academy of Sciences of the United States of America*, **106**, 16446-16450.

Dehorter, N., Ciceri, G., Bartolini, G., Lim, L., del Pino, I. & Marin, O. (2015) Tuning of fast-spiking interneuron properties by an activity-dependent transcriptional switch. *Science*, **349**, 1216-1220.

Denman, D.J. & Contreras, D. (2014) The structure of pairwise correlation in mouse primary visual cortex reveals functional organization in the absence of an orientation map. *Cerebral cortex*, **24**, 2707-2720.

Desimone, R. & Duncan, J. (1995) Neural mechanisms of selective visual attention. *Annual review of neuroscience*, **18**, 193-222.

DiCarlo, J.J. & Cox, D.D. (2007) Untangling invariant object recognition. *Trends Cogn Sci*, **11**, 333-341.

DiCarlo, J.J., Zoccolan, D. & Rust, N.C. (2012) How does the brain solve visual object recognition? *Neuron*, **73**, 415-434.

Dreher, B., Fukada, Y. & Rodieck, R.W. (1976) Identification, classification and anatomical segregation of cells with X-like and Y-like properties in the lateral geniculate nucleus of old-world primates. *The Journal of physiology*, **258**, 433-452.

Drew, P.J., Duyn, J.H., Golanov, E. & Kleinfeld, D. (2008) Finding coherence in spontaneous oscillations. *Nature neuroscience*, **11**, 991-993.

Dur-e-Ahmad, M., Imran, M. & Gul, A. (2011) Calcium dynamics in dendritic spines: a link to structural plasticity. *Mathematical biosciences*, **230**, 55-66.

Ebrahimi, S. & Okabe, S. (2014) Structural dynamics of dendritic spines: molecular composition, geometry and functional regulation. *Biochimica et biophysica acta*, **1838**, 2391-2398.

Ecker, A.S., Berens, P., Cotton, R.J., Subramaniyan, M., Denfield, G.H., Cadwell, C.R., Smirnakis, S.M., Bethge, M. & Tolias, A.S. (2014) State dependence of noise correlations in macaque primary visual cortex. *Neuron*, **82**, 235-248.

Ecker, A.S., Berens, P., Keliris, G.A., Bethge, M., Logothetis, N.K. & Tolias, A.S. (2010) Decorrelated neuronal firing in cortical microcircuits. *Science*, **327**, 584-587.

Essen, D.C. & Zeki, S.M. (1978) The topographic organization of rhesus monkey prestriate cortex. *The Journal of physiology*, **277**, 193-226.

Fabre-Thorpe, M., Richard, G. & Thorpe, S.J. (1998) Rapid categorization of natural images by rhesus monkeys. *Neuroreport*, **9**, 303-308.

Felleman, D.J. & Van Essen, D.C. (1991) Distributed hierarchical processing in the primate cerebral cortex. *Cerebral cortex*, **1**, 1-47.

Fox, R. & Blake, R.R. (1971) Stereoscopic vision in the cat. *Nature*, **233**, 55-56.

Frick, A., Feldmeyer, D., Helmstaedter, M. & Sakmann, B. (2008) Monosynaptic connections between pairs of L5A pyramidal neurons in columns of juvenile rat somatosensory cortex. *Cerebral cortex*, **18**, 397-406.

Fries, P. (2005) A mechanism for cognitive dynamics: neuronal communication through neuronal coherence. *Trends Cogn Sci*, **9**, 474-480.

Fries, P. (2015) Rhythms for Cognition: Communication through Coherence. *Neuron*, **88**, 220-235.

Fries, P., Nikolic, D. & Singer, W. (2007) The gamma cycle. *Trends Neurosci*, **30**, 309-316.

Fries, P., Reynolds, J.H., Rorie, A.E. & Desimone, R. (2001) Modulation of oscillatory neuronal synchronization by selective visual attention. *Science*, **291**, 1560-1563.

Fujisawa, S., Amarasingham, A., Harrison, M.T. & Buzsaki, G. (2008) Behavior-dependent short-term assembly dynamics in the medial prefrontal cortex. *Nature neuroscience*, **11**, 823-833.

Garner, A. & Mayford, M. (2012) New approaches to neural circuits in behavior. *Learning & memory*, **19**, 385-390.

Geerling, J.C. & Loewy, A.D. (2006) Aldosterone-sensitive neurons in the nucleus of the solitary tract: efferent projections. *The Journal of comparative neurology*, **497**, 223-250.

Ghisovan, N., Nemri, A., Shumikhina, S. & Molotchnikoff, S. (2008) Synchrony between orientation-selective neurons is modulated during adaptation-induced plasticity in cat visual cortex. *BMC Neurosci*, **9**, 60.

Gilbert, C.D. & Wiesel, T.N. (1979) Morphology and intracortical projections of functionally characterised neurones in the cat visual cortex. *Nature*, **280**, 120-125.

Grady, C.L., Haxby, J.V., Horwitz, B., Schapiro, M.B., Rapoport, S.I., Ungerleider, L.G., Mishkin, M., Carson, R.E. & Herscovitch, P. (1992) Dissociation of object and spatial vision in human extrastriate cortex: age-related changes in activation of regional cerebral blood flow measured with [(15) o]water and positron emission tomography. *Journal of cognitive neuroscience*, **4**, 23-34.

Gray, C.M., Engel, A.K., Konig, P. & Singer, W. (1990) Stimulus-Dependent Neuronal Oscillations in Cat Visual Cortex: Receptive Field Properties and Feature Dependence. *The European journal of neuroscience*, **2**, 607-619.

Gray, C.M., Konig, P., Engel, A.K. & Singer, W. (1989) Oscillatory responses in cat visual cortex exhibit inter-columnar synchronization which reflects global stimulus properties. *Nature*, **338**, 334-337.

Gray, C.M. & Singer, W. (1989) Stimulus-specific neuronal oscillations in orientation columns of cat visual cortex. *Proceedings of the National Academy of Sciences of the United States of America*, **86**, 1698-1702.

Grienberger, C. & Konnerth, A. (2012) Imaging calcium in neurons. *Neuron*, **73**, 862-885.

Grossberg, S. (1976) Adaptive pattern classification and universal recoding: I. Parallel development and coding of neural feature detectors. *Biological cybernetics*, **23**, 121-134.

Gutnisky, D.A. & Dragoi, V. (2008) Adaptive coding of visual information in neural populations. *Nature*, **452**, 220-224.

Hagmann, P., Cammoun, L., Gigandet, X., Gerhard, S., Grant, P.E., Wedeen, V., Meuli, R., Thiran, J.P., Honey, C.J. & Sporns, O. (2010) MR connectomics: Principles and challenges. *Journal of neuroscience methods*, **194**, 34-45.

Han, F., Caporale, N. & Dan, Y. (2008) Reverberation of recent visual experience in spontaneous cortical waves. *Neuron*, **60**, 321-327.

Hansen, B.J., Chelaru, M.I. & Dragoi, V. (2012) Correlated variability in laminar cortical circuits. *Neuron*, **76**, 590-602.

Harris, K.D. & Mrsic-Flogel, T.D. (2013) Cortical connectivity and sensory coding. *Nature*, **503**, 51-58.

Hasegawa, S., Sakuragi, S., Tominaga-Yoshino, K. & Ogura, A. (2015) Dendritic spine dynamics leading to spine elimination after repeated inductions of LTD. *Scientific reports*, **5**, 7707.

Hebb, D.O. (1949) The organization of behavior. New York: *John Wiley and Sons.*

Hellwig, B. (2000) A quantitative analysis of the local connectivity between pyramidal neurons in layers 2/3 of the rat visual cortex. *Biological cybernetics*, **82**, 111-121.

Helmstaedter, M., Staiger, J.F., Sakmann, B. & Feldmeyer, D. (2008) Efficient recruitment of layer 2/3 interneurons by layer 4 input in single columns of rat somatosensory cortex. *J Neurosci*, **28**, 8273-8284.

Herry, C. & Johansen, J.P. (2014) Encoding of fear learning and memory in distributed neuronal circuits. *Nature neuroscience*, **17**, 1644-1654.

Heywood, C.A., Gadotti, A. & Cowey, A. (1992) Cortical area V4 and its role in the perception of color. *The Journal of neuroscience : the official journal of the Society for Neuroscience*, **12**, 4056-4065.

Hubel, D.H. & Wiesel, T.N. (1959) Receptive fields of single neurones in the cat's striate cortex. *The Journal of physiology*, **148**, 574-591.

Hubel, D.H. & Wiesel, T.N. (1962) Receptive fields, binocular interaction and functional architecture in the cat's visual cortex. *The Journal of physiology*, **160**, 106-154.

Hubel, D.H. & Wiesel, T.N. (1965) Receptive Fields and Functional Architecture in Two Nonstriate Visual Areas (18 and 19) of the Cat. *Journal of neurophysiology*, **28**, 229-289.

Hubel, D.H. & Wiesel, T.N. (1968) Receptive fields and functional architecture of monkey striate cortex. *The Journal of physiology*, **195**, 215-243.

Hubel, D.H. & Wiesel, T.N. (1969) Visual area of the lateral suprasylvian gyrus (Clare-Bishop area) of the cat. *The Journal of physiology*, **202**, 251-260.

Jayakumar, J., Hu, D. & Vidyasagar, T.R. (2012) Sparseness of coding in area 17 of the cat visual cortex: a comparison between pinwheel centres and orientation domains. *Neuroscience*, **225**, 55-64.

Jia, H., Rochefort, N.L., Chen, X. & Konnerth, A. (2010) Dendritic organization of sensory input to cortical neurons in vivo. *Nature*, **464**, 1307-1312.

Johnson, D.H., Gruner, C.M., Baggerly, K. & Seshagiri, C. (2001) Information-theoretic analysis of neural coding. *Journal of computational neuroscience*, **10**, 47-69.

Jung, C.K. & Herms, J. (2014) Structural dynamics of dendritic spines are influenced by an environmental enrichment: an in vivo imaging study. *Cerebral cortex*, **24**, 377-384.

Just, M.A., Carpenter, P.A. & Varma, S. (1999) Computational modeling of high-level cognition and brain function. *Human brain mapping*, **8**, 128-136.

Kampa, B.M., Roth, M.M., Gobel, W. & Helmchen, F. (2011) Representation of visual scenes by local neuronal populations in layer 2/3 of mouse visual cortex. *Frontiers in neural circuits*, **5**, 18.

Kapadia, M.K., Westheimer, G. & Gilbert, C.D. (1999) Dynamics of spatial summation in primary visual cortex of alert monkeys. *Proceedings of the National Academy of Sciences of the United States of America*, **96**, 12073-12078.

Kasai, H., Fukuda, M., Watanabe, S., Hayashi-Takagi, A. & Noguchi, J. (2010) Structural dynamics of dendritic spines in memory and cognition. *Trends in neurosciences*, **33**, 121-129.

Kaschube, M., Schnabel, M., Lowel, S., Coppola, D.M., White, L.E. & Wolf, F. (2010) Universality in the evolution of orientation columns in the visual cortex. *Science*, **330**, 1113-1116.

Kellner, Y., Fricke, S., Kramer, S., Iobbi, C., Wierenga, C.J., Schwab, M.E., Korte, M. & Zagrebelsky, M. (2016) Nogo-A controls structural plasticity at dendritic spines by rapidly modulating actin dynamics. *Hippocampus*.

Kenet, T., Bibitchkov, D., Tsodyks, M., Grinvald, A. & Arieli, A. (2003) Spontaneously emerging cortical representations of visual attributes. *Nature*, **425**, 954-956.

Kepecs, A. & Fishell, G. (2014) Interneuron cell types are fit to function. *Nature*, **505**, 318-326.

Keysers, C., Xiao, D.K., Foldiak, P. & Perrett, D.I. (2001) The speed of sight. *Journal of cognitive neuroscience*, **13**, 90-101.

Ko, H., Hofer, S.B., Pichler, B., Buchanan, K.A., Sjostrom, P.J. & Mrsic-Flogel, T.D. (2011) Functional specificity of local synaptic connections in neocortical networks. *Nature*, **473**, 87-91.

Ko, H., Mrsic-Flogel, T.D. & Hofer, S.B. (2014) Emergence of feature-specific connectivity in cortical microcircuits in the absence of visual experience. *The Journal of neuroscience : the official journal of the Society for Neuroscience*, **34**, 9812-9816.

Korn, H. & Faure, P. (2003) Is there chaos in the brain? II. Experimental evidence and related models. *Comptes rendus biologies*, **326**, 787-840.

Kuceyeski, A., Navi, B.B., Kamel, H., Relkin, N., Villanueva, M., Raj, A., Toglia, J., O'Dell, M. & Iadecola, C. (2015) Exploring the brain's structural connectome: A quantitative stroke lesion-dysfunction mapping study. *Human brain mapping*, **36**, 2147-2160.

Leergaard, T.B., Hilgetag, C.C. & Sporns, O. (2012) Mapping the connectome: multi-level analysis of brain connectivity. *Front Neuroinform*, **6**, 14.

Logothetis, N.K., Pauls, J., Bulthoff, H.H. & Poggio, T. (1994) View-dependent object recognition by monkeys. *Curr Biol*, **4**, 401-414.

Loop, M.S. & Bruce, L.L. (1978) Cat color vision: the effect of stimulus size. *Science*, **199**, 1221-1222.

Losonczy, A. & Magee, J.C. (2006) Integrative properties of radial oblique dendrites in hippocampal CA1 pyramidal neurons. *Neuron*, **50**, 291-307.

Markram, H., Toledo-Rodriguez, M., Wang, Y., Gupta, A., Silberberg, G. & Wu, C. (2004) Interneurons of the neocortical inhibitory system. *Nature reviews. Neuroscience*, **5**, 793-807.

Marlsburg, C. (1981) The Correlation Theory of Brain Function. *Departmental Technical Report*

Marshall, L., Helgadottir, H., Molle, M. & Born, J. (2006) Boosting slow oscillations during sleep potentiates memory. *Nature*, **444**, 610-613.

Massimini, M., Huber, R., Ferrarelli, F., Hill, S. & Tononi, G. (2004) The sleep slow oscillation as a traveling wave. *The Journal of neuroscience : the official journal of the Society for Neuroscience*, **24**, 6862-6870.

Maunsell, J.H. & Gibson, J.R. (1992) Visual response latencies in striate cortex of the macaque monkey. *Journal of neurophysiology*, **68**, 1332-1344.

McMahon, T.T., Hansen, M., Stelmack, J., Oliver, P. & Viana, M.A. (1993) Saccadic eye movements as a measure of the effect of low vision rehabilitation on reading rate. *Optom Vis Sci*, **70**, 506-510.

Melchitzky, D.S., Gonzalez-Burgos, G., Barrionuevo, G. & Lewis, D.A. (2001) Synaptic targets of the intrinsic axon collaterals of supragranular pyramidal neurons in monkey prefrontal cortex. *The Journal of comparative neurology*, **430**, 209-221.

Miles, R. (1990) Synaptic excitation of inhibitory cells by single CA3 hippocampal pyramidal cells of the guinea-pig in vitro. *The Journal of physiology*, **428**, 61-77.

Miller, J.E., Ayzenshtat, I., Carrillo-Reid, L. & Yuste, R. (2014) Visual stimuli recruit intrinsically generated cortical ensembles. *Proceedings of the National Academy of Sciences of the United States of America*, **111**, E4053-4061.

Milner, P.M. (1974) A model for visual shape recognition. *Psychol Rev*, **81**, 521-535.

Mohajerani, M.H., Chan, A.W., Mohsenvand, M., LeDue, J., Liu, R., McVea, D.A., Boyd, J.D., Wang, Y.T., Reimers, M. & Murphy, T.H. (2013) Spontaneous cortical activity alternates between motifs defined by regional axonal projections. *Nature neuroscience*, **16**, 1426-1435.

Molotchnikoff, S. & Rouat, J. (2012) Brain at work: time, sparseness and superposition principles. *Front Biosci (Landmark Ed)*, **17**, 583-606.

Moran, J. & Desimone, R. (1985) Selective attention gates visual processing in the extrastriate cortex. *Science*, **229**, 782-784.

Movshon, J.A. (1975) The velocity tuning of single units in cat striate cortex. *The Journal of physiology*, **249**, 445-468.

Nadasdy, Z. (2000) Spike sequences and their consequences. *J Physiol Paris*, **94**, 505-524.

Nauhaus, I., Nielsen, K.J., Disney, A.A. & Callaway, E.M. (2012) Orthogonal micro-organization of orientation and spatial frequency in primate primary visual cortex. *Nature neuroscience*, **15**, 1683-1690.

Niell, C.M. & Stryker, M.P. (2008) Highly selective receptive fields in mouse visual cortex. *The Journal of neuroscience : the official journal of the Society for Neuroscience*, **28**, 7520-7536.

Niessing, J. & Friedrich, R.W. (2010) Olfactory pattern classification by discrete neuronal network states. *Nature*, **465**, 47-52.

Nir, Y., Mukamel, R., Dinstein, I., Privman, E., Harel, M., Fisch, L., Gelbard-Sagiv, H., Kipervasser, S., Andelman, F., Neufeld, M.Y., Kramer, U., Arieli, A., Fried, I. & Malach, R. (2008) Interhemispheric correlations of slow spontaneous neuronal fluctuations revealed in human sensory cortex. *Nature neuroscience*, **11**, 1100-

1108.

Nowak, L.G., Azouz, R., Sanchez-Vives, M.V., Gray, C.M. & McCormick, D.A. (2003) Electrophysiological classes of cat primary visual cortical neurons in vivo as revealed by quantitative analyses. *Journal of neurophysiology*, **89**, 1541-1566.

Ohki, K., Chung, S., Ch'ng, Y.H., Kara, P. & Reid, R.C. (2005) Functional imaging with cellular resolution reveals precise micro-architecture in visual cortex. *Nature*, **433**, 597-603.

Perin, R., Berger, T.K. & Markram, H. (2011) A synaptic organizing principle for cortical neuronal groups. *Proceedings of the National Academy of Sciences of the United States of America*, **108**, 5419-5424.

Perkel, D.H., Gerstein, G.L. & Moore, G.P. (1967) Neuronal spike trains and stochastic point processes. I. The single spike train. *Biophysical journal*, **7**, 391-418.

Petreanu, L., Mao, T., Sternson, S.M. & Svoboda, K. (2009) The subcellular organization of neocortical excitatory connections. *Nature*, **457**, 1142-1145.

Poulet, J.F. & Petersen, C.C. (2008) Internal brain state regulates membrane potential synchrony in barrel cortex of behaving mice. *Nature*, **454**, 881-885.

Quiroga, R.Q. (2012) Spike sorting. *Curr Biol*, **22**, R45-46.

Quiroga, R.Q., Reddy, L., Kreiman, G., Koch, C. & Fried, I. (2005) Invariant visual representation by single neurons in the human brain. *Nature*, **435**, 1102-1107.

Ramo´ n y Cajal, S. (1923) Recuerdos de mi vida: Historia de mi labor cientı´fica *(Madrid: Alianza Editorial)*

Ratte, S., Hong, S., De Schutter, E. & Prescott, S.A. (2013) Impact of neuronal properties on network coding: roles of spike initiation dynamics and robust synchrony transfer. *Neuron*, **78**, 758-772.

Ray, S. & Maunsell, J.H. (2015) Do gamma oscillations play a role in cerebral cortex? *Trends Cogn Sci*, **19**, 78-85.

Renart, A., de la Rocha, J., Bartho, P., Hollender, L., Parga, N., Reyes, A. & Harris, K.D. (2010) The asynchronous state in cortical circuits. *Science*, **327**, 587-590.

Rey, H.G., Pedreira, C. & Quian Quiroga, R. (2015) Past, present and future of spike sorting techniques. *Brain Res Bull*, **119**, 106-117.

Ribot, J., Aushana, Y., Bui-Quoc, E. & Milleret, C. (2013) Organization and origin of spatial frequency maps in cat visual cortex. *The Journal of neuroscience : the*

official journal of the Society for Neuroscience, **33**, 13326-13343.

Rolls, E.T. & Tovee, M.J. (1994) Processing speed in the cerebral cortex and the neurophysiology of visual masking. *Proc Biol Sci*, **257**, 9-15.

Rousselet, G.A., Fabre-Thorpe, M. & Thorpe, S.J. (2002) Parallel processing in high-level categorization of natural images. *Nature neuroscience*, **5**, 629-630.

Rubin, G.S. & Turano, K. (1992) Reading without saccadic eye movements. *Vision research*, **32**, 895-902.

Rubinov, M. & Sporns, O. (2010) Complex network measures of brain connectivity: uses and interpretations. *NeuroImage*, **52**, 1059-1069.

Sadeh, S., Clopath, C. & Rotter, S. (2015) Processing of Feature Selectivity in Cortical Networks with Specific Connectivity. *PloS one*, **10**, e0127547.

Saleem, K.S., Pauls, J.M., Augath, M., Trinath, T., Prause, B.A., Hashikawa, T. & Logothetis, N.K. (2002) Magnetic resonance imaging of neuronal connections in the macaque monkey. *Neuron*, **34**, 685-700.

Salin, P.A., Kennedy, H. & Bullier, J. (1995) Spatial reciprocity of connections between areas 17 and 18 in the cat. *Canadian journal of physiology and pharmacology*, **73**, 1339-1347.

Salinas, E. & Sejnowski, T.J. (2001) Correlated neuronal activity and the flow of neural information. *Nature reviews. Neuroscience*, **2**, 539-550.

Schmolesky, M.T., Wang, Y., Hanes, D.P., Thompson, K.G., Leutgeb, S., Schall, J.D. & Leventhal, A.G. (1998) Signal timing across the macaque visual system. *Journal of neurophysiology*, **79**, 3272-3278.

Scholl, B. & Priebe, N.J. (2015) Neuroscience: The cortical connection. *Nature*, **518**, 306-307.

Schwindel, C.D., Ali, K., McNaughton, B.L. & Tatsuno, M. (2014) Long-term recordings improve the detection of weak excitatory-excitatory connections in rat prefrontal cortex. *The Journal of neuroscience : the official journal of the Society for Neuroscience*, **34**, 5454-5467.

Sengpiel, F., Baddeley, R.J., Freeman, T.C., Harrad, R. & Blakemore, C. (1998) Different mechanisms underlie three inhibitory phenomena in cat area 17. *Vision research*, **38**, 2067-2080.

Seung, H.S. (2011) Neuroscience: Towards functional connectomics. *Nature*, **471**, 170-172.

Shatz, C.J. & Stryker, M.P. (1978) Ocular dominance in layer IV of the cat's visual cortex and the effects of monocular deprivation. *The Journal of physiology*, **281**, 267-283.

Sherrington CS (1906). The integrative action of the nervous system, *Yale University Press*

Shimono, M. & Beggs, J.M. (2015) Functional Clusters, Hubs, and Communities in the Cortical Microconnectome. *Cerebral cortex*, **25**, 3743-3757.

Siegle, J.H., Pritchett, D.L. & Moore, C.I. (2014) Gamma-range synchronization of fast-spiking interneurons can enhance detection of tactile stimuli. *Nature neuroscience*, **17**, 1371-1379.

Singer, W. (1999) Neuronal synchrony: a versatile code for the definition of relations? *Neuron*, **24**, 49-65, 111-125.

Singer, W. (2013) Cortical dynamics revisited. *Trends Cogn Sci*, **17**, 616-626.

Smith, M.A. & Kohn, A. (2008) Spatial and temporal scales of neuronal correlation in primary visual cortex. *The Journal of neuroscience : the official journal of the Society for Neuroscience*, **28**, 12591-12603.

Sporns, O. (2011) The human connectome: a complex network. *Annals of the New York Academy of Sciences*, **1224**, 109-125.

Sporns, O., Tononi, G. & Kotter, R. (2005) The human connectome: A structural description of the human brain. *PLoS computational biology*, **1**, e42.

Stanley, G.B. (2013) Reading and writing the neural code. *Nature neuroscience*, **16**, 259-263.

Stepanyants, A., Hirsch, J.A., Martinez, L.M., Kisvarday, Z.F., Ferecsko, A.S. & Chklovskii, D.B. (2008) Local potential connectivity in cat primary visual cortex. *Cerebral cortex*, **18**, 13-28.

Steriade, M. (1997) Synchronized activities of coupled oscillators in the cerebral cortex and thalamus at different levels of vigilance. *Cerebral cortex*, **7**, 583-604.

Stettler, D.D., Yamahachi, H., Li, W., Denk, W. & Gilbert, C.D. (2006) Axons and synaptic boutons are highly dynamic in adult visual cortex. *Neuron*, **49**, 877-887.

Swindale, N.V. (1997) Visual cortex: a cat's-eye view of the visual system. *Current biology : CB*, **7**, R387-389.

Swindale, N.V. (1998) Orientation tuning curves: empirical description and estimation of parameters. *Biological cybernetics*, **78**, 45-56.

Symonds, L.L. & Rosenquist, A.C. (1984) Laminar origins of visual corticocortical connections in the cat. *The Journal of comparative neurology*, **229**, 39-47.

Tiesinga, P. & Sejnowski, T.J. (2009) Cortical enlightenment: are attentional gamma oscillations driven by ING or PING? *Neuron*, **63**, 727-732.

Tsuda, I. & Fujii, H. (2007) Chaos reality in the brain. *Journal of integrative neuroscience*, **6**, 309-326.

Tye, K.M. & Deisseroth, K. (2012) Optogenetic investigation of neural circuits underlying brain disease in animal models. *Nature reviews. Neuroscience*, **13**, 251-266.

Tyler, C.J., Dunlop, S.A., Lund, R.D., Harman, A.M., Dann, J.F., Beazley, L.D. & Lund, J.S. (1998) Anatomical comparison of the macaque and marsupial visual cortex: common features that may reflect retention of essential cortical elements. *The Journal of comparative neurology*, **400**, 449-468.

Ugolini, G. (2011) Rabies virus as a transneuronal tracer of neuronal connections. *Advances in virus research*, **79**, 165-202.

Van Hooser, S.D. (2007) Similarity and diversity in visual cortex: is there a unifying theory of cortical computation? *The Neuroscientist : a review journal bringing neurobiology, neurology and psychiatry*, **13**, 639-656.

Vinck, M., Womelsdorf, T., Buffalo, E.A., Desimone, R. & Fries, P. (2013) Attentional modulation of cell-class-specific gamma-band synchronization in awake monkey area v4. *Neuron*, **80**, 1077-1089.

Wang, Q., Webber, R.M. & Stanley, G.B. (2010) Thalamic synchrony and the adaptive gating of information flow to cortex. *Nature neuroscience*, **13**, 1534-1541.

Wang, X.J. & Buzsaki, G. (1996) Gamma oscillation by synaptic inhibition in a hippocampal interneuronal network model. *The Journal of neuroscience : the official journal of the Society for Neuroscience*, **16**, 6402-6413.

Watson, B.O. & Buzsaki, G. (2015) Neural syntax in mental disorders. *Biological psychiatry*, **77**, 998-1000.

Wertz, A., Trenholm, S., Yonehara, K., Hillier, D., Raics, Z., Leinweber, M., Szalay, G., Ghanem, A., Keller, G., Rozsa, B., Conzelmann, K.K. & Roska, B. (2015) PRESYNAPTIC NETWORKS. Single-cell-initiated monosynaptic tracing reveals layer-specific cortical network modules. *Science*, **349**, 70-74.

Whittington, M.A., Traub, R.D. & Jefferys, J.G. (1995) Synchronized oscillations in interneuron networks driven by metabotropic glutamate receptor activation. *Nature*, **373**, 612-615.

Womelsdorf, T., Lima, B., Vinck, M., Oostenveld, R., Singer, W., Neuenschwander, S. & Fries, P. (2012) Orientation selectivity and noise correlation in awake monkey area V1 are modulated by the gamma cycle. *Proceedings of the National Academy of Sciences of the United States of America*, **109**, 4302-4307.

APPENDIX:

Article 1. Bachatene, L., **Bharmauria, V.,** Cattan, S., Chanauria, N., Rouat, J. & Molotchnikoff, S. (2015a) Electrophysiological and firing properties of neurons: Categorizing soloists and choristers in primary visual cortex. *Neuroscience letters*, **604**, 103-108.

Article 2. Bachatene, L., **Bharmauria, V.,** Cattan, S., Chanauria, N., Rouat, J. & Molotchnikoff, S. (2015b) Summation of connectivity strengths in the visual cortex reveals stability of neuronal microcircuits after plasticity. *Bmc Neurosci*, **16**.

Article 3. Bachatene, L.,* **Bharmauria, V.,*** Cattan, S.,* Rouat, J. & Molotchnikoff, S. (2015d) Reprogramming of orientation columns in visual cortex: a domino effect. *Sci Rep-Uk*, **5**.

Article 4. Bachatene, L., **Bharmauria, V**., Cattan, S., Rouat, J. & Molotchnikoff, S. (2015c) Modulation of functional connectivity following visual adaptation: homeostasis in V1. *Brain research*, **1594**, 136-153.

Article 5. Jeyabalaratnam, J., **Bharmauria, V.,** Bachatene, L., Cattan, S., Angers, A. & Molotchnikoff, S. (2013) Adaptation shifts preferred orientation of tuning curve in the mouse visual cortex. *PloS one*, **8**, e64294.

Article 6. Cattan, S., Bachatene, L., **Bharmauria, V.,** Jeyabalaratnam, J., Milleret, C. & Molotchnikoff, S. (2014) Comparative analysis of orientation maps in areas 17 and 18 of the cat primary visual cortex following adaptation. *European Journal of Neuroscience*, **40**, 2554-2563.

Article 7. Bachatene, L., **Bharmauria, V.,** Cattan, S. & Molotchnikoff, S. (2013) Fluoxetine and serotonin facilitate attractive-adaptation-induced orientation plasticity in adult cat visual cortex. *The European Journal of neuroscience*, **38**, 2065-2077.

Article 8. Bachatene, L., **Bharmauria, V**., Rouat, J. & Molotchnikoff, S. (2012) Adaptation-induced plasticity and spike waveforms in cat visual cortex. *Neuroreport*, **23**, 88-92.

Chapter 1: Bachatene, L.,* **Bharmauria, V.,*** Molotchnikoff, S. (2012) Adaptation and Neuronal Network in Visual Cortex. Visual Cortex—Current status and perspectives, doi.org/10.5772/46011

Neuroscience Letters 604 (2015) 103–108

Contents lists available at ScienceDirect

Neuroscience Letters

journal homepage: www.elsevier.com/locate/neulet

Research paper

Electrophysiological and firing properties of neurons: Categorizing soloists and choristers in primary visual cortex

Lyes Bachatene[a,b], Vishal Bharmauria[a,b], Sarah Cattan[a,b], Nayan Chanauria[a,b], Jean Rouat[a,b], Stéphane Molotchnikoff[a,b,*]

[a] Laboratoire de Neurosciences de la vision, Département de Sciences Biologiques, Université de Montréal, Montréal, QC, Canada
[b] Neurosciences Computationnelles et Traitement Intelligent des Signaux NECOTIS, Université de Sherbrooke, Québec, Canada

HIGHLIGHTS

- Neurons in cats' V1 exhibit variability in correlation with the population rate.
- Population coupling highly depends on the neuronal firing rate.
- Thin spike cells highly correlate their firing with the population.
- Broad spike cells fire independently being more soloists.

ARTICLE INFO

Article history:
Received 8 June 2015
Received in revised form 30 July 2015
Accepted 31 July 2015
Available online 3 August 2015

Keywords:
Soloists
Choristers
Visual cortex
Thin spike neurons
Broad spike neurons
Visual processing
Firing rate

ABSTRACT

Visual processing in the cortex involves various aspects of neuronal properties such as morphological, electrophysiological and molecular. In particular, the neural firing pattern is an important indicator of dynamic circuitry within a neuronal population. Indeed, in microcircuits, neurons act as soloists or choristers wherein the characteristical activity of a 'soloist' differs from the firing pattern of a 'chorister'. Both cell types correlate their respective firing rate with the global populational activity in a unique way. In the present study, we sought to examine the relationship between the spike shape (thin spike neurons and broad spike neurons) of cortical neurons recorded from V1, their firing levels and their propensity to act as soloists or choristers. We found that thin spike neurons, which exhibited higher levels of firing, generally correlate their activity with the neuronal population (choristers). On the other hand, broad spike neurons showed lower levels of firing and demonstrated weak correlations with the assembly (soloists). A major consequence of the present study is: estimating the correlation of neural spike trains with their neighboring population is a predictive indicator of spike waveforms and firing level. Indeed, we found a continuum distribution of coupling strength ranging from weak correlation-strength (attributed to low-firing neurons) to high correlation-strength (attributed to high-firing neurons). The tendency to exhibit high- or low-firing is conducive to the spike shape of neurons. Our results offer new insights into visual processing by showing how high-firing rate neurons (mostly thin spike neurons) could modulate the neuronal responses within cell-assemblies.

1. Introduction

Sensory information is represented in the cortex by networks of co-activated neurons which coordinate their firing activity, thus forming functional assemblies [25]. Encoding stimulus attributes involves a variety of strategies considering the anatomical and functional divergence within neuronal populations. Indeed, based on their intrinsic electrophysiological properties, cortical cells are classified into different types such as regular-spiking (RS), fast-rhythmic-bursting (FRB), fast-spiking (FS) and intrinsically bursting (IB) neurons [35]. Despite the fact that neurons exhibit large panoply of firing properties, their correlated activities within assemblies efficiently code the stimulus features rather than the independent spiking of each involved neuron [25]. As a matter of fact, it is largely reported that neurons coding for similar attributes exhibit high levels of correlation and are thus functionally strongly

Abbreviations: CCG, cross-correlogram; HF, high firing; LF, low firing.

* Corresponding author at: Département de Sciences Biologiques Université de Montréal CP 6128 Succ. Centre-Ville Montréal, QC H3C 3J7, Canada.

http://dx.doi.org/10.1016/j.neulet.2015.07.049
0304-3940/

connected to each other [1,7,12,20,34,39] yet, the debate remains controversial [28,29,32,38]. However, in spite of the stimulus-selective correlation aspect, each neuron may also show coupling with its neighboring local population [27] as if it belongs to a "neuronal orchestra" [15]. It was recently shown in the mouse primary visual cortex and monkey area V4 that, regardless of neuronal preferences, population coupling may lead to discrimination between the choristers (highly coupled) and soloists (weakly coupled) [27]. These two groups differ in many aspects. For instance, highly correlated neurons may receive stronger synaptic drive from neighboring cells [27]. In addition, noise correlation (R_{sc}) is higher for choristers than soloists in IT cortex [18]. Anatomical differences were also observed since the cortical laminar distribution for these types of units is distinct [18]. In mouse V1, population coupling varies between the narrow-spiking and regular-spiking neurons; however, this difference was reported to be smaller than the class-variability [27]. In the present investigation, we sought to examine the relationship between the cell-type (thin spike and broad spike neurons), the firing rate (high-firing and low-firing) and the population coupling of above classes in adult anesthetized cats (columnar-organized cortex). We found that thin spike neurons systematically exhibited higher firing levels than broad spike neurons. In addition, high-firing (HF) neurons displayed higher coupling strength than the low-firing (LF) neurons.

We report that within a sub-network, LF neurons (which were mostly broad spike neurons and weakly coupled) and HF neurons (mainly thin spike neurons and highly coupled) likely play distinct roles in information coding where high-firing neurons may orchestrate the sensory selectivity of the neighboring cells.

2. Materials and methods

2.1. Ethical approval

Animal surgery procedures and electrophysiological recordings followed the guidelines of the Canadian Council on Animal Care and were approved by the Institutional Animal Care and Use Committee of the University of Montreal. Animals were supplied by the Division of Animal Resources of the University of Montreal. The experiments were conducted in accordance with the Guide for Care and Use of Laboratory Animals of the National Institutes of Health (USA).

Details of animal surgery, electrophysiology, visual stimulation and isolation of neurons are described in Bachatene et al. [4].

2.2. Cross-correlation computations

Cross-correlogram shows the conditional probability of a spike at time $t_0 + t$ on the condition that there is a reference event (or reference spike, spike-by-spike analysis) at time t_0. The spike train of each neuron was cross-correlated with the population rate activity (the multi-unit activity) at its preferred orientation (Fig. 1A). Time axis is divided into bins. The first bin is defined as: XMin, XMin + Bin. The next bin is XMin + Bin, XMin + Bin × 2, *etc.* We calculated the distances from each spike to all spikes of the spike train as follows:

$$d[i] = t_s[i] - \mathrm{ref}[k]$$

where t_s[i] represents the spike train, and ref[k] is each timestamp.

Bin counts were then divided by the number of reference events to normalize the counts per bin into probabilities. 95% statistical threshold for the significance of the bins was used. Each bin-width was set at 1 ms and a Gaussian filter width of 3 bins was used. Probabilities were calculated from the counts/bin as follows:

$$P = \frac{N}{T} \times b$$

where N/T is the neuron frequency and b represents the bin size of the calculated firing of the neuron. T represents the total time interval and N the number of spikes within this interval.

The 95% confidence limit was calculated assuming that the expected bin count (C) has a Poisson distribution:

$$C = P \times N\mathrm{ref}$$

where Nref is the number of reference events.

The 95% confidence limit is calculated as follows:

$$\text{Low Conf.} = x \text{ such that } \mathrm{Prob}(S < x) = 0.005$$

$$\text{High Conf.} = y \text{ such that } \mathrm{Prob}(S > y) = 0.005$$

where S represents a random variable which has a Poisson distribution with parameter C.

Raw cross-correlograms were corrected by using a shift-predictor procedure in order to eliminate the putative significant peaks resulting from the coincident firing due to simultaneous visual drive during each trial [4,13].

3. Results

3.1. Coupling strength strategy

We performed electrophysiological recordings in primary visual cortex of adult anesthetized cats ($n = 8$) that were visually stimulated (drifting sine-wave grating patches covering the excitatory fields, spatial frequency = 0.24 cycle/°, temporal frequency = 1.0–2.0 Hz, contrast = 80%, orientations: from 0° to 157.5°, 25 trials, stimulus duration: 4.1 s [5]). Recordings were performed from multiple cortical sites using multi-channel electrodes. Spiking responses were sorted from the multi-unit activity. In addition to the distinct waveforms, the isolation of cells was based on the classical procedure, *i.e.*, principal component analysis, autocorrelograms and cluster separation (Mahalanobis distance and mean cluster distance) [5,8].

We cross-correlated the firing activity of each neuron with the firing of the global population of neurons (multi-unit activity) using the shift-corrected cross-correlation computation (see Section 2 for details). Fig. 1A shows the population coupling strategy: raster plots of three simultaneously recorded cells and their coupling strength indicated by the peak straddling zero in the corresponding correlograms along with the population rate (three superimposed cross-correlograms with the respective color code for each neuron) are displayed. In this example, the green cell exhibited larger correlation-strength than the blue and purple cells. The histogram distribution of all values for correlation-strengths is displayed in Fig. 1B. Note that the values of coupling strengths were normalized (minimum value corresponds to zero, maximum value corresponds to 1) due to the variability between all experiments ($n = 73$ neurons). The absence of a bimodal mode suggests that the coupling strength ranges from low to high values. However, differences were observed based on two parameters: the spike-type and the firing rate (see next Sections).

3.2. Spike-types and coupling strength

In total, 73 neurons were isolated and classified into two major types, namely thin spike neurons ($n = 30$) and broad spike neurons ($n = 43$). Spike-width was quantified as the interval between the

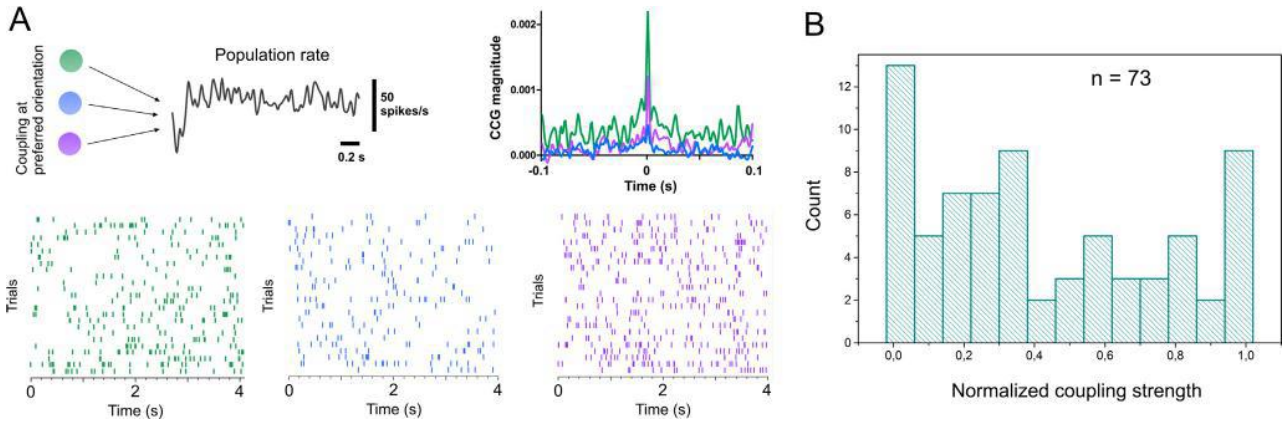

Fig. 1. Correlation strategy.
(A) Schematic representation of the correlation procedure between three recorded neurons and the populational rate. Raster plots of the spiking activity of the neurons and respective superimposed cross-correlograms are displayed. (B) Histogram distribution of the coupling strengths for all experiments ($n = 73$).

trough and peak of the average spike wave-shape of the neuron, allowing for the distinction between broad waveforms (spike-width $\geq$0.5 ms) and narrow waveforms (spike-width <0.5 ms) [4,9,22,31]. An example is shown in Fig. 2A where thin spike neurons and broad spike cells have distinct waveform with a trough-to-peak latency of 0.33 ms and 0.55 ms, respectively. Superimposed spike-waveforms of 20 cells are shown for each type in Fig. 2B. The bold traces represent the average waveforms. Fig. 2C illustrates the distribution of the thin spike neurons (black) and the broad spike neurons (orange) depending on their trough-to-peak interval (trough-to-peak interval <0.5 ms, mean = 0.30 $\pm$ 0.04 ms, for thin spike cells, trough-to-peak interval $\geq$0.5 ms, mean = 0.52 $\pm$ 0.04 ms, for broad spike cells [4,9,22,31]). Averaged spike-widths are displayed in Fig. 2D.

Fig. 2E illustrates the respective cross-correlation of a thin spike neuron and a broad spike neuron (the spike shapes are represented above each CCG) with the populational activity. Indeed, the correlation-strength indicated by the significant peaks in the cross-correlograms was notably different for the thin spike neurons (black CCG, CCG magnitude = 0.005) and the broad spike neurons (orange CCG, CCG magnitude = 0.0003). Fig. 2F and G display examples of cross-correlograms between the populational activity and the firing rate of thin spike cells (black) and broad spike cells (orange), respectively. This tendency was observed for all sampled neurons. The averaged values were 0.003 $\pm$ 0.0009 and 0.001 $\pm$ 0.0004 for thin spike cells and broad spike cells, respectively (t-test, $p < 0.05$, Fig. 2H).

3.3. *Firing rate, spike-type and categorization of soloists and choristers*

Correlating the spike trains of each neuron with the population rate generates two notable behaviors within the assembly: neurons acting as soloists show a weak correlation index whereas neurons acting as choristers exhibit strong correlation with the population activity. It has been suggested that soloists are distinct from choristers in many aspects such as the synaptic connectivity [27] and the laminar distribution [18]. We examined the relationship between the waveform type, the firing rate and the correlation-strength of the cells' firing with the population activity. Typical examples of response-frequency plots to optimal orientation are shown in Fig. 3A (same neurons as in Fig. 2F, G). The relationship between the firing rate and the presented oriented stimuli is displayed in Fig. 3B; polar plots of two neurons (thin and broad spikes) exhibit differences in their orientation tuning and firing rate. It may be worthwhile to underline that poorly tuned cells are often associated with thin spike neurons whereas highly tuned neurons are related to broad spike neurons [2,3,6,10,16,17,21,24,36].

Moreover, we found that thin spike cells presented higher levels of firing rate in comparison to broad spike cells (responses measured for optimal orientations, Fig. 3C, t-test, $p < 0.01$).

In addition, we sought to examine the relationship between the firing rate and the coupling strength. Fig. 3D illustrates these correlations for all experiments. We observed significantly higher correlations between the firing rate and the coupling activity as the R-squared ranged from 0.75 to 0.99.

4. Discussion

In the current study, we classified simultaneously recorded neurons from primary visual cortex of adult anesthetized cats into thin spike neurons and broad spike neurons and studied their firing rate patterns. These two parameters (spike waveforms and firing rate level) were then related to the coupling strength of neurons with the neighboring population. The firing activity of a neuron characterized as a 'chorister' is highly correlated with the firing rate of the global population. On the other hand, a 'soloist' tends to be more autonomous, exhibiting independent firing [23,27]. Here we found a systematic relationship between the cell-class, the firing pattern and the correlation-strength of neurons. Despite the large diversity of cell-types, cortical neurons coordinate their spiking activity forming functional sub-networks which, when co-activated encode the attributes of stimuli [25]. It is extensively reported that sensory neurons may exhibit different levels of correlation depending largely on their selectivity to specific sets of stimuli [1,7,12,20,34,39], though the debate persists [28,29,32,38].

It has been reported that the correlation properties are inherent characteristics of neurons [27]. Indeed, for both stimulation condition and spontaneous activity, soloists and choristers maintain their distinct firing-patterns such as carrying more general information for choristers than soloists [23,27]. On other hand, this correlation seems to be independent of neuronal sparseness and plays a key role in predicting visual search efficiency in humans [18].

Moreover, in rodent sensory cortex, it has been shown that soloists and choristers can be dissociated based on several features. Soloists were reported to be less functionally connected as they were driven less effectively by optogenetic activation [27]. Significant distinction in noise correlation, which represents the

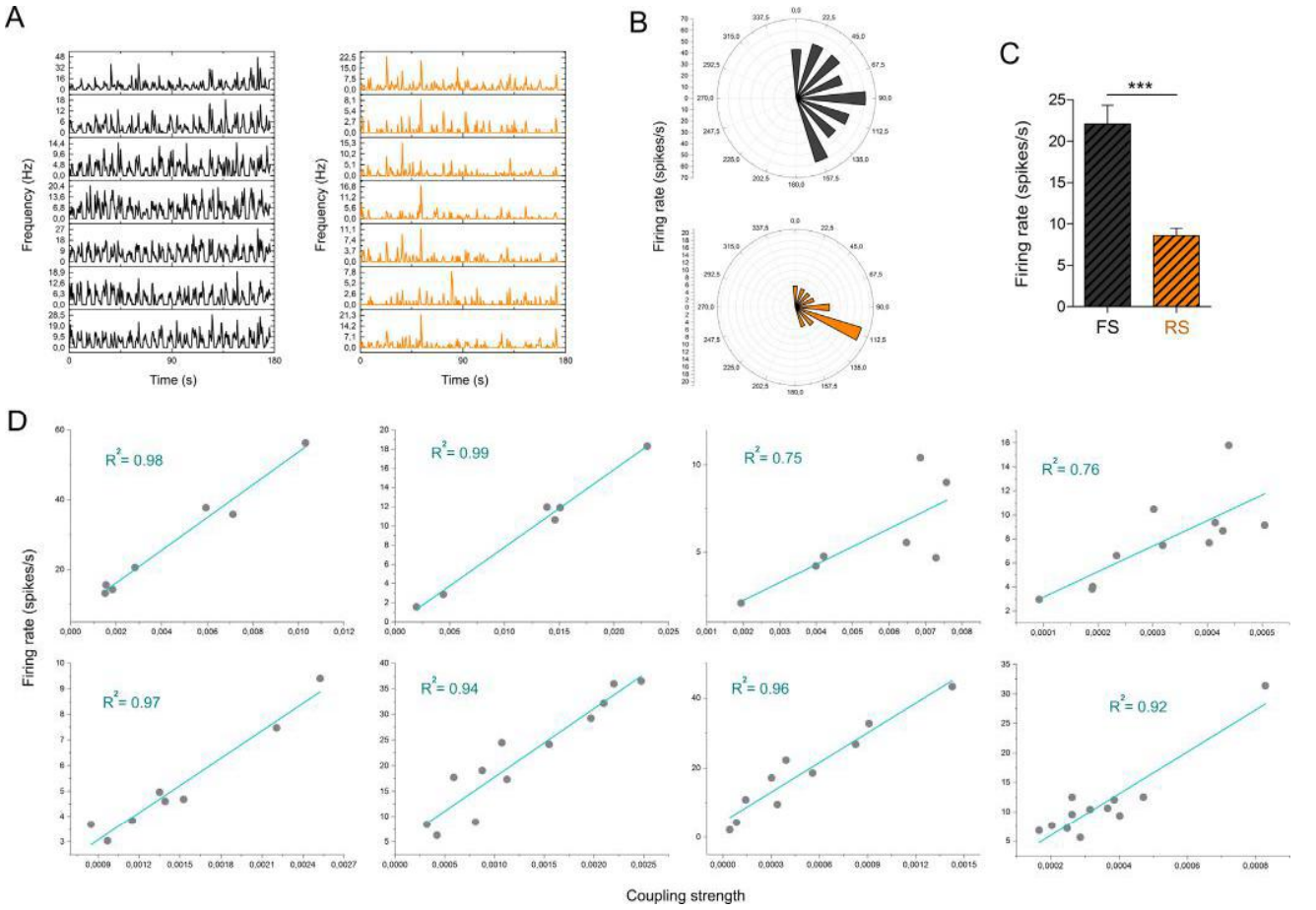

Fig. 3. Firing rate, spike-type and coupling strength.
(A) Frequency plots of typical examples of thin spike neurons (black) and broad spike neurons (orange). Note the differences on *Y*-axis scales. (B) Polar plots of two neurons showing the relationship between the stimulus and the firing rate. The broad spike neuron (orange) exhibit higher selectivity (sharply tuned). (C) Global statistics on the difference in firing rate levels between thin spike neurons and broad spike neurons. (D) Regression analyses between the firing rate and the correlation-strength for all experiments. *R*-squared values are indicated for each graphic (For interpretation of the references to color in this figure legend, the reader is referred to the web version of this article.).

correlation coefficient of spike count responses to the presentation of a stimulus [11], has also been reported; noise correlation (R_{sc}) was much higher for choristers than for soloists in IT cortex [18]. Laminar differences were observed in macaque IT where soloists are common at 0.2 and 1.2 mm depth, whereas choristers are rare in layer 4 and are located in non-granular output layers [18]. In the present investigation, we report that in cat's primary visual cortex, which exhibits a columnar organization, thin spike neurons exhibited higher firing levels and tend to differ in their coupling with their ensemble from broad spike neurons exhibiting lower firing levels and weaker population coupling. It has been reported that thin spike neurons and broad spike neurons exhibit different tuning properties [2,3,6,10,16,17,21,24,36]; thin spike cells being poorly tuned to orientation stimuli whereas broad spike cells being more highly tuned.

Furthermore, in cat's visual cortex, large number of excitatory neurons exhibit narrow spikes making the spike-width a non-valid parameter, therefore not permitting the distinction between pyramidal cells and inhibitory interneurons [26]. A recent study demonstrated that in cat V1, neurons show similar diversity in their spike-widths. In addition, neurons with a broad spike exhibit higher correlation levels between each other [31]. On the contrary, we found that correlating the spiking activity of each spike-waveform with the population activity shows the opposite trend: cells with a narrow spike-shape (also highly firing) exhibited greater coupling strengths than cells with a broad spike-shape. It is to be emphasized that on a cell–pair basis, the firing rates and peak magnitudes in CCG's are unrelated [14,30,33].

Complex circuitry mechanisms of individual neurons and the assemblies they form are involved in visual information processing [19]. Thus, measuring correlated spike-trains between neurons and the entire group predicts the spike shape and the firing rate pattern as the coupling level can be distinguishable between broad spike neurons (mainly LF neurons) and thin spike neurons (mainly HF neurons). Synchrony within a restricted space such as a cortical orientation domain can be accomplished by their specific relationships [37].

Combined with our recent finding which confers to the thin spike neurons higher gamma activity [8], these findings provide new insights into visual information processing. Indeed, within a cell-assembly comprising different cell-types, HF neurons may modulate the inputs and contribute to the selectivity of broad spike neurons in a recurrent "broad spike–thin spike" neuronal ensemble. A schematic model of a neuronal population is illustrated in Fig. 4 where a stimulus is coded by a cell-assembly; the HF neurons (black) are more correlated with the neuronal ensemble. This may occur to ensure an efficient firing of neurons preferring the presented stimulus. LF neurons (orange) are less coupled to the population but exhibit correlations with neighboring neurons preferring the same orientation.

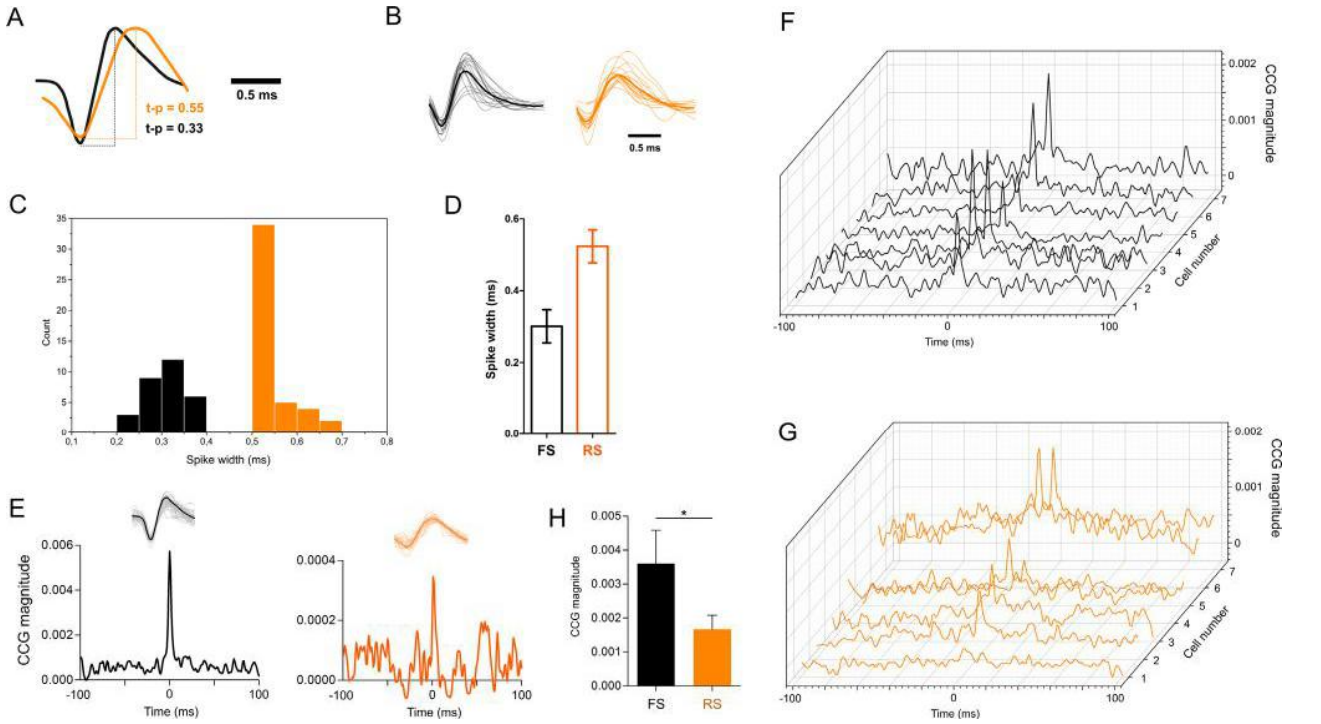

Fig. 2. Population coupling and types of neurons.
(A) Examples of two simultaneously recoded neurons showing the measurements of the spike-widths (trough-to-peak intervals). (B) Superimposed spike-waveforms of 20 cells from each type. The bold traces represent the average waveforms. (C) Histogram distribution of the trough-to-peak intervals for all neurons ($n = 73$). Orange and black histograms reflect the broad spike and the thin spike cells, respectively. (D) Averaged spike-widths for each cell-type. (E) Cross-correlograms between two neurons (the respective spike-waveforms are shown above each CCG) and the global spiking activity of the neuronal population. *X*-axis represents the time-window and *Y*-axis indicates the magnitude of the CCG. (F and G) Cross-correlograms between a group of thin spike cells (black) and the population rate (F), and between broad spike cells (orange) and the populational rate (G). (H) Global statistics on the correlation-strength for all neurons ($n = 73$) (For interpretation of the references to color in this figure legend, the reader is referred to the web version of this article.).

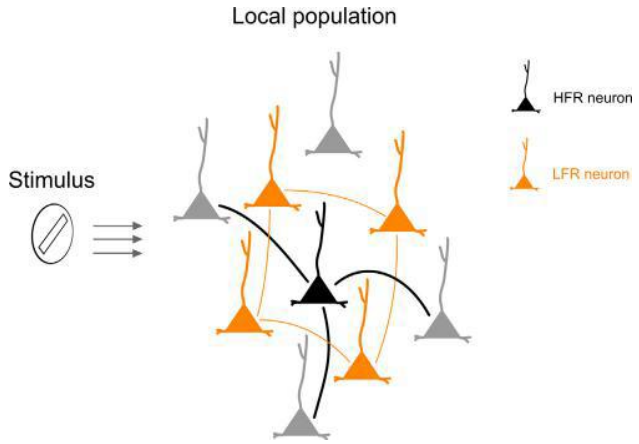

Fig. 4. Schematic model of a neuronal ensemble and the respective putative functional connections between thin spike neurons (HF neurons) and broad spike cells (LF neurons). (For interpretation of the references to color in the text, the reader is referred to the web version of this article.)

Conflict of interest

The authors have no conflicts of interest to declare.

Acknowledgements

Funding were supported by CRSNG (Conseil de Recherches en Sciences Naturelles et en Génie) and FRQ-NT (Fonds de recherche du Québec—Nature et technologies).

References

[1] K.D. Alloway, S.A. Roy, Conditional cross-correlation analysis of thalamocortical neurotransmission, Behav. Brain Res. 135 (2002) 191–196.
[2] B.V. Atallah, W. Bruns, M. Carandini, M. Scanziani, Parvalbumin-expressing interneurons linearly transform cortical responses to visual stimuli, Neuron 73 (2012) 159–170.
[3] R. Azouz, C.M. Gray, L.G. Nowak, D.A. McCormick, Physiological properties of inhibitory interneurons in cat striate cortex, Cereb. Cortex 7 (1997) 534–545.
[4] L. Bachatene, V. Bharmauria, S. Cattan, J. Rouat, S. Molotchnikoff, Modulation of functional connectivity following visual adaptation: homeostasis in V1, Brain Res. 1594 (2015) 136–153.
[5] L. Bachatene, V. Bharmauria, S. Cattan, J. Rouat, S. Molotchnikoff, Reprogramming of orientation columns in visual cortex: a domino effect, Sci. Rep. 5 (2015) 9436.
[6] L. Bachatene, V. Bharmauria, J. Rouat, S. Molotchnikoff, Adaptation-induced plasticity and spike waveforms in cat visual cortex, Neuroreport 23 (2012) 88–92.
[7] P. Bartho, H. Hirase, L. Monconduit, M. Zugaro, K.D. Harris, G. Buzsaki, Characterization of neocortical principal cells and interneurons by network interactions and extracellular features, J. Neurophysiol. 92 (2004) 600–608.
[8] V. Bharmauria, L. Bachatene, S. Cattan, N. Chanauria, J. Rouat, S. Molotchnikoff, Stimulus-dependent augmented gamma oscillatory activity between the functionally connected cortical neurons in the primary visual cortex, Eur. J. Neurosci. 41 (2015) 1587–1596.
[9] D.S. Bortone, S.R. Olsen, M. Scanziani, Translaminar inhibitory cells recruited by layer 6 corticothalamic neurons suppress visual cortex, Neuron 82 (2014) 474–485.
[10] J.A. Cardin, L.A. Palmer, D. Contreras, Stimulus feature selectivity in excitatory and inhibitory neurons in primary visual cortex, J. Neurosci. 27 (2007) 10333–10344.
[11] M.R. Cohen, A. Kohn, Measuring and interpreting neuronal correlations, Nat. Neurosci. 14 (2011) 811–819.
[12] J. Csicsvari, H. Hirase, A. Czurko, G. Buzsaki, Reliability and state dependence of pyramidal cell-interneuron synapses in the hippocampus: an ensemble approach in the behaving rat, Neuron 21 (1998) 179–189.
[13] Y. Dong, S. Mihalas, F. Qiu, R. von der Heydt, E. Niebur, Synchrony and the binding problem in macaque visual cortex, J. Vis. 8 (2008) 1–34.

[14] F. Duret, S. Shumikhina, S. Molotchnikoff, Neuron participation in a synchrony-encoding assembly, BMC Neurosci. 7 (2006) 72.
[15] A. Grinvald, A. Arieli, M. Tsodyks, T. Kenet, Neuronal assemblies: single cortical neurons are obedient members of a huge orchestra, Biopolymers 68 (2003) 422–436.
[16] S.B. Hofer, H. Ko, B. Pichler, J. Vogelstein, H. Ros, H. Zeng, E. Lein, N.A. Lesica, T.D. Mrsic-Flogel, Differential connectivity and response dynamics of excitatory and inhibitory neurons in visual cortex, Nat. Neurosci. 14 (2011) 1045–1052.
[17] H. Hu, J. Gan, P. Jonas, Interneurons, Fast-spiking, parvalbumin(+) GABAergic interneurons: from cellular design to microcircuit function, Science 345 (2014) 1255263.
[18] C.P. Hung, D. Cui, Y.P. Chen, C.P. Lin, M.R. Levine, Correlated activity supports efficient cortical processing, Front. Computat. Neurosci. 8 (2014) 171.
[19] H. Ko, Neuroscience. Functional organization of synaptic connections in the neocortex, Science 346 (2014) 555.
[20] H. Ko, S.B. Hofer, B. Pichler, K.A. Buchanan, P.J. Sjostrom, T.D. Mrsic-Flogel, Functional specificity of local synaptic connections in neocortical networks, Nature 473 (2011) 87–91.
[21] S.J. Kuhlman, E. Tring, J.T. Trachtenberg, Fast-spiking interneurons have an initial orientation bias that is lost with vision, Nat. Neurosci. 14 (2011) 1121–1123.
[22] Y.T. Li, B.H. Liu, X.L. Chou, L.I. Zhang, H.W. Tao, Strengthening of Direction Selectivity by Broadly Tuned and Spatiotemporally Slightly Offset Inhibition in Mouse Visual Cortex, Cereb. Cortex (2014), http://dx.doi.org/10.1093/cercor/bhu049 [Epub ahead of print].
[23] C.P. Lin, Y.P. Chen, C.P. Hung, Tuning and spontaneous spike time synchrony share a common structure in macaque inferior temporal cortex, J. Neurophysiol. 112 (2014) 856–869.
[24] D.A. McCormick, B.W. Connors, J.W. Lighthall, D.A. Prince, Comparative electrophysiology of pyramidal and sparsely spiny stellate neurons of the neocortex, J. Neurophysiol. 54 (1985) 782–806.
[25] J.E. Miller, I. Ayzenshtat, L. Carrillo-Reid, R. Yuste, Visual stimuli recruit intrinsically generated cortical ensembles, Proc. Natl. Acad. Sci. U. S. A. 111 (2014) E4053–E4061.
[26] L.G. Nowak, R. Azouz, M.V. Sanchez-Vives, C.M. Gray, D.A. McCormick, Electrophysiological classes of cat primary visual cortical neurons in vivo as revealed by quantitative analyses, J. Neurophysiol. 89 (2003) 1541–1566.
[27] M. Okun, N.A. Steinmetz, L. Cossell, M.F. Iacaruso, H. Ko, P. Bartho, T. Moore, S.B. Hofer, T.D. Mrsic-Flogel, M. Carandini, K.D. Harris, Diverse coupling of neurons to populations in sensory cortex, Nature 521 (2015) 511–515.
[28] B.J. Palanca, G.C. DeAngelis, Does neuronal synchrony underlie visual feature grouping? Neuron 46 (2005) 333–346.
[29] P.R. Roelfsema, V.A. Lamme, H. Spekreijse, Synchrony and covariation of firing rates in the primary visual cortex during contour grouping, Nat. Neurosci. 7 (2004) 982–991.
[30] E.T. Rolls, A. Treves, The neuronal encoding of information in the brain, Prog. Neurobiol. 95 (2011) 448–490.
[31] D.P. Schulz, M. Sahani, M. Carandini, Five key factors determining pairwise correlations in visual cortex, J. Neurophysiol. (jn 94) (2015) 02015.
[32] M.N. Shadlen, J.A. Movshon, Synchrony unbound: a critical evaluation of the temporal binding hypothesis, Neuron 24 (1999) 67–77.
[33] S. Shumikhina, J. Guay, F. Duret, S. Molotchnikoff, Contextual modulation of synchronization to random dots in the cat visual cortex, Exp. Brain Res. 158 (2004) 223–232.
[34] A. Stepanyants, J.A. Hirsch, L.M. Martinez, Z.F. Kisvarday, A.S. Ferecsko, D.B. Chklovskii, Local potential connectivity in cat primary visual cortex, Cereb. Cortex 18 (2008) 13–28.
[35] M. Steriade, Neocortical cell classes are flexible entities, Nat. Rev. Neurosci. 5 (2004) 121–134.
[36] H.A. Swadlow, Efferent neurons and suspected interneurons in binocular visual cortex of the awake rabbit: receptive fields and binocular properties, J. Neurophysiol. 59 (1988) 1162–1187.
[37] P. Tiesinga, T.J. Sejnowski, Cortical enlightenment: are attentional gamma oscillations driven by ING or PING? Neuron 63 (2009) 727–732.
[38] C. van der Togt, S. Kalitzin, H. Spekreijse, V.A. Lamme, H. Super, Synchrony dynamics in monkey V1 predict success in visual detection, Cereb. Cortex 16 (2006) 136–148.
[39] Y. Yoshimura, J.L. Dantzker, E.M. Callaway, Excitatory cortical neurons form fine-scale functional networks, Nature 433 (2005) 868–873.

Bachatene *et al. BMC Neurosci (2015) 16:64*
DOI 10.1186/s12868-015-0203-1

BMC Neuroscience

RESEARCH ARTICLE Open Access

Summation of connectivity strengths in the visual cortex reveals stability of neuronal microcircuits after plasticity

Lyes Bachatene[1,2], Vishal Bharmauria[1,2], Sarah Cattan[1,2], Nayan Chanauria[1,2], Jean Rouat[1,2] and Stéphane Molotchnikoff[1,2*]

Abstract

Background: Within sensory systems, neurons are continuously affected by environmental stimulation. Recently, we showed that, on cell-pair basis, visual adaptation modulates the connectivity strength between similarly tuned neurons to orientation and we suggested that, on a larger scale, the connectivity strength between neurons forming sub-networks could be maintained after adaptation-induced-plasticity. In the present paper, based on the summation of the connectivity strengths, we sought to examine how, within cell-assemblies, functional connectivity is regulated during an exposure-based adaptation.

Results: Using intrinsic optical imaging combined with electrophysiological recordings following the reconfiguration of the maps of the primary visual cortex by long stimulus exposure, we found that within functionally connected cells, the summed connectivity strengths remain almost equal although connections among individual pairs are modified. Neuronal selectivity appears to be strongly associated with neuronal connectivity in a "homeodynamic" manner which maintains the stability of cortical functional relationships after experience-dependent plasticity.

Conclusions: Our results support the "homeostatic plasticity concept" giving new perspectives on how the summation in visual cortex leads to the stability within labile neuronal ensembles, depending on the newly acquired properties by neurons.

Keywords: Visual cortex, Plasticity, Summation, Correlation, Adaptation

Background

Visual processing in the brain highly depends on physiological connectivity of neurons to establish functional circuits in the visual cortex. Specific neuronal connections are framed between stimulus selective neurons (functional circuits) within cell-assemblies that process visual information [1]. These recruited functional circuits, when co-activated, encode the attributes of stimuli [2] and are believed to be crucial for visual perception [1]. It is well established that neurons sharing similar selectivity vigorously and strongly connect with each other in response to the visual stimulation [1, 3, 4].

In a recent report [5], we showed that neurons exhibit changes in the correlation-strength after adaptation for their original optimal and new acquired optimal orientations suggesting that adaptation impacts the strength of their functional connections. These previous data were investigated on cell-pairs basis and focused exclusively on cells sharing similar orientations before and after adaptation phase. Hence the previous report was not centered on the large spectrum of orientations. In the present paper, seeking a deeper understanding how connectivity-strength is modified, we further broadened analyses by investigating the connection strengths between cells selective to a wide range of orientations as revealed within a cluster of neurons. Thus, crosscorrelograms

[1] Laboratoire de Neurosciences de la vision, Département de Sciences Biologiques, Université de Montréal, CP 6128 Succ. Centre-Ville, Montréal, QC H3C 3J7, Canada
Full list of author information is available at the end of the article

were computed between all cells of a cluster irrespective of the axis of the preferred orientation. The magnitudes of the central pic were computed to derive the strength of inter-neuronal functional relationships and then we investigated the modulation of crosscorrelogram pics following adaptation. In addition, the present paper focuses on a summative model which explains how within cell-assemblies formed by similarly tuned and differently tuned neurons, the summed connectivity strength remained relatively unchanged during plasticity. We recorded visual responses from neuronal units and populations using extracellular electrophysiological recordings and intrinsic optical imaging. Brain plasticity is an inherent feature of cortical neurons that is inevitable for animals to adapt to the environment. The cortical organization is well known to be malleable mostly during early stages of life [6, 7]. For instance, visual neurons of animals raised in a forced, stripped environment exhibit orientation-preference shifts toward the imposed stimulus [7]. Such plastic changes have been widely observed at neuronal [8–11] and populational levels [10, 12, 13]. In principle, these changes are attributed to visual deprivation or visual training (adaptation).

Crosscorrelations have been widely employed to reveal the putative functional connections between neurons [14–16]. We crosscorrelated the spiking activity of simultaneously recorded neurons to reveal the functional relationships between them.

Our results are in line with the concept of homeostatic plasticity [17–19]. Indeed, a homeostatic process is established in order to stabilize the initial global connectivity strength of the neuronal group [19]. This regulatory activity is considered as a complementary process to the Hebbian plasticity wherein changes of synaptic strength are observed in order to redefine the properties of neuronal-assemblies [19–21].

Methods

Ethical approval

Animal surgery procedures and electrophysiological recordings followed the guidelines of the Canadian Council on Animal Care and were approved by the Institutional Animal Care and Use Committee of the University of Montreal. Animals were supplied by the Division of Animal Resources of the University of Montreal. The experiments were conducted in accordance with the Guide for Care and Use of Laboratory Animals of the National Institutes of Health (USA).

Animal surgery

Briefly, electrophysiological recordings and optical imaging were performed within layer II/III of V1 area of adult anaesthetized cats (Felis catus). Eight adult cats (2.5–3.5 kg, age 12–24 months) of either sex were used for this study. General anaesthesia was maintained by artificial ventilation with a mixture of N_2O/O_2 (70:30) supplemented with 0.5 % isoflurane (AErrane, Baxter, Toronto, ON, Canada) for the duration of the experiment. The following parameters were monitored throughout the experiment: the EEG, the expired CO_2, the temperature and the heart rate. At the end of each experiment, euthanasia was achieved with a lethal dose of pentobarbital sodium (Somnotol, MTC Pharmaceuticals, Cambridge, ON, Canada; 100 mg kg^{-1}) by intravenous injection. Details are described in Bachatene et al. [5].

Electrophysiology

Visual stimuli were generated with a VSG 2/5 graphic board (Cambridge Research Systems, Rochester, England) and displayed on a 21-in. monitor (Sony GDM-F520 Trinitron, Tokyo, Japan) placed 57 cm from the cat's eyes, with 1024 × 768 pixels, running at 100 Hz frame refresh. Stimuli were drifting sine-wave grating square patches (~2°–5°) covering the excitatory RF (unidirectional movement). Patches characteristics were set to evoke optimal responses: contrast at 80 %, mean luminance at 40 cd/m^2, optimal spatial and temporal frequencies set within the 0.1–0.5 cycles/deg. and 1.0–2.0 Hz range, respectively. In all cases the above parameters were chosen with the aim of evoking the maximal discharges. After manual RF characterization, nine oriented stimuli centered on the preferred orientation were selected and used for the rest of the experiment. Test orientations were applied in random order. Each oriented stimulus was presented in blocks of 25 trials lasting 4.1 s each, with a random inter-trial interval (1.0–3.0 s) during which no stimuli were presented. Thus, a recording session lasted for 25–30 min. Peri-stimulus time histograms were recorded. Once control orientation tuning curves were characterized, an adapting non-preferred stimulus was presented continuously for 3 or 12 min and 24 min in one experiment. The adapting stimulus was a drifting grating whose orientation was randomly selected in the range 22.5°–67.5° off of the neuron's preferred orientation. All other stimulus parameters were kept constant, at control values, throughout the recordings. Neurons were isolated from multi-unit activity using autocorrelograms, principal component analysis, spike wave-shapes and cluster separation. Details are described in Bachatene et al. [5].

Optical imaging

Detailed account of intrinsic optical imaging is available in Cattan et al. [12]. Intrinsic optical imaging allows assessment of the activity of a large population of cells.

Thus, we used this technique to visualize the range of shift propagation following adaptation.

After craniotomy, the dura mater was removed, a round chamber (15 mm in diameter) was fixed with dental cement above one hemisphere's area 17 and the chamber was filled with mineral oil and closed with a cover glass.

Achromatic gratings were to stimulate all cortical area within the imaging window to obtain orientation maps in control and post-adaptation sessions (contrast: 75 %; generated by VSG software; Cambridge Research Systems, Rochester, UK), presented randomly in order to avoid stimulus-order bias with rotation in eight different orientations from 0° to 157.5°, spatial frequency: 0.3 cycles/°, temporal frequency: 1 Hz). Each trial started with the presentation of a black screen for 15 s, and this was followed by the presentation of every orientation (12 s). For each presented orientation spanning 12 s, the grating was kept stationary during the first 6 s to remove the cortical activity resulting from the stimulus onset, and this was followed by drifts in one direction for the next 3 s and then in the reverse direction for 3 s to maximize cortical responses. The stimulation was full-screen. From these recordings, we generated control polar orientation maps. Then we presented a patch as an adapter for 12 min (full screen stimulus). Immediately after adaptation, we stimulated again all cortical area within the imaging window by presenting full screen stimuli as in the control phase. The polar map obtained post-adaptation was compared with the control map to evaluate the spatial spread of local adaptation.

Data acquisition and processing

The cortex was illuminated with 630-nm light. Cortex images were captured with a CCD camera (Dalsa 1 M60P; Dalsa, Waterloo, Ontario, Canada), composed of two 50-mm f1.2 lenses arranged in tandem, and focused 500 μm below the cortical surface. Images were digitised with Imager 3001 (Optical Imaging, Germantown, NY, USA), with a spatial resolution of 1024 × 1024 pixels (binned 2 × 2), and a temporal resolution of 20-ms frame duration. Image analysis was performed with MATLAB programs (MathWorks, Natick, MA, USA).

Thirty images were recorded for every orientation. As the last images showed more activity than the initial images, the average of the last 10 images (21–30) was divided by the average of the first 20 images (1–20). This calculation was performed to remove the non-specific activity in initial images, while preserving the specific activity recorded mostly in the last frames. Then, the generalised indicator function method [22] was applied. In short, this method extracts the frames that account for as much of the signal as possible by using principal component analysis, and optimises the differences between signal and noise.

Pixel shifts

To quantify changes in the orientation of pixels between control and post-adaptation polar maps, the amplitude of the shift in orientation was calculated from pairs of pixels located at the same position in the two maps.

$$s_{i,j} = \min\left(\left|p2_{i,j} - p1_{i,j}\right|, 180 - \left|p2_{i,j} - p1_{i,j}\right|\right)$$

where s is the shift-amplitude associated with the pair of pixels at the map position (i, j); p1 the pixel-orientation in the first map and, p2 the orientation of the same pixel in the second map. The shift-map comprised of all the shifts calculated for each position.

Connectivity strength, crosscorrelograms and shift predictor

Crosscorrelograms (CCG's) were performed in order to compare the spike distribution of each neuron of the pair within a time-frame; one neuron is set as reference and the second as target; this allows us to show the firing of the target neuron at a specific time-spread in relation to the firing of the reference neuron.

Time axis is divided into bins. The first bin is defined as: XMin, XMin + Bin. The next bin is XMin + Bin, XMin + Bin*2, etc. We calculated the distances from each spike to all spikes of the spike train as follows:

$$d[i] = ts[i] - ref[k]$$

where ts[i] represents the spike train, and ref[k] is each timestamp.

Bin counts were then divided by the number of reference events to normalize the counts per bin into probabilities. 95 % statistical threshold for the significance of the bins was used. Each bin-width was set at 1 ms. The connectivity strengths were calculated from the counts/bin as follows:

$$CS = F \times b$$

where F is the neuron frequency and b represents the bin size of the calculated firing of the neuron.

The neuron frequency F was calculated as follows:

$$F = \frac{N}{T}$$

where T represents the total time interval and N the number of spikes within this interval.

The 95 % confidence limit was calculated assuming that the expected bin count (EBC) has a Poisson distribution:

$$EBC = CS \times Nref$$

where Nref is the number of reference events.

The 95 % confidence limit is calculated as follows:

$$Low\ \ Conf. = x\ such\ that\ Prob(S < x) = 0.005$$

$$High\ Conf. = y\ such\ that\ Prob(S > y) = 0.005$$

where S represents a random variable which has a Poisson distribution with parameter EBC.

Raw CCG's were corrected by subtracting a shift-predictor algorithm in order to eliminate the putative significant peaks due to the simultaneous stimulation of both cells during each trial.

Results

To investigate the temporal relationships of spikes between cells of recorded assemblies, we performed optical imaging and extracellular electrophysiological recordings in V1 of adult anaesthetized cats based on an exposure-learning procedure (Fig. 1a). Optical imaging allows examining orientation shifts of a population of neurons [12] whereas electrophysiology permits recording a small number of neurons. Orientation preference maps were generated in order to compare the orientation layout before and after stimulus exposure: 3 or 12 min presentation of one particular orientation. An example of orientation maps is shown in Fig. 1b for both conditions (pre and post-adaptation periods). In addition to the optical imaging, electrophysiological recordings reveal, at the single cell scale, the orientation preference of cells and the changes of their selectivity after adaptation (orientation maps and neuronal tuning curves are shown in Fig. 1c, simulated data [23]). Colored dots within the circles depict orientation domains before (left) and following adaptation (right). Two orientation tuning curves are illustrated. Crosscorrelogram (CCG) analysis was used to unveil the putative inter-neuronal functional connections between neurons within a cell-assembly [15]. Raw CCGs were shift-corrected to eliminate the putative significant peaks due to the simultaneous stimulation of both cells (Fig. 1d). In this example, the CCG shows a significant peak within 10 ms time-window before zero mark. This suggests that cell A functionally projects onto cell B (cell B being the reference cell and cell A was set as a target neuron).

Stability of pixel proportion in orientation domains

In the following section, we examined the orientation selectivity on a populational level using intrinsic brain imaging. For this purpose, area 17 was probed in order to perform computations of pixel-changes of orientation and pixel-distribution in the region of interest.

To attribute the observed shifts in orientation maps to the effect of adaptation, we performed control tests of the stability of the maps over a period of time (1 h). From these maps, pinwheel spots and regions between two iso-orientation domains were identified and traced in both maps. An example of two generated maps is illustrated in Fig. 2a. A shift map was generated between test 1 and test

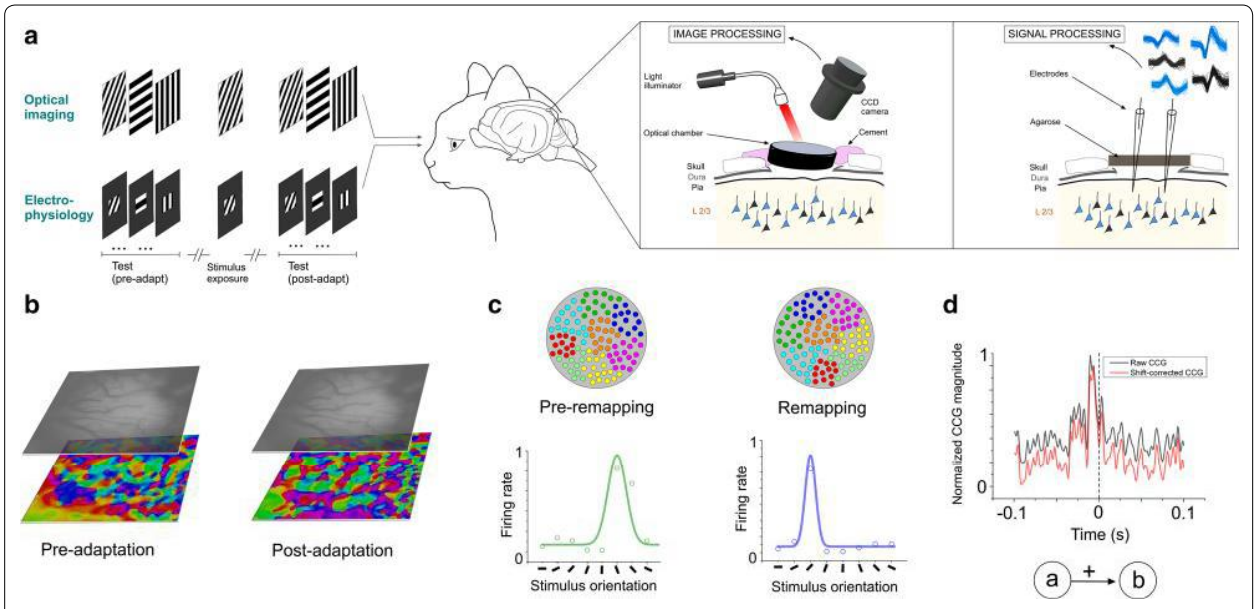

Fig. 1 Neuronal recordings, orientation selectivity and crosscorrelation. **a** Visual stimulations, oriented gratings are presented randomly; one non-preferred grating is used for stimulus-exposure as adaptation (duration: 12 min). Visual responses are measured using intrinsic optical imaging and electrophysiological recordings. **b** Examples of orientation maps pre- and post-adaptation. **c** Model of plasticity of orientation maps and tuning curves shifts of one neuron (simulated data). **d** Raw (*gray*) and corrected (*red*) crosscorrelograms showing a mono-projection from neuron "a" to neuron "b"

2. We observed small shifts in the frontiers between iso-orientation domains. This may be attributed to the small displacement of the pixels which may result from cortical movement, animal breathing…etc. However, in the shift map between pre- and post-adaptation, the shifts are more likely to happen in several regions of the map (see the description of Fig. 2d below).

As a further control of the stability of both maps, Pearson coefficient was computed between test 1 and test 2. We found a Pearson coefficient of 0.49 which is equivalent to a map similarity-index of 0.7 as previously shown [13, 43–45].

The spatial coordinates of each pinwheel was computed to test the stability of both orientation maps as shown in Fig. 2b for X-axis (red) and Y-axis (blue). The black dot represents the example shown in Fig. 2c (pinwheel 5). The similarity of both profiles is suggestive of the stability of the maps and thus the changes may be related to adaptation effect.

Following 12 min of stimulus exposure to one particular oriented grating (generally 90°), we observed a rearrangement of the orientation map characterized by pixel-shifts after adaptation. Figure 2d illustrates an orientation map generated from intrinsic optical imaging computations. In this investigation, we focused on the distribution of pixels for each orientation inside the region of interest for control and post-adaptation maps. This region of interest was selected based on pinwheel organization which is common to species such as cats and monkeys [24, 25].

To assess the magnitude of orientation shifts after visual adaptation, pixels were subtracted between the control and post adaptation steps. The result of this subtraction identified as pixel-shifts map is displayed in Fig. 2d (lower right); the color-scale represents the shift-intensity.

It is interesting to highlight that the global proportion of pixels is maintained, in other words, a new cortical map emerges following adaptation with a new distribution of pixels for each orientation, yet the proportion remained unchanged (One-way Anova test between pre- and post-adaptation, $p > 0.05$, Fig. 2e).

Functional connectivity modulation

The previous results indicate that following adaptation, neurons modified their original orientation selectivity;

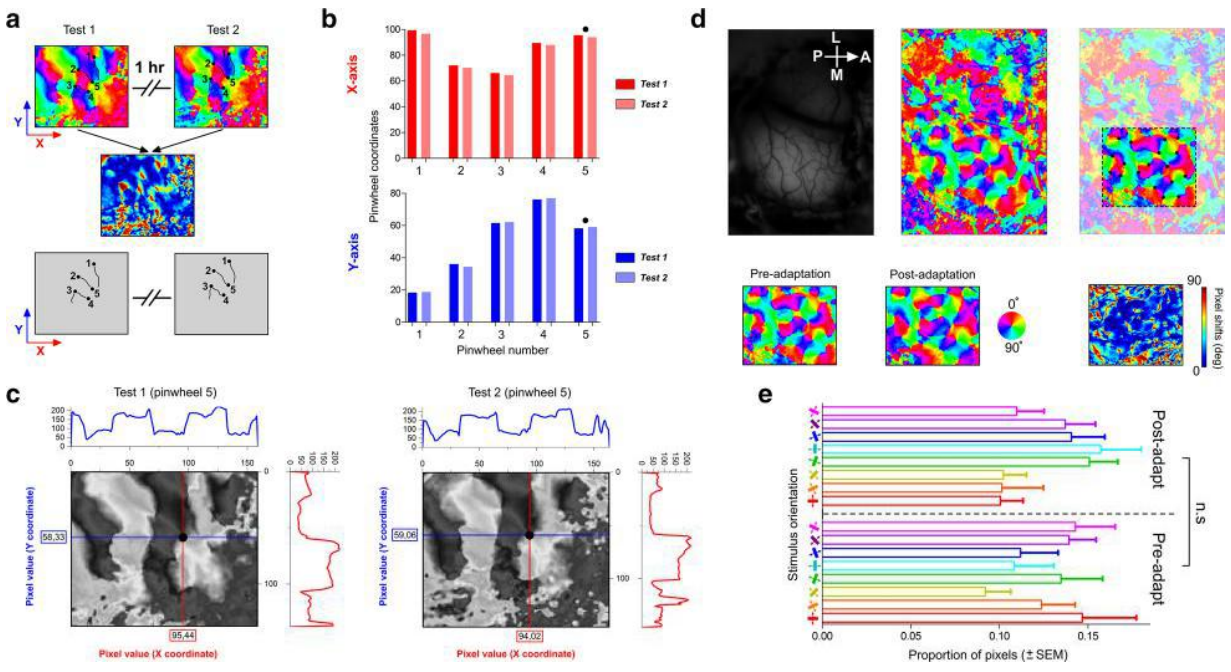

Fig. 2 Orientation maps stability and Pixel proportions in orientation maps. **a** Two orientation maps generated at two intervals (1 h). Pinwheels and zones separating iso-orientation domains were traced within each map. The shift map in illustrated below both orientation maps (test 1 and test 2). **b** Spatial coordinates (*x* and *y axes*) of each pinwheel during both tests. The *black dot* indicates the pinwheel presented in (**c**). **c** Profile plot of pinwheel 5 with its respective coordinates for both tests. **d** Orientation maps pre- and post-adaptation, each color represents one specific orientation. The *dashed rectangle* indicates the region of interest wherein each *black dot* represents a pinwheel. Pixel-shifts map generated using pixel-by-pixel subtraction between the two maps (pre- and post-adaptation) and is shown on the *lower right part*. **e** Pixel proportions of all orientations for both pre- and post-adaptation conditions

hence the pixel-distribution of each orientation was reorganized. However the global distribution of orientations remained unmodified which is in line with previous report [23]. This raises one question: how the relationships between cells are modulated to maintain the equal distribution of orientations? Therefore, it becomes interesting to investigate how time-relationships between spikes of recorded neurons are changed. For this, we investigated the functional connectivity between neurons regardless of their orientation selectivity within sub-networks in pre- and post-adaptation phases. We recorded simultaneously the extracellular activity of groups of cells around two distinct electrodes (400 microns). Six examples of neuronal responses are shown in Fig. 3a (three cells from each site). Orientation tuning curves of all cells obtained from the raw data (response matrices) before and after adaptation are shown. Neuronal firing activity was crosscorrelated for all the possible neuron-pairs between the recorded sites. Based on the highest significant peaks across the CCGs of all pairs (pairs are coded by colored squares, the first colored square in the CCG represents the reference neuron, Fig. 3b, in this example all reference neurons were from site 1), putative functional connections were revealed within the networks and are further described in the next section. The spike waveforms of each neuron are displayed in Fig. 3b (left).

Coordinated adjustment of synaptic weights in the circuits

We generated a connectivity circuit between the simultaneously recorded neurons shown previously (Fig. 4a). In the illustration, the value of CCG magnitude reflecting connection strength is indicated above each connecting-line, and is proportional to the thickness of the latter. The computations of CCG magnitudes of all summed pairs ($n = 7$) indicated a non-significant difference between the mean magnitude in pre- and post-adaptation conditions (paired two-tailed t test, $p > 0.05$, Fig. 4b). The sums (ΣP) of CCG magnitudes before and after visual adaptation were 0.14 and 0.13 respectively.

Another example is illustrated by a connectivity matrix (4×4 cells from two sites, Fig. 4c); it shows that the total connectivity strength remains unchanged following adaptation (the sums of CCG magnitudes were 0.11 and 0.10 before and after adaptation, respectively) despite the fact that functional connections are redeployed between different cells within the neuronal network (Fig. 4c). The connectivity matrices were found to be significantly different (Pearson coefficient = 0.11). Hence, there is an emergence of a new functional network within the same assembly that is characterized by the merging of both novel orientation selectivity's and new links between cells wherein the functional strengths may weaken or strengthen. This suggests that there is a coordinated adjustment of synaptic strengths within the circuits leading to a rearrangement of functional connectivity with a change of orientation selectivity. However and most importantly, the overall proportion of connections is stable (histogram in Fig. 4d, left). The total values in all experiments pre- and post-adaptation point toward such stability (the summed CCG magnitude remained same at both pre and post-adaptation conditions, $\Sigma P = 0.08$, $n = 135$ cells, histogram in Fig. 4d, right).

Interplay between selectivity and connectivity

Based on our findings, we propose a plastic neuronal network model which links the selectivity of neurons to their respective connectivity following plastic changes (Fig. 5). We found that the sum of the connectivity strength is equal at pre- and post-adaptation conditions. Mathematically, the total connectivity volume of a cell-assembly is the sum of all the individual contributions to the connectivity matrix; the connectivity strength is redistributed within the network following a "steady-selectivity-connectivity rule" so that the total connectivity volume of the entire assembly remains constant. This rule could be represented by the following equation:

$$W = \sum_{i=1}^{n} CSi$$

$$CS = \frac{N \times b}{t}$$

where W is the total connectivity weight within the network, CS is the measure of the individual Connectivity Strength for each cell-pair and n is the number of neuron-pairs, t represents the total time interval, N the number of spikes within this interval, and b represents the bin size of the calculated firing of the neuron (see "Methods").

Correlations as a function of adaptation-duration and distance between electrodes

Finally, the effect of the time of adaptation on the connectivity-strength summation was investigated. For this purpose, three adaptation-durations were used: 3 min, 12 min and 24 min (Fig. 6a–c, respectively). The results indicate that the summed connectivity strengths are maintained post-adaptation with no significant effect of the time of adaptation. The results were: $\Sigma P = 1.2$ pre-adaptation and $\Sigma P = 1.2$ post-adaptation for both 3 and 12 min adaptation-duration, and $\Sigma P = 1.1$ pre-adaptation and $\Sigma P = 1.08$ for 24 min adaptation. Another parameter which has been tested is the distance between the recorded neurons. Multi-channel electrodes allowed simultaneously recording locally clustered cells as well

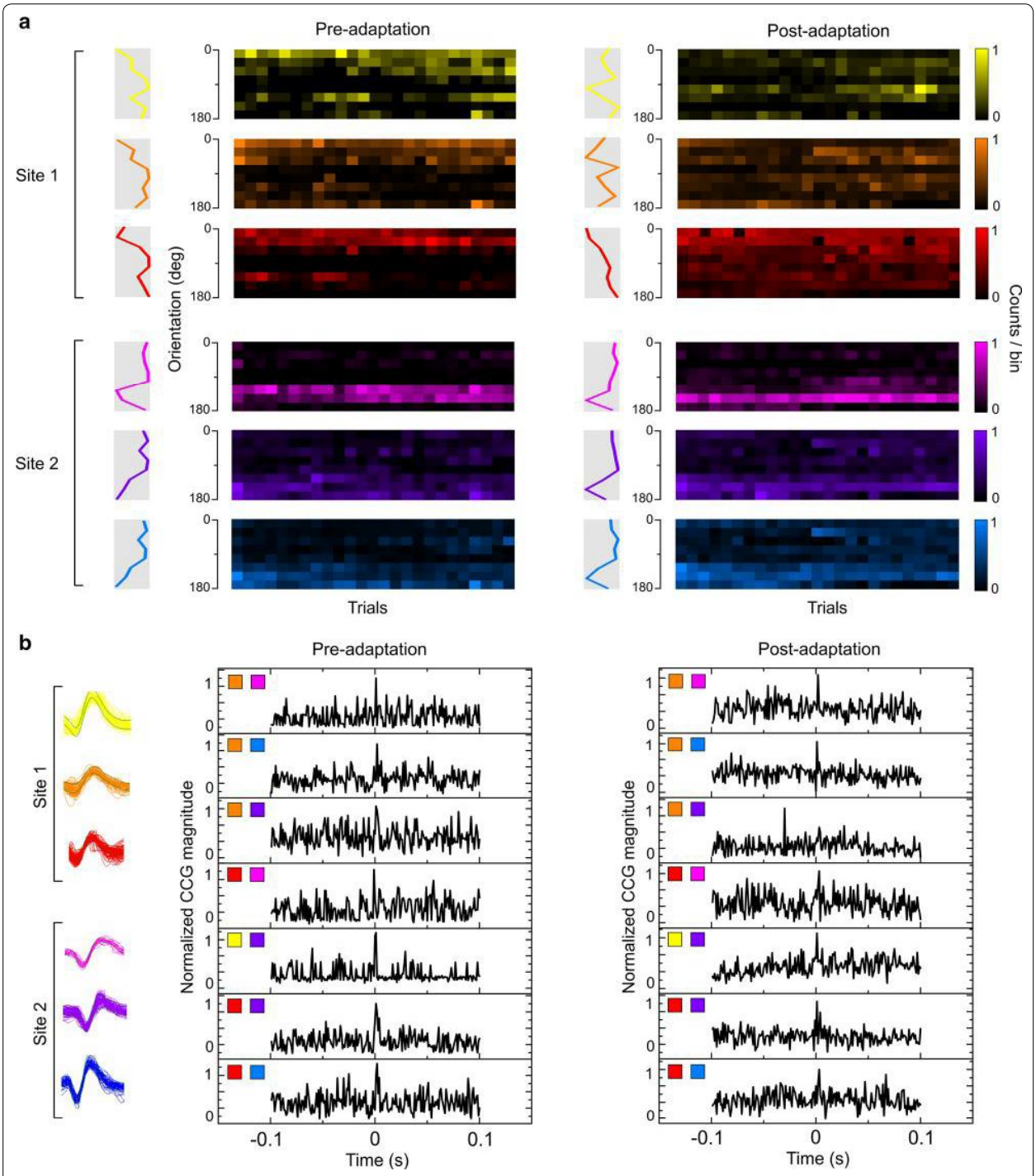

Fig. 3 Modulation of functional connectivity. **a** Neuronal responses of six neurons recorded from two different sites. Colored matrices correspond to the measured responses at each trial (*X-axis*) and at all presented orientations (*Y-axis*). On the *left* are shown the raw tuning curves of each neuron. **b** Significant CCG's between pairs of neurons from (**a**). The spike waveforms are displayed on the *left*

as cells separated by up to 800 microns. The correlation-strength was then examined between neurons recorded from the same electrode tip (local, Fig. 6d) and between neurons recorded from distinct electrodes (distal, Fig. 6d). The results show significant differences between the connectivity strength of locally recorded neurons and the

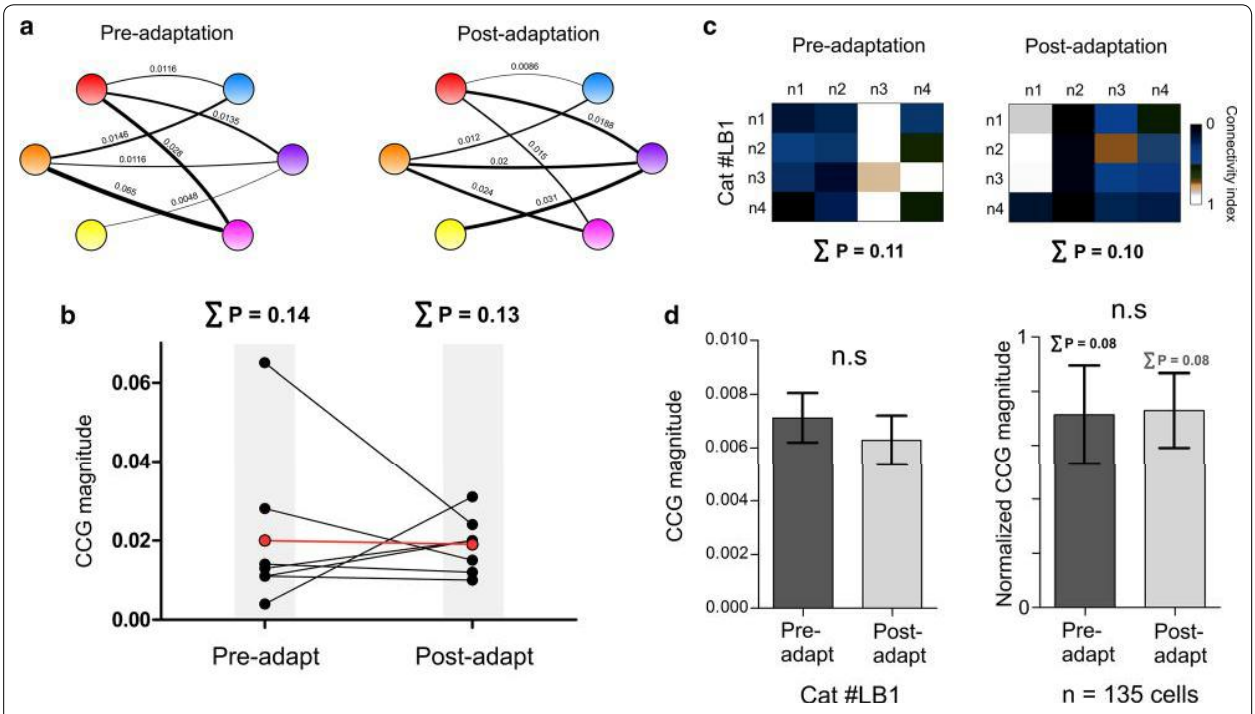

Fig. 4 Connectivity dynamics of neuronal microcircuits. **a** Neuronal microcircuits and connectivity strength dynamics. The *thickness of lines* corresponds to the connectivity level. **b** Comparison between connectivity indices pre- and post-adaptation conditions. *Red dots* represent the mean connectivity strength. *Sums* are indicated above each condition. **c** Connectivity matrix of a different neuronal group showing the connectivity strength between all pairs. **d** Comparative histograms of the previous example (*left*) and global results (*right*)

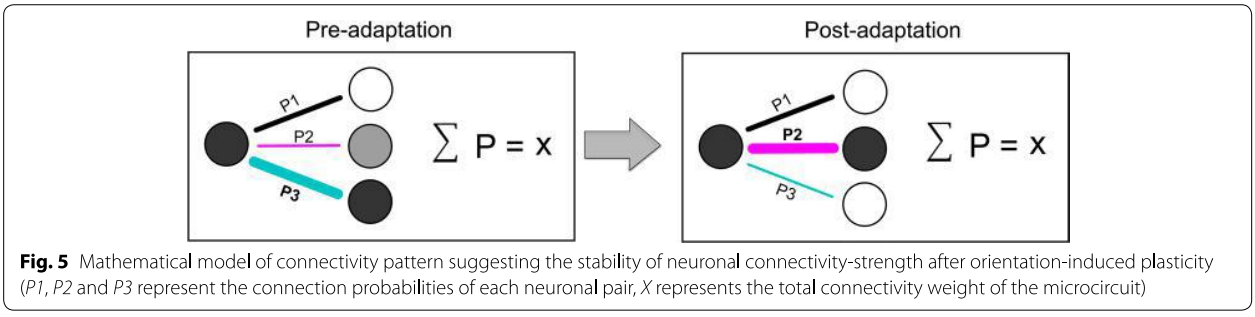

Fig. 5 Mathematical model of connectivity pattern suggesting the stability of neuronal connectivity-strength after orientation-induced plasticity (*P1*, *P2* and *P3* represent the connection probabilities of each neuronal pair, *X* represents the total connectivity weight of the microcircuit)

connectivity strength of distal neurons. These differences were observed for both pre- and post-adaptation phases (t-test, $p < 0.01$, Fig. 6d). Interestingly, for distal pairs, significant difference was also observed between pre- and post-adaptation phases with an increased average of the CCG magnitude (t-test, $p < 0.01$, Fig. 6d). This could be explained by an expansion of functional connections between neurons belonging to distinct microcircuits.

Discussion

Sensory systems are continuously affected by the external environmental attributes [26]. The visual system is highly altered by experience wherein neuronal properties and neuronal circuits undergo important changes during development [6, 7]. These modifications may persist during adulthood as a consequence of large panoply of strategies such as visual deprivation [27, 28], retinal lesions [29] or adaptive sensory experience (short, long or repetitive visual exposure) [9–12, 30–32]. It appears that visual stimulation recruits functional groups of neurons which, when co-activated, process the visual stimuli properties [2]. Thus, the visual input from one microcircuit may affect the information provided to different downstream cell-assemblies [12, 26].

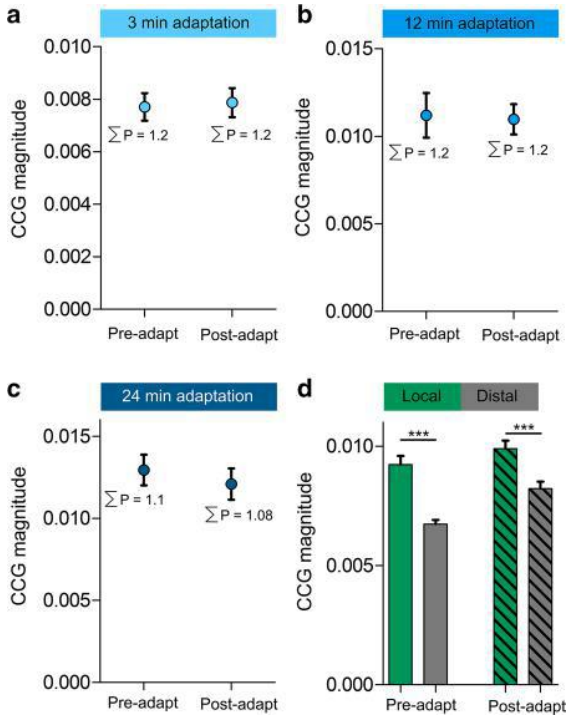

Fig. 6 Correlations as a function of adaptation-duration [3 min in (**a**), 12 min in (**b**) and 24 min in (**c**)] and distance between neurons (**d**). The results indicate no significant difference in the summed connectivity-strengths between different adaptation-durations. However, significant differences were observed between locally recorded neurons (higher CCG magnitude) and neurons recorded from distinct electrode tips (lower CCG magnitude)

Methodological considerations

From intrinsic optical imaging recordings, pixel-by-pixel subtraction computations allow the quantification of the difference between two orientation maps (in our case pre- and post-adaptation maps). It was thus important to test the stability of the maps as a control; indeed, the recorded signal may be contaminated by ambient noise due to breath-induced movement, light intensity change, cortical movement… etc. We have measured the light intensity of all generated images and found no difference between all animals as well as between all recording sessions. Despite the inherent presence of noise, the generated maps clearly contained well-organized regions with iso-orientation domains that converge at the center of pinwheels. This regular pattern cannot be attributed to random noise. In addition, orientation preference maps remained unchanged when tested twice (if no adaptation is applied) (Fig. 2a–c).

The dynamic of neuronal connectivity

Brain processing is intimately related to how important the dynamic of complexly connected microcircuits is. Visual neurons within layers 2/3 are selectively interconnected leading to the emergence of independent fine-scale circuits entrenched in the cortical architecture [1]. In line with our data, experience-dependent plasticity leads to modifications of the connectivity patterns within the neuronal network. However, it has been proposed that a homeostatic process is established in order to stabilize the global connectivity strength of the neuronal group [19]. This regulating activity is considered as a complementary process to the Hebbian plasticity where changes in synaptic strengths are observed after plasticity in order to refine the properties of neuronal-assemblies [19–21]. In young animals for instance, stimulus adaptation leads to the development of orientation maps. Exposing kittens to a single oriented environment shifted the optimal orientations of many neurons to the experienced orientation [7]. Hence, experience is a significant factor in determining the plastic changes operating in orientation maps [7]. In adulthood, there have been studies reporting the adapting ability of the visual cortex to external stimuli: orientation, contrast, motion, direction and spatial frequency [9–11, 30, 31, 33]. Stimulus exposure (adaptation) which mimics the learning process changes neuronal properties; this may be attributed to changes in dynamics of neuronal cell-assemblies wherein neurons acquire new optimal properties [8, 11, 32]. Recent findings assign a high contribution of adaptation to neuronal response uniformity within a population of cells sharing neuronal and feature selectivity [5, 34]. Moreover, it has been shown that adaptation enhances the spike-synchrony in the gamma frequency range in V4 [35] as well as in V1 [36]. This gamma-modulation of synchrony is coupled with an improvement of feature encoding [35, 36].

Functional cell-assemblies are newly formed wherein neurons sharing similar stimulus preference exhibit high connectivity profile [4, 37]. On the other hand, during the critical period and learning in adulthood, synaptic strengths have to be modified in order to regulate the neuronal properties changes due to multiple synaptic drives and maintain a stable level of firing [17]. In line with our findings, homeostatic scaling was proposed as a strategy to normalize the global synaptic connectivity strength to compensate the Hebbian plasticity which modifies the inter-cellular connectivity in relation to the neuronal selectivity [38]. Homeostatic plasticity prevents an over-increase or over-decrease of the firing activity levels due to long-term potentiation (LTP) or long-term depression (LTD) which modify the connectivity strength in order to change the neuronal selectivity features [39–41]. Another scenario would be the change in excitation-inhibition equilibrium that could lead to critical effects on neuronal spiking activity and information processing

[18, 42]. Maintaining stable excitation-inhibition ratio could thus prevent an exceeding augmentation or diminution of global strengths within networks allowing sensory processing to remain stable [18].

Conclusion

The concept of neuronal homeostasis implies that synaptic weights could be limited to an optimal level in order to regulate the total connectivity ratio within the assemblies. Indeed, the increase of synaptic strengths within a group of neurons may lead to the decrease of other connections as a trade-off allowing, therefore, the formation of new functional microcircuits after plasticity.

Abbreviations

OSI: orientation selectivity index; CS: connectivity strength; RF: receptive field; CCG: crosscorrelogram.

Authors' contributions

LB performed the experiments and analyzed the data including the statistical analyses. VB, SC and NC contributed to data analyses and writing of the paper. SM conceived the study and contributed to data analyses. LB and SM wrote the manuscript. JR contributed to data analyses. All authors read and approved the final manuscript.

Author details

[1] Laboratoire de Neurosciences de la vision, Département de Sciences Biologiques, Université de Montréal, CP 6128 Succ. Centre-Ville, Montréal, QC H3C 3J7, Canada. [2] Neurosciences Computationnelles et Traitement Intelligent des Signaux (NECOTIS), Département de Génie Électrique et Génie Informatique, Université de Sherbrooke, Sherbrooke, QC, Canada.

Acknowledgements

We thank Dr Milad Toubal and Simon Brodeur for their useful comments on the manuscript.

Competing interests

The authors declare that they have no competing interests.

Received: 22 May 2015 Accepted: 30 September 2015
Published online: 09 October 2015

References

1. Yoshimura Y, Dantzker JL, Callaway EM. Excitatory cortical neurons form fine-scale functional networks. Nature. 2005;433(7028):868–73. doi:10.1038/nature03252.
2. Miller JE, Ayzenshtat I, Carrillo-Reid L, Yuste R. Visual stimuli recruit intrinsically generated cortical ensembles. Proc Natl Acad Sci USA. 2014;111(38):E4053–61. doi:10.1073/pnas.1406077111.
3. Alloway KD, Roy SA. Conditional cross-correlation analysis of thalamocortical neurotransmission. Behav Brain Res. 2002;135(1–2):191–6.
4. Ko H, Hofer SB, Pichler B, Buchanan KA, Sjostrom PJ, Mrsic-Flogel TD. Functional specificity of local synaptic connections in neocortical networks. Nature. 2011;473(7345):87–91. doi:10.1038/nature09880.
5. Bachatene L, Bharmauria V, Cattan S, Rouat J, Molotchnikoff S. Modulation of functional connectivity following visual adaptation: homeostasis in V1. Brain Res. 2015;1594:136–53. doi:10.1016/j.brainres.2014.10.054.
6. Hensch TK. Critical period plasticity in local cortical circuits. Nat Rev Neurosci. 2005;6(11):877–88. doi:10.1038/nrn1787.
7. Sengpiel F, Stawinski P, Bonhoeffer T. Influence of experience on orientation maps in cat visual cortex. Nat Neurosci. 1999;2(8):727–32. doi:10.1038/11192.
8. Bachatene L, Bharmauria V, Cattan S, Molotchnikoff S. Fluoxetine and serotonin facilitate attractive-adaptation-induced orientation plasticity in adult cat visual cortex. Eur J Neurosci. 2013;38(1):2065–77. doi:10.1111/ejn.12206.
9. Bachatene L, Bharmauria V, Rouat J, Molotchnikoff S. Adaptation-induced plasticity and spike waveforms in cat visual cortex. NeuroReport. 2012;23(2):88–92. doi:10.1097/WNR.0b013e32834e7e71.
10. Dragoi V, Sharma J, Sur M. Adaptation-induced plasticity of orientation tuning in adult visual cortex. Neuron. 2000;28(1):287–98.
11. Ghisovan N, Nemri A, Shumikhina S, Molotchnikoff S. Long adaptation reveals mostly attractive shifts of orientation tuning in cat primary visual cortex. Neuroscience. 2009;164(3):1274–83. doi:10.1016/j.neuroscience.2009.09.003.
12. Cattan S, Bachatene L, Bharmauria V, Jeyabalaratnam J, Milleret C, Molotchnikoff S. Comparative analysis of orientation maps in areas 17 and 18 of the cat primary visual cortex following adaptation. Eur J Neurosci. 2014;40(3):2554–63. doi:10.1111/ejn.12616.
13. Godde B, Leonhardt R, Cords SM, Dinse HR. Plasticity of orientation preference maps in the visual cortex of adult cats. Proc Natl Acad Sci USA. 2002;99(9):6352–7. doi:10.1073/pnas.082407499.
14. Denman DJ, Contreras D. The structure of pairwise correlation in mouse primary visual cortex reveals functional organization in the absence of an orientation map. Cereb Cortex. 2014;24(10):2707–20. doi:10.1093/cercor/bht128.
15. Perkel DH, Gerstein GL, Moore GP. Neuronal spike trains and stochastic point processes. I. The single spike train. Biophys J. 1967;7(4):391–418. doi:10.1016/S0006-3495(67)86596-2.
16. Reid RC. From functional architecture to functional connectomics. Neuron. 2012;75(2):209–17. doi:10.1016/j.neuron.2012.06.031.
17. Surmeier DJ, Foehring R. A mechanism for homeostatic plasticity. Nat Neurosci. 2004;7(7):691–2. doi:10.1038/nn0704-691.
18. Turrigiano G. Homeostatic synaptic plasticity: local and global mechanisms for stabilizing neuronal function. Cold Spring Harb Perspect Biol. 2012;4(1):a005736. doi:10.1101/cshperspect.a005736.
19. Turrigiano GG. Homeostatic plasticity in neuronal networks: the more things change, the more they stay the same. Trends Neurosci. 1999;22(5):221–7.
20. Hebb DO. The organization of behavior: a neuropsychological theory. New York: Wiley and Sons; 1949.
21. Shatz CJ. Impulse activity and the patterning of connections during CNS development. Neuron. 1990;5(6):745–56.
22. Yokoo T, Knight BW, Sirovich L. An optimization approach to signal extraction from noisy multivariate data. NeuroImage. 2001;14(6):1309–26. doi:10.1006/nimg.2001.0950.
23. Bachatene L, Bharmauria V, Cattan S, Rouat J, Molotchnikoff S. Reprogramming of orientation columns in visual cortex: a domino effect. Sci Report. 2015;5:9436. doi:10.1038/srep09436.
24. Ohki K, Matsuda Y, Ajima A, Kim DS, Tanaka S. Arrangement of orientation pinwheel centers around area 17/18 transition zone in cat visual cortex. Cereb Cortex. 2000;10(6):593–601.
25. Okamoto T, Ikezoe K, Tamura H, Watanabe M, Aihara K, Fujita I. Predicted contextual modulation varies with distance from pinwheel centers in the orientation preference map. Sci Report. 2011;1:114. doi:10.1038/srep00114.
26. Patterson CA, Wissig SC, Kohn A. Adaptation disrupts motion integration in the primate dorsal stream. Neuron. 2014;81(3):674–86. doi:10.1016/j.neuron.2013.11.022.
27. He HY, Hodos W, Quinlan EM. Visual deprivation reactivates rapid ocular dominance plasticity in adult visual cortex. J Neurosci Off J Soc Neurosci. 2006;26(11):2951–5. doi:10.1523/JNEUROSCI.5554-05.2006.
28. Shibata K, Kawato M, Watanabe T, Sasaki Y. Monocular deprivation boosts long-term visual plasticity. Curr Biol CB. 2012;22(9):R291–2. doi:10.1016/j.cub.2012.03.010.
29. Keck T, Scheuss V, Jacobsen RI, Wierenga CJ, Eysel UT, Bonhoeffer T, et al. Loss of sensory input causes rapid structural changes of inhibitory neurons in adult mouse visual cortex. Neuron. 2011;71(5):869–82. doi:10.1016/j.neuron.2011.06.034.
30. Kohn A, Movshon JA. Adaptation changes the direction tuning of macaque MT neurons. Nat Neurosci. 2004;7(7):764–72. doi:10.1038/nn1267.

31. Nemri A, Ghisovan N, Shumikhina S, Molotchnikoff S. Adaptive behavior of neighboring neurons during adaptation-induced plasticity of orientation tuning in VI. BMC Neurosci. 2009;10:147. doi:10.1186/1471-2202-10-147.
32. Patterson CA, Wissig SC, Kohn A. Distinct effects of brief and prolonged adaptation on orientation tuning in primary visual cortex. J Neurosci Off J Soc Neurosci. 2013;33(2):532–43. doi:10.1523/JNEUROSCI.3345-12.2013.
33. Marshansky S, Shumikhina S, Molotchnikoff S. Repetitive adaptation induces plasticity of spatial frequency tuning in cat primary visual cortex. Neuroscience. 2011;172:355–65. doi:10.1016/j.neuroscience.2010.10.017.
34. Benucci A, Saleem AB, Carandini M. Adaptation maintains population homeostasis in primary visual cortex. Nat Neurosci. 2013;16(6):724–9. doi:10.1038/nn.3382.
35. Wang Y, Iliescu BF, Ma J, Josic K, Dragoi V. Adaptive changes in neuronal synchronization in macaque V4. J Neurosci Off J Soc Neurosci. 2011;31(37):13204–13. doi:10.1523/JNEUROSCI.6227-10.2011.
36. Hansen BJ, Dragoi V. Adaptation-induced synchronization in laminar cortical circuits. Proc Natl Acad Sci USA. 2011;108(26):10720–5. doi:10.1073/pnas.1102017108.
37. Ko H, Cossell L, Baragli C, Antolik J, Clopath C, Hofer SB, et al. The emergence of functional microcircuits in visual cortex. Nature. 2013;496(7443):96–100. doi:10.1038/nature12015.
38. Turrigiano GG, Nelson SB. Hebb and homeostasis in neuronal plasticity. Curr Opin Neurobiol. 2000;10(3):358–64.
39. Burrone J, O'Byrne M, Murthy VN. Multiple forms of synaptic plasticity triggered by selective suppression of activity in individual neurons. Nature. 2002;420(6914):414–8. doi:10.1038/nature01242.
40. Turrigiano GG, Leslie KR, Desai NS, Rutherford LC, Nelson SB. Activity-dependent scaling of quantal amplitude in neocortical neurons. Nature. 1998;391(6670):892–6. doi:10.1038/36103.
41. Turrigiano GG, Nelson SB. Homeostatic plasticity in the developing nervous system. Nat Rev Neurosci. 2004;5(2):97–107. doi:10.1038/nrn1327.
42. Nelson SB, Turrigiano GG. Strength through diversity. Neuron. 2008;60(3):477–82. doi:10.1016/j.neuron.2008.10.020.
43. Gödecke I, Bonhoeffer T. Development of identical orientation maps for two eyes without common visual experience. Nature. 1996;379(6562):251–4.
44. Chapman B, Stryker MP, Bonhoeffer T. Development of orientation preference maps in ferret primary visual cortex. J Neurosci. 1996;16(20):6443–53.
45. Schuett S, Bonhoeffer T, Hübener M. Pairing-induced changes of orientation maps in cat visual cortex. Neuron. 2001;32(2):325–37.

SCIENTIFIC REPORTS

OPEN

SUBJECT AREAS:
STRIATE CORTEX
CORTEX

Received
21 October 2014

Accepted
2 March 2015

Published
24 March 2015

Reprogramming of orientation columns in visual cortex: a domino effect

Lyes Bachatene[1,2], Vishal Bharmauria[1,2], Sarah Cattan[1,2], Jean Rouat[1,2] & Stéphane Molotchnikoff[1,2]

[1]Département de Sciences Biologiques, Université de Montréal, Montréal, QC, Canada, H3C 3J7, [2]Neurosciences Computationnelles et Traitement Intelligent des Signaux (NECOTIS, Département de Génie Électrique et Génie Informatique, Université de Sherbrooke, Sherbrooke, Québec, Canada, J1K 2R1).

Cortical organization rests upon the fundamental principle that neurons sharing similar properties are co-located. In the visual cortex, neurons are organized into orientation columns. In a column, most neurons respond optimally to the same axis of an oriented edge, that is, the preferred orientation. This orientation selectivity is believed to be absolute in adulthood. However, in a fully mature brain, it has been established that neurons change their selectivity following sensory experience or visual adaptation. Here, we show that after applying an adapter away from the tested cells, neurons whose receptive fields were located remotely from the adapted site also exhibit a novel selectivity in spite of the fact that they were not adapted. These results indicate a robust reconfiguration and remapping of the orientation domains with respect to each other thus removing the possibility of an orientation hole in the new hypercolumn. These data suggest that orientation columns transcend anatomy, and are almost strictly functionally dynamic.

Since the seminal investigations of Hubel and Wiesel in 1962[1], it has been extensively established that the visual cortex is organized for orientation selectivity in a columnar fashion from pial membrane to the white matter. That is, most neurons assembled in a vertical column are selective to the same axis of orientation in response to an edge presented within their respective receptive field (RF). Indeed, if an electrode penetrates the cortex in an oblique direction, the preferred neuronal orientation rotates in a methodical fashion by about 16.5° for every traveling step of 0.09 mm of the recording tip, as it crosses from one orientation column to the next. Such systematic progression implies that, once a few reference preferred orientations of neurons are determined, it is conceivable to predict the orientation sequence. This organization rests on the notion that columnar organization is an outcome of segregated architecture of inter-neuronal connections leading to a relatively inflexible layout of striate organization. For instance, LGN neurons aligned along an axis connect to a single cortical cell[2,3] giving rise to the orientation selectivity.

Yet, a few observations[4–6] have reported that these columnar organizations are highly variable, even in the same species.

Interestingly, recent experiments showed that following the continuous or frequent application of non-optimal stimuli, orientation in our case (called adapter to which neurons initially responded poorly), neurons change their stimulus selectivity[7–14]. For orientation, depending on the duration of adaptation, neurons in area 17 shift the peak of their orientation tuning curve either in the direction of the adapter (attractive shift) or away from the adapter (repulsive shift). Whatever the direction of the shift, the newly acquired optimal orientation presents a two-fold problem. The new selectivity following adaptation may be represented twice inside the hypercolumn, and alternatively, the emergence of a novel preferred orientation creates an orientation hole since the original axis is now deleted.

A basic question then arises: do cells in neighboring columns also shift their optimal orientation even if they were not exposed to the adapting stimulus, in order to restore the uniquely fashioned regularity of orientation processing? Heuristically, this invites another question: does the entire orientation hypercolumn exhibit an altered organization? In other words, are Hubel and Wiesel columns modifiable depending on the stimulation history or, in contrast, do orientation columns retain their original orientation selectivity in spite of the fact that the neighboring column changes its orientation-preference?

Our results allow us to argue that columnar organization is a processing unit rather than an anatomically based structure. The direct implication of our described investigations is that the orientation column organization classically supported by structural connections between neurons in V1 must be reassessed. We demonstrate that original preferred orientations of neurons are changed following local adaptation executed at some distance from tested cells.

Although shifts in orientation tuning of the adapted cells were described in previous reports[9–11], we were particularly interested in exploring what occurred in the non-adapted cells, i.e., if one group of cells changes its preferred orientation following adaptation, do the cells belonging to other and non-adapted orientation columns change their preferred orientation concurrently as well?

Results

Orientation preference and goodness of fits. In total, 266 cells were recorded in area 17 of anesthetized cats. Neurons were classified into two groups of cells on the basis of their orientation selectivity which was determined by the orientation selectivity index (OSI, see methods). In line with the previous reports[8,15–17], neurons having an OSI superior or equal to 0.4 are classified as sharply tuned cells. This classification led to 218 orientation-selective neurons while 48 cells were broadly tuned. In the present investigation, tuned neurons had an OSI of 0.5 ± 0.02 and 0.4 ± 0.02 for adapted and non-adapted sites respectively, whereas broadly tuned neurons exhibited an OSI of 0.08 ± 0.004 and 0.07 ± 0.005 for adapted and non-adapted sites, respectively (Fig. 1a). In addition, we computed the Gaussian fits from the raw tuning curves to precisely compute the preferred orientation (pre- and post-adaptation) thus allowing the calculation of shift of the peak of the orientation tuning curve. For both sites, i.e., adapted and non-adapted, significant differences were observed between tuned (mean $R^2 = 0.73 \pm 0.1$ for adapted sites, mean $R^2 = 0.76 \pm 0.1$ for non-adapted sites, Fig. 1b) and untuned neurons (mean $R^2 = 0.23 \pm 0.1$ for adapted sites, mean $R^2 = 0.26 \pm 0.1$ for non-adapted sites, Fig. 1b). Due to their poor orientation selectivity, all untuned cells were excluded from further analyses.

Comparison of the orientation selectivity index for all neurons from adapted and non-adapted sites before and after adaptation was performed. The values were respectively: $OSI_{pre\text{-}adaptation} = 0.44 \pm 0.01$ and $OSI_{post\text{-}adaptation} = 0.49 \pm 0.01$ (n = 218). The R-squared derived from the Gaussian fits were also computed for both conditions; the $R^2_{pre\text{-}adaptation} = 0.7 \pm 0.008$, the $R^2_{post\text{-}adaptation} = 0.7 \pm 0.01$ (n = 218).

Typical results. As expected from previous investigations, peaks of orientation tuning curves shift following visual adaptation in anesthetized cats that were conventionally prepared for recording neurons' electrical activity. Recorded unit activity was filtered, amplified and displayed on oscilloscope and computer screens. Figure 2 shows the typical results. Three receptive fields (RF) are displayed on the top left. In this example, the center to center distance was 4° between RF's A and B and 5° between RF's A and C. Only RF A was locally adapted (see methods for details), and all three fields were stimulated one-by-one with an identical drifting sine-wave grating patch positioned at the center of each excitatory field (stimuli properties were constant). RF's B and C are positioned on opposite sides relative to the adapted area. In the first stage, multi-unit orientation tuning curves were determined from recorded cumulative activities (multiunit responses) from all three areas. Each RF was stimulated in isolation, that is, gratings were applied alternatively in each field, and it is important to emphasize that we never stimulated excitatory fields simultaneously, in order to exclude direct cross talk between groups of cells. Additionally, the spontaneous activity of unstimulated cells remained unchanged when the companion field was excited (see example in Fig. 3c).

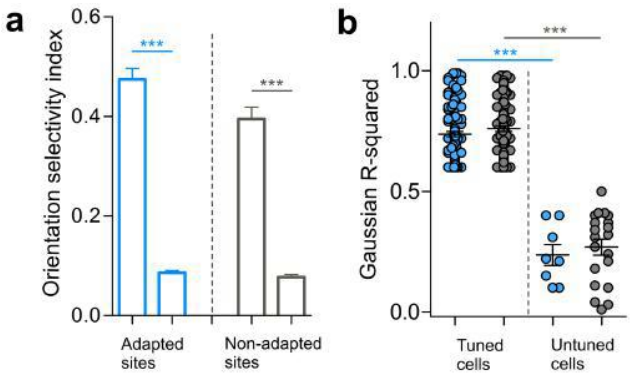

Figure 1 | Orientation selectivity and goodness of fits. (a) Histograms showing the mean values of orientation selectivity indices (OSI's) for both sites. Significant differences lead to the classification of cells into broadly tuned cells and orientation-selective neurons. (b) Differences of the Gaussian R-squared between tuned and untuned cells in both sites (adapted sites in blue, non-adapted sites in gray).

In the second phase, the adapting grating was placed within RF A at an orientation 45° off the optimal axis, as determined in the first phase, of this particular field. Other parameters of the sine-wave patch remained unchanged. The adaptation phase lasted 12 minutes without interruption and no stimulation was applied to companion RF's that remained dark. Single units were isolated from the multi-unit activity and Gaussian tuning curves were computed. The sorted waveforms at each site are displayed in the upper left part of the figure. The adaptation of RF A induced the classical shifts of the peak of the orientation tuning curves of cells belonging to this particular field. Trial-by-trial Pearson correlations of spike-counts (TC) between simultaneously recorded cells were computed in order to ascertain that cells are well isolated (Supplementary Fig. S1).

Figure 2 shows the classical attractive shifts in the adapted field for all three recorded units. This adaptation (adapting orientation indicated by downward red arrow head, in all figures; light colors in raw curves indicate error bars in all figures; Gaussian R-squared and OSI's are shown above each tuning curve) induced a roughly equal attractive displacement of the peak of the orientation tuning curves: 60.49°, 71.04°, and 96.22° for blue, green, and pink cells, respectively (first row, horizontal colored arrows in Fig. 2). However, and quite unexpectedly, neurons belonging to the non-adapted site B (located 4° away) also shifted their respective optimal orientation tuning curves. The orientation tuning curve of the orange neuron shifted in the repulsive direction (68.9°), while red and purple units displaced their respective optimal peaks towards the adapter (49.3° and 86.1° for red and purple neurons, respectively, middle row). Cells belonging to the third non-adapted site C (bottom row) also shifted their respective orientation tuning curves (22.1° for sky neuron, 38.3° for green neuron, and 27.4° for gray neuron) in the attractive direction, that is, the novel orientation approached the adapter. It is worthwhile to emphasize that, at this site the amplitude of the shift is smaller perhaps due to the larger distance separating both receptive fields (A and C, see Fig. 2 insert). Thus, in spite of the fact that cells excited within RF's B and C were not adapted, they reacted by showing new preferred orientations. Furthermore, the response magnitude of the novel optimal orientation was about equal to the strength of the original preferred orientation. Other examples are shown in a supplementary figure (Fig. S2).

Receptive-fields separation. The excitatory receptive field dimensions of the multi-unit activity extended from 2.5° to 4° (average = 3.8 ± 0.4°). All RF's were centrally located within a 15° radius from fovea (Fig. 3a). The adapting stimulus had equal dimensions and covered the excitatory receptive area. Measurements of receptive field size in area 17 as a function of eccentricity indicate that within a radius of 15° of fovea, RF dimensions rarely extend 5°[18,19]. The average distance separating the adapted and non-adapted fields was 8.0 ± 3.0° (histogram distribution shown in Fig. 3b, the downward triangle indicates the mean value). Most significantly, the absence of cross-influences between units excited through distant receptive fields was tested by measurement of spontaneous activity because the latter is weak and it readily fluctuates if a stimulus

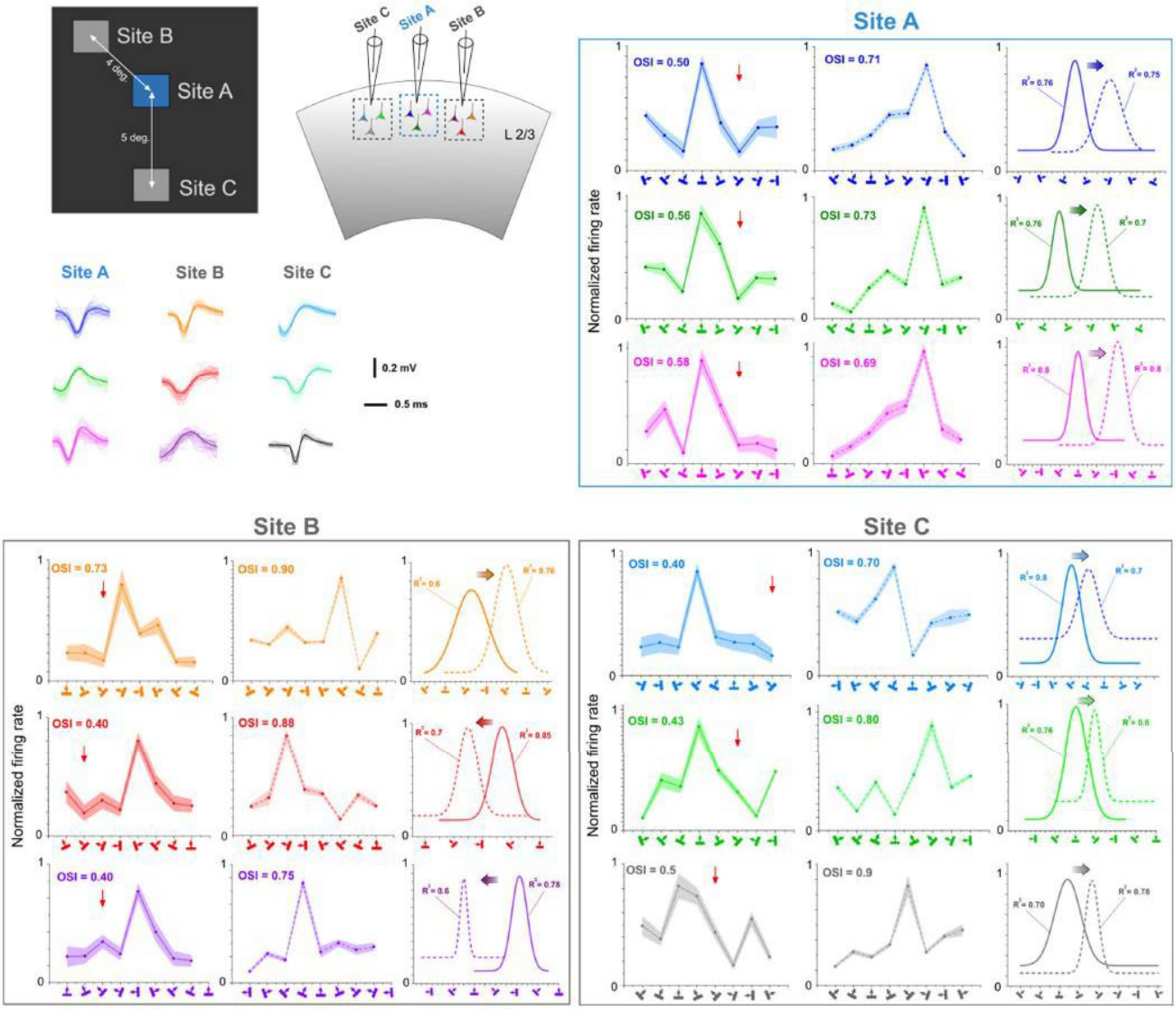

Figure 2 | Typical examples of shifts of orientation tuning curve peaks. Tuning shifts are underlined by horizontal colored arrows. The downward red arrow heads indicate the adapting orientation in this and all figures. Upper left insert shows the respective positions of three receptive fields. Only receptive field A was adapted. Waveforms of respective sorted out action potentials are shown below the insert. Tuning curves pre- and post-adaptation are illustrated for each stimulated site (Upper right row: site A, lower left row: site B, lower right row: site C). The curves represent raw data and Gaussian fits. Light colors indicate error bars. Orientations of gratings are depicted on X-axis. OSI's and R-squared are indicated for each tuning curve.

encroaches on the periphery of the companion receptive field. An example is displayed in Fig. 3c, indicating the levels of spontaneous firing while at the same time when the distant companion RF is stimulated with the selected range of orientations. In this example the distance separating both receptive fields was 6°. The spontaneous firing remained unchanged for all applied orientations (X-axis) and for every trial (a single dot stands for one trial presentation of the sine-wave grating applied for 4.1 s; one-way ANOVA: $p > 0.05$, Shapiro-Wilk normality test: $w = 0.9$, Bartlett's test for variances: $p = 0.8$). The average firing at spontaneous activity in control conditions was 15.8 Hz and in adaptation 15.76 Hz (t-test: $p > 0.05$, Shapiro-Wilk normality test: $w = 0.9$, $F = 1.2$). It must also be emphasized that RF's were never stimulated concurrently (see methods). Thus, RF's were sufficiently far apart in order to avoid overlapping surrounds. In addition, we observed non-significant differences of spontaneous activity across all the presented orientations within all RF's when stimulating the adjacent RF's pre- and post-adaptation (one-way ANOVA: $p > 0.05$, Shapiro-Wilk normality test: $w = 0.8$, Bartlett's test for variances: $p = 0.8$, Fig. 3d). Another example is illustrated in Fig. 3e. It shows the spiking activity of neurons from one RF (RF A, blue, *i.e.*, non-stimulated) during the stimulation of the adjacent RF (RF B, gray), and during the stimulation of the RF itself (RF A). Conversely, the activity was computed in a similar fashion for RF B when RF A was stimulated, and when RF B was stimulated.

We observed a significant difference between these two conditions for both RF's (unpaired t-test, $p < 0.05$, Shapiro-Wilk normality test: $w = 0.9$, $F = 1.7$, Fig. 3e). Furthermore, stimulating one RF did not modify the firing at spontaneous activity (red arrow, Fig. 3e). This is highly incompatible, had we encroached the boundaries of the companion RF.

Preferred orientation stability. It is important to confirm that optimal orientations do not fluctuate spontaneously. Many investigations have shown that for any given cell, although response magnitude varies, the preferred orientation remains remarkably

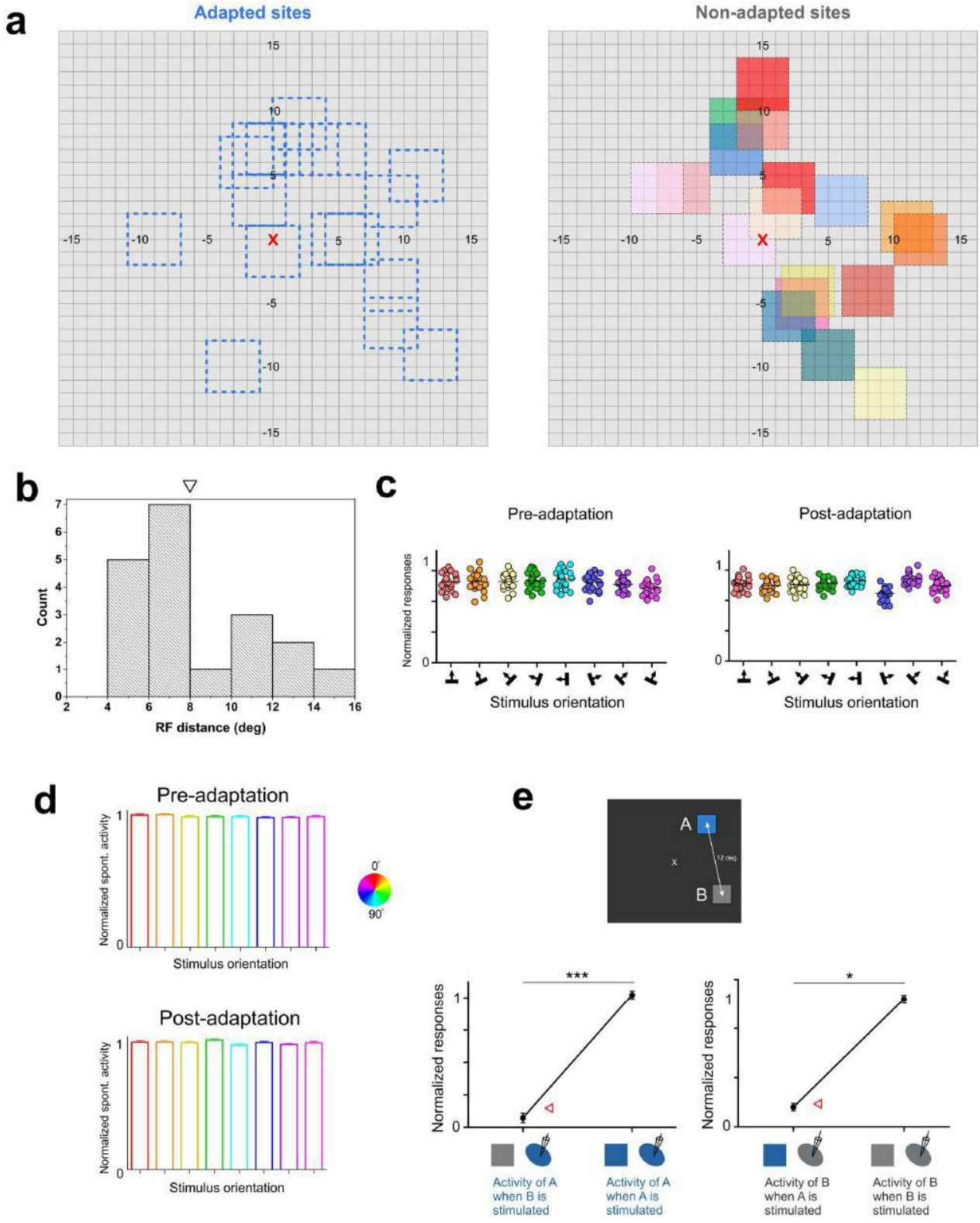

Figure 3 | Location of receptive fields and spontaneous activity. (a) Distribution of adapted (left) and non-adapted (right) receptive fields. Color codes of non-adapted sites correspond to colors of Figure 4a. The receptive field (RF) locations are relative to the fixation point which is underlined by the red cross. (b) Histogram distribution of RF-distances between adapted and non-adapted sites. The downward triangle represents the mean value of RF distance. (c) Absence of spontaneous activity (SA) modulations of one unit when the companion cell is stimulated within its RF at tested orientations. Distance between receptive fields: 6°. The total lack of modulation of SA suggests an absence of overlap between both RF's. (d) Global results of spontaneous activity of one site while stimulating the adjacent one in both pre- and post-adaptation conditions. (e) Example of multi-unit activity of one RF during the stimulation of the companion RF and during the stimulation of the RF itself. Statistical differences were observed between these conditions. Red triangles indicate the level of spontaneous activity of the RF of interest.

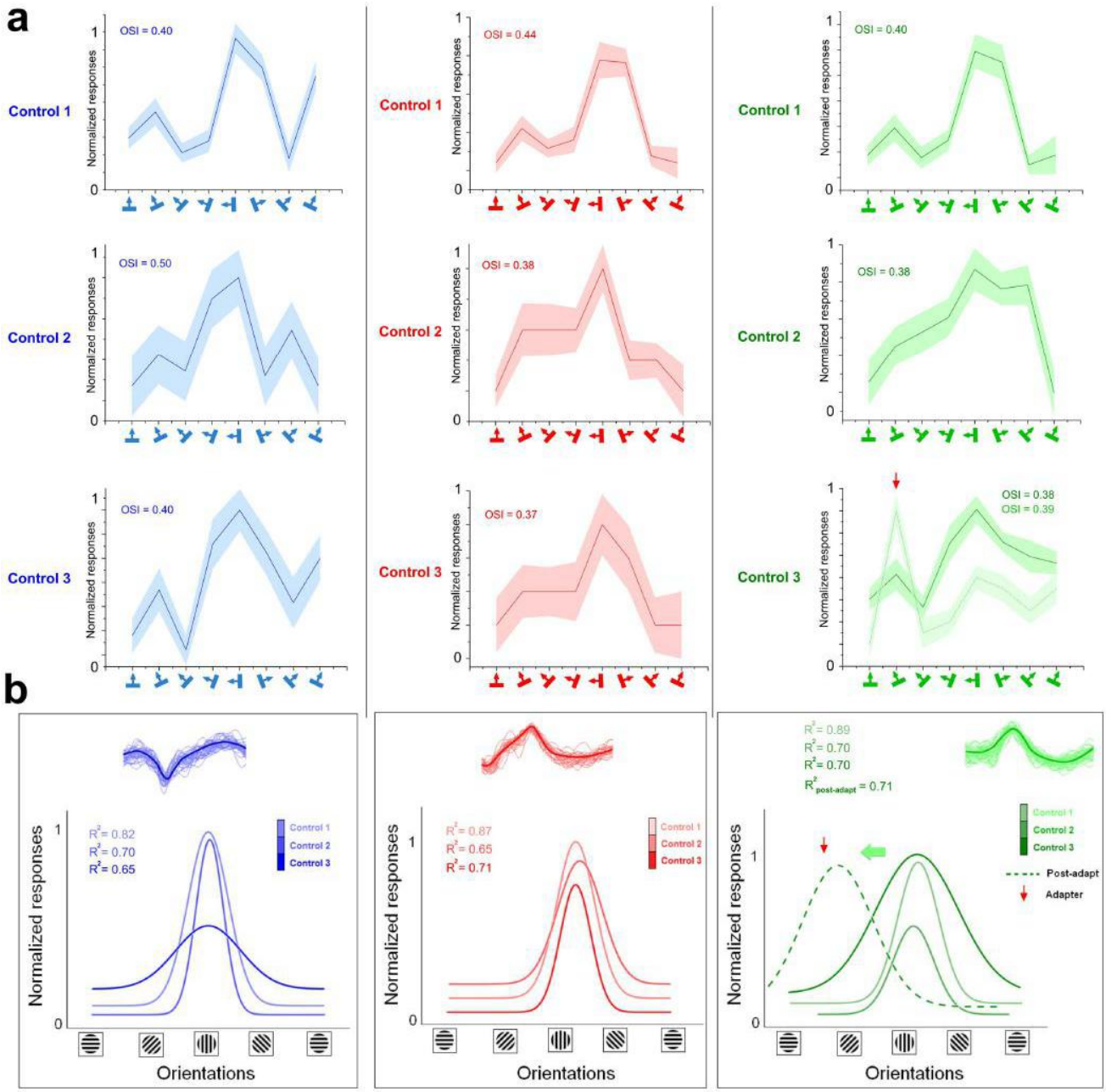

Figure 4 | Tuning stability. (a) Raw tuning curves of three neurons at different time-windows (90 min between control 1, control 2, and control 3). As an additional example, the green cell (right) shows the post-adaptation tuning curve (dashed tuning curve, red arrow head corresponds to the adapting orientation) demonstrating the classical observed tuning shift (horizontal green arrow); Y-axis is the normalized amplitude of the cell's firing. (b) Gaussian fits derived from raw data. Spike-waveforms for every neuron are shown above the Gaussian curves.

constant for several days[3,20,21]. Nevertheless, we proceeded with an additional control by measuring orientation tuning curves of three cells during a four hour period (about 90 min separated each recording session, Fig. 4). Raw responses are shown in Fig. 4a and Gaussian fits for each cell are illustrated in Fig. 4b. While the evoked firing rates vary in amplitude, the optimal response (normalized) is elicited by the same orientation in all three recorded neurons. Following these retests, adaptation (12 minutes) was carried out that resulted in a shift of the peak of the tuning curve (see example in Fig. 4, right, the green cell shifted by 45° in the attractive direction).

Shifts in non-adapted sites. Figure 5a illustrates the range of orientation shifts on a cell to cell basis (the short horizontal line indicates the average shifts for a particular cluster of cells). Clusters, *i.e.*, cells recorded from the same site, are identified on the X-axis and the Y-axis indicates shift-range of every unit belonging to non-adapted neurons. In total, 108 units were analyzed. Notice that the first two groups of neurons (labeled "LS1-135" and "Second attempt") are same units tested twice in order to ascertain the consistency of shifts in cells at the non-adapted locus. In this example, the mean magnitudes of shifts were 19.7° (first attempt) and 15.6° (second attempt). Therefore, it can be deduced that orientation shifts at non-adapted sites are the consequence of adaptation executed at some distance from the tested location. Although the average shift-magnitudes were about equal, it should be emphasized that within a single cluster (cells likely to be physically close to each other) some

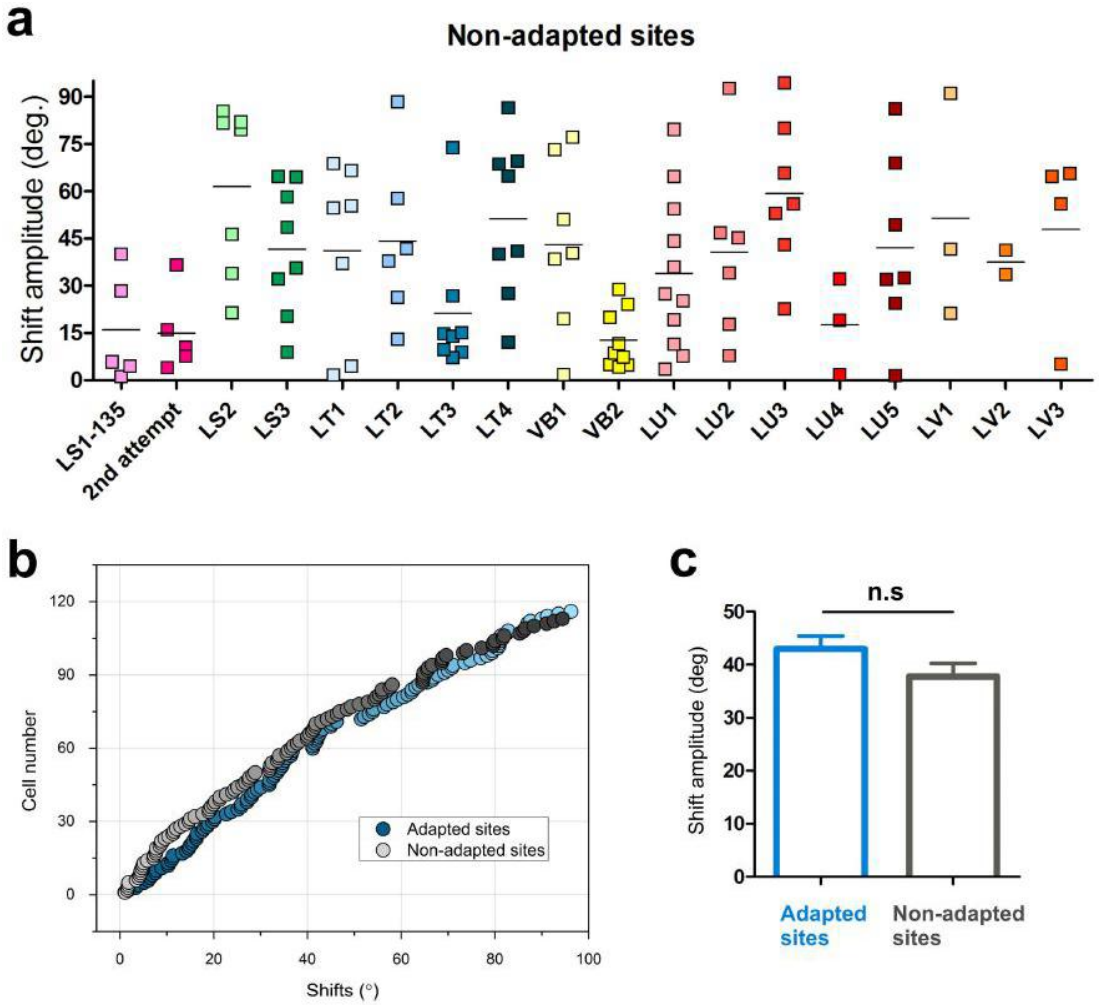

Figure 5 | General survey. (a) Shift-magnitude of every neuron in every cluster; Y-axis: shift amplitude, horizontal line: mean-shift for the corresponding cluster. Notice that the recording "LS1 135" is repeated (second attempt). X-axis: cluster code. For sake of clarity, cells recorded from closely positioned electrodes are grouped within one cluster. (b) Cumulative plots of orientation shifts, magnitudes in increasing order; the close parallelism between both curves suggests that in adapted (blue) and non-adapted (gray) cells, the shifts are comparable. (c) The equal average magnitude shifts confirm that there is no difference between adapted and non-adapted sites.

units significantly shifted their preferred orientation, whereas other neighboring cells failed to change their preferred orientation, hence suggesting that orientation changes are specific characteristics belonging to some neurons (cluster LU3 for instance). This last result indicates that changes of orientation may not be attributed to a general surge of excitation (see below). These results corroborate recent reports showing that within a large population of neurons in sensory cortices, there are embedded sub-networks of units whose selectivity is modifiable depending on a particular stimulus protocol[22]. Such a manifold potential for modification depending on groups of particular cells leads to the conclusion that within a pool of neurons, a class of cells maintains its initial property (original orientation); while another group of intermingled units has a potential to change its optimal stimulating feature to a newly acquired orientation. This heterogeneous organization echoed by dissimilar shifts following adaptation could allow the preservation of an overall stable network yet allowing adaptation to novel conditions of the visual environment.

In Fig. 5b, absolute orientation shifts' magnitudes are plotted in increasing order for every tested cell (cells are not paired, adapted site = 110; non-adapted site = 108). The very similar profiles of cumulative-type curves of shifts in adapted and non-adapted sites are indicative that in both sites the peaks of the orientation tuning curves are displaced with equal magnitude. Although the change of orientation in individual cells may vary, the overall mean shift-amplitude is about equal in adapted and non-adapted cells: 42.9° and 37.7°, respectively (Fig. 5c, t-test: $p > 0.05$, Shapiro-Wilk normality test: $w = 0.9$, $F = 1$). These data suggest that when a group of neurons modifies its orientation selectivity, some other cells follow the change in an equivalent magnitude. Analogously, it is like the domino effect: once the first block falls the other blocks tilt and fall accordingly. That is, a full set of orientation axes is represented with no orientation-hole. Alternatively, if such collective shifts were deficient, one orientation (shifted) would be represented twice since it would closely match an already present axis. Such double presentation of one axis of orientation appears incompatible with the notion that a single hypercolumn contains full range of orientations.

The above results along with data reported in the literature suggest that, following adaptation, the original equilibrium between multiple synaptic drives is ruptured. Consequently a novel optimal orientation arises[9,23]. In addition, we observed significant changes of another parameter: the tuning bandwidth. Indeed, the overall bandwidth at half magnitude is significantly narrower after adaptation for both sites (Control: 32.1 ± 1.7°; post-adaptation: 26.9 ± 1.4°, unpaired

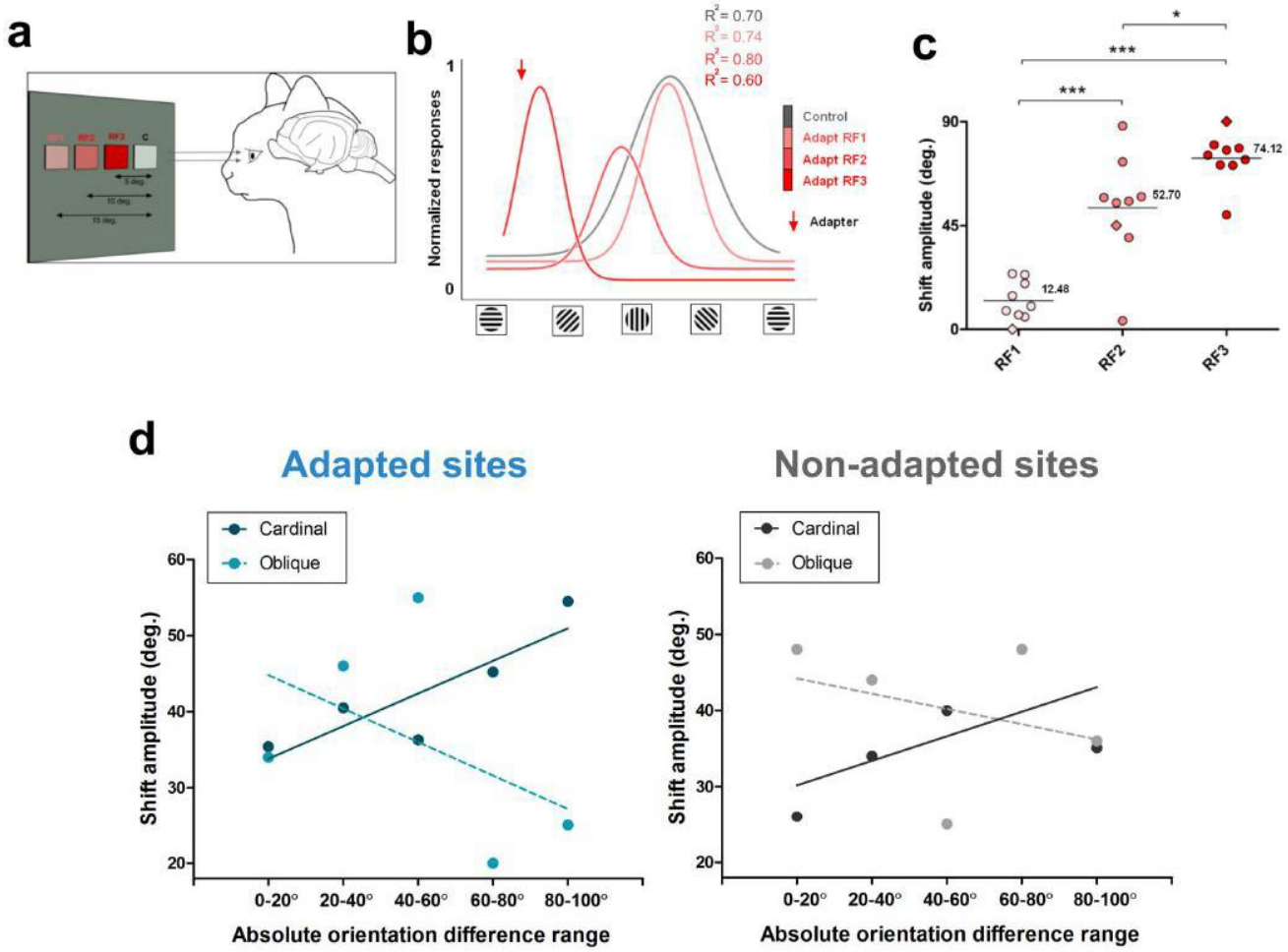

Figure 6 | Inter-receptive-field distances. (a) Experimental set up of stimulation and visual adaptation in relation to inter-RF distances. (b) Typical example of tuning curves of one neuron, responses normalized. The adapting site was approached in steps of 5° from 15° (RF1) — the largest distance separating both fields to the closest gap: 5° (RF3). The example shows that as the adapting field gets closer to the control receptive field, the stimulated neurons elicited larger shifts of the orientation tuning curve towards the adapter (downward red arrow). (c) Global distribution of the averaged shift-magnitudes in relation to inter-RF distances (same cells in all conditions). (d) Shift-amplitudes in adapted and non-adapted sites in relation to the original preferred orientation prior to adaptation, the broken line represents cells whose initial preferred orientation was oblique, while the solid line stands for units whose initial preferred orientations were cardinal (vertical or horizontal, see text for details). X-axis: absolute orientation differences between preferred orientation and the adapting orientation.

t-test: $p < 0.05$, Shapiro-Wilk normality test: $w = 0.8$, $F = 1.3$). This narrowing of the bandwidth following adaptation is coherent with the slight augmentation of the OSI after adaptation as described above.

Relationships between magnitude of shifts and inter-RF distance and orientation differences. We then examined the spatial extension of adaptation. We measured the amplitude of shifts in relation to the distance separating the two stimulated loci measured from center to center (Fig. 6a–c). The adapting grating was applied in steps at three distances: 5°, 10°, and 15° from the tested site (Fig. 6a, tested site identified by letter C). When both RF's were separated by 15°, the tuning curves of neurons were not modified in strong fashion, although the shifts were significant (average shift = 12.48°). Then, as the adapted field approached the tested field to 10° (RF2), the neurons shifted their optimal orientation with increased amplitude in the attractive direction (average shift = 52.70°). At the third adapted site (RF3) located 5° off the tested field (RF C), neurons showed an even larger shift, (average shift = 74.12°) (Fig. 6b, c). Figure 6c shows the distribution of shift amplitudes over a neuronal population ($n = 9$). It demonstrates the relationships between the distance separating both RF's and the shift amplitude (Shapiro-Wilk normality test: $w = 0.8$, t-test RF1-RF2, $p < 0.05$; t-test RF2-RF3, $p < 0.05$; t-test RF1-RF3, $p < 0.05$). Thus changes of orientation selectivity spread over a distance of up to 15°.

Previously[9] it has been reported that in adapted receptive fields cells tuned to cardinal orientations have larger shift-amplitudes when the orientation difference between the adapter and the original orientation increased. Conversely, cells tuned to oblique orientations exhibited larger shift amplitudes when the orientation difference was small, and shifts decreased as this gap increased. Figure 6d illustrates the shifts magnitudes between adapted and non-adapted sites when cells were grouped in relation to their initial optimal orientation. Thus cells with original cardinal orientations: 90° ± 22° and 0° ± 22° (solid line) were dissociated from cells with initial oblique orientation, 45° ± 22° (broken line). Furthermore, for these analyses, neurons were grouped into five 20° orientation classes (Fig. 6d). Interestingly, the same relationships were observed in both adapted and non-adapted sites. These data could signify that in order to maintain constancy of orientation organization following the shifts in the adapted and non-adapted sites, the cortical network rectifies its original orientation layout to maintain its orientation selectivity dis-

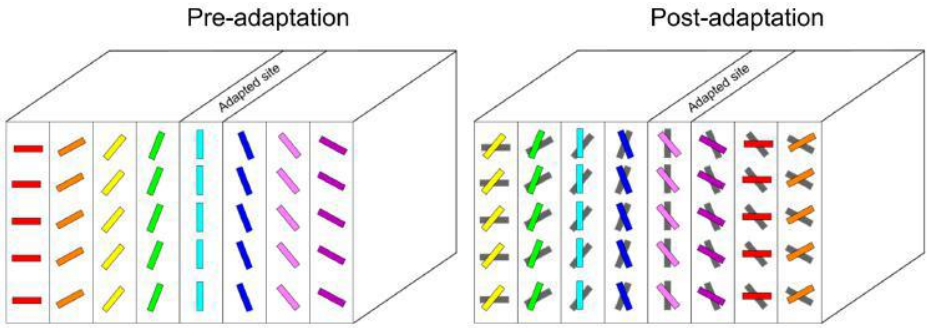

Figure 7 | Schematic model illustrating cortical reorganization following visual adaptation. "Ice cube" model exhibiting orientation columns. After adaptation, a tilt of orientation axis is displayed. Notice an absence of orientation hole.

tribution. In other words, a group of neurons in area 17 displaces the peaks of its orientation tuning curve in relation to the orientation of the neighboring neurons as reference axis.

Discussion

The results demonstrate that preferred orientation of neurons in the visual cortex changes following a relatively short period (12 min) of localized adaptation taking place remotely from the tested (non-adapted) receptive field. Data from our experiments have the following implications: (1) selectivity of orientation organization in area 17 is not attributed to a determined anatomically based and/or ontogenetic layout of a neuronal network. Rather, orientation column design appears to be a labile formation changing its selectivity depending on the history and more generally stimuli conditions exciting neighboring neurons; in other words, local persistent stimulus leads to unmapping and remapping of cortical orientation domains (Fig. 7). Thus, a cross-mutual influence may redraw what has been thought to be an immutable organization of the orientation layout. (2) It appears that orientation columns are a functional construction rather than strictly anatomical, one based on parallel segregation of input fibers emanating from the retina, and then from the lateral geniculate nucleus (LGN). These results may appear astonishing since orientation columns in the visual system are thought to be rather stable after the critical period that follows birth because coding visual trigger features necessitates highly discriminatory neuronal properties[24].

Methodological considerations. It may be argued that shifts in orientation are the consequences of spontaneous fluctuations of levels of firing rates. Although such a hypothesis may not be rejected, nonetheless, numerous experimental results argue against this eventuality. Recently, it has been shown that orientation selectivity in identified units remains stable over several days[20]. In addition, it is unlikely that response-changes may be ascribed to random fluctuations of cellular excitability. Several authors have demonstrated that orientation selectivity is invariant[3], as the jitter of the optimal orientation is small ($<5^{\circ}$). Finally, the response modulations of cells in the adapted and non-adapted sites are constrained roughly to the adapter and the initial preferred orientations. For instance, evoked responses close to the adapter are augmented while, in parallel, responses to the original preferred orientation are weakened[9]; such dual modulations in opposite directions cannot be reconciled with global fluctuations of excitability. Collectively, all of these arguments indicate that it is very unlikely that the described specific discharge modulations are due to spontaneous surges of excitability. Moreover, anesthesia eliminates the impact of attention. Imposing an orientation to a particular neuron for twelve minutes while the animal is paralyzed and anaesthetized is a situation that clearly does not replicate natural conditions. This is a compromise needed to induce neurons to change their preferred orientation. In many reports, it has been shown that imposing a sensory or appropriately timed electrical stimulus induces neuronal property changes within minutes[25–29], which is a time scale congruent with adaptation duration of the described experiments. Although the change in preferred orientation may last for many minutes[30] and may be ten times longer than adaptation duration[7], data suggest that the brain's network is dynamic as it is attuned to the environmental conditions. This may imply that functional column changes are transient yet lasting for many minutes.

Twelve minutes of continuous adaptation may raise the question of the duration of recovery. Literature reports that even after two hours following adaptation; only half of the neurons recover their original selectivity[7,27,30]. Indeed, while capturing the activity of both sites (adapted and non-adapted) post-adaptation; we started first with the adapted site by presenting it the grating corresponding to the original optimal orientation, thereafter, showing the grating corresponding to the original optimal of non-adapted site. In a systematic fashion, after the presentation of these gratings corresponding to the original optimal controls in both sites, we presented the adapter-grating alternatively to both sites (adapted then non-adapted). As evident from our data that most of the neurons exhibited shifts of the tuning curves superior to 10 degrees (both sites) post-adaptation (90% from the adapted sites, 80% from the non-adapted sites, Fig. 5a), thus indicating that they are indeed the result of the adaptation process.

Another methodological aspect may be clarified. In order to avoid surround cross-influence between the receptive fields, neurons stimulated by each site were never excited simultaneously (see Fig. 8). In this study, the average distance separating the adapted and non-adapted fields was $8.0 \pm 3.0^{\circ}$. It has been shown that far-surround radius in V1 averaged $5.5 \pm 2.64^{\circ}$[31]. This reduces the probability of extensive overlapping of both RF's. To our knowledge, no study has demonstrated that stimulating the surround of RF affects the orientation selectivity of neurons. Rather, the stimulation of the periphery results in the modulation of the firing rate (see Fig. 6b). Furthermore, as mentioned above, the spontaneous activity of each RF was never affected by the stimulation of the companion RF.

Mechanisms. Our results are supported by several recent reports. In mouse it has been demonstrated that a single dendritic branch exhibits, over a short distance, synaptic inputs with a large spectrum of orientation channels allowing mutual influences[32]. Whole-cell recording in rodent V1 shows large sub-threshold depolarization evoked by non-preferred orientations[33–35]. After adaptation, the impact of an applied orientation takes over the cell's excitability causing the emergence of a novel optimal orientation due to a specific excitatory drive, wherein one input dominates over other inputs, thus, driving the synaptic strength above threshold that provides the cell its orientation selectivity. Recently in human, it was demonstrated that when the neuronal processing is disturbed,

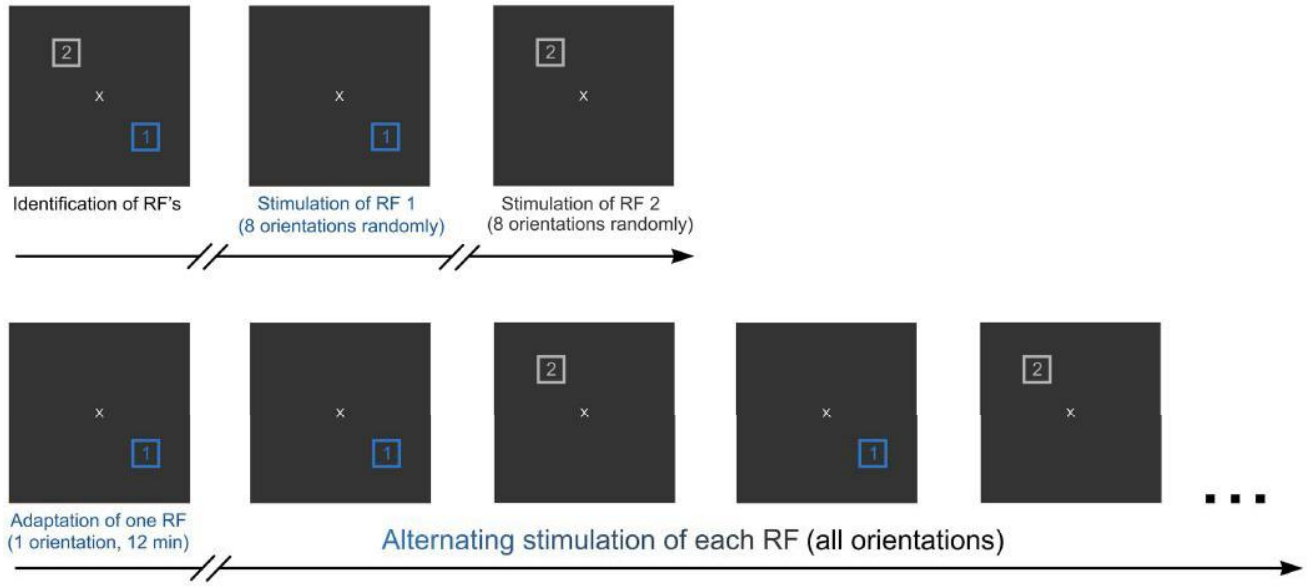

Figure 8 | Visual stimulation and adaptation protocols. Upper part: initial stimulation (control). Lower part: adaptation process and post-adaptation recordings.

another cortical area takes over the task to maintain subject performance[36]. These investigations, although at different levels, suggest that single cells or cortical areas may modify their destined commitment to specific functions or tasks following changing conditions, and thus shift the responses to new stimulating environments[37]. The above assumptions are supported by recent reports describing "classes of neurons that accumulate information from an entire cortical column and broadcasts outputs to distant targets"[22].

Neurons in the primary visual cortex receive polysynaptic inputs not only from neighboring cells, but also from a network of distal cortical sites. Indeed, feed-forward and feedback connections are extensive. Thus, area 17 neurons' preferred orientations are not exclusively resulting from feed-forward inputs originating from aligned lateral geniculate nucleus cells[2], since elicited responses are also influenced by long-range connections[38,39]. In particular, the cat's secondary visual cortex (area 18) exhibits strong reciprocal relations with area 17[40], which relays parvocellular inputs to area 18. Monier et al.[25] demonstrated by recording membrane potentials intracellularly that a single cortical cell is receiving inputs from a large variety of synaptic inputs. They came to the conclusion that the diversity of input combinations may be reflected in homogeneities of intra-cortical patterns of connectivity leading to changeable properties. It is to be expected that once the adaptation modifies the balance between inputs and specifically the gradient between excitatory and inhibitory synaptic weights, the neurons become susceptible to exhibit a novel optimal orientation. Because of the extensive intra-cortical network a particular neuron that modifies its selectivity influences other cells with which it is directly or indirectly connected, thus contributing to modifications of the orientation selectivity of an entire network (Fig. 7). Such neuronal dynamics have been described in the auditory cortex[41].

In conclusion, our results strongly suggest that orientation selectivity is a rapidly modifiable characteristic that is adjusted by specific neurons depending on the behavior of cells surrounding the tested neurons. Thus, orientation columns transcend anatomy, and are functionally dynamic entities.

Methods

Ethical approval. Animal surgery and electrophysiological procedures followed the guidelines of the Canadian Council on Animal Care and were approved by the Institutional Animal Care and Use Committee of the University of Montreal. Animals were supplied by the Division of Animal Resources of the University of Montreal.

Animal preparation. Electrophysiological recordings were performed using multielectrodes within area 17 of adult domestic cats. Adult cats (2.5–3.5 kg, age 12–24 months) of either sex, sedated with acepromazine maleate (Atravet, Wyeth-Ayerst, Guelph, ON, Canada; 1 mg kg^{-1}, intramuscular) and atropine sulfate (ATRO-SA, Rafter, Calgary, AB, Canada; 0.04 mg kg^{-1}, intramuscular), were anaesthetized with ketamine hydrochloride (Rogarsetic, Pfizer, Kirkland, QC, Canada; 25 mg kg^{-1}, intramuscular) maintained with 0.3% isoflurane (AErrane, Baxter, Toronto, ON, Canada). Lidocaine hydrochloride (Xylocaine, AstraZeneca, Missis-sauga, ON, Canada; 2%) was injected subcutaneously as a local anaesthetic during surgery. A tracheotomy was performed for artificial ventilation, and one forelimb vein was cannulated to administer a nutritive solution containing a paralyzing agent. Animals were then placed in a stereotaxic apparatus. Xylocaine gel (Astra Pharma, Mississauga, ON, Canada; 5%) was applied on the pressure points. For the remaining preparations and recording, paralysis was induced with 40 mg and maintained with 10 mg kg^{-1} h^{-1} gallaminetriethiodide (Flaxedil, Sigma Chemical, St. Louis, MO, USA; intravenous) administered in 5% dextrose lactated Ringer's nutritive solution. General anaesthesia was maintained by artificial ventilation with a mixture of N_2O/O_2 (70 : 30) supplemented with 0.5% isoflurane (AErrane, Baxter, Toronto, ON, Canada) for the duration of the experiment. Proper depth of anaesthesia was ensured throughout the experiment by monitoring the EEG, the electrocardiogram and expired CO_2. In addition the heart rate remained unmodified after skin stimulation. The end-tidal CO_2 partial pressure was kept constant between 25 and 30 mmHg. A heating pad was used to maintain a body temperature of 37.5°C. Tribrissen (Schering-Plough, Pointe-Claire, QC, Canada; 30 mg kg^{-1} per day, subcutaneous) and Duplocillin (Intervet, Withby, ON, Canada; 0.1 ml kg^{-1}, intramuscular) were administered to the animals to prevent bacterial infection. The pupils were dilated with atropine sulfate (Isopto-Atropine, Alcon, Mississauga, ON, Canada; 1%) and the nictitating membranes were retracted with phenylephrine hydrochloride (Mydfrin, Alcon, Mississauga, ON, Canada; 2.5%). The loci of the area centrales were inferred from the positions of the blind spots, which were ophthalmoscopically focused and back projected onto a translucent screen. Plano contact lenses with artificial pupils (5 mm diameter) were placed on the cat's eyes to prevent the cornea from drying (University of Montréal, PQ, Canada).

At the end of each experiment, euthanasia was achieved with a lethal dose of pentobarbital sodium (Somnotol, MTC Pharmaceuticals, Cambridge, ON, Canada; 100 mg kg^{-1}) by intravenous injection.

Electrophysiology and visual stimulation. Neurons from several recording sites in layers 2/3 were simultaneously recorded. Electrodes were lowered either tangentially (with a 20–30° angle, tetrode arrangements) or vertically (four electrodes, inter-electrode separation: 400 µm, Frederick Haer & Co, Bowdoinham, ME, USA; 2–10 MΩ at 1 kHz). The signal from the microelectrodes was amplified, band-pass filtered (300 Hz–3 kHz), digitized, and recorded with a 0.05 ms temporal resolution (Spike2, CED, Cambridge, England). In all cases at least two excitatory receptive fields were outlined. We paid particular consideration that surrounds of receptive fields were not overlapping.

Firstly, in order to minimize direct cross-influence between both sites, respective cells were never stimulated at the same time (Fig. 8). Secondly, the spontaneous spiking activity of each neuronal population belonging to one RF was recorded during the stimulation of the adjacent RF (see results). Finally, the surround influence in

responses evoked from excitatory area could modulate the magnitude of responses but the neuronal selectivity remained unaffected (see Fig. 6b).

Each site was stimulated with drifting sine-wave grating patches covering the excitatory fields (Spatial Frequency = 0.24 cycle/°, Temporal frequency = 1.0–2.0 Hz, Contrast = 80%). Cells were sequentially stimulated in pseudorandom presentation of gratings. The grating was placed in the center of the aggregate RF of the sampled units. We measured tuning with eight equally spaced orientations (22.5° interval) of the drifting sinusoidal grating. It is to be underlined that the gratings were presented only for one direction. Stimuli were presented in each receptive field in isolation, thus each group of cells was stimulated alternatively in order to eliminate direct cross influence between neurons (Fig. 8). Adapting and stimulating gratings were identical in size and characteristics. Prior to adaptation, respective tuning curves were obtained revealing the preferred orientation in each site that elicited the maximal firing rates. In the following step, only one site was adapted by applying a non-preferred orientation up to 90° off the initial preferred orientation of the neurons (usually evoking a weak response) continuously for twelve minutes. While the adaptation happened over one site, the second site was unstimulated. After adaptation, orientation tuning curves were re-investigated in the same manner as before adaptation.

Cell isolation. Given that the multi-unit activity was recorded concurrently from the same tips using multi-electrodes, it was essential to ascertain that cells were well isolated, because the same unit may exhibit sufficiently different waveforms (for instance, magnitude in relation to distance between recording tip), and thus belong to different clusters in principal component analysis.

Cell-separation was based on spike-waveforms, cluster-isolation using first principal components analyses, autocorrelograms, and trial-count correlation (TC). No more than 5 cells were recorded from the same electrode tip. TC denotes the trial by trial Pearson correlation-coefficient between simultaneously recorded firing of two neurons in response to the presentation of an identical stimulus. In response to the presentation of the same stimulus, the same unit fires identically, regardless of spike amplitude. In order to eliminate such occurrences we correlated neural activities of every cell-pair for every applied trial (25 trials, same stimulus, duration 4.1 s). Since optimal orientations eliciting maximal firing rates were chosen for this computation, and considering a relatively long time-window of analyses (4.1 s), we should expect a high value for correlation if it were the same unit, because such time windows of analyses are sufficiently large to capture the full strength of correlation. Indeed, correlations are underestimated if the counting window is too short. In all analyzed cells the TC was extremely weak (TC < 0.3). Such extremely feeble TC establishes that both spike trains do not originate from the same neuron (see Supplementary Fig. S1). Autocorrelograms preclude contamination by spikes of other units. Anesthesia and paralysis of animals reduced the possibility of similar modulations of firing patterns in cells of the same clusters due to rapid eye motion or attention.

Data analysis. Once single cells were sorted out off-line from multi-unit spike trains accumulated during data acquisition, Gaussian tuning curves were constructed from raw data. We fitted our raw data with the Gaussian function to determine with precision the preferred orientation of neurons and then measured shifts in orientation preference. We used the following Gaussian function:

$$y = y0 + \left(\frac{A}{w\sqrt{\pi/2}}\right)\cdot e^{-2\left(\frac{x-xc}{w}\right)^2} \qquad \text{(Equation1)}$$

where y0 is the offset, Xc is the center, w is the width, and A represents the area under the Gaussian fit.

The shifts of peaks of tuning curves between pre- and post-adaptation conditions were calculated from the Gaussian fits using the following formula:

$$Shift = |Xc\ post - Xc\ pre| \qquad \text{(Equation2)}$$

where Xc is the central value derived from the Gaussian fit.

Orientation selectivity index (OSI) was calculated from data as the difference between firing rate (FR) at preferred and orthogonal orientations as follows:

$$OSI = \frac{FR\ pref - FR\ ortho}{FR\ pref + FR\ ortho} \qquad \text{(Equation3)}$$

The closer the OSI is to one, the stronger the orientation selectivity (see results).

It has been shown previously that averaged shifts inferior to 5° were not significant[9], however we consider all the shifts in the present investigation.

One-way ANOVA (95% confidence limit) statistical tests were used to compare the spontaneous firing activity between all presented stimuli. Statistical comparisons were performed using unpaired sample two-tailed t-test (95% confidence limit) for unpaired data. Shapiro-Wilk normality test (significance threshold = 0.05) was used for the normal distribution of data, and Fisher test to compare variances for all student tests.

Bartlett's test was performed to compare variances for ANOVA tests.

1. Hubel, D. H. & Wiesel, T. N. Receptive fields, binocular interaction and functional architecture in the cat's visual cortex. *J Physiol.* **160**, 106–154 (1962).
2. Jin, J., Wang, Y., Swadlow, H. A. & Alonso, J. M. Population receptive fields of ON and OFF thalamic inputs to an orientation column in visual cortex. *Nat Neurosci.* **14**, 232–238 (2011).
3. Henry, G. H., Bishop, P. O., Tupper, R. M. & Dreher, B. Orientation specificity and response variability of cells in the striate cortex. *Vision Res.* **13**, 1771–1779 (1973).
4. Horton, J. C. & Adams, D. L. The cortical column: a structure without a function. *Philos Trans R Soc Lond B Biol Sci.* **360**, 837–862 (2005).
5. Kaas, J. H., Krubitzer, L. A. & Johanson, K. L. Cortical connections of areas 17 (V-I) and 18 (V-II) of squirrels. *J Comp Neurol.* **281**, 426–446 (1989).
6. Swindale, N. V., Shoham, D., Grinvald, A., Bonhoeffer, T. & Hubener, M. Visual cortex maps are optimized for uniform coverage. *Nat Neurosci.* **3**, 822–826 (2000).
7. Dragoi, V., Sharma, J. & Sur, M. Adaptation-induced plasticity of orientation tuning in adult visual cortex. *Neuron* **28**, 287–298 (2000).
8. Dragoi, V., Rivadulla, C. & Sur, M. Foci of orientation plasticity in visual cortex. *Nature* **411**, 80–86 (2001).
9. Ghisovan, N., Nemri, A., Shumikhina, S. & Molotchnikoff, S. Long adaptation reveals mostly attractive shifts of orientation tuning in cat primary visual cortex. *Neuroscience* **164**, 1274–1283 (2009).
10. Ghisovan, N., Nemri, A., Shumikhina, S. & Molotchnikoff, S. Visual cells remember earlier applied target: plasticity of orientation selectivity. *PloS one* **3**, e3689 (2008).
11. Kohn, A. Visual adaptation: physiology, mechanisms, and functional benefits. *J Neurophysiol.* **97**, 3155–3164 (2007).
12. Kohn, A. & Movshon, J. A. Adaptation changes the direction tuning of macaque MT neurons. *Nat Neurosci.* **7**, 764–772 (2004).
13. Krekelberg, B., van Wezel, R. J. & Albright, T. D. Adaptation in macaque MT reduces perceived speed and improves speed discrimination. *J Neurophysiol.* **95**, 255–270 (2006).
14. Hietanen, M. A., Crowder, N. A., Price, N. S. & Ibbotson, M. R. Influence of adapting speed on speed and contrast coding in the primary visual cortex of the cat. *J Physiol.* **584**, 451–462 (2007).
15. Atallah, B. V., Bruns, W., Carandini, M. & Scanziani, M. Parvalbumin-expressing interneurons linearly transform cortical responses to visual stimuli. *Neuron* **73**, 159–170 (2012).
16. Ringach, D. L., Shapley, R. M. & Hawken, M. J. Orientation selectivity in macaque V1: diversity and laminar dependence. *J Neurosci.* **22**, 5639–5651 (2002).
17. Denman, D. J. & Contreras, D. The structure of pairwise correlation in mouse primary visual cortex reveals functional organization in the absence of an orientation map. *Cereb Cortex.* **24**, 2707–2720 (2014).
18. Freeman, J. & Simoncelli, E. P. Metamers of the ventral stream. *Nat Neurosci.* **14**, 1195–1201 (2011).
19. Orban, G. A., Kennedy, H. & Bullier, J. Velocity sensitivity and direction selectivity of neurons in areas V1 and V2 of the monkey: influence of eccentricity. *J Neurophysiol.* **56**, 462–480 (1986).
20. Lutcke, H., Margolis, D. J. & Helmchen, F. Steady or changing? Long-term monitoring of neuronal population activity. *Trends Neurosci.* **36**, 375–384 (2013).
21. Frenkel, M. Y. *et al.* Instructive effect of visual experience in mouse visual cortex. *Neuron* **51**, 339–349 (2006).
22. Harris, K. D. & Mrsic-Flogel, T. D. Cortical connectivity and sensory coding. *Nature* **503**, 51–58 (2013).
23. Bachatene, L., Bharmauria, V., Cattan, S. & Molotchnikoff, S. Fluoxetine and serotonin facilitate attractive-adaptation-induced orientation plasticity in adult cat visual cortex. *Eur J Neurosci.* **38**, 2065–2077 (2013).
24. Shtoyerman, E., Arieli, A., Slovin, H., Vanzetta, I. & Grinvald, A. Long-term optical imaging and spectroscopy reveal mechanisms underlying the intrinsic signal and stability of cortical maps in V1 of behaving monkeys. *J Neurosci.* **20**, 8111–8121 (2000).
25. Monier, C., Chavane, F., Baudot, P., Graham, L. J. & Fregnac, Y. Orientation and direction selectivity of synaptic inputs in visual cortical neurons: a diversity of combinations produces spike tuning. *Neuron* **37**, 663–680 (2003).
26. Fregnac, Y. *et al.* A Re-Examination of Hebbian-Covariance Rules and Spike Timing-Dependent Plasticity in Cat Visual Cortex in vivo. *Front Synaptic Neurosci.* **2**, 147 (2010).
27. Godde, B., Leonhardt, R., Cords, S. M. & Dinse, H. R. Plasticity of orientation preference maps in the visual cortex of adult cats. *Proc Natl Acad Sci U S A.* **99**, 6352–6357 (2002).
28. Schuett, S., Bonhoeffer, T. & Hubener, M. Pairing-induced changes of orientation maps in cat visual cortex. *Neuron* **32**, 325–337 (2001).
29. Yao, H., Shi, L., Han, F., Gao, H. & Dan, Y. Rapid learning in cortical coding of visual scenes. *Nat Neurosci.* **10**, 772–778 (2007).
30. Nemri, A., Ghisovan, N., Shumikhina, S. & Molotchnikoff, S. Adaptive behavior of neighboring neurons during adaptation-induced plasticity of orientation tuning in VI. *BMC Neurosci.* **10**, 147 (2009).
31. Shushruth, S., Ichida, J. M., Levitt, J. B. & Angelucci, A. Comparison of spatial summation properties of neurons in macaque V1 and V2. *J Neurophysiol.* **102**, 2069–2083 (2009).
32. Jia, H., Rochefort, N. L., Chen, X. & Konnerth, A. Dendritic organization of sensory input to cortical neurons in vivo. *Nature* **464**, 1307–1312 (2010).
33. Lien, A. D. & Scanziani, M. Tuned thalamic excitation is amplified by visual cortical circuits. *Nat Neurosci.* **16**, 1315–1323 (2013).

34. Li, Y. T., Ibrahim, L. A., Liu, B. H., Zhang, L. I. & Tao, H. W. Linear transformation of thalamocortical input by intracortical excitation. *Nat Neurosci.* **16**, 1324–1330 (2013).
35. Van Hooser, S. D., Heimel, J. A., Chung, S. & Nelson, S. B. Lack of patchy horizontal connectivity in primary visual cortex of a mammal without orientation maps. *J Neurosci.* **26**, 7680–7692 (2006).
36. Zanto, T. P., Chadick, J. Z., Satris, G. & Gazzaley, A. Rapid functional reorganization in human cortex following neural perturbation. *J Neurosci.* **33**, 16268–16274 (2013).
37. Reid, R. C. From functional architecture to functional connectomics. *Neuron* **75**, 209–217 (2012).
38. Ringach, D. L. Haphazard wiring of simple receptive fields and orientation columns in visual cortex. *J Neurophysiol.* **92**, 468–476 (2004).
39. Gilbert, C. D. & Wiesel, T. N. Columnar specificity of intrinsic horizontal and corticocortical connections in cat visual cortex. *J Neurosci.* **9**, 2432–2442 (1989).
40. Bullier, J., McCourt, M. E. & Henry, G. H. Physiological studies on the feedback connection to the striate cortex from cortical areas 18 and 19 of the cat. *Exp Brain Res.* **70**, 90–98 (1988).
41. Froemke, R. C., Merzenich, M. M. & Schreiner, C. E. A synaptic memory trace for cortical receptive field plasticity. *Nature* **450**, 425–429 (2007).

Acknowledgments

This study was supported by grants to S.M. (NSERC, FQRNT).

Author contributions

L.B., V.B. and S.C. contributed equally to this work. S.M. designed the study, contributed to data analyses and wrote the manuscript. J.R. contributed to data analyses.

Additional information

Supplementary information accompanies this paper at http://www.nature.com/scientificreports

Competing financial interests: The authors declare no competing financial interests.

How to cite this article: Bachatene, L., Bharmauria, V., Cattan, S., Rouat, J. & Molotchnikoff, S. Reprogramming of orientation columns in visual cortex: a domino effect. *Sci. Rep.* 5, 9436; DOI:10.1038/srep09436 (2015).

BRAIN RESEARCH 1594 (2015) 136–153

Available online at www.sciencedirect.com

ScienceDirect

www.elsevier.com/locate/brainres

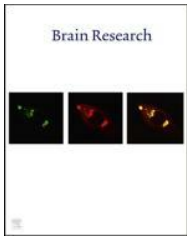

Research Report

Modulation of functional connectivity following visual adaptation: Homeostasis in V1

L. Bachatene[a,b], V. Bharmauria[a,b], S. Cattan[a,b], J. Rouat[a,b], S. Molotchnikoff[a,b,*]

[a]Laboratoire de Neurosciences de la Vision, Département de Sciences Biologiques, Université de Montréal, C.P. 6128, Succursale Centre-ville, Montréal, QC, Canada H3C 3J7

[b]Neurosciences Computationnelles et Traitement Intelligent des Signaux—NECOTIS, Université de Sherbrooke, Sherbrooke, QC, Canada

ARTICLE INFO

Article history:
Accepted 26 October 2014
Available online 31 October 2014

Keywords:
Cortical plasticity
Crosscorrelation
Functional connectivity
Visual adaptation
Neuronal network
Homeostasis

ABSTRACT

Sensory neurons exhibit remarkable adaptability in acquiring new optimal selectivity to unfamiliar features when a new stimulus becomes prevalent in the environment. In conventionally prepared adult anesthetized cats, we used visual adaptation to change the preferred orientation selectivity in V1 neurons. Cortical circuits are dominated by complex and intricate connections between neurons. Cross-correlation of cellular spike-trains discloses the putative functional connection between two neurons. We sought to investigate changes in these links following a 12 min uninterrupted application of a specific, usually non-preferred, orientation. We report that visual adaptation, mimicking training, modulates the magnitude of crosscorrelograms suggesting that the strength of inter-neuronal relationships is modified. While individual cell-pairs exhibit changes in their response correlation strength, the average correlation of the recorded cell cluster remains unchanged. Hence, visual adaptation induces plastic changes that impact the connectivity between neurons.

1. Introduction

The brain has a remarkable capacity for plastic modifications where cortical areas are able to switch to a new selection-preference in relation to the stimulus. For instance, V1 neurons are selective for stimuli features such as orientation, spatial frequency, direction and speed (Dragoi et al., 2000; Hubel and Wiesel, 1959; Hubel and Wiesel, 1968; Kohn and Movshon, 2004; Marshansky et al., 2011; Movshon, 1975), but can modify their selectivity in order to functionally reorganize the visual cortex as an "adapted cortex" to altered stimulation. Primary visual neurons are organized into cortical domains exhibiting specific connections (Hubel and Wiesel, 1959, 1968; Stratford et al., 1996; Yoshimura et al., 2000).

Visual training impinges upon the spiking activity of neuronal populations (Bachatene et al., 2012, 2013; Dragoi

Abbreviations: CCG, crosscorrelogram; OSI, orientation selectivity index; RF, receptive field; TC, trial-count correlation; V1, primary visual cortex

*Corresponding author at: Laboratoire de Neurosciences de la Vision, Département de Sciences Biologiques, Université de Montréal, C.P. 6128, Succursale Centre-ville, Montréal, QC, Canada H3C 3J7. Fax: +1 514 343 2293.

http://dx.doi.org/10.1016/j.brainres.2014.10.054
0006-8993/

et al., 2000; Ghisovan et al., 2009; Kohn and Movshon, 2004; Patterson et al., 2013), hence it may influence the dynamic modulation of functional relationships between cells. Indeed, the primary visual cortex recalibrates its inputs to reconfigure information processing which results in modified neuronal connectivity after plasticity phenomenon (Fahle, 2004).

Many studies have shown that neuronal connectivity is related to the stimuli preference of neurons; cellular projections are higher between neurons sharing similar preferred features (Ko et al., 2011; Stepanyants et al., 2008). For example, cells exhibiting similar orientation selectivity are grouped into orientation columns (Alloway and Roy, 2002; Bartho et al., 2004; Csicsvari et al., 1998; Hubel and Wiesel, 1959, 1968; Yoshimura et al., 2005). Following cortical plasticity, the neurons change their selectivity (Bachatene et al., 2012; Dragoi et al., 2000; Ghisovan et al., 2009) and the cortex is reorganized (Dragoi et al., 2000; Godde et al., 2002), however, the mechanisms conferring a novel circuitry on cortical neurons are as yet unknown. Here, we seek to examine the impact of adaptation on connectivity between V1 neurons. Crosscorrelation computations signify inter-neuronal relationships that are indicative of functional connections emerging from coordinated neural activities of involved neurons (Bartho et al., 2004; Denman and Contreras, 2013; Fujisawa et al., 2008; Hata et al., 1991; Konig et al., 1995; Perkel et al., 1967). Moreover, crosscorrelograms (CCG) calculate a peak-strength which yields an index of connectivity between neurons (Alloway and Roy, 2002; Wise et al., 2010). Significant peaks within a short time-window in the CCG's are indicative of putative functional linkages between units (Bartho et al., 2004; Denman and Contreras, 2013; Fujisawa et al., 2008; Kara and Reid, 2003; Perkel et al., 1967). In the present investigation, we used crosscorrelation analyses to examine connection probabilities between V1 neuronal pairs sharing similar pre- and post-adaptation orientation-selectivity in order to reveal plastic changes in dynamic functional connectivity. In other words, how is the neural coding altered after experience-dependent plasticity? We report that visual adaptation considerably modulates the peaks-strengths among individual neuron-pairs, however, on average, peaks-strengths are not significantly different pre- and post-adaptation. Such adjustments involving cell-pairs in V1 while preserving the global time relationships between neuronal spikes allow constancy within neuronal properties of an assembly of cells and at the same time adaptability to visual stimuli modifications (Benucci et al., 2013).

2. Results

We measured extracellular spiking activity of V1 neurons in response to visual orientation gratings after spike sorting protocol within layers II/III. The current investigation was focused on how visual adaptation (prolonged presentation of a non-preferred orientation stimulus within the receptive field of neurons) affects this functional dynamic. In total, 166 cells were recorded, and 105 pairs were selected based on the similarity of orientation-preference pre- and post-adaptation.

2.1. *Peaks-strengths pre- and post-adaptation: A typical cell-pair example*

The computations in Fig. 1 display a typical example of CCG analysis for a cell-pair (both cells exhibited $\pm 22^\circ$ similar pre- and post-adaptation selectivity). We first isolated single units from multi-unit spiking activity (see methods). Fig. 1A illustrates two simultaneously recorded cells sorted by spike wave-shapes (top), cluster distribution derived from principal component analysis (below) and autocorrelograms (right), the latter showing an absence of event (refractory period) at 0 on the time-scale.

The raster plots and peri-stimulus time histograms are shown in Fig. 1B. The inserted histograms (on the right) display the push-pull effect at both orientations of interest, the spiking activity at the initial optimal orientation declines post-adaptation, and the firing rate at the new preferred orientation (evoking weak responses pre-adaptation) increases after visual adaptation. This is demonstrated by the respective tuning curves for both neurons (Fig. 1C). The raw orientation tuning curves revealed that both cells had $\pm 22^\circ$ similar preferred orientation (pink neuron: 3.9 ± 2.06 Hz at 67.5°, blue neuron: 3.19 ± 1.21 Hz at 90°). After 12 min of visual adaptation to a non-preferred orientation (indicated by the downward black arrows), both tuning curves shifted their peaks to 157.5° and 0° for pink and blue neurons, respectively (pink neuron: 3.7 ± 1.65 Hz at 157°, blue neuron: 1.6 ± 0.94 Hz at 0°). Thereafter, shift-corrected CCG's were computed to reveal the dynamic functional links between cell-pairs (see methods for details). Fig. 1D represents the CCG's analysis for neurons shown in Fig. 1A at similar original and novel preferred orientations (pre-adaptation condition is displayed on the left and post-adaptation on the right). In this example, neuron 1 (pink unit) was set as the reference neuron and neuron 2 (blue unit) as the target unit. The peaks-strengths at the original optimal orientation decreased from 0.040 to 0.015 after adaptation with a large decorrelation (see also next section for general distribution). However, for the new optimal orientation, we observed a decrease from 0.040 to 0.034 and the correlation was maintained (significant peak). This reflects the dynamic functional linkage due to visual adaptation. It is to be mentioned that the aim of this study was to investigate direct functional relationships between specific neurons. Therefore, the analyses were focused on significant peaks offset from zero mark in the CCG, such analysis is a useful method to interpret the putative functional links between neurons (Bartho et al., 2004; Csicsvari et al., 1998; Denman and Contreras, 2013; Fujisawa et al., 2008).

2.2. *Adaptation influences the correlation between units*

The next figure illustrates on a global scale the changing strength of connectivity (as reflected from the peaks-strengths) for all neuronal pairs sharing the same pre- and post-adaptation orientation-selectivity. Fig. 2A shows, on a cell-pair basis, the correlation of the peaks-strengths for the highest bins ($>95\%$, time-window ± 5 ms) in the CCG's prior and post-adaptation, at original optimal orientation (left graph) and new optimal orientation (right graph). For the original optimal orientation, we obtained 87 cases of significant CCG's (peaks above 95% of the confidence line) before and/or after adaptation. At the new optimal orientation, 75 significant cases were obtained.

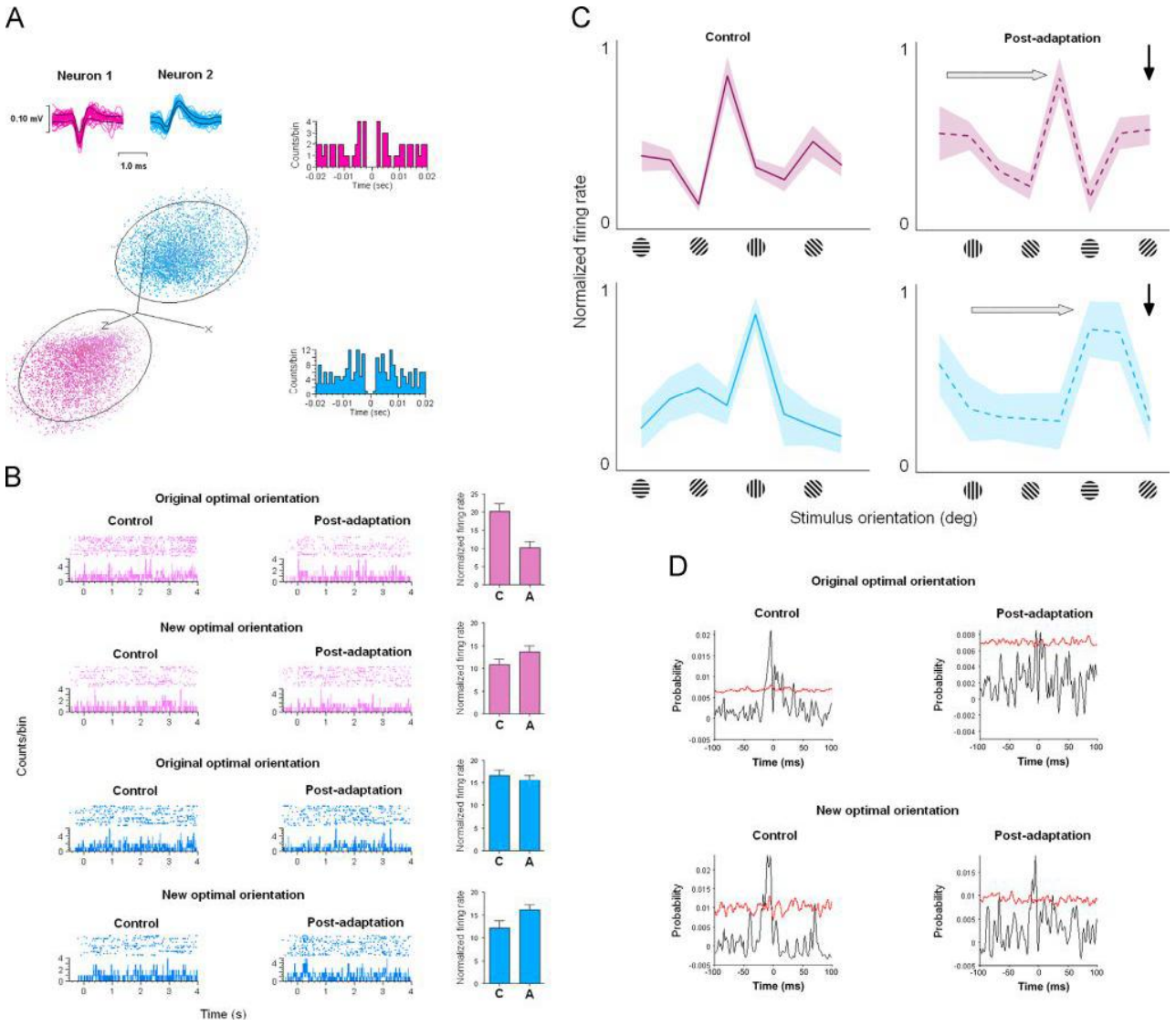

Fig. 1 – Typical example. (A) Two neurons (pink and blue units) sorted using spike waveforms, principal component analyses, and autocorrelograms. (B) Raster plots and peri-stimulus time histograms for both cells (at the initial optimal orientation and the new optimal orientation). The values of the mean firing activity are displayed in the histograms (on the right, C for control and A for adaptation). (C) Orientation tuning curves of both neurons for control (solid lines) and post-adaptation (dashed lines) conditions, corresponding lighter colors represent error bars. Horizontal gray arrows show the direction of shifts of tuning curves and the black downward arrows represent the adapting orientation. The two neurons are tuned to a $\pm 22^{\circ}$ similar oriented stimulus. (D) Shift-corrected crosscorrelograms of both neurons for their similar original optimal and new optimal gratings (left: control, right: post-adaptation). (For interpretation of the references to color in this figure legend, the reader is referred to the web version of this article.)

Thereafter, we correlated the peaks-strengths of neuronal pairs pre- and post-adaptation for both orientations (original and new optimal). The resultant linear regression analysis is shown in Fig. 2A. The dotted line in each graph represents the best-fit 45° line passing through the origin. The peak-strength before adaptation is indicated on the X-axis, whereas the Y-axis shows the peak-strength following adaptation. The solid black line in each graph corresponds to the linear regression trend with the value of the coefficient of determination (R^2). R^2 equals 0.17 and 8.10^{-5} for the original optimal orientation (left) and the new optimal orientation (right), respectively. Such a wide distribution of dots points to the fact that adaptation redistributes (decrease or increase of the peaks-strengths) the time-relationship between spiking activities of neuronal pairs, even though the cells are sharing the same orientation-selectivity following adaptation. We suggest that adaptation disturbs the original inter-neuronal relationships, thereby either erasing or establishing new functional connections to frame novel connectomes as a result of the emergence of newly acquired firing patterns of involved neurons.

The number of cases for diminution and augmentation of the peaks-strengths are as follows: at original optimal orientation,

we found 49 cases (56%) of diminution and 38 cases (44%) of augmentation ($n=87$), whereas, for new optimal orientation, a decrease was observed in 45 cases (60%), versus 30 cases (40%) of increase ($n=75$) (see next section for details).

Fig. 2B represents the total distribution of the peaks-strengths for all cell-pairs pre- (green) and post-adaptation (orange) at the original optimal orientation (left) and the newly acquired orientation (right). Below are shown the respective non-linear regression curves with the relative coefficients of determination (Original optimal: $R^2_{control}=0.99$, $R^2_{post\text{-}adaptation}=0.99$, New optimal: $R^2_{control}=0.97$, $R^2_{post\text{-}adaptation}=0.97$).

In spite of the decorrelation following adaptation on cell-pair basis as evident from Fig. 2A, we note that in Fig. 2B, the very close superposition of the cumulative distribution of dots and curves indicates an absence of difference in global modification of the peaks-strengths in both conditions (control and post-adaptation) at each orientation of interest (original optimal and new optimal), thus suggesting that even though functional connections may change at the cell-pair basis, it is, however, likely on a populational scale that there is an inherent stability (homeostasis) to the network. Furthermore, we compared the functional connectivity between neurons sharing a $\pm 22^\circ$ orientation-preference-range and between differently tuned neurons (superior to 22° of orientation-preference-range, Fig. 2C). We found a significant difference between these two groups (two-tailed t-test, $p<0.05$). These results suggest that even though visual adaptation modifies the peaks-strengths of crosscorrelograms that may reflect the functional connections between neurons, cells that exhibit newly similar orientations remain more strongly connected in comparison to differently tuned cells. In addition, we calculated the peaks-strengths at the adapting orientation. Overall, the modulations of the peaks-strengths set the latter at about the same average values (Fig. 2D).

2.3. *Modulation of peak-strengths*

Fig. 3 shows the population analysis of the peaks-strengths for both orientations of interest (original optimal and new optimal). We averaged the peaks-strengths for all neuronal pairs in pre-adaptation condition, and thereafter, the increase and decrease post-adaptation. Fig. 3A displays all cellular pairs showing a decline of the peaks; the mean probabilities pre- and post-adaptation were 0.029 and 0.011 respectively for the original optimal orientation ($n=49$, left, significant decrease of 0.018, two-tailed t-test, $p<0.05$). The same tendency is observed for the new optimal orientation ($n=45$, right), i.e., a significant decline of 0.019 from 0.032 to 0.013 (paired two-tailed t-test, $p<0.05$). Fig. 3B displays the group of pairs reacting with an increase in probability following adaptation (significant two-tailed paired t-tests for augmentation of the peaks-strengths for both original and new optimal orientations). Interestingly, the enhancement of the peak-strength for the new optimal orientation (right) is superior to the enhancement of the peak for the original optimal orientation (left); these increases are 0.027 and 0.015, respectively (one-tailed unpaired t-test, $p<0.05$). This is the highest modulation for this group of cells that acquire a new optimal orientation.

These sets of data and particularly the regression analysis (Figs. 2 and 3) suggest that even after visual adaptation, on average, the peaks-strengths are altered, yet, the constant application of the grating influences the time correlation of individual pairs of neurons in a flexible fashion. These computations suggest a lack of uniformity which, in turn, points toward the fact that adaptation adjusts the functional relationship between involved neurons. We suggest that such versatility in inter-neuronal relationships promotes flexibility, and, consequently, plasticity. To test whether these variations were due to spontaneous fluctuations of firing, peaks-strengths were compared for original orientations prior to, post-adaptation, and subsequently 1 h after adaptation (recovery). An example of crosscorrelograms between two cells is illustrated in Fig. 3C (left). It shows the effect of adaptation on the correlation between spike trains of these two neurons and the recovery of the magnitude level 1 h after adaptation. The maximal peaks of CCG's in this example were 0.06, 0.013 and 0.061 for control, post-adaptation and recovery, respectively. Other examples in Fig. 3C (right, upper part) show the variability of correlation due to adaptation process as the peak strength values return to control levels after recovery. These examples indicate that visual adaptation modulates the magnitude of the peak strength between correlated neuronal spike trains.

Globally, the average values were 0.022 ± 0.003, 0.019 ± 0.002, 0.022 ± 0.003 for control, post-adaptation and recovery, respectively (Fig. 3C right, lower part, random sample, $n=41$).

Additionally, we compared the CCG-magnitudes between the stimulus-condition and the non-stimulus-condition (spontaneous activity of the recorded neurons), and found a significant difference (two-tailed t-test, $p<0.05$). Crosscorrelogram-magnitudes during spontaneous activity were very low, suggesting that connectivity-strength is due to the presentation of stimulus rather than spontaneous neuronal firing (Fig. 3D). Moreover, stimulation was repeated in order to compare the CCG-values at different times. Fig. 3E shows an example of two CCG's between two neurons at time t_1 (attempt 1) and t_2 (attempt 2); the time-laps between both attempts was 1 h. The values of the CCG-peaks were 0.040 and 0.039, respectively. Taken together, these results demonstrate that the CCG's remain constant.

2.4. *Dynamics of correlation*

Firing rate of neurons pre- and post-visual adaptation is changed mostly for two main orientation classes: the original optimal orientation and the new acquired optimal orientation. It is changed in such a way that we generally notice a decline of evoked firing activity for the original preferred stimulus and an increase of elicited discharges for the new preferred stimulus by an already described push-pull mechanism, therefore leading to the observed shifts after the adaptation process (Bachatene et al., 2012, 2013; Ghisovan et al., 2009). We thus calculated a Fano factor ($F=\sigma^2/\mu$) by dividing the variance (σ^2) by the mean firing rate (μ) of every neuron from each pair; we then compared these factors in pre- and post-adaptation conditions. Fig. 4A shows the modulation of the Fano Factor for original (top) and new optimal (bottom) orientations. This factor increased from 0.49 to 0.57 for the original preferred orientation (paired two-tailed t-test, $p<0.05$) and decreased from 0.58 to 0.48 for the new preferred orientation (paired two-tailed t-test, $p<0.05$). These reverse trends show that spike patterns are more variable for the original optimal orientation and steadier for the new preferred

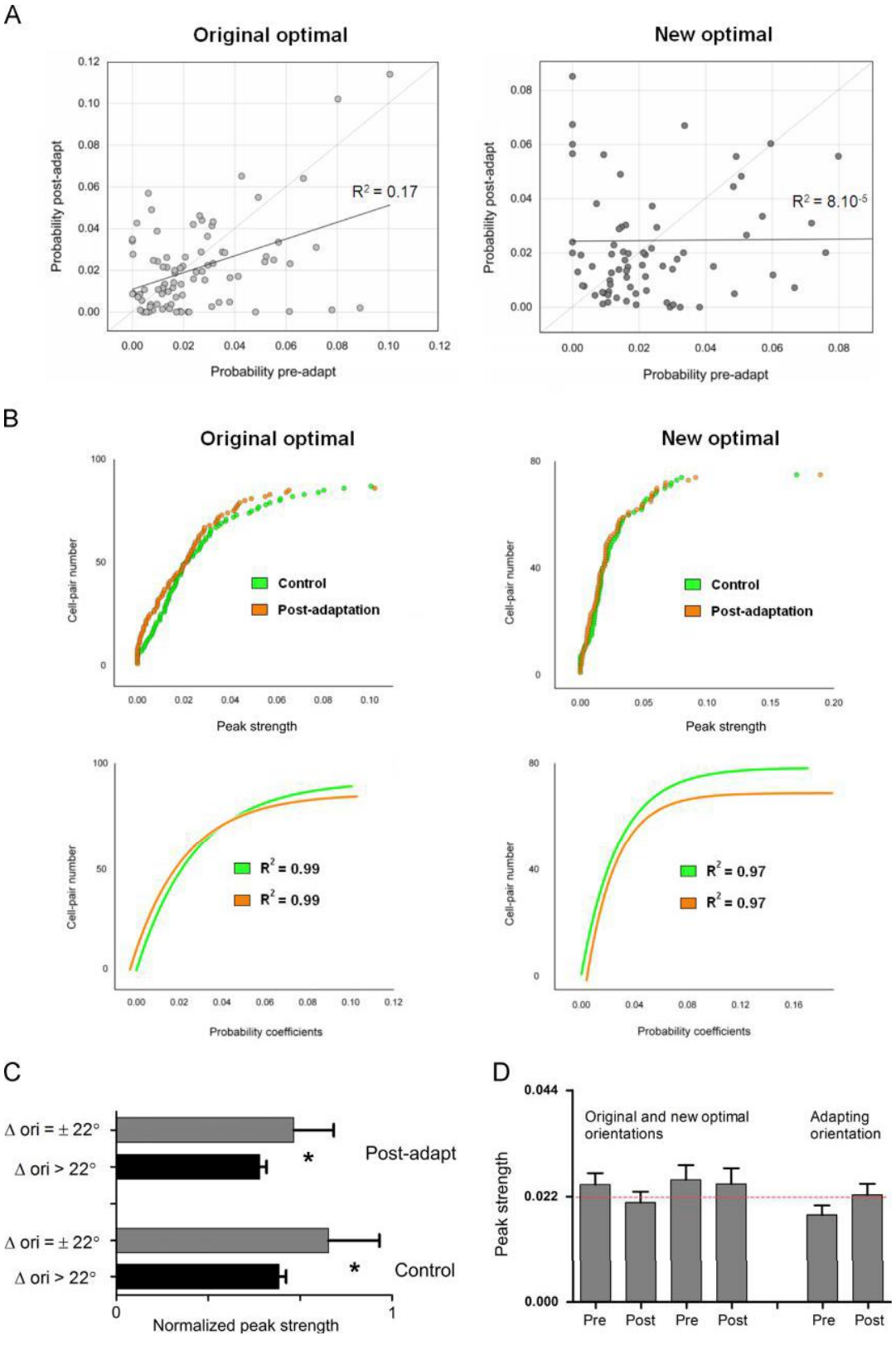
A
Original optimal
New optimal
Probability post-adapt
Probability pre-adapt
R² = 0.17
R² = 8.10⁻⁵
B
Original optimal
New optimal
Cell-pair number
Peak strength
Control
Post-adaptation
R² = 0.99
R² = 0.99
R² = 0.97
R² = 0.97
Probability coefficients
C
Δ ori = ± 22°
Δ ori > 22°
Post-adapt
Control
Normalized peak strength
D
Peak strength
Original and new optimal orientations
Adapting orientation
Pre
Post

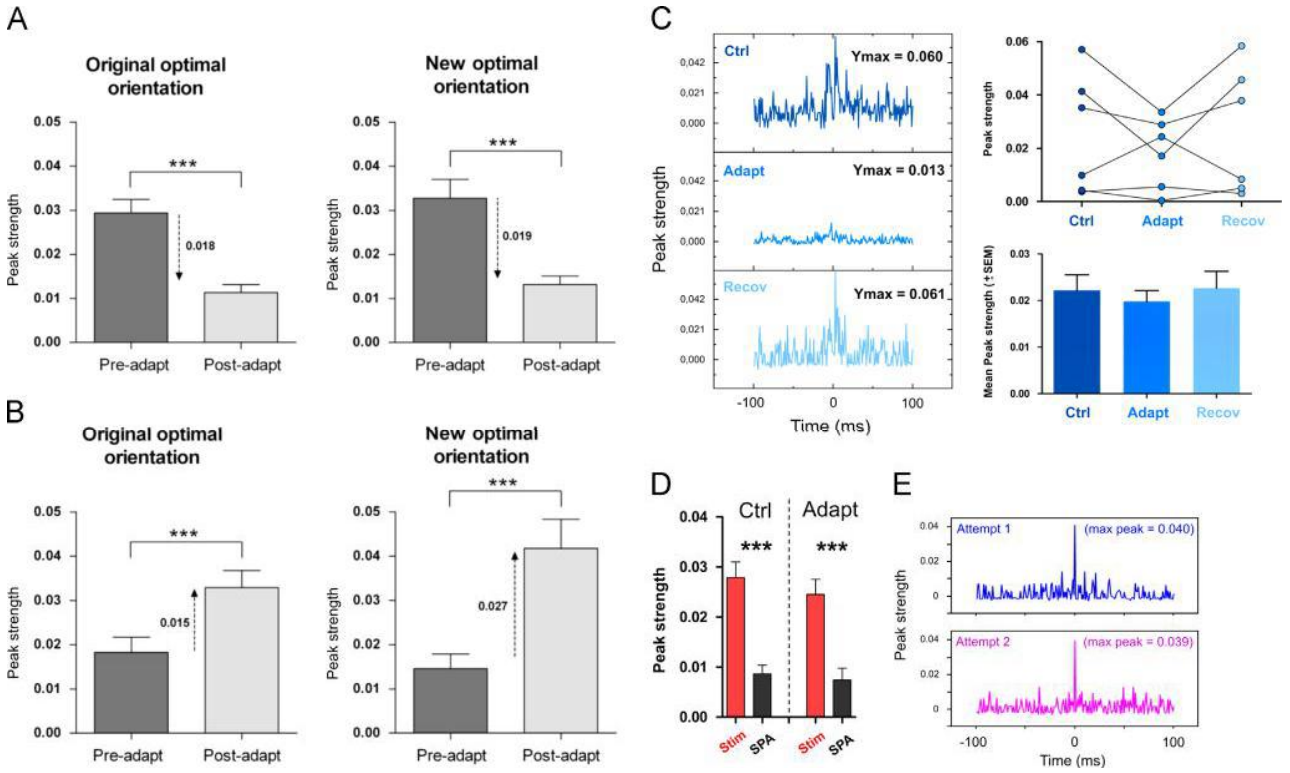

Fig. 3 – Population analyses of the modulation of peaks-strengths and spontaneous activity. (A) Cases of diminution of the mean peaks-strengths post-adaptation for the original optimal orientation (left) and the new optimal orientation (right), significant declines of 0.018 (two-tailed *t*-test, $p<0.05$) and 0.019 (two-tailed *t*-test, $p<0.05$) were observed for both orientations, respectively. (B) Cases of augmentation of the mean peaks-strengths following adaptation for both orientations (original and new optimal), the increase of mean peak-strength for the new optimal orientation is almost 50% superior to the increase for the original optimal (0.027 and 0.015, respectively). (One-tailed unpaired *t*-test, 95% significance level, $p=0.03$). (C) Left: example of CCG's between spike trains of two neurons. The peak magnitudes were 0.06, 0.013 and 0.061 for control, post-adaptation and recovery (1 h after adaptation process), respectively. Right, upper: other examples of correlation variability for these three conditions. Right, lower: random sample test of averaged peaks strengths ($n=41$) between control, post-adaptation and recovery period. Error bars in the histogram indicate the standard error of the mean. The observed peaks were 0.022 ± 0.003, 0.019 ± 0.002, 0.022 ± 0.003, respectively. (D) Averaged peak-strength (control and post-adaptation) for two conditions: during visual stimulation (red histograms) and during spontaneous activity (black histograms). Significant difference was observed for both conditions. (E) Example of two CCG's at two different times (two attempts separated by 1 h). This example shows the stability of the peak-strength over a period of time. (For interpretation of the references to color in this figure legend, the reader is referred to the web version of this article.)

Fig. 2 – Correlation of peaks-strengths pre- and post-adaptation. (A) Linear regression analyses of the peaks-strengths for the original optimal orientation (left, 87 significant cases found, $n=105$) and for the new acquired optimal orientation (right, 75 significant cases found, $n=105$). The dotted line indicates best-fit 45° line passing through the origin. *X*-axis and *Y*-axis show the peaks-strengths pre- and post-adaptation, respectively. Solid black line in each graph displays the linear regression trend ($R^2=0.17$ for the original optimal orientation, $R^2=8.10^{-5}$ for the new optimal orientation). (B) Total distribution of peaks-strengths for all cell-pairs, green dots and curves represent pre-adaptation condition, orange dots and curves show post-adaptation condition. Results for the original optimal orientation are on the left and for new optimal orientation on the right. Below are illustrated the respective non-linear regression curves (original optimal: $R^2_{control}=0.99$, $R^2_{post\text{-}adaptation}=0.99$, new optimal: $R^2_{control}=0.97$, $R^2_{post\text{-}adaptation}=0.97$). (C) Difference of connectivity strength between closely tuned neurons (gray bars) and differently tuned neurons (black bars) for control and post-adaptation. The peak-strength is significantly higher for closely tuned neurons in both conditions. (D) Averaged peak-strength at all orientations of interest (original and new optimal orientations on the left, adapting orientation on the right). The red dashed line represents the mean peak-strength (0.022) which is maintained post-adaptation. (For interpretation of the references to color in this figure legend, the reader is referred to the web version of this article.)

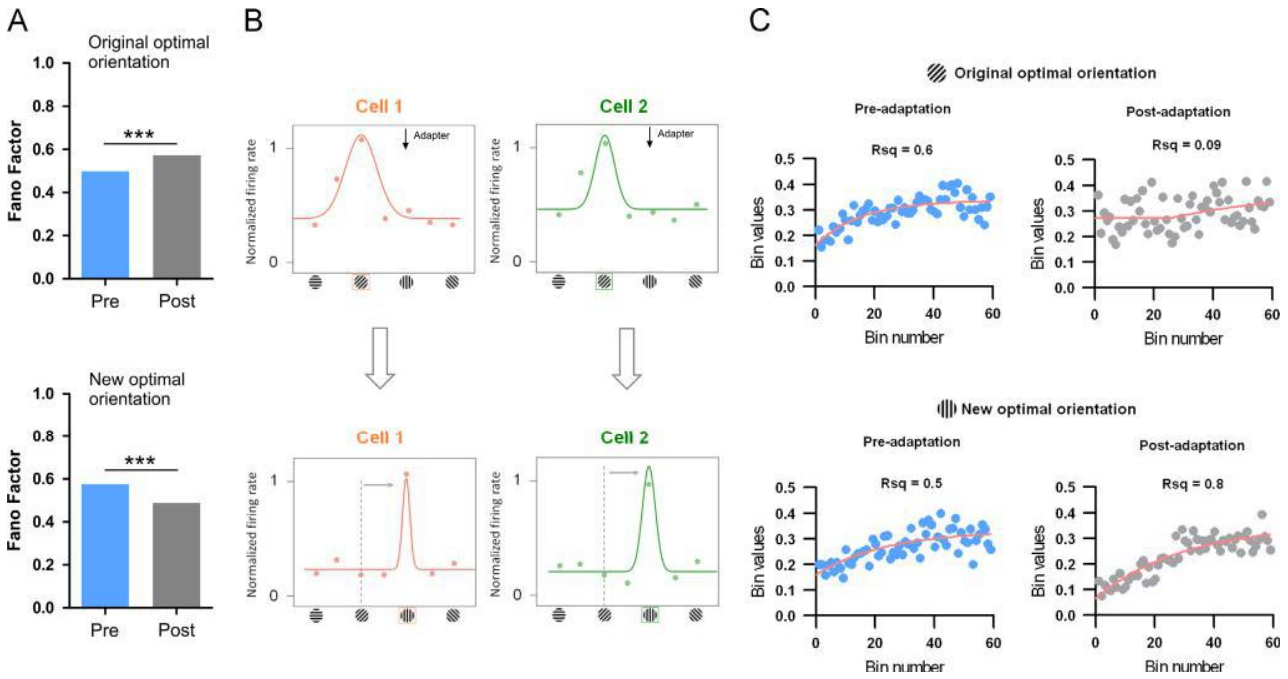

Fig. 4 – Variability of firing-responses. (A) Fano factors were calculated by dividing the variance (σ^2) by the mean firing rate (μ) of every neuron from each pair at original (left) and new optimal (right) orientations. This factor increased from 0.49 to 0.57 for the original preferred orientation (paired two-tailed *t*-test, $p<0.05$) and decreased from 0.58 to 0.48 for the new preferred orientation (paired two-tailed *t*-test, $p<0.05$). (B) Gaussian orientation tuning curves plotted from raw data of two neurons. (C) Probabilities values within each bin (7 ms) during the stimulus period of presentation (4.1 s) for the same neurons. We observed a large decorrelation for the original orientation ($R^2_{\text{pre-adaptation}}=0.6$, $R^2_{\text{post-adaptation}}=0.09$, top) whereas the correlation is stable for the new optimal orientation ($R^2_{\text{pre-adaptation}}=0.5$, $R^2_{\text{post-adaptation}}=0.8$, bottom).

orientation after adaptation. A typical example of response variability is shown in Fig. 4B and C; Gaussian tuning curves of two neurons are illustrated in Fig. 4B, the common preferred orientation for both cells is a 45° angle prior to adaptation. The new optimal orientation coincides with a vertically oriented angle (90°, which corresponds to the adapting orientation indicated by a black arrow in the plot) for both units post-adaptation. Probability values within each bin (7 ms) are plotted along the stimulus period of presentation (4.1 s) in Fig. 4C. These plots illustrate the large decorrelation for the original orientation ($R^2_{\text{pre-adaptation}}=0.6$, $R^2_{\text{post-adaptation}}=0.09$, top), whereas the correlation is conserved (stable) for the new optimal orientation ($R^2_{\text{pre-adaptation}}=0.5$, $R^2_{\text{post-adaptation}}=0.8$, bottom).

2.5. *Relationship with neuronal behavior*

Adapting neurons to a non-preferred stimulus leads to two major effects on the orientation tuning curves. Neurons acquire a new optimal orientation close to the adapter in an attractive shift. The second effect is a shift away from the adapter. Despite the fact that adaptation maintains the functional connectivity by rebalancing the excitation–inhibition and maintaining this ratio, we observed significant differences between attracted and retracted conditions (Fig. 5). Indeed, for the original optimal orientation (Fig. 5A), the new optimal orientation (Fig. 5B), and the adapting orientation (Fig. 5C), the CCG-magnitude was superior for attracted neurons (paired two-tailed *t*-test, $p<0.05$). This result may indicate a predictive effect of the neuronal behavior by estimating the strength of connectivity between neurons.

2.6. *Spike waveforms and tuning bandwidth*

Cortical processing involves a necessary interplay between different neuronal types. Two major classes of neurons are classically distinguished: regular-spiking and fast-spiking cells (Bachatene et al., 2012; Bortone et al., 2014). Fast-spiking neurons were identified by a narrow spike waveform (trough-to-peak time less than 0.5 ms, Fig. 6A) whereas regular-spiking neurons had a longer trough-to-peak interval (greater than 0.5 ms, Fig. 6A) (Bortone et al., 2014). An example of two neurons is shown in Fig. 6B indicating the respective spike wave-shapes of each neuron. The crosscorrelation computations were carried out between regular spiking neurons, between fast spiking neurons, and between both types of neurons. No significant difference was observed between cell types, that is, visual adaptation rebalances the functional connectivity strength among neurons by maintaining the global connectivity strength within neuronal networks made of regular-spiking and fast-spiking neurons (Fig. 6C).

Neurons in area 17 are remarkably selective for orientation (Hubel and Wiesel, 1959). The sharpness of orientation selectivity can be gauged by measuring the bandwidth at half height of the orientation Gaussian tuning curve (Moore et al., 2005;

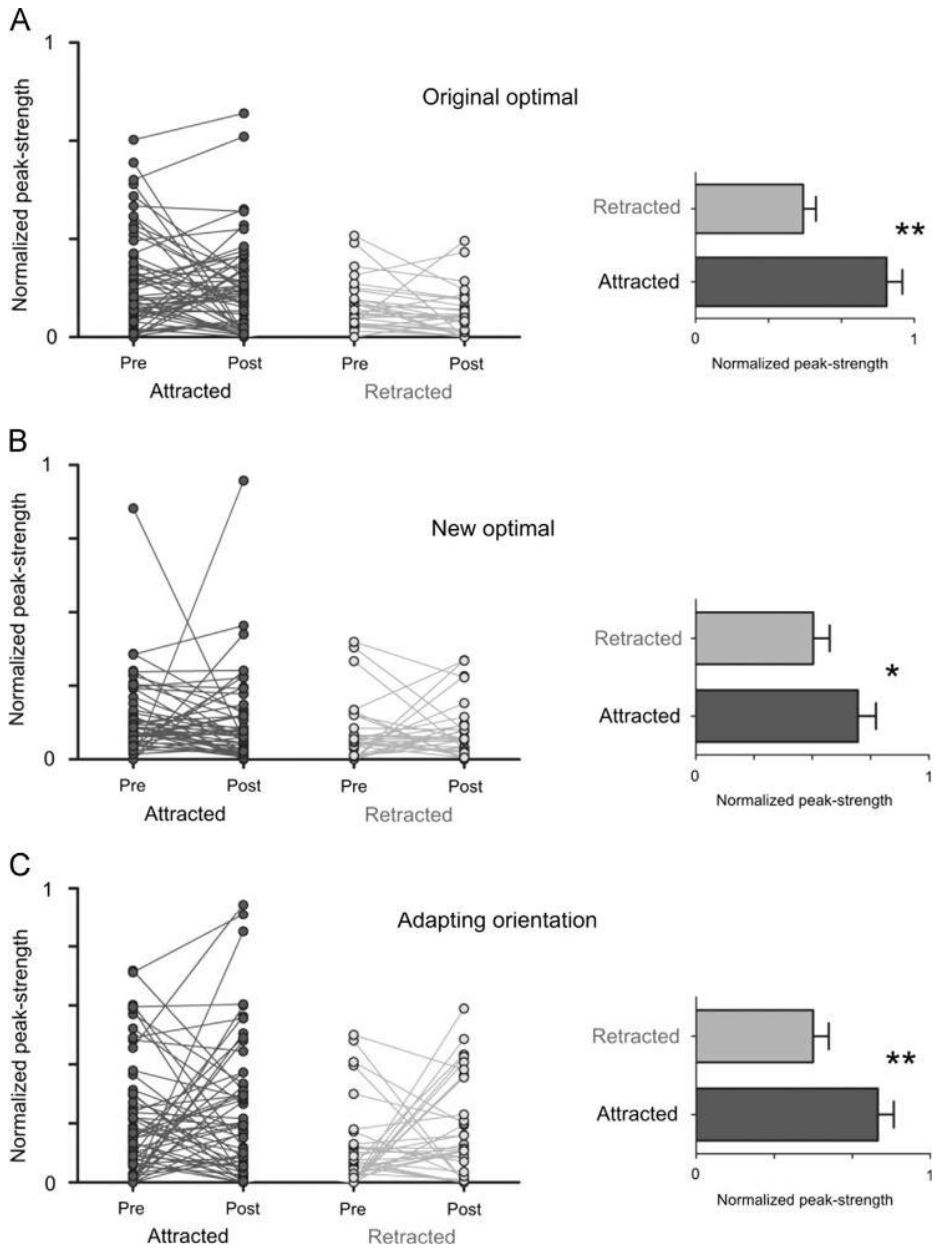

Fig. 5 – Relationship to neuronal behavior. (A) Differences of peak-strength pre- and post-adaptation between attracted and retracted neurons at the original optimal orientation. Histograms on the right side represent the average. The results demonstrate significant differences between attracted and retracted neurons (higher peak-strength for attracted neurons). (B and C) Similar to A for new optimal orientation and adapting orientation, respectively.

Ringach et al., 2002). In the next analyses, we compared the peak-strength-modulation in relation to the tuning bandwidth. Fig. 6D shows the changes in the latter before and after adaptation. Cell-classes are grouped depending on whether, following adaptation, the peak-strength decreased (red dots) or increased (green dots). Note that original and new optimal orientations are used as peak markers for tuning curves. Overall, the tuning bandwidth at half magnitude (FWHM: full width at half magnitude) is slightly diminished. Interestingly, the narrowest bandwidth belongs to a particular group of neurons exhibiting the largest augmentation in the peaks-strengths (bandwidth values: green dots, original preferred orientation, non-significant from 29.41 to 21.20, new optimal orientation significant from 26.47 to 17.33, non-parametric Mann–Whitney test, $p<0.05$, see Fig. 6D, right, green dots). Such a decrease strongly implies that adaptation induces the development of a jointly novel preferred orientation with a finer tuning curve. In addition, this specific group of cells exhibited the strongest enhancement of the peak-strength suggesting a closer time relationship between spike trains of involved cells.

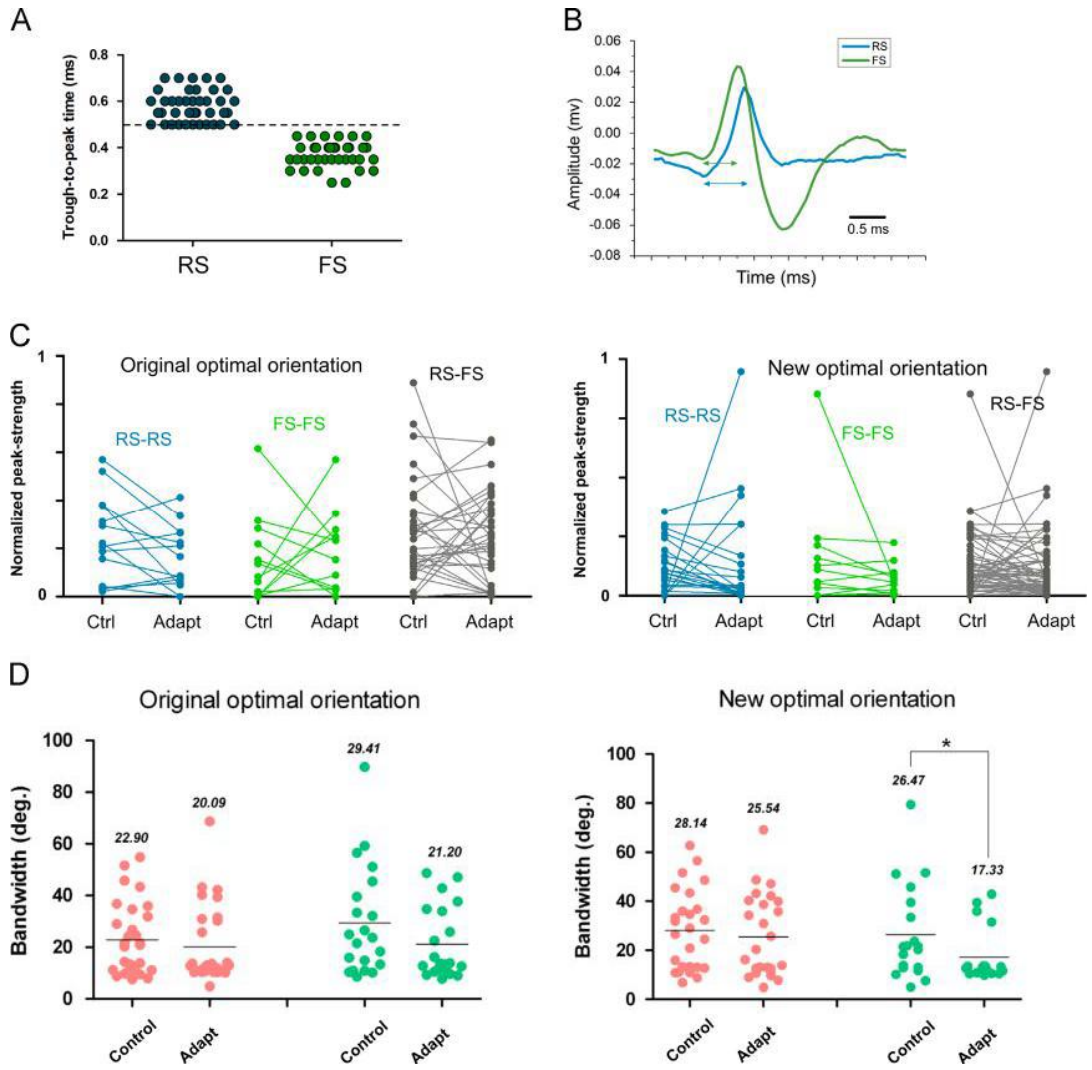

Fig. 6 – Spike wave-forms and tuning bandwidth. (A) Separation of spikes based on trough-to-peak time, regular spikes had a trough-to-peak time greater than 0.5 ms (blue dots) and fast spikes had a smaller value (inferior to 0.5 ms, green dots). (B) Example of two neurons with two different spike-shapes (blue unit: regular-spiking cell, green unit: fast-spiking cell). (C) Peak-strength modulation of all possible groups (RS–RS: blue plots, FS–FS: green plots, RS–FS: gray plots). No significant difference was observed between these spike-types. (D) Connection probability and tuning bandwidth. Tuning bandwidths measured (full width at half magnitude) for the original and the new optimal orientations. Neuronal pairs were classified in relation to the augmentation (green dots) or the diminution (red dots) of the peaks-strengths post-adaptation. The higher decrease of bandwidth is occurring for new optimal orientation (26.4° to 17.3°, Mann–Whitney test, 95% significance level, $p<0.05$). (For interpretation of the references to color in this figure legend, the reader is referred to the web version of this article.)

2.7. *Dynamics of a microcircuit: Restructuring the neuronal assembly by adaptation*

In previous sections, we demonstrated that the relationships between cells are modulated by adaptation. Indeed, some functional connections are strengthened while others are weakened, as revealed by CCG analyses. These modifications occur while both cells shift their preferred orientation to exhibit an almost identical new optimal orientation.

In the next section, we expand our analysis by constructing a peak-strength-matrix in a homogenous population, i.e., a group of simultaneously recorded neurons responding to the same original preferred stimulus and shifting their tuning curves after adaptation to the same new preferred orientation. Fig. 7 illustrates a typical example of a cluster of five cells recorded simultaneously and constituting a microcircuit with putative projections corresponding to the strength of connectivity as derived by crosscorrelation data. In Fig. 7A, orientation tuning curves (error bars indicate the standard error of the mean) and Gaussian fits of all cells are shown with their respective spike-waveforms (color codes apply to all the parts of this figure, where the black lines of spike waveforms specify the template window of spike sorting). All five cells responded similarly to the same optimal orientation (45° angle) before adaptation. After adaptation (orientation of the adapter equals 90°), a 90° oriented angle eliciting the highest discharge rate

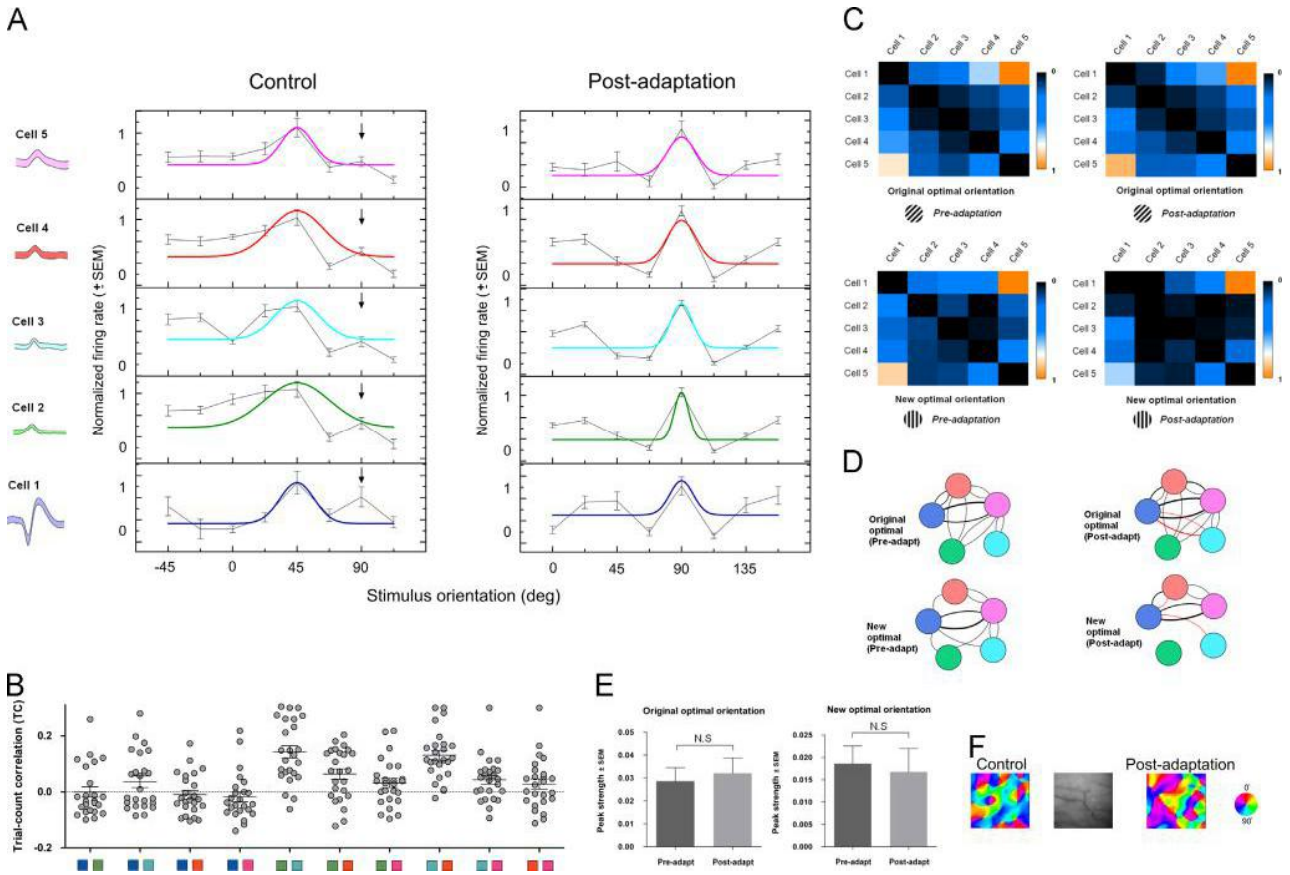

Fig. 7 – Cell-assembly computations. (A) Orientation tuning curves and Gaussian fits of five neurons (respective waveforms shown on the left) recorded simultaneously and responding preferentially to 45° grating before adaptation. All neurons shifted their original optimal orientation to reach 90° grating (corresponding to the adapter, downward black arrow in the plots), error bars in the tuning curves indicate standard error of the mean. (B) Cluster separation of all five neurons using the Trial-count correlation (*TC*), scatter plots are displayed for each neuronal pair of the entire group, mean *TC*'s values are indicated by the horizontal bars. (C) Connectivity matrices of peak-strengths for original optimal orientation at control condition (top left) and post-adaptation (top right), and for the new optimal orientation at control (bottom left) and post-adaptation (bottom right). Colored scale indicates the normalized peaks-strengths. (D) Putative connections plotted from the matrices indicating the strength of connectivity (thickness of projections); red lines indicate newly formed connections after adaptation. (E) Comparative histograms of averaged peaks-strengths for the entire matrices between both conditions for original optimal orientation (top) and new optimal orientation (bottom). (F) Example of an orientation-map generated using optical imaging. It shows the changes of the entire map post-adaptation. (For interpretation of the references to color in this figure legend, the reader is referred to the web version of this article.)

corresponds to the new acquired preferred orientation. Fig. 7B illustrates the trial-count correlation computations (*TC*) for all possible pairs among the cluster, the mean *TC* values are indicated by horizontal bars. The exceedingly weak values indicate that spike trains originate from distinct cells (see methods for details). The matrices comparing the peaks-strengths are displayed in Fig. 7C. Adaptation modified the structure of the matrices; some connections are strengthened while others are weakened, and few remain unchanged (for example, cell 1–cell 5 pair, see Fig. 7C; cell 1 projects on cell 5 almost with equal peak-strength pre- and post-adaptation, whereas cell 5 reverse projects with varying peak-strength before and after adaptation). The values of probabilities are indicated by the color scale on the right of each matrix. These matrices allowed plotting cell-assemblies for each case and each orientation of interest. Indeed, the linkage between similarly selective neurons within a group is modified as some connections emerge, while others are inhibited and some cells were functionally disconnected, for instance the green cell. Fig. 7D shows a microcircuit of the presented neurons putatively connected, red lines represent the newly formed projections after adaptation (in the displayed network, the red connection indicated the change of direction from cyan cell to blue cell) and the thickness of lines highlights the strength of projections between units.

Furthermore, for the same cell-assembly, we averaged the peaks-strengths of all connections for both orientations, in order to compare the global strength of functional connectivity between the same assembly prior to and post-adaptation (Fig. 7E). The mean values for the peaks-strengths of matrices

were not significant for both orientations (paired two-tailed *t*-test, $p=0.21$ and 0.39 for original optimal and new optimal orientations, respectively).

This analysis underscores the following: adapting cells to a non-preferred orientation induces two major effects; first there is a change of the preferred orientation and second there is a modification of the connectivity of the neuronal network and consequently its dynamics. Overall, connectivity strength is maintained and redistributed to different neurons for the broadcast of the learned feature. An example of changes of an orientation polar map is shown in Fig. 7F with a new orientation-configuration established post-visual adaptation (Cattan et al., 2014).

3. Discussion

We examined functional time-relationships between spike trains of primary visual cortical neurons by computing cross-correlation analyses for specific pairs of cells stimulated visually. Pairs of neurons were selected on the basis of their similar orientation-selectivity axis and post-adaptation behavior which lead to acquiring of same preferred orientation (for both neurons) after we imposed a visual "training" to non-preferred grating for 12 min. Crosscorrelogram data processing is a powerful in-situ tool for establishing the functional interactions between cells within sensory systems by indicating time-delay spiking activity between two neurons, where one neuron's spikes are set as reference to another neuron's spikes (target); therefore, it indicates putative functional projections between cells when it displays significant peaks within a short time-window reflecting direct functional relationships (Bartho et al., 2004; Denman and Contreras, 2013; Fujisawa et al., 2008; Konig et al., 1995; Perkel et al., 1967). In this report, we aimed to investigate the linkage dynamics between neuron-pairs prior and post-visual adaptation to a non-preferred oriented grating in order to reveal the extent of changes in neuronal connectivity after cells adopted new orientation-selectivity. Adaptation induced the following main results: the peaks-strengths that reflect cellular connectivity are disturbed and recalibrated after adaptation. Furthermore, the highest increase of the peak-strength belonged to cells that exhibited the sharpest bandwidth. In conclusion, there is an emergence of a novel sub-network after adaptation.

3.1. *Methodological considerations*

It was important to ask whether the disclosed functional connections were due to some physiological parameters such as anesthesia or attention. The brain state of an anesthetized animal might control the number of responsive neurons and the magnitude of the firing rate. Rhythmic oscillations which permit the synchronization of neuronal population may also be recorded in an anesthetized state (Poulet and Petersen, 2008). Moreover, the sequence of stimuli presentations is unrelated to the spontaneous oscillatory activity of cortical rhythms of the anesthetized animals (Xing et al., 2012). Furthermore, the stimuli were applied in a random fashion with inter-stimulus time intervals varying from 1 to 3 s. Since the recordings were done in the anesthetized cats, the response output of the cells for the presented stimulus cannot be attributed to the attention parameters (de Kock and Sakmann, 2009).

Time-relationships between action potentials of neurons in the circuits may go undetected due to low firing rates of neurons; however, this does not necessarily mean that temporal locking of neurons cannot be elicited with low firing rates of neurons. It has been demonstrated that the firing rates and peaks in CCG's are unrelated (Duret et al., 2006; Rolls and Treves, 2011; Shumikhina et al., 2004).

In addition to the classical cells' isolation using spike waveshapes, principal component analyses, and autocorrelation, it was important to ascertain that the isolated cells emerged from distinct templates; therefore we performed trial-count-correlation (*TC*) between every possible pair of neurons in order to compare the firing pattern between cells. To this aim, we used a 1 ms resolution. All correlations had a value inferior to 0.25 which ascertains that spike-trains emerged from different cells. Furthermore, we carried out these count correlations on a time-window of 4.1 s across all trials that corresponded to the presentation of the stimuli. Given that we divided the 4.1 s epoch into 1 ms time-bins (1 ms resolution), the probability of synchronous spikes in the same template within this short time-window is exceedingly low.

3.2. *Crosscorrelation and functional connections*

Crosscorrelation computations have been used in neurophysiological analyses in order to reveal functional linkages between spike trains of two neurons recorded simultaneously (Perkel et al., 1967). A synaptic connection can be attributed to correlation only under certain circumstances (Reid, 2012), however, a time-relationship between the firing activity two neurons may be considered as a clue to temporal projections between two cells as the temporal delay in the crosscorrelograms may suggest modifications in wiring. Temporal connections can be demonstrated by an increase in the firing probability of the postsynaptic neuron (Bharmauria et al., 2014; Reid, 2012).

A typical CCG is generated with the aim of disclosing the significance level and strength of connectivity between two cells within a specific time-frame. Depending on the peak-position in the CCG's, the analyses revealed the spike timing of both neurons in relation to each other. However, it is worth noting that a typical CCG may lead to biased significant peaks due to the co-stimulation of both neurons at each trial of the stimulus cycle. In order to circumvent and lessen this potential bias, we employed the shuffling minus subtraction algorithm based on neuron firing rates, and subtracted it from the raw CCG's which eliminated evoked firing (Dong et al., 2008).

We examined neuronal connectivity between cell-pairs within a time-window of ± 5 ms primarily to unveil putative direct synaptic connections between cells. It has been demonstrated in the macaque MT area that neuronal crosscorrelation between pairs of cells is mostly short-termed within a time-window of 10–100 ms (Bair et al., 2001). Though in several investigations various time-windows have been taken into consideration ranging from 3 ms to 10 ms (Bartho et al., 2004) to reveal the functional connections between the involved neurons, nonetheless a time window of ± 5 ms is most frequently used and is reasonably short.

In addition to disclosing functional projections between neurons, the crosscorrelation technique allows for the evaluation of the strength of neuronal connectivity (through peak-strength) as it is significant in understanding variations of cell-assemblies in response to experience (Bock et al., 2011). We investigated the changing of probability-indices prior to and after visual adaptation in order to uncover the modulation mechanisms of neuronal relationships (see next section for details). Indeed, this adaptation process leads to modifications of neural spiking activity attributed to push-pull mechanisms (Bachatene et al., 2012; Bachatene et al., 2013; Ghisovan et al., 2009; Kohn and Movshon, 2004). It has been demonstrated previously that long adaptation of neurons to a non-preferred stimulus, which is orientation in our experiments, for the most part leads to a decrease in firing activity for the original optimal orientation, and in contrast, a firing increase for the new preferred orientation (Bachatene et al., 2012, 2013; Ghisovan et al., 2009). It was relevant to explore whether the probability modulation of neuronal connectivity is related to the firing rates of neurons, as previously shown. However, we found no significant correlation between the peak-strengths and the firing rates in our results, as previously described (Duret et al., 2006; Ghisovan et al., 2008; Rolls and Treves, 2011). In addition, results indicated no relationship between spike waveforms which are attributed to specific putative cellular types, and peak strength fluctuations post-adaptation.

3.3. *Neuronal connectivity and orientation-selectivity*

Neurons within the primary visual cortex are "orientation-detectors", and respond maximally to a properly oriented stimulus presented in their receptive field (Hubel and Wiesel, 1959). Several studies have demonstrated the ability of V1 neurons to adjust their stimulus-selectivity in order to restructure the primary visual cortex as an "adapted cortex" to the imposed visual environment by a persistent adaptation to a specific stimulus. For instance, such modifications have been reported for orientation (Bachatene et al., 2012, 2013; Dragoi et al., 2000; Ghisovan et al., 2009; Kohn and Movshon, 2004), spatial frequency (Marshansky et al., 2011), direction of motion (Kohn and Movshon, 2004) and speed (Movshon, 1975). By changing their preferred features, neurons acquire new optimal properties for a short or long period of time depending on the visual training duration (Bachatene et al., 2013; Ghisovan et al., 2009; Patterson et al., 2013). In V1, cells are scattered within cortical domains and connected to each other laterally and vertically. Horizontal connections are characterized as long range connections between neurons preferring similar stimulus features (Das and Gilbert, 1995; Sompolinsky et al., 1990) which are functionally connected to each other at large distances (Hata et al., 1991; Ts'o et al., 1986). Vertical connections are described as inputs to layers II and III from layer IV of the visual cortex (Stratford et al., 1996; Yoshimura et al., 2000) which receives its inputs from LGN (Alonso et al., 1996). From layers II and III, the connections descend to layers V and VI (Stratford et al., 1996).

As suggested by crosscorrelogram analysis, neuronal connectivity has been reported to be high between cells with similar preferred parameters due in part to specific connections between cortical domains having similar tuning properties (Alloway and Roy, 2002; Alonso et al., 1996; Bartho et al., 2004; Csicsvari et al., 1998; Yoshimura et al., 2005). Indeed the correlation between neurons sharing reciprocal tuning properties is well established (Kohn and Smith, 2005; Zohary et al., 1994). Neuronal connections within the cortex are very specific, mostly depending on the properties of the responses of neurons (Alonso, 2002). For instance, in macaque visual cortex, it has been shown that correlation varies with stimulus condition and this variation is stronger between neurons sharing similar direction tuning curves (Bair et al., 2001). In mouse primary visual cortex, it has been reported that significant pair-wise synchrony is related to orientation preference between neurons (Denman and Contreras, 2013). Neuronal connectivity can also be related to specific stimulus preference; it has been demonstrated that in mouse visual cortex, the similarity of neuronal activity to a specific feature of the stimulus affects the connection-probabilities; for example, neurons sharing similar selectivity for oriented stimuli exhibit more connectedness with each other than neurons having orthogonal orientation selectivity (Ko et al., 2011).

These findings provide evidence that stimuli features influence the temporal pattern of neuronal activity (Gray et al., 1990). Nevertheless, following plastic modifications, connectivity patterns among neuronal pairs in V1 have yet to be explored. In the present paper, we sought to examine how the peaks-strengths calculated from crosscorrelation analyses between pair-wise neurons sharing stimulus-feature selectivity are modulated following a long duration visual "training."

Following the critical period, neurons programmed to connect to distinctive neurons that share homogenous orientation-selectivity start responding to a new acquired orientation after visual adaptation, and therefore switch on to connect a different neuronal population to participate in a different sub-network of cells. Indeed, some authors have demonstrated in mouse visual cortex a reorganization of the connectivity configuration. This is related to a higher proportion of links between neurons with similar visual responses, while connections were eliminated between visually unresponsive units, yet the overall connectedness remained unchanged (Ko et al., 2013).

Although peaks-strengths on average were not significantly different, individual pairs appeared to increase or decrease their respective peaks, suggesting that the adaptation process redeploys the strength of projections between neurons to restructure the entire linkage-dynamic of the neuronal population in response to the changing stimuli environment. For instance, the forceful presentation of a particular stimulus (a different orientation in our experiments) results in the disappearance of some relationships and the appearance of new projections. Understanding the temporal relations between neurons within sub-networks could help us to decipher how visual processing is altered under specific changes of environmental conditions and how the plastic capacity of neuronal networks lead to the acquisition of new features. Although our stimulation conditions are artificial (stimulus exposure), it still mimics training or forcing cells to respond to a particular trigger feature which in turn, may serve as basis for learning process.

An alternative possibility may be hypothesized. Neurons are connected with excitatory (*E*) and inhibitory (*I*) fibers and their spiking output is the net outcome of these antagonistic influences. Thus adaptation may strengthen and weaken excitatory and inhibitory connections, respectively, in order to unlock cellular time-relationships in involved cortical areas whereby a new *E*–*I* equilibrium might be considered as a possible scenario for the neuronal variability dynamic after visual adaptation. The fluctuations of neuronal alterability due to adaptation effects may rebalance the *E*–*I* ratio and contribute to the stability of the total inter-neuronal variability (Kasamatsu et al., 2001). It has been shown in layers 2/3 of the mouse visual cortex that *E*–*I* ratios are equalized across pyramidal cells (Xue et al., 2014). Our results are in concordance with the equalization of excitation–inhibition ratios after adaptation (Fig. 7D and E).

This is in line with recent findings which assign an important contribution of adaptation to neuronal homeostasis within a population of cells sharing neuronal response uniformity, as well as visual feature selectivity (Benucci et al., 2013). We reported that adaptation restructures the neural code following plasticity by maintaining the connectivity strength within the cellular network and redistributing this linkage to different neurons within the assembly (see Fig. 7D and E). In models of cross-orientation, feature-selectivity is induced by inhibitory connections between cells with different orientation preferences (Alonso, 2002). Furthermore, it has been shown that in relation to differences in orientation-selectivity between two neurons, excitatory, inhibitory and common input correlations occur mostly in neuronal pairs with a difference of orientation preference inferior to 45° (Hata et al., 1991). Moreover, adaptation may provide a 'window of opportunity' for recipient neurons to modify excitatory/inhibitory balance in order to reorganize the spiking cortical activity (Stanley, 2013). Indeed, complex feedforward-feedback mechanisms emerge within the primary visual cortex in order to reorganize the signal processing following plasticity (Fahle, 2004).

Therefore, we postulate that orientation-selective neuronal pairs modify the strength of connections following adaptation in order to recalibrate the neural code.

Such rapid changes may not be accounted by structural modifications, there are most likely due to modification of equilibrium between excitation and inhibition influences to a recorded cell which allows silent synapses to become effective. For instance, in mouse visual cortex, it has been demonstrated that a single dendritic branch receive synaptic drives from a large spectrum of orientations (Jia et al., 2010).

Excitatory and inhibitory cells coordinate time-related firing activity to maintain the neuronal population output during visual information processing.

4. Conclusion

Visual adaptation of neurons to non-optimal stimuli suggests the adaptability of neuronal code to visual stimuli. In the primary visual cortex, neurons respond in coordination with neighboring cells to the trigger features, and encode stimuli properties by constituting cell assemblies (Kampa et al., 2011; Lee and Reid, 2011; Wallace and Kerr, 2010) wherein cells are anatomically connected by forming synaptic contacts or by interacting through synchronous time-relationships. To reveal how this local circuitry of different neurons in the visual cortex is set up and modulated in response to different visual stimulation conditions is of prime importance to understanding the mechanisms of information processing.

5. Experimental procedures

5.1. *Ethical approval*

Animal surgery procedures and electrophysiological recordings followed the guidelines of the Canadian Council on Animal Care and were approved by the Institutional Animal Care and Use Committee of the University of Montreal. Animals were supplied by the Division of Animal Resources of the University of Montreal. The experiments were conducted in accordance with the Guide for Care and Use of Laboratory Animals of the National Institutes of Health (USA).

5.2. *Animal surgery*

Electrophysiological recordings were performed using multi-electrodes within V1 area of adult domestic cats (*Felis catus*). Eleven adult cats (2.5–3.5 kg, age 12–24 months) of either sex, sedated with acepromazine maleate (Atravet, Wyeth-Ayerst, Guelph, ON, Canada; 1 mg kg^{-1}, intramuscular) and atropine sulfate (ATRO-SA, Rafter, Calgary, AB, Canada; 0.04 mg kg^{-1}, intramuscular), were anesthetized with ketamine hydrochloride (Rogarsetic, Pfizer, Kirkland, QC, Canada; 25 mg kg^{-1}, intramuscular) maintained with 0.3% isoflurane (AErrane, Baxter, Toronto, ON, Canada). Lidocaine hydrochloride (Xylocaine, AstraZeneca, Missis-sauga, ON, Canada; 2%) was injected subcutaneously as a local anesthetic during surgery. A tracheotomy was performed for artificial ventilation, and one forelimb vein was cannulated. Animals were then placed in a stereotaxic apparatus. Xylocaine gel (Astra Pharma, Mississauga, ON, Canada; 5%) was applied on the pressure points. For the remaining preparations and recording, paralysis was induced with 40 mg and maintained with 10 mg kg^{-1} h^{-1} gallamine triethiodide (Flaxedil, Sigma Chemical, St. Louis, MO, USA; intravenous) administered in 5% dextrose lactated Ringer's nutritive solution. General anesthesia was maintained by artificial ventilation with a mixture of N_2O/O_2 (70:30) supplemented with 0.5% isoflurane (AErrane, Baxter, Toronto, ON, Canada) for the duration of the experiment. Proper depth of anesthesia was ensured throughout the experiment by monitoring the EEG, the electrocardiogram and expired CO_2. In addition the heart rate remained unmodified after skin stimulation. The end-tidal CO_2 partial pressure was kept constant between 25 and 30 mmHg. A heated pad was used to maintain a body temperature of 37.5 °C. Tribrissen (Schering-Plough, Pointe-Claire, QC, Canada; 30 mg kg^{-1} per day, subcutaneous) and Duplocillin (Intervet, Withby, ON, Canada; 0.1 ml kg^{-1}, intramuscular) were administered to the animals to prevent bacterial infection. The pupils were dilated with atropine sulfate (Isopto-Atropine, Alcon, Mississauga, ON, Canada; 1%)

and the nictitating membranes were retracted with phenylephrine hydrochloride (Mydfrin, Alcon, Mississauga, ON, Canada; 2.5%). The loci of the area centrales were inferred from the positions of the blind spots, which were ophthalmoscopically focused and back projected onto a translucent screen. In order to verify the stability of the eye this procedure was repeated at the end of tests. Plano contact lenses with artificial pupils (5 mm diameter) were placed on the cat's eyes to prevent the cornea from drying (University of Montréal, PQ, Canada).

At the end of each experiment, euthanasia was achieved with a lethal dose of pentobarbital sodium (Somnotol, MTC Pharmaceuticals, Cambridge, ON, Canada; 100 mg kg^{-1}) by intravenous injection.

5.3. *Electrophysiology*

Multi-unit activity in the primary visual cortex was carried out with tungsten microelectrode (Frederick Haer & Co, Bowdoinham, ME, USA; 2–10 MΩ at 1 kHz). Each set of electrodes, consisting of a four microelectrode in linear array (inter-electrode spacing of 400 μm) enclosed in stainless steel tubing, was controlled by a separate micromanipulator. The signal from the microelectrodes was amplified, band-pass filtered (300 Hz–3 kHz), digitized and recorded with a 0.05 ms temporal resolution (Spike2, CED, Cambridge, England). We recorded at an average of 400–500 μm cortical depth from two recording sites (Average of three neurons recorded per electrode per session). Action potentials were sorted out using a window discriminator for further off-line analyses. Multiunit signals from one electrode included well-isolated single units. The spike sorting method was based on cluster classification in reduced space (Spike2, CED). The stability of each cell's activity across conditions was verified qualitatively by visual control of the clusters disposition and of the waveforms shape. Autocorrelograms and principal component analysis were systematically performed to insure proper single cell capture (refractory period for autocorrelograms). Spike-count correlation was used to ascertain that spikes emerged from different neurons. 85% of neurons were included in the data analyses.

5.4. *Visual stimulation*

Stimulation was monocular (dominant eye, the opposite eye was shut). After clearly detectable activity was obtained, the multiunit receptive fields (RF) were mapped as the minimum response fields (Barlow et al., 1967) by using a hand-held ophthalmoscope. RF edges were determined by moving a light bar from the periphery toward the center until a response was elicited. Eye-screen distance was 57 cm. These preliminary tests revealed qualitative properties such as dimensions, velocity preference, orientation and directional selectivity. Visual stimuli were generated with a VSG 2/5 graphic board (Cambridge Research Systems, Rochester, England) and displayed on a 21-in. monitor (Sony GDM-F520 Trinitron, Tokyo, Japan) placed 57 cm from the cat's eyes, with 1024 × 768 pixel, running at 100 Hz frame refresh. Stimuli were drifting sine-wave grating patches (~2° to 5°) covering the excitatory RF (Maffei and Fiorentini, 1973). Patches characteristics were set to evoke optimal responses: contrast at 80%, mean luminance at 40 cd m^{-2}, optimal spatial and temporal frequencies set within the 0.1–0.5 cycles/deg. and 1.0–2.0 Hz range, respectively. The blank screen was uniformly gray (~35 cd m^{-2}). In all cases the above parameters were chosen with the aim of evoking the maximal discharges. V1 neurons are known to respond well to sine wave drifting gratings (Bardy et al., 2006). After manual RF characterization, nine oriented stimuli centered on the preferred orientation were selected and used for the rest of the experiment. With a 22.5° interval between orientations, tuning curves covered 180°. Test orientations were applied in random order. Each oriented stimulus was presented in blocks of 25 trials lasting 4.1 s each, with a random inter-trial interval (1.0–3.0 s) during which no stimuli were presented. Thus, a recording session lasted for 25–30 min. Peri-stimulus time histograms were recorded. Once control orientation tuning curves were characterized, an adapting non-preferred stimulus was presented continuously for 12 min. The adapting stimulus was a drifting grating whose orientation was randomly selected in the range 22.5 to 67.5° off of the neuron's preferred orientation (Fig. 8A). All other stimulus parameters were kept constant, at control values, throughout the recordings. During this adaptation period no recordings were performed. Immediately after adaptation, orientation tuning curves was measured starting with the adapting and control preferred orientations to prevent an unlikely premature recovery, as these two orientations were the center of interest, while the remaining orientations were recorded in random order.

5.5. *Cells' isolation*

Given that the multi-unit activity was recorded concurrently from same tips using multi-electrodes, it was essential to ascertain that cells were well isolated, because the same unit may exhibit sufficiently different waveforms (for instance magnitude in relation to distance between recording tip), and thus belong to different clusters in principal component analysis. Cell-separation was based on spike-waveforms, cluster-isolation using first principal components analyses, autocorrelograms and trial-count correlation (*TC*). Cluster analysis was performed using Spike2 (CED, Cambridge, England) in a 3-dimensional plot. The isolation distance was calculated using the Mahalanobis distance; it defines boundaries of constant probability around the multi-dimensional center of the distribution. This estimation allows the separation of a cluster from the nearest cluster. All clusters within Mahalanobis distance of 2.5 were considered for analysis (Bharmauria et al., 2014).

Trial-count correlation (*TC*) denotes the trial by trial Pearson correlation-coefficient between simultaneously recorded firing of two neurons in response to the presentation of the identical stimulus. In response to the same grating, the same unit fires identically regardless of spike amplitude. In order to eliminate such occurrences, we correlated neural activities of each cell-pair for every applied trial (25 trials, same stimulus, duration 4.1 s). Given that optimal orientations eliciting maximal firing rates were chosen for this computation as well as a relatively long time-window analysis (4.1 s), we would have expected a high value for correlation if it had been the same unit, because such a time-window analysis is sufficiently large

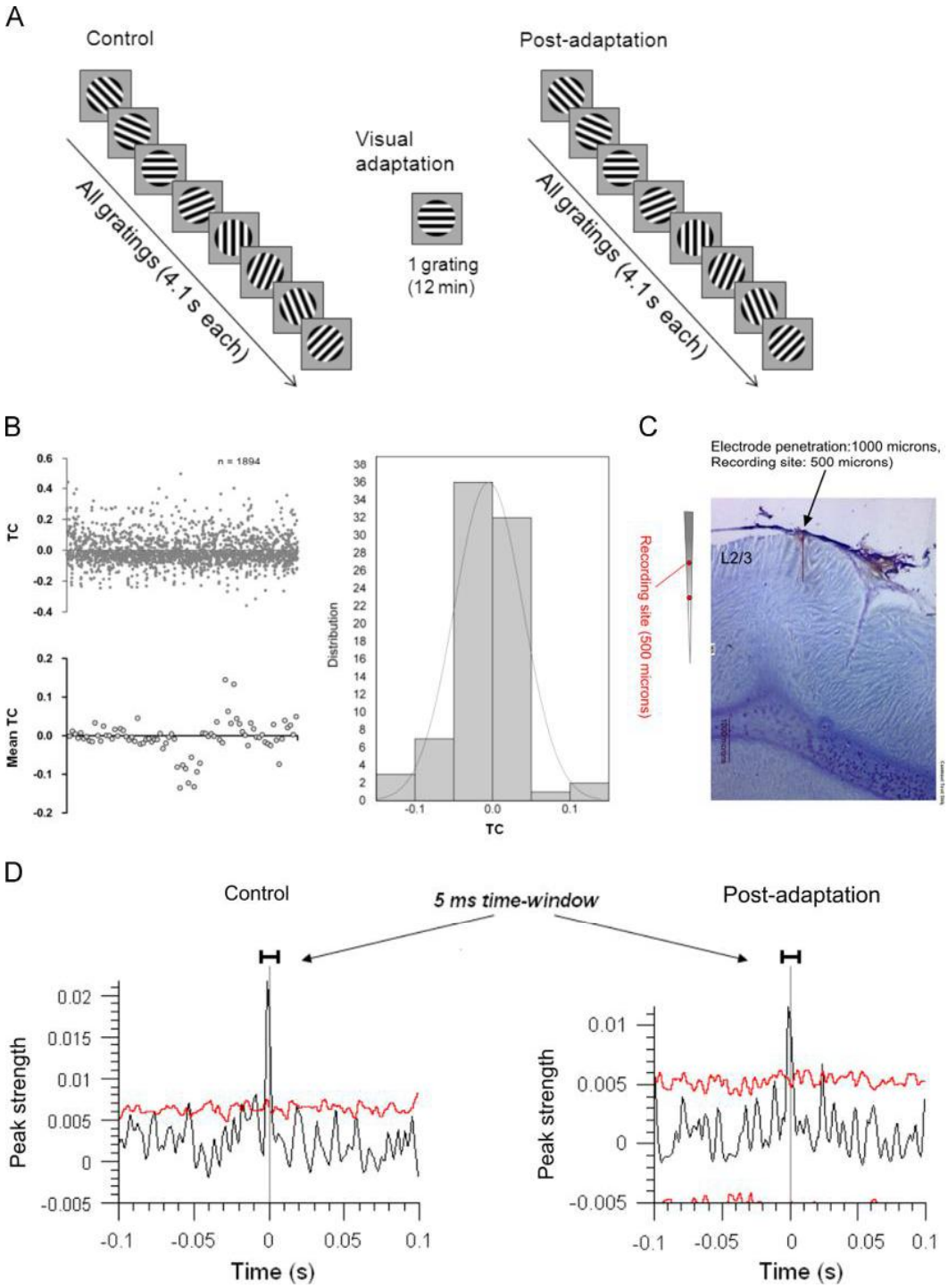

Fig. 8 – Visual stimulation, cell separation and crosscorrelation. (A) Time course stimulus. Left: control condition, 8 orientations presented in random order within the receptive fields of recorded neurons in 25 trials (4.1 s each trial, 1–3 s interval time). Middle: one grating (non-preferred orientation in control) is presented continuously (12 min). Right: post-adaptation condition, all orientations are projected as in the control step. (B) Trial-count correlation (*TC*). Upper left side: *TC* values for all trials ($n=1894$) accumulated over all selected neuron-pairs. Downer left side: averaged *TC* values for each cell pair ($TC=-0.005$). Right side: histogram-distribution of the averaged *TC* for each neuronal pair, gray curve represents the normal distribution curve. (C) Histological brain slice showing the electrode penetration and the recording site. (D) Examples of crosscorrelogram analyses indicating the ± 5 ms time range (time-delay of putative direct synaptic connections between cells). Red line indicates the 95% statistical threshold for the bin's significance; *Y*-axis shows the peak-strength computed from the counts/bin. (For interpretation of the references to color in this figure legend, the reader is referred to the web version of this article.)

to capture the full strength of correlation (Bair et al., 2001; Kohn and Smith, 2005; Reich et al., 2001). Indeed correlations would be underestimated if the counting window is too short (Cohen and Kohn, 2011). In spite of such conditions, the found correlations were exceedingly low (average $TC = -0.005$, see Fig. 8B). Pairs exhibiting correlations superior to 0.25 were eliminated from further analyses (as a general rule). This very weak correlation in spike response patterns (close to zero) indicates that the spikes arise from different units, hence the cells fire in an independent fashion. Fig. 8B illustrates the trial-count correlation analysis performed for the cells and recorded from the same electrode tip within each group.

Fig. 8B depicts the TC values for all trials ($n = 1894$) accumulated over all selected neuron-pairs (the average TC value for each cell pair equals to -0.005). The distribution of the average TC for each neuronal pair is shown in the figure (gray curve represents the normal distribution curve). The correlation values are clustered around zero and never exceed 0.25, which is in agreement with earlier published data (Cohen and Kohn, 2011; Ecker et al., 2010; Maruyama and Ito, 2013). This ascertains that firing patterns of the two selected neurons are different and ensures the cells' isolation.

Autocorrelograms preclude contamination by spikes of other units. Anesthesia and animal paralysis reduce the possibility of similar modulations of firing patterns in cells of same clusters due to rapid eye motion or attention (de Kock and Sakmann, 2009).

5.6. Data analysis and statistical computations

Once single cells were sorted out off-line from multi-unit spike trains accumulated during data acquisition, orientation tuning curves were constructed from raw data. Because orientation tuning is best described by Gaussian-like functions, we fitted our raw data with the von Mises function (Swindale, 1998). This allowed us to determine with precision the preferred orientation of neurons and then measure shifts in orientation preference. The von Mises function is defined as:

$$M(\theta) = A \times e^{b[\cos(\theta - c)]} + d$$

where A is the value of the function at the preferred orientation, c, and b is a width parameter. An additional parameter, d, represents the spontaneous firing rate of the cell (Kohn and Movshon, 2004; Swindale, 1998). The above calculations are necessary because tuning curves derived from raw data may be imperfect in determining the preferred orientation since the interval between the stimulus orientations is relatively large, 22.5°. In the cat, over 90% of V1 neurons are well tuned to stimulus orientation (Bishop and Henry, 1972). It was, however, necessary to ensure that cells in our sample were properly tuned for orientation. We measured an orientation selectivity index (OSI) by dividing the firing rate at orthogonal orientations by the firing rate for the preferred orientation, and subtracting the result from one (Liao et al., 2004; Ramoa et al., 2001). The closer the OSI is to one, the stronger the orientation selectivity. Adaptation induced shifts were measured as the distance between peak positions of the fitted tuning curves before and after conditioning. To assess the statistical significance of tuning shifts, curve fits were generated separately for each of the 25 trials, and the mean difference was tested by a paired t-test. Shifts in preferred orientation larger than 5° were statistically significant (paired sample two-tailed t-test, $p < 0.05$). Tuning bandwidths were calculated based on the full width at half magnitude of the Gaussian tuning curves. Statistical analyses were performed with Graphpad Prism (GraphPad Software Inc., La Jolla, California, USA). Student's t-tests were computed to compare the peaks-strengths between control and post-adaptation conditions, and to compare bandwidths between different classes. Ninety-five percent confidence-interval was used. Gaussian curves were fitted using the following equation:

$$y = y0 + \left(A \div \left(w \times \sqrt{\left(\frac{\pi}{2}\right)}\right)\right) \times e^{(-2\times((x-xc)/w)^2)}$$

where $y0$ is the offset, xc is the center, w is the width and A represents the area.

Non-linear regression analyses were computed using this equation:

$$y = y0 + A1 \times (1 - e^{(-x/t1)}) + A2 \times (1 - e^{(-x/t2)})$$

where $y0$ is the offset, $A1$ and $A2$ are the amplitudes, $t1$ and $t2$ are the widths.

5.7. Crosscorrelograms, shift predictor and confidence limits

We generated CCG's between simultaneously recorded spike trains of cell-pairs at specific orientations, i.e., the original optimal orientation and the new optimal orientation of each pair of neurons. Cell-pairs were selected based on their similarity of spiking discharge for these two preferred orientations using an orientation range of ±22.5°.

CCG's were performed in order to compare the spike distribution of each neuron of the pair within a time-frame; one neuron is set as reference and the second as target; this allows us to show the firing of the target neuron at a specific time-spread in relation to the firing of the reference neuron.

Time axis is divided into bins. The first bin is defined as: XMin, XMin+Bin. The next bin is XMin+Bin, XMin+Bin × 2, etc. We calculated the distances from each spike to all spikes of the spike train as follows:

$$d[i] = ts[i] - ref[k]$$

where $ts[i]$ represents the spike train, and $ref[k]$ is each timestamp.

Bin counts were then divided by the number of reference events to normalize the counts per bin into probabilities. Fig. 8D illustrates the parameters of CCG's; the red line represents the 95% statistical threshold for the significance of the bins. Each bin-width was set at 1 ms, Y-axis corresponds to the peak-strength calculated from the counts/bin as follows:

$$P = F \times b$$

where F is the neuron frequency and b represents the bin size of the calculated firing of the neuron (Abeles, 1982).

The neuron frequency F was calculated as follows:

$$F = \frac{N}{T}$$

where T represents the total time interval and N the number of spikes within this interval.

The 95% confidence limit was calculated assuming that the expected bin count (C) has a Poisson distribution:

$C = P \times Nref$

where *Nref* is the number of reference events.

The 95% confidence limit is calculated as follows:

Low Conf. $= x$ such that Prob $(S < x) = 0.005$

High Conf. $= y$ such that Prob $(S > y) = 0.005$

where S represents a random variable which has a Poisson distribution with parameter C.

The bins which fit into the ± 1 ms around the center were classified as synchrony events (putative common afferent input to both neurons). Raw CCG's were corrected by subtracting a shift-predictor algorithm in order to eliminate the putative significant peaks due to the simultaneous stimulation of both cells during each trial. We used linear regression analysis with 95% confidence interval for the entire population of the recorded neuron-pairs to determine the modulation of the peak-strength for the two major specific preferred stimuli (original and newly acquired orientations).

Acknowledgments

This work was supported by grants to S.M.

The Natural Sciences and Engineering Research Council of Canada (Grant no. 6943-2010RGPIN). Fonds québécois de la recherche sur la nature et les technologies.

REFERENCES

Abeles, M., 1982. Quantification, smoothing, and confidence limits for single-units' histograms. J. Neurosci. Methods 5, 317–325.

Alloway, K.D., Roy, S.A., 2002. Conditional cross-correlation analysis of thalamocortical neurotransmission. Behav. Brain Res. 135, 191–196.

Alonso, J.M., Usrey, W.M., Reid, R.C., 1996. Precisely correlated firing in cells of the lateral geniculate nucleus. Nature 383, 815–819.

Alonso, J.M., 2002. Neural connections and receptive field properties in the primary visual cortex. Neuroscientist 8, 443–456.

Bachatene, L., Bharmauria, V., Rouat, J., Molotchnikoff, S., 2012. Adaptation-induced plasticity and spike waveforms in cat visual cortex. Neuroreport 23, 88–92.

Bachatene, L., Bharmauria, V., Cattan, S., Molotchnikoff, S., 2013. Fluoxetine and serotonin facilitate attractive-adaptation-induced orientation plasticity in adult cat visual cortex. Eur. J. Neurosci. 38, 2065–2077.

Bair, W., Zohary, E., Newsome, W.T., 2001. Correlated firing in macaque visual area MT: time scales and relationship to behavior. J. Neurosci. 21, 1676–1697.

Bardy, C., Huang, J.Y., Wang, C., FitzGibbon, T., Dreher, B., 2006. 'Simplification' of responses of complex cells in cat striate cortex: suppressive surrounds and 'feedback' inactivation. J. Physiol. 574, 731–750.

Barlow, H.B., Blakemore, C., Pettigrew, J.D., 1967. The neural mechanism of binocular depth discrimination. J. Physiol. 193, 327–342.

Bartho, P., Hirase, H., Monconduit, L., Zugaro, M., Harris, K.D., Buzsaki, G., 2004. Characterization of neocortical principal cells and interneurons by network interactions and extracellular features. J. Neurophysiol. 92, 600–608.

Benucci, A., Saleem, A.B., Carandini, M., 2013. Adaptation maintains population homeostasis in primary visual cortex. Nat. Neurosci. 16, 724–729.

Bharmauria, V., Bachatene, L., Cattan, S., Rouat, J., Molotchnikoff, S., 2014. Synergistic activity between primary visual neurons. Neuroscience 268, 255–264.

Bishop, P.O., Henry, G.H., 1972. Striate neurons: receptive field concepts. Invest. Ophthalmol. 11, 346–354.

Bock, D.D., Lee, W.C., Kerlin, A.M., Andermann, M.L., Hood, G., Wetzel, A.W., Yurgenson, S., Soucy, E.R., Kim, H.S., Reid, R.C., 2011. Network anatomy and in vivo physiology of visual cortical neurons. Nature 471, 177–182.

Bortone, D.S., Olsen, S.R., Scanziani, M., 2014. Translaminar inhibitory cells recruited by layer 6 corticothalamic neurons suppress visual cortex. Neuron 82, 474–485.

Cattan, S., Bachatene, L., Bharmauria, V., Jeyabalaratnam, J., Milleret, C., Molotchnikoff, S., 2014. Comparative analysis of orientation maps in areas 17 and 18 of the cat primary visual cortex following adaptation. Eur. J. Neurosci. 40, 2554–2563.

Cohen, M.R., Kohn, A., 2011. Measuring and interpreting neuronal correlations. Nat. Neurosci. 14, 811–819.

Csicsvari, J., Hirase, H., Czurko, A., Buzsaki, G., 1998. Reliability and state dependence of pyramidal cell-interneuron synapses in the hippocampus: an ensemble approach in the behaving rat. Neuron 21, 179–189.

Das, A., Gilbert, C.D., 1995. Long-range horizontal connections and their role in cortical reorganization revealed by optical recording of cat primary visual cortex. Nature 375, 780–784.

de Kock, C.P., Sakmann, B., 2009. Spiking in primary somatosensory cortex during natural whisking in awake head-restrained rats is cell-type specific. Proc. Natl. Acad. Sci. U.S.A 106, 16446–16450.

Denman, D.J., Contreras, D., 2013. The structure of pairwise correlation in mouse primary visual cortex reveals functional organization in the absence of an orientation map. Cereb. Cortex.

Dong, Y., Mihalas, S., Qiu, F., von der Heydt, R., Niebur, E., 2008. Synchrony and the binding problem in macaque visual cortex. J. Vis. 8 (30), 1–16.

Dragoi, V., Sharma, J., Sur, M., 2000. Adaptation-induced plasticity of orientation tuning in adult visual cortex. Neuron 28, 287–298.

Duret, F., Shumikhina, S., Molotchnikoff, S., 2006. Neuron participation in a synchrony-encoding assembly. BMC Neurosci 7, 72.

Ecker, A.S., Berens, P., Keliris, G.A., Bethge, M., Logothetis, N.K., Tolias, A.S., 2010. Decorrelated neuronal firing in cortical microcircuits. Science 327, 584–587.

Fahle, M., 2004. Perceptual learning: a case for early selection. J. Vis. 4, 879–890.

Fujisawa, S., Amarasingham, A., Harrison, M.T., Buzsaki, G., 2008. Behavior-dependent short-term assembly dynamics in the medial prefrontal cortex. Nat. Neurosci. 11, 823–833.

Ghisovan, N., Nemri, A., Shumikhina, S., Molotchnikoff, S., 2008. Synchrony between orientation-selective neurons is modulated during adaptation-induced plasticity in cat visual cortex. BMC Neurosci 9, 60.

Ghisovan, N., Nemri, A., Shumikhina, S., Molotchnikoff, S., 2009. Long adaptation reveals mostly attractive shifts of orientation tuning in cat primary visual cortex. Neuroscience 164, 1274–1283.

Godde, B., Leonhardt, R., Cords, S.M., Dinse, H.R., 2002. Plasticity of orientation preference maps in the visual cortex of adult cats. Proc. Natl. Acad. Sci. U.S.A 99, 6352–6357.

Gray, C.M., Engel, A.K., Konig, P., Singer, W., 1990. Stimulus-dependent neuronal oscillations in cat visual cortex: receptive

field properties and feature dependence. Eur. J. Neurosci. 2, 607–619.
Hata, Y., Tsumoto, T., Sato, H., Tamura, H., 1991. Horizontal interactions between visual cortical neurones studied by cross-correlation analysis in the cat. J. Physiol. 441, 593–614.
Hubel, D.H., Wiesel, T.N., 1959. Receptive fields of single neurones in the cat's striate cortex. J. Physiol. 148, 574–591.
Hubel, D.H., Wiesel, T.N., 1968. Receptive fields and functional architecture of monkey striate cortex. J. Physiol. 195, 215–243.
Jia, H., Rochefort, N.L., Chen, X., Konnerth, A., 2010. Dendritic organization of sensory input to cortical neurons in vivo. Nature 464, 1307–1312.
Kampa, B.M., Roth, M.M., Gobel, W., Helmchen, F., 2011. Representation of visual scenes by local neuronal populations in layer 2/3 of mouse visual cortex. Front. Neural Circuits 5, 18.
Kara, P., Reid, R.C., 2003. Efficacy of retinal spikes in driving cortical responses. J. Neurosci. 23, 8547–8557.
Kasamatsu, T., Polat, U., Pettet, M.W., Norcia, A.M., 2001. Colinear facilitation promotes reliability of single-cell responses in cat striate cortex. Exp. Brain Res. 138, 163–172.
Ko, H., Hofer, S.B., Pichler, B., Buchanan, K.A., Sjostrom, P.J., Mrsic-Flogel, T.D., 2011. Functional specificity of local synaptic connections in neocortical networks. Nature 473, 87–91.
Ko, H., Cossell, L., Baragli, C., Antolik, J., Clopath, C., Hofer, S.B., Mrsic-Flogel, T.D., 2013. The emergence of functional microcircuits in visual cortex. Nature 496, 96–100.
Kohn, A., Movshon, J.A., 2004. Adaptation changes the direction tuning of macaque MT neurons. Nat. Neurosci. 7, 764–772.
Kohn, A., Smith, M.A., 2005. Stimulus dependence of neuronal correlation in primary visual cortex of the macaque. J. Neurosci. 25, 3661–3673.
Konig, P., Engel, A.K., Roelfsema, P.R., Singer, W., 1995. How precise is neuronal synchronization?. Neural Comput 7, 469–485.
Lee, W.C., Reid, R.C., 2011. Specificity and randomness: structure-function relationships in neural circuits. Curr. Opin. Neurobiol. 21, 801–807.
Liao, D.S., Krahe, T.E., Prusky, G.T., Medina, A.E., Ramoa, A.S., 2004. Recovery of cortical binocularity and orientation selectivity after the critical period for ocular dominance plasticity. J. Neurophysiol. 92, 2113–2121.
Maffei, L., Fiorentini, A., 1973. The visual cortex as a spatial frequency analyser. Vision Res. 13, 1255–1267.
Marshansky, S., Shumikhina, S., Molotchnikoff, S., 2011. Repetitive adaptation induces plasticity of spatial frequency tuning in cat primary visual cortex. Neuroscience 172, 355–365.
Maruyama, Y., Ito, H., 2013. Diversity, heterogeneity and orientation-dependent variation of spike count correlation in the cat visual cortex. Eur. J. Neurosci. 38, 3611–3627.
Moore, B.D.t., Alitto, H.J., Usrey, W.M., 2005. Orientation tuning, but not direction selectivity, is invariant to temporal frequency in primary visual cortex. J. Neurophysiol. 94, 1336–1345.
Movshon, J.A., 1975. The velocity tuning of single units in cat striate cortex. J. Physiol. 249, 445–468.
Patterson, C.A., Wissig, S.C., Kohn, A., 2013. Distinct effects of brief and prolonged adaptation on orientation tuning in primary visual cortex. J. Neurosci. 33, 532–543.
Perkel, D.H., Gerstein, G.L., Moore, G.P., 1967. Neuronal spike trains and stochastic point processes. I. The single spike train. Biophys. J. 7, 391–418.
Poulet, J.F., Petersen, C.C., 2008. Internal brain state regulates membrane potential synchrony in barrel cortex of behaving mice. Nature 454, 881–885.
Ramoa, A.S., Mower, A.F., Liao, D., Jafri, S.I., 2001. Suppression of cortical NMDA receptor function prevents development of orientation selectivity in the primary visual cortex. J. Neurosci. 21, 4299–4309.
Reich, D.S., Mechler, F., Victor, J.D., 2001. Independent and redundant information in nearby cortical neurons. Science 294, 2566–2568.
Reid, R.C., 2012. From functional architecture to functional connectomics. Neuron 75, 209–217.
Ringach, D.L., Shapley, R.M., Hawken, M.J., 2002. Orientation selectivity in macaque V1: diversity and laminar dependence. J. Neurosci. 22, 5639–5651.
Rolls, E.T., Treves, A., 2011. The neuronal encoding of information in the brain. Prog. Neurobiol. 95, 448–490.
Shumikhina, S., Guay, J., Duret, F., Molotchnikoff, S., 2004. Contextual modulation of synchronization to random dots in the cat visual cortex. Exp. Brain Res. 158, 223–232.
Sompolinsky, H., Golomb, D., Kleinfeld, D., 1990. Global processing of visual stimuli in a neural network of coupled oscillators. Proc. Natl. Acad. Sci. U.S.A 87, 7200–7204.
Stanley, G.B., 2013. Reading and writing the neural code. Nat. Neurosci. 16, 259–263.
Stepanyants, A., Hirsch, J.A., Martinez, L.M., Kisvarday, Z.F., Ferecsko, A.S., Chklovskii, D.B., 2008. Local potential connectivity in cat primary visual cortex. Cereb .Cortex. 18, 13–28.
Stratford, K.J., Tarczy-Hornoch, K., Martin, K.A., Bannister, N.J., Jack, J.J., 1996. Excitatory synaptic inputs to spiny stellate cells in cat visual cortex. Nature 382, 258–261.
Swindale, N.V., 1998. Orientation tuning curves: empirical description and estimation of parameters. Biol. Cybern. 78, 45–56.
Ts'o, D.Y., Gilbert, C.D., Wiesel, T.N., 1986. Relationships between horizontal interactions and functional architecture in cat striate cortex as revealed by cross-correlation analysis. J. Neurosci. 6, 1160–1170.
Wallace, D.J., Kerr, J.N., 2010. Chasing the cell assembly. Curr. Opin. Neurobiol.
Wise, A.K., Cerminara, N.L., Marple-Horvat, D.E., Apps, R., 2010. Mechanisms of synchronous activity in cerebellar Purkinje cells. J. Physiol. 588, 2373–2390.
Xing, D., Shen, Y., Burns, S., Yeh, C.I., Shapley, R., Li, W., 2012. Stochastic generation of gamma-band activity in primary visual cortex of awake and anesthetized monkeys. J. Neurosci. 32 (13873-80a).
Xue, M., Atallah, B.V., Scanziani, M., 2014. Equalizing excitation–inhibition ratios across visual cortical neurons. Nature 511, 596–600.
Yoshimura, Y., Sato, H., Imamura, K., Watanabe, Y., 2000. Properties of horizontal and vertical inputs to pyramidal cells in the superficial layers of the cat visual cortex. J. Neurosci. 20, 1931–1940.
Yoshimura, Y., Dantzker, J.L., Callaway, E.M., 2005. Excitatory cortical neurons form fine-scale functional networks. Nature 433, 868–873.
Zohary, E., Shadlen, M.N., Newsome, W.T., 1994. Correlated neuronal discharge rate and its implications for psychophysical performance. Nature 370, 140–143.

OPEN ACCESS Freely available online

PLOS ONE

Adaptation Shifts Preferred Orientation of Tuning Curve in the Mouse Visual Cortex

Jeyadarshan Jeyabalaratnam, Vishal Bharmauria, Lyes Bachatene, Sarah Cattan, Annie Angers, Stéphane Molotchnikoff*

Université de Montréal, Département des Sciences Biologiques, Montréal, Canada

Abstract

In frontalized mammals it has been demonstrated that adaptation produces shift of the peak of the orientation tuning curve of neuron following frequent or lengthier presentation of a non-preferred stimulus. Depending on the duration of adaptation the shift is attractive (toward the adapter) or repulsive (away from the adapter). Mouse exhibits a salt-and-pepper cortical organization of orientation maps, hence this species may respond differently to adaptation. To examine this question, we determined the effect of twelve minutes of adaptation to one particular orientation on neuronal orientation tuning curves in V1 of anesthetized mice. Multi-unit activity of neurons in V1 was recorded in a conventional fashion. Cells were stimulated with sine-wave drifting gratings whose orientation tilted in steps. Results revealed that similarly to cats and monkeys, majority of cells shifted their optimal orientation in the direction of the adapter while a small proportion exhibited a repulsive shift. Moreover, initially untuned cells showing poor tuning curves reacted to adaptation by displaying sharp orientation selectivity. It seems that modification of the cellular property following adaptation is a general phenomenon observed in all mammals in spite of the different organization pattern of the visual cortex. This study is of pertinence to comprehend the mechanistic pathways of brain plasticity.

Citation: Jeyabalaratnam J, Bharmauria V, Bachatene L, Cattan S, Angers A, et al. (2013) Adaptation Shifts Preferred Orientation of Tuning Curve in the Mouse Visual Cortex. PLoS ONE 8(5): e64294. doi:10.1371/journal.pone.0064294

Editor: Manabu Sakakibara, Tokai University, Japan

Received February 6, 2013; **Accepted** April 10, 2013; **Published** May 23, 2013

Funding: Natural Sciences and Engineering Research Council 8290 AND Fonds de Recherche du Quebec - Nature et Technolgies - 137773. The funders had no role in study design, data collection and analysis, decision to publish, or preparation of the manuscript.

Competing Interests: The authors have declared that no competing interests exist.

Introduction

In general, neurons in the sensory cortices respond preferentially to stimulus features eliciting maximal firing rates. Brain has a remarkable tendency to change its neuronal properties in response to the stimulus [1–5], though most of these original properties and connections are wired during the developmental critical period [6,7].

It has been shown that the cortical neurons can adapt when a non-preferred stimulus is imposed on them for shorter or lengthier durations [8–18]. Adaptation leads to either attractive or repulsive shifts in neuronal tuning (orientation, spatial frequency, speed, motion direction). An attractive shift is a shift when the tuning curve of a neuron shifts toward the adapter, whereas a repulsive shift relates to the shift of the tuning curve away from the adapting stimulus. Moreover, investigations in cat and monkey visual cortices have shown that shorter adaptation durations lead to frequent repulsive shifts [10,11], whereas longer and repetitive adaptations induce majority of attractive shifts [14–17].

Neurons in the visual cortices of higher vertebrates such as cats, monkey and humans are arranged in a columnar fashion [19], whereas cells are arranged in a salt-and-pepper fashion in mice and rats [20,21]. Recently it has been shown that majority of neighboring cells in cat exhibit similar shifts (toward the adapter in majority) of tuning curves, and only 25% of groups of cells showed different direction of shifts following adaptation [13]. The salt-and-pepper organization implies that neurons with different orientation preferences are close to each other. The close proximity of these neurons may favor functional relations between them which consequently may lead to specifically different reactions following adaptation in comparison to cats and monkeys.

In this paper we report the effect of an imposed oriented sine-wave drifting grating on visual neurons in mice for a long time (12 min). Data show that attractive shifts are more frequent amongst orientation selective neurons. Interestingly, a number of cells that were originally poorly tuned (untuned) to orientation displayed selectivity following adaptation. We found that the shifts are not as systematic as in cats and monkeys, and this could be attributed to the salt-and-pepper functional organization of the cortex. Hence, it seems reasonable to postulate that columnar arrangement of neurons displays more methodical shift-pattern. Thus, we conclude that long adaptation leads to change in neuronal properties in response to the adapter, and this further consolidates the previous findings [1,14,15,16] that forceful application of a stimulus modifies the neuronal selectivity.

Materials and Methods

Ethical approval

The animal preparation and recording procedures followed the guidelines of the Canadian Council on Animal Care and were approved by the Institutional Animal Care and Use Committee of University of Montreal. Animals were provided by the Division of Animal Resources of University of Montreal.

Animal preparation

CD-1 strain adult mice aged from 9 to 11 weeks were used in this study. For recording from visual cortex the animals were anesthetized with 10% urethane (1.5 g/kg) injected intraperitoneally. Atropine sulphate (0.5 mg/kg) was administered subcutaneously to prevent accumulation of secretion in the trachea. Lidocaine hydrochloride 2% (Xylocaine) was applied at surgical and pressure sites as a local anesthetic. Pinch reflexes were used to assess the depth of anesthesia. The mice were then placed in a custom made stereotaxic apparatus allowing visual stimulation of the entire contralateral visual field and the skull was secured in a head holder, which eliminated head movement. The section of the skull and dura mater (2.5×2.5 mm) over the visual cortex was dissected out. Mystacial macro vibrissae were cut to preclude obstruction of the visual field. Corneal desiccation of the stimulated eye was prevented by applying a thin layer of silicone oil while allowing a clear optical transmission. Eye movements were negligible within the period of recordings. The unstimulated eye was closed.

Electrophysiological recordings and stimuli

Evoked extracellular neuronal activity was recorded with a glass microelectrode filled with 0.9% NaCl inserted in V1. Both multi-unit and single-unit activities were recorded from superficial layers (<1 mm). The signal from the microelectrode was filtered (300 Hz–3 kHz), amplified, displayed on oscilloscope and audio-monitored. Then multi-unit activity was digitized and recorded with data acquisition software (Spike 2, Cambridge Electronic Design, CED Limited, Cambridge, England). The off-line spike sorting method was based on cluster classification in reduced space. The stability of each cell's activity across conditions was verified qualitatively by visual control of the clusters disposition, the waveforms shape and auto-correlograms showing a total depression at its center. As we began by recorded multi-unit electrical activities, no attempt was made to stimulate the receptive fields. In mice the excitatory receptive field is rarely smaller than 10° [23]. The stimulating grating covered ±30° horizontally and ±30° vertically of the mouse monocular field.

Stimulation was monocular. For the entire study, visual stimuli were drifting full-contrast square wave gratings generated with a VRG Volante 34020 graphic board (Vision Research Graphics, New Hampshire, USA). Stimuli were presented on a 21-in. monitor (60 Hz refresh rate, Mitsubishi FHS6115SLK Color Display Monitor, Tokyo, Japan) with 1024×512 pixels placed 28.5 cm from the mouse's eye. Temporal frequency and velocity were constant at 0.07 cycles/deg and 4 deg/s respectively. These parameters were maintained constant throughout the duration of the experiment. The center of the monitor was positioned at about 45° azimuth 0° elevation.

Visual stimulation protocol

Six orientations equally spaced were selected and used for this study covering a span of 90°. Test orientations were presented in a random order. Each oriented stimulus was presented in blocks of 25 trials lasting 4.1 s each with a random inter-trial interval (1.0–3.0 s) during which no stimulus was presented. We recorded peri-stimulus time histograms (PSTH) of multi-unit activity.

Once control orientation tuning curves were characterized, an adapting stimulus was presented continuously for 12 min. The adapting stimulus was a quasi full field drifting grating whose orientation was 45°. During this adaptation period no recordings were performed. Immediately after adaptation, orientation tuning curves were measured starting with the adapting orientation while the remaining orientations were recorded in a random order. Following a recovery period of 60 min, another orientation tuning curve measurement was performed.

Data analysis

Single cells were sorted out off-line from the multi-unit activity recorded during data acquisition. Evoked responses were derived from peri-stimulus time histograms which provided cellular firing rates. Orientation tuning curves were constructed from raw data and fitted using the Gaussian function. This allowed us to determine the preferred orientation of neurons with precision and then measure shifts in orientation preference. Since orientation tuning is best described with Gaussian-like functions, we fitted our raw data with the von Mises function [22]. This allowed us to determine the preferred orientation of neurons and then measure shifts in orientation preference. The von Mises function is defined as:

$$M(\theta) = A \cdot e^{b[\cos(\theta - c)]} + d$$

where A is the value of the function at the preferred orientation, c, and b is a width parameter. An additional parameter, d, represents the spontaneous firing rate of the cell [22,24]. We analyzed cells whose tuning fitted well von Mises function over the (90°) range of sampled orientations. The above calculations are necessary because tuning curves derived from raw data may be imperfect in determining the preferred orientation as the interval between the presented orientations is relatively large. A fit was considered satisfactory if it accounted for at least 80% of the variance in the data.

It was also necessary to ensure that cells in our sample were properly tuned for orientation. We measured an orientation selectivity index (OSI) by dividing the firing rate at orthogonal orientations (baseline of the tuning curves) by the firing rate for the preferred orientation, and subtracting the result from 1 [25]. The closer the OSI is to 1, the stronger the orientation selectivity because it means that the ratio baseline/preferred orientation is small, implying that the firing rate at the preferred orientation is much greater than the baseline-firing rate. No significant difference was found between OSI values measured from raw or fitted data. The figures we present in the results section are from raw and fitted data.

Results

We investigated the orientation tuning curves of V1 neurons following the adaptation protocol. Neurons were sorted from the multi-unit activity recorded in the primary visual cortex of anesthetized mouse. A total of 108 cells were sorted out and are shown in Table 1. In the first step we presented gratings randomly at varied orientations to generate orientation tuning curves. Following twelve minutes of adaptation at 45°, tuning curves were fitted again. A recovery from adaptation effects was carried out about sixty minutes after adaptation phase. Orientation tuning curves were fitted using a Gaussian function (see Material and methods).

Out of investigated 108 cells 14 (13%) cells were characterized with attractive shifts, whereas tuning curves of 4 (3.7%) cells repelled away from the adapter. 17(15.7%) neurons displayed no significant shift, that is, they retained their original preferred orientation. Other cells were categorised as follows: 22 UT neurons (20.4%), that is, untuned neurons that showed no preferred orientation tuning curves (OSI = 0.10) before adaptation, but exhibited tuning after an adaptation of 12 min (OSI≥0.70); 47 cells were UU neurons (43.5%), that is, neurons

Table 1. Classification of cells after adaptation.

	Attractive	Repulsive	No-shift	Other (67.6%)		
Total cells, n = 108 cells	14 (13%)	4 (3.7%)	17 (15.7%)	22 UT (20.4%)	47 UU (43.5%)	4 TU (3.7%)

Legend: UT: Untuned to Tuned, UU: Untuned to Untuned, TU: Tuned to Untuned.
doi:10.1371/journal.pone.0064294.t001

which displayed no preferred orientation prior and post-adaptation; and finally 4 TU neurons (3.7%) which were tuned before adaptation, but behaved with no orientation selectivity post-adaptation. In summary this table indicates that out of all originally orientation selective neurons which changed their tuning after adaptation, most of them responded with attractive shifts. It also demonstrates that adaptation may have varied effects on neurons. It may induce orientation selectivity in cells originally lacking an optimal orientation, and may even potentiate originally tuned neurons to lose their selectivity. Finally, a large proportion of cortical cells in V1 in mice exhibited poor tuning and was insensitive to adaptation.

Adaptation-induced plasticity of orientation tuning curves

In all cases the adapting orientation was applied on the flank of the tuning curve, the offset generally was 30° from the optimal orientation. Curve fits were generated for each of the 25 trials and Student's t-test was done between control and adaption conditions to evaluate the significance of orientation shifts on the single cell basis.

Figure 1 describes a typical example of an attractive shift (toward the adapter). Blue tuning curves correspond to values before adaption. Since this study is centered on shifts of tuning curves and to ease comparison between cells, optimal orientations were normalized to 0°. These curves show that although response magnitude fluctuates from one presentation to the next (in the example range 0.14 Hz to 0.64 Hz) the jitter for optimal orientation is small (<5°). Initial optimal orientation was 90° (normalized to 0°). Immediately after twelve minutes of adaptation, the orientation selectivity was tested again with identical stimuli (red tuning curves). Following adaptation, the preferred orientation shifted in direction of the adapter (arrow head adapter oriented at −45°). The acquired new optimal orientation is −20°. Thus the cell showed a significant attractive shift of 20° (optimal orientation, paired sample two-tailed t-test, $P<0.0001$, interrupted vertical lines represent the averaged optimal orientation). In addition, this change in orientation selectivity is accompanied by an increase (26.7%) of the responsivity. About sixty minutes (recovery period) after the end of adaptation protocol, the original preferred orientation was reinstated (illustrated by the green tuning curves). On the right (Figure 1), waveforms of action potentials recorded during each step of this recording are displayed. Identical waveforms ascertain that responses were produced by the same unit during all phases of the study.

Figure 2 illustrates three typical behaviors of neurons after adaptation. The upper row displays the tuning curves as derived from raw data (error bars indicate SEM). Lower plots illustrate trial-by-trial Gaussian fitted orientation tuning curves pre and post-adaptation. The first cell (Figure 2A) showed a significant attractive shift of 49° following adaptation (paired sample two-tailed t-test, $P<0.0001$). The second cell (Figure 2B) showed a significant repulsive shift of 35° after adaptation (paired sample two-tailed t-test, $P = 0.0032$). The third cell (Figure 2C) is an example of a typical refractory neuron that shows no significant shift. Indeed the preferred orientation is unchanged in spite of variability of the evoked discharges from trial to trial [26], (paired sample two-tailed t-test, $P>0.1$).

Moreover, these plots underline the fact that there is a strong decline of responses evoked by the original preferred orientation, regardless of the direction of the shifts. In these examples the magnitude of responses to the initial preferred orientation declined to the level of the remote flank orientations. In addition these examples illustrate the response enhancements of novel peak responses. Additionally, activity driven by orientations outside the range of the adapter and original optimal orientation is unchanged (Figure 2), suggesting that imposing a particular orientation for several minutes impacts mechanisms influencing original and the novel optimal orientations. These data point toward the fact that adaptation effects are mostly constrained around the adapter and the original optimal orientations. It signifies that the peak shifts are not the consequence of the global modulation of neuronal activity.

The mean shift was calculated for a subset of 18 cells (originally tuned cells showing significant shifts). For this computation, cells displaying attractive and repulsive shifts were pooled together to assess the overall significance of shift-magnitude. Shifts in orientation preference of amplitude larger than 5° were all significant ($P<0.05$, t-test) and represented 89% of the cells (16/18 cells). The absolute average amplitude of significant shifts was 53.64°±8.40°. The mean amplitude of significant attractive shifts

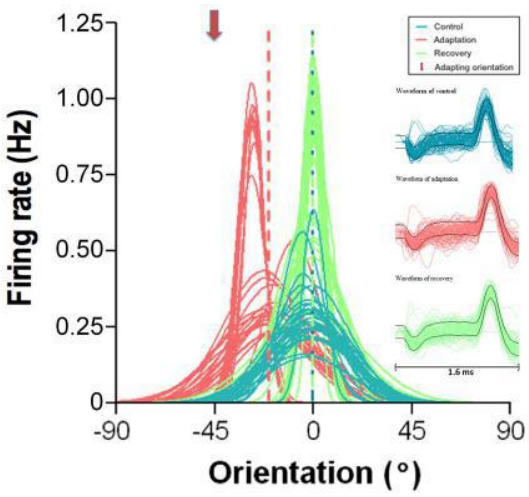

Figure 1. Typical example of an attractive shift. Twenty-five presentations of each orientation. Gaussian fits and orientation are normalized in this and other figures: optimal orientation is marked zero. Vertical broken lines indicate optimal orientations. Downward arrowhead indicates adapting orientation in this and all figures. Horizontal Right inserts show spike waveforms recorded during each phase of the recordings. Bar equals 1.6 ms.
doi:10.1371/journal.pone.0064294.g001

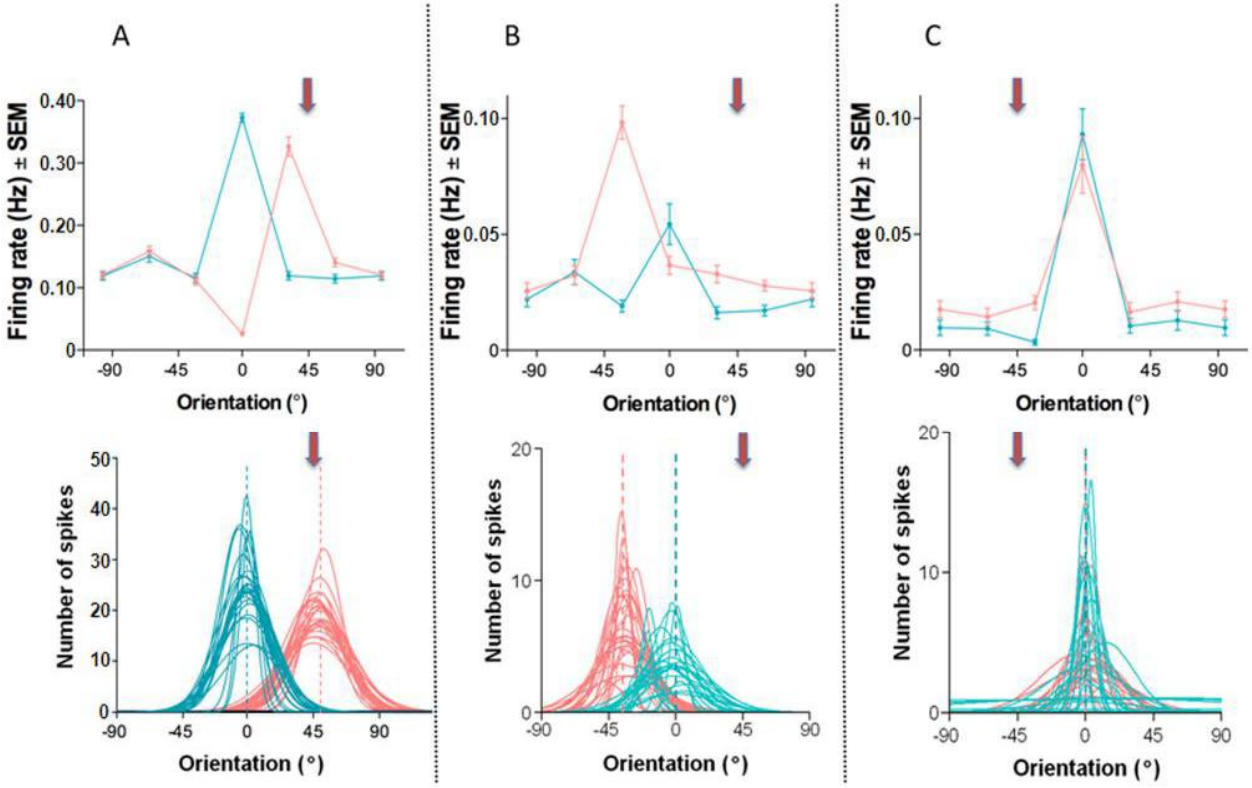

Figure 2. Three examples of orientation shifts. From left to right (**A**) attractive, (**B**) repulsive and (**C**) no shift. Upper row: Raw data, error bars indicate SEM. Bottom row: Gaussian fits, same cells as in the upper row.
doi:10.1371/journal.pone.0064294.g002

was 60.91°±12.61° and 20.25°±0.74° for repulsive shifts respectively.

Figure 3A shows the distribution of orientation-class preference for this pool of neurons. The population of neurons was divided into five orientation classes of ±18°. Similarly to cats, vertical and horizontal orientations seem to dominate this distribution (that is cardinal orientations). The survey shown in Figure 3B indicates that cardinal orientations exhibit bigger shifts 72±8.3° than oblique orientations. The displacement of the peak of the tuning curve in this case averaged 38±7.0°, that is, almost half of the shift-magnitude induced at cardinal orientations ($p = 0.0287$, t-test). However, this difference may be attributed to frequent application of an oblique adapter (45°).

Orientation tuning curve emergence

Contrary to what is observed in cats and monkeys where most of the cells exhibit orientation selectivity (significant orientation tuning curve) in V1, in mice a fairly large (>50%) proportion of neurons failed to show selectivity for a specific orientation [23]. For instance, in Figure 4 the unit responded to any orientation with an almost equal firing rate (approximately 15 spikes per trial) to all presented orientations (blue). The weak responsiveness is shown in the upper PSTH (Figure 4, tracing 3) Quite interestingly, and unexpectedly, following a period of twelve minutes of adaptation to a grating oriented at 45°, the same cell displayed a robust orientation tuning curve whose preferred orientation was horizontal (0°) and the OSI = 0.92. The PSTH in tracing 4 illustrates the firing rate corresponding to the acquired optimal orientation. It is important to underline that this particular unit was recorded simultaneously within the same cluster of neurons that yielded the cell in Figure 2A. Thus, although both units were close to each other, only one neuron disclosed a typical tuning curve prior to adaptation. After adaptation both cells showed orientation tuning curves which indicates that the second cell (Figure 4) acquired this property through adaptation.

Effects of adaptation on responses magnitude

The average adaptation-induced response modulations are compared in Figure 5. The quantification is focused on three responses: the initial preferred response, the response to the adapter and finally the acquired optimal response. The upper row (Figure 5A–C) shows results related to repulsive shifts. These computations indicate that responses evoked by the original optimal orientation are considerably diminished (−96.83%). This decline of initial optimal firing is recorded quite systematically, and has been reported in previous studies carried out on other mammals [15,24]. In addition, the evoked discharges in response to the adapting orientation also decreased by 96.94%. Thus, applying an orientation up to 90° off the preferred axis of orientation depresses responses on the flank of the tuning curve facing the adapter. By contrast, responses on the opposite flank relative to the adapter are augmented although this increase is insignificant, (62.72% % $P>0.01$). The global result however is that the repulsive shift is attributed to depression of responses on the slope of tuning curve facing the adapting orientation.

In comparison, the profile of response modulations for attractive shifts is quite different following adaptation (Figure 5D–F). Responses evoked by the original optimal orientation are strongly depressed (−48.47% $p<0.05$, t-test), in a fashion similar to repulsive shifts (see above). But in contrast to the repulsive shifts,

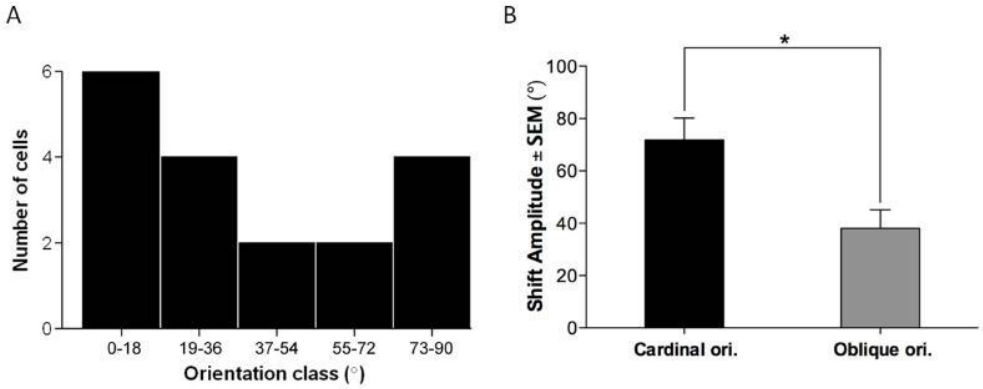

Figure 3. Distribution of orientation-class preference and shift magnitude significance. (**A**) Neurons divided into five orientation classes of 18°. Vertical and horizontal orientations dominate (that is cardinal orientations). (**B**) The relationship between shift-magnitude and significance level indicates that cardinal orientations have larger shift than cells whose orientation is oblique.
doi:10.1371/journal.pone.0064294.g003

responses produced by orientations close to the adapter are significantly enhanced leading to attractive shifts. Indeed, the acquired preferred orientation (Figure 5F) is the result of an average increase by 66% ($p<0.05$, t-test) in the firing rate evoked by orientation close to or corresponding to the adapter. This dual effect: decline of evoked responses to the initial optimal orientation and enhancement of discharges on the adapting flank may be the result of a push-pull process suggested for cats and monkeys [15,24,27,28] that underwent similar experimental protocol.

Discussion

Our results suggest that as for other mammals with eyes in frontal plane, mice cortical cells shift their peaks of orientation tuning curves in response to adaptation. This appears particularly interesting since these animals lack a columnar organization of the orientation domains as demonstrated in cats and monkeys. As a matter of fact investigations have suggested that mouse cortex exhibits salt-and-pepper type of organization for orientation, that is, a large spectrum of axes of orientations are interspersed over a small cortical distance; instead of a progressive tilt of orientation preference as recording electrode moves tangentially in shorter steps from one column to the next [7,19].

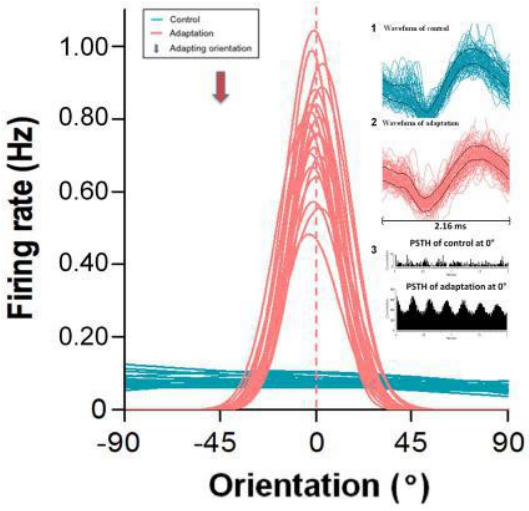

Figure 4. Example of a neuron untuned to orientation. Prior to adaptation (in blue) no orientation evokes a stronger response. Following adaptation (in red) a clear optimal orientation emerges. Right inserts, tracing 1 and 2 show spike waveforms recorded during each phase of the recordings, bar equals 2.16 ms. Tracings in 3 illustrates PSTHs of evoked responses prior to (upper) and following (lower) adaptation respectively.
doi:10.1371/journal.pone.0064294.g004

Thus, in spite of this organizational difference orientation tuning curves are susceptible to relatively long period of adaptation: cells adopt new preferred orientations. Globally these results suggest that such shifts are a general property that would be applicable to all mammals. A general rule may be proposed for mammals: imposing a non-preferred stimulus for several minutes induces a modification of the preferred stimulus that was established since birth or during the critical period. Our results are quite synonymous with the data recorded by Frenkel et al., 2006 [12] describing selective response potentiation. This facilitation of responses relates to selective increase of responsiveness following corresponding exposure to the grating stimuli. In addition to orientation [29], other properties such as spatial frequency [9,17], speed [24], direction [5,30–33], patterned plaid [34], ocular dominance [35] are also triggered following frequent presentation of appropriate stimuli. Similar data have been reported in the auditory system [36,37].

This type of plasticity may be explained with results for mice reported by Jia et al., 2010 [38]. Using double high-speed two-photon imaging and electrophysiological recordings, it has been demonstrated that a single dendritic branch receives synaptic connections from neurons selective to different orientations [38,39]. Such large range indicates that many or all orientations may be efficient in exciting a single cortical cell. These studies demonstrate that each contact generates synaptic response as measured through calcium fluxes. Therefore, activating an alternate group of synapses shifts the optimal orientation. Because weak responses evoked by non-preferred orientation (flank orientation) are barely modified by adaptation, it seems that adaptation affects almost exclusively the initial optimal orientation (decline) and the new acquired orientation (facilitation). It has been suggested that this dual modulation is attributed to a push-pull mechanism [15,24,28,40].

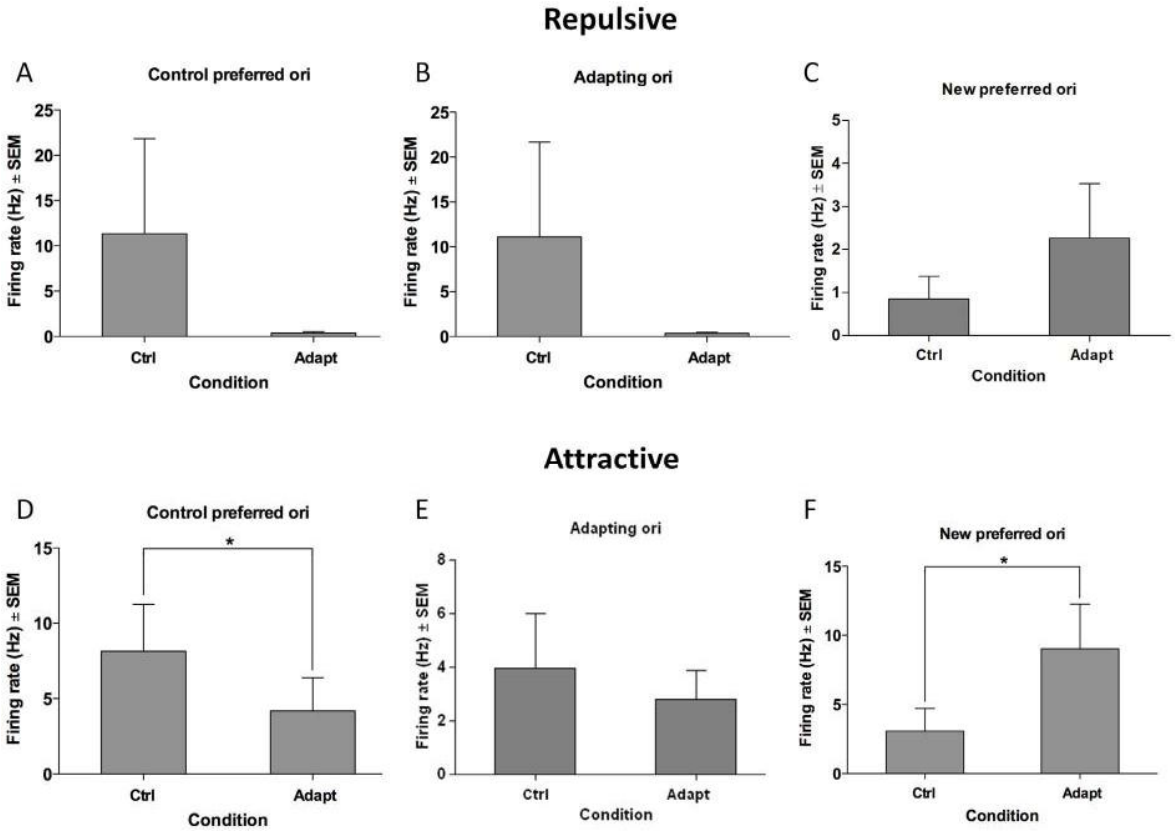

Figure 5. Comparative response modulations induced by adaptation. Upper row: repulsive shifts. Lower row: attractive shifts. Three responses are computed: Original preferred, responses to adapter, new preferred. Star indicates significant level $p<0.05$. Abbreviations, Ori: orientation, Ctrl: control, Adapt: adaptation
doi:10.1371/journal.pone.0064294.g005

Methodological considerations

It is unlikely that response modulations reported in the present paper are attributed to a random and sudden surge of electrical activity. Data show that flank orientations remained unchanged although these responses were weak. In addition evoked responses to the adapter are enhanced while responses to the initial preferred orientation are decreased. Such dual effects are irreconcilable with a uniform and global fluctuation of firing rates. Also, response modifications are roughly constrained around the adapter and the original optimal orientation. It is worth to signal that orientations are applied randomly. It may be argued that orientation tuning curves vary in relation to cell's discharge variability or stimuli dimensions. However, as shown in the present paper although response magnitude changes from trial to trial, the jitter of optimal orientation remains quite small. Since adapting orientation is applied uninterruptedly for twelve minutes, it may be argued that our results are due to change of luminosity induced by prolonged adaptation. This eventuality is unlikely. Shou et al., 1996 [41] reported that prolonged exposure to drifting gratings induces a global decline of responsiveness in most cells. In addition, facilitation of responses was a rare occurrence and no tuning shifts were recorded [42]. Finally, it is important to mention that firing increase makes it unlikely that neuronal fatigue is associated in adaptation mechanisms. In cats it has been shown that orientation change is not occurring at the LGN (lateral geniculate nucleus) level since cells at this level are unoriented. Thus, this sort of plasticity originates at cortical level [9,10]. Finally, in the salamander retina [43] and cats adaptation to contrast modulates evoked responses. However, these changes are occurring in a few seconds, consequently they are not comparable to modulation observed in the present study.

Comparison with other mammals

Several investigations report orientation attractive and repulsive shifts [1,14,15,27]. Equally, in adult and mature cortices, other visual properties demonstrated changes following various adaptation protocols. Although the presented results are similar to those obtained in other species, several differences are noteworthy.

In mice a large proportion of cells are poorly tuned [23], and also in our study in which we employed a quasi full field presentation of gratings. We did not stimulate local receptive field as multi-unit recordings were carried out. However after adaptation the same cells exhibited a classical tuning curve even though the same stimuli were applied. Such emergence of orientation tuning curves was unreported in cat's study, may be because in cats most cortical cells are tuned to orientation in V1. This lack of orientation selectivity in mice may be attributed to the fact that cortical cells are connected by afferent axons displaying a large range of orientations [38]. Thus there is no bias favoring one orientation. Adaptation would induce a preference allowing one orientation to strengthen its drive over the remaining inputs. This argument seems reasonable for attractive shifts as the highest changes are close to the adapter. Alternatively, as we used large stimuli adaptation to one orientation, and this may cause a

disinhibition of surround suppression which in turn results in an attractive shift. The same reasoning is conflicting with repulsive shifts. One may assume that the adapter weakens the inputs driven by the latter, which in turn facilitates responses on the opposite side of the tuning curve. Such description was advanced for repulsive shifts in cats [14,15] and monkeys [24,27].

It has been suggested that tuning function of individual cells is the result of converging and overlapping inputs. In mice this situation may be the result of an absence of clear and extensive columnar organization. Therefore cells with different preferred orientations are close to each other. This assumption is supported by above cited data reported in Jia et al., 2010 [38]. Such arrangement favors large shift of synaptic equilibrium depending on the stimuli conditions. Another difference with other animals deserves attention. Cells lacking orientation selectivity demonstrate a clear tuning curve after adaptation. Such emergence of orientation selectivity was unexpected. However, it is compatible with previous explanation stating that a single neuron receives a large spectrum of oriented inputs and following a forceful application of one particular orientation favors synaptic excitation associated with the adapter which leads to the emergence of an orientation tuning curve. Furthermore, this statement is in line with a recent report of Makino and Malinow [44] who identified grouped synaptic changes induced by experience at individual dendritic branches in the barrel cortex. They showed changes of synaptic spines in a grouped manner. In parallel, it has been demonstrated that exposing mice to grating stimuli of one orientation produces increase of responses to the applied stimulus [12,45]. Hence our data suggest that synaptic modifications are occurring within relatively brief time window.

In conclusion, the results of the current paper are reasonable to suggest that despite the cortical organization, the neurons in either columnar or salt-and-pepper fashioned mammals exhibit behavioral shifts in response to longer adaptation periods. Nevertheless, the shift pattern in column-fashioned animals is more systematic than in mammals with salt-and-pepper orientation map.

Author Contributions

Conceived and designed the experiments: SM. Performed the experiments: JJ LB VB SC. Analyzed the data: JJ VB LB SC AA SM. Contributed reagents/materials/analysis tools: AA. Wrote the paper: JJ VB SM.

References

1. Kohn A (2007) Visual adaptation: physiology, mechanisms, and functional benefits. J. Neurophysiol. 97: 3155–3164.
2. Daoudal G, Debanne D (2003) Long-term plasticity of intrinsic excitability: learning rules and mechanisms. Learn Mem 10: 456–465.
3. Kokovay E, Shen Q, Temple S (2008) The incredible elastic brain: how neural stem cells expand our minds. Neuron 60: 420–429.
4. McCoy PA, Huang H, Philpot BD (2009) Advances in understanding visual cortex plasticity. Curr. Opin. Neurobiol. 19: 298–304.
5. Levinson E, Sekuler R (1976) Adaptation alters perceived direction of motion. Vision Res 16: 779–781.
6. Sur M, Schummers J, Dragoi V (2002) Cortical plasticity: time for a change. Curr Biol. 12: R168–170.
7. Hubel DH, Wiesel TN (1962) Receptive fields, binocular interaction and functional architecture in the cat's visual cortex. J Physiol 160: 106–154.
8. Clifford CW (2002) Perceptual adaptation: motion parallels orientation. Trends Cogn Sci 6: 136–143.
9. Bouchard M, Gillet P-C, Shumikhina S, Molotchnikoff S (2008) Adaptation changes the spatial frequency tuning of adult cat visual cortex neurons. Exp Brain Res 188: 289–303.
10. Dragoi V, Rivadulla C, Sur M (2001) Foci of orientation plasticity in visual cortex. Nature 411: 80–86.
11. Dragoi V, Sharma J, Sur M (2000) Adaptation-induced plasticity tuning in adult visual cortex. Neuron 28: 287–298.
12. Frenkel MY, Sawtell NB, Diogo ACM, Yoon B, Neve RL, et al. (2006) Instructive effect of visual experience in mouse visual cortex. Neuron 51: 339–349.
13. Nemri A, Ghisovan N, Shumikhina S, Molotchnikoff S (2009) Adaptive behaviour of neighboring neurons during adaptation-induced plasticity of orientation tuning in V1. B.M.C. Neurosci. 10: 147.
14. Ghisovan N, Nemri A, Shumikhina S, Molotchnikoff S (2008) Visual cells remember earlier applied target: plasticity of orientation selectivity. *PLoS One* 3:e3689.
15. Ghisovan N, Nemri A, Shumikhina S, Molotchnikoff S (2009) Long adaptation reveals mostly attractive shifts of orientation tuning in cat primary visual cortex. Neuroscience 164: 1274–1283.
16. Bachatene L, Bharmauria V, Rouat J, Molotchnikoff S (2012) Adaptation-induced plasticity and spike waveforms in cat visual cortex. NeuroReport 23: 88–92.
17. Marshansky S, Shumikhina S, Molotchnikoff S (2011) Repetitive adaptation induces plasticity of spatial frequency tuning in cat primary visual cortex. Neuroscience 172: 355–365.
18. O'Hashi KO, Miyashita M, Tanaka S (2007) Experience-dependent orientation plasticity in the visual cortex of rats chronically exposed to a single orientation. Neurosci Res. 58: 86–90.
19. Espinosa JS, Stryker MP (2012) Development and plasticity of the primary visual cortex. Neuron 75:230–249.
20. Wang KH, Majewska A, Schummers J, Farley B, Hu C, et al. (2006) In vivo two-photon imaging reveals a role of arc in enhancing orientation specificity in visual cortex. Cell 126: 389–402.
21. Ohki K, Reid RC (2007) Specificity and randomness in the visual cortex. Curr Opin Neurobiol. 17:401–7.
22. Swindale NV (1998) Orientation tuning curves: empirical description and estimation of parameters. Biol Cybern. 78: 45–56.
23. Mangini NJ, Pearlman AL (1980) Laminar distribution of receptive field properties in the primary visual cortex of the mouse. J Comp Neurol. 193: 203–222.
24. Kohn A, Movshon JA (2004) Adaptation changes the direction tuning of macaque MT neurons. Nature. Neurosci. 7: 764–772.
25. Ramoa AS, Mower AF, Liao D, Jafri SI (2001) Suppression of cortical NMDA receptor function prevents development of orientation selectivity in the primary visual cortex. J Neurosci 21: 4299–4309.
26. Molotchnikoff S, Rouat J (2012) Brain at work: time, sparseness and superposition principles. Front Biosci. 17: 583–606.
27. Patterson CA, Wissig SC, Kohn A (2013) Distinct effects of brief and prolonged adaptation on orientation tuning in primary visual cortex. J. Neurosci 33: 532–543.
28. Hietanen MA, Crowder NA, Price NS, Ibbotson MR (2007) Influence of adapting speed on speed and contrast coding in the primary visual cortex of the cat. J Physiol 584: 451–462.
29. Schoups A, Vogels R, Qian N, Orban G (2001) Practising orientation identification improves orientation coding in V1 neurons. Nature. 412: 549–553.
30. Priebe N, Lampl I, Ferster D (2010) Mechanisms of direction selectivity in cat primary visual cortex as revealed by visual adaptation. J. Neurophysiol 104: 2615–2623.
31. Saul AB, Cynader MS (1989) Adaptation in single units in visual cortex: The tuning of after effects in the temporal domain. Vis Neurosci 2: 609–620.
32. Schlack A, Albright TD (2007) Remembering visual motion: Neural correlates of associative plasticity and motion recall in cortical area MT. Neuron 53: 881–890.
33. Tolias A, Keleris GA, Smirnakis SM, Logothetis NK, (2005) Neurons in macaque area V4 acquire directional tuning after adaptation to motion stimuli. Nature Neurosci. 8: 591–593.
34. Movshon JA, Lennie P (1979) Pattern-selective adaptation in visual cortical neurones. Nature 278: 850–852.
35. Vetencourt JFM, Sale A, Vigi A, Baroncelli L, De Pasquale R, et al. (2008) The antidepressant fluoxetine restores plasticity in the adult visual cortex. Science 320: 385–388.
36. Weinberger N (1998) Physiological memory in primary auditory cortex: Characteristics and mechanisms. Neurobiol Learn Memory 70: 226–251.
37. Eggermont J, Pienkowski M (2009) Effects of adaptation on spectrotemporal receptive fields in primary auditory cortex. NeuroReport 20: 1198–1203.
38. Jia H, Rochefort NL, Chen X, Konnerth A (2010) Dendritic organization of sensory input to cortical neurons in vivo. Nature 464: 1307–1312.
39. Ko H, Hofer SB, Pichler B, Buchanan KA, Sjöström PJ, et al. (2011) Functional specificity of local synaptic connections in neocortical networks. Nature 473: 87–91.
40. Frégnac Y, Pananceau M, René A, Huguet N, Marre O, et al. (2010) A re-examination of Hebbian-covariance rules and spike timing-dependent plasticity in cat visual cortex in vivo. Frontiers in Synaptic Neurosci 2: 1–20.
41. Shou T, Li X, Zhou Y, Hu B (1996) Adaptation of visual evoked responses of relay cells in the dorsal lateral geniculate nucleus of the cat following prolonged exposure to drifting gratings. Vis Neurosci 13: 605–613.
42. Kohn A, Movshon JA (2003) Neuronal adaptation to visual motion in area MT of the macaque. Neuron 39: 681–691.
43. Baccus SA, Meister M (2002) Fast and slow contrast adaptation in retinal circuitry. Neuron 36: 909–919.

44. Makino H, Malinow R (2011) Compartmentalized versus global synaptic plasticity on dendrites controlled by experience. Neuron 72:1001–1011.

45. McCurry LC, Shepherd JD, Tropea D, Wang KH, Bear MF, et al. (2010) Loss of Arc renders the visual cortex impervious to the effects of sensory experience or deprivation. Nature Neurosci. 13: 450–457.

EJN European Journal of Neuroscience

FENS Federation of European Neuroscience Societies

European Journal of Neuroscience, Vol. 40, pp. 2554–2563, 2014 doi:10.1111/ejn.12616

NEUROSYSTEMS

Comparative analysis of orientation maps in areas 17 and 18 of the cat primary visual cortex following adaptation

Sarah Cattan,[1] Lyes Bachatene,[1] Vishal Bharmauria,[1] Jeyadarshan Jeyabalaratnam,[1] Chantal Milleret[2] and Stéphane Molotchnikoff[1]

[1]Département de sciences biologiques, Université de Montréal, Pavillon Marie-Victorin, C.P. 6128, succ. Centre-ville, Montréal, QC, H3C 3J7, Canada

[2]Neural Bases of Spatial Memory and Navigation, CIRB – Collège de France (CNRS UMR 7241, INSERM U1050, UPMC ED 158, MEMOLIFE PSL), Paris, France

Keywords: learning, optical imaging, orientation tuning, plasticity, visual cortex

Abstract

Object orientations in the visual field are columned into specific orientation domains in the primary visual cortex [area 17 (A17) and area 18 (A18)] of cats. At the single-cell level, adapting A17 neurons to a non-preferred orientation (adaptor) shifts their preferred orientation either towards the adaptor (attractive shift) or away from it (repulsive shift). As A17 and A18 are reciprocally connected, we sought to determine how changes in preferred orientations in A18 neurons are correlated with changes recorded in A17 anesthetised cats. To this end, we simultaneously traced populations of neurons in A17 and A18, using intrinsic optical imaging, before and after long (12 min) and short (3 min) adaptations. The comparison of A17 and A18 maps pre-adaptation and post-adaptation showed that variance in shift amplitudes is greater in A18 than A17 for short adaptations. Our results indicate a rapid reconfiguration of functional maps that may spread to many cortical areas.

Introduction

In spite of numerous investigations, how the external environment is represented in internal brain states is a domain yet to be comprehensively explored. However, it is now widely accepted that neurons coordinate their activity in fine-scale networks to process the sensory information (Hebb, 1949; Lindquist & Barrett, 2012; Miller & Buschman, 2013; Sporns, 2013). These circuits are flexible, allowing neurons to adapt in response to frequent changes in inputs from the environment (De Jong *et al.*, 2012; Grossberg, 2013). Therefore, sub-networks or microcircuits may be considered as a dynamic system, wherein – at a given point in time – environmental conditions transiently induce a steady state of the neuronal system. For instance, if an environmental input varies sufficiently to reach a threshold level, the neuronal system becomes unstable and progresses to another state of disambiguation, thus reflecting the impact of new inputs. Such progression in brain-state changes results from rules that still remain poorly understood.

To understand these mechanisms, plastic modifications (in our analogy, the switch to another steady state) can be artificially induced in the brain by presenting a stimulus that is unusual as compared with natural conditions (with variations in shape, color, motion, and duration). This process of imposition of stimulus is called adaptation (Kohler, 1962). In the primary visual cortex [area 17 (A17)], adaptation studies have been carried out with a drifting sine-wave grating, called an adaptor, which is applied within the boundaries of the cellular receptive field for variable amounts of time (a few milliseconds to several hours) (Harris & Calvert, 1989; Dragoi *et al.*, 2000; Kohn, 2007; Zhang *et al.*, 2009). After adaptation, most neurons change (shift) their original preferred orientation and acquire a new optimal orientation. Neurons typically show two behaviors post-adaptation: attractive shifts and repulsive shifts. An attractive shift corresponds to the displacement of the preferred orientation of a neuron towards the adaptor; a repulsive shift corresponds to the movement away from it.

Previous studies have suggested that the shift depends on the duration of the adaptation: shifts are mainly repulsive (i.e. neurons respond less to the adaptor) for shorter adaptations (< 6 min) (Dragoi *et al.*, 2000; Ghisovan *et al.*, 2009), and mostly attractive for adaptations exceeding 10 min (Ghisovan *et al.*, 2009; Bachatene *et al.*, 2012, 2013). In addition, the shift amplitude seems to be augmented as a function of the gap between the adaptor and the initial preferred orientation (Dragoi *et al.*, 2000; Kohn, 2007). Here, we compared the effects of short (3 min) and long (12 min) periods of adaptation on orientation shifts in A17 and area 18 (A18) neuronal populations by using cortical activity imaging (optical imaging).

A17 neurons' preferred orientations are not exclusively derived from direct feed-forward inputs [i.e. lateral geniculate nucleus (LGN)], because elicited responses are also influenced by local and long-range connections (Gilbert & Wiesel, 1989; Chavane *et al.*, 2011). Furthermore, extensive feedback loops from other cortical areas contribute to the setting of A17 neuronal tuning, even in the absence of any visual stimulation (Bullier *et al.*, 1988;

Correspondence: Stéphane Molotchnikoff, as above.

Received 6 February 2014, revised 7 April 2014, accepted 10 April 2014

Shibata *et al.*, 2011; Muckli & Petro, 2013). In particular, the cat A18 shows strong reciprocal connections with A17 (Symonds & Rosenquist, 1984; Salin *et al.*, 1995), which relay X geniculate cells' inputs to A18 (Freund *et al.*, 1985; Dreher *et al.*, 1992). In addition to structural connectivity, it has already been shown that these areas undergo functional interactions in orientation tuning, as inactivation of A17 changes the orientation sensitivity of A18 cells (Chabli *et al.*, 1998). Thus, recording adaptation influences in A17 and A18 simultaneously may contribute to further understanding of neuronal interactions and information processing within these areas.

Materials and methods

Animal preparation

Six anesthetised adult cats (*Felis catus*) of either sex, supplied by the Division of Animal Resources of the University of Montreal, were used. Experiments were carried out in accordance with the guidelines approved by the NIH in the USA, the Canadian Council on Animal Care and the Institutional Animal Care and Use Committee of University of Montréal (CDEA) regarding the care and use of animals for experimental procedures. The experimental protocols were approved by the CDEA.

Cats were first sedated with acepromazine maleate [1 mg/kg, intramuscular (i.m.), Atravet; Wyeth-Ayerst, Guelph, Ontario, Canada] and atropine sulfate (0.04 mg/kg, i.m., Atrosa; Rafter, Calgary, Alberta, Canada), and anesthetised with ketamine hydrochloride (25 mg/kg, i.m., Rogarsetic; Pfizer, Kirkland, Quebec, Canada). Anesthesia was sustained during surgery with isoflurane ventilation (2%, AErrane; Baxter, Toronto, Ontario, Canada). After surgery, cats were paralysed by perfusion of gallaminetriethiodide (40 mg, intravenous, Flaxedil; Sigma Chemical, St Louis, MO, USA), fixed in a stereotaxic apparatus, and artificially ventilated with O_2/N_2O (30 : 70) containing isoflurane (0.5%). Paralysis was maintained by perfusion of gallaminetriethiodide (10 mg/kg per h) in 5% dextrose lactated Ringer's nutritive solution.

A round chamber (15 mm in diameter) was fixed with dental cement (Jet; Lang Dental MFG, Chicago, IL, USA) above one hemisphere's A17 and A18 [antero-posterior −5 to 5, latero-medial 0 to −10, according to the Tusa *et al.* (1979) stereotaxic map; see Fig. 1A]. After craniotomy, the dura mater was removed, and the chamber was filled with mineral oil (viscosity, 150 mPa.s; Fluka, Sigma-Aldrich, Steinheim, Germany) and closed with a cover glass.

The pupils were dilated with atropine sulfate (1%, Isopto-Atropine; Alcon, Mississauga, Ontario, Canada), and the nictitating membranes were retracted with phenylephrine hydrochloride (2.5%, Mydfrin; Alcon). Contact lenses with artificial pupils (diameter, 5 mm; University of Montreal, Quebec, Canada) were placed on the cat's eyes to prevent the cornea from drying. The contralateral eye was covered with a mask.

Visual stimuli

An entire sequence of stimulation was ordered as follows: a control session directly followed by a 3-min or 12-min adaptation, a post-adaptation session, a 90-min period during which random dots of different contrasts were presented in full-screen to prevent the potential effects of visual deprivation (Watroba *et al.*, 2001), and a recovery session (Fig. 1B). Typically, control results were compared with post-adaptation and recovery results to estimate the effect of adaptation and de-adaptation processes, respectively.

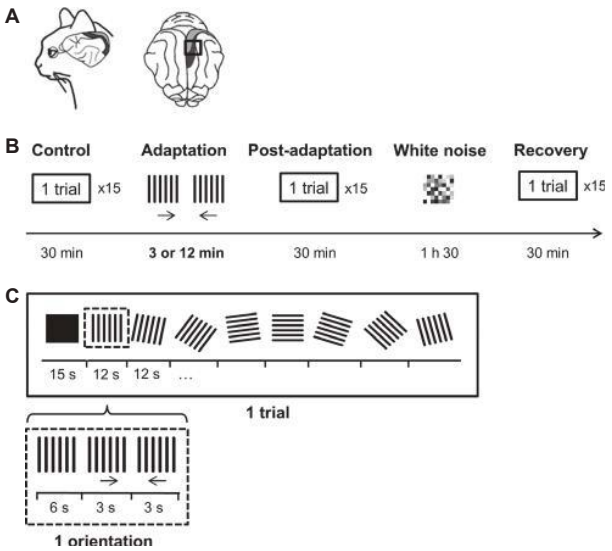

FIG. 1. Sequence of stimulus presentation. (A) Craniotomy location (bold square) on the cat stereotaxic map. A17 is shown in gray and A18 in dark. (B) Succession of all presented stimuli. The black square in B was repeated at least 15 times for each condition. (C) Stimulus sequence presented during one trial (inside the black rectangle). Stimulus details for the presentation of an orientation are framed in dashed square. Stimulus durations are indicated under the black line. Small horizontal black arrows under some gratings indicate the direction of the drift.

Achromatic gratings (contrast, 75%; generated by VSG software; Cambridge Research Systems, Rochester, UK), presented randomly (in order to avoid stimulus-order bias) with rotation in eight different orientations (0, 22.5, 45, 67.5, 90, 112.5, 135, and 167.5 °), were used as stimuli to obtain orientation maps in control, post-adaptation and recovery sessions (Fig. 1C, top). A spatial frequency of 0.3 cycles/degree was chosen to stimulate A17 and A18 equally (Tani *et al.*, 2012). Each trial started with the presentation of a black screen for 15 s, and this was followed by the presentation of every orientation (12 s). For each presented orientation spanning 12 s, the grating was kept stationary during the first 6 s to remove the cortical activity resulting from the stimulus onset, and this was followed by drifts to the left for the next 3 s and then to the right for the last 3 s to maximise cortical responses (Fig. 1C, bottom). The temporal frequency of the drift was set at 1 Hz. Although this temporal frequency is appropriate to elicit responses in A17 (Movshon *et al.*, 1978), A18 is sufficiently activated at this frequency to develop orientation maps. To average cortical responses for each orientation, 15 trials were performed.

The stimulus used for adaptation was a 90 ° grating (adapting orientation or adaptor) drifting alternatively in left and right directions during 3 min or 12 min of adaptation.

Visual stimuli were presented full-screen on a 21-inch monitor (Sony GDM-F520 Trinitron, Tokyo, Japan) placed at 57 cm from the cat's eyes.

Data acquisition

The cortex was illuminated with 630-nm light, because, at this wavelength, optimal cortical activation is reflected by light absorption (related to the oxygen saturation of hemoglobin) and light scattering (related to the synaptic transmission) (Cohen, 1973). Cortex images were captured with a CCD camera (Dalsa 1 M60P; Dalsa, Waterloo, Ontario, Canada), composed of two 50-mm f1.2 lenses arranged in

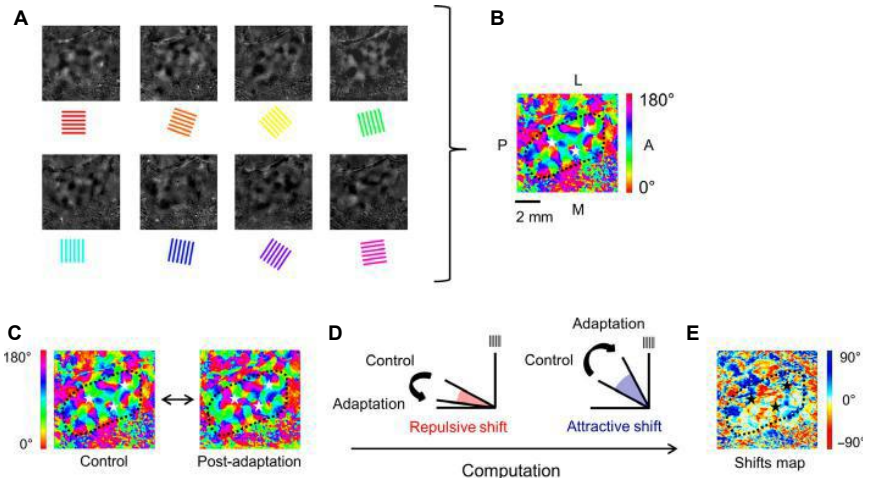

FIG. 2. Construction of maps. (A) Single condition maps obtained after denoising for each presented orientation (specified by colored gratings under images; colors are matched to the color scale in B). (B) Polar map resulting from the vector sum of maps in A. The color scale represents the pixels' preferred orientations. (C) Polar maps without intensity for control and post-adaptation. (D) Shift calculation from the polar representation of control and adaptation maps. The grating above the *y*-axis represents the adapting orientation (vertical, 90 °). (E) Shift map: the color scale represents the shift amplitude (as calculated in D; the red scale represents repulsive shifts, and the blue scale represents attractive shifts). The area of interest is delimited by a black dashed line. Black and white stars are position references. A, anterior; L, lateral; M, median; P, posterior.

tandem, and focused 500 μm below the cortical surface (corresponding approximately to the cat's cortical layer III). Images were digitised with Imager 3001 (Optical Imaging, Germantown, NY, USA), with a spatial resolution of 1024 × 1024 pixels (binned 2 × 2), and a temporal resolution of 20-ms frame duration. As the cortical activity causes light absorption, the areas activated by the presentation of one orientation appear darker on the picture taken by the camera, thus giving rise to black spots on denoised images (Fig. 2A).

For each orientation, recordings of the cortex were obtained for 3 s during the stationary stimulus and for 3 s during the drifting stimulus in either direction.

Data processing

Image analysis was performed with MATLAB programs (MathWorks, Natick, MA, USA).

Denoising

Thirty images were recorded for every orientation. As the last images showed more activity than the initial images, the average of the last 10 images (21–30) was divided by the average of the first 20 images (1–20). This calculation was performed to remove the non-specific activity in initial images, while preserving the specific activity recorded mostly in the last frames. Then, the generalised indicator function method (Yokoo *et al.*, 2001) was applied. In short, this method extracts the frames that account for as much of the signal as possible by using principal component analysis, and optimises the differences between signal and noise. For each orientation, a single condition map was generated by summing the resulting image for this orientation across all trials. Black spots corresponding to cortical activity are clearly visible on the maps obtained for each presented orientation (Fig. 2A).

Polar maps

Each pixel of a single condition map was associated with a vector with a magnitude corresponding to the pixel value (i.e. a decimal number corresponding to the amount of light received by the camera), and the direction representing the presented orientation. The sum of the pixel–vectors situated at the same position on the map was calculated across all single condition maps. The resulting direction represents the preferred orientation of each pixel, and the resulting magnitude corresponds to the theoretical response intensity for this orientation. Polar maps of the preferred orientation of pixels and were generated for each condition (Fig. 2B).

Orientation maps

On polar maps, orientations were represented on a continuous scale. To statistically compare pixel orientations, we grouped them to match the eight presented orientations (Fig. 3A). As they were separated by 22.5 °, orientations falling within the range (presented orientation ± 11.25 °) were grouped. For instance, all pixel values within (33.75; 56.25) were replaced by 45 °. Examples of orientation maps for control, post-adaptation and recovery conditions for two areas located in A17 and in A18 are shown in Fig. 3B. It should be noted that orientation domains vary with adaptation.

Shift amplitude and categorisation

To quantify changes in pixel orientation between any two polar maps relative to the adapting orientation, a shift was calculated for the corresponding pixel (pair) on each map as follows:

$$s = \min(|\, p_1 - a \,|, |\, 180 - p_1 + a \,|) - \min(|\, p_2 - a \,|, |\, 180 - p_2 + a \,|) \quad (1)$$

where s is the shift amplitude associated with the pair of pixels, p_1 is the pixel direction in the first map, p_2 is the direction of the same pixel in the second map, and a is the adapting orientation. If s is positive, the difference between p_1 and a is larger than the difference between p_2 and a, which means that the pixel in the second map is closer to the adapting orientation than that in the first map. This type of shift is classified as attractive. On

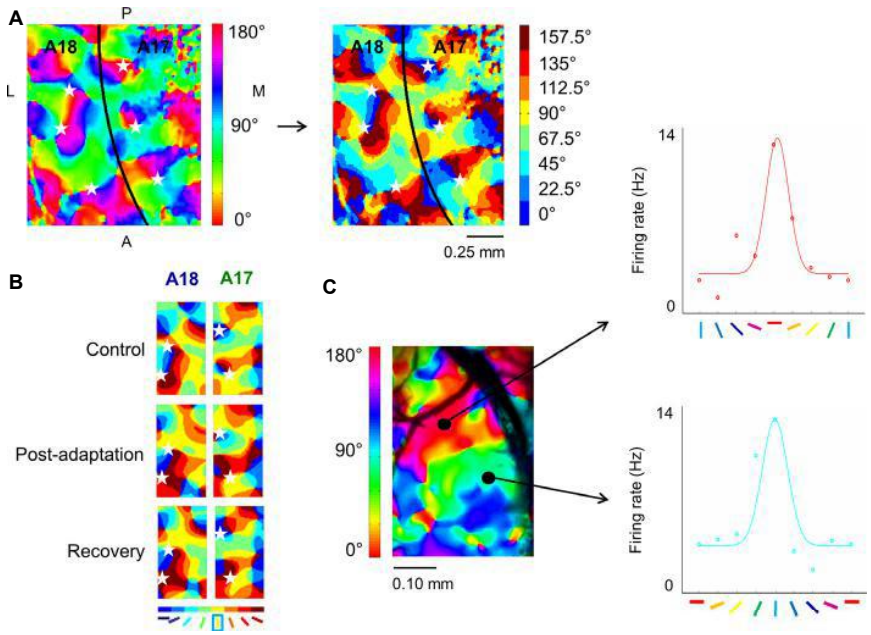

FIG. 3. Polar maps and electrophysiology. (A) Pixel orientations of the polar maps (left) are regrouped into the eight presented orientations (right). Selected locations in A17 and A18 are shown in B. (B) Changes in pinwheel organisation at the same locations in A17 and A18 (columns) in the control (upper row), following adaptation (middle row) and recovery (lower row) conditions. The orientation inside the blue square under the colored bar indicates the adapting orientation. (C) Correspondence between orientation maps and electrophysiological multi-unit recordings. Left: positions of microelectrodes (black points) are indicated on the polar map. Associated tuning curves are presented on the right (R = 0.80, red curve; R = 0.64, blue curve). White stars are position references. A, anterior; L, lateral; M, median; P, posterior.

the contrary, if s is negative, the pixel in the second map is further from the adapting orientation than that in the first map, and the shift is categorised as repulsive (see Fig. 2C,D for an intuitive representation of shift categorisation, and Fig. 2E as an example of a shift-amplitude map). As one pixel can be associated with two angles (for instance, 0 and 180 ° represent the same stimulus), in such cases we took the minimal angle with respect to the adaptor. Shift amplitudes of <5 ° were considered to be statistically insignificant ($P < 0.01$, t-test) and were not categorised.

Statistics

The results for 3-min and 12-min adaptation were averaged over four and six cats, respectively. Because orientations (represented on the same map) and conditions (control, post-adaptation and recovery maps derived from the same cat) are dependent variables, we used repeated measure ANOVAS (to compare orientations and conditions) along with *post hoc* Tukey or Dunnett multiple comparison tests and paired two-tailed t-tests.

The Pearson coefficient was calculated to quantify the 'goodness of curves' fits and the correlation between data matrices. To assess the significance of the difference between two correlation coefficients, we constructed 95% confidence intervals with the Fisher r-to-z transformation.

Electrophysiological control

In a few experiments, conventional electrophysiological recordings were performed after adaptation to confirm the orientation maps and the optimal orientation as derived from multicellular tuning curves. The protocol is based on the study of Bachatene *et al.* (2013).

First, optical imaging was performed and a polar map was computed (see above). The polar map was overlaid with an image of cortical blood vessels taken with the optical imaging camera. The recording wavelength for the camera was set at 546 nm for better visualisation of blood vessels (Grinvald *et al.*, 1999). Thereafter, two well-defined orientation domains were chosen for electrophysiological recordings in each area. A tungsten microelectrode was positioned within each selected domain with reference to the blood vessel pattern. Tuning curves were calculated by the use of multi-unit spike trains accumulated during data acquisition (the spontaneous activity was subtracted), and modeled with a Gaussian-like function as described below:

$$y = y_o + \frac{A}{w\sqrt{\frac{\pi}{2}}} \cdot e^{-2\left(\frac{x-\mu}{w}\right)} \quad (2)$$

where y_o is the offset, A is the area of the Gaussian, w is the standard deviation, and μ is the center of the Gaussian.

An example of electrophysiological control is shown in Fig. 3C, where two electrodes were placed in 0 and 90 ° domains corresponding to red and light blue areas, respectively, on the polar map (on the left). We found that, in these areas, cells were globally tuned to 0 and 90 °, respectively (see associated tuning curves in Fig. 3C, right), which coincide with optical imaging data.

Results

To compare adaptation influences in A17 and A18, orientation and intensity maps were created before and after adaptation procedures. Recovery maps were generated 90 min after the end of adaptation. As it has previously been reported that neurons recover their original preferred selectivity at a rate 12 times slower than the adaptation

rate (Dragoi *et al.*, 2000; Nemri *et al.*, 2009), we expected that most neurons would recover their original preferred selectivity after 3 min of adaptation, and two-thirds of neurons after 12 min of adaptation. Typical examples of control, post-adaptation and recovery orientation maps are shown in Fig. 3B.

Orientation proportions remain the same post-adaptation

The proportion of pixels for each orientation, determined from orientation maps, is shown in Fig. 4. Pixel-proportion averages (or pixel frequencies as we term them, normalised to 1 on the *y*-axis, 1 corresponding to 100%) were determined for A17 and A18 under all experimental conditions, following 3 min or 12 min of adaptation. We found a classic slight bias favoring the vertical orientation (in A18, $P < 0.01$ for recovery after 3 min of adaptation, $P < 0.05$ for post-adaptation and recovery after 12 min of adaptation; in A17, $P < 0.05$ for post-adaptation, and $P < 0.01$ for recovery after 12 min of adaptation; ANOVA and Dunnett test). This is probably attributable to a neuronal preference for cardinal orientations in the cat A17 (Wang *et al.*, 2003; Huang *et al.*, 2006; Ghisovan *et al.*, 2009). Moreover, there were no significant differences in the proportions of pixels representing orientations between control, adaptation and recovery conditions ($P > 0.06$; ANOVA). It may be worth underlining that the distribution shows the preferred orientation of pixels at a given time, and does not provide information about pixel-wise changes that may have occurred because of adaptation. We therefore analysed pixel shifts between control and post-adaptation maps.

The direction of neuronal orientation shifts depends on the remoteness of the original preferred orientation from the adaptor

Thereafter, we measured the proportion of pixels that shifted their orientation in either direction, and the magnitude of these shifts, after 3 min and 12 min of adaptation. Figure 5 illustrates these data, grouped into orientation classes of 22.5°. In each histogram, attractive shifts are represented by blue bars, and repulsive shifts are represented by red bars. The computation for shift-direction categorisation is explained in Materials and methods.

The proportions and magnitudes of shifts were systematically and significantly different across orientations ($P < 0.003$; ANOVA). In both adaptation protocols (3 min and 12 min), the proportions and amplitudes of repulsive transfers were higher for orientations close to the adapting orientation ($P < 0.01$ between 0 and 90° in all cases; Tukey test). For instance, after 3 min of adaptation in A17 (Fig. 5A, left), pixels whose initial preferred orientation was closer to the adaptor showed a higher rate of repulsive shifts (top). In addition, these repulsive shifts occurred with higher magnitudes (bottom).

For attractive shifts, the distribution for orientation proportions and amplitude of shifts showed an opposite pattern. In both areas, for orientations close to the adaptor (90°), the proportion of pixels that showed an attractive direction was smaller. The number of pixels showing attractive shifts increased (Fig. 5A,B, top) with the gap between initially preferred orientations and the adaptor. An analogous U-shaped distribution was computed for shift magnitude (Fig. 5A,B, bottom). In A17, after 3 min of adaptation (Fig. 5A, left), shift proportions and amplitudes changed from one orientation to another in a similar fashion ($P < 0.0001$; ANOVA). Both the proportion of shifted pixels and the amplitude were significantly increased at 90° with respect to the flank orientations (i.e. 0, 22.5, 45 and 157.5° for shift proportions; 0, 22.5 and 157.5° for shift amplitudes; $P < 0.05$; Tukey test).

Additionally, at the flanks and the adapting orientation, the pixel proportions and shift amplitudes were significantly different for attractive and repulsive shifts ($P < 0.03$ at 0 and 90°; *t*-test). This supports the idea that shift behavior depends on the orientation distance between the original preferred orientation and the adaptor. However, for both attractive and repulsive shifts, the differences in amplitude of shifts and pixel proportions was insignificant between

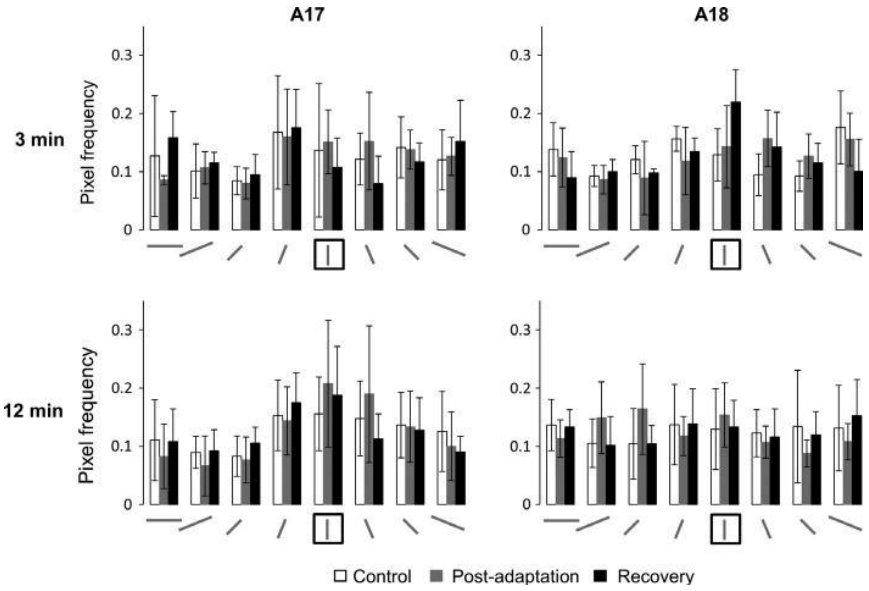

FIG. 4. Orientation representation across conditions. The first row and first column represent 3 min of adaptation and A17 location, respectively; the second row and the second column represent 12 min of adaptation and A18 location, respectively. The average pixel frequencies for each orientation are shown for control, adaptation and recovery conditions on the *y*-axis. The oriented bar inside the bold squares indicates the adapting orientation; error bars represent the standard deviation.

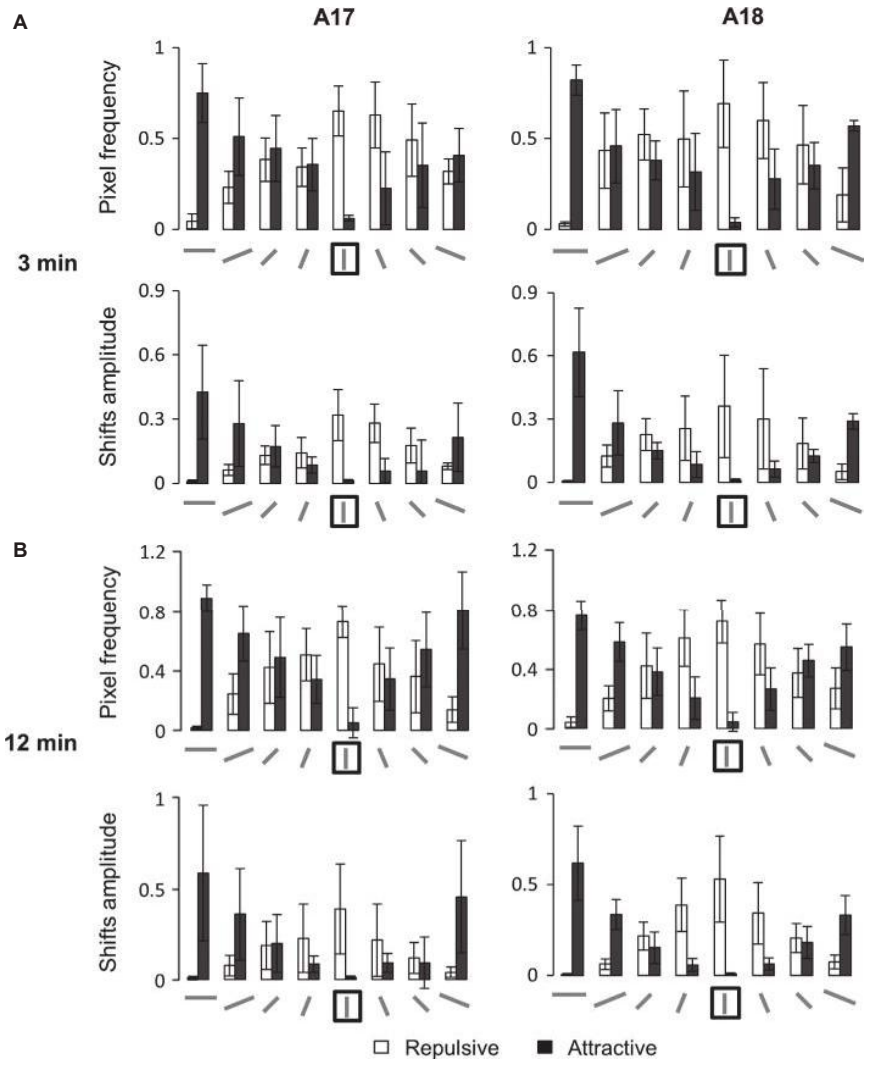

FIG. 5. Pixel frequencies of orientation distribution and magnitude of shifts. The first column represents A17 location, and the second column represents A18 location. (A) Average frequencies of attractive and repulsive shifts for each control orientation (upper row) and average amplitudes of attractive and repulsive shifts for each control orientation (bottom row) for 3 min of adaptation. (B) Average frequencies of attractive and repulsive shifts for each control orientation (upper row), and average amplitudes of attractive and repulsive shifts for each control orientation (bottom row) for 12 min of adaptation. The oriented bar inside the bold squares indicates the adapting orientation. Error bars represent the standard deviation.

A17 and A18 ($P > 0.1$ for all orientations, *t*-test). We conclude that, in both areas, adaptation affects the average shift amplitude and pixel proportion in a similar manner.

The same behavior was observed after 12 min of adaptation (Fig. 5B); that is, no significant difference was found, indicating that duration of adaptation may not influence adaptation mechanisms.

Orientation-map modifications are greater in A18 than in A17

The matrices in Fig. 6A show the modification of pixel orientation induced by adaptation. For example, we chose all pixels corresponding to 45 ° orientation in the post-adaptation orientation map. Then, we selected the pixels situated at the same locations in the control orientation map, and noted the initial orientation of these particular pixels. Thereafter, the proportion of pixels that shifted their orientation to the same value (e.g. from 45 to 65 °) in each selected orientation was calculated. These proportions are represented in a matrix, wherein the rows represent the orientation on the post-adaptation map, and the columns represent orientation on control maps. Matrices can be inferred in the following way: for example, in the matrix corresponding to 3 min of adaptation in A17 (top left), the pixels post-adaptation at 0 ° (first row of the matrix; each colored square represents the pixel proportion at the control orientation) were originally distributed (prior to adaptation) as follows: 0.32 at 0 ° (yellow square), 0.14 at 22.5 °, 0.06 at 45 °, 0.03 at 67.5 °, 0.03 at 90 °, 0.07 at 112.5 °, 0.1 at 135 °, and 0.25 at 157.5 ° (see the color bar in Fig. 6A for proportions). The matrices underscore a general trend of shift amplitudes: if the majority of pixels are distributed close to the diagonal (i.e. the post-adaptation orientation), this indicates that shifts are mostly small; conversely, if pixels are more evenly distributed, this implies that shifts can be greater or smaller irrespective of initial orientation, leading to more variability in shift amplitudes. Notably, the highest proportions (>0.2, green on the figure) are distributed along the diagonal of the matrix. This unequivocal diagonal

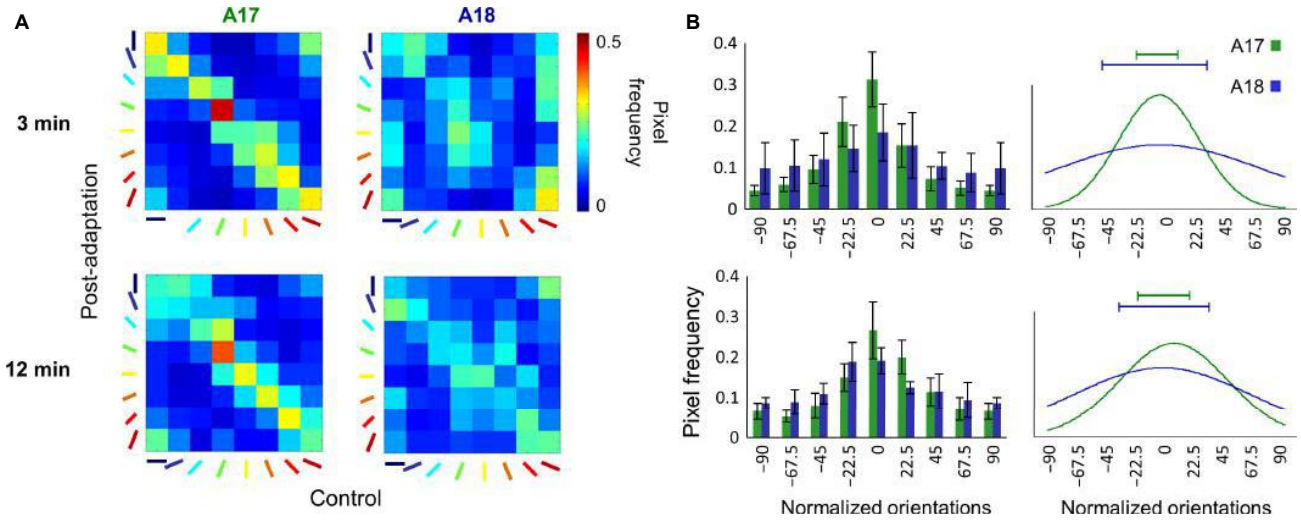

FIG. 6. Variability of shift amplitudes in A17 and A18. The first row represents 3 min of adaptation, and the second row represents 12 min of adaptation. (A) The first column represents A17 location, and the second column represents A18 location. In each matrix, the columns represent the frequency of pixels at all control orientations, and rows represent new orientations after adaptation. (B) Left: average of pixel frequencies for every control orientation, i.e. for each column in A. Orientations are normalised: zero always corresponds to the post-adaptation orientation (matrix rows). Error bars represent the standard deviation. Right: Gaussian fits for each distribution. Interval bars above the curves indicate the standard deviation. $R = 0.87$ and $R = 0.81$ for A17 at 3 min and 12 min of adaptation, respectively. $R = 0.67$ and $R = 0.69$ for A18 at 3 min and 12 min of adaptation, respectively.

distribution indicates that, following adaptation, a substantial population of cells maintains orientation selectivity that is approximately the same as that recorded in the control condition.

Furthermore, correlation of 3-min and 12-min adaptation matrices in A17 showed a close similarity ($R = 0.82$), implying that the redistribution of shift amplitudes was not greatly affected by the duration of adaptation in A17. Interestingly, in A18 (Fig. 6A right), such pronounced diagonal distribution was almost completely absent for short adaptation (correlation analysis showed that A17 and A18 matrices for 3 min of adaptation were very different; $R = 0.46$), and was even more dispersed for long adaptation (12 min). Indeed, the Pearson coefficient between matrices for 3 min and 12 min of adaptation in A18 ($R = 0.53$) was significantly lower ($P < 0.05$, Fisher transformation; see Materials and methods) than the Pearson coefficient in A17 ($R = 0.82$), indicating that effect of adaptation duration on shift amplitudes was stronger in A18. Additionally, in A18, the highest proportions of pixels were not evenly distributed along the diagonal, unlike in A17. For example, in the case of 3 min of adaptation, among neurons that were selective to 45 ° orientation post-adaptation, 23% of them were tuned to 157.5 ° prior to adaptation. This difference indicates that, in A18, the initial and post-adaptation orientations can be very distant.

To illustrate these observations in depth, the averaged distribution of pixels is shown in both areas (Fig. 6B). In these histograms, the distributions (matrices lines) were first normalised by attributing 0 ° to the post-adaptation orientation, and the average was then calculated over columns (Fig. 6B, left). Thereafter, Gaussian curves were fitted to the data (Fig. 6B, right). In line with the results of the matrices (Fig. 6A), the mean distribution in A18 (blue curve), as expected, was flatter than in A17 (green curve) for 3 min or 12 min of adaptation. Furthermore, for 3 min of adaptation, the variance in shift magnitude was significantly higher in A18 ($P < 0.01$ for 3 min, $P = 0.13$ for 12 min; Fisher test) than in A17. Thus, it appears that cells in A18 are more sensitive to adaptation than cells in A17.

In summary, Fig. 6 demonstrates that the variance in shift amplitudes was larger in A18 than in A17. However, Fig. 5 shows that, on average, the amplitudes of attractive and repulsive shifts were similar in A17 and A18. These results may seem contradictory, but it is important to underline that shift amplitudes were calculated differently in both cases: in Fig. 6, pixel shifts were established relative to post-adaptation orientation, whereas in Fig. 5, shifts were segregated into attractive and repulsive relative to the adapting orientation. Furthermore, the increase in shift-amplitude variance (although significant for 3 min of adaptation) seems much too small to affect the overall average of shift magnitudes in A17 and A18 (mean shift magnitudes were not significantly different in A17 and A18; $P = 0.57$ and $P = 0.56$ for 3 min and 12 min of adaptation, respectively).

Altogether, this leads us to conclude that adaptation affects A17 and A18 in similar ways, but produces more variable effects in A18.

Discussion

In the present study, we explored the simultaneous effects of short (3 min) and long (12 min) adaptations on orientation maps in A17 and A18. In both areas, the distribution of pixels shows that, after adaptation, the orientation selectivity of the neuronal population is modified. Neurons that originally preferred orientations distant from the adaptor showed high-amplitude attractive shifts, whereas, neurons originally tuned to orientations close to the adaptor showed repulsive shifts with higher amplitude. There were no differences in overall proportions of attractive and repulsive shifts for short or long adaptation duration. That is, globally, the proportion of pixels post-adaption remained balanced. In addition, the higher variability in A18 may suggest that this area is potentially more flexible than A17 in responding to changes induced by adaptation.

Methodological considerations

Stimulation preferences in A17 and A18

A17 and A18 were simultaneously stimulated with a spatial frequency of 0.3 cycles/degree. Although this spatial frequency is non-optimal for both A17 and A18, it allows simultaneous generation of

responses in both areas (Issa *et al.*, 2000; Tani *et al.*, 2012). The temporal frequency (1 Hz) is also non-optimal for A18, but sufficient to excite this area. It has been found that orientation tuning and temporal frequencies are unrelated (Moore *et al.*, 2005). Furthermore, orientation maps established at different spatial frequencies have revealed that pixel orientations do not change but become less responsive for non-optimal spatial frequencies (Ribot *et al.*, 2013). As all results are derived from orientation maps, and not from response intensity maps, we conclude that differential activity between A17 and A18 should not affect our results. It can be argued that non-optimal activation of neurons during adaptation moderates the orientation-map variation. However, we emphasise that adaptation results when a non-optimal stimulus is presented for a certain period of time. At the single-cell level, adaptation is always performed with orientation gratings, spatial frequencies or contrast levels that elicit poor responses in control conditions (Ohzawa *et al.*, 1982; Bouchard *et al.*, 2008; Bachatene *et al.*, 2013).

Adaptation protocol duration

In our experiments, continuous adaptation was performed for several minutes. Some authors argue that this kind of adaptation does not emulate natural conditions, but employs stimuli of very short durations presented frequently to approach the conditions of natural visual fixations (Müller *et al.*, 1999; Patterson *et al.*, 2013). However, long adaptation is more potent in inducing plasticity and, consequently, stronger variations in neuronal responses. Others consider that response modulations of preferred orientations post-adaptation reveal after-effects (Benucci *et al.*, 2013). However, adaptation effects are constrained approximately around the original preferred orientation and the newly acquired orientation – responses at the original preferred orientation decline, while cells start responding to the novel optimal orientation with increased discharges (Dragoi *et al.*, 2000; Ghisovan *et al.*, 2009; Nemri *et al.*, 2009; Jeyabalaratnam *et al.*, 2013). Such a dual effect is difficult to reconcile with global after-effects. As after-effects are generally rapid (almost immediate), they are unlikely to produce the described changes in orientation selectivity following adaptation. As neuronal connections are dynamic, adaptation may lead to a transition of the neuronal network to a different equilibrium, reflecting new background conditions as a consequence of adaptation. For this reason, we believe that adaptive processes can be recorded either during or after adaptation.

Bias caused by map instability

Our results are based on pixel shifts between control and post-adaptation maps. Therefore, it is important that orientation maps remain stable over time. Otherwise, a fraction of shifts may result from random variations in pixel orientations, introducing noise into the results. As various studies have shown that maps are stable during development (Chapman *et al.*, 1996; Gödecke *et al.*, 1997) and even for as long as 1 year (Shtoyerman *et al.*, 2000), we may reasonably assume that shifts are not attributable to instability in maps. Furthermore, the dual and opposite (almost mirror-like) shifts in pixel orientation depending upon the gap between the original and adapting orientations argue against random fluctuation of orientations.

It also has to be noted that, in our experiment, shifts between control and post-adaptation maps are equivalent to shifts between control and recovery maps. It has been shown that the rate of recovery is 11.9 times slower than the rate of adaptation (Dragoi *et al.*, 2000; Nemri *et al.*, 2009). In Nemri *et al.* (2009), only 50% of neurons recovered their original orientation 90 min after 12 min of adaptation. We suppose that our recovery rate is not sufficient to induce significant differences in shifts between adaptation and recovery maps. In addition, successive adaptations modified the strength of response to the preferred orientation or spatial frequency, indicating that cells keep a trace of previous adaptation (Ghisovan *et al.*, 2008; Marshansky *et al.*, 2011). It suggests that adaptation generates structural modifications of cells, making it difficult for them to recover.

Possible functional mechanisms

Attractive and repulsive shifts

In mice, a dendritic branch of a single neuron receives connections from cells responding to different orientations (Jia *et al.*, 2010). On the same grounds, if a cat's cortical cells have a similar organisation – which is supported by studies showing that local connections are established with adjacent neurons with different orientation tunings (Buzás *et al.*, 2006; Sato *et al.*, 2012) – then it is reasonable to assume that a neuron's newly acquired preferred orientation is a consequence of the recalibrated balance between synaptic clusters (Bachatene *et al.*, 2013). Thus, during adaptation, the synapses of neurons originally excited by the adaptor are weakened, allowing other connections matching remote orientations to take over, leading to repulsive shifts. The above interpretations have been corroborated by several studies that reported a decrease in firing rate after adaptation in response to an adaptor (Maffei *et al.*, 1973; Vautin & Berkley, 1977; Wang *et al.*, 2010; Patterson *et al.*, 2013). Moreover, Dragoi *et al.* (2000) and Benucci *et al.* (2013) have found that the suppression of neuronal responses is stronger for orientations close to the adaptor, whereas the responses of neurons for orientations distant from the adaptor are facilitated. On the other hand, adaptation can also reinforce synapses activated by the adaptor, thereby inducing attractive shifts (Ghisovan *et al.*, 2008; Marshansky *et al.*, 2011; Bachatene *et al.*, 2012, 2013).

Previous studies (Müller *et al.*, 1999; Dragoi *et al.*, 2000; Felsen *et al.*, 2002; Ghisovan *et al.*, 2009) have shown that, for short adaptation durations (<6 min), response suppression leads to repulsive shifts. As the adaptation duration increases, cell responses to the adapting orientation are facilitated. We did not find any correlation between the duration of adaptation and the direction of shifts. A possible explanation is that we recorded global cortical activity, and not only firing of single cells. During intracellular recordings, adaptation induces tonic somatic hyperpolarisation without changes in synaptic inputs (Carandini & Ferster, 1997). Thus, modulation of firing rate can be screened among the large sub-threshold membrane potential variations and may be revealed by intrinsic imaging.

Interaction between A17 and A18

We also found that shift-amplitude variability is larger in A18. This may be attributable to differences in the connections of A17 and A18. Indeed, although both areas have extensive reciprocal connections, A18 neurons additionally receive inputs from Y geniculate cells (Holländer & Vanegas, 1977; Tani *et al.*, 2012). Both X and Y cells have been shown to be selective with regard to orientation (Hochstein & Shapley, 1976a; Suematsu *et al.*, 2012). However, Y cells present a more complex receptive field than X cells (Hochstein & Shapley, 1976b; Bullier & Norton, 1979), eliciting non-linear responses for contrast, spatial frequencies, and orientation tuning

(Hochstein & Shapley, 1976a; Soodak *et al.*, 1987). Thus, the differential responses to orientation of X and Y cells may induce differences in tuning in A17 and A18. Nevertheless, there is no proven demonstration of the involvement of Y cells in orientation detection in cats (Dreher *et al.*, 1992). Thus, the involvement of the LGN in A18 variability remains unclear.

The gating role of feedback connections may also account for this variability. This mechanism leads to selection of relevant inputs from the sea of LGN inputs (Desimone, 1998; Harris, 2012; Luczak *et al.*, 2013; Muckli & Petro, 2013) through excitatory connections from the LGN that transiently facilitate specific evoked neuronal firing in primary sensory areas (Larkum, 2013), or periodic transient inhibitory connections suppressing neuronal responses by hyperpolarising cortical cells. It has been shown that A18 modulates A17 responses, either by enhancing or by diminishing neuronal firing rates, without drastically changing their orientation or velocity tuning (Martinez-Conde *et al.*, 1999). Thus, A17 may be less prone to plastic modifications than A18, in that A17 outputs are 'gated' by A18 and other cortical areas.

Moreover, the functional properties of A18 cells' receptive fields (temporal and spatial frequency) are suggestive of a large axonal convergence of X and Y inputs (Bisti *et al.*, 1985; Dreher *et al.*, 1992).

Overall, such an organisation may contribute to an increase in the variability of A18 responses, which, in turn, makes A18 cells more susceptible to adaptation.

Adaptation mechanisms in environment learning

Adaptation may be related to learning of recurrent visual features (Ghisovan *et al.*, 2008). When an object remains unchanged for a long period or is applied repetitively (in our case, the adapting orientation), information corresponding to neurons responding to this object is no longer relevant. As a result, the response of these neurons decreases (thus leading to repulsive shifts), most probably for two reasons. First, a majority of neurons become more sensitive to new objects (in our case, other orientations or properties such as color and contrast) (Neitz *et al.*, 2002; Kwon *et al.*, 2009; Zhang *et al.*, 2009). A minority continue to respond to the original preferred stimulus; however, the firing rate of the neurons decreases. This decrease in neuronal firing compensates for increased synchronous activity between neurons (Wang *et al.*, 2010; Hansen & Dragoi, 2011). On the other hand, neurons that initially did not respond to the unchanged object tend to 'learn' it; that is, they respond more when this feature is continuously presented within their receptive field. Indeed, a second episode of adaptation, carried out after >1 h of the first adaptation, strengthens the attractive shift magnitude (Ghisovan *et al.*, 2008; Marshansky *et al.*, 2011). However, this response, in turn, could be suppressed if it became too strong. Thus, the perception of orientation may result from the constant equilibrium between neuronal connections (Webster, 2011; Maya-Vetencourt & Origlia, 2012).

Conclusions

The shifts in preferred orientations are largely dependent on the original preferred orientation in relation to the adaptor orientation: attractive shifts mainly occur away from the adaptor, whereas repulsive shifts mainly occur close to the adaptor. We found that adaptation affects A17 and A18 in the same manner. However, shift magnitudes in A18 show more variability, suggesting that A17 is less plastic than A18.

Acknowledgements

This study was supported by grants to S. Molotchnikoff (NSERC and FQRNT). We thank Jérôme Ribot for his expert advice on optical imaging analysis and for helpful comments, Martin Villeneuve for his help with optical imaging experiments, and Philippe Cattan for useful comments on the manuscript.

Abbreviations

A17, area 17; A18, area 18; i.m., intramuscular; LGN, lateral geniculate nucleus.

References

Bachatene, L., Bharmauria, V., Rouat, J. & Molotchnikoff, S. (2012) Adaptation-induced plasticity and spike waveforms in cat visual cortex. *NeuroReport*, **23**, 88–92.

Bachatene, L., Bharmauria, V., Cattan, S. & Molotchnikoff, S. (2013) Fluoxetine and serotonin facilitate attractive-adaptation-induced orientation plasticity in adult cat visual cortex. *Eur. J. Neurosci.*, **38**, 2065–2077.

Benucci, A., Saleem, A.B. & Carandini, M. (2013) Adaptation maintains population homeostasis in primary visual cortex. *Nat. Neurosci.*, **16**, 724–729.

Bisti, S., Carmignoto, G., Galli, L. & Maffei, L. (1985) Spatial-frequency characteristics of neurones of area 18 in the cat: dependence on the velocity of the visual stimulus. *J. Physiol.*, **359**, 259–268.

Bouchard, M., Gillet, P.-C., Shumikhina, S. & Molotchnikoff, S. (2008) Adaptation changes the spatial frequency tuning of adult cat visual cortex neurons. *Exp. Brain Res.*, **188**, 289–303.

Bullier, J. & Norton, T.T. (1979) Comparison of receptive-field properties of X and Y ganglion cells with X and Y lateral geniculate cells in the cat. *J. Neurophysiol.*, **42**, 274–291.

Bullier, J., McCourt, M.E. & Henry, G.H. (1988) Physiological studies on the feedback connection to the striate cortex from cortical areas 18 and 19 of the cat. *Exp. Brain Res.*, **70**, 90–98.

Buzás, P., Kovács, K., Ferecskó, A.S., Budd, J.M.L., Eysel, U.T. & Kisvárday, Z.F. (2006) Model-based analysis of excitatory lateral connections in the visual cortex. *J. Comp. Neurol.*, **499**, 861–881.

Carandini, M. & Ferster, D. (1997) A tonic hyperpolarization underlying contrast adaptation in cat visual cortex. *Science*, **276**, 949–952.

Chabli, A., Ruan, D.Y. & Molotchnikoff, S. (1998) Influences of area 17 on neuronal activity of simple and complex cells of area 18 in cats. *Neuroscience*, **84**, 685–698.

Chapman, B., Stryker, M.P. & Bonhoeffer, T. (1996) Development of orientation preference maps in ferret primary visual cortex. *J. Neurosci.*, **16**, 6443–6453.

Chavane, F., Sharon, D., Jancke, D., Marre, O., Frégnac, Y. & Grinvald, A. (2011) Lateral spread of orientation selectivity in V1 is controlled by intracortical cooperativity. *Front. Syst. Neurosci.*, **5**, 1–26.

Cohen, L.B. (1973) Changes in neuron structure during action potential propagation and synaptic transmission. *Physiol. Rev.*, **53**, 373–418.

De Jong, M.C., Kourtzi, Z. & van Ee, R. (2012) Perceptual experience modulates cortical circuits involved in visual awareness. *Eur. J. Neurosci.*, **36**, 3718–3731.

Desimone, R. (1998) Visual attention mediated by biased competition in extrastriate visual cortex. *Philos. T. Roy. Soc. B.*, **353**, 1245–1255.

Dragoi, V., Sharma, J. & Sur, M. (2000) Adaptation-induced plasticity of orientation tuning in adult visual cortex. *Neuron*, **28**, 287–298.

Dreher, B., Michalski, A., Cleland, B.G. & Burke, W. (1992) Effects of selective pressure block of Y-type optic nerve fibers on the receptive-field properties of neurons in area 18 of the visual cortex of the cat. *Visual Neurosci.*, **9**, 65–78.

Felsen, G., Shen, Y., Yao, H., Spor, G., Li, C. & Dan, Y. (2002) Dynamic modification of cortical orientation tuning mediated by recurrent connections. *Neuron*, **36**, 945–954.

Freund, T.F., Martin, K.A. & Whitteridge, D. (1985) Innervation of cat visual areas 17 and 18 by physiologically identified X- and Y-type thalamic afferents. I. Arborization patterns and quantitative distribution of postsynaptic elements. *J. Comp. Neurol.*, **242**, 263–274.

Ghisovan, N., Nemri, A., Shumikhina, S. & Molotchnikoff, S. (2008) Visual cells remember earlier applied target: plasticity of orientation selectivity. *PLoS ONE*, **3**, e3689.

Ghisovan, N., Nemri, A., Shumikhina, S. & Molotchnikoff, S. (2009) Long adaptation reveals mostly attractive shifts of orientation tuning in cat primary visual cortex. *Neuroscience*, **164**, 1274–1283.
Gilbert, C.D. & Wiesel, T.N. (1989) Columnar specificity of intrinsic horizontal and corticocortical connections in cat visual cortex. *J. Neurosci.*, **9**, 2432–2442.
Gödecke, L., Kim, D.-S., Bonhoeffer, T. & Singer, W. (1997) Development of orientation preference maps in area 18 of kitten visual cortex. *Eur. J. Neurosci.*, **9**, 1754–1762.
Grinvald, A., Shoham, D., Shmuel, A., Glaser, D., Vanzetta, I., Shtoyerman, E., Slovin, H., Wijnbergen, C., Hildesheim, R. & Arieli, A. (1999) In-vivo optical imaging of cortical architecture and dynamics. In Johansson, H. & Windhorst, U. (Eds), *Modern Techniques in Neuroscience Research*. Springer, Berlin Heidelberg, pp. 893–969.
Grossberg, S. (2013) Adaptive resonance theory: how a brain learns to consciously attend, learn, and recognize a changing world. *Neural Networks*, **37**, 1–47.
Hansen, B.J. & Dragoi, V. (2011) Adaptation-induced synchronization in laminar cortical circuits. *Proc. Natl. Acad. Sci. USA*, **108**, 10720–10725.
Harris, K.D. (2012) Cell assemblies of the superficial cortex. *Neuron*, **76**, 263–265.
Harris, J.P. & Calvert, J.E. (1989) Contrast, spatial frequency and test duration effects on the tilt aftereffect: implications for underlying mechanisms. *Vision Res.*, **29**, 129–135.
Hebb, D.O. (1949) *The Organization of Behavior: A Neuropsychological Theory*. Wiley, New York.
Hochstein, S. & Shapley, R.M. (1976a) Linear and nonlinear spatial subunits in Y cat retinal ganglion cells. *J. Physiol.*, **262**, 265–284.
Hochstein, S. & Shapley, R.M. (1976b) Quantitative analysis of retinal ganglion cell classifications. *J. Physiol.*, **262**, 237–264.
Holländer, H. & Vanegas, H. (1977) The projection from the lateral geniculate nucleus onto the visual cortex in the cat. A quantitative study with horseradish-peroxidase. *J. Comp. Neurol.*, **173**, 519–536.
Huang, L., Shou, T., Chen, X., Yu, H., Sun, C. & Liang, Z. (2006) Slab-like functional architecture of higher order cortical area 21a showing oblique effect of orientation preference in the cat. *NeuroImage*, **32**, 1365–1374.
Issa, N.P., Trepel, C. & Stryker, M.P. (2000) Spatial frequency maps in cat visual cortex. *J. Neurosci.*, **20**, 8504–8514.
Jeyabalaratnam, J., Bharmauria, V., Bachatene, L., Cattan, S., Angers, A. & Molotchnikoff, S. (2013) Adaptation shifts preferred orientation of tuning curve in the mouse visual cortex. *PLoS ONE*, **8**, e64294.
Jia, H., Rochefort, N.L., Chen, X. & Konnerth, A. (2010) Dendritic organization of sensory input to cortical neurons *in vivo*. *Nature*, **464**, 1307–1312.
Kohler, I. (1962) Experiments with goggles. *Sci. Am.*, **206**, 62–86.
Kohn, A. (2007) Visual adaptation: physiology, mechanisms, and functional benefits. *J. Neurophysiol.*, **97**, 3155–3164.
Kwon, M., Legge, G.E., Fang, F., Cheong, A.M.Y. & He, S. (2009) Adaptive changes in visual cortex following prolonged contrast reduction. *J. Vision*, **9**, 1–16.
Larkum, M.E. (2013) The yin and yang of cortical layer 1. *Nat. Neurosci.*, **16**, 114–115.
Lindquist, K.A. & Barrett, L.F. (2012) A functional architecture of the human brain: emerging insights from the science of emotion. *Trends Cogn. Sci.*, **16**, 533–540.
Luczak, A., Bartho, P. & Harris, K.D. (2013) Gating of sensory input by spontaneous cortical activity. *J. Neurosci.*, **33**, 1684–1695.
Maffei, L., Fiorentini, A. & Bisti, S. (1973) Neural correlate of perceptual adaptation to gratings. *Science*, **182**, 1036–1038.
Marshansky, S., Shumikhina, S. & Molotchnikoff, S. (2011) Repetitive adaptation induces plasticity of spatial frequency tuning in cat primary visual cortex. *Neuroscience*, **172**, 355–365.
Martinez-Conde, S., Cudeiro, J., Grieve, K.L., Rodriguez, R., Rivadulla, C. & Acuña, C. (1999) Effects of feedback projections from area 18 layers 2/3 to area 17 layers 2/3 in the cat visual cortex. *J. Neurophysiol.*, **82**, 2667–2675.
Maya-Vetencourt, J.F. & Origlia, N. (2012) Visual cortex plasticity: a complex interplay of genetic and environmental influences. *Neural Plast.*, **2012**, 1–14.
Miller, E.K. & Buschman, T.J. (2013) Cortical circuits for the control of attention. *Curr. Opin. Neurobiol.*, **23**, 216–222.
Moore, B.D. 4th, Alitto, H.J. & Usrey, W.M. (2005) Orientation tuning, but not direction selectivity, is invariant to temporal frequency in primary visual cortex. *J. Neurophysiol.*, **94**, 1336–1345.
Movshon, J.A., Thompson, I.D. & Tolhurst, D.J. (1978) Spatial and temporal contrast sensitivity of neurones in areas 17 and 18 of the cat's visual cortex. *J. Physiol.*, **283**, 101–120.
Muckli, L. & Petro, L.S. (2013) Network interactions: non-geniculate input to V1. *Curr. Opin. Neurobiol.*, **23**, 195–201.
Müller, J.R., Metha, A.B., Krauskopf, J. & Lennie, P. (1999) Rapid adaptation in visual cortex to the structure of images. *Science*, **285**, 1405–1408.
Neitz, J., Carroll, J., Yamauchi, Y., Neitz, M. & Williams, D.R. (2002) Color perception is mediated by a plastic neural mechanism that is adjustable in adults. *Neuron*, **35**, 783–792.
Nemri, A., Ghisovan, N., Shumikhina, S. & Molotchnikoff, S. (2009) Adaptive behavior of neighboring neurons during adaptation-induced plasticity of orientation tuning in V1. *BMC Neurosci.*, **10**, 1–9.
Ohzawa, I., Sclar, G. & Freeman, R.D. (1982) Contrast gain control in the cat visual cortex. *Nature*, **298**, 266–268.
Patterson, C.A., Wissig, S.C. & Kohn, A. (2013) Distinct effects of brief and prolonged adaptation on orientation tuning in primary visual cortex. *J. Neurosci.*, **33**, 532–543.
Ribot, J., Aushana, Y., Bui-Quoc, E. & Milleret, C. (2013) Organization and origin of spatial frequency maps in cat visual cortex. *J. Neurosci.*, **33**, 13326–13343.
Salin, P.A., Kennedy, H. & Bullier, J. (1995) Spatial reciprocity of connections between areas 17 and 18 in the cat. *Can. J. Physiol. Pharm.*, **73**, 1339–1347.
Sato, T.K., Nauhaus, I. & Carandini, M. (2012) Traveling waves in visual cortex. *Neuron*, **75**, 218–229.
Shibata, K., Watanabe, T., Sasaki, Y. & Kawato, M. (2011) Perceptual learning incepted by decoded fMRI neurofeedback without stimulus presentation. *Science*, **334**, 1413–1415.
Shtoyerman, E., Arieli, A., Slovin, H., Vanzetta, I. & Grinvald, A. (2000) Long-term optical imaging and spectroscopy reveal mechanisms underlying the intrinsic signal and stability of cortical maps in V1 of behaving monkeys. *J. Neurosci.*, **20**, 8111–8121.
Soodak, R.E., Shapley, R.M. & Kaplan, E. (1987) Linear mechanism of orientation tuning in the retina and lateral geniculate nucleus of the cat. *J. Neurophysiol.*, **58**, 267–275.
Sporns, O. (2013) Network attributes for segregation and integration in the human brain. *Curr. Opin. Neurobiol.*, **23**, 162–171.
Suematsu, N., Naito, T. & Sato, H. (2012) Relationship between orientation sensitivity and spatiotemporal receptive field structures of neurons in the cat lateral geniculate nucleus. *Neural Networks*, **35**, 10–20.
Symonds, L.L. & Rosenquist, A.C. (1984) Corticocortical connections among visual areas in the cat. *J. Comp. Neurol.*, **229**, 1–38.
Tani, T., Ribot, J., O'Hashi, K. & Tanaka, S. (2012) Parallel development of orientation maps and spatial frequency selectivity in cat visual cortex. *Eur. J. Neurosci.*, **35**, 44–55.
Tusa, R.J., Rosenquist, A.C. & Palmer, L.A. (1979) Retinotopic organization of areas 18 and 19 in the cat. *J. Comp. Neurol.*, **185**, 657–678.
Vautin, R.G. & Berkley, M.A. (1977) Responses of single cells in cat visual cortex to prolonged stimulus movement: neural correlates of visual aftereffects. *J. Neurophysiol.*, **40**, 1051–1065.
Wang, G., Ding, S. & Yunokuchi, K. (2003) Difference in the representation of cardinal and oblique contours in cat visual cortex. *Neurosci. Lett.*, **338**, 77–81.
Wang, Q., Webber, R.M. & Stanley, G.B. (2010) Thalamic synchrony and the adaptive gating of information flow to cortex. *Nat. Neurosci.*, **13**, 1534–1541.
Watroba, L., Buser, P. & Milleret, C. (2001) Impairment of binocular vision in the adult cat induces plastic changes in the callosal cortical map. *Eur. J. Neurosci.*, **14**, 1021–1029.
Webster, M.A. (2011) Adaptation and visual coding. *J. Vis.*, **11**, 1–23.
Yokoo, T., Knight, B.W. & Sirovich, L. (2001) An optimization approach to signal extraction from noisy multivariate data. *NeuroImage*, **14**, 1309–1326.
Zhang, P., Bao, M., Kwon, M., He, S. & Engel, S.A. (2009) Effects of orientation-specific visual deprivation induced with altered reality. *Curr. Biol.*, **19**, 1956–1960.

EJN fens EUROPEAN JOURNAL OF NEUROSCIENCE

European Journal of Neuroscience, Vol. 38, pp. 2065–2077, 2013 doi:10.1111/ejn.12206

NEUROSYSTEMS

Fluoxetine and serotonin facilitate attractive-adaptation-induced orientation plasticity in adult cat visual cortex

Lyes Bachatene, Vishal Bharmauria, Sarah Cattan and Stéphane Molotchnikoff
Department of Biological Sciences, University of Montreal, Montreal, QC, Canada

Keywords: adaptation, fluoxetine, plasticity, serotonin, visual cortex

Abstract

Neurons in V1 display orientation selectivity by responding optimally to a preferred orientation edge when it is presented within their receptive fields. Orientation plasticity in striate cortex occurs either by ocular deprivation or by imposition of a non-preferred stimulus for several minutes. Adaptation of neurons to a non-optimal orientation induces shifts of tuning curves towards the adapting orientation (attractive shift) or away from it (repulsive shift). Here, we investigated the effects of the neurotransmitter serotonin and antidepressant fluoxetine (a selective serotonin reuptake inhibitor) on the modulation of adaptation-induced orientation plasticity. We show that serotonin and fluoxetine promote mostly attractive shifts. Attractive shifts augmented in magnitude towards adapter, whereas repulsive neurons reversed their behavior in the direction of the forced orientation. Furthermore, neurons which retained their original preferred orientation expressed plasticity by shifting their tuning curves after drug administration mostly towards adapter. Our data suggest a pre-eminent role of fluoxetine by inducing and facilitating short-term plasticity in V1.

Introduction

Neurons in the primary visual cortex are selective to stimulus properties such as orientation (Hubel & Wiesel, 1959, 1968). Cells respond optimally when the preferred stimulus is applied within their respective receptive fields. Properties that deviate from the preferred characteristics evoke weaker responses. Over a range of axes of orientation, it is common to obtain a typical Gaussian fit of the tuning curve that reveals the preferred orientation. Such curves are established during the critical period that follows birth (Chiu & Weliki, 2003; Tanaka *et al.*, 2009). Several laboratories have demonstrated that frequent or prolonged presentation of a non-preferred orientation induces modifications of the tuning curves of neurons (Dragoi *et al.*, 2000; Ghisovan *et al.*, 2009; Nemri *et al.*, 2009; Bachatene *et al.*, 2012). This presented non-preferred stimulus to which a neuron generally responds poorly is called an adapter and the process of stimulus presentation for a specific period is referred to as adaptation. In this framework, adaptation is a method that points towards the 'forced' application of a non-preferred orientation (Krekelberg *et al.*, 2006; Stroud *et al.*, 2012). After adaptation, the peak of a neuron's tuning curve shifts either towards the adapting orientation (attractive shifts) or away from it (repulsive shifts). Similar results have been obtained for other features, namely spatial frequency (Marshansky *et al.*, 2011), direction of motion (Kohn & Movshon, 2004) and speed (Movshon, 1975). Interestingly, the adaptation-induced plasticity occurs in the adult, and hence in a fully mature brain well beyond the critical period that follows birth. Investigations have concluded that visual plasticity can be restored after ocular deprivation by electrical stimulation of the locus coeruleus (Kasamatsu *et al.*, 1985), or can be modulated by several substances such as acetylcholine and noradrenaline (Bear & Singer, 1986), and L-threo-DOPS (Mataga *et al.*, 1992). Moreover, it has been shown that over- expression of the protein Lynx1 restricts plasticity in V1 by contributing to the stability of cortical networks in the presence of cholinergic innervations. Conversely, ablating Lynx1 improves cholinergic circuitries and may restore plasticity in mice (Morishita *et al.*, 2010). In monocular deprived adult rats, ocular dominance plasticity may be reinstated by a decline of both GABAergic transmission and expression of chondroitin sulfate proteoglycans (Harauzov *et al.*, 2010). Some authors have shown that down-regulation of chondroitin sulfate proteoglycans coupled with reverse lid-suturing in adult rats restores ocular dominance (Pizzorusso *et al.*, 2002, 2006). This is supported by an augmentation of both visual acuity and dendritic spine density (Pizzorusso *et al.*, 2006). However, in adult cat V1, the recovery from monocular deprivation is insufficiently re-established after administration of chondroitinase (Vorobyov *et al.*, 2013). Such physiological and molecular mechanisms of visual plasticity are of high therapeutic importance for visual system pathologies, e.g. amblyopia (Maya-Vetencourt & Origlia, 2012).

Recently, Maya-Vetencourt *et al.* (2008, 2011) have shown that in adult rats, ocular-dominance plasticity is restored after long-term treatment with the antidepressant fluoxetine. Furthermore, it has been shown that administration of fluoxetine to patients with ischemic stroke leads to an increase of motor recovery in comparison with placebo subjects (Chollet *et al.*, 2011). In line with the above published data, we sought to examine the effects of serotonin and fluoxetine on shifts of orientation tuning curves of neurons following adaptation in adult anesthetized cats. We show that serotonin

Correspondence: Dr S. Molotchnikoff, as above.

Received 2 January 2013, revised 26 February 2013, accepted 28 February 2013

and fluoxetine mostly potentiate attractive shifts, suggesting a facilitatory effect on orientation plasticity after adaptation.

Material and methods

Ethical approval

Electrophysiological recordings were performed on the primary visual cortex of nine adult domestic cats (*Felis catus*). Animal surgery procedures and electrophysiological recordings followed the guidelines of the Canadian Council on Animal Care and were approved by the Institutional Animal Care and Use Committee of the University of Montreal. Animals were supplied by the Division of Animal Resources of the University of Montreal.

Animals, anesthesia and surgical procedures

Adult cats (2.5–3.5 kg, age 12–24 months) of either sex, sedated with acepromazine maleate (1 mg/kg, i.m., Atravet; Wyeth-Ayerst, Guelph, ON, Canada) and atropine sulfate (0.04 mg/kg, i.m., ATRO-SA; Rafter, Calgary, AB, Canada), were anesthetized with ketamine hydrochloride (25 mg/kg, i.m., Rogarsetic; Pfizer, Kirkland, QC, Canada) maintained with 0.3% isoflurane (AErrane; Baxter, Toronto, ON, Canada). Lidocaine hydrochloride (2%, Xylocaine; AstraZeneca, Missis-sauga, ON, Canada) was injected subcutaneously as a local anesthetic during surgery. A tracheotomy was performed for artificial ventilation, and one forelimb vein was cannulated. Animals were then placed in a stereotaxic apparatus. Xylocaine gel (5%; Astra Pharma, Mississauga, ON, Canada) was applied on the pressure points. For the remaining preparations and recording, paralysis was induced with 40 mg and maintained with 10 mg/kg/h gallamine triethiodide (i.v., Flaxedil; Sigma Chemical, St. Louis, MO, USA) administered in 5% dextrose lactated Ringer's nutritive solution. General anesthesia was maintained by artificial ventilation with a mixture of N_2O/O_2 (70 : 30) supplemented with 0.5% isoflurane (AErrane; Baxter) for the duration of the experiment. Proper depth of anesthesia was ensured throughout the experiment by monitoring the EEG, the electrocardiogram and expired CO_2. In addition, heart rate remained unmodified after skin stimulation. End-tidal CO_2 partial pressure was kept constant between 25 and 30 mmHg. A heated pad was used to maintain a body temperature of 37.5 °C. Tribrissen (30 mg/kg/day, s.c.; Schering-Plough, Pointe-Claire, QC, Canada) and Duplocillin (0.1 mL/kg, i.m.; Intervet, Withby, ON, Canada) were administered to the animals to prevent bacterial infection. The pupils were dilated with atropine sulfate (1%, Isopto-Atropine; Alcon, Mississauga, ON, Canada) and the nictitating membranes were retracted with phenylephrine hydrochloride (2.5%, Mydfrin; Alcon). The loci of the area centrales were inferred from the positions of the blind spots, which were ophthalmoscopically focused and back projected onto a translucent screen. To verify the stability of the eye this procedure was repeated at the end of tests. Plano contact lenses with artificial pupils (5 mm diameter) were placed on the cat's eyes to prevent the cornea from drying (University of Montréal, PQ, Canada).

At the end of each experiment, the animals were killed via a lethal dose of pentobarbital sodium (100 mg/kg, Somnotol; MTC Pharmaceuticals, Cambridge, ON, Canada) by intravenous injection.

Electrophysiological recordings

Multi-unit activity in the primary visual cortex was carried out with tungsten microelectrodes (2–10 MΩ at 1 kHz; Frederick Haer & Co, Bowdoinham, ME, USA). Each set of electrodes, consisting of four microelectrodes in linear array (inter-electrode spacing 400 μm) enclosed in stainless steel tubing, was controlled by a separate micromanipulator. The signal from the microelectrodes was amplified, band-pass filtered (300 Hz–3 kHz), digitized and recorded with a 0.05-ms temporal resolution (Spike2, CED, Cambridge, UK). We recorded at an average of 400–500 μm cortical depth from two recording sites. Each recording site yielded up to eight neurons. Action potentials were sorted using a window discriminator for further off-line analyses. Multi-unit signals from one electrode usually included up to seven well-isolated single units. The spike sorting method was based on cluster classification in reduced space (Spike2, CED). The stability of each cell's activity across conditions was verified qualitatively by visual control of the cluster disposition and of the waveform shape. Auto-correlograms were systematically performed to ensure proper single-cell capture (deep at zero).

Visual stimulation (adaptation protocol) and drug administration

Stimulation was monocular (dominant eye, the opposite eye was shut). After clearly detectable activity was obtained, the multiunit receptive fields (RFs) were mapped as the minimum response fields (Barlow *et al.*, 1967) by using a hand-held ophthalmoscope. RF edges were determined by moving a light bar from the periphery towards the centre until a response was elicited. Eye–screen distance was 57 cm. These preliminary tests revealed qualitative properties such as dimensions, velocity preference, orientation and directional selectivity. Visual stimuli were generated with a VSG 2/5 graphic board (Cambridge Research Systems, Rochester, UK) and displayed on a 21-inch monitor (Sony GDM-F520 Trinitron, Tokyo, Japan) placed 57 cm from the cat's eyes, with 1024 × 768 pixels, running at 100 Hz frame refresh. Stimuli were drifting sine-wave grating patches (~2° to 5°) covering the excitatory RF (Maffei & Fiorentini, 1973).

Patch characteristics were set to evoke optimal responses: contrast at 80%, mean luminance at 40 cd/m^2, optimal spatial and temporal frequencies set within 0.1–0.5 cycles/degree and 1.0–2.0 Hz, respectively. The blank screen was uniformly gray (~ 35 cd/m^2). In all cases the above parameters were chosen with the aim of evoking maximal discharges. V1 neurons are known to respond well to sine wave drifting gratings (Bardy *et al.*, 2006). After manual RF characterization, nine oriented stimuli centered on the preferred orientation were selected and used for the rest of the experiment. With a 22.5° interval between orientations, tuning curves covered 180°. Test orientations were applied in random order. Each oriented stimulus was presented in blocks of 25 trials lasting 4.1 s each, with a random inter-trial interval (1.0–3.0 s) during which no stimuli were presented. Thus, a recording session lasted for 25–30 min. Peristimulus time histograms were recorded. Once control orientation tuning curves were characterized, an adapting non-preferred stimulus was presented continuously for 12 min. The adapting stimulus was a drifting grating whose orientation was randomly selected in the range 22.5–67.5° from the neuron's preferred orientation. It has been shown previously that larger gaps between optimal and adapting orientations are less efficient in inducing orientation shifts (Ghisovan *et al.*, 2009). All other stimulus parameters were kept constant, at control values, throughout the recordings. During this adaptation period no recordings were performed. Immediately after adaptation, orientation tuning curves was measured starting with the adapting and control preferred orientations to prevent an unlikely

premature recovery, as these two orientations were the center of interest, while the remaining orientations were recorded in random order. Following a recovery period of 60–90 min, another tuning curve measurement was performed.

After the recovery period, we applied topically on the cortical surface a custom-cut filter paper (1 × 1 mm) soaked in 10 mM serotonin or fluoxetine; we also used γ-aminobutyric acid (GABA) as a control test for drug diffusion as this drug suppresses all electrical activity (see Results).

Data analysis

Once single cells were sorted off-line from multi-unit spike trains accumulated during data acquisition, orientation tuning curves were constructed from the raw data. Because orientation tuning is best described by Gaussian-like functions, we fitted our raw data with the von Mises function (Swindale, 1998). This allowed us to determine with precision the preferred orientation of neurons and then measure shifts in orientation preference. The von Mises function is defined as $M(\theta) = A.e^{\,b[\cos(\theta - c)]} + d$, where A is the value of the function at the preferred orientation, c, and b is a width parameter. An additional parameter, d, represents the spontaneous firing rate of the cell (Swindale, 1998; Kohn & Movshon, 2004). The above calculations are necessary because tuning curves derived from raw data may be imperfect in determining the preferred orientation given that the interval between the stimulus orientations is relatively large, 22.5°. In the cat, over 90% of V1 neurons are well tuned to stimulus orientation (Bishop & Henry, 1972). It was, however, necessary to ensure that cells in our sample were properly tuned for orientation. We measured an orientation selectivity index (OSI) by dividing the firing rate at orthogonal orientations by the firing rate for the preferred orientation, and subtracting the result from 1 (Ramoa *et al.*, 2001; Liao *et al.*, 2004). The closer the OSI is to 1, the stronger the orientation selectivity. To compare the mean OSI between control, post-adaptation and post-drug administration, a one-way ANOVA statistical test was performed with a significance level of 95%. We also correlated the OSI of each neuron with the amplitude of shift and used linear regression with 95% confidence interval to verify the relation. Adaptation-induced shifts were measured as the distance between peak positions of the fitted tuning curves before and after conditioning. To assess the statistical significance of tuning shifts, curve fits were generated separately for each of the 25 trials, and the mean difference was tested by a paired t-test. Shifts in preferred orientation larger than 5° were statistically significant (paired sample two-tailed t-test, $P < 0.01$). Furthermore, paired two-tailed Student's tests were carried out to verify the significance of differences between experimental conditions. In addition to the amplitude of shifts, we computed the modulation of responses for orientation classes (original optimal, adapter, new optimal and a flank orientation before and after adaptation). We used a one-tailed Wilcoxon rank test with 95% confidence interval to compare the response amplitude before and after the tests. Thereafter, we compared the amplitude of response between two specific classes of orientations (prior to drug administration versus post-drug administration, see Fig. 6) using a two-way ANOVA statistical test (95% significance level). Moreover, the firing rate of spontaneous activity (firing rate of the neurons when a black screen was presented, no stimulus) was compared between control, post-adaptation, recovery and drug conditions and a one-way ANOVA statistical test was used to compare the mean firing response between these conditions with a 95% significance level. All statistical tests described in the results were computed using the numerical software GraphPad Prism version 5 (GraphPad Software Inc., La Jolla, CA, USA).

Results

The present experiments were aimed at investigating the effects of the neurotransmitter serotonin and antidepressant fluoxetine (a selective serotonin reuptake inhibitor, SSRI) on shifts of orientation tuning curves of neurons following adaptation on adult cats of either sex. No difference was observed between males and females in the results presented below. After a classical visual stimulation protocol to determine the Gaussian orientation tuning curves, we established the shifts of tunings of the recorded neurons after adaptation prior to drug application. Thereafter, we proceeded with drug testing on the same neurons. After the recovery period from the first adaptation, we administered serotonin or fluoxetine topically with a custom-cut filter paper soaked in 10 mM solution deposited on the surface of the primary visual cortex (adjacent to the recording electrode shaft). In addition, drug diffusion was assessed by recording responses from neighboring sites. Moreover, we used the potent inhibitory GABA (10^{-2} M) to supplement our results regarding substance diffusion. Figure 1 illustrates the experiments aimed at showing that the drug's effect is limited to a tissue volume inferior to 400–500 μm. The general set-up is displayed in Fig. 1A. A typical example of multi-unit recordings is shown in Fig. 1B. It demonstrates that the diffusion of drugs was restricted to a volume inferior to ~ 400–500 μm. On the left, we show two electrodes positioned laterally (inter-electrode distance 400 μm), while on the right, the recording tips are vertically spaced along the electrode shank (inter-recording site distance 500 μm). The application of GABA next to electrode #2 (E2) reduced considerably the multi-neuronal activity while the electrical activity under electrode #1 (E1) remained unaffected. Similarly, in depth recordings (right side), the most superficial site (site 2) illustrates the firing decline, whereas 500 μm below, the multi-neuronal firing remains unmodified by serotonin. Although serotonin may decrease the general activity of neurons (Licata *et al.*, 1993; Zhong & Yan, 2011; Avesar & Gulledge, 2012), these cells maintain a tuning curve as one specific orientation evokes the maximal firing rate relative to other orientations. The experimental protocol is shown schematically in Fig. 1C. The test began by determining the orientation tuning curves by randomly presenting sine-wave gratings at eight orientations wherein the preferred orientation evokes the highest firing rate. In the next phase, a non-preferred orientation is applied uninterruptedly for 12 min to induce adaptation. This initial step, for most cells, ascertains the shift of the peak of the tuning curve for the unit under investigation. The recovery of the original tuning curve is achieved about 60–90 min after the cessation of first adaptation: consequently, the original tuning curve is reinstated. After the recovery period, the drug was topically applied. Immediately after administration of the substance, we carried out a second adaptation for the same duration (12 min) with the same non-preferred orientation (as the first adaptation), and the entire process was repeated.

The present paper describes data recorded from single unit analysis. Of 139 isolated neurons, 68 were tested with serotonin (four cells were eliminated and eight units were unclassified) and 71 neurons were investigated with fluoxetine (one unit was eliminated and 10 were unclassified). Neurons were eliminated when their firing activity was lost during the experiment, and as a consequence they could not be traced. Unclassified neurons refer to neurons for which the tuning curve could not be determined. We also calculated the OSI of each neuron as 1 – (firing rate at orthogonal orientation/firing

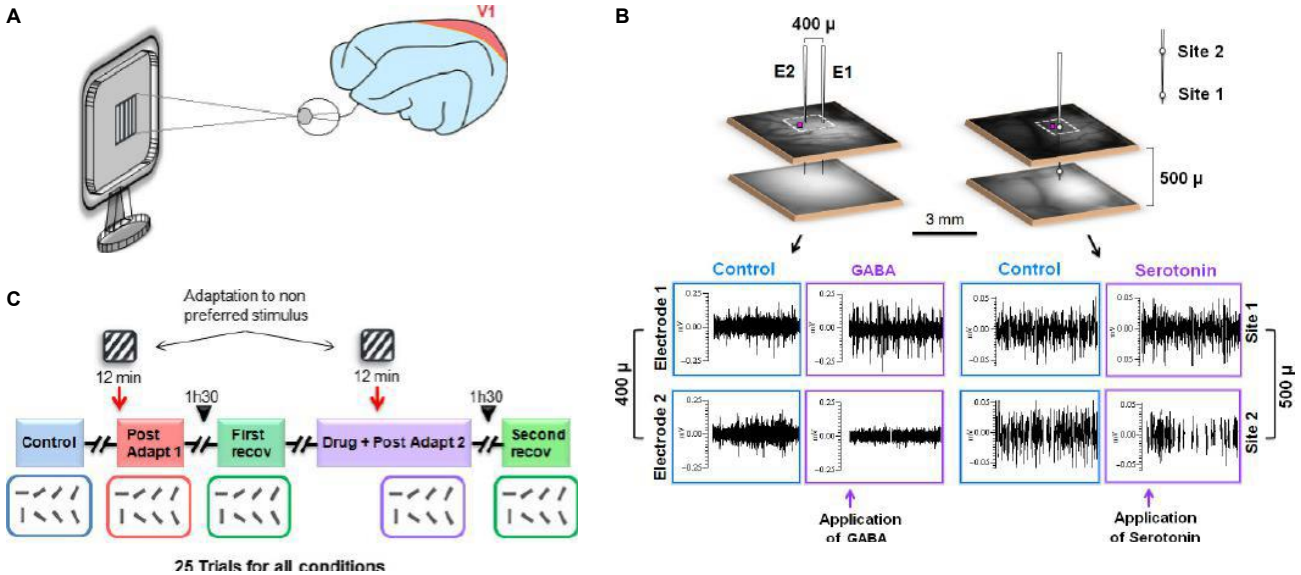

FIG. 1. Experimental procedures and drug diffusion. (A) Visual stimulation on adult cat striate cortex. (B) Electrophysiological recordings using multi electrodes (left cortex) and multisite electrode (right cortex); small square beside the electrode (E2 and site 2) represents the filter paper soaked with the drug. Below are shown the firing rates of multi-unit activity using GABA (left cortex) and serotonin (right cortex) for drug diffusion. (C) Experimental time course. All the orientations are randomly presented on the screen in 25 trials with arbitrary intervals.

rate at preferred orientation); the closer the OSI is to 1, the stronger the orientation-selectivity. We also correlated the orientation selectivity index with the amplitude of shift for each neuron. The mean OSI was superior to 0.7 for each condition ($OSI_{control}$ = 0.78, $OSI_{post\text{-}adaptation}$ = 0.73, $OSI_{post\text{-}drug\ administration}$ = 0.82), and no significant difference was observed between these conditions (one-way ANOVA: F = 1.77, P = 0.17, see Supporting Information Fig. S2A). Results from the correlation between the OSI and the amplitude of shifts showed no significant correlation after adaptation (linear regression: F = 0.05, P = 0.81) or after drug administration (linear regression: F = 0.02, P = 0.88).

Serotonin and fluoxetine facilitate adaptation-induced plasticity

Previous studies have shown that prolonged adaptation of 12 min to a non-preferred stimulus leads to shifts of peaks of orientation tuning curves towards the adapting orientation in most of cases (attractive shift) (Ghisovan *et al.*, 2008, 2009; Nemri *et al.*, 2009; Bachatene *et al.*, 2012). Figure 2A and B present an example of the effect of serotonin on the attractive shifts. In these figures, the spike waveform at every stage of the study is shown in rectangular boxes, i.e. the neuron was traced throughout all steps of the recording. The red triangle represents the adapting orientation in this and all subsequent figures. The upper two plots show the orientation tuning curve of a cell as derived from the raw data, i.e. spike counts. Horizontal orientation (optimal orientation = 1.65°, derived from Gaussian fits) evoked the highest firing rate specifying the preferred orientation of the neuron (blue curve). The adapting orientation (112.5°), applied uninterruptedly for 12 min, induced a new optimal orientation (red curve) at 46.82°. In this case, the amplitude of the attractive shift was 45.17°. The lower curves are obtained after Gaussian fits as derived from raw values (Control R^2 = 0.7, Adaptation R^2 = 0.9, Recovery R^2 = 0.9, Serotonin R^2 = 0.5). Following the recovery (green curve) of the original preferred orientation (1.31°), serotonin was applied over the cortex (see Fig. 1). The impact of the drug resulted in an increase of shift by 110.29° from 1.31° to 111.6° (Fig. 2B). Indeed, in the presence of serotonin, the new preferred orientation coincided with the adapter (shift increased from 45.17° to 110.29°).

Comparable results were obtained with fluoxetine (Fig. 2C and D, Control R^2 = 0.5, Adaptation R^2 = 0.6, Recovery R^2 = 0.8, Fluoxetine R^2 = 0.6). Prior to fluoxetine application, the attractive shift was 23.06° (original preferred: 65.98°, adapter set at 135°, following adaptation optimal axis = 89.04°). Fluoxetine administration increased the attractive shift to 106.13°, which displaced the peak of the tuning curve further towards the adapting orientation (Fig. 2D).

It is worth underlining that adaptation declines the responses evoked by the initial optimal orientation (Ghisovan *et al.*, 2008). Interestingly, in some cases the attractive translation is partial, i.e. the adaptation-induced shift failed to reach the adapter (Fig. 2A and C), particularly if the gaps separating adapting and the initial optimal orientations were too large. Following the adaptation procedure accompanied by serotonin or fluoxetine (Fig. 2B and D, respectively), the amplitude of the attractive shift increased (amplified shift effect) in the presence of the drug and attained that of the adapter, suggesting the effectiveness of both drugs in driving the peak of the tuning curve towards the adapter. The new optimal orientation coincided with the imposed orientation in 74% of neurons treated with serotonin, and in 73% of neurons treated with fluoxetine. No specific properties (cortical depth, firing rate or specific receptive field) were found for neurons which acquired a new preferred orientation similar to the adapter.

Refractory neurons

Twenty-two per cent of neurons that we term 'refractory' did not display any significant shift of their orientation tuning curves after first adaptation, i.e. they maintained their original preferred orientation following the first adaptation. In our experiments, a shift is considered significant if it is > 5° (shifts below to this threshold are insignificant, paired sample two-tailed t-test, P > 0.01, Ghisovan

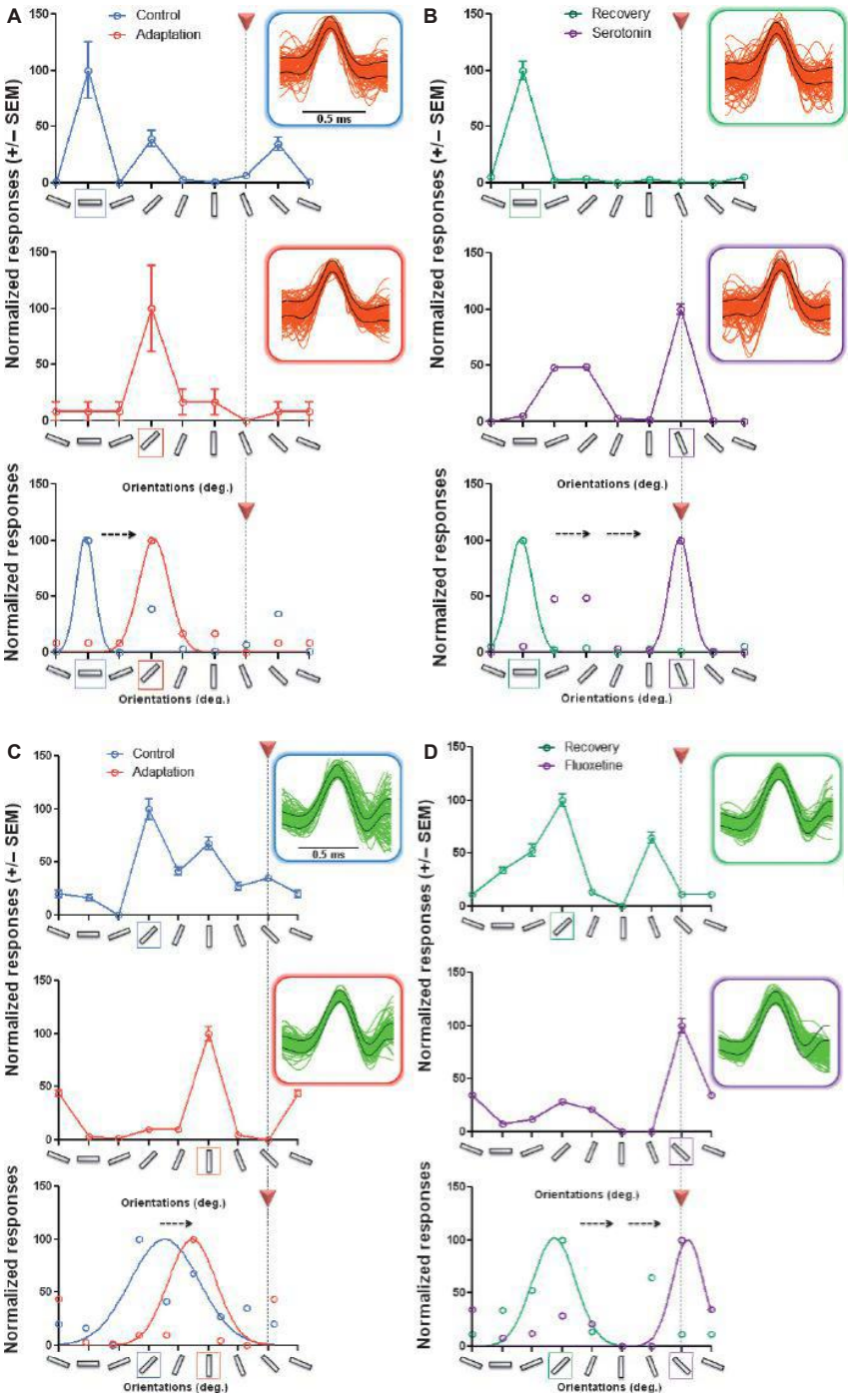

FIG. 2. Amplified attractive effect of serotonin and fluoxetine. (A) Raw data and Gaussian fit of normalized responses of one neuron for control (blue) and post-adaptation (red). Red triangle represents adapting orientation. Gaussian fits show shift of the tuning curve (attractive shift, 45.17°). (B) Raw data and Gaussian fit of normalized responses of the same neuron for recovery (green) and after the second adaptation during serotonin application (purple); the new attractive shift is 110.29°. Orange spikes represent waveforms of the same neuron for all conditions. (C, D) Same results for a different neuron, during fluoxetine administration (attractive shift post-adaptation 23.06°, amplified attractive shift during fluoxetine application 106.13°). Green spikes show the waveforms of the same cell.

et al., 2009). Thus, refractory neurons retained their original optimal orientation following an initial adaptation period to a non-preferred stimulus or showed a very small jitter of their peak inferior to 5°. Figure 3 illustrates that administration of serotonin (Fig. 3A and B, Control $R^2 = 0.9$, Adaptation $R^2 = 0.9$, Recovery $R^2 = 0.9$, Serotonin $R^2 = 0.8$) or fluoxetine (Fig. 3C and 3D, Control $R^2 = 0.8$, Adaptation $R^2 = 0.8$, Recovery $R^2 = 0.7$, Fluoxetine $R^2 = 0.9$) prompted a significant shift of the peaks in the post-adaptation

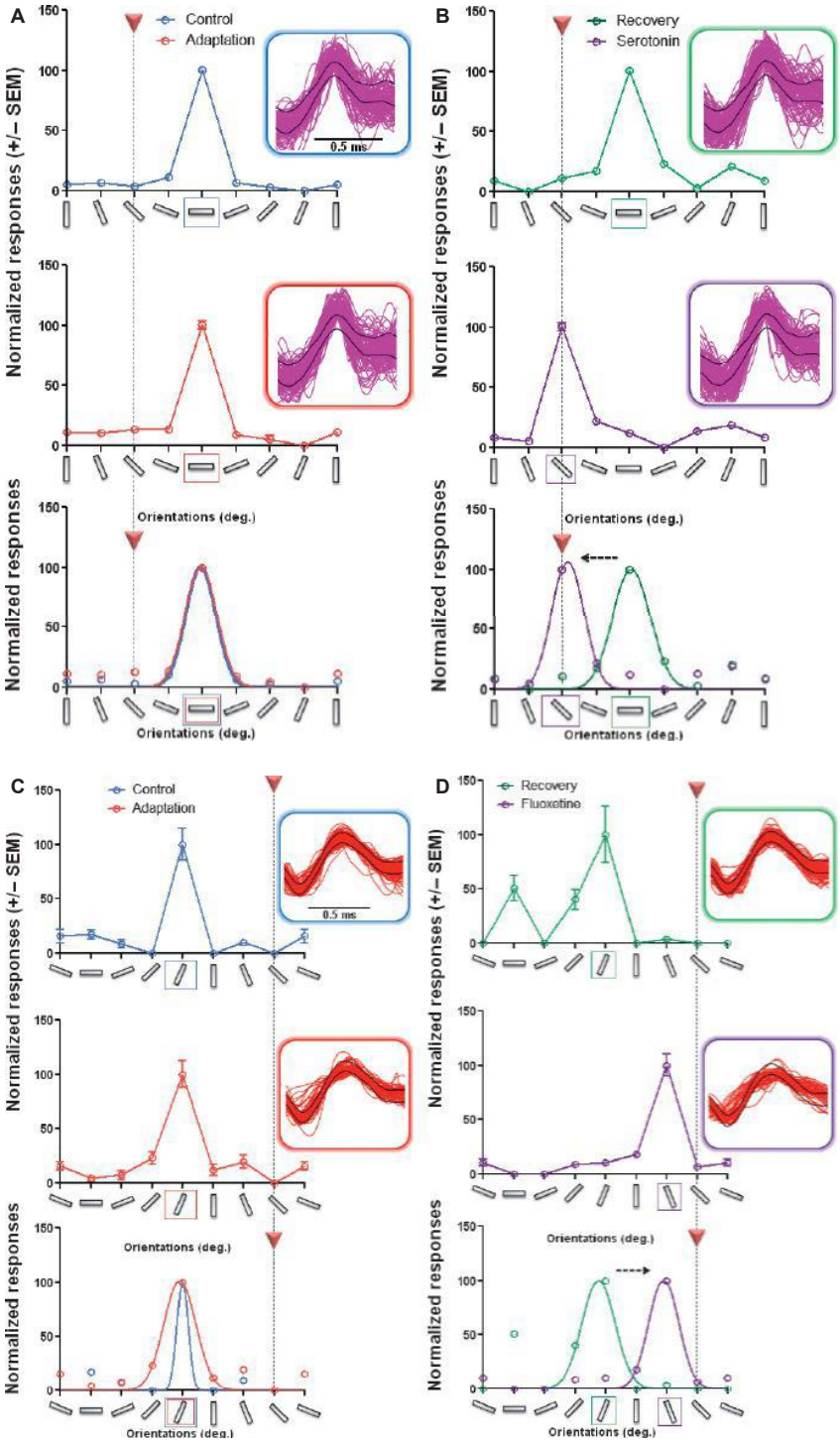

FIG. 3. Induction of attractive shift by the action of serotonin and fluoxetine. (A) Raw data and Gaussian fit of normalized responses of one neuron for control and post-adaptation conditions (blue and red curves, respectively). Red triangle represents the adapter. Gaussian fits below show a non-significant shift after the first adaptation. (B) Raw data and Gaussian fit of normalized responses of the same cell for recovery and second adaptation in the presence of serotonin (green and purple curves, respectively). Pink spikes represent waveforms of the same cell for the entire procedure. The tuning curve shifted toward the adapter in the presence of the drug. (C, D) Similar induction of an attractive shift for another neuron during fluoxetine administration. Red spikes represent waveforms of the same neuron.

period. In sections B and D, administration of serotonin (B) and fluoxetine (D) displaced the orientation tuning curves towards the adapting orientation (attractive shift 42.33° and 48.02°, respectively). In most refractory cells, shifts were attractive (91%, $n = 11$ for serotonin experiments, 93%, $n = 14$ for fluoxetine experiments) (see also Fig. 5).

Serotonin and fluoxetine reverse the repulsive shifts

Although 12 min of adaptation induces attractive shifts in about two-third of neurons, a fairly large number of units do exhibit repulsive shifts. In the present investigation, 32% of neurons ($n = 56$, serotonin experiments) and 25% of neurons ($n = 60$, fluoxetine experiments) responded with repulsive shifts after the first adaptation. In the following section, comparative effects of serotonin and fluoxetine are described, wherein the repulsive shifts post-first adaptation were reversed towards the adapter. Figure 4 illustrates such reversal of the orientation-selectivity (Control $R^2 = 0.8$, Adaptation $R^2 = 0.5$, Recovery $R^2 = 0.5$, Serotonin $R^2 = 0.6$). For instance, in Fig. 4A the first adaptation displaced the peak of the tuning curve by 79.32° away from the adapter (optimal orientation 119.7°, adapter set at 135° and new optimal orientation 40.38°). During serotonin application, a repeated adaptation resulted in optimal orientation corresponding to the adapter: 142.5° (Fig. 4B). Comparable results were recorded with fluoxetine (Control $R^2 = 0.5$, Adaptation $R^2 = 0.6$, Recovery $R^2 = 0.7$, Fluoxetine $R^2 = 0.8$). Indeed, Fig. 4C shows a repulsive shift (31.68° as obtained from Gaussian fits) after the first adaptation for the illustrated neuron (purple spike). Following the second adaptation in the presence of fluoxetine (Fig. 4D), we observed an attractive effect towards the imposed orientation (adapter set at 22.5°), and thus fluoxetine cancels the repulsive shift and induces an attractive change of the peak of the orientation tuning curve (attractive shift 8.25°, from Gaussian fit).

Modulations of shifts following serotonin and fluoxetine applications

Figure 5A and B display for every analysed cell the changes of shift magnitudes and displacement direction of orientation tuning curve peak induced by serotonin and fluoxetine. Cells are grouped into three major classes according to the direction of the shift following the first adaptation: from left to right these are repulsive to attractive, attractive to attractive (increase of attractive shift) and no shift to attractive, whereas the other two groups with very few neurons (six units for serotonin experiments in Fig. 5A, and ten units for fluoxetine experiments in Fig. 5B) did not display an attractive facilitatory effect. Drugs were applied after the first adaptation following recovery of the original orientation-selectivity. The shifts following the first adaptation are depicted by red circles, whereas shifts in the presence of serotonin or fluoxetine are indicated by purple squares (serotonin) and purple circles (fluoxetine). Paired two-tailed Student's tests were used to compare the amplitude of shifts after the first adaptation versus the second adaptation with administration of the drug. The effects of serotonin are displayed in Fig. 5A. Eighteen neurons (32%, $n = 56$) reacted with a repulsive shift after the first adaptation with an average amplitude shift of 25.4 ± 19.4°. Seventeen of these neurons reversed the initial repulsive shift towards the opposite direction: attractive, the average amplitude of the new shift was 24 ± 19.2° (paired two-tailed t-test: $t = 7.9$, $P < 0.0001$, see Fig. 5A, first column from left), and one neuron remained unaffected by the drug (see proportion of unaffected neurons). Twenty-seven neurons (48%, $n = 56$) reacted attractively as a result of the first adaptation. Twenty-three of these neurons responded with significant augmented shifts (averaged shift following the first adaptation 15.1 ± 9.6°, averaged shift with serotonin reached 33 ± 29.4°; paired two-tailed t-test: $t = 3.4$, $P = 0.002$, second column from left). Interestingly, 11 neurons (20%, $n = 56$) that retained their orientation-selectivity after the first adaptation (averaged shift amplitude = 2.2 ± 2.0°, i.e. not significant) exhibited a large attractive shift for 10 neurons (new averaged shift amplitude = 23 ± 17.1°, paired two-tailed t-test: $t = 3.8$, $P = 0.0039$), although one neuron remained unaffected. This suggests a facilitating role of serotonin in inducing attractive shifts. In addition to these three major classes, a few cells (3%, $n = 56$) reacted by shifting their peak from attractive to repulsive translation (fourth column from left) and four units (7%, $n = 56$) remained unaffected by the drug (right column). The horizontal bars underline the mean values of tuning shifts.

In Fig. 5B, on a cell-by-cell basis, we show the changes of shift magnitudes after the second adaptation while fluoxetine was applied to the cortex. The same global trend of results was obtained: the drug potentiates attractive shifts, i.e. repulsive displacement reversed to attractive shifts (25%, $n = 60$), attractive shifts remaining attractive although the increase is insignificant (averaged shift after the first adaptation equals 22 ± 11.1°, and the averaged shift after the second adaptation with fluoxetine administration is 27 ± 25.4°; paired two-tailed t-test: $t = 0.9$, $P = 0.37$). Thirteen cells failed to change their orientation-selectivity once the first adaptation was carried out, and these cells exhibited strong attractive displacements as fluoxetine was deposited (2.6 ± 1.3° shift after the first adaptation, this shift reached 23.5 ± 14.2° post-adaptation and fluoxetine administration; paired two-tailed t-test: $t = 4.9$, $P = 0.0003$).

Thus, these results suggest that serotonin and fluoxetine (an SSRI) (Manji *et al.*, 2001; Castrén, 2005; Kaneko *et al.*, 2007; Briscoe *et al.*, 2008) potentiate attractive shifts following adaptation, and as a consequence these drugs facilitate the emergence of responses to a new preferred orientation close to the adapter.

The results presented above show the important role of these two drugs in facilitating neuronal adaptation-induced plasticity within the primary visual cortex. Note that for the amplified effect of the drugs (attractive to attractive), tests were significant for serotonin (paired two-tailed t-test: $t = 3.4$, $P = 0.002$) with an increase in amplitude of shifts of more than 50%, whereas for fluoxetine, attractive shift modifications were not significant (paired two-tailed t-test: $t = 0.9$, $P = 0.37$), suggesting that the facilitatory effect is due to direct serotoninergic actions, while the smaller effect of fluoxetine would be due to an indirect path such as inhibition of serotonin reuptake, which is pronounced after chronic administration (Maya-Vetencourt *et al.*, 2008; Wang *et al.*, 2008). Indeed, in a recent investigation, it has been shown that the effect of fluoxetine on polysynaptic transmission is relatively small in comparison with the action of serotonin (Komlosi *et al.*, 2012).

Modulations of response magnitude following serotonin and fluoxetine applications

Figure 6A and B compare response modulations during serotonin and fluoxetine applications for the group of neurons that increased the attractive effect during drug administration. In addition to responses obtained at the flanks of the tuning curve, we focused these analyses on the evoked discharges in response to three orientations: original optimal orientation, the adapter and new optimal orientation. Colored squares (in accordance with the orientation classes) represent average changes in response amplitude relative to the baseline, which corresponds to the response magnitude recorded before testing. These control responses are normalized (100%) in the computations of Fig. 6. As indicated in the Methods, in the absence of drugs, we carried out an adaptation protocol to ensure that indeed the unit is shifting the peak of its orientation curve. One-tailed Wilcoxon rank tests (95% confidence interval) were computed to compare the response amplitude before and after adaptation for each orientation class. Two-way ANOVA (95% significance level)

was used to compare the amplitude of response between two specific classes of orientations: prior to drug administration versus post-drug administration. Blue squares show changes in response amplitude for the original optimal orientation (control). As expected from the previous results, this response amplitude decreased after adaptation. For serotonin and fluoxetine experiments, we found that this

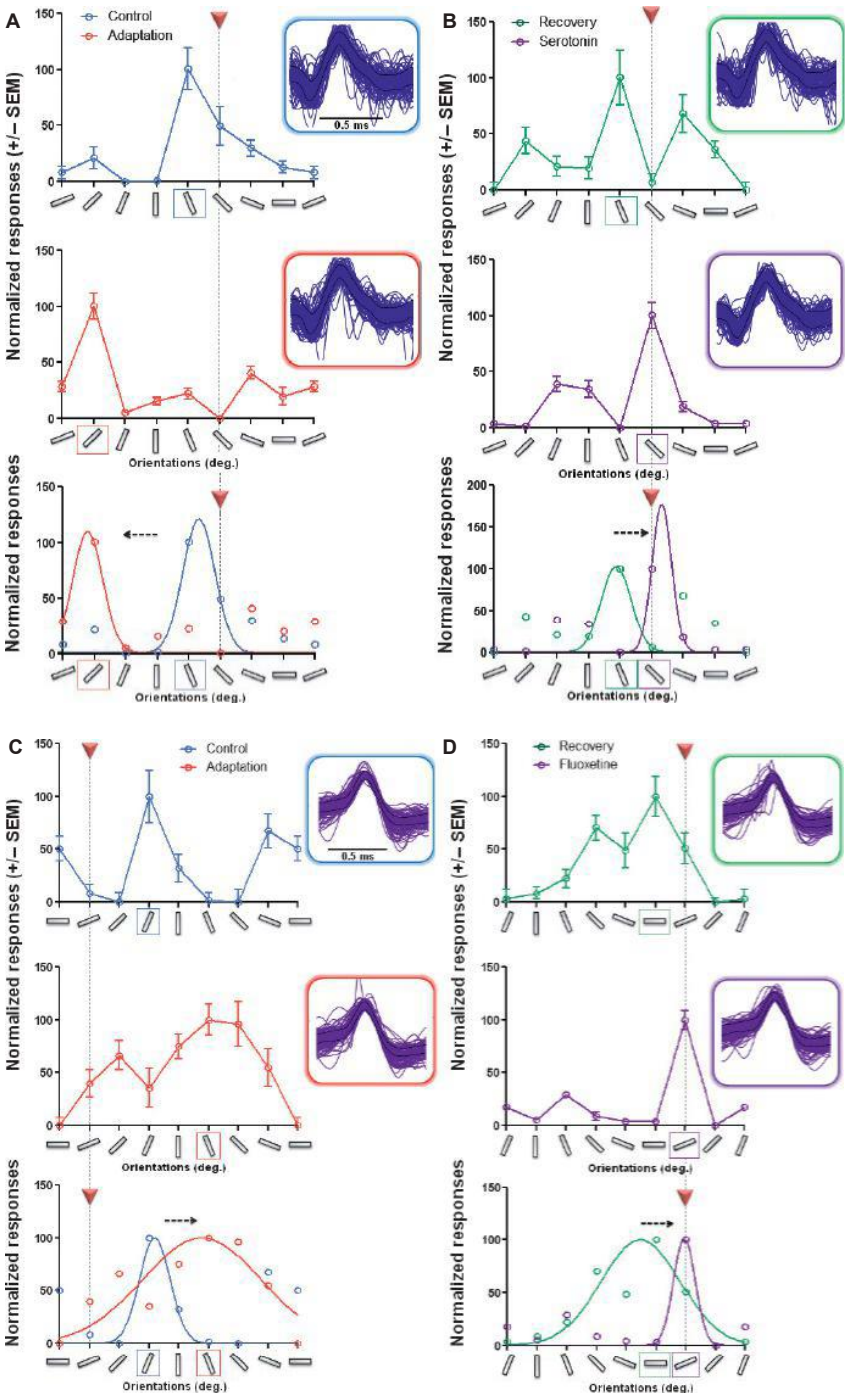

FIG. 4. Inversion of shift by serotonin and fluoxetine. (A) Raw data and Gaussian fit of normalized responses of one neuron for control (blue curve) and after the first adaptation process (red curve). The red triangle indicates the imposed orientation during adaptation. Note the shift of the tuning curve away from the adapter (repulsive shift). (B) Raw data and Gaussian fit of normalized responses of the same recorded cell for recovery (green curve) and after the second adaptation during serotonin deposition (purple curve). Blue spikes represent waveforms of the same neuron over all steps. The drug inversed the shift of the tuning curve towards the adapting orientation (see Gaussian fits below). (C, D) Same effect (inversion of repulsive shift) for a different presented neuron (purple spikes indicating the same cell for all conditions) in the presence of fluoxetine.

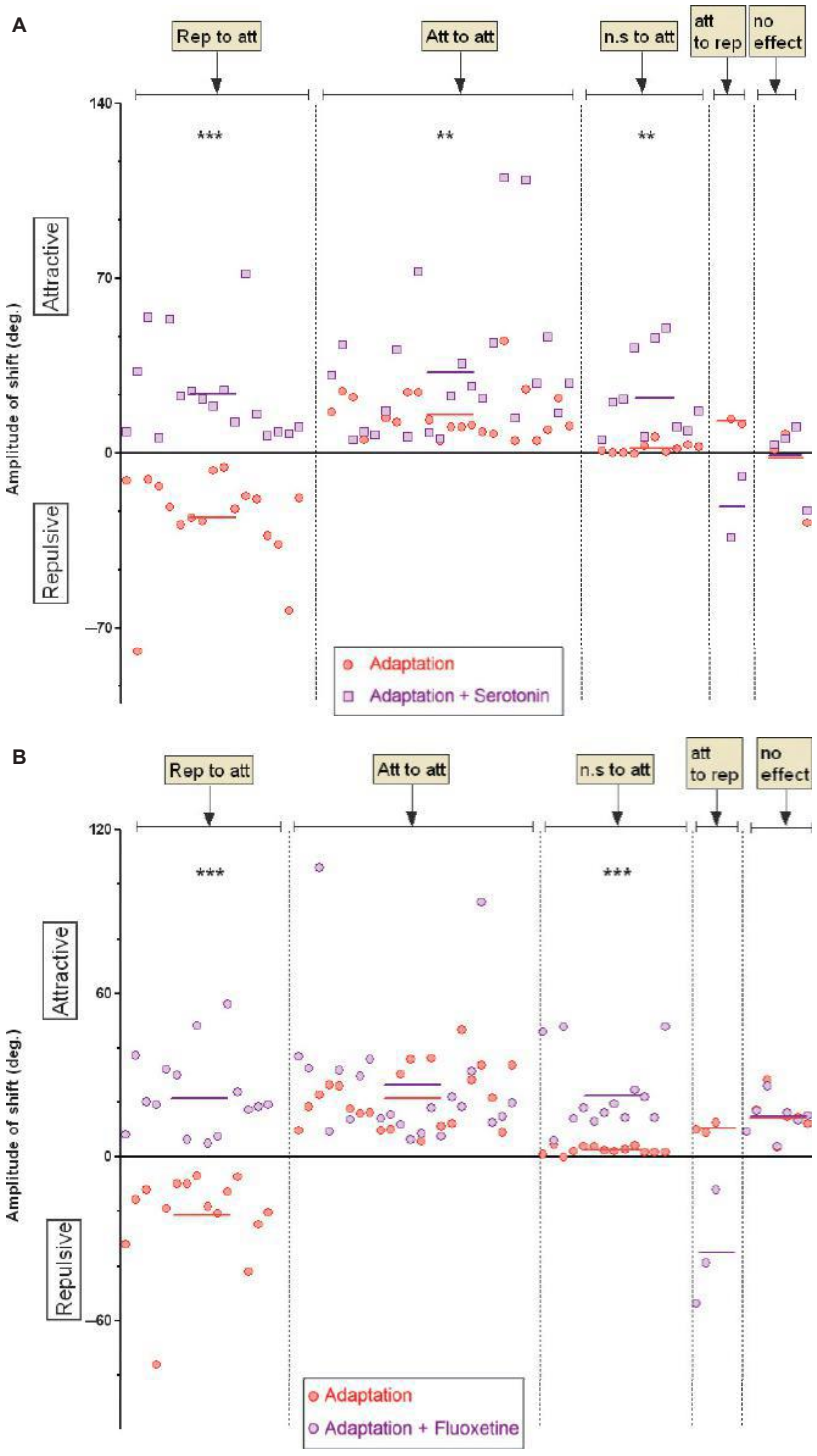

FIG. 5. Modulation of shift-magnitudes for every analysed neuron. (A) Global distribution of neurons for serotonin experiments. Red circles represent shifts of each neuron after the first adaptation, and purple squares represent shifts of the same neurons after the second adaptation during serotonin administration. Horizontal bars indicate the average shift of each group for both conditions. The lower side represents the repulsive side, i.e. the shifts away from the adapter, and the upper side represents the attractive side, i.e. the shifts towards the adapter. The first group (left) shows the reversal effect of serotonin from repulsive to attractive shift (for values see Results). The second group shows the amplified attractive effect. The third group represents refractory neurons; the drug induced an attractive shift (see Results). The fourth group represents a small proportion of neurons which reverse their shifts from attractive to repulsive (two neurons). The last group (right) shows the population of neurons which was not affected by serotonin (no effect). (B) Fluoxetine showed a similar tendency. Red circles show shifts of each analysed cell after the first adaptation, and purple circles represent shifts of the same cells after the second adaptation during fluoxetine administration, stars (***) indicate the significance level of the statistical test (see text).

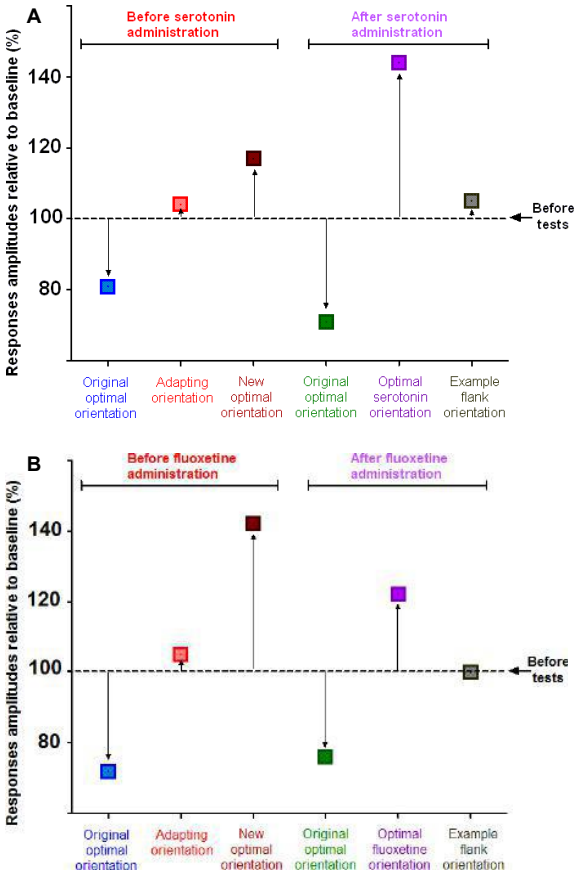

FIG. 6. Graph representing changes in response amplitudes for different orientations. (A) Graph of response amplitudes for serotonin experiments. Colored squares represent averaged changes in response amplitude following a specific stimulus (orientation) in several conditions relative to baseline (normalized firing rate before adaptation = 100%). Blue squares show the change in response amplitude for the original optimal orientation (control), which decreased after adaptation. Red squares show the change in response amplitude for the adapter, which increased post-adaptation. Brown squares show modifications in response amplitude for the new optimal orientation, which increased after adaptation. Green squares represent the new original optimal orientation, which decreased post-adaptation. Purple squares show the change in response amplitude for the preferred orientation during application of serotonin; the response amplitude increased. Gray squares illustrate an example of flank orientation; the response amplitude remained mainly similar. (B) Similar to A, for fluoxetine experiments.

original optimal response decreased in response magnitudes by −19% (Wilcoxon matched-paired signed rank test, $P = 0.020$) and −28% (Wilcoxon matched-paired signed rank test, $P = 0.004$) prior to their application, respectively. Red squares show mean response enhancements to the adapter: attractive shifts + 4.08% (Wilcoxon matched-paired signed rank test, $P = 0.46$) for serotonin experiments and + 5% (Wilcoxon matched-paired signed rank test, $P = 0.20$) for fluoxetine experiments. Brown squares indicate the average change in response amplitude for the new preferred orientation. These discharges increased by 17% (Wilcoxon matched-paired signed rank test, $P = 0.002$) after adaptation for serotonin experiments, and augmented by 42% (Wilcoxon matched-paired signed rank test, $P = 0.0003$) post-adaptation for fluoxetine experiments. The modulation of response magnitude during the drug administration is shown by the three colored squares of the right side in each figure. Green squares represent the original optimal orientation, and in a fashion similar to the first step (before drug administration) these responses declined by 29% (Wilcoxon matched-paired signed rank test, $P = 0.001$) for serotonin tests and 24% (Wilcoxon matched-paired signed rank test, $P = 0.0001$) for fluoxetine experiments. Purple squares represent modifications in firing amplitude for the new preferred orientation after application of serotonin (Fig. 6A) or fluoxetine (Fig. 6B). The magnitude of these responses increased by 44% (Wilcoxon matched-paired signed rank test, $P = 0.04$) for neurons administered with serotonin, and by 22% (Wilcoxon matched-paired signed rank test, $P = 0.0005$) for neurons administered with fluoxetine. Gray squares indicate flank orientations (67.5–90° from the optimal orientation); these weak responses fail to change following drug application. Thus, this suggests that the influence of

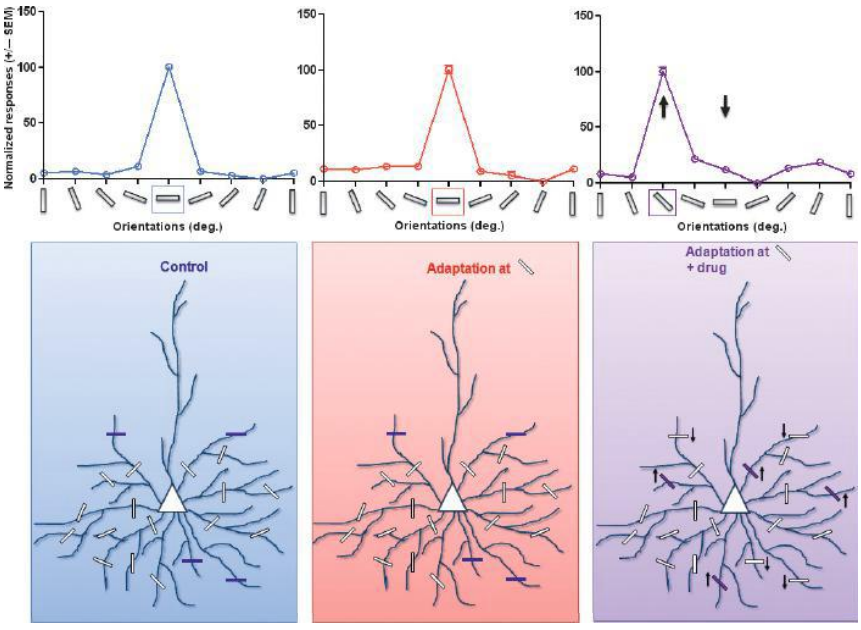

FIG. 7. Proposed model for adaptation and action of drug mechanisms. Example of a refractory neuron based on results with respective tuning curves for each condition: control (blue), post-adaptation (red) and post-administration of the drug (purple). White bars represent all the preferred orientations for each segment of the dendrite. After the first adaptation, the preferred orientation remained as for the control (horizontal). After the second adaptation during drug administration, the synaptic weight for the adapter increased and the synaptic weight for the original optimal decreased (push–pull).

serotonin as well as fluoxetine on response amplitude is limited to adapted and original orientations, i.e. it is not a global effect.

It is noticeable that the response magnitude of neurons is considerably modulated throughout the experiments for specific orientations (described above), but it is interesting that firing magnitudes of neurons post-drug administration adaptation (purple square) are not significantly changed in comparison with prior to drug administration (brown square) (two-way ANOVA test: $F = 1.33$, $P = 0.25$ for serotonin experiments, $F = 1.7$, $P = 0.30$ for fluoxetine experiments). In particular, no additional strengthening was observed. Hence, it is worth noting that the effect of both drugs is overwhelming on the shift magnitude rather than firing rates. It may be due to saturation of the discharge rates. It can be inferred that both drugs modulate the plasticity by affecting mostly the selectivity range of a neuron rather than its evoked firing. Furthermore, spontaneous activity remained unchanged after administration of the drug (one-way ANOVA: $F = 0.11$, $P = 0.95$, see Supporting Information Fig. S2B).

Discussion

The results described may be summarized as follows: the neurotransmitter serotonin and SSRI fluoxetine facilitate movement of the peak of orientation tuning curve in the direction of the adapter, thus producing attractive shifts. Indeed, in the absence of drugs, about 30% of cells displaced their optimal orientation in the repulsive direction, whereas in the presence of both drugs, the proportion of repulsive shifts is quite small: only a few cells exhibited repulsive direction. In addition, the magnitude of attractive shifts increased under the influence of both agents and particularly with serotonin. Interestingly, the firing rates were not increased in a significant fashion. The differential effects suggest that both drugs promote orientation-selectivity rather than the strength of the evoked discharges.

Comparative results

In previous studies, we have shown that successive adaptation enhances the firing rate of responses to the new optimal orientation. Consequently, the responses following the second adaptation (drug application) may be partially due to reiteration of the adaptation procedures and not entirely attributed to the presence of drugs. However, in these previous reports (Ghisovan *et al.*, 2008), shifts in the orientation tuning curves following the second adaptation were relatively small in magnitude (magnitude of shifts between the two adaptation periods were ~ 15.7–19.5° and ~ 15.6–13.6° for attractive and repulsive shifts, respectively). This contrasts strikingly with the present results. The average attractive shift was 24° under the influence of serotonin and 23.4° under the influence of fluoxetine in the case of reversal from repulsive to attractive displacements, whereas the shift increased on average to 33° with serotonin and 27° with fluoxetine for cells displaying an attractive shift after the first attempt. Furthermore, and notably during drug deposition, only very few neurons displayed repulsive shifts after adaptation: 5% for both serotonin and fluoxetine experiments. Without drugs, the proportion of repulsive shifts remained much higher: 16% (Ghisovan *et al.*, 2008). Neurons which maintained their original preferred orientation after the first adaptation protocol changed their refractory reaction under the influence of both drugs. Indeed, for neurons tested with serotonin, the average shift increased significantly (paired two-tailed *t*-test: $t = 3.8$, $P = 0.0039$), and for neurons tested with the antidepressant fluoxetine, neurons that were refractory after the first adaptation showed a significant shift (paired two-tailed *t*-test: $t = 4.9$, $P = 0.0003$) after the second adaptation during drug administration. Thus, serotonin and fluoxetine induce attractive shifts, promoting sensitization of refractory neurons to 'learn' the imposed stimulus. This suggests that the action of both substances is biasing the synaptic drive in favor of the adapter. It can be attained by changing the cellular threshold resulting in a higher firing rate of the neurons with a preferred orientation similar to that of the adapter. This could explain why the spontaneous activity remained unchanged. There seems to be a dual effect of the second adaptation: without drugs it is the response magnitude that is enhanced (to the adapter) while displacement of the peak of the orientation tuning curve remained to a large extent unmodified (see above). In the presence of drugs, it is the magnitude of the shifts that is augmented, with a strong bias towards attractive direction.

Interestingly, response magnitudes evoked by flank orientations are not significantly changed; the influence of drugs is restricted to the adapter and to the original preferred orientation.

Sensitization to the adapter

Both drugs were closely associated with reactivation of brain plasticity. Maya-Vetencourt *et al.* (2008) unambiguously showed in rats that long-term chronic treatment of fluoxetine (in drinking water) reduces GABAergic inhibition and simultaneously increases brain-derived neurotrophic factor (BDNF) expression, allowing the reinstatement of ocular dominance plasticity in adult rats. It appears that this antidepressant compound increases glutamatergic synaptic transmission. It has also been suggested that fluoxetine restructures branches of dendritic extremities (Chen *et al.*, 2011), has neurodevelopmental effects (Homberg *et al.*, 2010), and potentiates neuron maturation and synaptic plasticity (Wang *et al.*, 2008). In adult rats, serotonin reinstates the induction of *N*-methyl-D-aspartate (NMDA)-dependent long-term potentiation (Park *et al.*, 2012). Furthermore, an increase of serotonin transmission augments the BDNF-trkB signaling path, which in turn promotes processes of plasticity (Maya-Vetencourt *et al.*, 2011). In addition, it is suggested that the 5-HT_{1A} receptor is associated with epigenetic remodeling of chromatin structure, leading to reactivation of cortical plasticity (Maya-Vetencourt *et al.*, 2011).

As we deposited serotonin, it is very likely that we increased the amount of serotonin in the tissue volume open to synaptic transmission and corresponding receptors. If their model (Maya-Vetencourt *et al.*, 2011) is applied to our data, this would suggest that both drugs lead to new equilibrium of the synaptic inputs, which in turn allows functional modification of neuronal circuits (Jaffer *et al.*, 2012). Results suggest that both drugs act on most active synapses (Chen *et al.*, 2011). Application of the adapter certainly produces a surge of action potentials during a brief time-window and high probability of synchronizing inputs upon the recipient neurons (Ghisovan *et al.*, 2008). Hence our protocol implies that cells driven by the adapter for several minutes impact the dendritic membrane in such a way that clusters of dendritic spines prevail in pushing the cell to fire maximally in response to orientations close to the adapter. Furthermore, our data suggest that these modifications may occur in a relatively short period of time, compatible with the time course of molecular cascades described above. Because our results show that the responses are roughly limited to the orientations close to the adapter, they are reminiscent of the stimulus-selective response potentiation (SRP) described by Frenkel *et al.* (2006), which requires activation of NMDA receptors. In support of this, it has been shown that serotonin enhances responses to the NMDA receptors in adult rats (Reynolds *et al.*, 1988).

Serotonin and fluoxetine fail to influence firing rates

Several investigations have been reported on neuronal selectivity to orientation for different species such as cats (Carandini & Ferster, 2000; Kisvárday *et al.*, 2000) and rodents (Jia *et al.*, 2010). Combining high-speed two-photon imaging with electrophysiological recordings (Jia *et al.*, 2010) and functional mapping with electrophysiological recordings or optical imaging followed by three-dimensional anatomical reconstruction (Kisvárday *et al.*, 2000), it has been demonstrated that a single dendritic branch receives synaptic connections from neurons selective to different orientations (Kisvárday *et al.*, 2000; Jia *et al.*, 2010). Such a large range indicates that many or all orientations may be efficient in exciting a single cortical cell. Although dendritic branches show synaptic contacts associated with a particular axis of orientation, these studies demonstrate that various orientations are interspersed and represented throughout the dendritic tree (Kisvárday *et al.*, 2000; Jia *et al.*, 2010). Therefore, activating an alternative group of synapses shifts the optimal orientation but not necessarily the discharge rates. The firing rate that is the neuronal output is susceptible to saturation (Carandini & Ferster, 2000) and hence once available receptors are saturated then the maximal rate of action potential firing is reached and no further increase is possible. It is also possible that the restriction of the firing rates may be due to inhibition.

Because weak responses evoked by unpreferred orientation (flank orientations) are barely modified by both drugs, it appears that each drug's action is constrained almost to the initial optimal orientation (decline) and the new acquired orientation (facilitation). It has been suggested that this dual modulation is attributed to a push–pull mechanism (Palmer & Davis, 1981; Ferster, 1988, 1992; Tolhurst & Dean, 1990; Troyer *et al.*, 1998; Shapley *et al.*, 2003; Ghisovan *et al.*, 2009), which appears to be sensitive to SSRIs.

Proposed model

Based on our findings, we suggest a model for how adaptation mechanisms might occur in the primary visual cortex at the neuronal level and how serotonin and fluoxetine could regulate post-adaptation mechanisms. The model takes into consideration that the output of primary visual cortex neurons is due to synaptic weight distributions within the dendritic tree of a neuron for every orientation. As a consequence, the maximum discharge occurs for specific orientations that solicit predominantly the corresponding synaptic links. The adaptation process tends to reorganize this distribution such that neurons change their synaptic weight favoring the imposed orientation or in the direction opposite to it, as has been described previously.

Based on our results, we show in the proposed model (Fig. 7) an example of a refractory neuron (same neuron as in Fig. 3). As tuning curves overlapped pre- and post-adaptation, this could be attributed to the same synaptic equilibrium, which is not disturbed and maintained post-adaptation (here 0° is the optimal for control and post-adaptation, no shift). Interestingly, serotonin or fluoxetine appears to recalibrate the synaptic cross-influence by a push–pull mechanism, possibly associated with the corresponding decrease and increase of synaptic strengths for the original optimal orientation and the adapter, respectively, thus leading to a shift. This mechanism could involve specific receptors to induce this push–pull effect.

Plasticity within the primary visual cortex is a key property which can contribute to cerebral treatments or cognitive mechanisms such as memory or learning. We have shown that the neurotransmitter serotonin and antidepressant fluoxetine (an SSRI) promote attractive shifts to an imposed stimulus and facilitate neuronal property changes in learning process of a new feature, thus facilitating cerebral plasticity in primary visual cortex neurons. We have revealed a pre-eminent role of serotonin, which could be involved in a push–pull mechanism responsible for response modulations due to serotoninergic affinity to its receptors. Fluoxetine would act either by inhibiting serotoninergic recapture, or by direct actions on the changes of properties of specialized neurons for orientation in V1. Our experiments showed a predominant role of serotonin and fluoxetine by improving the "training" capacity of the refractory neurons, as well as a facilitation of plasticity for the repulsive neurons in relation to adaptation, by guiding the primary visual neurons to learn an unfamiliar feature of an image.

Supporting Information

Additional supporting information can be found in the online version of this article:
Fig. S1. Example tuning curves showing the local effect of the drug.
Fig. S2. Orientation selectivity index and spontaneous activity.

Acknowledgement

This study was supported by grants to S.M. (NSERC, FQRNT).

Abbreviations

5-HT, 5-hydroxytryptamine; BDNF, brain-derived neurotrophic factor; GABA, γ-aminobutyric acid; NMDA, *N*-methyl-D-aspartate; OSI, orientation selectivity index; RF, receptive field; SRP, stimulus-selective response potentiation; SSRI, selective serotonin reuptake inhibitor; trkB, tyrosine-related kinase B.

References

Avesar, D. & Gulledge, A.T. (2012) Selective serotonergic excitation of callosal projection neurons. *Front. Neural Circuits*, **6**, 12.
Bachatene, L., Bharmauria, V., Rouat, J. & Molotchnikoff, S. (2012) Adaptation-induced plasticity and spike waveforms in cat visual cortex. *NeuroReport*, **23**, 88–92.
Bardy, C., Huang, J.Y., Wang, C., FitzGibbon, T. & Dreher, B. (2006) "Simplification" of responses of complex cells in cat striate cortex: suppressive surrounds and "feedback" inactivation. *J. Physiol.*, **574**, 731–750.
Barlow, H.B., Blakemore, C. & Pettigrew, J.D. (1967) The neural mechanism of binocular depth discrimination. *J. Physiol.*, **193**, 327–342.
Bear, M.F. & Singer, W. (1986) Modulation of visual cortical plasticity by acetylcholine and noradrenaline. *Nature*, **320**, 172–176.
Bishop, P.O. & Henry, G.H. (1972) Striate neurons: receptive field concepts. *Invest. Ophthalmol.*, **11**, 346–354.
Briscoe, V.J., Ertl, A.C., Tate, D.B., Dawling, S. & Davis, S.N. (2008) Effects of a selective serotonin reuptake inhibitor, fluoxetine, on counterregulatory responses to hypoglycemia in healthy individuals. *Diabetes*, **57**, 2453–2460.
Carandini, M. & Ferster, D. (2000) Membrane potential and firing rate in cat primary visual cortex. *J. Neurosci.*, **20**, 470–484.
Castrén, E. (2005) Is mood chemistry? *Nat. Rev. Neurosci.*, **6**, 241–246.
Chen, J.L., Lin, W.C., Cha, J.W., So, P.T., Kubota, Y. & Nedivi, E. (2011) Structural basis for the role of inhibition in facilitating adult brain plasticity. *Nat. Neurosci.*, **14**, 587–594.
Chiu, C. & Weliki, M. (2003) The role of neural activity in the development of orientation selectivity. In Chalupa, L.M. & Werner, J. (Eds), *The Visual Neurosciences*. MIT Press, Cambridge, MA, pp. 117–125.
Chollet, F., Tardy, J., Albucher, J.F., Thalamas, C., Berard, E., Lamy, C., Bejot, Y., Deltour, S., Jaillard, A., Niclot, P., Guillon, B., Moulin, T., Marque, P., Pariente, J., Arnaud, C. & Loubinoux, I. (2011) Fluoxetine for motor recovery after acute ischaemic stroke (FLAME): a randomised placebo-controlled trial. *Lancet Neurol.*, **10**, 123–130.
Dragoi, V., Sharma, J. & Sur, M. (2000) Adaptation-induced plasticity of orientation tuning in adult visual cortex. *Neuron*, **28**, 287–298.

Ferster, D. (1988) Spatially opponent excitation and inhibition in simple cells of the cat visual cortex. *J. Neurosci.*, **8**, 1172–1180.
Ferster, D. (1992) The synaptic inputs to simple cells of the cat visual cortex. *Prog. Brain Res.*, **90**, 423–441.
Frenkel, M.Y., Sawtell, N.B., Diogo, A.C.M., Yoon, B., Neve, R.L. & Bear, M.F. (2006) Instructive effect of visual experience in mouse visual cortex. *Neuron*, **51**, 339–349.
Ghisovan, N., Nemri, A., Shumikhina, S. & Molotchnikoff, S. (2008) Visual cells remember earlier applied target: plasticity of orientation selectivity. *PLoS ONE*, **3**, e3689.
Ghisovan, N., Nemri, A., Shumikhina, S. & Molotchnikoff, S. (2009) Long adaptation reveals mostly attractive shifts of orientation tuning in cat primary visual cortex. *Neuroscience*, **164**, 1274–1283.
Harauzov, A., Spolidoro, M., DiCristo, G., De Pasquale, R., Cancedda, L., Pizzorusso, T., Viegi, A., Berardi, N. & Maffei, L. (2010) Reducing intracortical inhibition in the adult visual cortex promotes ocular dominance plasticity. *J. Neurosci.*, **30**, 361–371.
Homberg, J.R., Schubert, D. & Gaspar, P. (2010) New perspectives on the neurodevelopmental effects of SSRIs. *Trends Pharmacol. Sci.*, **31**, 60–65.
Hubel, D.H. & Wiesel, T.N. (1959) Receptive fields of single neurones in the cat's striate cortex. *J. Physiol.*, **148**, 574–591.
Hubel, D.H. & Wiesel, T.N. (1968) Receptive fields and functional architecture of monkey striate cortex. *J. Physiol.*, **195**, 215–243.
Jaffer, S., Vorobyov, V., Kind, P.C. & Sengpiel, F. (2012) Experience-dependent regulation of functional maps and synaptic protein expression in the cat visual cortex. *Eur. J. Neurosci.*, **35**, 1281–1294.
Jia, H., Rochefort, N.L., Chen, X. & Konnerth, A. (2010) Dendritic organization of sensory input to cortical neurons *in vivo*. *Nature*, **464**, 1307–1312.
Kaneko, Y., Kashiwa, A., Ito, T., Ishii, S., Umino, A. & Nishikawa, T. (2007) Selective serotonin reuptake inhibitors, fluoxetine and paroxetine, attenuate the expression of the established behavioral sensitization induced by methamphetamine. *Neuropsychopharmacol.*, **32**, 658–664.
Kasamatsu, T., Watabe, K., Heggelund, P. & Scholler, E. (1985) Plasticity in cat visual cortex restored by electrical stimulation of the locus coeruleus. *Neurosci. Res.*, **2**, 365–386.
Kisvárday, Z.F., Crook, J.M., Buzás, P. & Eysel, U.T. (2000) Combined physiological–anatomical approaches to study lateral inhibition. *J. Neurosci. Meth.*, **103**, 91–106.
Kohn, A. & Movshon, J.A. (2004) Adaptation changes the direction tuning of macaque MT neurons. *Nat. Neurosci.*, **7**, 764–772.
Komlosi, G., Molnar, G., Rozsa, M., Olah, S., Barzo, P. & Tamas, G. (2012) Fluoxetine (prozac) and serotonin act on excitatory synaptic transmission to suppress single layer 2/3 pyramidal neuron-triggered cell assemblies in the human prefrontal cortex. *J. Neurosci.*, **32**, 16369–16378.
Krekelberg, B., Van Wezel, R.J. & Albright, T.D. (2006) Adaptation in macaque MT reduces perceived speed and improves speed discrimination. *J. Neurophysiol.*, **95**, 255–270.
Liao, D.S., Krahe, T.E., Prusky, G.T., Medina, A.E. & Ramoa, A.S. (2004) Recovery of cortical binocularity and orientation selectivity after the critical period for ocular dominance plasticity. *J. Neurophysiol.*, **92**, 2113–2121.
Licata, F., Li Volsi, G., Maugeri, G., Ciranna, L. & Santangelo, F. (1993) Serotonin-evoked modifications of the neuronal firing rate in the superior vestibular nucleus: a microiontophoretic study in the rat. *Neuroscience*, **52**, 941–949.
Maffei, L. & Fiorentini, A. (1973) The visual cortex as a spatial frequency analyser. *Vision Res.*, **13**, 1255–1267.
Manji, H.K., Drevets, W.C. & Charney, D.S. (2001) The cellular neurobiology of depression. *Nat. Med.*, **7**, 541–547.
Marshansky, S., Shumikhina, S. & Molotchnikoff, S. (2011) Repetitive adaptation induces plasticity of spatial frequency tuning in cat primary visual cortex. *Neuroscience*, **172**, 355–365.
Mataga, N., Imamura, K. & Watanabe, Y. (1992) L-threo-3,4-dihydroxyphenylserine enhanced ocular dominance plasticity in adult cats. *Neurosci. Lett.*, **142**, 115–118.
Maya-Vetencourt, J.F. & Origlia, N. (2012) Visual cortex plasticity: a complex interplay of genetic and environmental influences. *Neural Plast.*, **2012**, 631965.
Maya-Vetencourt, J.F., Sale, A., Viegi, A., Baroncelli, L., De Pasquale, R., O'Leary, O.F., Castrén, E. & Maffei, L. (2008) The antidepressant fluoxetine restores plasticity in the adult visual cortex. *Science*, **320**, 385–388.
Maya-Vetencourt, J.F., Tiraboschi, E., Spolidoro, M., Castrén, E. & Maffei, L. (2011) Serotonin triggers a transient epigenetic mechanism that reinstates adult visual cortex plasticity in rats. *Eur. J. Neurosci.*, **33**, 49–57.
Morishita, H., Miwa, J.M., Heintz, N. & Hensch, T.K. (2010) Lynx1, a cholinergic brake, limits plasticity in adult visual cortex. *Science*, **330**, 1238–1240.
Movshon, J.A. (1975) The velocity tuning of single units in cat striate cortex. *J. Physiol.*, **249**, 445–468.
Nemri, A., Ghisovan, N., Shumikhina, S. & Molotchnikoff, S. (2009) Adaptive behavior of neighboring neurons during adaptation-induced plasticity of orientation tuning in VI. *BMC Neurosci.*, **10**, 147.
Palmer, L.A. & Davis, T.L. (1981) Receptive-field structure in cat striate cortex. *J. Neurophysiol.*, **46**, 260–276.
Park, S.W., Jang, H.J., Cho, K.H., Kim, M.J., Yoon, S.H. & Rhie, D.J. (2012) Developmental switch of the serotonergic role in the induction of synaptic long-term potentiation in the rat visual cortex. *Korean J. Physiol. Pha.*, **16**, 65–70.
Pizzorusso, T., Medini, P., Berardi, N., Chierzi, S., Fawcett, J.W. & Maffei, L. (2002) Reactivation of ocular dominance plasticity in the adult visual cortex. *Science*, **298**, 1248–1251.
Pizzorusso, T., Medini, P., Landi, S., Baldini, S., Berardi, N. & Maffei, L. (2006) Structural and functional recovery from early monocular deprivation in adult rats. *Proc. Natl. Acad. Sci. USA*, **103**, 8517–8522.
Ramoa, A.S., Mower, A.F., Liao, D. & Jafri, S.I.A. (2001) Suppression of cortical NMDA receptor function prevents development of orientation selectivity in the primary visual cortex. *J. Neurosci.*, **21**, 4299–4309.
Reynolds, J.N., Baskys, A. & Carlen, P.L. (1988) The effects of serotonin on *N*-methyl-D-aspartate and synaptically evoked depolarizations in rat neocortical neurons. *Brain Res.*, **456**, 286–292.
Shapley, R., Hawken, M. & Ringach, D.L. (2003) Dynamics of orientation selectivity in the primary visual cortex and the importance of cortical inhibition. *Neuron*, **38**, 689–699.
Stroud, A.C., Ledue, E.E. & Crowder, N.A. (2012) Orientation specificity of contrast adaptation in mouse primary visual cortex. *J. Neurophysiol.*, **108**, 1381–1391.
Swindale, N.V. (1998) Orientation tuning curves: empirical description and estimation of parameters. *Biol. Cybern.*, **78**, 45–56.
Tanaka, S., Tani, T., Ribot, J., O'Hashi, K. & Imamura, K. (2009) A postnatal critical period for orientation plasticity in the cat visual cortex. *PLoS ONE*, **4**, e5380.
Tolhurst, D.J. & Dean, A.F. (1990) The effects of contrast on the linearity of spatial summation of simple cells in the cat's striate cortex. *Exp. Brain Res.*, **79**, 582–588.
Troyer, T.W., Krukowski, A.E., Priebe, N.J. & Miller, K.D. (1998) Contrast-invariant orientation tuning in cat visual cortex: thalamocortical input tuning and correlation-based intracortical connectivity. *J. Neurosci.*, **18**, 5908–5927.
Vorobyov, V., Kwok, J.C., Fawcett, J.W. & Sengpiel, F. (2013) Effects of digesting chondroitin sulfate proteoglycans on plasticity in cat primary visual cortex. *J. Neurosci.*, **33**, 234–243.
Wang, J.W., David, D.J., Monckton, J.E., Battaglia, F. & Hen, R. (2008) Chronic fluoxetine stimulates maturation and synaptic plasticity of adult-born hippocampal granule cells. *J. Neurosci.*, **28**, 1374–1384.
Zhong, P. & Yan, Z. (2011) Differential regulation of the excitability of prefrontal cortical fast-spiking interneurons and pyramidal neurons by serotonin and fluoxetine. *PLoS ONE*, **6**, e16970.

Adaptation-induced plasticity and spike waveforms in cat visual cortex

Lyes Bachatene[a], Vishal Bharmauria[a], Jean Rouat[a,b] and Stéphane Molotchnikoff[a,b]

Orientation-selective neurons shift their preferred orientation after being adapted to a nonpreferred orientation. These shifts of the peaks of tuning curves may be in the attractive or repulsive direction in relation to the adapter orientation. In anesthetized cats, we recorded evoked electrical responses from the visual cortex in a conventional manner. The recorded spikes in cortex may present two typical waveforms: regular spikes or fast spikes. However, there is no evidence whether the shapes of spikes are related to the attractive or repulsive shifts of orientation tuning curves of cells. Our results show that after adaptation the recorded cells with both attractive and repulsive shifts display one or the other shape of spike. However, the magnitude of shifts is systematically higher for regular spikes, which is attributed to putative pyramidal cells, whereas tuning curves for fast spikes have smaller magnitudes and are evoked by putative interneurons. *NeuroReport* **00:000–000** © **2011 Wolters Kluwer Health | Lippincott Williams & Wilkins.**

NeuroReport 2011, **00**:000–000

Keywords: adaptation, fast spikes, interneurons, neurophysiology, pyramidal cells, regular spikes, visual cortex

[a]Department of Biological Sciences, University of Montreal, Montreal and [b]Department of Electrical and Computer Engineering, University of Sherbrooke, Sherbrooke, Quebec, Canada

Correspondence to Dr Stéphane Molotchnikoff, PhD, Department of Biological Sciences, University of Montreal, Montreal, Quebec, Canada
Tel: +1 514 343 6111 x6616; fax: +1 514 343 2293;

Received 13 October 2011 **accepted** 23 October 2011

Introduction

Neurons in the mammalian visual cortex are tuned to respond to visual stimuli such as contour orientation, motion direction, and speed [1–3]. In previous studies, it has been shown that it is possible to modify the preferred stimulus which optimally excites neurons by applying a nonpreferred adaptation stimulus [4,5] in adult visual cortex. Adaptation studies in recent years have presented a more complex picture where prolonged exposure to a nonpreferred orientation has shown modifications in neurons' preferred orientations [4,6,7]. Longer adaptation durations ($\geq$ 6 min) were shown to induce attractive shifts more frequently than repulsive shifts [6,8,9], but repeated or prolonged exposure to an adapter is also known to reduce neuronal responsiveness to that same stimulus, especially if it is the neuron's preferred stimulus [10].

Preference for orientation is considered relatively stable in the primary visual cortex (V1) as an emergent property that is established early in life following the so-called critical period [11]. Classically, spike waveforms allow dissociating two functional cell-groups into excitatory pyramidal cells and inhibitory interneurons [12,13]; hence, it is worth investigating how these two cell types react to adaptation. To this aim, we dissociated the recorded cells and analyzed their respective orientation tunings before and after adaptation to a nonpreferred orientation. This study deciphers whether after adaptation there is a relation between behaviour (attractive or repulsive) of cells and their respective waveforms. The most novel and interesting finding in our results was that the regular-spiking cells always shifted with higher magnitude than fast-spiking cells after adaptation. Furthermore, both types of cells shifted their peaks of orientations in either direction.

Methods

Animal preparation and electrophysiological recordings

Experiments were carried with the approval of Université de Montréal animal care committee following the guidelines of the Canadian Council on Animal Care. Anesthetized and paralyzed cats were prepared for electrophysiological recordings in upper layers of visual cortex (two to three, recording depths 250–1500 μm) in a conventional manner fully described previously [8,9,14]. A brief account is provided below.

Adaptation protocol

After manual receptive field characterization (all receptive fields were within 15° of area centralis), nine electrically generated, oriented drifting gratings were selected and centered on the preferred orientation for the entire experiment. Tuning curves covered 180° (22.5° intervals). Test orientations were presented in monocular manner in random order. Each oriented stimulus was presented in blocks of 25 trials (4.1 s each) with a random intertrial interval (1.0–3.0 s) during which no stimulus was presented. Once control orientation tuning curves were characterized, an adapting oriented stimulus was presented continuously for 12 min. The adapting stimulus was a drifting grating whose orientation was generally set within 22.5 to 67.5° of the neurons' preferred orientations. No recordings were performed during this

0959-4965 © 2011 Wolters Kluwer Health | Lippincott Williams & Wilkins DOI: 10.1097/WNR.0b013e32834e7e71

adaptation period. Immediately after adaptations, orientation tuning curves were measured starting with the adapting and control preferred orientations, whereas the remaining orientations were recorded in random order.

Data analysis

Once single cells were sorted out offline from multiunit spike trains accumulated during data acquisition (Spike 2, Cambridge Electronic Design, CED Limited, Cambridge, England), orientation tuning curves were constructed from raw data and fitted with the Gaussian function. This allowed us to determine the preferred orientation of neurons with precision and then measure shifts in orientation preference. The Gaussian function is defined as

$$y = b + \mathrm{rmx} \times \exp\{-[(x - x0)^2] / 2s^2\},$$

where b is the baseline, rmx is max firing rate, x is used orientation, $x0$ is optimal orientation, and s is sigma.

In the present study, over 82% of V1 neurons were well tuned to stimulus orientation. However, it was necessary to ensure that cells in our sample were properly tuned for orientation. In our experiments, 25 consecutive measurements of a neuron's response to the same stimulus yielded 25 slightly different tuning curves. Adaptation-induced shifts were measured as the distance between peak positions of the fitted tuning curves before and after conditioning. To assess the statistical significance of tuning shifts, curve fits were generated separately for each of the 25 trials, and the mean difference was tested by a paired t-test. In all cases, shifts in preferred orientation greater than 5° are statistically significant (paired sample two-tailed t-test, $P < 0.01$) [9].

Cells were sorted out offline from multiunit activity of the recording site and were analyzed cell by cell (single-unit activity). We measured the degree of shift for each cell. This allowed us to classify the cells on the basis of their behavior: attractive or repulsive, or with no shift (preferred orientation remained within 5° of the initial optimal orientation). The spike waveforms were dissociated in the ascending phase of the action potential by measuring the slope (dv/dt) of each spike within an interval of 0.2 ms. This computation allowed us to separate the regular-spiking cells from the fast-spiking cells [15,16].

Polar plots that calculate the bandwidth of each cell were constructed on the basis of its response at all orientations. Chi-square test was done to estimate significance of difference between the bandwidth of fast spikes and regular spikes.

Results

We recorded the multiunit activity of cells for stimulations at nine orientations in the primary visual cortex of anesthetized cats before and after adapting the neurons for a period of 12 min. We analyzed the single-unit activity of cells by spike sorting and we sorted out 73 cells (Table 1).

Figure 1a shows the distribution of regular and fast spikes according to dv/dt (slope) calculations in a time window of 0.2 ms. Both groups are clearly distinguished. In Fig. 1b, waveforms of all 73 cells were overlaid illustrating the difference between spike shapes, wherein red waveforms stand for fast-spiking cells ($n = 23$), whereas green

Table 1 Classification of cells after adaptation

		Attractive	Repulsive	No shift
Total cells ↓ → n=73 cells		42 (57%)	18 (25%)	13 (18%)
Regular spikes	50 (68%)	30 (41%)	14 (19%)	6 (8%)
Fast spikes	23 (32%)	12 (16%)	4 (6%)	7 (10%)

Fig. 1

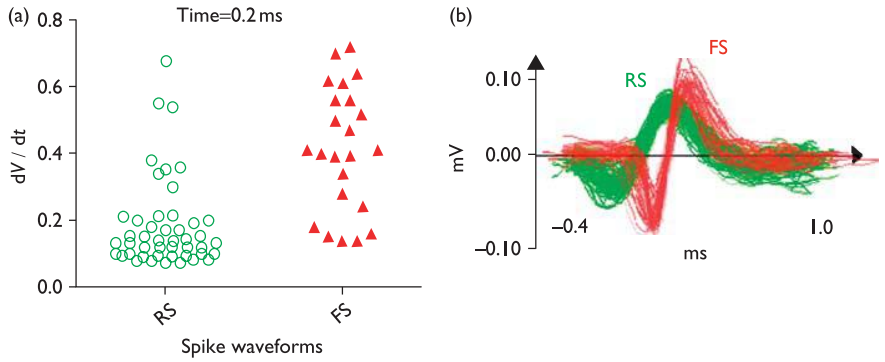

Comparison between regular spikes (RS) and fast spikes (FS). (a) Distribution of RS and FS based on dv/dt (slope) in a time window of 0.2 ms. (b) Superposition of RS and FS from all cells.

indicates regular-spiking cells ($n = 50$). Furthermore, we compared the distribution pattern of spikes for the rising phase of waveforms. We found that regular spikes and fast spikes were distinct by their ascending phase, that is, regular spikes always had a lesser slope than fast spikes (Fig. 1a and b). Also, after aligning the waveforms of fast spikes and regular spikes at the same origin we observed that regular spikes peak earlier than fast spikes by a phase difference of (almost) 0.1 ms (Fig. 1b).

We then classified neurons on the basis of their behavior (attractive, repulsive, no shift) and shape (regular or fast). Overall results are summarized in Table 1. Figure 2 illustrates a typical example. In Fig. 2a and b, Gaussian tuning curves are plotted for two individual cells for all 25 trials. Waveforms for these cells are illustrated in Fig. 2c and d. The cell in Fig. 2a shifted by 20°, whereas the cell in Fig. 2b shifted by 15°. Both units shifted in the attractive direction (*t*-test, $P < 0.05$), even though they belonged to different groups. Consistent with published data [4,5], regular-spiking cells had a sharper tuning curve for orientation, whereas fast-spiking cells exhibited a broader tuning curve. Indeed, both types of cells react in attractive or repulsive directions. The polar plot (Fig. 2e) exhibiting the bandwidth illustrates the representative difference characterizing both types of cells. Fast-spiking cells responded strongly to more orientations creating broadly tuned bandwidths than regular-spiking cells that responded strongly to a few orientations (roughly optimal) creating narrowly tuned bandwidths (Fig. 2e) because discharge rates declined rapidly as the angle of orientation tilted away from the preferred axis [1,2,9–11]. Chi-square tests compared the responses at every tested orientation and showed a significant difference between both bandwidths ($P < 0.0001$, $\alpha < 0.05$, $n = 8$ orientations).

Fig. 2

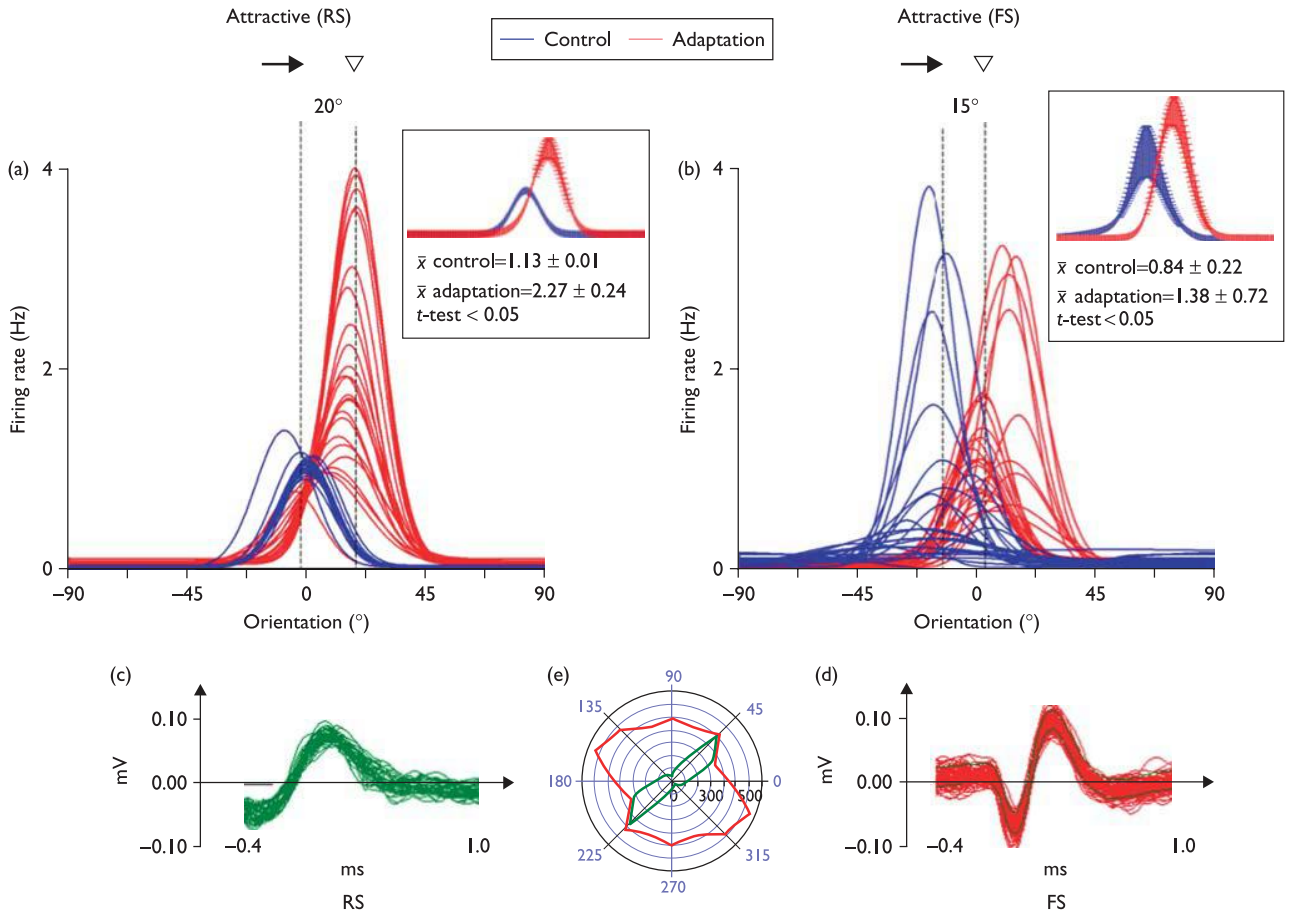

An example of an attractive orientation tuning shift for a fast-spiking (FS) cell and a regular-spiking (RS) cell. (a) Cell displayed a 20° attractive shift following adaptation in the case of a regular waveform of the spike. Downward triangle indicates the adapting orientation. (b) Cell displayed a 15° attractive shift following adaptation in the case of a fast waveform of the spike. Downward triangle indicates the adapting orientation. (c) Example of an RS waveform. (d) Example of an FS waveform. (e) Polar plots (fast and regular cell superimposed) of two cells: RS cell and FS cell.

Fig. 3

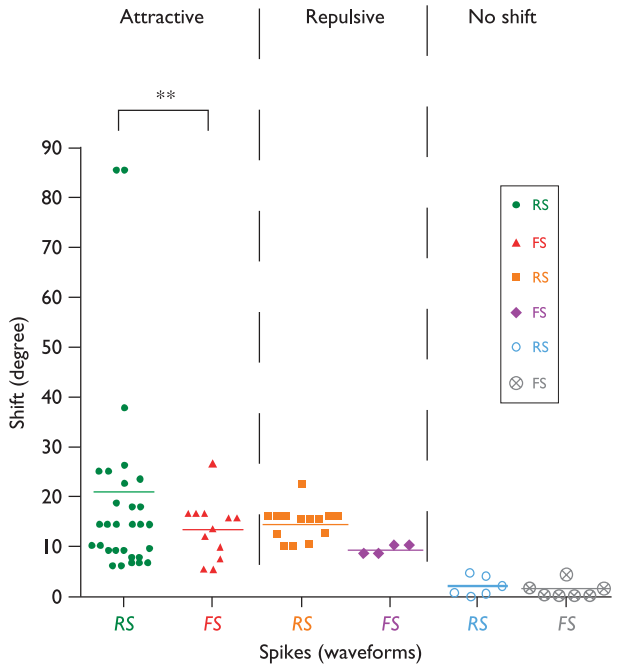

Distribution of two classes of spikes according to postadaptation shift of attractive, repulsive, and no shift cells. This figure demonstrates that magnitudes of attractive and repulsive shifts are higher in regular-spiking (RS) cells than the fast-spiking (FS) cells (Fisher test between RS attractive cells and FS attractive cells: *P*-value <0.05). The maximum value of the shift was 85.5° and 26.7°, respectively, for RS and FS cells. The small number ($n=4$) of FS cells with repulsive reaction precludes statistical computations, yet the trend appears clear that the peaks of the orientation tuning curves for RS cells in the repulsive direction were also displaced to a larger extent.

Moreover, as shown in Fig. 3, regular-spiking cells for attractive behavior shifted within a range of 5–85.5° (average shift 21°) and the fast-spiking cells shifted within a range of 6–27° (average shift 14°; Fisher test, $P < 0.05$). Similarly, regular-spiking cells for repulsive behavior shifted within a range of 10–23° (average shift 15°) and the fast-spiking cells shifted to 9°.

Discussion

The results of our study indicate that both types of functionally identified cells exhibit, following relatively long adaptation (12 min), shifts of their peaks of the orientation tuning curves in both directions, attractive and repulsive. The most interesting result that we found after induced adaptation to a nonpreferred orientation is that the regular-spiking cells and the fast-spiking cells shift in a consistent pattern with respect to each other, though to different degrees.

Therefore, directions of shifts are independent of types of waveforms. As expected from previous studies attractive shifts were more frequent [8]. Such common behavior suggests that neurons reacted collectively irrespective of the cell type. Our conclusion is in line with an earlier investigation showing that in most cases all cells recorded by a single electrode tip shift in the same direction [9]. These observations suggest that adaptation impacts a neuronal network, where a large proportion of cells change their preferred orientation jointly. However, fast-spiking units shift with a smaller magnitude than regular-spiking units. Various studies have indicated that fast-spiking cells are interneurons [17–21] with broader bandwidths of their tuning curves [15,22]. Their broader orientation tuning is a sign that these neurons are driven by a large spectrum of orientations with approximately equal strength. In that case, it is likely that each oriented input is contributing to the cell's response(s) with about comparable magnitude. Therefore, if one assumes that adaptation affects mostly the testing orientation, the other inputs maintain their excitatory drive producing relatively higher firing rates. The net result is a relatively lesser shift of the peak of the tuning curve.

On the other hand, the regular-spiking cells are pyramidal cells [21,23,24] with narrower bandwidths [15,22] exhibiting much sharper tuning curves. Consequently, the range of orientations generating higher firing rate is small, presumably due to a combination of inhibitory inputs [18] sharpening the bandwidths. Thus, optimal responses are produced by a smaller range of oriented input. Therefore, the modified equilibrium between excitation and inhibition that was induced by adaptation results in larger shifts because imposed orientation potentiate response, while remote orientations contribute less to the tuning curves. Indeed, in line with previous reports [4,8,9] responses evoked by flanked orientations did not change significantly.

Based on our findings, we hypothesize that in the primary visual cortex of cat after adaptation the pyramidal cells and interneurons interact and communicate with each other in an organized way to respond to orientation stimuli.

Conclusion

To our knowledge, this study is the first to show that the regular-spiking cells always shift more than the fast-spiking cells after adaptation to stimuli. We may conclude that in primary visual cortex of the cat, pyramidal cells and interneurons interact with each other in parallel to respond to induced adaptation stimuli. Pyramidal cells set the orientation selectivity and the interneurons regulate this selectivity.

Acknowledgements

Conflicts of interest

There are no conflicts of interest.

References

1 Hubel DH, Wiesel TN. Receptive fields of single neurones in the cat's striate cortex. *J Physiol* 1959; **148**:574–591.
2 Hubel DH, Wiesel TN. Receptive fields and functional architecture of monkey striate cortex. *J Physiol* 1968; **195**:215–243.

3 Movshon JA. The velocity tuning of single units in cat striate cortex. *J Physiol* 1975; **249**:445–468.
4 Dragoi V, Sharma J, Sur M. Adaptation-induced plasticity of orientation tuning in adult visual cortex. *Neuron* 2000; **28**:287–298.
5 Kohn A, Movshon JA. Neuronal adaptation to visual motion in area MT of the Macaque. *Neuron* 2003; **39**:681–691.
6 Ghisovan N, Nemri A, Shumikhina S, Molotchnikoff S. Visual cells remember earlier applied target: plasticity of orientation selectivity. *PLoS ONE* 2008; **3**:e3689.
7 Yap H, Dan Y. Stimulus timing-dependent plasticity in cortical processing of orientation. *Neuron* 2001; **32**:315–323.
8 Ghisovan N, Nemri A, Shumikhina S, Molotchnikoff S. Long adaptation reveals mostly attractive shifts of orientation tuning in cat primary visual cortex. *Neuroscience* 2009; **164**:1274–1283.
9 Nemri A, Ghisovan N, Shumikhina S, Molotchnikoff S. Adaptive behaviour of neighboring neurons during adaptation-induced plasticity of orientation tuning in V1. *BMC Neurosci* 2009; **10**:147.
10 Maffei L, Fiorentini A, Bisti S. Neural correlate of perceptual adaptation to grating. *Science* 1973; **182**:1036–1038.
11 Chiu C, Weliki M. The role of neural activity in the development of orientation selectivity. In: Chalupa LM, Werner J, editors. *The visual neurosciences*. Cambridge, MA: MIT Press 2003. pp. 117–125.
12 Ison MJ, Mormann F, Cerf M, Koch C, Fried I, Quiroga RQ. Selectivity of pyramidal cells and interneurons in the human medial temporal lobe. *J Neurophysiol* 2011; **106**:1713–1721.
13 Wilson FA, O'Scalaidhe SP, Goldman-Rakic PS. Functional synergism between putative gamma-aminobutyrate-containing neurons and pyramidal neurons in prefrontal cortex. *Proc Natl Acad Sci* 1994; **91**:4009–4013.
14 Marshansky S, Shumikhina S, Molotchnikoff S. Repetitive adaptation induces plasticity of spatial frequency tuning in cat primary visual cortex. *Neuroscience* 2011; **13**:355–365.
15 Kuhlman SJ, Tring E, Trachtenber JT. Fast-spiking interneurons have an initial orientation bias that is lost with vision. *Nat Neurosci* 2011; **14**: 1121–1123.
16 Ge R, Qian H, Wang J. Physiological synaptic signals initiate sequential spikes at soma of cortical pyramidal neuron. *Mol Brain* 2011; **4**:1.
17 González-Burgos G, Krimer LS, Povysheva NV, Barrionuevo G, Lewis DA. Functional properties of fast spiking interneurons and their synaptic connections with pyramidal cells in primate dorsolateral prefrontal cortex. *J Neurophysiol* 2005; **93**:942–953.
18 Fries P, Nikolic D, Singer W. The gamma cycle. *Trends Neurosci* 2007; **30**:309–316.
19 Gouwens NW, Zeberg H, Tsumoto K, Tateno T, Aihara K, Robinson HPC. Synchronization of firing in cortical fast-spiking interneurons at gamma frequencies: a phase-resetting analysis. *PLoS Comput Biol* 2010; **6**:e1000951.
20 Povysheva NV, González-Burgos G, Zaitsev AV, Kroner S, Barrionuevo G, Lewis DA, Krimer LS. Properties of excitatory synaptic responses in fast-spiking interneurons and pyramidal cells from monkey and rat prefrontal cortex. *Cereb Cortex* 2005; **16**:541–552.
21 Galarreta M, Hestrin S. Electrical and chemical synapses among parvalbumin fast-spiking GABAergic interneurons in adult mouse neocortex. *Proc Nat Acad Sci* 2002; **99**:12438–12443.
22 Hofer SB, Ko H, Pichler B, Vogelstein J, Ros H, Zeng H, *et al*. Differential connectivity and response dynamics of excitatory and inhibitory neurons in visual cortex. *Nat Neurosci* 2011; **14**:1045–1054.
23 McCormick DA, Connors BW, Lighthall JW, Prince DA. Comparative electrophysiology of pyramidal and sparsely spiny stellate neurons of the neocortex. *J Neurophysiol* 1985; **54**:782–806.
24 Chang Y, Luebke JI. Electrophysiological diversity of layer 5 pyramidal cells in the prefrontal cortex of the Rhesus monkey: in vitro slice studies. *J Neurophysiol* 2007; **98**:2622–2632.

Chapter 15

Adaptation and Neuronal Network in Visual Cortex

Lyes Bachatene, Vishal Bharmauria and Stéphane Molotchnikoff

Additional information is available at the end of the chapter

http://dx.doi.org/10.5772/46011

1. Introduction

Complex mechanisms from retina to different visual areas allow us to read these lines. The visual system is inevitable for the way we interact with our surroundings as majority of our impressions, memories, feelings are bound to the visual perception. Millions of cortical neurons are implicated and programmed specifically to frame this incredible interface (perception) for us to interact with the world. Neurons in the visual cortex respond essentially to the variations in luminance occurring within their receptive fields, where each neuron fires maximally by acting as a filter for stimulus features such as orientation, motion, direction and velocity, with an appropriate combination of these properties [1-5].

The seminal work of Hubel and Wiesel on the visual cortex of cat [1, 2, 6-8], has been instrumental in establishing the anatomical and physiological aspects of the visual cortex. Many studies by various investigators on the visual cortex of different animals, thereafter, have been phenomenal in understanding the brain in general and the vision in particular; yet, neuronal mechanisms involved in processing of stimuli still elude our complete understanding of cortical functioning. These findings have been crucial in unravelling the organization of the visual cortex. The visual cortex reorganises itself in the postnatal development, within a specific period called 'the critical period' [9], which is a period characterised with pronounced brain plasticity. In recent years, the focus of the research has been to comprehend the 'reorganization' of neuronal framework, especially after the so called 'critical period' [10-12] in response to various conditions and its ability to adapt accordingly. This amazing tendency of brain to change its neuronal connections and properties is termed 'plasticity' [13]. Two common approaches to study the reorganization of visual cortex are frequently applied: deprivation and induced adaptation. Deprivation refers to the removal of sensory inputs, whereas induced adaptation refers to the forceful application of a sensory input. Consequently, neurons communicate dynamically with each

other in a specific way self-assembling, auto-calibrating, memorizing and adapting to different stimuli properties, thus responding accordingly to several experiences [14-16].

The aim of this chapter is to primarily focus on how the linkage between cells changes following plastic modifications of cortical neuronal properties, that is, how the reorganization of the cortical network is modulated following adaptation-induced plasticity, as it is inferred by cross-correlating the action potentials of the neurons in the primary visual cortex. We begin with the general architecture of visual cortex (particularly cat visual cortex), followed by a brief introduction to plasticity and adaptation. Then, we cite an example of modification of the neuronal connections before and after adaptation as revealed by cross-correlation method. Based on this example, we propose a model for changing functional connections prior and post adaptation and conclude with how neurons change their functional relationships when forcefully adapted to a non-optimal stimulus.

2. Visual system: Organization

2.1. Introduction

Visual area constitutes about 25 % of the cortex in humans with approximately 5 billion neurons. The study of the visual cortex has revealed many of these visual regions such as V1, V2, V3, V4 and MT on the basis of their anatomical architecture, topography and physiological properties [17, 18]. These regions are involved in processing of multitude of informations (shape, orientation, color, movement, size etc) resulting from the visual pathways, thus making up an image applied to retina.

The cortical area of higher mammals such as cats, monkeys and humans is generally divided into modules of selectivity (e.g. the visual cortex is divided into areas of selectivity called orientation columns). Several characteristics of the visual system of mammals appear to be common to many species [19, 20], though the neurons are distributed in a salt and pepper fashion in the visual cortex of lower animals such as rats and mice, lacking the orientation domains [21, 22]. Research on animal models is used on a large scale to study and investigate the structure and function of the visual system. Monkeys, cats, and mice are commonly used in neurophysiological experiments for understanding cortical mechanisms in general and visual pathways in particular [23].

2.2. From retina to visual areas

Visual perception begins in the retina where the received light is transformed into electrical signal by a biochemical cascade produced in the rods and cones. The retinal ganglion cells relay the message to the lateral geniculate body (LGN) which consists of six layers [24]. Each layer receives information from the retinal hemi-field of one eye. The axon terminals of ganglion cells which project on each layer form a precise retinotopic map. This retinotopy denotes the spatial organization of neuronal responses to visual stimuli. Indeed, in many parts of the brain, neurons that respond to stimulation from a given portion of the visual field are located right next to the neurons whose receptive fields cover adjacent portions.

Therefore, all the neurons in these brain regions form a topographical map of the visual field from its projection onto the retina.

From the LGN, axons are organized into thalamocortical fibres forming the optic radiations. These optic radiations project onto the cortex in specialized visual areas. The distribution of fibres in the cortex can reproduce the visual field on the cortical layer, and the stimulation of a small cortical area leads to the appearance of bright spots called 'phosphenes' [25] in a specific location of the visual field. Visual areas begin in the occipital lobe, and the primary visual cortex or area 17 is the main entrance to cortex for thalamic relay cells [24]. The primary visual cortex is organized into functional modules. Neurons with similar receptive fields are organized into columns [26, 27]. Visual neurons have other fundamental properties, such as the direction selectivity of cells in the layer IVβ, and the selectivity for speed [3, 6]. There is another system of alternating columns, which corresponds to the separation of afferents from both eyes. These are the ocular dominance columns. The ocular dominance columns represent bands of cortical tissue alternately occupied by afferents from the left eye or right eye [28-30]. These bands are particularly pronounced at the cortical layer IV, which receives the afferent endings of the lateral geniculate nucleus. Thus the visual cortex is organized into functional maps of orientation, spatial frequency, ocular dominance, temporal frequency which are interrelated to each other [31-33].

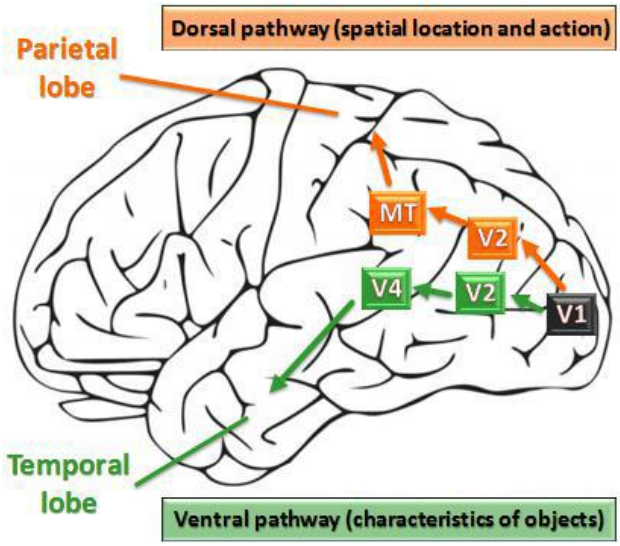

Figure 1. Parallel organization of the visual system

Many findings have led to the discovery of thirty different cortical areas that contribute to visual perception. The primary areas (V1) and secondary areas (V2) are surrounded by many other tertiary or associative visual areas such as V3, V4, V5 (or MT) involved in processing various attributes of trigger features [18, 34]. Areas V3 and V3A are selective to the form of stimuli [35], and neurons of area V4 are selective to colors [36]. Area V5 or MT (middle temporal) is an area where majority of cells are sensitive to motion and direction, and none of which are selective to color [37].

Moreover, the parallel organization of visual system is involved in the establishment of two major visual pathways: Ventral and dorsal pathways which are indispensable for the object recognition [38, 39]. Figure 1 illustrates the parallel organization of visual system, two major pathways: Green part corresponds to the ventral pathway in the cortex ending in the temporal lobe [38, 40]. It is involved in the processing of information on the characteristics of the objects (shapes, colours, materials), that is, object recognition including faces. Orange part corresponds to the dorsal pathway in the cortex ending in the parietal lobe [38, 40]. This path is associated with spatial vision (action / location) of objects, and is involved in processing of action in space.

3. Neuron types in primary visual cortex

3.1. Pyramidal cells and interneurons

The grey matter in the primary visual cortex is divided into six layers namely I, II, III, IV, V, VI (Figure 2) which comprise of different types of neurons [41, 42]. Two types of neurons are mainly observed: pyramidal cells and interneurons which can be physiologically separated and are the focus of interest in this chapter, that is, how they modify their properties and change linkage with each other post-adaptation. Pyramidal cells are excitatory neurons projecting onto other brain regions [43, 44] whereas stellate cells which are the recipient cells from the relay cells of the LGN correspond to the local excitatory interneurons [45]. In addition, there are interneurons that are inhibitory in nature [45]. Figure 2 illustrates the layers and cell types in primary visual cortex. Each layer has specific cell types and connectivity in primary visual cortex. Layer IV contains many stellate cells, small neurons with dendrites arranged radially around the cell body. Pyramidal cells are found in layers II-III, V and VI and are the only type of neurons that send axons outside the cortex. These neurons exhibit two levels of their dendritic extension: basal level close to the cell body and relatively long apical dendritic branches extending sometimes over the entire thickness of the cortex.

Classically, spike waveforms allow cells' distinction into two functional cell-groups, that is, excitatory pyramidal cells and inhibitory interneurons [11, 46, 47]. Figure 3 illustrates a typical example of cells distinguished based on their waveforms: fast spike and regular spike. Figure 3a corresponds to a fast spike with steeper ascending slope of the action potential and represents the putative interneuron [11], whereas Figure 3b corresponds to a regular spike which exhibits a slower ascending slope and represents the putative pyramidal cell [11].

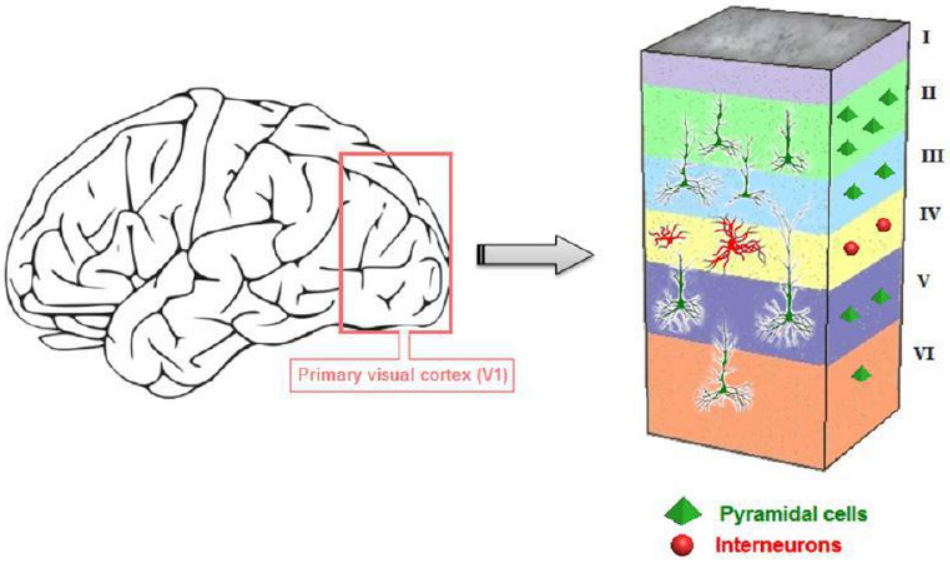

Figure 2. Organization of the primary visual cortex

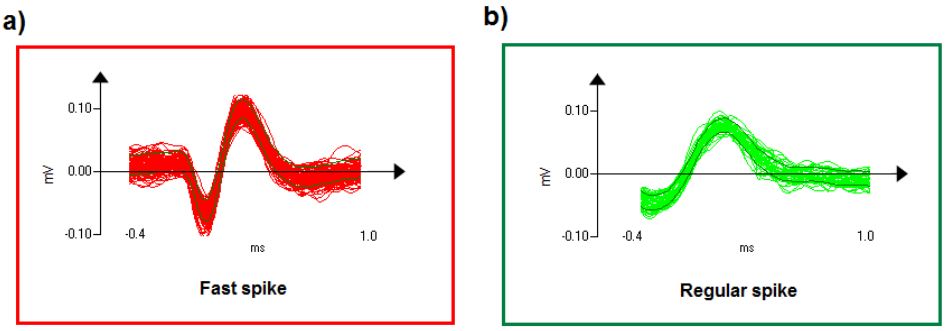

Figure 3. Spike waveforms for putative interneurons (a) and putative pyramidal cells (b)

3.2. Receptive fields

Visual information from the LGN cells firstly projects onto the stellate interneurons in layer IV, which have concentric receptive fields similar to those of LGN neurons [24, 48]. Neurons of layer IV project vertically onto other cortical layers. In layers II / III, cortical cells exhibit a radical transformation of the receptive field organization, where cells respond preferentially to stimuli with properties such as a bar or an edge that has specific characteristics namely orientation, direction, length, width, and motion [3, 6, 49].

Cells in these layers are classified into simple, complex and hypercomplex cells based on their dark or light-edge properties [6]. Simple cell is a cell which has an ON-OFF sub field,

that is, it responds to ON or OFF stimuli in the receptive field and has adjacent excitatory and inhibitory areas [6]. Complex neurons have receptive fields larger than those of simple neurons. They are also selective for orientation, but the precise position of the stimulus within the receptive field is less critical because they have no defined ON or OFF sub-areas. That is why a movement of the stimulus through the receptive field is a potent stimulus for some complex neurons [6, 50, 51]. A complex cell does not have adjacent excitatory and inhibitory areas in the receptive field and responds to whole of the receptive field regardless of the exactitude of the stimulus area, though complex cells can be direction-specific [6]. A hypercomplex cell appears to result, when the axons of complex neurons with different orientations converge on it. A hypercomplex cell is selective to lines of a defined length, and if the stimulus exceeds this length the response is diminished due to inhibitory extremities in addition to antagonistic flanks [6].

Neurons in primary visual cortex are connected laterally and vertically to each other. Lateral or horizontal connections are specified as long range connections between neurons preferring similar stimulus features [52, 53] which are functionally connected to each other at large distance [54, 55]. Vertical connections are specified as inputs to layers II and III from layer IV of the visual cortex [56, 57] which receives its inputs from LGN [58]. From layers II and III, the connections descend to layers V and VI [57].

Cats have a high performance visual system close to that of primates, making it a very coveted subject for researches to reveal the functional aspects of this complex system [59, 60]. Approaches to study the visual system are based on functional electrophysiology, where animals are anaesthetized and paralyzed for electrophysiological recordings by lowering microelectrodes into regions of interest within the visual area and visually stimulating the neurons [6, 11, 49, 61].

4. Plasticity and adaptation in the visual cortex

Neurons in the mammalian visual cortex are tuned to respond to visual stimuli such as contour orientation, motion, direction, and speed [3, 6, 59]. Preference for orientation in orientation columns is considered relatively stable in the primary visual cortex (V1) as an emergent property that is established early in the life, following the so-called critical period [9].

Studies from various laboratories have shown that in a fully mature brain, neuronal network restructures itself beyond the postnatal critical period that follows birth [11, 49, 61-65]. Recent investigations revealed the ability of visual neurons to respond to different stimuli conditions (deprivation or imposition) by changing their optimal properties acquired after birth. This adaptation of neurons for visual perception suggests the existence of neuronal plasticity in adults, hence a mature brain.

Adaptation-induced-plasticity of orientation in primary visual cortex is characterized by authors as the ability of cortical neurons to change their preferred orientation following a long [11, 61, 63] or short [62, 65] exposure to a non-preferred orientation for the primary

visual cortex neurons in cats, e.g. Long adaptation leads to the shift of orientation tuning towards attractive direction [61]. In a similar fashion, repetitive adaptation to a non-preferred spatial frequency reveals the spatial frequency tuning shifts in cat visual cortex [49]. In general, imposing a particular stimulus induces instructive process to modify neuronal properties, for example, when in the visual cortex of awake mice a single orientation grating stimulus is repeatedly presented; it leads to augmentation of responses evoked exclusively by testing stimulus, that is, the experience led to enhancement of response [66]. In experiments where animals are anaesthetized (e.g. a cat in the experiment described later on) the shifts of peaks of tuning curves following adaptation (described in figure 4) are not attributed to attention modulations. Consequently, these shifts result from basic neuronal processes outside the frame of attentional processes that might impact response magnitudes.

Adaptation studies in recent years have presented a more complex picture where prolonged exposure to a non-preferred orientation has shown modifications in neurons' preferred orientations. After adaptation to a non preferred orientation, obtained tuning curve for the new preferred orientation (after adaptation) can shift in two directions relative to the original preferred orientation: attractive or repulsive [11, 61, 63, 64]. An attractive shift is a shift of the tuning curve towards the adapting orientation. On the other hand; a repulsive shift is a shift of the tuning curve in the opposite side of the adapting orientation. Figure 4 illustrates types of shifts post-adaptation. Figure 4a corresponds to an attractive shift, in which blue tuning curve represents control optimal orientation (before adaptation), and red tuning curve represents new optimal orientation (after adaptation).The tuning curve shifted towards the adapting orientation. Figure 4b corresponds to the repulsive shift, in which blue tuning curve represents control optimal orientation (before adaptation), and red tuning curve represents new optimal orientation (after adaptation). The tuning curve shifted away from the adapting orientation. Red arrows depict adapting orientation (non-preferred orientation in control).

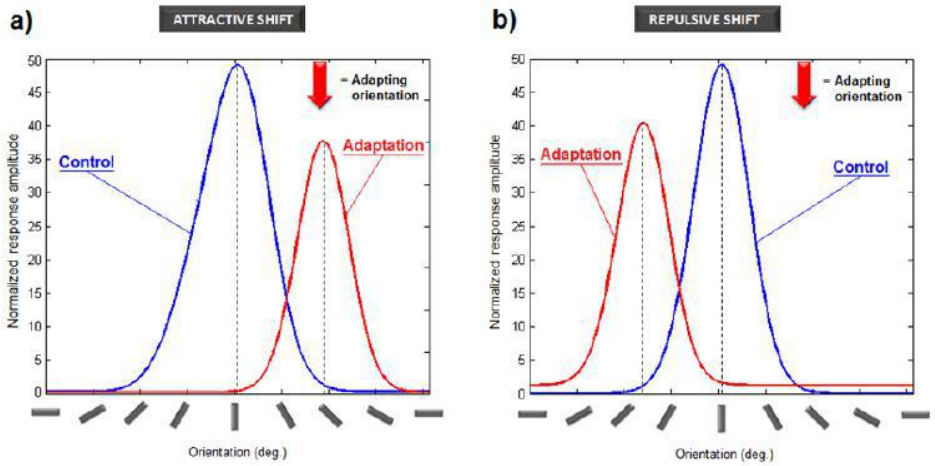

Figure 4. Types of shifts post-adaptation

Attractive shifts are more frequent than repulsive shifts in longer adaptation durations (≥ 6 min) [11, 61]. Repeated or prolonged exposure to an adapter diminished neuronal responses evoked by the original optimal properties, furthermore in parallel, if it is the neuron's preferred stimulus [61]. Optical imaging investigations in recent years have also revealed the impact of adaptation-induced-plasticity, showing that orientation maps in V1 can be modified by imposing one particular orientation [62, 65, 67].

5. Crosscorrelograms and neuronal relationships in visual cortex

As reviewed above [11, 49, 61-65], adaptation- induced studies on visual cortex can reveal a great deal about the functioning of the visual cortex. Crosscorrelogram analysis is an efficient tool to establish the functional connectivity between neurons. Ever since the crosscorrelogram approach was introduced [68], it has proved to be an invaluable tool to determine how specific neurons interact with each other. A crosscorrelogram is a histogram used to infer the connectivity between two neurons, where one neuron is reference and other target. The histogram shows us when the spikes of target neuron are related in time to the spikes of reference neuron. The technique has been instrumental in revealing widespread incidences of neuronal synchrony and neuronal time-relationships among various cortical areas [64, 70-78]. For instance, as revealed by crosscorrelogram analysis, synchrony has been reported to be strong between cells with similar preferred parameters due in part to specific connections between cortical domains having similar tuning properties. Thus, based on the crosscorrelogram analysis, the functional network connections can be established between the neurons [58, 71, 79-81].

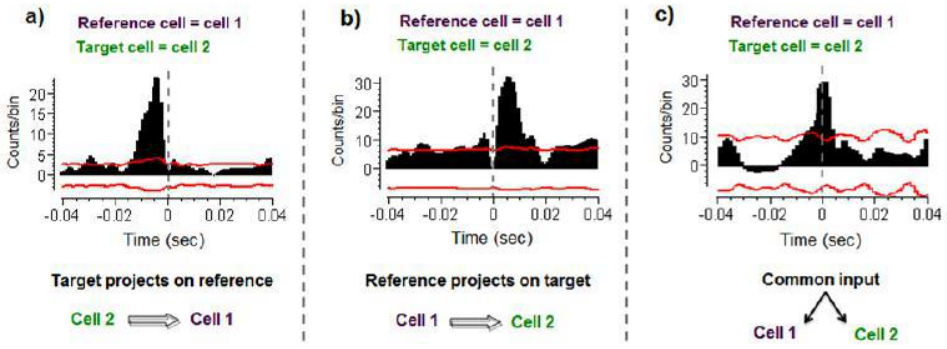

Figure 5. Crosscorrelograms between two neurons (reference and target)

A typical crosscorrelogram between two neurons to interpret the relation between them is obtained by keeping one of the neurons as reference and calculating the spikes of the other neuron with reference to it. An investigator generally is interested in one of the following patterns as illustrated in figure 5, while he is interpreting crosscorrelograms. Figure 5 illustrates the time relations between two neurons as revealed by shifted and corrected

crosscorrelograms when one neuron is reference and other target. A shifted crosscorrelogram is a histogram obtained, when the spikes of the reference cell are shifted by one or two cycles of stimulation. This eliminates the possibility of stimulus-induced-relationship between two neurons. After this the shifted crosscorrelogram is subtracted (corrected) to remove the stimulus-locked -component. Figure 5a corresponds to target cell projecting onto the reference cell. Target neuron fires few milliseconds before the reference cell since the peak of the crosscorrelogram appears few milliseconds before zero, that is, offset from zero, within 5ms. This means there is an excitation from target to the reference cell [79, 81]. Figure 5b corresponds to the reference cell projecting onto the target cell. Target neuron fires few milliseconds after the reference cell since the peak of the crosscorrelogram appears few milliseconds after zero, within 5ms. This means the excitation is from reference cell to the target cell [79, 81]. Figure 5c corresponds to the synchrony between two neurons, as the peak straddles zero [73, 82]. This means there is a common excitatory input to both neurons most likely from other neuron or neurons. Though, various time windows have been taken into consideration ranging from 3ms to 10 ms [72, 79] to reveal the functional connections between the involved neurons, but a time window within 5ms is most frequently used.

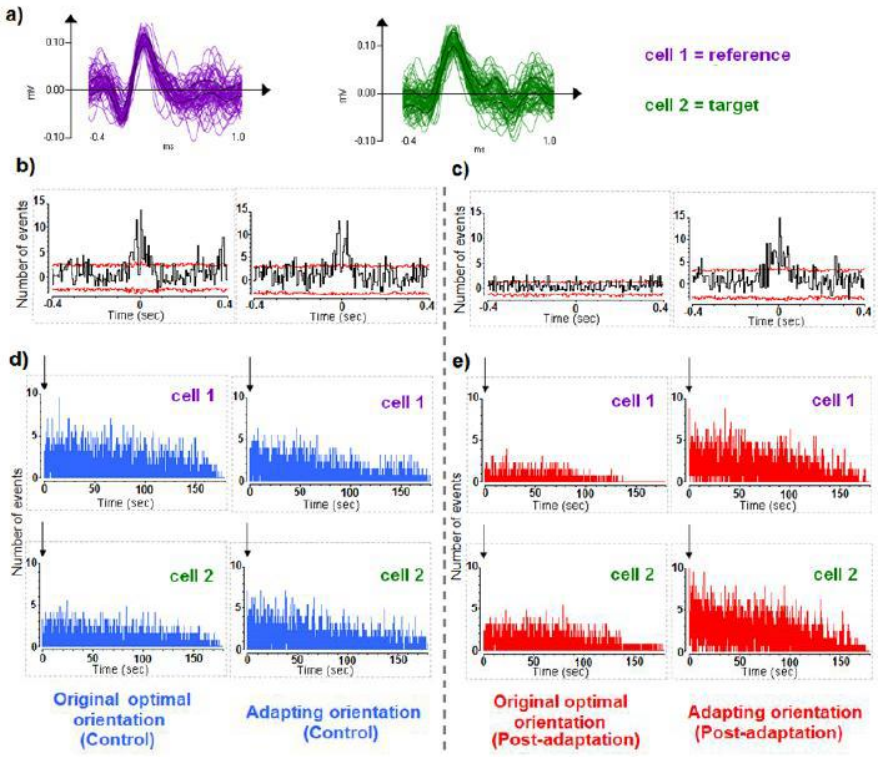

Figure 6. Differential effects of adaptation on synchrony for responses evoked by original orientation and adapting orientation

Figure 6 corresponds to differential effects of adaptation on synchrony for responses evoked by original orientation and adapting orientation. Figure 6a represents respective spike-waveforms for cell 1 and cell 2. Figure 6b shows crosscorrelograms between cell 1 and cell 2 before adaptation (control). The centered peak corresponds to synchrony. Fig 6c represents crosscorrelograms between cell 1 and cell 2 after adaptation. Synchrony disappeared for original optimal orientation while it persists for responses evoked by adapter. Figure 6d shows respective Peri-Stimulus Time Histograms (PSTH's) for cells in control (before adaptation). Figure 6e corresponds to respective Peri-Stimulus Time Histograms (PSTH's) for cells after adaptation. The downward black arrows indicate onset of the drifting sine-wave patch positioned in the receptive field.

Since adaptation modifies the optimal properties of neurons, whether orientation, direction or spatial frequency, it seems reasonable to postulate that these modifications following adaptation induce a rapid reorganization of the inter-neuronal relationships, as revealed by crosscorrelogram analyses. For instance, a recipient neuron programmed since birth to be connected to a specific neuron that responds optimally to one specific property, all of a sudden starts responding optimally to another stimulus, and begins participating in a different network with other neuron- as if breaking its allegiance to the neuron it is programmed to be connected since birth.

6. Network formation

Neurons do not respond in isolation to the trigger features, but in coordination with surrounding neurons. Thus, they encode stimuli features by forming cell assemblies, where in the involved neurons are time related with each other. Recent investigations have revealed the ability of visual neurons to respond to different stimuli conditions by changing their optimal properties acquired after birth. Most of these studies have been done by visual deprivation [9, 83-86], whereas only a few have centered on induced adaptation [11, 62, 64, 87]. This adaptation of neurons to non-optimal stimuli suggests the adaptability of neuronal code to visual stimuli.

Neuronal connections in the cortex generally occur locally [79, 88]. Visual cortex is a highly specialized functional area where the neurons coordinate locally to encode the visual scenes [89, 90, 91]. To reveal how this local circuitry of different neurons in visual cortex is set up and modulated in response to different visual stimuli is of prime importance to understand the mechanisms of information processing. Crosscorrelogram strategy discussed above can be effectively applied to form a neuronal network in response to visual stimuli. Thus, it can be an efficient tool in deciphering the changes in the neuronal code post-adaptation, hence, the mechanisms of plastic modifications can be revealed.

For example, in the Figure 7 we show the network of connections prior and post adaptation between three neurons recorded simultaneously from the same electrode lowered into the primary visual cortex of an anaesthetized cat. In this experiment, a stimulating sine-wave drifting grating was set to excite cells optimally. Shifted and corrected crosscorrlegrams

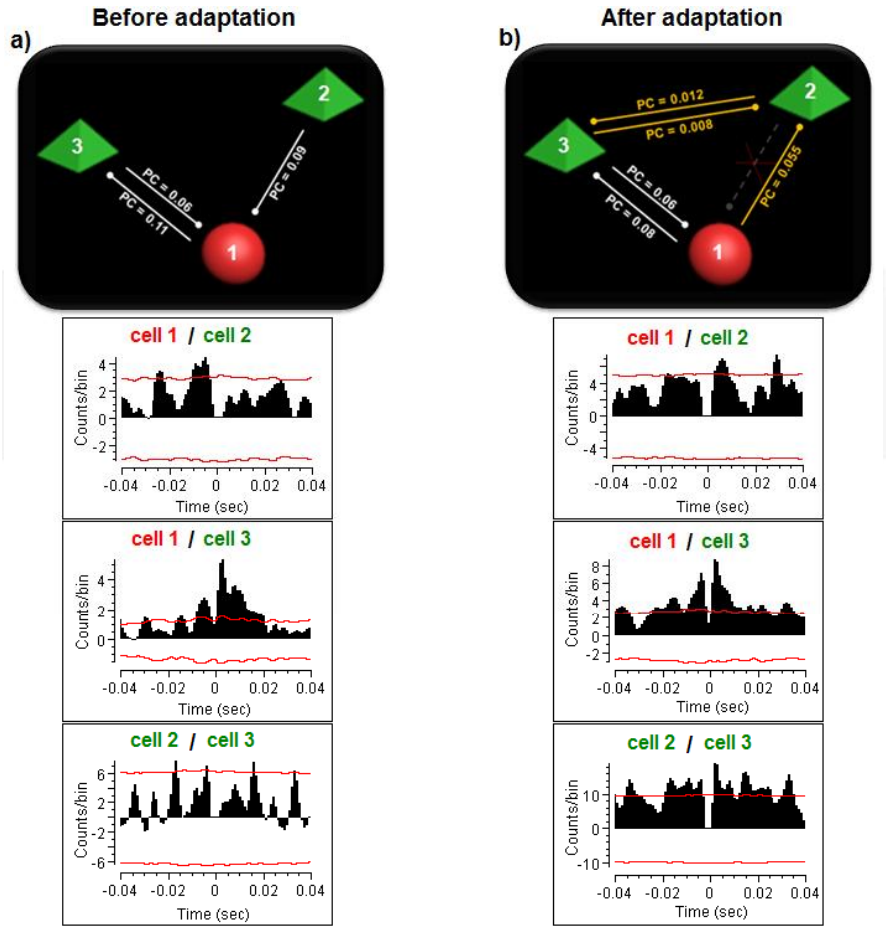

Figure 7. Functional relationships between simultaneously recorded cells before and after adaptation

between all the involved neurons were obtained. A time window of 5 ms before or after the zero in the shifted and corrected crosscorrelogram is taken into account for the projection to be valid. The physiological connectivity (synaptic connections, common input) between cells occurs on very small time scales, less than 3 ms [79, 81]. Since we consider a time window of 10 ms in crosscorrelograms for establishing connections, therefore, this connectivity only reflects that the cells function (irrespective of physical connectivity) in coordination with each other in a time-window of 10 ms following a presented stimulus. Figure 7a illustrates the functional connections between three neurons as revealed by their respective crosscorrelograms (shifted and corrected). White projections correspond to established connections before adaptation. Figure 7b illustrates the new functional connections between same neurons as revealed by their respective crosscorrelograms (shifted and corrected). Yellow projection corresponds to the new connection established after adaptation. Dotted

gray projection represents the disappeared projection. PC corresponds to the probability coefficient of the connections. Solid green pyramid represents a pyramidal cell and the solid red sphere represents an interneuron. Red curve line indicates 95% significance level.

This changing of connections indicates that the functional relationships between neurons are modified depending on the stimulus features. For instance, following the forceful presentation of a particular stimulus (in this example a different orientation) results in disappearance of some relationships, and appearance of new relationships.

Based on the above example, we hypothesize and propose a model how the network of neurons is modulated prior and post adaptation as revealed by the functional time-relationship of neurons between them. Figure 8 depicts the functional connections between the same neurons before and after adaptation. White projections in figure 8a show the projections that cells have onto each other before adaptation, whereas figure 8b depicts how the network changes in the same group of neurons after adaptation. Some of the connections between the cells remain distinct (white projections) whereas some connections disappear (dotted gray arrows) with appearing new connections (yellow projections).

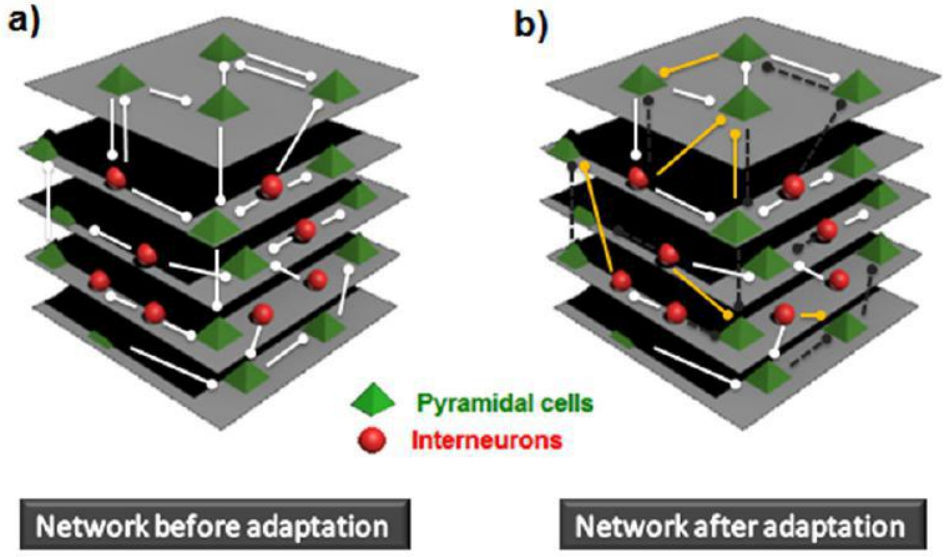

Figure 8. Network model before and after adaptation

7. Conclusion

This chapter reviewed the changes in the cellular properties post-adaptation. Indeed, the optimal trigger features may change following the prolonged application of a stimulus to which the cell responded feebly before adaptation. This phenomenon has been virtually observed in all mammals which have been tested so far. Also in parallel, following

adaptation the inter-neuronal relationships are modified. This suggests that the entire cortical network reorganises itself post adaptation, that is, a new cortex is formed, as if designed for changed properties.

To sum it up, it is of prime importance to understand the plastic modifications of brain for various fundamental and medical reasons. This chapter underlined the importance of imposed adaptation studies within brain, particularly in primary visual cortex based on the crosscorrelogram analysis, framing a premise to better understand the functional connectivity [79, 92] and mechanisms in local neuronal circuits between various identified neurons, at least between the pyramidal cells and interneurons before and after adaptation. and post adaptation, thus, could help us to decipher the mechanisms of information processing, hence the neuronal codes governing them.

Author details

Lyes Bachatene* and Vishal Bharmauria*
Department of Biological Sciences, University of Montreal, Montreal, Canada

Stéphane Molotchnikoff**
Department of Biological Sciences, University of Montreal, Montreal, Canada

8. References

[1] Hubel DH, Wiesel TN (1959) Receptive Fields of Single Neurones in the Cat's Striate Cortex. J Physiol. 148: 574-591.
[2] Hubel DH, Wiesel TN (1968) Receptive Fields and Functional Architecture of Monkey Striate Cortex. J Physiol. 195: 215-243.
[3] Movshon JA (1975) The Velocity Tuning of Single Units in Cat Striate Cortex. J Physiol. 249: 445-468.
[4] Martinez LM, Wang Q, Reid RC, Pillai C, Alonso JM, Sommer FT, Hirsch JA (2005) Receptive Field Structure Varies with Layer in the Primary Visual Cortex. Nat Neurosci. 8: 372-379.
[5] Bishop PO, Henry GH (1972) Striate Neurons: Receptive Field Concepts. Invest Ophthalmol. 11: 346-354.
[6] Hubel DH, Wiesel TN (1962) Receptive Fields, Binocular Interaction and Functional Architecture in the Cat's Visual Cortex. J Physiol.160: 106-154.
[7] Hubel DH, Wiesel TN (1963a) Shape and Arrangement of Columns in Cat's Striate Cortex. J Physiol. 165: 559-568.
[8] Hubel DH, Wiesel TN (1963b) Receptive Fields of Cells in Striate Cortex of Very Young, Visually Inexperienced Kittens. J Neurophysiol. 26: 994-1002.

* Both Authors Contributed Equally
** Corresponding Author

[9] Tanaka S, Tani T, Ribot J, O'Hashi K, Imamura K (2009) A Postnatal Critical Period for Orientation Plasticity in the Cat Visual Cortex. PLoS One. 4: e5380.
[10] Chiu C, Weliki M. 2003 The role of neural activity in the development of orientation selectivity. The visual neurosciences. 117–125Cambridge, MA: MIT Press. pp.
[11] Bachatene L, Bharmauria V, Rouat J, Molotchnikoff S (2012) Adaptation-induced Plasticity and Spike Waveforms in Cat Visual Cortex. Neuroreport. 23: 88-92.
[12] Southwell DG, Froemke RC, Alvarez-Buylla A, Stryker MP, Gandhi SP (2010) Cortical Plasticity Induced by Inhibitory Neuron Transplantation. Science. 327: 1145-1148.
[13] Buonomano DV, Merzenich MM (1998) Cortical Plasticity: From Synapses to Maps. Annu Rev Neurosci. 21: 149-186.
[14] Laughlin SB, Sejnowski TJ (2003) Communication in Neuronal Networks. Science. 301: 1870-1874.
[15] Singer W (2011) Dynamic Formation of Functional Networks by Synchronization. Neuron. 69: 191-193.
[16] Buzsáki G (2010) Neural Syntax: Cell Assemblies, Synapsembles, and Readers. Neuron. 68: 362-385.
[17] Kujovic M, Zilles K, Malikovic A, Schleicher A, Mohlberg H, Rottschy C, Eickhoff SB, Amunts K (2012) Cytoarchitectonic Mapping of the Human Dorsal Extrastriate Cortex. Brain Struct Funct. [Epub ahead of print]
[18] Felleman DJ, Van Essen DC (1991) Distributed Hierarchical Processing in the Primate Cerebral Cortex. Cereb Cortex. 1: 1-47.
[19] Kaschube M, Schnabel M, Löwel S, Coppola DM, White LE, Wolf F (2010) Universality in the Evolution of Orientation Columns in the Visual Cortex. Science. 330: 1113-1116.
[20] Tyler CJ, Dunlop SA, Lund RD, Harman AM, Dann JF, Beazley LD, Lund JS (1998) Anatomical Comparison of the Macaque and Marsupial Visual Cortex: Common Features That May Reflect Retention of Essential Cortical Elements. J Comp Neurol. 400: 449-468.
[21] Ohki K, Chung S, Ch'ng YH, Kara P, Reid RC (2005) Functional Imaging with Cellular Resolution Reveals Precise Micro-architecture in Visual Cortex. Nature. 433: 597-603.
[22] Van Hooser SD (2007) Similarity and Diversity in Visual Cortex: Is There a Unifying Theory of Cortical Computation? Neuroscientist. 13: 639-656.
[23] Casagrande VA, Xu X (2004) Parallel visual pathways: a comparative perspective. The Visual Neurosciences. pp. 494-506 Cambridge, MA: MIT Press.
[24] Gilbert CD, Wiesel TN (1979) Morphology and Intracortical Projections of Functionally Characterised Neurones in the Cat Visual Cortex. Nature. 280: 120-125.
[25] Davis FA, Bergen D, Schauf C, McDonald I, Deutsch W (1976) Movement Phosphenes in Optic Neuritis: A New Clinical Sign. Neurology. 26: 1100-1104.
[26] Hubel DH, Wiesel TN, Stryker MP (1977) Orientation Columns in Macaque Monkey Visual Cortex Demonstrated by the 2-Deoxyglucose Autoradiographic Technique. Nature. 269: 328-330.
[27] Blasdel GG, Salama G (1986) Voltage-sensitive Dyes Reveal a Modular Organization in Monkey Striate Cortex. Nature. 321: 579-585.

[28] Adams DL, Sincich LC, Horton JC (2007) Complete Pattern of Ocular Dominance Columns in Human Primary Visual Cortex. J Neurosci. 27: 10391-10403.
[29] Horton JC, Hocking DR (1996) Intrinsic Variability of Ocular Dominance Column Periodicity in Normal Macaque Monkeys. J Neurosci. 16: 7228-7239.
[30] Shatz CJ, Stryker MP (1978) Ocular Dominance in Layer IV of the Cat's Visual Cortex and the Effects of Monocular Deprivation. J Physiol. 281: 267-283.
[31] Carandini M, Sengpiel F (2004) Contrast Invariance of Functional Maps in Cat Primary Visual Cortex. J Vis. 4: 130-143.
[32] Issa NP, Trepel C, Stryker MP (2000) Spatial Frequency Maps in Cat Visual Cortex. J Neurosci. 20: 8504-8514.
[33] Issa NP, Rosenberg A, Husson TR (2008) Models and Measurements of Functional Maps in V1. J Neurophysiol. 99: 2745-2754.
[34] Van Essen DC, Felleman DJ, DeYoe EA, Olavarria J, Knierim J (1990) Modular and Hierarchical Organization of Extrastriate Visual Cortex in the Macaque Monkey. Cold Spring Harb Symp Quant Biol. 55: 679-696.
[35] Essen DC, Zeki SM (1978) The Topographic Organization of Rhesus Monkey Prestriate Cortex. J Physiol. 277: 193-226.
[36] Heywood CA, Gadotti A, Cowey A (1992) Cortical Area V4 and its Role in the Perception of Color. J Neurosci. 12: 4056-4065.
[37] Born RT, Bradley DC (2005) Structure and Function of Visual Area MT. Annu Rev Neurosci. 28: 157-189.
[38] Mishkin, M., Ungerleider, L., & Macko, K (1983) Object Vision and Spatial Vision: Two Cortical Pathways.Trends in Neuroscience. 6: 414-417.
[39] DiCarlo JJ, Zoccolan D, Rust NC (2012) How Does the Brain Solve Visual Object Recognition? Neuron. 73: 415-434.
[40] Milner, D. A., & Goodale, M. (1995).The visual brain in action. Oxford University Press
[41] Lin CS, Friedlander MJ, Sherman SM (1979) Morphology of Physiologically Identified Neurons in the Visual Cortex of the Cat. Brain Res. 172: 344-348.
[42] Peters A (1984) Identified neurons in visual cortex.Trends in Neurosci. 7 :375–378
[43] González-Burgos G, Krimer LS, Povysheva NV, Barrionuevo G, Lewis DA (2005) Functional Properties of Fast Spiking Interneurons and their Synaptic Connections with Pyramidal Cells in Primate Dorsolateral Prefrontal Cortex. J Neurophysiol. 93: 942-953.
[44] Povysheva NV, Gonzalez-Burgos G, Zaitsev AV, Kröner S, Barrionuevo G, Lewis DA, Krimer LS (2006) Properties of Excitatory Synaptic Responses in Fast-spiking Interneurons and Pyramidal Cells From Monkey and Rat Prefrontal Cortex. Cereb Cortex. 16: 541-552.
[45] Markram H, Toledo-Rodriguez M, Wang Y, Gupta A, Silberberg G, Wu C (2004) Interneurons of the Neocortical Inhibitory System. Nat Rev Neurosci. 5: 793-807.
[46] Ison MJ, Mormann F, Cerf M, Koch C, Fried I, Quiroga RQ (2011) Selectivity of Pyramidal Cells and Interneurons in the Human Medial Temporal Lobe. J Neurophysiol. 106: 1713-1721.

[47] Wilson FA, O'Scalaidhe SP, Goldman-Rakic PS (1994) Functional Synergism Between Putative Gamma-Aminobutyrate-Containing Neurons and Pyramidal Neurons in Prefrontal Cortex. Proc Natl Acad Sci U S A. 91: 4009-4013.
[48] Gilbert CD (1977) Laminar Differences in Receptive Field Properties of Cells in Cat Primary Visual Cortex. J Physiol. 268: 391-421.
[49] Marshansky S, Shumikhina S, Molotchnikoff S (2011) Repetitive Adaptation Induces Plasticity of Spatial Frequency Tuning in Cat Primary Visual Cortex. Neuroscience. 172: 355-365.
[50] Wilson JR, Sherman SM (1976) Receptive-field Characteristics of Neurons in Cat Striate Cortex: Changes with Visual Field Eccentricity. J Neurophysiol. 39: 512-533.
[51] Pettigrew JD, Nikara T, Bishop PO (1968) Responses to Moving Slits by Single Units in Cat Striate Cortex. Exp Brain Res. 6: 373-390.
[52] Das A, Gilbert CD (1995) Long-range Horizontal Connections and Their Role in Cortical Reorganization Revealed by Optical Recording of Cat Primary Visual Cortex. Nature. 375: 780-784.
[53] Sompolinsky H, Golomb D, Kleinfeld D (1990) Global Processing of Visual Stimuli in a Neural Network of Coupled Oscillators. Proc Natl Acad Sci U S A. 87: 7200-7204.
[54] Ts'o DY, Gilbert CD, Wiesel TN (1986) Relationships Between Horizontal Interactions and Functional Architecture in Cat Striate Cortex as Revealed by Cross-correlation Analysis. J Neurosci. 6: 1160-1170.
[55] Hata Y, Tsumoto T, Sato H, Tamura H (1991) Horizontal Interactions between Visual Cortical Neurones Studied by Cross-correlation Analysis in the Cat. J Physiol. 441: 593-614.
[56] Yoshimura Y, Sato H, Imamura K, Watanabe Y (2000) Properties of Horizontal and Vertical Inputs to Pyramidal Cells in the Superficial Layers of the Cat Visual Cortex. J Neurosci. 20: 1931-1940.
[57] Stratford KJ, Tarczy-Hornoch K, Martin KA, Bannister NJ, Jack JJ (1996) Excitatory Synaptic Inputs to Spiny Stellate Cells in Cat Visual Cortex. Nature. 382: 258-261.
[58] Alonso JM, Usrey WM, Reid RC (1996) Precisely Correlated Firing in Cells of the Lateral Geniculate Nucleus. Nature. 383: 815-819.
[59] De Weerd P, Vandenbussche E, De Bruyn B, Orban GA (1990) Illusory Contour Orientation Discrimination in the Cat. Behav Brain Res. 39: 1-17.
[60] Bravo M, Blake R, Morrison S (1988) Cats See Subjective Contours. Vision Res. 28: 861-865.
[61] Ghisovan N, Nemri A, Shumikhina S, Molotchnikoff S (2009) Long Adaptation Reveals Mostly Attractive Shifts of Orientation Tuning in Cat Primary Visual Cortex. Neuroscience.164: 1274-1283.
[62] Dragoi V, Sharma J, Sur M (2000) Adaptation-induced Plasticity of Orientation Tuning in Adult Visual Cortex. Neuron. 28: 287-298.
[63] Nemri A, Ghisovan N, Shumikhina S, Molotchnikoff S (2009) Adaptive Behavior of Neighboring Neurons During Adaptation-induced Plasticity of Orientation Tuning in VI. BMC Neurosci. 10: 147.

[64] Ghisovan N, Nemri A, Shumikhina S, Molotchnikoff S (2008) Visual Cells Remember Earlier Applied Target: Plasticity of Orientation Selectivity. PLoS One. 3: e3689.
[65] Dragoi V, Rivadulla C, Sur M (2001) Foci of Orientation Plasticity in Visual Cortex. Nature. 411: 80-86.
[66] Frenkel MY, Sawtell NB, Diogo AC, Yoon B, Neve RL, Bear MF (2006) Instructive Effect of Visual Experience in Mouse Visual Cortex. Neuron. 51: 339-349.
[67] Voussoughi A, Shumikhina S, Milleret C, Molotchnikoff S (2010) Adaptation Modifies the Organization of Orientation Maps in Adult Cat Visual Cortex. II. Pinwhell Reorganization. Soc. Neurosci:371.22
[68] Perkel DH, Gerstein GL, Moore GP (1967) Neuronal Spike Trains and Stochastic Point Processes. I. The Single Spike Train. Biophys J. 7: 391-418.
[69] König P, Engel AK (1995) Correlated Firing in Sensory-Motor Systems. Curr Opin Neurobiol. 5: 511-519.
[70] Singer W, Engel AK, Kreiter AK, Munk MH, Neuenschwander S, Roelfsema PR (1997) Neuronal Assemblies: Necessity, Signature and Detectability. Trends Cogn Sci. 1: 252-261.
[71] Alloway KD, Roy SA (2002) Conditional Cross-correlation Analysis of Thalamocortical Neurotransmission. Behav Brain Res.135: 191-196.
[72] Singer W, Gray CM (1995) Visual Feature Integration and the Temporal Correlation Hypothesis. Annu Rev Neurosci. 18: 555-586.
[73] Shumikhina S, Guay J, Duret F, Molotchnikoff S (2004) Contextual Modulation of Synchronization to Random Dots in the Cat Visual Cortex. Exp Brain Res. 158: 223-232.
[74] König P, Engel AK, Singer W (1996) Integrator or Coincidence Detector? The Role of the Cortical Neuron Revisited. Trends Neurosci. 19: 130-137.
[75] Softky WR, Koch C (1993) The Highly Irregular Firing of Cortical Cells is Inconsistent with Temporal Integration of Random EPSPs. J Neurosci. 13: 334-350.
[76] Abeles M. (1982) Local cortical circuits: an electrophysiological study. 67-69 Berlin:Springer-Verlag.
[77] Takahashi N, Kitamura K, Matsuo N, Mayford M, Kano M, Matsuki N, Ikegaya Y (2012) Locally Synchronized Synaptic Inputs. Science. 335: 353-356.
[78] Duret F, Shumikhina S, Molotchnikoff S (2006) Neuron Participation in a Synchrony-encoding Assembly. BMC Neurosci. 7: 72.
[79] Barthó P, Hirase H, Monconduit L, Zugaro M, Harris KD, Buzsáki G (2004) Characterization of Neocortical Principal Cells and Interneurons by Network Interactions and Extracellular Features. J Neurophysiol. 92: 600-608.
[80] Yoshimura Y, Callaway EM (2005) Fine-scale Specificity of Cortical Networks Depends on Inhibitory Cell Type and Connectivity. Nat Neurosci. 8: 1552-1559.
[81] Csicsvari J, Hirase H, Czurko A, Buzsáki G (1998) Reliability and State Dependence of Pyramidal Cell-interneuron Synapses in the Hippocampus: An Ensemble Approach in the Behaving Rat. Neuron. 21: 179-189.
[82] Ghisovan N, Nemri A, Shumikhina S, Molotchnikoff S (2008) Synchrony between Orientation-selective Neurons is Modulated During Adaptation-induced Plasticity in Cat Visual Cortex. BMC Neurosci. 9: 60.

[83] He HY, Hodos W, Quinlan EM (2006) Visual Deprivation Reactivates Rapid Ocular Dominance Plasticity in Adult Visual Cortex. J Neurosci. 26: 2951-2955.
[84] Daw NW, Fox K, Sato H, Czepita D (1992) Critical Period for Monocular Deprivation in the Cat Visual Cortex. J Neurophysiol. 67: 197-202
[85] Yaka R, Yinon U, Wollberg Z (1999) Auditory Activation of Cortical Visual Areas in Cats After Early Visual Deprivation. Eur J Neurosci. 11: 1301-1312.
[86] Mower GD, Christen WG (1985) Role of Visual Experience in Activating Critical Period in Cat Visual Cortex. J Neurophysiol. 53: 572-589.
[87] Gutnisky DA, Dragoi V (2008) Adaptive Coding of Visual Information in Neural Populations.Nature. 452: 220-4.
[88] Angulo MC, Staiger JF, Rossier J, Audinat E (2003) Distinct Local Circuits Between Neocortical Pyramidal Cells and Fast-spiking Interneurons in Young Adult Rats. J Neurophysiol. 89: 943-953.
[89] Lee WC, Reid RC (2011) Specificity and Randomness: Structure-function Relationships in Neural Circuits. Curr Opin Neurobiol. 21: 801-807.
[90] Kampa BM, Roth MM, Göbel W, Helmchen F (2011) Representation of Visual Scenes by Local Neuronal Populations in Layer 2/3 of Mouse Visual Cortex. Front Neural Circuits. 5: 18.
[91] Wallace DJ, Kerr JN (2010) Chasing the Cell Assembly. Curr Opin Neurobiol. 20: 296-305.
[92] Holmgren C, Harkany T, Svennenfors B, Zilberter Y (2003) Pyramidal Cell Communication Within Local Networks in Layer 2/3 of Rat Neocortex. J Physiol. 551: 139-153.

VISHAL BHARMAURIA

Neurophysiology of Visual System (LAB F-180)
Department of Biological Sciences
University of Montreal, C.P. 6128, succursale Centre-ville
Montréal QC, Canada H3C 3J7
Ph: 514-343-6111 ext 1238
Cellular: 514-867-1777
vishal.bharmauria(at)umontreal.ca

417, Rue Ouimet
St-Laurent, Quebec
Canada, H4L 3N6

EDUCATION:

❖ **PhD in Neurosciences –Neurophysiology** **2011- present**
Department of Biological Sciences
University of Montréal
Title: Studying the encoding of visual stimuli in the primary visual cortex.

❖ **Master of Biotechnology (M.Sc)** **2005-2007**
Himachal Pradesh University, India (First Division)
Title: To study the genetic variation and polymorphism in *Emblica officinalis*.

❖ **Bachelor of Biotechnology (B.Sc)** **2001-2004**
Himachal Pradesh University, India (First Division)

REASEARCH DOMAIN:

- Neurosciences • Neurophysiology • Cerebral plasticity • Neuronal encoding • Neural Circuits

CONTRIBUTION SUMMARY:

Until now I have published **eight *(8)*** first-author papers (one combined first-author), **seven *(7)*** co-author papers, **one** chapter (combined first author). During my PhD, I have attended 4 major international conferences, published several abstracts and presented in many national level conferences. Two papers are under review. Currently, I am learning fMRI from a colleague.

❖ **Articles published:**

1. **Bharmauria V,** Bachatene L, Cattan S, Chanauaria N, Etindele-Sosso FA, Molotchnikoff S (2016). Interplay of orientation selectivity and the power of low- and high-gamma bands in cat visual cortex. *Neuroscience Letters* 620: 14-19

2. **Bharmauria V,** Bachatene L, Cattan S, Chanauaria N, Rouat J, Molotchnikoff S (2015). High noise correlation between functionally connected neurons in emergent V1 microcircuits. *Exp. Brain Research* 234: 523-532

3. **Bharmauria V,** Bachatene L, Cattan S, Brodeur, Chanauaria N, Rouat J, Molotchnikoff S (2015). Network-selectivity and stimulus-discrimination in the primary visual cortex: cell assembly dynamics. *Eur. J. Neuroscience* 43: 204-219

4. Bachatene L, **Bharmauria V**, Cattan S, Chanauria N, Rouat J, Molotchnikoff S (2015). Summation of connectivity strengths in the visual cortex reveals stability of neuronal microcircutis after plasticity. *BMC Neurosci.* 16:64

5. Bachatene L, **Bharmauria V,** Cattan S, Chanauria N, Rouat J, Molotchnikoff S (2015). Electrophysiological and firing properties of neurons: categorizing soloists and choristers in primary visual cortex. *Neurosci. Letters* 604:103-108

6. **Bharmauria V,** Bachatene L, Cattan S, Chanauaria N, Rouat J, Molotchnikoff S (2015). Stimulus- dependent augmented gamma oscillatory activity between the functionally connected cortical neurons in the primary visual cortex. *Eur. J. Neurosci*. 41:1587-1596

7. Bachatene L, **Bharmauria V**, Cattan S, Molotchnikoff S (2015). Modulation of functional connectivity following visual adaptation. *Brain Res.* 1594:136-153

8. Bachatene L*, **Bharmauria V***, Cattan S*, Rouat J, Molotchnikoff S (2015). Reprogramming of orientation columns in visual cortex: a domino effect. *Sci. Rep.* DOI:10.1038/srep09436. *equally contributed

9. Cattan S, Bachatene L, **Bharmauria V,** Jeyabalaratnam J, Milleret C, Molotchnikoff S (2014). Comparative analysis of orientation maps in areas 17 and 18 of the cat primary visual cortex following adaptation. *Eur. J. Neurosci*. 3:2554-2563

10. **Bharmauria V,** Bachatene L, Cattan S, Rouat J, Molotchnikoff S (2014). Synergistic activity between primary visual neurons. *Neuroscience* 268:255-264

11. Jeyabalaratnam J, **Bharmauria V,** Bachatene L, Cattan S, Angers A, Molotchnikoff S (2013). Adaptation shifts preferred orientation of tuning curve in the mouse visual cortex. *PLoS One* 5:e64294

12. Bachatene L, **Bharmauria V**, Cattan S, Molotchnikoff S (2013). Fluoxetine and serotonin facilitate attractive-adaptation-induced orientation plasticity in adult cat visual cortex. *Eur. J. Neurosci.* 38:2065-2077

13. Bachatene L**, Bharmauria V,** Rouat J, Molotchnikoff S (2012). Adaptation-induced plasticity and spike waveforms in cat visual cortex. *Neuroreport* 23:88-92

14. **Bharmauria V,** Narang N, Verma V, Sharma S (2010). Efficient DNA isolation from Emblica officinalis for effective PCR. *Sci. Research and Essays* 5:105-109

15. **Bharmauria V,** Narang N, Verma V, Sharma S (2009). Genetic variation and polymorphism in the Himalayan nettle plant Urtica dioica based on RAPD marker. *J. Med Plant Research* 3:166-170

❖ **Articles submitted:**

16. Cattan S, Bachatene L, **Bharmauria V,** Chanauria N, Ribot J, Milleret C, Molotchnikoff S (2015). Pinwheel centers exhibit more plasticity than iso-orientation domains in the cat (*Felis catus*) primary visual cortex. (SREP-15-33431) Scientific Reports

❖ **Chapters:**

1. Bachatene L*, **Bharmauria V***, Molotchnikoff S (2012). Adaptation and neuronal network in visual cortex. *Visual Cortex - Current Status and Perspectives*, ISBN: 978-953-51-0760-6, InTech, doi: 10.5772/46011. *equally contributed

❖ **Abstracts:**

2016

1. Chanauria N, **Bharmauria V**, Bachatene L, Cattan S, Etindele-Sosso FA, Rouat J, Molotchnikoff S. Functional synchrony between the supra and infragranular neurons in the cat V1 pre- and post-adaptation: a homeostatic interplay. (2016, School of Optometry)

2. Mansouri H, El-ezzi A, Etindele-Sosso FA, Bachatene L, **Bharmauria V**, Molotchnikoff S. Effet de la Ketamine sur le mécanisme d'adaptation à l'orientation chez la souris (Submitted Symposium Sciences Biologiques, 2016)

3. **Bharmauria V**, Clevet E. Modèle d'encodage du système visuel (2016, NECOTIS meeting)

4. Chanauria N, **Bharmauria V**, Bachatene L, Cattan S, Etindele-Sosso FA, Rouat J, Molotchnikoff S. Cross-correlation investigation of neurons in supra and infragranular layers in cat V1 before and following adaptation. (Submitted CERNEC, 2016).

5. Etindele-Sosso FA, Chanauria N, Cattan S, **Bharmauria V**, Bachatene L, Molotchnikoff S. Étude de la sélectivité neuronale post-stimulation visuelle chez la souris. (Submitted CERNEC, 2016).

2015

1. **Bharmauria V,** Bachatene L**,** Cattan S, Chanauria N, Molotchnikoff S. The 50-ms window of opportunity inV1 microcircuits. (SfN 2015).

2. Chanauria N, **Bharmauria V**, Bachatene L, Cattan S, Rouat J, Molotchnikoff S. Cross-correlation investigation of neurons in supra and infragranular layers in cat V1 before and following adaptation. (SfN 2015).

3. Bachatene L, **Bharmauria V**, Cattan S, Chanauria N, Rouat J, Molotchnikoff S. Characterizing soloists and choristers in primary visual cortex. (SfN 2015).

4. Bachatene L, Cattan S, **Bharmauria V**, Chanauria N, Rouat J, Molotchnikoff S. Correlation and summation in the visual cortex reveal stable neuronal assemblies (Journée scientifique, centre de recherche en neuropsychologie et cognition, 13-14 March 2015).

5. Bachatene L, **Bharmauria V**, Cattan S, Chanauria N, Rouat J, Molotchnikoff S. Sommation et correlation dans le cortex visuel (Journée scientifique, département des sciences biologiques, UdeM, 11 March 2015)

6. Cattan S, Bachatene L, **Bharmauria V**, Chanauria N, Molotchnikoff S. Modéliser les phénomènes d'adaptation dans le cortex visuel à l'aide de réseaux de neurones. (Journée scientifique, département des sciences biologiques, UdeM, 11 March 2015).

7. Chanauria N, **Bharmauria V**, Bachatene L, Cattan S, Molotchnikoff S. Comparative effects of adaptation on supra (layer 2/3) and infragranular (layer 5/6) layers in the adult cat visual cortex. (Journée scientifique, centre de recherche en neuropsychologie et cognition, 13-14 March 2015).

8. Chanauria N, **Bharmauria V**, Bachatene L, Cattan S, Molotchnikoff S. Comparative effects of adaptation on supra (layer 2/3) and infragranular (layer 5/6) layers in the adult cat visual cortex. (Journée scientifique, département des sciences biologiques, UdeM, 11 March 2015).

9. Balti M, Masri S, **Bharmauria V**, Bachatene L, Cattan S, Chanauria N, Molotchnikoff S. Souris vs Chat: lequel a la plus grande plasticité cérébrale? (Journée scientifique, département des sciences biologiques, UdeM, 11 March 2015).

2014

1. Bachatene L, Cattan S, **Bharmauria V**, Chanauria N, Rouat J, Molotchnikoff S. Plasticity in the visual cortex: Emergence of new orientation maps (Society for Neuroscience, Nov 2014, Published #819.10/FF28)

2. Rouat J, Bachatene L, Cattan S, Adeli M, **Bharmauria V**, Chanauria N, Molotchnikoff S. Noise and brain plasticity? (HUMAIN BRAIN PROJECT Workshop : Stochastic Neural Computation, November 27, 2014)

3. Molotchnikoff S, Bachatene L, **Bharmauria V**, Cattan S. Orientation columns : do they exist ? (Annual meeting, Federation of European Neuroscience Societies, Milano, July 5-9, 2014)

4. Chanauria N, **Bharmauria V**, Bachatene L, Cattan S, Rouat J, Molotchnikoff S. Comparative effects of adaptation on supra- and infra-granular layers in cat's visual cortex (Society for Neuroscience, Nov 2014, Published #819.19/GG5)

5. Cattan S, **Bharmauria V**, Bachatene L, Jeyabalaratnam J, Ribot J, Milleret C, Chanauria N, Molotchnikoff S.Les zones de fort gradient d'orientation sont plus plastiques dans le cortex visuel primaire du chat. (Journée scientifique du groupe de recherche en sciences de la vision, 4 April 2014)

6. Nehme I, Ishak M, Jeyabalaratnam J, Bachatene L, **Bharmauria V**, Cattan S, Molotchnikoff S. Examens des propriétés cellulaires du cortex visuel de la souris suite à une adaptation (Journée scientifique, département des sciences biologiques, UdeM, 26 March 2014)

2013

1. Bachatene L, **Bharmauria V**, Cattan S, Jeyabalaratnam J, Molotchnikoff S. Correlating neuronal activity after adaptation-induced-plasticity in V1 (Society for Neuroscience, Nov 2013, Published #260.05/OO8)

2. Bachatene L, **Bharmauria V**, Cattan S, Molotchnikoff S. Plasticité dans le cortex visuel (Colloque UdeM/ groupe Neurosciences Computationnelles et Traitement Intelligent des Signaux, 1March 2013).

3. Bachatene L, **Bharmauria V**, Cattan S, Molotchnikoff S. Effets des antidépresseurs sur la plasticité du cortex visuel (Journée scientifique, département des sciences biologiques, UdeM, 21 March 2013)

4. Cattan S, Bachatene L, **Bharmauria V**, Molotchnikoff S. Représentations des orientations dans les aires V1 et V2 après adaptation par la method d'imagerie intrinsèque (Colloque UdeM/ groupe Neurosciences Computationnelles et Traitement Intelligent des Signaux, 1 March 2013)

5. **Bharmauria V**, Bachatene L, Cattan S, Jeyabalaratnam J, Rouat J, Molotchnikoff S. Synergistic activity in V1 neuronal assembly (Society for Neuroscience, Nov 2013, Published #638.06/DD1)

6. Cattan S, Bachatene L, **Bharmauria V**, Molotchnikoff S. Effets de l'adaptation et des antidépresseurs sur la plasticité du cortex visuel (Journée scientifique, centre de recherche en neuropsychologie et cognition, 05-06April 2013)

7. **C**attan S, **Bharmauria V**, Bachatene L, Jeyabalaratnam J, Ribot J, Milleret C, Chanauria N, Molotchnikoff S.Orientation-domains exhibit more plasticity than pinwheel-centers in V1 (Society for Neuroscience, Nov 2013, Published #260.06/OO9

8. Suissa L, Yahia MA, Megarbané L, Jeyabalaratnam J, Bachatene L, **Bharmauria V**, Cattan S, Angers A, Molotchnikoff S. L'effet de la sérotonine et de la fluoxétine sur la quantité de MAPK dans le cortex visuel

primaire de la souris suite à l'adaptation (Journée scientifique, département des sciences biologiques, UdeM, 21 March 2013)

2012

1. Bachatene L, **Bharmauria V**, Cattan S, Rouat J, Molotchnikoff S. Serotonin and Fluoxetine Increase Adaptation-induced Orientation Plasticity in Adult Cat's Visual Cortex (Society for Neuroscience, Oct 2012, Published #572.09/FF10)

2. Bachatene L, **Bharmauria V**, Cattan S, Rouat J, Molotchnikoff S. Serotonin and Fluoxetine Increase Adaptation-induced Orientation Plasticity in Adult Cat's Visual Cortex (Réunion annuelle Réseau de recherché en santé de la vision du FRQS – 19 Oct 2012)

3. Bachatene L, **Bharmauria V**, Cattan S, Molotchnikoff S. Effets de la sérotonine et de la fluoxetine sur la plasticité du cortex visuel primaire (Journée scientifique de l'école d'Optométrie, Groupe de Recherche en Sciences de la Vision, March 2012)

4. Cattan S, Bachatene L, **Bharmauria V**, Ribot J, Milleret C, Molotchnikoff S. Adaptation-induced plasticity in V2. (Réunion annuelle Réseau de recherché en santé de la vision du FRQS – 19 Oct 2012

5. **Bharmauria V**, Bachatene L, Cattan S, Rouat J, Molotchnikoff S. Network-selectivity between Primary Visual Cortical Neurons: Connectome Dynamics (Society for Neuroscience, Oct 2012, Published #572.07/FF8)

6. Cattan S, Bachatene L, **Bharmauria V**, Ribot J, Milleret C, Molotchnikoff S. Adaptation-induced plasticity in V2 (Society for Neuroscience, Oct 2012, Published #572.08/FF9)

7. Brodeur S, **Bharmauria V**, Bachatene L, Rouat J, Molotchnikoff S. Investigating functional connectivity maps through simulation of cortical networks (Society for Neuroscience, Oct 2012, Published #572.06/FF7)

8. Passarelli Y, Clini L, Jeyabalaratnam J, Bachatene L, **Bharmauria V**, Cattan S, Forget R, Angers A, Molotchnikoff S. Effet de la sérotonine sur la cascade moléculaire de la plasticité du cortex visuel chez la souris (Symposium du département des Sciences Biologiques, April 2012 p.19)

2011

1. Bachatene L, **Bharmauria V**, Molotchnikoff S. Adaptation induced plasticity in pyramidal cells and interneurons in visual cortex (Ann. Meeting Réseau Vision, Nov 2011, Québec

❖ **Talks**

1. **Bharmauria V,** Bachatene L**,** Cattan S, Chanauria N, Molotchnikoff S. Augmented gamma-activity between functionally connected neurons in V1 (Journée scientifique du groupe de recherche en sciences de la vision, 27m March 2015).

2. **Bharmauria V,** Cattan S. Big Data Problem (Colloque coinjoint, UdeM – UdeS, NECOTIS, 20 Feb 2015).

3. **Bharmauria V**, Bachatene L, Cattan S, Molotchnikoff S. Network selectivity and stimulu discrimination inV1: Connectome dynamics (Journée Scientifique de l'École d'Optométrie, 22 March 2013).

4. **Bharmauria V**, Bachatene L, Cattan S, Molotchnikoff S. Network selectivity between primary visual neurons (Journée scientifique de l'axe cerveau et perception du réseau vision – 24 May 2012)

5. **Bharmauria V**, Bachatene L, Cattan S, Molotchnikoff S. Language of brain (Colloque UdeM/ groupe Neurosciences Computationnelles et Traitement Intelligent des Signaux, 1 March 2013).

6. **Bharmauria V**, Bachatene L, Cattan S, Rouat J, Molotchnikoff S. Connectome Dynamics (Colloque FQRNT/UdeM/UdeS – NECOTIS 30 August 2012)

7. **Bharmauria V**, Bachatene L, Cattan S, Jeyabalaratnam J, Passarelli Y, Clini L, Rouat J, Molotchnikoff S Formation des circuits neuronaux en réponse aux stimuli visuels (Symposium du département de sciences biologiques, April2012, p.19)

8. **Bharmauria V**, Bachatene L, Cattan S, Rouat J, Molotchnikoff S. Network selectivity between primary visual cortical neurons : dynamics of connectome (Réunion annuelle Réseau de recherché en santé de la vision du FRQS – 19 Oct 2012)

9. **Bharmauria V**, Bachatene L, Cattan S, Rouat J, Molotchnikoff S. Neuronal circuit formation in response to visual stimuli (Journée scientifique du Centre de recherche en Neurophysiologie et Cognition, March 2012, St Sauveur)

10. **Bharmauria V**, Molotchnikoff S. Decoding the visual stimuli by neuronal network formation. (5 Dec 2011Necotis meeting

INVITED TALKS:

1. **Bharmauria V.** The dynamics of connectome. Dr. Sophie Breton's Course (2013)

2. **Bharmauria V.** Spikes and oscillations. Dr. Karim Jerbi's Lab meeting (2015)

SCHOLARSHIPS:

1. Bourses d'exemption des droits supplémentaires de scolarité pour étudiants internationaux (Fee-waiver scholarship from the Graduate studies), University of Montreal, (Sep 2011- Sep 2013) **$30,000**

2. Research Scholarship for Graduate studies (PhD), CERNEC (Centre de recherche en Neurophyschologie et Cognition), (Nov 2013-Nov 2014) **(COMPETITIVE)** **$10,000**

3. Bourse de fin d'études doctorales (Scholarship for finishing doctoral studies), Univrsity of Montreal, (August2015-present) **(COMPETITIVE)** **$12,000**

4. Bourse d'études du GRSV: École d'Optometrie, *Université de Montréal, Canada* (Année 2012)

CONTRIBUTION TO STUDENT SUPERVISION (Supervisor: Dr. Stéphane Molotchnikoff):

1. Bachelor Student Afef Ouelhazi , Anastasia El Azzi, Hidayat Mansouri 2015 – present
"Effect of Ketamine on visual cortical plasticity"
University of Montreal

2. Bachelor Student Samir Masri, Malik Balti Jan 2014 – Jul 2014
"Effect of serotonin on neuronal plasticity in mouse V1"
University of Montreal

3. Bachelor Student Vanessa Diab, Sarah Massol Jan 2014 – Jul 2014
"Investigating neuronal circuitries in mouse V1"
University of Montreal

4. Bachelor Student Laurent Suissa, Lynn Megarbane, Massicylia Ait Yahia Jan 2013 – Jul 2013
"Effect of Serotonin and Fluoxteine on MAP kinase in mouse V1"
University of Montreal

5. Bachelor Student Jeyabalaratnam Jeyadarshan Jan 2012 – July 2012
"Effect of adaptation on neuronal selectivity in mouse V1"
University of Montreal

6. Bachelor Student Raefat El Jammal Jan 2012 – Jul 2012
"Effect of aaptation on molecular cascades in mouse V1"
University of Montreal

7. Bachelor Student Yannick Passarelli, Livia Clini Jan 2012 – Jul 2012
"Effect of Serotonin on molecular cascades in mouse V1"
University of Montreal

BIBLIOMETRIC MEASURES:

Total citations: 70
H-index: 6
I-index: 2
International conferences attended: 4, 14 posters presented

MEMBERSHIP:

SFN (Society for Neuroscience)
CERNEC (Centre de recherche en Neurophyschologie et Cognition)
NECOTIS (Neurosciences Computationnelles et Traitement Intelligent des Signaux)
AMI (Association of Microbiologists of India)

WORK EXPERIENCE:

1. **Teaching Assistant (Auxiliaire d'enseignement)**
   Département de Sciences Biologiques, Université de Montréal (Sep 2011- present)
   - ❖ Physiologie nerveuse et musculaire (BIO3661): Demonstrator
   - ❖ Principles de Physiologie animale (BIO1634): Demonstrator
   - ❖ Respiration, circulation et excrétion (BIO3674): Demonstrator
   - ❖ Physiologie animale comparée 1 (BIO2620): Demonstrator
   - ❖ Physiologie animale comparée 2 (BIO2625): Demonstrator

2. **Lecturer,** Genetics and Instrumental methods of Analysis, Shoolini Institute of Life Sciences **(** July 2007-Dec 2008)

3. **Lecturer (Voluntary),** Molecular Biology and Genetics**,** Shoolini University (Oct 2009-August 2010)

ARTICLES REVIEWED: 11

1. 5 (ISBN 980-953-307-044-0**)** (Visual Cortex- Current Status and Perspective**s)**
2. 1 (EJN-2015-01-22445) (European Journal of Neuroscience)
3. 1 (IJAS-12-131) (International Journal of Agricultural Sciences)
4. 2 (AJPP-12-008) (AJPP-12-587) (African Journal of Pharmacy and Pharmacology)
5. 1 (AJAR-12- 130) (African Journal of Agricultural Research)
6. 1 (JMPR-11-999) (Journal of Medicinal Plants Research)

OTHER SKILLS AND ACHIEVEMENTS:

- Programming Skills: Elementary Matlab, Elementary Python, Adobe photoshop
- Interests: Cricket, Music, Movies, Trekking, Painting, Writing
- Languages: English, Hindi, Punjabi, Elementary French
- Captained the School and College Cricket teams
- Founding member of University Montreal Cricket Club
- Ex-Secretary, University Montreal Cricket Club
- Member of Champion team of Quebec Cricket Federation Premier League, 2014 and 2015
- Directed a play (In the Light)

Internship:

1. Research project on Genetic markers on Himalayan Plants *(Urtica dioca and Emblica officinalis*) (2006)
2. Worked voluntarily in AIIMS (All India Institute of Medical sciences) to develop a Multiplex PCR, Department of Laboratory Medicine (Feb 2009-May 2009)
3. Worked voluntarily in JNU (Jawaharlal Nehru University) on a fungus *Pirifromaspora indica* (July 2009)
4. 45 days training in G- Biosciences, Noida, India, 2007.
5. 15 day course in Computational Neurosciences: "7th Ottawa Summer School in Computational Neurosciences", University of Ottawa, 2014.
6. Spike 2 Course, New Orleans, during Society for Neuroscience meeting.

REFERENCES: Available upon request